Electrophilic Ring Bond Activation of $2H$-Azaphosphirene Complexes

Dissertation

zur Erlangung des Doktorgrades (Dr. rer. nat.)
der Mathematisch-Naturwissenschaftlichen Fakultät
der
Rheinischen Friedrich-Wilhelms-Universität Bonn

vorgelegt von

Holger Helten

aus Bonn

Bonn, 2009

Angefertigt mit Genehmigung der Mathematisch-Naturwissenschaftlichen Fakultät
der Rheinischen Friedrich-Wilhelms-Universität Bonn

Zwei Dinge sind zu unserer Arbeit nötig: Unermüdliche Ausdauer und die Bereitschaft, etwas, in das man viel Zeit und Arbeit gesteckt hat, wieder wegzuwerfen.

Albert Einstein

This Thesis contains results previously published

H. Helten, S. Fankel, O. Feier-Iova, M. Nieger, A. Espinosa Ferao, R. Streubel, *Strong Evidence for an Unprecedented Borderline Case of Dissociation and Cycloaddition in Open-Shell 1,3-Dipole Chemistry: Transient Nitrilium Phosphane-Ylide Complex Radical Cations, Eur. J. Inorg. Chem.* **2009**, 3226−3237.

H. Helten, G. von Frantzius, G. Schnakenburg, J. Daniels, R. Streubel, *How To Tune Acid-Induced Ring Enlargement Reactions – The Strange Case of 2H-Azaphosphirene Complexes and Its Surprising Dichotomy, Eur. J. Inorg. Chem.* **2009**, 2062−2065.

H. Helten, M. Engeser, D. Gudat, R. Schilling, G. Schnakenburg, M. Nieger, R. Streubel, *Protonation of 2H-Azaphosphirene Complexes: P–N Bond Activation and Ring-Expansion Reactions, Chem. Eur. J.* **2009**, *15*, 2602−2616.

H. Helten, C. Neumann, A. Espinosa, P. G. Jones, M. Nieger, R. Streubel, *Evidence for Ligand-Centered Reactivity of a 17e Radical Cationic 2H-Azaphosphirene Complex, Eur. J. Inorg. Chem.* **2007**, 4669−4678.

Publications on related topics

S. Fankel, H. Helten, G. von Frantzius, G. Schnakenburg, J. Daniels, V. Chu, C. Müller, R. Streubel, *Novel Access to Azaphosphiridine Complexes and First Applications Using Brønsted Acid-induced Ring Expansion Reactions*, submitted.

R. Streubel, M. Beckmann, C. Neumann, S. Fankel, H. Helten, O. Feier-Iova, P. G. Jones, M. Nieger, *Synthesis, Structure, and Ring-Expansion Reactions of a 3-Ferrocenyl-Substituted 2H-Azaphosphirene Tungsten Complex, Eur. J. Inorg. Chem.* **2009**, 2090−2095.

H. Helten, J. Marinas Pérez, J. Daniels, R. Streubel, *First Brønsted Acid-Induced Ring Expansion of an Oxaphosphirane Complex: A Combined Experimental and DFT Study, Organometallics* **2009**, *28*, 1221−1226.

Conference contributions

H. Helten, A. Espinosa, R. Streubel, Summer School 2009 Computational Chemistry and Spectroscopy, September 22.–25. **2009**; *"DFT Calculations of Open-Shell 2H-Azaphosphirene Complexes. Nitrile Insertion via Transient Nitrilium Phosphane-Ylide Complex Radical Cations"*, poster.

A. Espinosa Ferao, S. Fankel, H. Helten, M. Nieger, R. Streubel, 12th International Symposium on Inorganic Ring Systems, Goa/India, August 16.–21. **2009**; *"Open-Shell Chemistry of 2H-Azaphosphirene Complex Radical Cations and their Acyclic Distonic Isomers – New Perspectives for Inorganic Ring Systems"*, OL-33 (A. Espinosa Ferao).

H. Helten, M. Engeser, D. Gudat, A. Espinosa Ferao, R. Streubel, 6th European Workshop on Phosphorus Chemistry, Florence/Italy, March 26.–27. **2009**; *"Oxidative and Acid Induced Ring Expansion of 2H-Azaphosphirene Complexes"*, P23.

H. Helten, A. Espinosa Ferao, R. Streubel, 7th Ferrocene Colloquium, Düsseldorf/Germany, Feb. 16.–18. **2009**; *"Ferrocenium Salt and Triflic Acid Induced Ring Expansion of 2H-Azaphosphirene Complexes"*, P11.

H. Helten, R. Streubel, SFB 624 Doktoranden-Workshop, October 9.–10. **2008**; *"Ferroceniumsalz- versus Triflatsäure-Induzierte 2H-Azaphosphiren-Ringerweiterung – ein Methodenvergleich"*, TP A3.

H. Helten, R. Streubel, D. Gudat, A. Espinosa, G. Schnakenburg, M. Nieger, International Conference on Heteroatom Chemistry – 08, Riverside, California, USA, August 14. **2007**; *"Bond Activation in Phosphorus Heterocyclic Chemistry"*, (oral contribution).

S. Fankel, H. Helten, A. Espinosa Ferao, R. Streubel, SFB 624, International Symposium "Complex Molecular Architectures on Surfaces", Bonn/Germany, October 12. **2006**; *"Preliminary Studies on Template-Directed Synthesis of N,P-Cavitand Complexes Having Ferrocene-1,1'-Diyl Bridges"*, P-A3-II.

H. Helten, M. Nieger, R. Streubel, 11th International Symposium on Inorganic Ring Systems, Oulu/Finland, July/August, **2006**; *"Novel Access to 2H-1,4,2-Diazaphosphole and 3H-1,3-Azaphosphole Complexes"*, P-88.

H. Helten, M. Nieger, R. Streubel, XXII International Conference on Organometallic Chemistry, Zaragoza/Spain, July, **2006**; *"Arenediyl-Bridged Biscarbene Complexes and the First 2H-Azaphosphirene Complex- / Carbene Complex-Difunctionalized Ferrocene"*, P-192.

R. Streubel, H. Helten, S. Fankel, J. Marinas Pérez, M. Nieger, A. Espinosa Ferao, XXII International Conference on Organometallic Chemistry, Zaragoza/Spain, July, **2006**; *"Novel Access to Mono- and Bis-Ferrocenyl-Substituted Phosphorus Heterocycles"*, P-53.

S. Fankel, H. Helten, M. Nieger, R. Streubel, XXII International Conference on Organometallic Chemistry, Zaragoza/Spain, July, **2006**; *"Preliminary Studies on Template-Directed Synthesis of N,P-Cavitand Complexes Having Ferrocenediyl Bridges"*, P-54.

H. Helten, R. Streubel, 1st Ph.D. Meeting on Main Group Element Chemistry, Graz/Austria, April 19. **2006**; *"Maskierte Phospheniumkomplexe als Synthesebausteine zum Aufbau von C,N,P-Heterocyclen"*, (oral contribution).

H. Helten, M. Nieger, R. Streubel, 3rd Ph.D. Meeting on Phosphorus Chemistry, Leipzig/Germany, March, **2006**; *"Masked Phosphenium Complexes as Building Blocks for C,N,P-Heterocycles"*, (oral contribution).

H. Helten, Schleiden/Germany, SFB 624, Workshop "Vom Design chemischer Schablonen zur Reaktionssteuerung", November 03.–04. **2005**; *"Ferrocenyl-Substituierte 2H-1,2,4-Diazaphosphol-Komplexe"*, (oral contribution).

H. Helten, S. Fankel, R. Streubel, Schleiden/Germany, SFB 624, Workshop "Vom Design chemischer Schablonen zur Reaktionssteuerung", November 03.–04. **2005**; *"Erste Untersuchungen zur Templatgesteuerten Synthese Polyfunktioneller N,P-Cavitanden"*, P-A3-II.

H. Helten, R. Streubel, GDCh-Jahrestagung 2005, Düsseldorf/Germany, September, **2005**; *"A Phosphenium Complex that Reacts Like a 1,3-Dipole"*, AC-037.

DANKSAGUNG

Contents

List of Figures

List of Schemes

List of Tables

Chapter 1

Introduction: Synthesis of Heterocycles via Ring Expansion

The chemistry of small ring systems[1] such as aziridines (**I**),[2–4] epoxides (oxiranes) (**II**),[3, 5–7] phosphiranes (**III**),[8, 9] and thiiranes (**IV**)[10] (Fig. 1.1) is dominated by *ring opening* reactions, the driving force for which is relief of ring strain.[1] This feature makes them highly versatile building blocks in synthetic organic chemistry[3, 4, 6–10] and drug design.[11] Their fundamental industrial utility becomes obvious in view of the large-scale production of poly(ethylene glycols)[12] and polyamines[13] through ring opening polymerization (ROP)[14] of epoxides[12] or aziridines,[13] respectively.
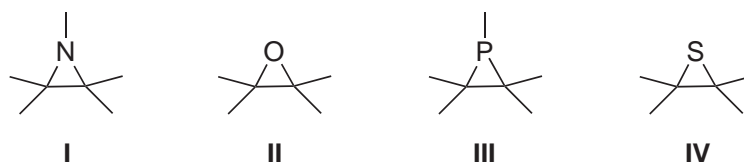
Figure 1.1: Saturated three-membered heterocycles: aziridines (**I**),[2–4] epoxides (**II**),[3, 5–7] phosphiranes (**III**),[8, 9] and thiiranes (**IV**).[10] Solid lines denote (here and in the following schemes and figures) common organic substituents.

In particular, the use of small ring systems for the synthesis of larger heterocycles via *ring expansion* is an important field of active research as it shall be illustrated by some selected examples in the following paragraphs. Such transformations provide access to heterocyclic compounds that are useful in various fields of application, for instance, as ligands in organometallic catalysis[15] or as essential intermediates in organic synthesis;[16] the outstanding importance of several kinds of heterocycles is due to their pharmacological activity.[17]

1.1 Ring Expansion of Saturated Three-Membered Heterocycles

Activated[1] aziridines react with a wide range of nucleophiles in general via C,N bond
cleavage to acyclic products (**V**) (Scheme 1.1, i).[4, 18, 20–22] Employment of π-systems
offers the possibility of ring expansion. Depending on the reactants and on the specific
reaction conditions the π-system can be inserted either into the C,N (ii) or into the
C,C bond of **I** (iii $\rightarrow$ iv or v $\rightarrow$ vi), which opens up ways to a variety of heterocyclic
compounds (**VI**, **VIII**).[3, 4]
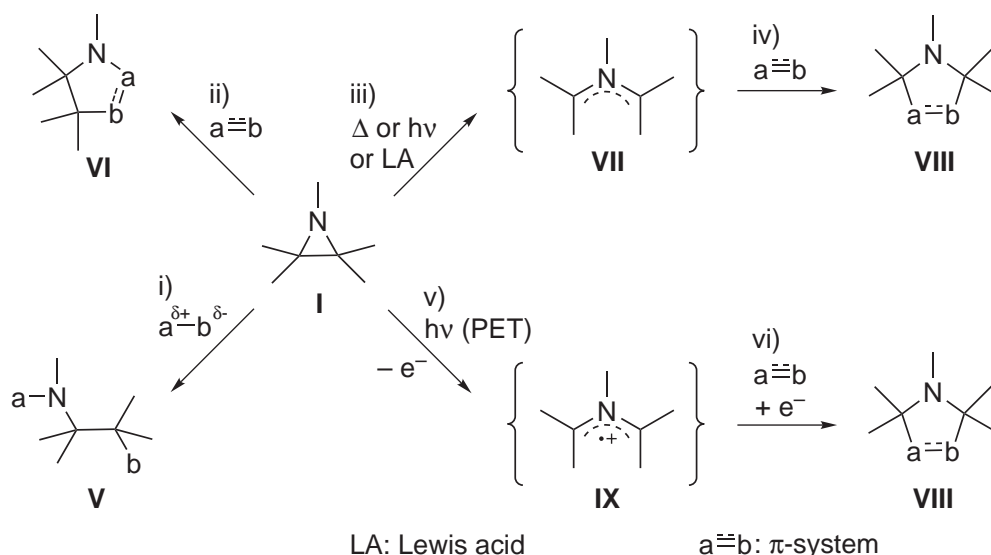
Scheme 1.1: Different reaction modes of aziridines (**I**):[3, 4] electrophilic or nucleophilic
ring opening to yield acyclic amines (**V**) (i),[4, 18–22] ring expansion affording heterocy-
cles **VI** via C,N bond cleavage (ii),[23–29] thermally,[30] photochemically,[23, 31] or Lewis
acid-induced[32] C,C bond cleavage with formation of transient azomethine ylides (**VII**)
(iii)[23, 30–33] and subsequent cycloaddition to give heterocycles **VIII** (iv),[23, 30–33] and
C,C bond cleavage under photoinduced electron transfer (PET) conditions with for-
mation of radical cationic azomethine ylides (**IX**) (v)[23, 33] followed by back electron
transfer and cycloaddition to yield heterocycles **VIII** (vi).[23, 33]

In most insertion reactions into the C,N bond of **I** (ii) alkenes and alkynes were
employed, which led to pyrrolidine or pyrroline derivatives.[23, 24] The use of CO_2
and CS_2 for ring expansion reactions giving 1,3-oxazolidin-2-ones and urethanes,[25]

---

[1]Aziridines are commonly classified as "activated" (towards the addition of nucleophiles) if they
contain a substituent at nitrogen that facilitates their ring opening such as COR, CO_2R, or SO_2R.[18]
Nonactivated aziridines are inert towards most nucleophiles[19] and require prior activation with a
Lewis[20, 21] or Brønsted[21, 22] acid.

as well as insertions of heterocumulenes such as carbodiimides, ketenimines, and iso-
cyanates have also been presented.[26] In contrast, not many reports involving nitriles
as π-components have found sizable entry into the literature. Such reactions required
N-tosyl- or N-alkoxycarbonylaziridines and harsh reaction conditions: high temper-
atures, addition of Lewis acids, and excess of nitrile (e.g., as solvent).[27] Lewis acid
promoted ring expansions with nitriles could be achieved under mild conditions only on
N-tosylaziridine derivatives that were activated further by a ring substituent capable
of stabilizing an evolving positive charge in the α-position.[28, 29]

The efficiency of Brønsted acids was impressively demonstrated on ring opening of
nonactivated aziridines with amine nucleophiles,[22] although in this case the *Lewis
acid* tris(pentafluorophenyl)borane was employed. It was observed that conversions
were significantly accelerated in the presence of water, and NMR spectroscopic reaction
monitoring revealed that $[(C_6F_5)_3B(OH_2)] \cdot H_2O$ was being formed *in situ*. This acted
as a strong *Brønsted acid*, which induced the ring opening process very effectively.[22]

The endocyclic C,C bond of aziridines can be cleaved via thermal[30] or photochem-
ical[23, 31] electrocyclic ring opening (Scheme 1.1, iii). In this way transient azome-
thine ylides (**VII**)[23, 30–32, 34] are generated, and their reactions with dipolarophiles
via [3+2] cycloaddition can afford five-membered heterocycles (**VIII**).[23, 30–32] Under
PET conditions,[23] pulse or γ radiolysis[33] aziridines are oxidized to radical cations,
which can undergo ring opening[2] (v) with formation of radical cationic azomethine
ylides (**IX**). Upon reactions with π-systems in combination with back electron trans-
fer from a photosensitizer (vi) heterocycles **VIII** were obtained; the exact sequence
is still unknown.[23] It has been shown that N-aryl substituted aziridines retain their
cyclic structure upon oxidation, and such radical cationic aziridines did not react with
dipolarophiles.[33] Ring expansions via C,C bond cleavage of appropriately substituted
aziridines could be induced also by Lewis acids,[32] which presumably involved inter-
mediately generated azomethine ylides as well. In this particular case the aziridine $\rightarrow$
azomethine ylide[3] rearrangement was induced by donor–acceptor complex formation
of the Lewis acid—not with the aziridine nitrogen—but with a carboxyl group at a
ring carbon center of the aziridine.[32]

Oxiranes (**II**)[3, 6, 7] and thiiranes (**IV**)[10] exhibit a comparably rich chemistry that
shall not be discussed further, here. In contrast, the chemistry of phosphiranes
(**III**),[8, 9] and phosphorus-carbon heterocycles in general,[9] has been largely undevel-
oped for a long time. The first phosphiranes (**III**) were synthesized in 1963,[35] almost
one century after the discovery of aziridine in 1888,[2] and since then their reactivity has

---

[2]In this case the ring opening process is not stereospecific.

[3]Azomethine ylides can also be generated from N-malonylimidates through acivation with a Lewis
acid.[34]

become a rapidly growing field of active research.[8,9] These heterocycles can undergo
an additional mode of ring bond cleavage that lacks analogous examples in aziridine
chemistry: the simultaneous homolytic cleavage of both endocyclic heteroatom–carbon
bonds.[8] Such thermally induced reactions afford an alkene along with a low coordi-
nated phosphorus fragment: a phosphanediyl,[36,37] a phosphanylidene oxide (in the
case of the thermolysis of phosphirane oxides),[38] or a phosphanylidene complex (in
case of phosphirane κP-metal complexes).[39,40] Its formation was in each case postu-
lated on the basis of trapping experiments[37–40] or intramolecular rearrangements.[36]
It has been shown that the cleavage of both P,C bonds of the phosphirane ring can also
occur upon attack of nucleophiles.[36,41,42] Reactions that address only one P,C ring
bond could be induced either by protic reagents or nucleophiles, whereas the polarity
of the P,C bond, thus, the regiochemistry of the ring opening is highly sensitive to the
substitution pattern at the phosphirane ring.[42–45] The nucleophilic reactivity of the
phosphorus lone pair of **II** is generally low, and reactions with acids or quaternizing
agents (RX) do not necessarily give the corresponding phosphiranium salts.[9] How-
ever, such reactions have been presented,[46,47] and in some instances ring opening was
observed upon quaternization.[46]

The majority of reports on ring expansions of phosphiranes concern internal rear-
rangements.[44,48] The first example of an *intermolecular* insertion reaction into a P,C
bond of the phosphirane ring system was described by Marinetti and Mathey.[44] Re-
action with enol ether **2** yielded ring enlargement of activated phosphirane complex **1**
by two carbon centers with formation of phospholane complex **3** (Scheme 1.2).[4]
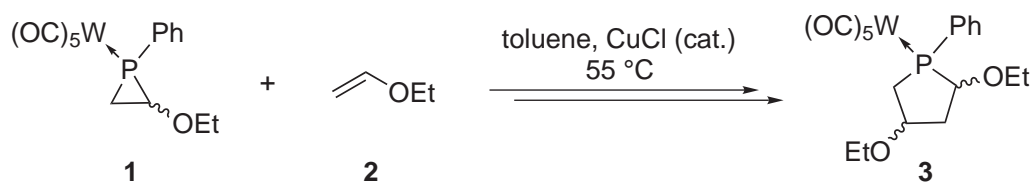
Scheme 1.2: Synthesis of phospholane complex **3** by ring expansion of phosphirane
complex **1** with enol ether **2**.[44]

Insertions of alkenes or alkynes into the P,C bond of a 2-alkylidenephosphirane com-
plex could be achieved via transition metal catalysis as a recent example showed.[49]

---

[4]The schemes displayed in this work do not always show stoichiometric reaction equations. In
general, they constitute descriptions of reaction progressions in terms of employed reactants, added
reagents, and formed products. Double arrows indicate that by-products were omitted (e.g., if cat-
alytic amounts of reagents were employed that might be consumed) or that several reaction steps
were omitted.

1.2 Ring Expansion of Unsaturated Three-Membered Heterocycles

Regarding the unsaturated three-membered heterocycles containing one group 15 element **X**–**XIII** (Fig. 1.2) an interesting trend is found. $1H$-Azirenes[5] (**X**)[50,51] are classified as unstable 4π-electron hetero-*antiaromatic* systems whose existence has been indicated only by trapping reactions until now.[50] Their chemistry is limited to the role as reactive intermediates,[51] and unidirectional isomerizations to $2H$-azirenes (**XI**) have been observed.[52] In contrast, the latter are stable heterocyclic compounds; their chemistry has extensively been explored in the last decades.[52,53]
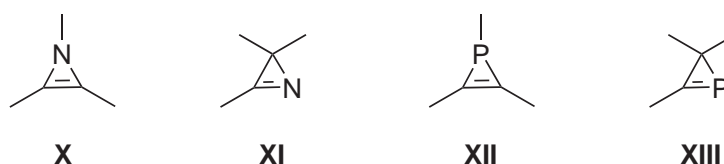
Figure 1.2: Unsaturated three-membered heterocycles with one group 15 element: $1H$-azirenes (**X**),[50,51] $2H$-azirenes (**XI**),[52,53] $1H$-phosphirenes (**XII**),[8,9,54] and $2H$-phosphirenes (**XIII**).[8,55–59]

A different situation is found for the isomeric phosphirenes **XII** and **XIII**. For $\sigma^2\lambda^3$-$2H$-phosphirenes (**XIII**), which are difficult to access,[8,55–59] an isomerization in the opposite direction (**XIII** → **XII**) was observed.[60]

2-Phosphino-$2H$-phosphirene **6** (Scheme 1.3), generated by [2+1] cycloaddition of phosphino(silyl)carbene **4**[61,62] with phosphaalkene **5**, could be characterized via NMR spectroscopy from the reaction mixture.[59] It rearranged quantitatively to $1\lambda^5,2\lambda^3$-diphosphete **7**.[59,63] This non-antiaromatic four-π-electron four-membered heterocycle was further converted to 1,2-dihydro-$1\lambda^3,2\lambda^3$-diphosphete **8** upon irradiation at 254 nm. The attempt to trap a BH_3 adduct of **6** resulted in ring expansion and formation of a BH_3 adduct of **7**.[59] Irradiation of **6** yielded isomerization to $1H$-phosphirene **9**; the latter did not undergo ring expansion upon further irradiation.

---

[5]*Azirene* is the denotation for this heterocycle according to the modified Hantzsch-Widman-Patterson system. However, the former denotation, *azirine*, is frequently used in the literature.
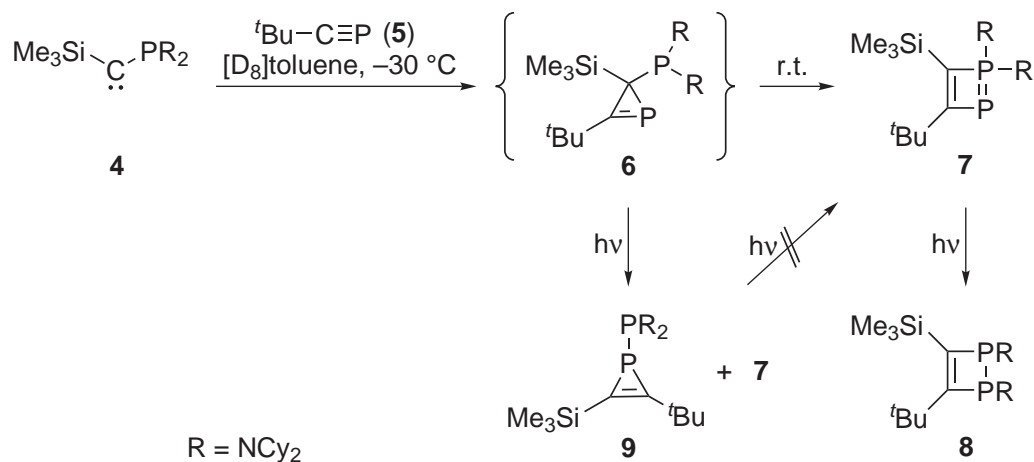
Scheme 1.3: Generation of 2-phosphino-$2H$-phosphirene **6**, intramolecular ring expansion to $1\lambda^5,2\lambda^3$-diphosphete **7**, photoinduced rearrangement of **7** to 1,2-dihydro-$1\lambda^3,2\lambda^3$-diphosphete **8**, and photoinduced isomerization of **6** to $1H$-phosphirene **9** (Cy = cyclohexyl).[59]

The more stable $1H$-phosphirenes (**XII**)[8,9,54] (Fig. 1.2) and κP-metal complexes thereof[8,9,64,65] can act as phosphanediyl sources (alike their saturated congeners **III**, Fig. 1.1) through thermal cleavage of both P,C bonds.[8,39] As in the case of **III** the nucleophilicity of the phosphorus lone pair of tervalent $1H$-phosphirenes is low.[8] However, phosphirenium salts[66] could be obtained by alkylation or bromination of the phosphorus center.[54] The ambivalence of the P,C bond in general becomes noticeable in the behavior of $1H$-phosphirenes towards electrophiles and nucleophiles.[8] Ring opening with P,C bond cleavage was observed upon protic[67] or nucleophilic[54] attack. It has been demonstrated that the regiochemistry for nucleophilic ring opening of a $1H$-phosphirene κP-metal complex (attack at C vs. P) may be dictated by steric factors.[54] Furthermore, some intramolecular rearrangement reactions have been described for the $1H$-phosphirene system that resulted in ring expansion.[68,69]

At high temperature pentacarbonyl metal complexes **10a–e** inserted CO into the P,C bond with formation of 2-keto-1,2-dihydrophosphete complexes **11a–e**, which can be regarded as phosphorus analogues of unsaturated β-lactams (Scheme 1.4).[70] The mechanism presumably involves an intermediate four-membered metallacycle.[70] This hypothesis was reinforced by the observation that $1H$-phosphirenes and their complexes readily insert 14-electron organometallic species, and it has been shown that a resulting nickelacycle was able to insert CO.[71] Transition metals could promote also the insertion of terminal alkynes into the $1H$-phosphirene ring of **10a,b**.[72,73]
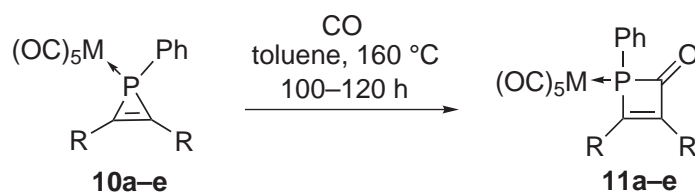
Scheme 1.4: Thermal insertion of CO into the P,C bond of $1H$-phosphirene complexes
10a–e (**a**: R = Ph, M = W; **b**: R = Et, M = W; **c**: R = Ph, M = Mo; **d**: R = Ph, M
= Cr; **e**: R = Et, M = Cr).[70]

Also transient terminal phosphanylidene complexes could be inserted into the P,C
bond of $1H$-phosphirene κP-tungsten complexes,[74] in a similar way iminophosphanes
reacted (via the phosphorus center) with phosphirene N-imines.[75] The formal in-
sertion of phosphanediyls or arsanediyls into the P,C bond of $1H$-phosphirenes was
achieved by reaction with dichlorophosphanes or dichloroarsanes.[76] In this case elec-
trophilic attack at phosphorus yielded a phosphirenium chloride that immediately
underwent intramolecular ring expansion; the intermediacy of the phosphirenium salt
was demonstrated by using $AlCl_3$ as a trap for the chloride ion.[76]

$2H$-Azirenes (**XI**)[52,53] (Fig. 1.2) proved to be highly versatile building blocks for
the synthesis of heterocycles.[52,53] Depending on the specific reaction conditions each
of the three ring bonds can selectively be cleaved[6] (Scheme 1.5).[53,77,78] Electrophilic
attack takes place at the nitrogen electron lone pair, while nucleophiles attack—in the
majority of cases—the doubly bonded C^3 atom (i).[53,79–84] Accordingly, hydrolysis of
the imine functionality of **XI** gives α-amino ketones.[79,81] This reactivity can also be
utilized for the synthesis of heterocycles. For example, N-acylation with acyl chlorides
in the presence of triethylamine affords oxazole derivatives via cyclization of interme-
diately formed N-acyl-2-chloroaziridines.[80] Furthermore, $2H$-azirene transition metal
complexes and metal-induced reactions of $2H$-azirenes have been described.[85,86] In
the presence of carbonyl complexes of group 6 transition metals dimerization reactions
were observed, which led to pyrazine derivatives.[86]

3-Amino-$2H$-azirenes react with carboxylic acids after protonation of the ring nitro-
gen atom via nucleophilic attack of the carboxylate at C^3 of a postulated $2H$-azirenium
intermediate (N-protonated $2H$-azirene; here with an amidinium substructure).[87] In-
tramolecular N-acylation and subsequent cleavage of the former C^3,N double bond
yields open chain α-amino acid derivatives.[87] If trifluoroacetamide is employed in-
stead, the initiatory 1,2-addition of the acidic NH functionality of the acetamide to

---

[6]Cleavage of the C^3,N bond is not shown in Scheme 1.5; it may occur upon previous electrophilic
or nucleophilic addition (via i) to this bond (vide infra). It should further be noted that the species
XIV and **XV** (like **XVI** and **XVIII**) constitute reactive intermediates. They undergo follow-up
reactions that might be useful for the synthesis of heterocycles as discussed in the following.

the C^3,N double bond is followed by a cyclization step, which finally affords $4H$-imidazole derivatives.[88] This ring expansion protocol was devised by Heimgartner and coworkers.[88] They further showed that it is also applicable to NH-acidic heterocycles, which leads upon reaction with 3-amino-$2H$-azirenes to new heterocycles with a ring enlarged by three atoms (C–C–N);[87,89] the overall applicability of this methodology is limited by the acidity of such reactants.[87,90] It is remarkable that—in spite of the versatile preparative applicability of this methodology—no clear-cut proof for transient $2H$-azirenium derivatives has been provided so far.[79,82,83,91,92]
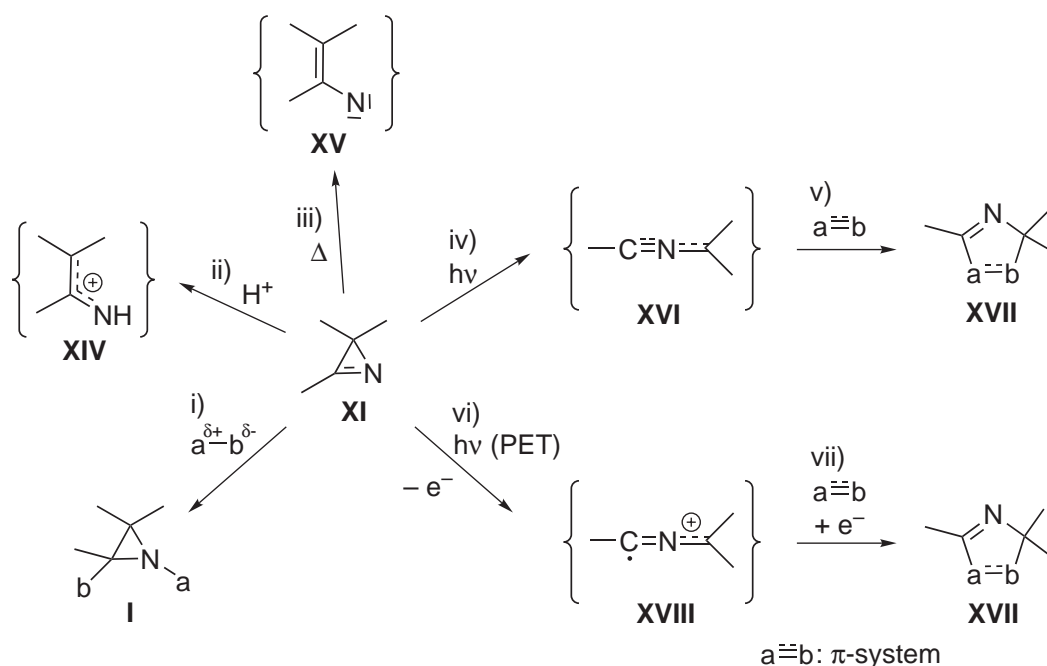
Scheme 1.5: Different reaction modes of $2H$-azirenes (**XI**):[52,53] electrophilic or nucleophilic addition to the C,N double bond to give aziridine derivatives (**I**) (i),[53,79–84] intermediate formation of 1-azaallyl cations (**XIV**) upon protonation (ii),[79,83,87,93,94] thermal generation of transient vinylnitrenes (**XV**) (iii),[95,96] nitrilium ylides (**XVI**)[77,97–103] via photochemical C,C bond cleavage (iv),[77,103] subsequent cycloaddition to give heterocycles **XVII** (v),[77,103] and C,C bond cleavage with generation of 2-azaallenyl radical cations (**XVIII**) under PET conditions (vi)[104] and subsequent reaction with a π-system to yield **XVII** (vii).[104]

An extension of this ring expansion protocol to less acidic reagents could successfully be achieved by Lewis acid activation of $2H$-azirenes using $BF_3 \cdot Et_2O$.[78,90,105] In the absence of external nucleophiles N-aryl-$2H$-azirene-3-amines **12a–i** reacted with $BF_3 \cdot Et_2O$ via electrophilic aromatic alkylation to substituted 2-amino-$3H$-indolium tetrafluoroborates **13a–i** (Scheme 1.6).[78,105] After hydrolysis this gave access to indoline-2-one derivatives (not shown).[78,105]
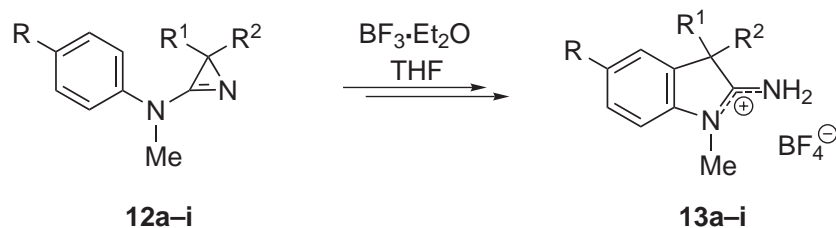
Scheme 1.6: Reactions of N-aryl-$2H$-azirene-3-amines **12a–i** with $BF_3 \cdot Et_2O$ leading to
2-amino-$3H$-indolium tetrafluoroborates **13a–i** (**a**: $R^1 = R^2 = Me$, $R = H$; **b**: $R^1 = Me$,
$R^2 = CH_2Ph$, $R = H$; **c**: $R^1 = Me$, $R^2 = CH_2CHMe_2$, $R = H$; **d**: R^1, $R^2 = -(CH_2)_3-$,
$R = H$; **e**: R^1, $R^2 = -(CH_2)_4-$, $R = H$; **f**: R^1, $R^2 = -(CH_2)_5-$, $R = H$; **g**: R^1, $R^2 =$
$-(CH_2)_6-$, $R = H$; **h**: $R^1 = R^2 = Me$, $R = OMe$; **i**: $R^1 = R^2 = Me$, $R = NO_2$).[105]

Another example for selective C^2,N bond cleavage was given by Ghosez and cowork-
ers.[82] Protonation of 3-amino-$2H$-azirene **14** with a strong Brønsted acid, "magic
acid"[106] (FSO_3H/SbF_5), in SO_2 at low temperature yielded instantaneously the open
chain amidinium salt **19** (Scheme 1.7). The reaction pathway via 1-azaallyl cation **16**
(cf. **XIV**, Scheme 1.5), where the stabilizing amidinium resonance form of **15** is no
longer operative, was largely excluded.[82] It was suggested that the facile rearrange-
ment of **14** should rely on the possibility of forming dication **17** under the applied
acidic conditions. This very unstable species could lose strain energy through cleavage
of the C^3,N bond to give **18** and finally product **19** after deprotonation.[82]
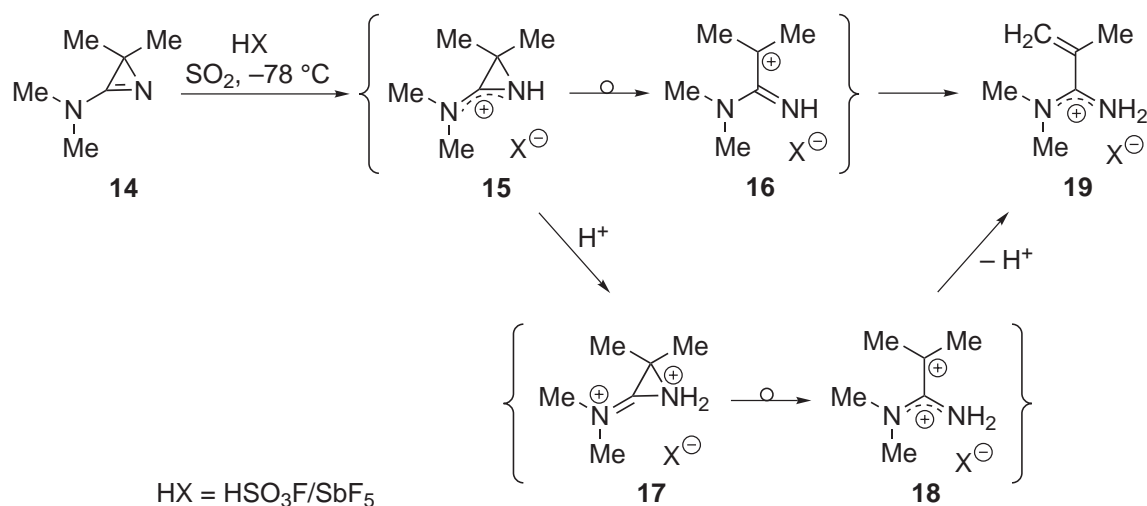
Scheme 1.7: Protonation and ring opening of 3-amino-$2H$-azirene **14**.[82]

Ring expansions of a 2H-azirene derivative via insertion of a π-system into the C^2,N bond were presented by Leonard and Zwanenburg.[79] Reaction of **20** with acetone or ethyl methyl ketone in the respective ketone as solvent induced by stoichiometric amounts of anhydrous perchloric acid yielded N-protonated oxazolinium salts **21a,b** (Scheme 1.8). After deprotonation the corresponding oxazoline derivatives **22a,b** were obtained. The authors stress that these reactions must be carried out under strict precautions to exclude water. Here, the perchloric acid was generated *in situ* from anhydrous *para*-toluene sulfonic acid and silver or magnesium perchlorate. Moreover, the employment of an acid that forms a non-nucleophilic corresponding anion[107] turned out to be essential for a clean reaction: while *in situ* generated fluoroboric acid gave similar good results, the use of anhydrous *para*-toluene sulfonic acid resulted in a complex mixture of products.[79]
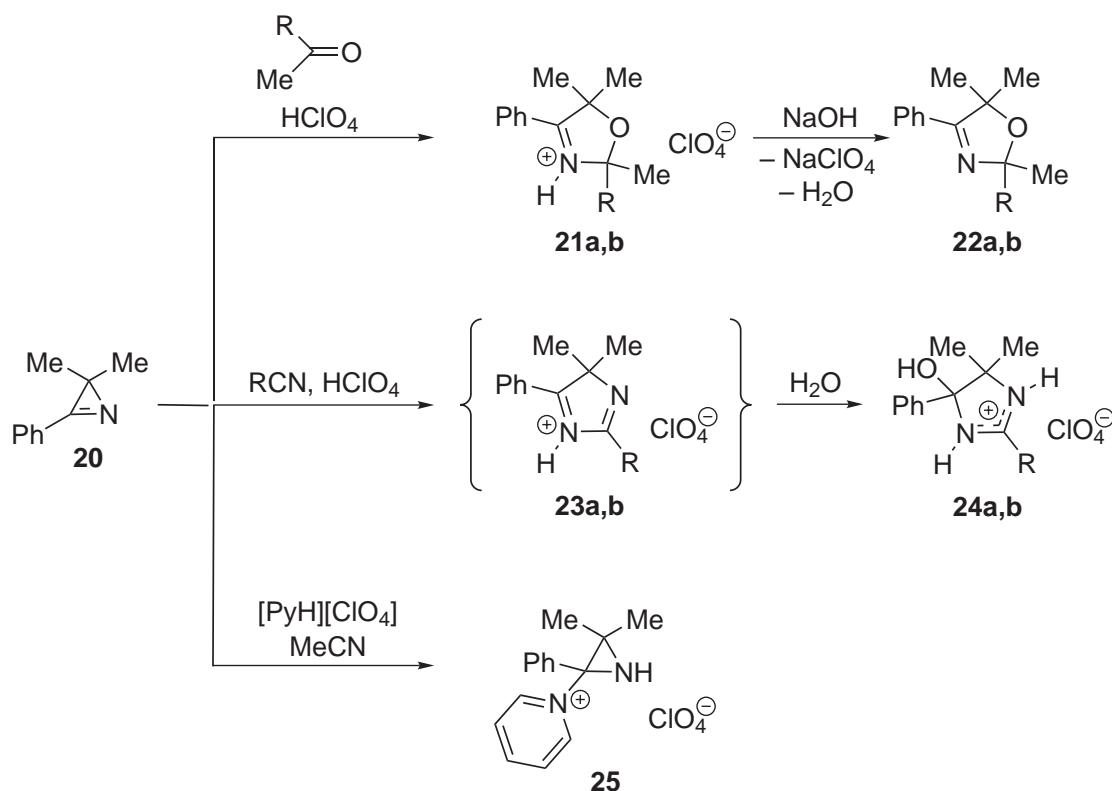
Scheme 1.8: Ring expansion of 2H-azirene **20** with ketone and nitrile derivatives (R = Me (**a**), Et (**b**)), and reaction of **20** with pyridinium perchlorate (Py = pyridine).[79]

Although likewise (water-free) conditions were chosen for acid-induced ring expansion of **20** with acetonitrile (as solvent), only the hydrolysis product **24a** could be isolated (Scheme 1.8); presumably it resulted from the addition of water to isoimidazolium cation **23a** that was intermediately formed;[79] an analogous observation was made in

the reaction of **20** with propionitrile.[79] The enhanced tendency of **23a,b** (in comparison to **21a,b**) to undergo hydrolysis presumably is the possibility to form the highly stabilized amidinium structure in the final products **24a,b**. Mechanistically, initial formation of a $2H$-azirenium cation that undergoes subsequent ring opening to an 1-azaallyl cation (**XIV**) (Scheme 1.5) was postulated, but no spectroscopic evidence was provided.[79] An alternative mechanism involving initial protonation of acetonitrile[108] followed by the nucleophilic attack of the azirene nitrogen was considered *"less likely in the light of the behavior of perchloric acid with bases in anhydrous acetonitrile."*[79]

Interestingly, $2H$-azirene **20** reacted with pyridinium perchlorate *in acetonitrile* to give a stable adduct, **25** (Scheme 1.8), formed by 1,2-addition of the pyridinium cation to the C^3,N double bond; no evidence for a ring expansion product (**23a** or **24a**) was obtained.[79]

Employment of the Lewis acid $BF_3 \cdot Et_2O$ to induce ring expansion of $2H$-azirene **26** with nitriles yielded imidazoles[7] **28a–h** (Scheme 1.9).[109] It is noteworthy that the reaction of **26** with acrylonitrile exclusively led to the formation of imidazole **28g**, and no products resulting from an insertion of the C,C double bond of acrylonitrile were observed. In the reaction with ethyl cyanoacetate the formation of **28h** competed with the insertion of the carbonyl group giving rise to the formation of oxazole derivative **29**. In each reaction two equivalents of $BF_3 \cdot Et_2O$ were employed, and the respective nitrile was used as solvent.
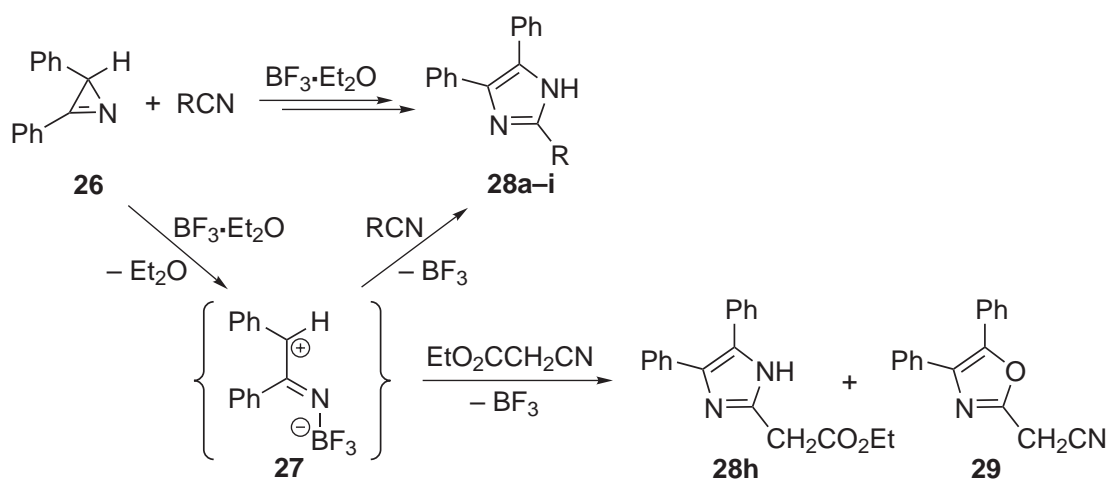
Scheme 1.9: Ring expansion of $2H$-azirene **26** with nitriles induced by $BF_3 \cdot Et_2O$ giving imidazoles **28a–h** (R = Me (**a**), $(CH_2)_9CH_3$ (**b**), ^tBu (**c**), Ph (**d**), CH_2Ph (**e**), $(CH_2)_4CN$ (**f**), $CH=CH_2$ (**g**), CH_2CO_2Et (**h**)) and oxazole **29**.[109]

---

[7]As $2H$-azirene **26** carries only one substituent at C^2, this enables the formation of the aromatic products.

It was suggested that the formation of a BF_3 adduct of **26** in the first step causes ring opening to give zwitterion **27** (analogous to 1-azaallyl cation **XIV**; Scheme 1.5).[109] This is followed by a Ritter-type[110] addition of the nitrile, subsequent cyclization, and tautomerization. Additional experiments with differently substituted $2H$-azirenes reinforced this hypothesis, as reactions were facilitated if the substituent at C^2 was capable of stabilizing the zwitterionic intermediate **27**.[109] Evidence for the Ritter-type adduct was obtained in the thermal reaction of 3-phenyl-$2H$-azirene with benzonitrile, which yielded phenacylamide as by-product that is a hydrolysis product of the proposed intermediate.[109] An alternative mechanism involving a BF_3 adduct of the nitrile was ruled out by comparison of the basicities of nitriles and 3-alkyl-$2H$-azirenes.[109]

Bertrand and coworkers presented ring expansion reactions of 2-phosphino-$2H$-azirene **30** (Scheme 1.10), which was synthesized by [2+1] cycloaddition of phosphino(silyl)carbene **4**[61] with benzonitrile.[111, 112] $1,2\lambda^5$-Azaphosphete **31** was obtained through intramolecular insertion of the phosphino substituent into the C^2,N bond of **30**.[111, 112] This occurred upon irradiation[112] or upon addition of catalytic amounts of transition metal complexes such as dichloro(p-cymene)ruthenium(II), $[Mo(CO)_4(NHC_5H_{10})_2]$, or $[Fe(Cp)(CO)_2]_2$.[111, 112]
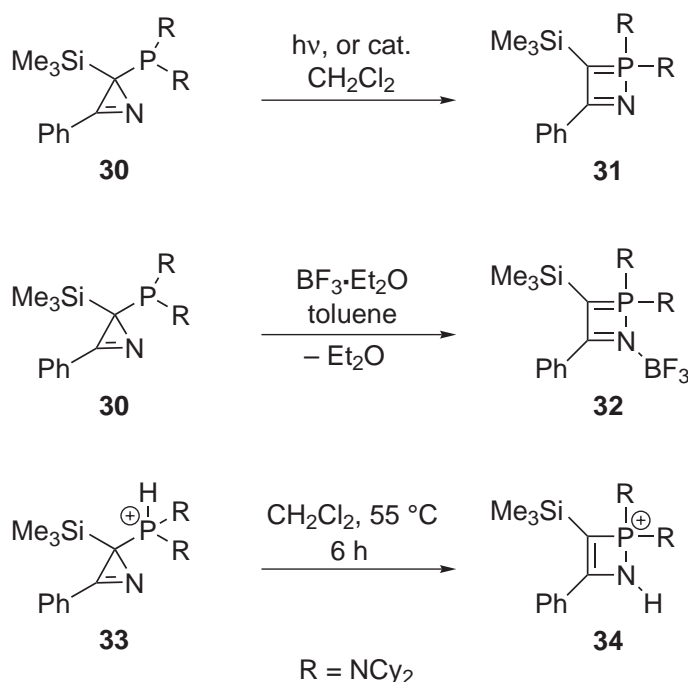
Scheme 1.10: Intramolecular ring expansion reactions of 2-phosphino-$2H$-azirene **30** and P-hydrogeno phosphonio azirene cation **33** (Cy = cyclohexyl; cat.: dichloro(p-cymene)-ruthenium(II), $[Mo(CO)_4(HNC_5H_{10})_2]$, or $[Fe(Cp)(CO)_2]_2$).[112]

Addition of one equivalent of $BF_3 \cdot Et_2O$ gave **32**, and heating of a CH_2Cl_2 solution of the *P*-hydrogeno phosphonio azirene cation **33**, generated by reaction of **30** with trifluoromethanesulfonic acid, afforded *N*-protonated azaphosphete **34**.[112] Further ring expansion reactions of **30** were presented that accounted for C^2,N bond cleavage.[112]

The C^2,N bond of $2H$-azirenes (**XI**) can be cleaved also thermally, which yields transient vinylnitrenes (**XV**) (Scheme 1.5, iii).[53, 96] The latter have proven to be useful intermediates for the synthesis of heterocycles as well.[53, 96] Cleavage of the C,C bond of **XI** (iv) is most effectively achieved by photochemical excitation of the $n-\pi^*$ transition,[77, 103] as thermal C,C bond cleavage requires very high temperatures.[101, 102] This provides transient nitrile ylides (**XVI**),[77, 97–103] which are 1,3-dipoles[97, 98] that react readily with a variety of dipolarophiles to give heterocycles **XVII** (v).[77, 103]

One-electron oxidation of $2H$-azirenes (**XI**) under PET conditions causes C,C bond cleavage with formation of transient 2-azaallenyl radical cations (**XVIII**) (Scheme 1.5, vi).[104] Alike neutral nitrilium ylides (**XVI**) they react preferentially with electron-poor π-systems to yield heterocycles **XVII** (vii),[104] whereas an increased reactivity is observed. The radical cations **XVIII** react even with common imines to give *N*-substituted imidazoles, and in the absence of suitable reaction partners dimerization is observed.[104] In contrast to the concerted nature of the cycloaddition reactions of nitrilium ylides (**XVI**), the reaction of 2-azaallenyl radical cations (**XVIII**) with dipolarophiles is a stepwise process.

1.3 Ring Expansion of Azaphosphirenes

Azaphosphirenes can also be regarded as heteroazirenes, and due to the analogy of phosphorus and carbon[113] as expressed by their diagonal relationship in the periodic table[8] a close relationship of their reactivities may be expected. However, it should be noted that the ring opening behavior of other heteroazirenes is rather non-uniform (or unknown in the case of oxazirenes) and nothing is known about their reactivity if these heterocycles are coordinated to a transition metal complex fragment.[114]

It is thus remarkable that none of the isomers of azaphosphirenes **XIX**–**XXI** (Fig. 1.3) has been isolated, so far. $1H$-Azaphosphirenes (**XIX**)[115] and $2H$-azaphosphirenes (**XX**)[116] have been postulated as reactive intermediates, and $3H$-azaphosphirenes (**XXI**) have only been subject of computational studies.[117]

---

[8]This analogy is even more pronounced if the phosphorus atom is coordinated due to an enhancement of its electronegativity and the tetrahedral arrangement of its environment.[113]
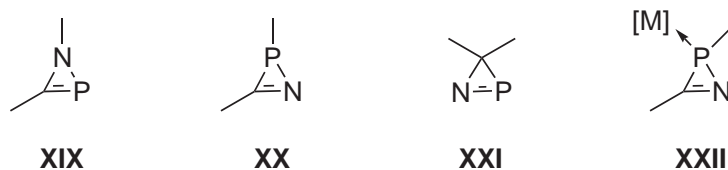
Figure 1.3:   Unsaturated three-membered heterocycles containing carbon, nitrogen, and phosphorus: 1H-azaphosphirenes (**XIX**),[115] 2H-azaphosphirenes (**XX**),[116] 3H-azaphosphirenes (**XXI**),[117] and 2H-azaphosphirene κP-metal complexes (**XXII**)[118–120] ([M]: organometallic fragment).

The first group 6 transition metal-coordinated 2H-azaphosphirenes (**XXII**) have been presented by Streubel et al.,[118] and various applications in heterocylic chemistry have been developed.[119,120] One remarkable structural feature of the three-membered ring of **XXII** is the similarity of its endocyclic P,C and P,N bond lengths as determined by single-crystal X-ray crystallography on various derivatives.[118,121–128] This, together with certain experimental findings (vide infra), underlines that the bonding of **XXII** should be described as a resonance hybrid of a three-membered ring having covalent P,C and P,N bonds and a π-donor/acceptor complex of a carbonitrile with a terminal phosphanylidene complex[119,123] according to the Dewar-Chatt-Duncanson model[129] (Scheme 1.11). Indeed, 2H-azaphosphirene complexes proved to be excellent precursors for terminal electrophilic phosphanylidene complexes (**XXIII**).[119] Unlike transient phosphanediyls, which are generally triplet species,[130] transient phosphanylidene metal(0) complexes of the general formula $[M(CO)_5(PR)]$ should have, according to their reactivity[131] and quantum chemical calculations,[132,133] a closed shell singlet ground state structure due to an effective backbonding by the transition metal center. Cleavage of both the P,C and the P,N bond of **XXII** (i) occurs already between 65 and 75 °C,[119] and in the presence of various π-systems[9] such as alkynes,[138–142] phosphaalkynes,[143] alkenes,[144] aldehydes,[118] ketones,[145] imines,[145] or nitriles[146] the corresponding three-membered heterocycle complexes **XXIV** were formed via [2+1] cycloaddition reaction of **XXIII** (ii).

Thermal decomposition of 2H-azaphosphirene tungsten complexes in the presence of dimethyl acetylenedicarboxylate (DMAD) led to 1H-phosphirene complexes *and* 2H-1,2-azaphosphole complexes.[139] As the latter resulted formally from ring expansion via cleavage of the P,C bond of **XXII**, the intermediacy of nitrilium phosphane ylide complexes (**XXV**), analogs of nitrilium ylides (**XVI**; cf. Scheme 1.5), was strongly suggested.[139] It was assumed that nitrilium phosphane ylide complexes are the primary

---

[9]The given temperature range refers to optimized conditions for reactions with π-systems. It should further be mentioned that also in the absence of trapping reagents interesting results were obtained.[134–137]

reaction products of the thermal decomposition of **XXII** (iii), which then generate phosphanylidene complexes (**XXIII**) via break of the P,C bond (v).[139]
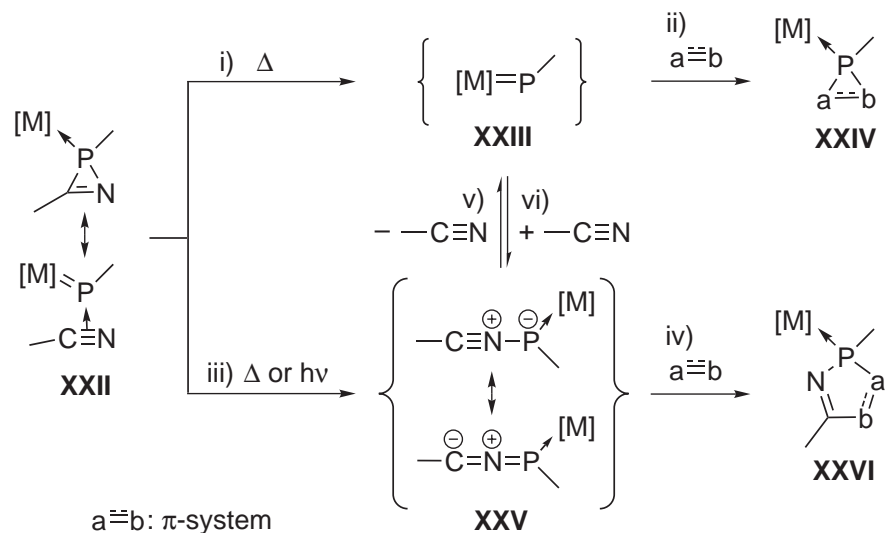
Scheme 1.11: Different reaction modes of $2H$-azaphosphirene complexes (**XXII**):[114,119] generation of terminal electrophilic phosphanylidene complexes (**XXIII**) (i),[118,138–146] their reaction with π-systems to yield heterocycles **XXIV** (ii),[118,138–146] thermal[114,126,139,146–160] or photochemical[114,153,161] generation of transient nitrilium phosphane ylide complexes (**XXV**) (iii),[114,126,139,146–160] and their reaction with dipolarophiles to yield **XXVI** (iv)[114,126,139,146–160] ([M] = Cr(CO)$_5$, Mo(CO)$_5$, W(CO)$_5$).

Conversely, through addition of carbonitriles the reverse reaction (vi) is promoted, leading to an enhancement of ring expansion products **XXVI** when subsequently trapped.[114] It was observed that the concentration of the added carbonitrile and the nature of its substituent are of importance to achieve a *transylidation*[10] reaction.[114,147] This led to rapid development of so-called *three-component reactions* using a $2H$-azaphosphirene complex, a carbonitrile, and a trapping reagent.[114] For example, outstanding results were achieved when carbonitriles with good π-donor substituents were employed such as cyanamides, which provide substantial stabilization of the transient nitrilium phosphane ylide complex (**XXV**);[114,126,146–154,156–160] effective stabilization of **XXV** could be achieved also by strongly electron-withdrawing substituents at the carbon center.[146] On the basis of this concept employment of different π-systems such as alkynes,[126,147–150] phosphaalkynes,[151] alkenes,[152] aldehydes,[114,153] ketones,[152,154] nitriles,[146,156–159] or heterocumulenes[160] gave access to a wide variety of five-membered heterocycles (**XXVI**); this methodology could also be adapted to photochemical conditions.[161]

---

[10]Likewise, the intermediacy of phosphacarbonyl ylides in the thermolysis of a $2H$-azaphosphirene complex in the presence of ketones[145] and aldehydes[162] was discussed.

One example is the thermal reaction of $2H$-azaphosphirene complex **35**[121, 122] with cyanamide derivatives **36a,b** and ethyl cyanoformate as trapping reagent (Scheme 1.12). This yielded a mixture of $2H$-1,3,2-diazaphosphole complexes **38a,b** and 1,3,2-oxazaphosphol-3-ene complexes **39a,b**.[146, 158] Here, transylidation had occurred, and [3+2] cycloaddition of nitrilium phosphane ylide complexes **37a,b** with either the cyano or the carbonyl functionality of EtO$_2$CCN gave the final products.[146, 158]
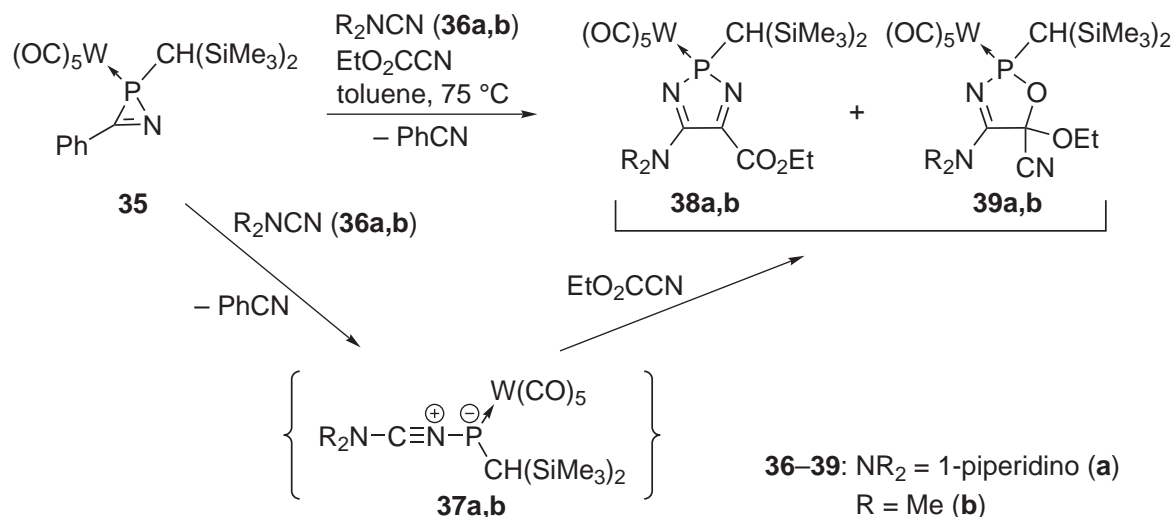
Scheme 1.12: Thermal reactions of $2H$-azaphosphirene complex **35** with cyanamide derivatives **36a,b** and ethyl cyanoformate.[146]

Reactions involving C-phenyl substituted nitrilium phosphane ylide complex **37c** have been observed when benzonitrile (**36c**) was employed in large excess or (better) as solvent.[146, 155] In this way thermal decomposition of $2H$-azaphosphirene complex **35** yielded $2H$-1,3,2-diazaphosphole complex **40** together with $2H$-1,4,2-diazaphosphole complex **41c** (Scheme 1.13), which are the two regioisomers of the [3+2] cycloaddition of **37c** with PhCN.[146, 155] Complex **41c** was not stable under these conditions and partially underwent decomplexation.[155] Due to its poor stability the liberated heterocycle could not be isolated, but its transformation into the corresponding heterocyclic P(V)-sulfide via oxidation with elemental sulfur was successful.[155] These examples demonstrate that the regiochemistry of [3+2] cycloaddition reactions of nitrilium phosphane ylide complexes (**XXV**) is largely influenced by their C-substituent; in some cases steric factors seemed to be crucial.[152]
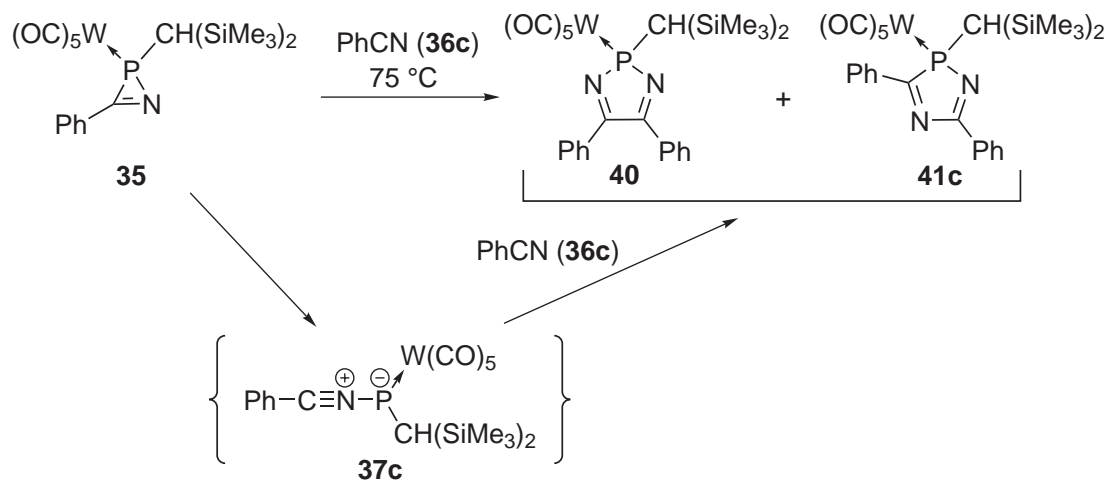
Scheme 1.13: Thermal decomposition of $2H$-azaphosphirene complex **35** in benzonitrile.[146, 155]

In the three-component reaction of **35** with nitrile **36a** and tetracyanoethylene (TCNE) besides the targeted 1,2-azaphosphol-5-ene complex **42** the formation of $2H$-1,4,2-diazaphosphole complex **41a** was observed (Scheme 1.14).[153, 163] As the reaction of *in situ* generated nitrilium phosphane ylide complex **37a** with benzonitrile in the absence of TCNE did not lead to **41a** but to its regioisomer,[146] it was concluded that complex **37a** was not an intermediate, here.[153, 163]
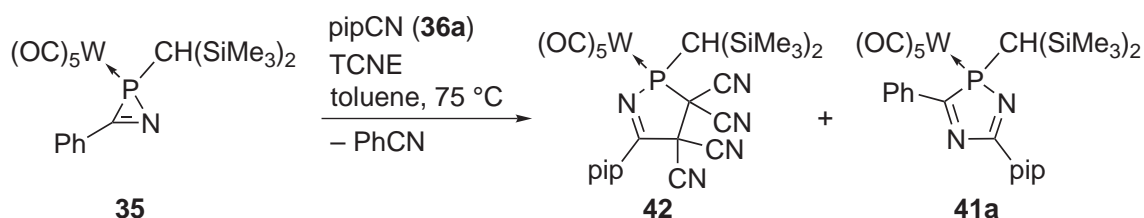
Scheme 1.14: Reaction of $2H$-azaphosphirene complex **35** with 1-piperidinecarbonitrile (pipCN; **36a**) and tetracyanoethylene (TCNE).[163]

When the reaction was carried out in neat 1-piperidinecarbonitrile (**36a**) the formation of **42** was completely suppressed, and complex **41a** was observed as the only product.[163] It turned out that the reaction can proceed also at ambient temperature, and when the reaction mixtures were heated catalytic amounts of TCNE were sufficient to induce complete conversion to **41a**.[163]

As it is well known that TCNE is able to act as oxidizing agent,[164, 165] a radical cation mechanism was suggested.[163] It was shown that such reactions can also be induced by

substoichiometric amounts of the typical single-electron oxidant ferrocinium[11] hexafluorophosphate ($[Fe(\eta^5\text{-}Cp)_2][PF_6]$).[127, 167–170] This opened up a more efficient route for the synthesis of $2H$-1,4,2-diazaphosphole complexes than the thermal or photochemical reactions described above. Reactions of $2H$-azaphosphirene complexes with carbonyl derivatives have also been described.[167–170] One restriction seemed to be steric hindrance as the insertion of a sterically encumbered ketone, benzophenone, failed.[170]

Despite all that, the knowledge about the reactivity of $2H$-azaphosphirene complexes towards nucleophiles and electrophiles is still very limited. For example, methyl iodide showed no reaction with **35**,[119] whereas [pentacarbonyl(tetrahydrofuran)tungsten(0)] afforded a dinuclear κN-,κP-coordinated $2H$-azaphosphirene complex that dissociated rapidly and irreversibly in solution at ambient temperature.[118]

Two further reactions illustrating the high and versatile reactivity of $2H$-azaphosphirene complexes deserve mentioning. Complex **35** reacts with triethylammonium chloride[125, 171] or water[148] with release of benzonitrile and formation of phosphane complexes **43** and **44**, respectively (Scheme 1.15). The exact mechanism of these reactions is still unknown.[171]
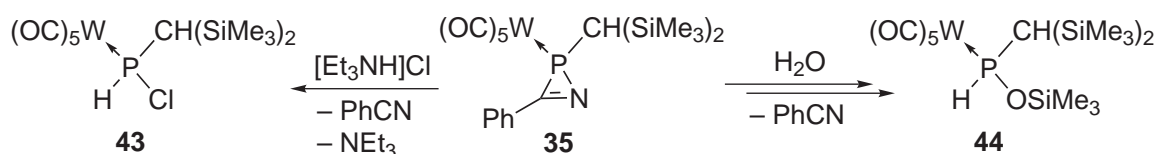
Scheme 1.15: Reactions of $2H$-azaphosphirene complex **35** with triethylammonium chloride[171] or water.[148]

---

[11]The recommended name for this cation is bis(η^5-cyclopentadienyl)iron(1+).[166] For clarity it is referred to as *ferrocinium*, which is preferred to *ferrocenium* to avoid ambiguities (i.e., confusion with protonated ferrocene), although the latter name is widely used. In the following its formula is abbreviated to $[FeCp_2]^{\bullet+}$ (i.e., "η^5-" omitted); the same was done for ferrocene.

Chapter 2

Objectives of this Thesis

The objective of this Thesis was to examine the reactivity of $2H$-azaphosphirene complexes towards cationic and neutral electrophiles that might be useful for ring expansion reactions with nitriles. This should be done via combined experimental and computational studies.

Chapter 3

SET-Induced Ring Expansion of $2H$-Azaphosphirene Complexes

For reactions of $2H$-azaphosphirene tungsten complex **35**[122, 172] with hetaryl carbonitriles **36d**–**g** C. Neumann employed $0.18-0.36$ equivalents of ferrocinium hexafluorophosphate, which was sufficient to induce complete conversion of **35** within a few hours (Scheme 3.1).[167, 173] He further investigated the influence of the C-substituent of the $2H$-azaphosphirene complex by using *ortho*-methylphenyl, *ortho*-methoxyphenyl, and *ortho*-dimethylaminophenyl substituted $2H$-azaphosphirene complexes for reactions with benzonitrile.[127, 167] These studies revealed that reaction rates significantly decreased with increasing donor ability of the aryl substituent. The *ortho*-dimethylamino substituted derivative showed only 20 % of conversion within 5 days, even in neat benzonitrile.[127, 167] Although the influence of the nature of the nitrile component was not investigated systematically, electron-poor derivatives seemed to be disadvantageous. For instance, reaction of complex **35** with ethyl cyanoformate resulted in a inseparable mixture of products. From the reaction of **35** with 2-cyanopyridine a product was isolated in 1 % yield, which was considered to be the desired 5-(2-pyridyl)-3-phenyl-$2H$-1,4,2-diazaphosphole complex. On the basis of new insights, presented in the following paragraphs, this result has to be reconsidered.

3.1 Experimental Investigations on the Reaction Course

2H-Azaphosphirene complex **35**[121, 122] was reacted with dimethyl cyanamide (**36b**) in the presence of substoichiometric amounts of ferrocinium hexafluorophosphate (0.18 equiv.) at ambient temperature (Scheme 3.1). This led to a bond- and regioselective insertion of **36b** into the P,N bond of **35**,[1] which afforded 5-dimethylamino-2H-1,4,2-diazaphosphole[2] complex **41b**.
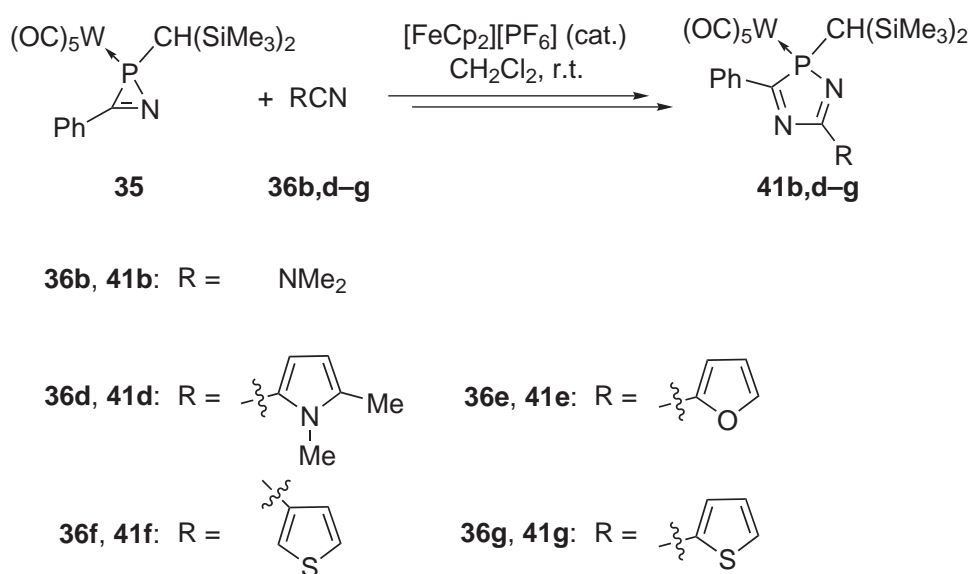
Scheme 3.1: Reactions of 2H-azaphosphirene complex **35** with nitrile derivatives **36b,d–g** in the presence of substoichiometric amounts of ferrocinium hexafluorophosphate.

Complex **41b** was purified using low-temperature column chromatography, thus giving 59 % of isolated yield. Its constitution was unambiguously identified via multinuclear NMR experiments, mass spectrometry, IR and UV/Vis spectroscopy, and confirmed by a single-crystal X-ray diffraction study (Fig. 3.3); the purity was examined by elemental analysis.

In Table 3.1 significant NMR spectroscopic data for **41b** are compiled together with corresponding data for derivatives **41a**[163] and **41d–g**,[173] 4H-1,2,4-diazaphosphole **45**,[174] and 2H-1,3,2-diazaphosphole complex **46**;[146] complex **47** is unknown. From

---

[1]Progressions of all reactions presented in this work were generally monitored by ^{31}P{^{1}H} NMR spectroscopy.

[2]The numbering of the ring atoms of heterocycles according to the modified Hantzsch-Widman-Patterson system is applied throughout this work.

the latter, complex **41b** can clearly be distinguished on the basis of ^{1}H,^{13}C long-range correlations of the ring carbons with the protons at the ring substituents (from 2D ^{1}H,^{13}C gsHMBC NMR experiments). $2H$-1,4,2-Diazaphosphole complexes can be distinguished from isomeric $4H$-1,2,4- and $2H$-1,3,2-diazaphosphole complexes already on the basis of the ^{31}P{^{1}H} NMR data as illustrated in the following.

Table 3.1: Selected NMR spectroscopic data for $2H$-1,4,2-diazaphosphole complexes **41a,b,d–g** (R = 1-piperidino (**a**),[163] NMe$_2$ (**b**), 1,5-dimethyl-2-pyrrolyl (**d**),[173] 2-furyl (**e**),[173] 3-thienyl (**f**),[173] 2-thienyl (**g**)), $4H$-1,2,4-diazaphosphole **45**,[174] and $2H$-1,3,2-diazaphosphole complex **46**;[146] $2H$-1,4,2-diazaphosphole complex **47** is unknown.

No.	$\delta(^{31}P)$	$|^1J_{WP}|$/Hz	$\delta(^{13}C^3)$	$|^{1+4}J_{PC^3}|$/Hz	$\delta(^{13}C^5)$	$|^{2+3}J_{PC^5}|$/Hz
41a[163]	100.1	240.5	200.0	24.7	163.4	–
41b†	101.8	241.6	200.3	25.5	165.0	–
41d[173]	108.4	233.9	198.8	23.5	162.3	5.8
41e[173]	110.6	230.6	202.1	22.7	160.2	3.8
41f[173]	109.1	229.8	201.8	22.8	165.0	4.9
41g	110.5	229.5	201.3	23.3	164.4	4.0
45‡[174]	19	–	190.35	27	179.56	15.1
	$\delta(^{31}P)$	$|^1J_{WP}|$/Hz	$\delta(^{13}C^5)$	$|^{2+3}J_{PC^5}|$/Hz	$\delta(^{13}C^4)$	$|^{2+3}J_{PC^4}|$/Hz
46[146]	149.8	257.1	165.0	2.5	162.4	9.4

All data recorded in CDCl$_3$ solution, except for † ^{13}C data recorded in C$_6$D$_6$, and ‡all data from C$_6$D$_6$ solution.

So far no example of a $4H$-1,2,4-diazaphosphole complex has been described, but the free ligand **45** is known.[174] It resonates at $\delta(^{31}P) = 19$,[174] and since coordination chemical shifts of five-membered phosphorus heterocycles due to complexation with a W(CO)$_5$ fragment are generally $\Delta\delta(^{31}P) \approx +25$ or less,[69, 155, 159, 175] the chemical shifts expected for $4H$-1,2,4-diazaphosphole tungsten complexes should be significantly lower than those of $2H$-1,4,2-diazaphosphole complexes. The phosphorus center of complex **46**, which is bonded to two nitrogen atoms, is more deshielded ($\delta(^{31}P) = 149.8$), and the magnitude of its tungsten–phosphorus coupling constant is considerably larger (257.1 Hz).

The ^{31}P{^{1}H} resonances of **41a,b** are $7-11$ ppm upfield from those of 5-hetaryl substituted complexes **41d–g**. Concerning their tungsten–phosphorus coupling constants a trend becomes apparent: $|^1J_{WP}|$ values increase with increasing donor ability of the substituent at C^5 in the order 2-thienyl $\approx$ 3-thienyl $<$ 2-furyl $<$ 1,5-dimethyl-2-pyrrolyl[3] $<<$ dialkylamino. The ring carbon atoms of **41a,b,d–g** display characteristic ^{13}C resonances. Typically, the C^3 centers resonate at very low field ($199-202$ ppm),[4] thus, they are even more deshielded than the ring carbons of 4H-1,2,4-diazaphosphole **45** ($\delta(^{13}$C$^3) = 190.35$, $\delta(^{13}$C$^5) = 179.56$)[174] or that of the W(CO)$_5$-coordinated 2H-azaphosphirene system (**35**: $\delta = 192.4$).[122, 124] Their phosphorus–carbon coupling constants are about $23-26$ Hz in magnitude. On the other hand, the C^5 centers resonate at significantly higher field ($160-165$ ppm), that is, in the same range as the ring carbons of complex **46**, which possesses two endocyclic PN=C units. The C^5 signals of **41a,b,d–g** have rather small phosphorus–carbon coupling constant magnitudes (**41d–g**: $4-6$ Hz), thus indicating that at least two scalar couplings contribute to these values; for complexes **41a,b** such couplings could not be resolved.

Investigations on the influence of the concentration of ferrocinium hexafluorophosphate on the reaction course were carried out for the reaction of **35** with 2-thiophene-carbonitrile (**36g**) as a good case in point. It was monitored by ^{31}P{^{1}H} NMR spectroscopy[5] at different [FeCp$_2$][PF$_6$] concentrations and at constant temperature (30 °C). As no resonances other than those of **35**, **41g**, and the hexafluorophosphate anion were detected, the time dependent formation of **41g** (Fig. 3.1) follows the same trend as the decay of **35**. Obviously, the ratio of [FeCp$_2$][PF$_6$] has a strong influence on the reaction progression, but it can be reduced to 0.03 equivalents ($\bullet$, 0.01 mol$\cdot$L^{-1}) without overall decrease in conversion. When only 0.02 equivalents ($\triangledown$) were used, the conversion leveled off at around 80 %, and in the presence of 0.01 equivalents ($\times$) saturation occurred at an early stage; even after 3 days the ratio of **41g** did not exceed 18 %. In the absence of [FeCp$_2$][PF$_6$] no conversion of **35** was observed within 10 days (not shown). For ratios of [FeCp$_2$][PF$_6$] $\geq$ 0.02 equivalents the data points

---

[3]The ease of electrophilic aromatic substitution at these heterocycles follows the same order: thiophene $<$ furan $<$ pyrrole.[176]

[4]In each case the C^3 resonance almost coincides with the carbon resonance of the CO ligand in *trans*-position to the heterocycle. Furthermore, the phosphorus–carbon coupling constant magnitudes of both centers are almost identical. A clear distinction can only be made if the satellites arising from couplings with ^{183}W ($I = 1/2$; relative abundance: 14.3 %) can be detected from highly resolved ^{13}C{^{1}H} NMR spectra. In this work $|^1J_{WC}|$ values of *trans*-CO carbon resonances were determined for several 2H-1,4,2-diazaphosphole complexes; in some cases the small $^2J_{WC}$ coupling constant magnitudes of the C^3 atoms could be estimated ($3-4$ Hz each). Careful analysis of the trends in chemical shifts and phosphorus–carbon coupling constant magnitudes revealed that some assignments that were previously published[153, 167, 173] might be wrong. Therefore, the respective data in Table 3.1 taken from the literature are shown together with the new assignments.

[5]Reaction monitoring by UV/Vis spectroscopy was limited by overlaps of absorption bands of reactants and products.

describe curves with a steep ascending slope after a comparatively flat trend at the start, and again a flattening at the end. Employment of more than 0.15 equivalents of [FeCp$_2$][PF$_6$] yielded no further acceleration.
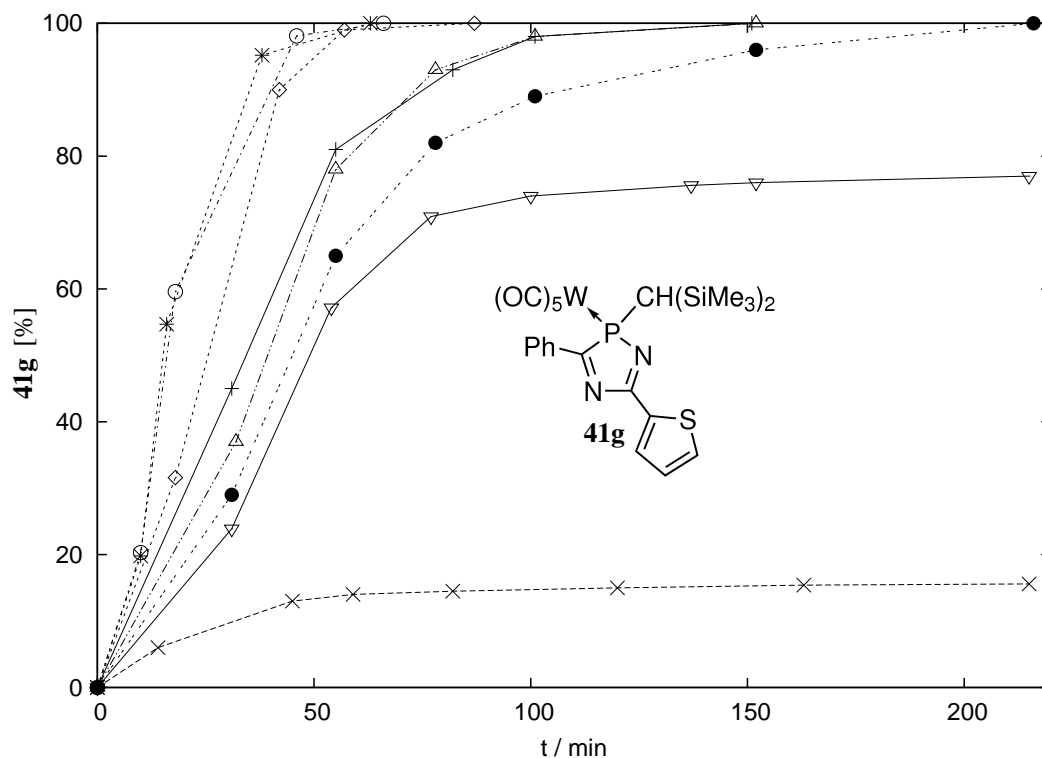
Figure 3.1: Ratio of **41g** (by ^{31}P$\{^1$H$\}$ NMR signal integration) against time for reactions of **35** with **36g** in the presence of varying amounts of [FeCp$_2$][PF$_6$]: $\times$ 0.01, $\triangledown$ 0.02, $\bullet$ 0.03, $\triangle$ 0.04, $+$ 0.05, $\diamond$ 0.10, $\odot$ 0.15, $*$ 0.20 equiv. (data points joined for clarity).

The generalizability of this result was examined for reactions of **35** with nitrile derivatives **36b,d–g** on small-scale by using 0.05 equivalents of [FeCp$_2$][PF$_6$] in each case. All reactions were complete within less than 6 hours at ambient temperature, and apart from the resonance of PF$_6^-$ no phosphorus-containing by-products were detected by ^{31}P$\{^1$H$\}$ NMR spectroscopy.

The reaction of **35** with **36g** using 0.05 equivalents of [FeCp$_2$][PF$_6$] was carried out on a preparative scale, and complex **41g** was purified via low-temperature column chromatography. In this way, the isolated yield was improved to about 91 %. Additionally, ferrocene was isolated[6] in 71 % yield (with respect to the amount of [FeCp$_2$][PF$_6$] em-

---

[6]Ferrocene was isolated via column chromatography and unambiguously identified by ^{1}H and ^{13}C NMR experiments. It has already been observed that approximately 10 % of ferrocene was formed in reactions that employed 0.18 equivalents of [FeCp$_2$][PF$_6$].[127, 169, 170]

ployed). Repeating the reaction of **35** with **36g** using 0.18 equivalents of [FeCp$_2$][PF$_6$] afforded a significantly lower yield of ferrocene (8 %).

In order to exclude that ferrocene is formed via oxidation of the nitrile, a CH$_2$Cl$_2$ solution of nitrile derivative **36g** and [FeCp$_2$][PF$_6$] was stirred for 2 hours at ambient temperature, thus, under the same conditions as used for the syntheses of **41b,d–g** but in the absence of the 2H-azaphosphirene complex. After evaporation of all volatiles the residue was subjected to column chromatography, and here, no ferrocene was obtained.[7] It was also ruled out that the ring expansion reaction is initiated by the hexafluorophosphate anion, by chosing a soluble PF$_6^-$ salt with an "innocent" cation, tetra-n-butylammonium hexafluorophosphate, which showed no effect on CH$_2$Cl$_2$ solutions of **35** and **36g**; no formation of **41g** was observed. It is concluded that oxidation of 2H-azaphosphirene complex **35** by the ferrocinium cation is the first step of the ring expansion pathway.[8]

In order to analyze the reaction progression in more detail, the reaction of **35** with **36g** was monitored at more frequent time intervals. Therefore, 0.025 equivalents of [FeCp$_2$][PF$_6$] were chosen to ensure an adequately slow but still complete reaction.[9] The results show a curve with a distorted S-type shape (Fig. 3.2). The fastest increase in the amount of **41g** was recorded between 29 and 42 % conversion.[10]

Putting all obtained information together this reaction progression can be explained by assuming a radical cation chain reaction mechanism (Scheme 3.2). The reaction is initiated by single-electron transfer (SET) from **35** to the ferrocinium cation (i) with formation of ferrocene and generation of radical cation **35**$^{\bullet+}$. At this point, no conclusion can be drawn if this species has a retained cyclic structure or if the ring might open up upon oxidation (see Computational Studies, Section 3.6). The chain propagation steps are ring expansion with the nitrile (**36**)[11] with formation of radical cationic species **41**$^{\bullet+}$ (ii), and reduction of **41**$^{\bullet+}$ by reactant **35** to yield the observed product **41** and radical cation **35**$^{\bullet+}$ (iii); the latter can restart the chain reaction.

---

[7]This furthermore assures that ferrocene is not present as impurity of the employed ferrocinium salt and that it is not formed via reaction with the solvent.

[8]The reaction of **35** and [FeCp$_2$][PF$_6$] in the absence of nitriles will be subject of Section 3.3.

[9]To guarantee that the entire amount of ferrocinium salt was dissolved at the start of the reaction, a solution of [FeCp$_2$][PF$_6$] and the nitrile (**36g**) was added to **35** in an NMR tube; this point was recorded as the reaction start (t = 0).

[10]A flat trend at the start of a reaction is also characteristic for autocatalytic reactions, and in reactions with a very low starting concentration of the autocatalytic species the peak of the rate is recorded at approximately 50 % conversion.[177]

[11]In the following the identifier add-on **b,d–g** is omitted for clarity.
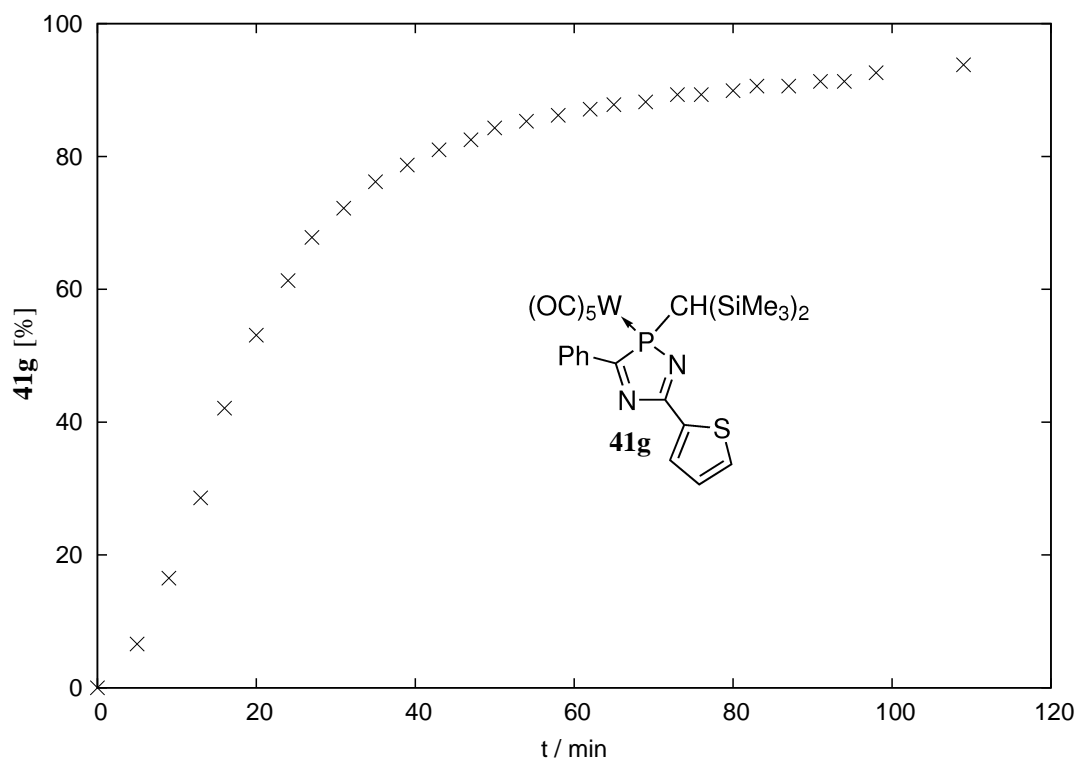
Figure 3.2: Ratio of **41g** (by $^{31}P\{^1H\}$ NMR signal integration) against time for the reaction of **35** with **36g** in the presence of 0.025 equivalents of $[FeCp_2][PF_6]$.
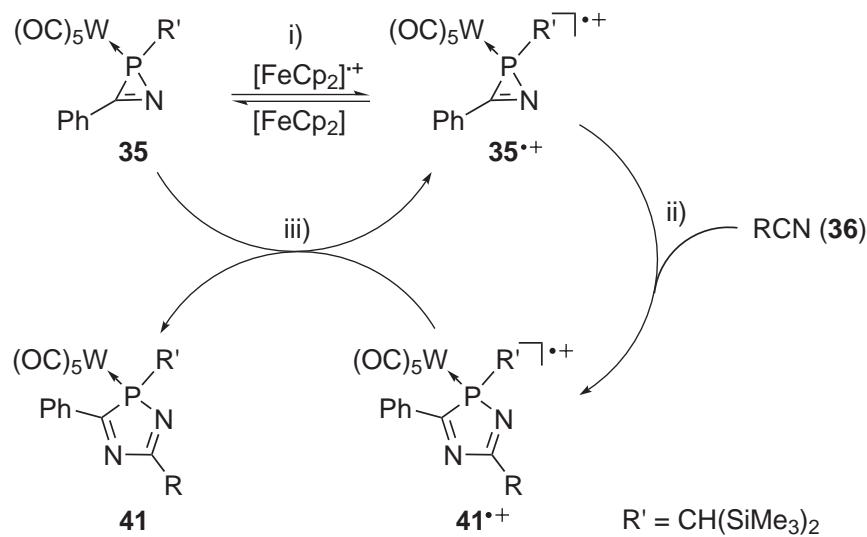
Scheme 3.2: Proposed chain reaction of $2H$-azaphosphirene complex **35** with nitriles (**36**) initiated by the ferrocinium cation.

Regarding the redox potentials of the participating species, as estimated experimentally (Section 3.5) or computationally (Section 3.6), it is not expected that the oxidation of **35** by $[FeCp_2]^{\bullet+}$ is quantitative. The SET reaction (i) should better be described as an endergonic equilibrium, which supports a low concentration of radical cation **35**$^{\bullet+}$. It should be noted that most synthetically applicable radical cation chain reactions require an endergonic SET pre-equilibrium to initiate selective follow-up reactions of highly electrophilic radical cations.[178]

According to Scheme 3.2 the rate of formation of **41** is given by:

$$\frac{d[\mathbf{41}]}{dt} = k_{iii}[\mathbf{35}][\mathbf{41}^{\bullet+}] - k_{-iii}[\mathbf{35}^{\bullet+}][\mathbf{41}], \tag{3.1}$$

and the variation of the radical cation concentration with time is determined by Eqs. (3.2) and (3.3).

$$\frac{d[\mathbf{35}^{\bullet+}]}{dt} = k_i[\mathbf{35}][[FeCp_2]^{\bullet+}] - k_{-i}[\mathbf{35}^{\bullet+}][[FeCp_2]] - k_{ii}[\mathbf{35}^{\bullet+}][RCN]$$
$$+ k_{iii}[\mathbf{35}][\mathbf{41}^{\bullet+}] - k_{-iii}[\mathbf{35}^{\bullet+}][\mathbf{41}], \tag{3.2}$$

$$\frac{d[\mathbf{41}^{\bullet+}]}{dt} = k_{ii}[\mathbf{35}^{\bullet+}][RCN] - k_{iii}[\mathbf{35}][\mathbf{41}^{\bullet+}] + k_{-iii}[\mathbf{35}^{\bullet+}][\mathbf{41}]. \tag{3.3}$$

Assuming that a quasi-stationary state is reached after an initiation phase at one point when the radical cation concentration does not further change, then it can be written: $d[\mathbf{35}^{\bullet+}]/dt = 0$ and $d[\mathbf{41}^{\bullet+}]/dt = 0$. By addition of Eqs. (3.2) and (3.3) the concentration of **35**$^{\bullet+}$ during the reaction reads:

$$[\mathbf{35}^{\bullet+}] = \frac{k_i}{k_{-i}} \frac{[[FeCp_2]^{\bullet+}]}{[[FeCp_2]]}[\mathbf{35}]. \tag{3.4}$$

The concentration of radical cation **41**$^{\bullet+}$ can be eliminated by addition of Eqs. (3.1) and (3.3), and after insertion of relation (3.4) into the resulting expression the rate of formation of **41** can be expressed as:

$$\begin{aligned}
\frac{d[\mathbf{41}]}{dt} &= k_{ii}\frac{k_i}{k_{-i}} \frac{[[FeCp_2]^{\bullet+}]}{[[FeCp_2]]}[\mathbf{35}][RCN] \\
&= k_{ii}K_i \frac{[[FeCp_2]^{\bullet+}]}{[[FeCp_2]]}[\mathbf{35}][RCN] \\
&\approx k_{2nd}[\mathbf{35}][RCN].
\end{aligned} \tag{3.5}$$

In Eq. (3.5) the quotient k_i/k_{-i} was substituted by the quilibrium constant K_i of the initiation step. As the value of K_i is very small, this must be compensated by a large

k_{ii} value according to a fast ring expansion of radical cation $\mathbf{35}^{\bullet+}$ (ii). Furthermore, a sufficiently high $[[FeCp_2]^{\bullet+}]/[[FeCp_2]]$ ratio is required. At the quasi-stationary state, when the reaction is successfully initiated, this ratio should remain approximately constant, hence, it can be combined with the constant factors k_{ii} and K_i in Eq. (3.5) to a quasi-second order rate constant k_{2nd}. So, regarding the curves in Figures 3.1 and 3.2, the reactions show second order characteristics towards the end. The dependency of the reaction rate in this time interval on the ferrocinium salt concentration is apparent from Eq. (3.5): k_{2nd} increases linearly with increasing $[[FeCp_2]^{\bullet+}]/[[FeCp_2]]$ ratio. The upper rate limit is probably connected to the solubility of $[FeCp_2][PF_6]$ in CH_2Cl_2, which was determined as $(1.00 \pm 0.06) \cdot 10^{-2}$ mol $\cdot$ L^{-1}, here.

The flat trend at the reaction start corresponds to an initiation phase when the concentration of the reactive species $\mathbf{35}^{\bullet+}$ is concurrently increased by two contributing reaction sequences: the chain propagation (iii) and its initiation (i). Especially for reactions with a low starting concentration of $[FeCp_2][PF_6]$ the quasi-stationary state is reached only after a comparatively long initiation period, which should cause the S-type curves observed. Obviously, a starting concentration of $3 \cdot 10^{-3}$ mol $\cdot$ L^{-1} of $[FeCp_2][PF_6]$ (Fig. 3.1, curve $\times$) is not sufficient for initiating the chain reaction successfully. For the reaction using $7 \cdot 10^{-3}$ mol $\cdot$ L^{-1} of $[FeCp_2][PF_6]$ (curve $\bigtriangledown$) it appears that a quasi-stationary state was reached at some point, but then the conversion dropped, and the reaction was terminated. Here, the $[FeCp_2]^{\bullet+}$ concentration was presumably too much depleted so that the reaction could not be re-initiated. For successfully initiated reactions it can be assumed that once the quasi-stationary state is reached the ratio of $[[FeCp_2]^{\bullet+}]/[[FeCp_2]]$ does not further change and equals its value at the end of the reaction, which can be estimated by the amount of isolated ferrocene. On the other hand, if a very low starting concentration of $[FeCp_2][PF_6]$ is employed, the $[[FeCp_2]^{\bullet+}]/[[FeCp_2]]$ ratio may change more significantly, not only at the start but also throughout the whole time span of the reaction progression. This explains why considerably more ferrocene is formed in such cases. Then, the last simplification of Eq. (3.5) is no more valid.

One potentially important reaction competing with step (iii) was not considered so far, that is, the reduction of $\mathbf{41}^{\bullet+}$ by ferrocene,

$$\mathbf{41}^{\bullet+} \;+\; [FeCp_2] \;\; \rightleftharpoons \;\; \mathbf{41} \;+\; [FeCp_2]^{\bullet+}. \tag{3.6}$$

It can be neglected at the start, but it might become more important towards the end of the reaction when the concentration of ferrocene is increased and at the same time reduction of $\mathbf{41}^{\bullet+}$ by $\mathbf{35}$ (iii) becomes less likely due to the depletion of the latter. Since reaction (3.6) yields formation of the initiator, $[FeCp_2]^{\bullet+}$, it cannot be regarded as conventional chain termination step, but depletion of $\mathbf{35}$ causes also that the re-

initiation becomes less likely. Participation of the alternative (3.6) may serve as an explanation for occurring chain termination in some cases. Here, the influence of k_{ii} becomes apparent: although a certain amount of initiator is still present in the reaction mixture, the ring expansion (ii) is not fast enough to yield in complete conversion. If the contribution of reaction (3.6) is considered in the overall deduction of the time law, the resulting expression becomes more complicated (than given by Eq. (3.5)), and the radical cation concentrations cannot be eliminated from the equation anymore.

A question still remains open that could not be answered within this work: what is the cation that replaces the ferrocinium ion, which is reduced during the reaction? Assuming that no further side-reactions take place it should be radical cation $41^{\bullet+}$. Unfortunately, analysis of the poorly soluble residue of the reaction mixture did not yield conclusive results (as earlier attempts[167]).

The trifluoromethanesulfonate (hereafter referred to as triflate) salts of Ag(I) and Cu(II),[12] known as strong oxidants,[13] were then investigated as single-electron transfer reagents[14] (Scheme 3.3).

$$M = Ag\ (n = 1),\ Cu\ (n = 2)$$
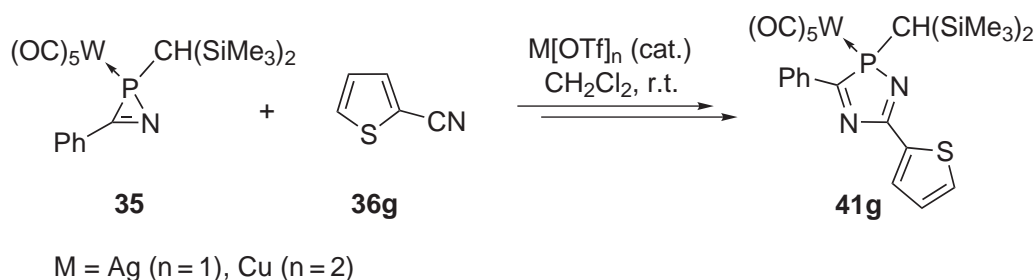
Scheme 3.3: Reactions of 2H-azaphosphirene complex **35** with nitrile **36g** in the presence of metal triflates (OTf$^-$ = CF$_3$SO$_3^-$).

Both metal triflates (0.19 equiv. each) gave highly selective reactions of complex **35** with nitrile **36g** in CH$_2$Cl$_2$ at ambient temperature to yield 2H-1,4,2-diazaphosphole complex **41g**. In the reaction with Ag[OTf] immediately upon addition a grey-brownish precipitate was observed, which points to the formation of elemental silver.

As for **41b** (Fig. 3.3) a single-crystal X-ray diffraction study was carried out on complex **41g** (Fig. 3.4).

---

[12]It has been shown that CuCl$_2$ can induce such ring expansion reactions to some extent.[119, 168]

[13]$E_{1/2}$(Ag$^+$/Ag)(CH$_2$Cl$_2$) = +0.65 V[179] and $E_{1/2}$(Cu[OTf]$_2$/Cu[OTf])(MeCN) = +0.40 V[179] vs. $E_{1/2}([FeCp_2]^+/[FeCp_2])$

[14]For reactions with Cu[OTf]$_2$ an outer-sphere ET mechanism has been evidenced by kinetic studies.[180]
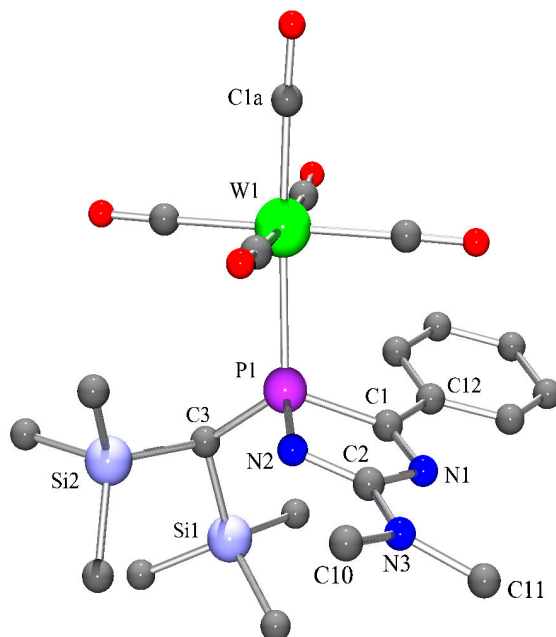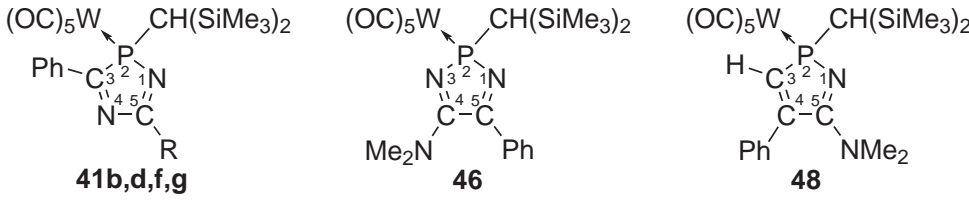
Figure 3.3: Molecular structure of complex **41b** in the crystal (hydrogen atoms omitted for clarity). Selected bond lengths [Å] and angles [°]: W(1)–C(1a) 1.989(5), W(1)–P(1) 2.5340(14), P(1)–N(2) 1.682(4), P(1)–C(1) 1.884(5), C(1)–N(1) 1.294(6), N(1)–C(2) 1.429(7), C(2)–N(2) 1.312(8), C(2)–N(3) 1.333(8), C(1)–C(12) 1.467(8), N(2)–P(1)–C(1) 90.7(2), P(1)–C(1)–N(1) 109.0(3), C(1)–N(1)–C(2) 110.5(4), N(1)–C(2)–N(2) 120.1(5), C(2)–N(2)–P(1) 109.2(4), N(2)–C(2)–N(3) 123.8(6).

Selected structural data for **41b,g**[15] are listed in Table 3.2 along with corresponding data for complexes **41d,f**, 2H-1,3,2-diazaphosphole complex **46**,[156] and 2H-1,2-azaphosphole complex **48**,[148] which exhibit some comparable structural features. While **41b** crystallizes in the monoclinic space group P2$_1$ (No. 4), complexes **41d,f,g** are isotypic and crystallize in the triclinic space group P$\bar{1}$ (No. 2). The bond lengths and angles within their diazaphosphole rings are almost identical with localized endocyclic nitrogen–carbon double bonds (about 1.29 Å) different from the situation of aromatic heterocycles such as 2H-1,2,3-diazaphospholes[181] and 2H-1,2,3-triazoles.[182] As in complex **46** the central phosphorus heterocycles of **41b,d,f,g** are essentially planar. The mean deviations from least-squares planes (with respect to all atoms of the particular ring system) are 0.031 (**41b**), 0.032 (**41d**), 0.031 (**41f**), and 0.029 Å (**41g**). This is contrary to 2H-1,2-azaphosphole complex **48**, which exhibits a slightly folded five-membered ring where the C^3 center deviates 0.160 Å from the best plane given by P–N^1–C^4–C^5.[153]

---

[15]The numbering of ring atoms according to the modified Hantzsch-Widman-Patterson system is applied for clarity. For example, C(1) in Figures 3.3 and 3.4 becomes C^3 and C(2) becomes C^5 (see Tab. 3.2). In all depicted molecular structures most atom labels are omitted for clarity; fully numbered pictures can be found in Appendix E.

Table 3.2: *A)* Selected bond lengths [Å], and *B)* angles [°] for 2H-1,4,2-diazaphosphole complexes **41b,d,f,g** (R = NMe$_2$ (**b**), 1,5-dimethyl-2-pyrrolyl (**d**),[173] 3-thienyl (**f**),[173] 2-thienyl (**g**)), 2H-1,3,2-diazaphosphole complex **46**,[156] and 2H-1,2-azaphosphole complex **48**.[148] *C)* Torsion angles [°] between ring planes of **41d,f,g** with respect to least-squares planes (all atoms of particular ring system involved).

41b,d,f,g   **46**   **48**

A) No.	W–P	P–N$^{1/3}$	P–C^3	N^1–C^5	C‡–C$^1_{phenyl}$	C^5–C$^2_{hetaryl}$ or C†–NMe$_2$
41b	2.5340(14)	1.682(4)	1.884(5)	1.312(8)	1.467(8)	1.333(8)
41d[173]	2.5324(13)	1.7006(39)	1.8701(45)	1.2946(59)	1.4876(60)	1.4228(62)
41f[173]	2.5321(5)	1.7042(14)	1.8767(16)	1.2903(21)	1.4675(23)	1.4592(22)
41g	2.5306(10)	1.707(3)	1.877(4)	1.293(5)	1.457(6)	1.441(5)
46[156]	2.4790(11)	1.736(3) 1.705(3)	–	1.291(5)	1.487	1.362(5)
48[148]	2.5123(10)	1.690(3)	1.810(4)	1.303(6)	1.470	1.360(5)

B)	C^3/N^3–P–N^1	P–N$^{1/3}$–C$^{5/4}$	N^1–C^5–N^4/C^4	C^5–N^4/C^4–C^3/N^3
41b	90.7(2)	109.2(4)	120.1(5)	110.5(4)
41d[173]	89.86(19)	109.80(31)	119.98(40)	109.92(37)
41f[173]	90.02(7)	109.31(12)	120.74(14)	110.33(14)
41g	90.1(2)	109.1(3)	121.0(3)	110.1(3)
46[156]	96.3(2)	107.8(3) 108.2(3)	114.0(3)	113.4(3)
48[148]	93.72(18)	109.9(3)	117.0(3)	110.0(4)

C)	Diazaphosphole−3-Ph	Diazaphosphole−5-hetaryl	3-Ph−5-hetaryl
41d[173]	6.7	1.9	5.3
41f[173]	4.2	2.8	2.3
41g*	4.3	3.5	3.5

‡C^3 (**41b,d,f,g**), C^5 (**46**), or C^4 (**48**). †C^5 (**41b**, **48**) or C^4 (**46**). *Only the values for the prevailing conformation given.

An interesting feature of complexes **41d,f,g** is the largely coplanar arrangement of the three ring systems (Tab. 3.2, *C*), thus pointing to extended π conjugation. The coplanarity is as pronounced as in 2,5-di(2-thienyl)phosphole complex **49** (Fig. 3.5),

which has interplanar angles between adjacent rings about 7.3° and 13.4°.[183] This is in marked contrast to the situation of 2H-1,3,2-diazaphosphole[156] and 2H-1,2-azaphosphole complexes.[148] For instance, the phenyl group of complex **46** subtends an interplanar angle to the five-membered heterocycle of 35.7°,[153] and in complex **48** this angle is about 54.6°.[148]
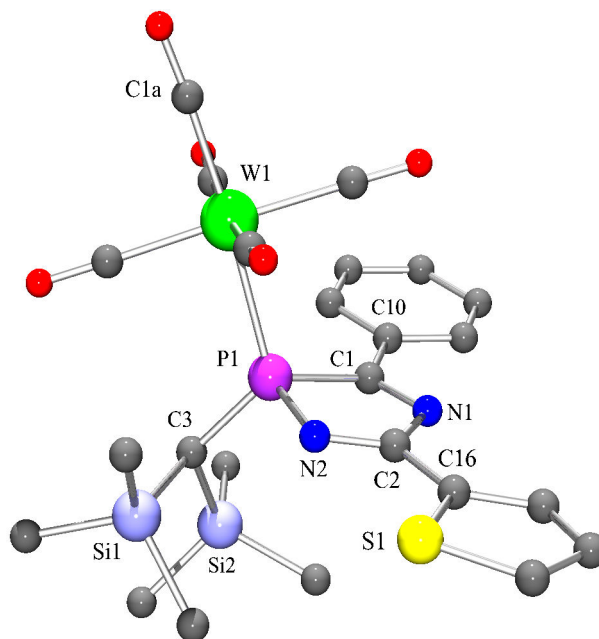
Figure 3.4: Molecular structure of complex **41g** in the crystal (hydrogen atoms omitted for clarity; only the prevailing conformation of the 2-thienyl substituent with respect to the diazaphosphole ring plane (81 %) shown). Selected bond lengths [Å] and angles [°]: W(1)–C(1a) 2.008(4), W(1)–P(1) 2.531(10), P(1)–N(2) 1.707(3), P(1)–C(1) 1.877(4), C(1)–N(1) 1.304(5), C(2)–N(2) 1.293(5), C(2)–C(16) 1.441(5), C(1)–C(10) 1.457(6), N(2)–P(1)–C(1) 90.1(2), P(1)–C(1)–N(1) 109.2(3), C(1)–N(1)–C(2) 110.1(3), N(1)–C(2)–N(2) 121.0(3), C(2)–N(2)–P(1) 109.1(3).

49
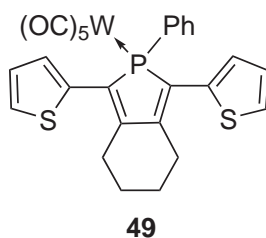
Figure 3.5: 2,5-Di(2-thienyl)phosphole complex **49**.[183]

The C,C distances between the 2H-1,4,2-diazaphosphole rings of **41d,f,g** and their aryl substituents are in the range of the lengths of conjugated C_{sp^2}(=N)–C_{Ar} bonds

(standard value: 1.476(14) Å[184]). The thienyl ring of **41g** exhibits a statistical disorder. This was observed also for complex **49**[183] and for the terminal rings of linear thiophene oligomers.[185] In the prevailing conformation (81 %) the thienyl and the 2*H*-1,4,2-diazaphosphole ring of **41g** adopt a *syn* arrangement (with respect to phosphorus and sulfur).

Also complex **41b** exhibits a coplanar arrangement of the phenyl substituent and the 2*H*-1,4,2-diazaphosphole ring (twist angle between least-squares planes: 8.9°). Additionally, a strong interaction of the dimethylamino nitrogen lone pair with the π electrons of the endocyclic C^5,N^1 bond is indicated as the C^5,N^1 and the C^5,NMe_2 bond lengths[16] are virtually identical. Different from complexes **46** and **48** the N center of the NMe_2 group is trigonal planar coordinated ($\Sigma\angle(N_{NR_3})$ 360.0°), and its nitrogen and carbon atoms deviate by only 0.081, 0.019, and 0.229 Å from the regression plane of the 2*H*-1,4,2-diazaphosphole ring. A consequence of the partial double bond character of the exocyclic C^5,N bond is a hindered rotation about this bond. This is in accordance with the observation of sets of two distinctly different ^{1}H and ^{13}C{^{1}H} resonances, showing that the nuclei of both methyl groups are magnetically inequivalent in solution. Noteworthy is that the P,N^1 bond of **41b** is significantly shorter compared to the P,N^1 bond of complex **41g**.

The phosphorus centers of complexes **41b,d,f,g** have distorted tetrahedral environments ($\Sigma\angle(P_{PR_3})$ 307.9° (**41b**), 309.6° (**41g**)). The tungsten–phosphorus bond lengths are about 2.53 Å, thus, substantially longer than in complexes **46** and **48**. The increase in W,P bond lengths in the order **46** < **48** < **41d,f,g** correlates with a decrease of the tungsten–phophorus coupling constant magnitudes within this series: **46** (257.1 Hz)[156] > **48** (236.8 Hz)[148] > **41d,f,g** (233.9, 229.8, 229.5 Hz). However, the $|^1J_{WP}|$ value of 5-dimethylamino-2*H*-1,4,2-diazaphosphole complex **41b** (241.6 Hz) is slightly larger than $|^1J_{WP}|$ of complex **48**, while its W,P bond is longer. As the W,P bond distances of complexes **41b,d,f,g** are in the same range, this seems to be a common feature of 2*H*-1,4,2-diazaphosphole complexes. Another remarkable feature of complexes **41b,d,f,g** is a small endocyclic angle at phosphorus of about 90°. Furthermore, they exhibit a comparatively long endocyclic P,C^3 bond (1.87−1.88 Å) while the length of the P,N^1 bond differs only marginally from the P,N bond lengths of complexes **46** and **48**.

The assumption of extended π-conjugated systems in 2*H*-1,4,2-diazaphosphole complexes **41d,f,g** should be deducible from their UV/Vis spetra as this should have a considerable influence on their electronic excitation energies. In the spectrum of **41g** (Fig. 3.6) the lowest-lying absorption maximum appears already at $\lambda_{max} = 435$ nm (lgϵ

---

[16]The standard length of a $C_{sp^2}=N_{sp^2}$ double bond was reported as 1.279(8) Å.[184]

= 3.55; n-pentane). Thus, this transition lies even lower than the longest-wavelength absorption of 2,5-di(2-thienyl)phosphole complex **49** (λ_{max} = 408 nm; THF).[183] For the latter it has been assigned to a π–π^* transition, while in the case of complex **41g** it can be assigned to a metal–ligand charge transfer (MLCT) process;[186] this is supported by time-dependent DFT (TD-DFT) calculations (Chapter 5) on **41b** and other $2H$-1,4,2-diazaphosphole complexes presented in Chapter 4. *Optical end absorption*[187] of **41g** appears already at λ_{onset} = 560 nm (cf. complex **49**: λ_{onset} = 475 nm[183]). A further band with higher intensity is found at λ_{max} = 317 nm (lgϵ = 4.40), which can be assigned to one or more nearly degenerate π–π^* transitions of the extended conjugated π system.
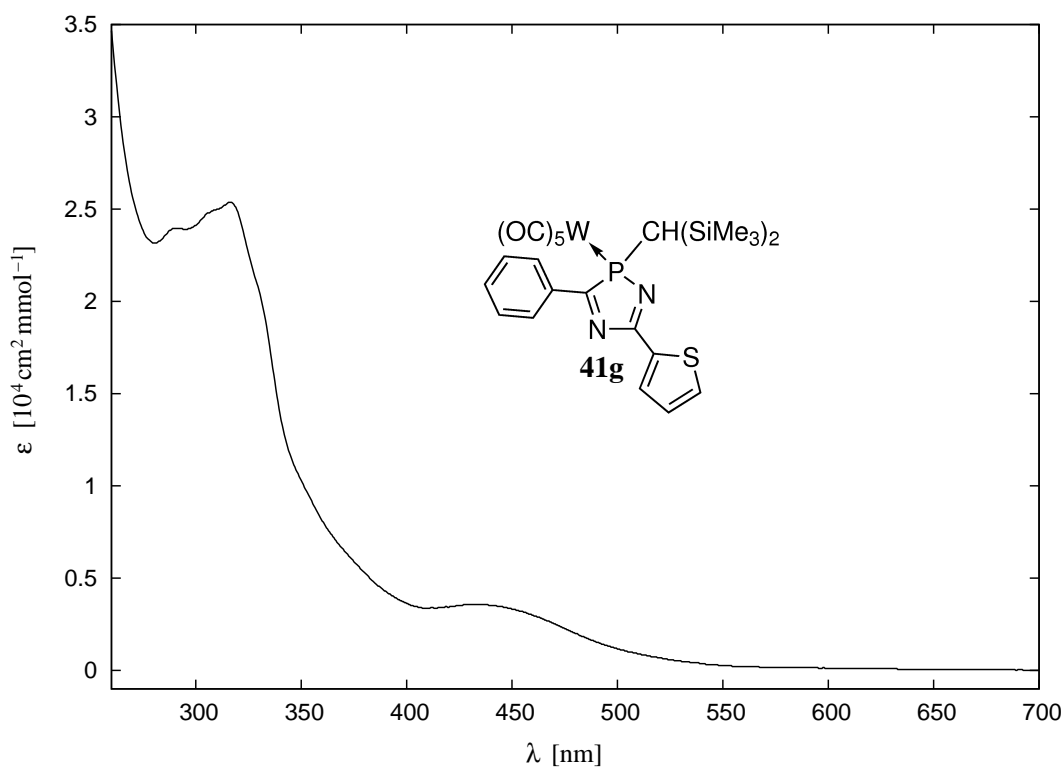
Figure 3.6: UV/Vis spectrum of complex **41g** (n-pentane).

The visible absorption of complex **41b** starts also at very long wavelength (λ_{onset} = 505 nm), even though this derivative has only two conjugated cyclic π systems. Due to an overlap with another band at λ_{max} = 350 nm the center of the lowest-lying transition at approximately 407 nm is only a rough estimate. The π–π^* transition band was observed at λ_{max} = 288 nm (lgϵ = 4.24). The most intense absorption maxima of complexes **41b** and **41g** are in the UV region at λ_{max} = 227 (lgϵ = 4.90) and 232 nm (lgϵ = 4.89), respectively.

Some interesting structure-reactivity relationships could be derived from mass spectrometric investigations on complexes **41b,g**. Upon electron impact (EI) the radical cations **41b,g**$^{\bullet+}$ were generated and detected (m/z 687 and 726). Their main fragmentation pathway is successive expulsion of CO or even loss of the whole W(CO)$_5$ fragment giving rise to the formation of the radical cationic heterocylic ligand systems **50b**$^{\bullet+}$ (m/z 363) and **50g**$^{\bullet+}$ (m/z 402) (Fig. 3.7). This reflects the relative weakness of the W,P bond of radical cationic (and presumably also neutral) 2H-1,4,2-diazaphosphole complexes.[17]

In contrast to complexes **46** and **48** fragmentation of the central 2H-1,4,2-diazaphosphole rings of **41b,g** occurred under EI conditions, which indicates a lower thermodynamic stability of this ring. So, upon ionization of both **41b** and **41g** signals were detected at m/z 533, 505, and 477, which result from loss of a nitrile unit (Me$_2$NCN or ThCN, respectively) and 3$-$5 CO ligands. Different conceivable structures for these radical cations are displayed in Figure 3.7: 2H-azaphosphirene complex structures **51**$^{\bullet+}$–**53**$^{\bullet+}$, nitrilium phosphane ylide complex structures **54**$^{\bullet+}$–**56**$^{\bullet+}$, and 1,3-azaphosphaallene complex structures **57**$^{\bullet+}$–**59**$^{\bullet+}$.[18] Furthermore, ring fragmentation with loss of Me$_2$NCN and additional loss of the entire W(CO)$_5$ moiety was observed for **41b** at m/z 293. The resulting fragment may have either one of the structures **60**$^{\bullet+}$–**62**$^{\bullet+}$. On the contrary, this signal was not present in the spectrum of complex **41g**. Instead, expulsion of benzonitrile from the heterocycle was observed (m/z 299). Likewise this cation should have one of the structures **63**$^{\bullet+}$–**65**$^{\bullet+}$. Finally, complete ring fragmentation via loss of both nitrile units and the pentacarbonyl metal fragment was observed in both cases (m/z 190). The resulting fragment may have the structure of radical cationic phosphaalkene **64**$^{\bullet+}$.

Upon fast atom bombardement (FAB, positive mode) expulsion of CO ligands was the major fragmentation pathway of complexes **41b,g**; the ratio of ring fragmentation is largely reduced. Interestingly, the protonated liberated heterocyclic ligand systems [**50b,g** + H]$^+$ (m/z 364 and 403) represented the base peaks in both cases. Radical cationic fragments that result from consecutive losses of CO ligands (not shown) are no intermediates in the formation of [**50b,g** + H]$^+$. Apparently, decomplexation occurs in a single step from the protonated molecules. These observations indicate that protonation causes a pronounced weakening of the W,P bond of 2H-1,4,2-diazaphosphole complexes **41b,g**. For comparison, the intensities of radical cationic heterocyclic ligands **50b,g**$^{\bullet+}$ under EI conditions were only 12 (**50b**$^{\bullet+}$) and 44 % (**50g**$^{\bullet+}$).

---

[17]For comparison, loss of the organometallic fragment was not observed for complex **46** under comparable ionization conditions.

[18]In the spectrum of complex **41b** the signal for at m/z 533 represented the base peak.
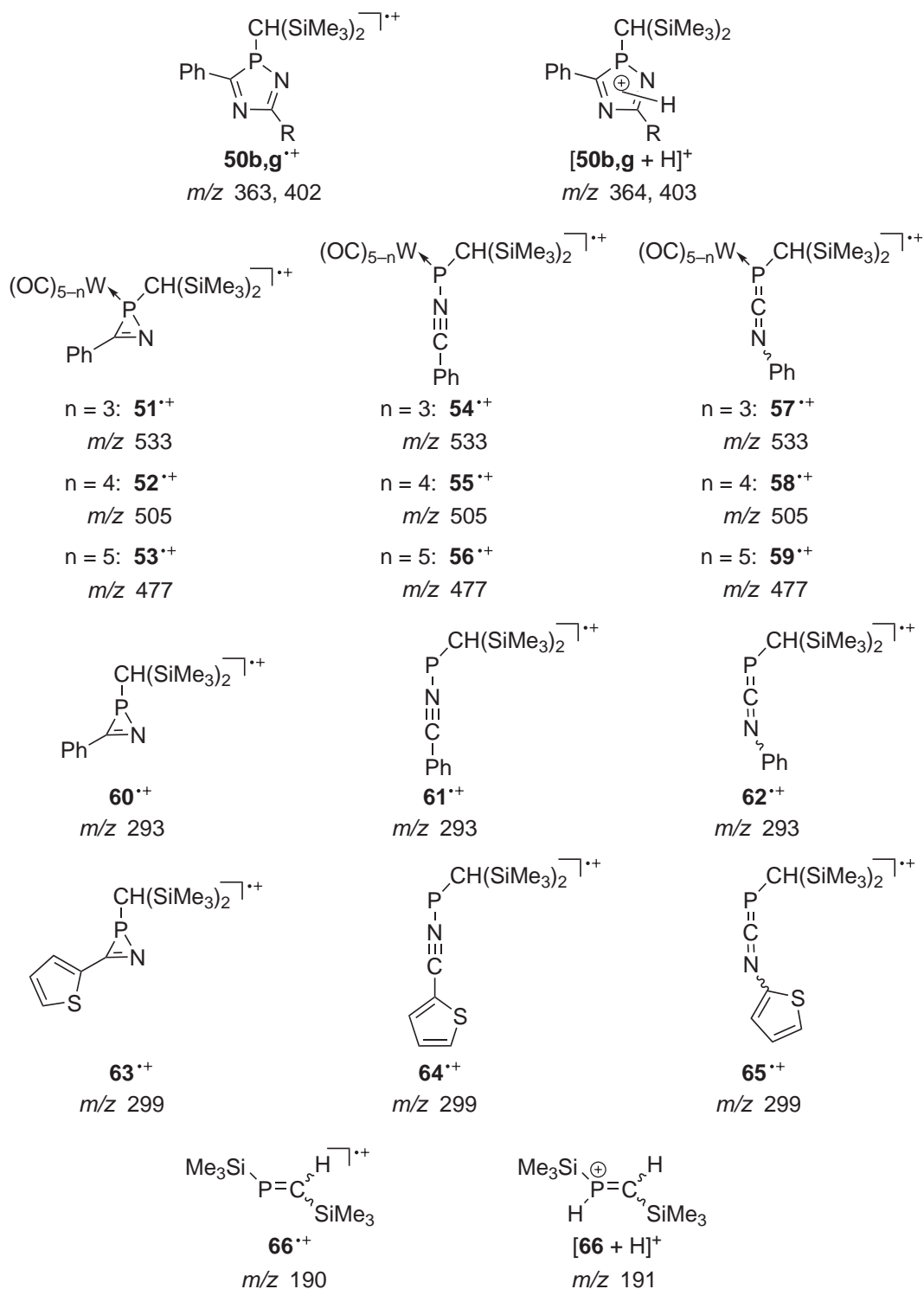
Figure 3.7: Assignment of cationic molecule fragments to m/z values detected upon ionization of complexes **41b,g** (R = NMe$_2$ (**b**), 2-thienyl (**g**)) under EI- (**50b,g**$^{\bullet+}$, **51**$^{\bullet+}$–**66**$^{\bullet+}$) or FAB-MS conditions ([**50b,g** + H]$^+$, **51**$^{\bullet+}$ or **54**$^{\bullet+}$ or **57**$^{\bullet+}$, **53**$^{\bullet+}$ or **56**$^{\bullet+}$ or **59**$^{\bullet+}$, [**64** + H]$^+$).

In the FAB spectrum of **41b** the peak corresponding to radical cation **51**$^{\bullet+}$, **54**$^{\bullet+}$, or **57**$^{\bullet+}$ was also detected (m/z 533; 22 %), and the radical cations corresponding to m/z 533 and 477 were formed via FAB from **41g** in 9 and 28 % abundance, respectively. The phosphaalkene fragment $[\mathbf{64} + \mathrm{H}]^+$ (m/z 191), which results from losses of two nitrile units and the organometallic fragment, appeared as protonated species in both spectra, hence, it was formed either in one step from the protonated molecule, or via the protonated heterocyclic ligand systems $[\mathbf{50b,g} + \mathrm{H}]^+$.[19]

3.2 Limitations of the SET-Induced Ring Expansion Methodology

In order to explore the applicability of the SET-induced ring expansion methodology three further nitrile derivatives were chosen: the parent nitrile HCN (**36h**), ethyl cyanoformate (**36i**), and pentafluorobenzonitrile (**36j**) (Scheme 3.4); the latter might be regarded as electron-poor nitrile derivatives. All reactions were carried out at ambient temperature using 0.18 equivalents of $[\mathrm{FeCp_2}][\mathrm{PF_6}]$.

36h, **41h**: R =   H

36i, **41i**: R =   CO$_2$Et   **36j**, **41j**: R =

Scheme 3.4: Reactions of 2H-azaphosphirene complex **35** with nitrile derivatives **36h–j** in the presence of substoichiometric amounts of ferrocinium hexafluorophosphate or tetraphenylborate.

In contrast to the reactions with **36b,d–g**, the reaction of **35** with HCN (**36h**) was unselective as revealed by ^{31}P NMR spectroscopy. Already after a short period (1.5 h) a variety of resonances were detected. One of them could be assigned to the desired

product **41h** ($\delta = 105.5$, $|^1J_{WP}| = 225.1$ Hz, $|^{3+4}J_{PH}| = 34.3$ Hz), although it could
not be isolated.[20] Even though an excess of **36h** was employed (2.6 equiv.), after 4
days the reaction mixture still contained 16 % of unreacted **35** (by ^{31}P NMR signal
integration) and only 20 % of **41h** besides numerous unidentified by-products.

Several by-products bearing a P,F bond were observed in the reaction of **35** with
electron-poor nitrile derivative **36i**. After 6 days 41 % of **35** remained unreacted, and
a product with a ^{31}P NMR resonance at $\delta = 110.7$ ($|^1J_{WP}| = 227.6$ Hz) was observed
(ca. 21 %). These data are too close to those of **41d–g**. Therefore, an assignment to
41i is not plausible. On the basis of the trend mentioned beforehand a lower $|^1J_{WP}|$
value should be expected for **41i**. Even more vexing was the finding that a by-product
having analogous ^{31}P NMR data was detected also in the reaction of **35** with HCN
(about 5 % after 4 d). The reaction of **35** with **36j** showed a similar behavior to that
of the reaction with **36i**, and also here a resonance at $\delta = 110.7$ was observed (12 %
after 6 d) as well as numerous by-products some of which showed $^1J_{PF}$ couplings, but
no evidence for the formation of the target product **41j** was obtained. After 6 days the
mixture contained 48 % of **35**, and ^{19}F{^{1}H} NMR spectroscopic monitoring revealed
that the entire amount of **36j** had remained unreacted.[21]

The ^{19}F resonance of the hexafluorophosphate anion decreased during the reaction,
and its ^{31}P{^{1}H} NMR resonance was after 6 days no longer detected. These results
reveal that the hexafluorophosphate counteranion, which is usually regarded as weakly
coordinating,[107] had taken part in the reaction course. However, the observation that
no reaction of **35** with **36g** takes place in the presence of [^{n}Bu$_4$N][PF$_6$] (Section 3.1)[22]
shows that the hexafluorophosphate ion does not play a crucial role for ring expansion
reactions of **35** as induced by [FeCp$_2$][PF$_6$], hence, the products with P,F bonds do
not constitute intermediates of this pathway. Instead, they should be regarded as
by-products resulting from reaction of transiently formed species with PF$_6^-$ through
fluoride transfer. As highly electrophilic cationic species are able to abstract fluoride
from the hexafluorophosphate anion,[188] here, this species presumably is the radical
cationic 2H-azaphosphirene complex **35**$^{\bullet+}$ (or an acyclic isomer thereof), which is
formed in the first step of the radical cation chain reaction (Scheme 3.2). Apparently,
the attack of nitrile derivatives **36h–j** is disfavored so that the rate constant k_{ii} of the
ring expansion is too small in these cases and side-reactions with the counteranion can
compete with the ring enlargement reaction.

---

[20]The synthesis of **41h** via another route is described in Section 4.1.3.

[21]In the perfluorophenyl region of the spectra only the resonances belonging to **36j** were detected
indicating that no conversion of **36j** had occurred even though an excess (6.4 equiv.) was employed.

[22]Also in the reaction with [^{n}Bu$_4$N][PF$_6$] products with a P,F bond were formed, but with significant
smaller ratios (< 1 % after 4 days) than in the reactions of **35** with **36h–j** and [FeCp$_2$][PF$_6$].

In order to suppress such side-reactions the hexafluorophosphate was exchanged for the weaker nucleophilic tetraphenylborate, which was tested for the reaction of **35** with 2-thiophenecarbonitrile (**36g**) with 0.2 equivalents of $[FeCp_2][BPh_4]$. A clean reaction afforded complex **41g** within 8 hours. Under the same conditions reactions of **35** with nitrile derivatives **36h–j** were re-investigated using this SET reagent. Also here, complex **41h** was obtained only as minor product, and the complex with the ^{31}P NMR resonance at $\delta = 110.6$ ($|^1J_{WP}| = 227.6$ Hz) was formed with a somewhat larger ratio (ca. 15 %); about 66 % of **35** remained unreacted (after 4 d). Reactions of **35** with **36i** and **36j** in the presence of $[FeCp_2][BPh_4]$ showed almost no conversion of **35** within one day. Nevertheless, the resonance at about 111 ppm emerged and increased slowly over several days in both reactions, and no conversion **36j** occurred.[23]

3.2.1 Reactions of a *C*-Ferrocenyl Substituted 2*H*-Azaphosphirene Complex

C-Ferrocenyl substituted 2*H*-azaphosphirene complex **67**[128] was reacted with succinonitrile (**36k**) in the presence of $[FeCp_2][PF_6]$ (Scheme 3.5). Because a twofold ring expansion was attempted, 0.5 equivalents of **36k** were employed. After a slow reaction complete conversion of **67** was evidenced by ^{31}P{^{1}H} NMR spectroscopy within 8 days, but only one resonance in the expected range for targeted complex **68** was detected ($\delta = 113.4$ $|^1J_{WP}| = 234.0$ Hz).[24] The product was separated by low-temperature column chromatography and subjected to multinuclear NMR experiments. The ^{1}H NMR spectrum showed two singlets at 4.14 and 4.22 ppm, each representing 5 protons by integration, attributable to unsubstituted cyclopendadienyl rings of ferrocenyl groups. Six resonances were detected between 4.25 and 5.25 ppm representing a total of 8 protons, thus giving rise to two mono-substituted ferrocenyl Cp rings. In principle, these observations would be consistent with the structure of **68**, but the spectrum showed only one resonance for the methine proton of a $CH(SiMe_3)_2$ moiety and two resonances of trimethylsilyl groups (9 H each), which is inconsistent with the constitution of **68**. The collected data are in good agreement with the structure of 3,5-diferrocenyl-2*H*-1,4,2-diazaphosphole complex **69l** (for ^{13}C{^{1}H} NMR data see below). This was supported by the molecular ion peak at m/z 936 in the FAB-MS spectrum and further confirmed by a single-crystal X-ray diffraction study (Fig. 3.8).

---

[23]As a good case in point, the reaction of **35** with **36j** was additionally examined in the presence of silver triflate. Also here, no reaction of **35** with **36j** occurred, and the resonance at about 111 ppm increased at the expense of that of **35**.

[24]Since a racemic mixture of 2*H*-azaphosphirene complex **67** was employed and the ring expansion is not expected to proceed diastereoselectively, complex **68** should be formed as a pair of enantiomers plus a *meso form*, therefore, two ^{31}P{^{1}H} NMR resonances were expected for **68**.
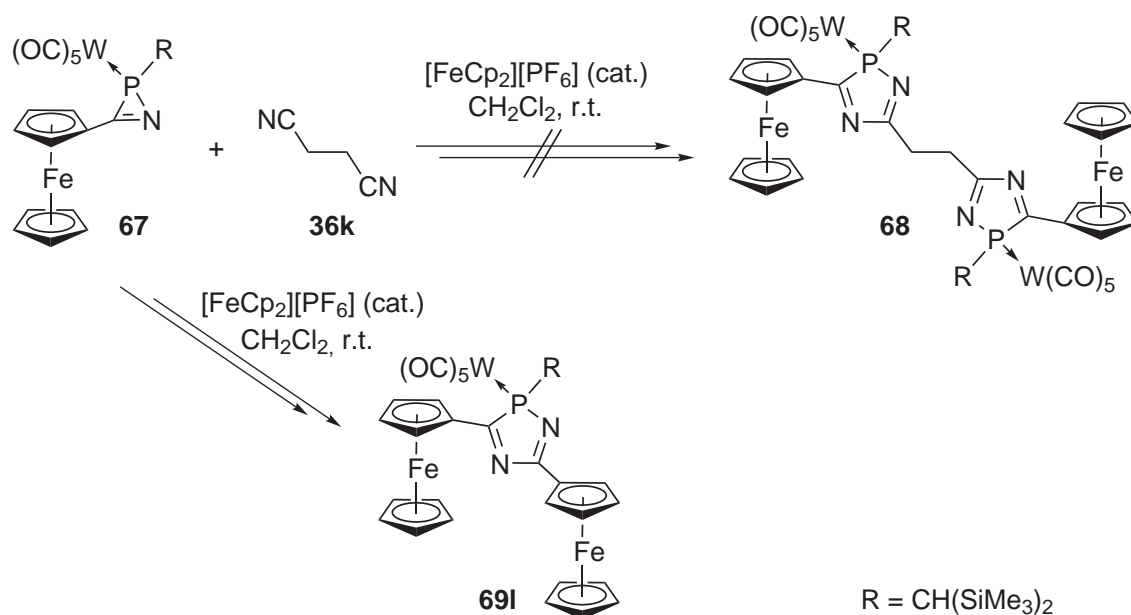
Scheme 3.5: Reaction of 2H-azaphosphirene complex **67** in the presence of succinonitrile
(**36k**) and substoichiometric amounts of ferrocinium hexafluorophosphate.
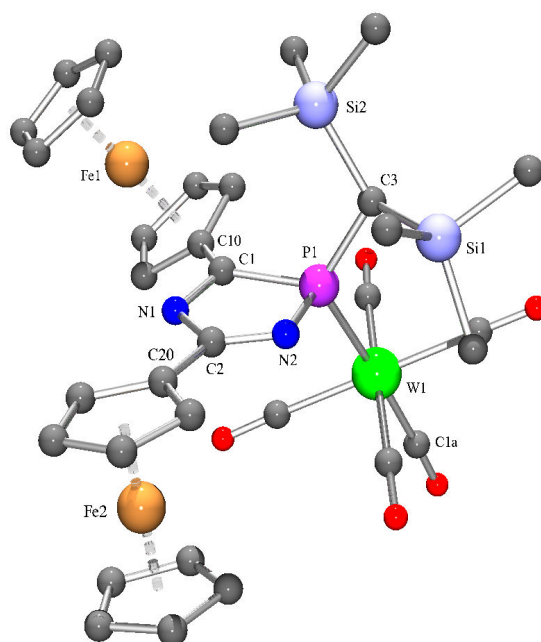
Figure 3.8: Molecular structure of complex **69l** in the crystal (hydrogen atoms omitted
for clarity). Selected bond lengths [Å] and angles [°]: W(1)–C(1a) 2.012(4), W(1)–
P(1) 2.5283(10), P(1)–N(2) 1.697(3), P(1)–C(1) 1.882(3), C(1)–N(1) 1.299(4), C(2)–N(2)
1.301(4), C(2)–C(20) 1.451(5), C(1)–C(10) 1.464(5), N(2)–P(1)–C(1) 90.40(15), P(1)–
C(1)–N(1) 108.6(3), C(1)–N(1)–C(2) 110.5(3), N(1)–C(2)–N(2) 120.4(3), C(2)–N(2)–P(1)
109.2(3).

While the $^{31}P\{^1H\}$ NMR spectroscopic data for complex **69l** are very similar to those of 5-hetaryl-2H-1,2,4-diazaphosphole complexes **41d–g**, the $^{13}C\{^1H\}$ NMR resonances of the ring carbon atoms C^3 ($\delta = 206.6$; $|^{1+4}J_{PC}| = 27.5$ Hz) and C^5 ($\delta = 175.1$; $|^{2+3}J_{PC}| = 5.8$ Hz) of **69l** are both shifted somewhat to lower field (compared to **41a,b,d–g**: $\Delta\delta(C^3) = 5{-}8$; $\Delta\delta(C^5) = 10{-}15$; cf. Tab. 3.1). Within this series complex **69l** exhibits the largest $|^{1+4}J_{PC^3}|$ value.

In the UV/Vis spectrum of **69l** (Fig. 3.9) a low-energy transition is observed at 404 nm (MLCT band), and the more intense $\pi{-}\pi^*$ absorption appears at $\lambda_{max} = 296$ nm. Thus, both bands are in the same range as those of complex **41b**, which also features two conjugated cyclic π systems. Another broad visible band appears at $\lambda_{max} = 539$ nm, which is assigned either to one or more nearly degenerate $d{-}d$ transitions of Fe(II),[189] or to a metal–ligand charge transfer process ($d_\pi{-}\pi^*$) occurring from the iron center to the acceptor-substituted cyclopendadienyl ring.[190, 191] This assignment is in accordance with the theoretical treatment (model III) by Marder and coworkers.[190]
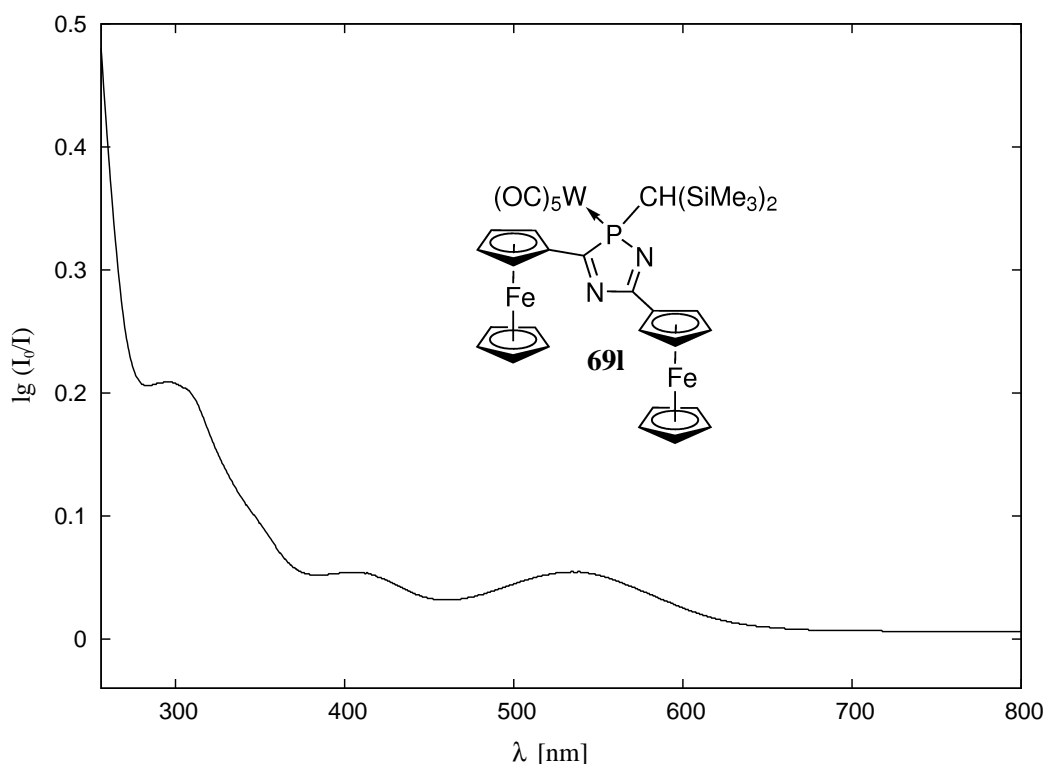
Figure 3.9: UV/Vis spectrum of complex **69l** (*n*-pentane).

Complex **69l** crystallizes in the monoclinic space group P $2_1/c$ (No. 14). The structural parameters of the central heterocycle of **69l** are similar to those of 5-hetaryl substituted complexes **41d,f,g** (cf. Tab. 3.2). It features localized C,N double bonds

(about 1.30 Å), a comparatively long endocyclic P,C bond, a long W,P bond, and
an acute endocyclic angle at phosphorus; the largest endocyclic bond angle is found
at C(2) as apex.[25] Notwithstanding the presence of two bulky ferrocenyl substituents
the phosphorus heterocycle is largely planar (mean deviation from least-squares plane:
0.038 Å). With respect to each other the two ferrocenyl-moieties exhibit a transoid
arrangement at the heterocycle. The cyclopentadienyl ring at C(2) (at the ferrocenyl
unit of Fe(2)) adopts a coplanar arrangement with the heterocycle as observed also
for the hetaryl substituents in **41d,f,g**; the torsion angle of the ring planes with re-
spect to least-squares planes is 6.9°. In contrast, the ferrocenyl unit at C(1) (around
Fe(1)) is out of the heterocyle ring plane, and the substituted Cp ring subtends an
interplanar angle of 31.8° with the phosphorus heterocycle (C(10) lies 0.140 Å above
the 2H-1,4,2-diazaphosphole ring plane). The reason for this distortion presumably
comes from the proximity to the bulky bis(trimethylsilyl)methyl group.

Complex **69l** represents the insertion product of ferrocenecarbonitrile (**36l**) into
the P,N bond of **67**, and since this nitrile was not added, it must stem from 2H-
azaphosphirene complex **67**. Indeed, reaction of **67** with ferrocinium hexafluorophos-
phate (0.32 equiv.) *in the absence* of any nitrile yielded complete conversion of **67** to
give **69l** as major product within 5 days at ambient temperature (Scheme 3.6, i).
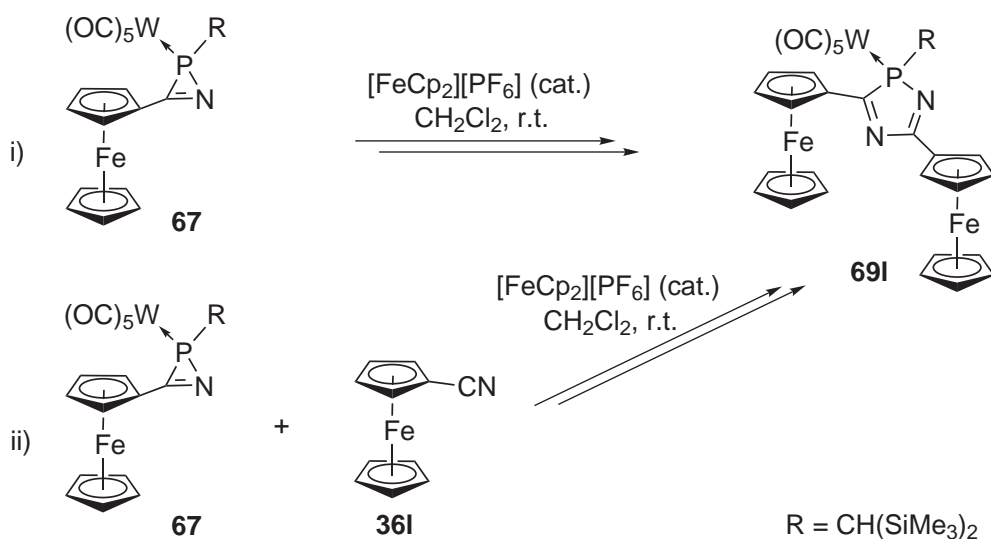
Scheme 3.6: SET-induced ring expansion of 2H-azaphosphirene complex **67** in the ab-
sence of nitriles or in the presence of ferrocenecarbonitrile **36l**.

The synthesis of **69l** was achieved in a clean reaction of **67** with ferrocenecarbo-
nitrile (**36l**) and 0.18 equivalents of [FeCp$_2$][PF$_6$] (Scheme 3.6, ii) whereby complex

---

[25]For atom numbering see Fig. 3.8.

69l was isolated in 66 % yield. It should be noted that in this case 67 % of ferrocene were obtained, while under comparable conditions reaction of **35** with 2-thiophene-carbonitrile (**36g**) gave only 8 % of ferrocene (cf. Scheme 3.1, Section 3.1). This correlates nicely with the oxidation potentials of the employed 2H-azaphosphirene complex derivatives (cf. Section 3.5).

Against this new background some earlier results appear in a new light. M. Schlenker[192] and O. Feier[193] described in their Diploma Theses ferrocinium hexafluorophosphate-induced reactions of 2H-azaphosphirene complex **67** with different nitrile derivatives and the formation of two reaction products (**A** and **B**; Tab. 3.3), which showed ^{31}P$\{^1$H$\}$ resonances in the expected range for 2H-1,4,2-diazaphosphole complexes in varying ratios.[128, 192, 193] The two products were interpreted as isomers of the respective target molecules, whereas the origin of the isomerism was interpreted in different ways.[128, 192, 193]

Table 3.3: ^{31}P$\{^1$H$\}$ NMR data and product shares for reactions of **67** with nitrile derivatives **36a,c,f,g,m–o** (**a**: 1-piperidinecarbonitrile,[128, 192] **c**: benzonitrile,[128, 192] **f**: 3-thiophenecarbonitrile,[128, 192] **g**: 2-thiophenecarbonitrile,[128, 192] **m**: acetonitrile,[128, 193] **n**: 2-pyridylacetonitrile,[193] **o**: malonitrile.[193])

	A		**B**		ratio **A** : **B**
R	$\delta(^{31}$P$)$	$|^1J_{WP}|$/Hz	$\delta(^{31}$P$)$	$|^1J_{WP}|$/Hz	
1-piperidino (**36a**)[128, 192]	105.0	240.5	–	–	1 : 0
3-thienyl (**36f**)[128, 192]	113.4	230.4	114.6	233.2	10 : 1
2-thienyl (**36g**)[128, 192]	114.7	230.5	114.5	*	8 : 1
phenyl (**36c**)[128, 192]	114.7	228.7	114.5	233.5	4 : 1
methyl (**36m**)†[128, 193]	111.9	230.2	113.5	233.9	1 : 1.3
CH$_2$-2-pyridyl (**36n**)[193]	–	–	113.2	235.2	0 : 1
CH$_2$CN (**36o**)[193]	–	–	112.8	231.4	0 : 1

*Not determined. †The two products were separated in this case, but the constitution of **B** was not identified; the given ratio refers to the ratio of isolated compounds.

The similarity of the data recorded for one of the products (denoted as **B**) strongly suggests that the corresponding resonances are assigned to the 3,5-diferrocenyl-2H-1,4,2-diazaphosphole complex **69l** in each case. Obviously, the ratio of this product increases with decreasing nucleophilicity of the employed nitrile derivative. In the reaction of **67** with strong nucleophilic cyanamide **36a** only the formation of **69a** was observed.

3.3 SET Reactions of 2H-Azaphosphirene Complexes in the Absence of Nitriles

In order to investigate the dependance of reaction progressions with [FeCp$_2$][PF$_6$] in the absence of nitriles on i) the C-substituent and ii) on the transition metal fragment of the 2H-azaphosphirene complex, a set of small-scale reactions was performed using 3-phenyl-2H-azaphosphirene tungsten, molybdenum, and chromium complexes **35**, **70**,[123] **71**,[123] and 3-ferrocenyl substituted derivatives **67**, **72**,[194] and **73**[194] (Tab. 3.4, A). All reactions were carried out in NMR tubes, and to ensure reasonable reaction times stoichiometric amounts of [FeCp$_2$][PF$_6$] were employed; progressions were monitored by ^{31}P{^{1}H} NMR spectroscopy.[26]

In each reaction symmetrically 3,5-disubstituted 2H-1,4,2-diazaphosphole complexes and/or their free ligands were observed (Tab. 3.4, B). In the following their identification is described and their formation rates are compared. In Figure 3.10 the ratios of these products (right hand side) and reactants (left hand side) are plotted against time; corresponding data are given in Table 3.5. With proceeding reaction time several resonances with large phosphorus–fluorine coupling constants were observed. In Table 3.4 (C) they are ordered columnwise according to similarity; they might belong to analogous, in some cases even to identical compounds.

During the reaction of **35** a resonance was detected at $\delta = 110.6$ ($|^1J_{WP}| = 227.8$ Hz), which increased at the expense of the signal of **35** and could be assigned to 3,5-diphenyl-2H-1,4,2-diazaphosphole complex **41c**.[146] Consequently, it is strongly suggested to assign the resonance with analogous data that was observed in reactions of **35** with **36h–j** (Section 3.2) to the same product. In reactions of **70** and **71** signals appeared at $\delta = 130.0$ (M = Mo) and 153.1 (M = Cr) corresponding to complexes **74c** and **75c**. This assignment based on a comparison with molybdenum complexes **74a** ($\delta = 120.0$),[163] **74b** ($\delta = 122.7$; Section 4.1.4) and chromium complexes **75a** ($\delta = 143.9$),[163] **75b** ($\delta = 146.3$; Section 4.1.4). The trends observed for tungsten complexes reveal that the resonance of 3,5-diphenyl-2H-1,4,2-diazaphosphole complex **41c** is shifted by 10.5 or 8.5 ppm to lower field with respect to corresponding 5-dialkylamino substituted derivatives **41a,b** (cf. Tab. 3.1). Therefore, the assignment appears reasonable.

---

[26]The investigations were carried out together with S. Fankel, who first has synthesized chromium complex **73**.[194]

Table 3.4: *A)* Reaction of 2H-azaphosphirene complexes **35**, **67**, and **70–73** with ferrocinium hexafluorophosphate in the absence of nitriles. *B)* ^{31}P$\{^1$H$\}$ NMR data for symmetrically 3,5-disubstituted 2H-1,4,2-diazaphosphole complexes **41c**, **74c**, **75c**, **69l**, **76l**, **77l** and their free ligands **50c**, **78l**. *C)* ^{31}P$\{^1$H$\}$ NMR data for products with one or two P,F bonds.

B)		M = W		M = Mo	M = Cr	
		$\delta(^{31}$P$)$ ($|^1 J_{WP}|$/Hz)		$\delta(^{31}$P$)$	$\delta(^{31}$P$)$	$\delta(^{31}$P$)$
Ar = Ph	**41c**:	110.6 (227.8)	**74c**:	130.0	**75c**: 153.1	**50c**: *
Ar = Fc	**69l**:	113.4 (234.0)	**76l**:	*	**77l**: 158.1	**78l**: 97.5

C) Ar	M		**85–87** triplet	**A–C** doublet	**79a–84a** doublet	**79b–81b** doublet	**88–90** doublet	**D** doublet	**E** doublet
	W	$\delta(^{31}$P$)$	233.4	198.5	197.3	193.3	*	18.5	17.8
		$|^1 J_{PF}|$/Hz	1068.1	836.7	822.7	857.0		1044.0	1065.6
Ph	Mo	$\delta(^{31}$P$)$	266.5	224.3	225.2	221.7	*	18.8	17.8
		$|^1 J_{PF}|$/Hz	1082.1	840.5	827.8	860.9		1044.0	1065.6
	Cr	$\delta(^{31}$P$)$	291.4	246.4	250.3	247.5	*	18.4	17.6
		$|^1 J_{PF}|$/Hz	1089.7	857.0	846.9	879.9		1044.0	1065.6
	W	$\delta(^{31}$P$)$	233.3	*	194.6	*	155.9	*	*
		$|^1 J_{PF}|$/Hz	1068.1		825.3		803.6		
Fc	Mo	$\delta(^{31}$P$)$	266.5	*	222.0	*	187.9	*	*
		$|^1 J_{PF}|$/Hz	1082.1		820.2		804.9		
	Cr	$\delta(^{31}$P$)$	291.6	*	246.2	*	216.2	*	*
		$|^1 J_{PF}|$/Hz	1091.0		846.9		826.5		

*Not observed

Quantitatively, the progressions showed a strong dependance on the pentacarbonyl metal fragment (Tab. 3.5). While the amount of tungsten complex **41c** increased to about 43 % within 5 days, rather little amounts of complexes **74c** and **75c** were observed.

Table 3.5: Ratio [%] of 2*H*-azaphosphirene complexes (reactants) and symmetrically 3,5-disubstituted 2*H*-1,4,2-diazaphosphole complexes (products) (by ^{31}P{^{1}H} NMR signal integration) for reactions shown in Table 3.4 (*A*) after 12–49 min (entry 1), 129–165 min (entry 2), 7–8 h (entry 3), 30–31 h (entry 4), and 5 d (entry 5).

| | | | Entry | | | | | | Entry | | | | |
Ar	M	Reactant	1	2	3	4	5	Product	1	2	3	4	5
Ph	W	**35**	92	80	72	40	0	**41c**	8	17	21	33	43
Ph	Mo	**70**	100	99	93	84	27	**74c**	0	0	2	2	0
Ph	Cr	**71**	99	97	93	79	23	**75c**	1	1	3	3	12
Fc	W	**67**	94	87	80	45	0	**69l**	6	10	14	28	50
Fc	Mo	**72**	100	97	84	74	29	**76l**	0	0	0	0	0
Fc	Cr	**73**	96	94	87	65	17	**77l**	3	3	2	5	4

Reactions of the 3-ferrocenyl substituted 2*H*-azaphosphirene complexes gave a similar picture (Fig. 3.10, C and D; Tab. 3.5). The rate of conversion of tungsten complex **67**, within the error margins, was equal to that of 3-phenyl derivative **35**; within 5 days about 50 % of **69l** was formed. For M = Cr a signal at $\delta = 158.1$ was detected, which is unambiguously assigned to complex **77l**.[27] In the reaction of molybdenum complex **72** no resonance was detected that might be ascribed to complex **76l**. In this case the emergence of a signal at $\delta = 97.5$ was observed, which was also found in the reaction of chromium complex **73**, thus, an assignment to the liberated ligand system **78l** is plausible.[28] Because **78l** is most likely formed via precedent formation of **76l** (M = Mo) or **77l** (M = Cr), respectively, it was reasonable to add the measured shares of **78l** to those of the corresponding complexes **76l** and **77l** (denoted as product* ratio in Fig. 3.10, E). In both cases the product* ratio passed a maximum and decreased with proceeding reaction time. This is presumably due to the low stability of the free ligand system **78l**.

---

[27]This derivative was synthesized by S. Fankel by the reaction of **73** with ferrocenecarbonitrile (**36l**) in the presence of [FeCp$_2$][PF$_6$].[194]

[28]For comparison, ligand **50c**, observed in the thermal reaction of **35** in benzonitrile,[155] resonated at $\delta = 103.2$ (see Section 1.3), thus, about 7 ppm upfield from its tungsten complex **41c**.[146, 155] Therefore, the assignment to **78l** is reinforced by a comparison with the data for **69l**.
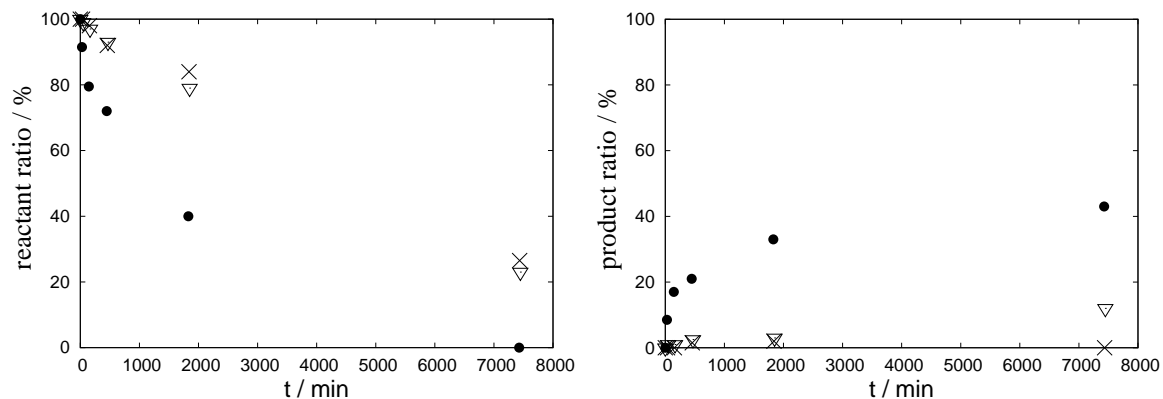
A) Reactant ratio against time (Ar = Ph).
●: M = W (**35**); ×: M = Mo (**70**);
▽ M = Cr (**71**).

B) Product ratio against time (Ar = Ph).
●: M = W (**41c**); ×: M = Mo (**74c**);
▽: M = Cr (**75c**).
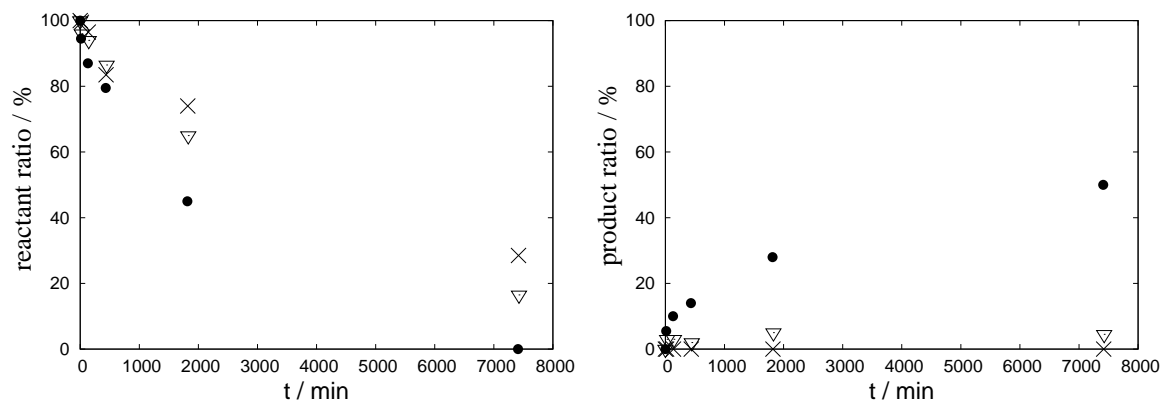
C) Reactant ratio against time (Ar = Fc).
●: M = W (**67**); ×: M = Mo (**72**);
▽: M = Cr (**73**).

D) Product ratio against time (Ar = Fc).
●: M = W (**69l**); ×: M = Mo (**76l**);
▽: M = Cr (**77l**).
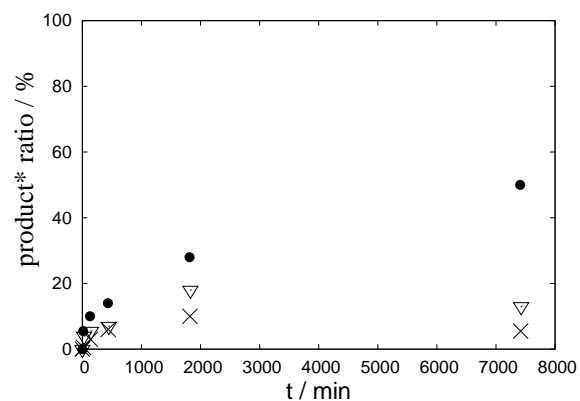
Figure 3.10: Ratio of reactants (left hand side) and products (right hand side) (by ^{31}P{^{1}H} NMR signal integration) against time for reactions shown in Table 3.4 (*A*). *In diagram E the ratio of ligand **78l** was added to the ratio of the respective complex (**76l** or **77l**).

E) Product* ratio against time (Ar = Fc).
●: M = W (**69l**); ×: M = Mo (**76l** + **78l**)*;
▽: M = Cr (**77l** + **78l**)*.

In each reaction one ^{31}P{^{1}H} NMR resonance was detected that appeared as a
triplet (**85–87**), thus revealing two *P*-bonded fluorine atoms. Since their recorded
NMR data agree for the reactions of both employed *C*-phenyl and -ferrocenyl substi-
tuted tungsten, molybdenum, and chromium complexes, in other words, they depend
only on the metal fragment, but not on the *C*-substituent of the 2*H*-azaphosphirene
complex employed, it can be concluded that neither the phenyl nor the ferrocenyl
moiety had remained in these compounds. By comparison with the ^{31}P (and ^{19}F)
NMR data for [(*tert*-butyldifluoro)phosphane]pentacarbonylmetal(0) complexes,[195]
which is for M = W: $\delta(^{31}\text{P}) = 235.1$ ($|^1J_{PF}| = 1089$ Hz) and $\delta(^{19}\text{F}) = -66$, for
M = Mo: $\delta(^{31}\text{P}) = 262.2$ ($|^1J_{PF}| = 1090$ Hz), and for M = Cr: $\delta(^{31}\text{P}) = 285.5$
($|^1J_{PF}| = 1095$ Hz), an assignment to {[bis(trimethylsilyl)methyl]difluorophosphane}-
pentacarbonylmetal(0) complexes **85–87** is strongly suggested.

Furthermore, fluorophosphane complexes **79a,b** were formed, which are described
in Section 4.3.2.[29] Their molybdenum and chromium analogs **80a,b**, **81a,b** could be
identified as the ^{31}P NMR chemical shifts systematically increase by $25-30$ ppm within
the series M = W < Mo < Cr,[30] reflecting the trend found for pentacarbonylphosphane
tungsten, molybdenum, and chromium complexes in general.[123, 148, 163, 175] Similarly,
resonances observed in the reactions of **67**, **72**, and **73** were assigned to complexes
82a–84a.[31] The ^{31}P{^{1}H} NMR data for the products denoted as **A**–**C** are very close to
those for complexes **79a–81a**, thus, they presumably have a comparable constitution.
In the reactions of **67**, **72**, and **73** after 5 days the resonances of fluorophosphane
complexes **88**,[196] **89**,[197] and **90**[197] were detected, which were synthesized by A.
Özbolat-Schön via another route. For the products denoted as **D** and **E** almost iden-
tical ^{31}P{^{1}H} NMR data were obtained in the reactions of each complex **35**, **70**, and
71, which strongly suggests that these products carry no metal fragment, and hence,
constitute the same product in each reaction.

The major results derived from these investigations are: 1) a metal-dependent in-
crease of reaction rates within the series M = Mo < Cr << W, 2) no significant dif-
ferences in rates between the series Ar = Ph and Ar = Fc, 3) partial decomplexation
of products in the cases of molybdenum and chromium complexes, and 4) formation
of by-products with P,F bonds in each case. The last-mentioned observation points
to the generation of highly electrophilic species that are able to abstract fluoride from
PF_6^-.

---

[29]Complexes **79a,b** were observed in the reaction of **35** with HBF$_4\cdot$Et$_2$O, and complex **79a** was
isolated from the reaction of **35** with BF$_3\cdot$Et$_2$O.

[30]^{183}W,^{31}P couplings of most by-products were not resolved in the reactions of **35** and **67** due to
their comparatively low abundances.

[31]Between the series Ar = Ph and Fc minor but still significant and systematic differences of the
phosphorus chemical shifts are apparent.

3.4   SET-Induced Ring Expansion of 2*H*-Azaphosphirene Complexes with Benzonitrile

In order to synthesize 3,5-diphenyl-2*H*-1,4,2-diazaphosphole molybdenum and chromium complexes **74c** and **75c**, complexes **70** and **71** were reacted with benzonitrile (**36c**) in the presence of 0.05 equivalents of [FeCp$_2$][PF$_6$] (Scheme 3.7). Both reactions were significantly slower than the reactions of tungsten complex **35** with aromatic carbonitriles **36d**–**g** (cf. Section 3.1) and remained incomplete after 24 hours (Fig. 3.11 and Tab. 3.6). In addition, decomplexation of the products **74c** and **75c** was observed during both reactions, which revealed that they were not stable under the applied *oxidative* reaction conditions.[32]
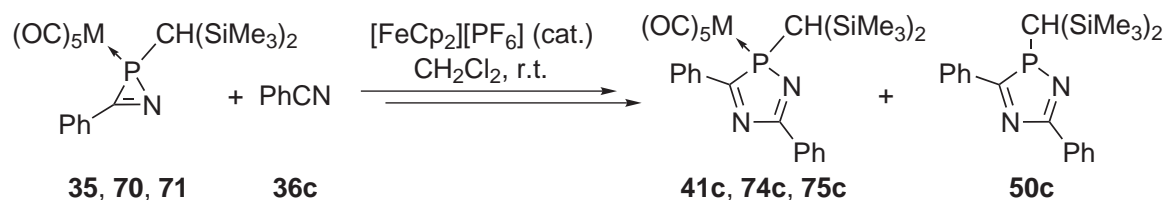
Scheme 3.7: Reactions of 2*H*-azaphosphirene complexes **35**, **70**, and **71** with benzonitrile (**36c**) in the presence of substoichiometric amounts of ferrocinium hexafluorophosphate (**35**, **41c**: M = W; **70**, **74c**: M = Mo; **71**, **75c**: M = Cr).
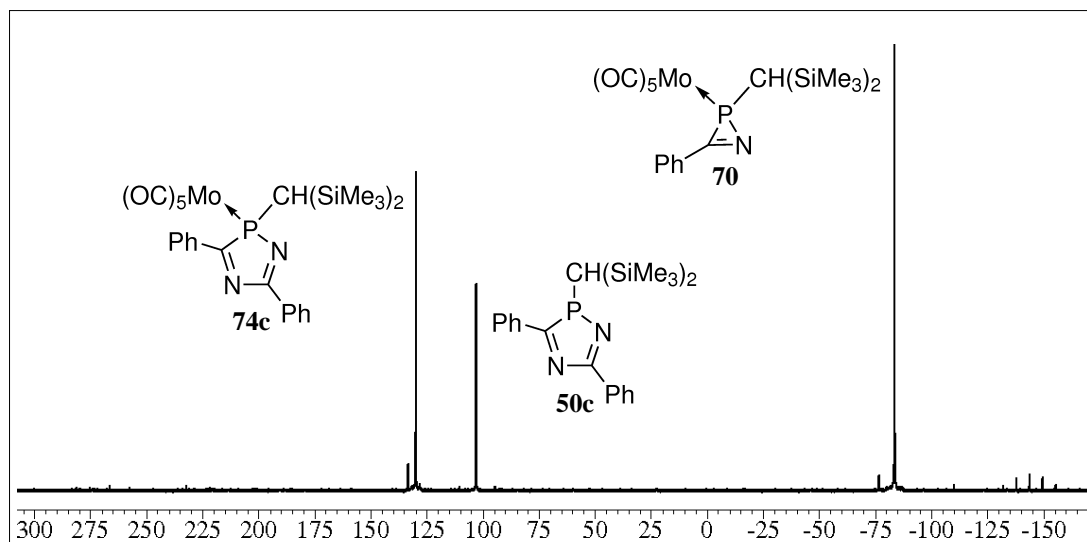
Figure 3.11: ^{31}P{^{1}H} NMR spectrum recorded during the reaction of molybdenum complex **70** with benzonitrile (**36c**) after 24 h (Scheme 3.7; 0.05 equiv. [FeCp$_2$][PF$_6$]).

---

[32]Employment of 0.18 equivalents of [FeCp$_2$][PF$_6$] for the reaction of **70** with **36c** yielded an acceleration, but the reaction still remained incomplete and decomplexation occurred.

Table 3.6: Ratio [%] of reactants **35** (M = W), **70** (M = Mo), and **71** (M = Cr), complexes **41c** (M = W), **74c** (M = Mo), and **75c** (M = Cr) (products), and ligand **50c** (by ^{31}P{^{1}H} NMR signal integration) for reactions shown in Scheme 3.7 after 24 h (0.05 equiv. [FeCp$_2$][PF$_6$]).

	Reactant	Product	Ligand
M = W	0	100	0
M = Mo	48	24	17
M = Cr	51	34	11

In order to find out if the reduced rate of these reactions was due to a lower reactivity of complexes **70**, **71** in comparison with tungsten complex **35** or possibly due to a lower nucleophilicity of benzonitrile (**36c**) compared to hetaryl carbonitriles **36d–g**, complexes **35** and **71** were reacted with **36c** under identical conditions (0.21 equiv. [FeCp$_2$][PF$_6$]), and the reactions were monitored by ^{31}P{^{1}H} NMR spectroscopy; the results are displayed in Figure 3.12.
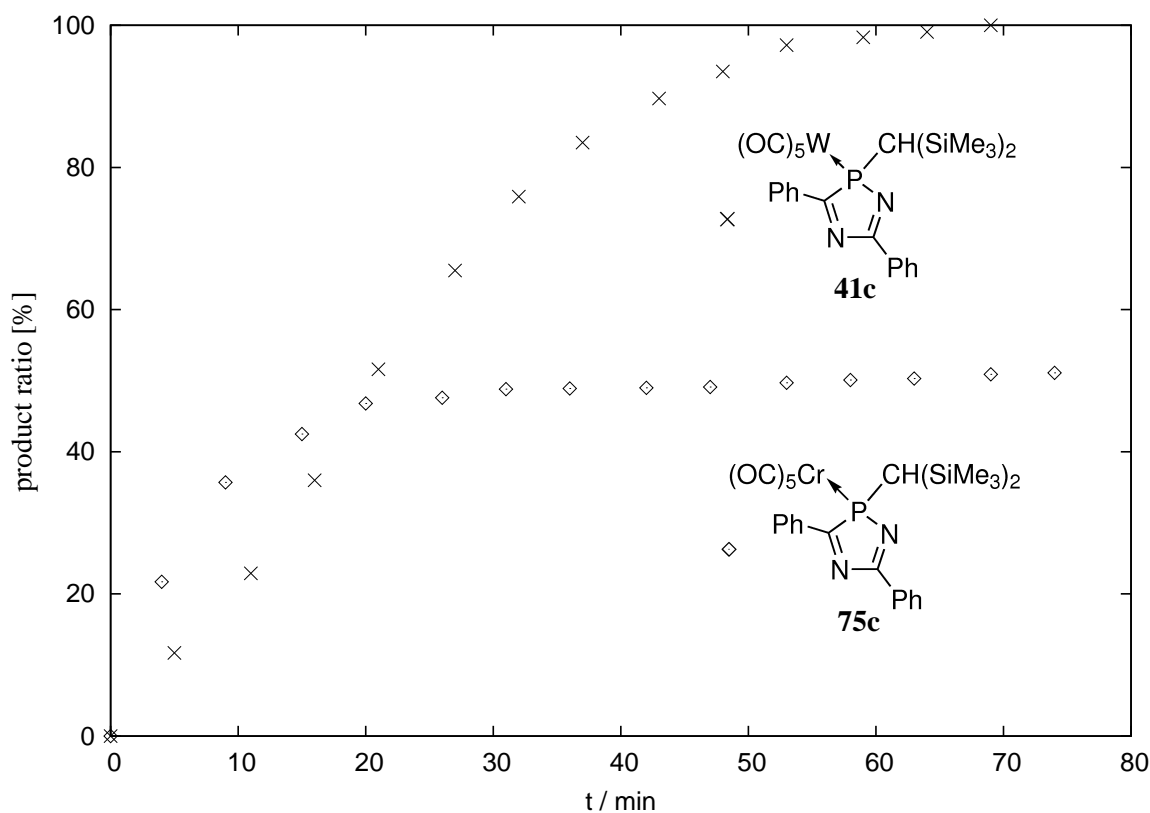
Figure 3.12: Ratio of **41c** (×) and **75c** (◇) (by ^{31}P{^{1}H} NMR signal integration) against time for reactions of **35** and **71** with **36c** (Scheme 3.7; 0.21 equiv. [FeCp$_2$][PF$_6$]).

Interestingly, both reactions showed a completely different course. For the reaction of **35** with **36c** the data points describe an S-shaped curve (as in the case of the reaction with nitrile **36g**; cf. Figures 3.1 and 3.2). In contrast, chromium complex **71** showed the highest reaction rate at the start. Initially it reacted even faster than complex **35**, but then the conversion leveled off at about 50 %. Obviously, the initiation occurs faster when M = Cr, which is presumably due to the lower oxidation potential of chromium complex **71** compared to complex **35** (see Section 3.5), but the chain propagation steps (ii and iii, Scheme 3.2, Section 3.1) might be too slow to complete the chain reaction. When the concentrations of reactants **71**, **36c** and initiator [FeCp$_2$][PF$_6$] are too much depleted or the total amount of [FeCp$_2$][PF$_6$] is consumed chain termination steps prevail.

3.5 Cyclic Voltammetric Investigations

Cyclic voltammetric (CV) measurements were carried out on $2H$-azaphosphirene tungsten, molybdenum, and chromium complexes **35**, **70**, **71** as well as on $2H$-1,4,2-diazaphosphole complexes **41b,g,m**, **69l**, and **126g**[33] (Fig. 3.13).
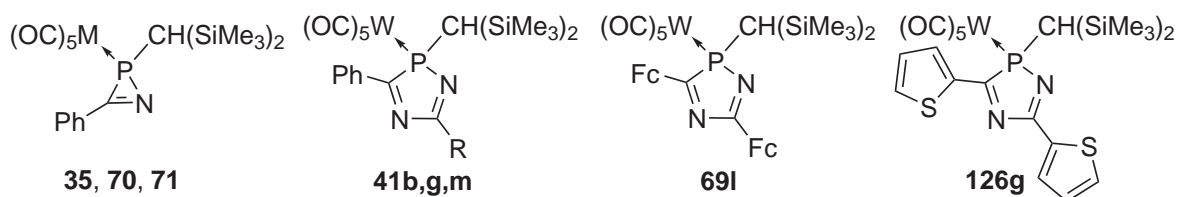
Figure 3.13: $2H$-Azaphosphirene complexes **35** (M = W), **70** (M = Mo), **71** (M = Cr) and $2H$-1,4,2-diazaphosphole complexes **41b,g,m** (R = NMe$_2$ (**b**), 2-thienyl (**g**), Me (**m**)), **69l**, **126g** investigated by cyclic voltammetry.

The voltammograms of $2H$-azaphosphirene complexes **35**, **70**, **71** show each an *irreversible* oxidation wave[34] between +1.0 and +1.4 V vs. AgCl/Ag (Fig. 3.14). This indicates fast follow-up reaction of the generated species presumably with the anion of the supporting electrolyte (PF$_6^-$), hence, the thermodynamic half cell potentials ($E_{1/2}$) cannot be obtained from these experiments. The anodic peak potentials (E_{pa}) of **35**, **70**, and **71** are in the same range (Tab. 3.7), whereas a slight increase within the series Cr < Mo < W is observed, but it should be noted that the value for **35** is only a rough estimate as the oxidation wave is overlapped by a second oxidation step (see Fig. 3.14, A).

In principle, this result reflects the trend of the ionization potentials of the group 6 transition metal atoms (652.8 (Cr), 685.0 (Mo), 770 kJ$\cdot$mol^{-1} (W)).[198] However, significantly smaller differences in ionization potentials were found for the hexacarbonyl complexes of these metals,[199–201] and a common $E_{1/2}$ value was reported for [Cr(CO)$_6$], [Mo(CO)$_6$], and [W(CO)$_6$] ($E_{1/2}$ = +1.53 V vs. SCE[35]).[202] The tricarbonyl-1,3,5-triphosphabenzene complexes [M(CO)$_3$(η^6-C$_3{}^t$Bu$_3$P$_3$)] of chromium and tungsten showed ionization potentials about 7.1 eV each, while the value reported for the corresponding molybdenum complex was 7.33 eV.[203] Nevertheless, DFT calculations presented in the following section stongly suggest that oxidation of $2H$-azaphosphirene complexes occurs at the transition metal center.

---

[33]The syntheses of complexes **41m** and **126g** are presented in Sections 4.1 and 4.1.2.

[34]Even at very high scan rates (up to 10 V$\cdot$s^{-1}) no reversible oxidation wave was observed.

[35]Aqueous standard calomel electrode.
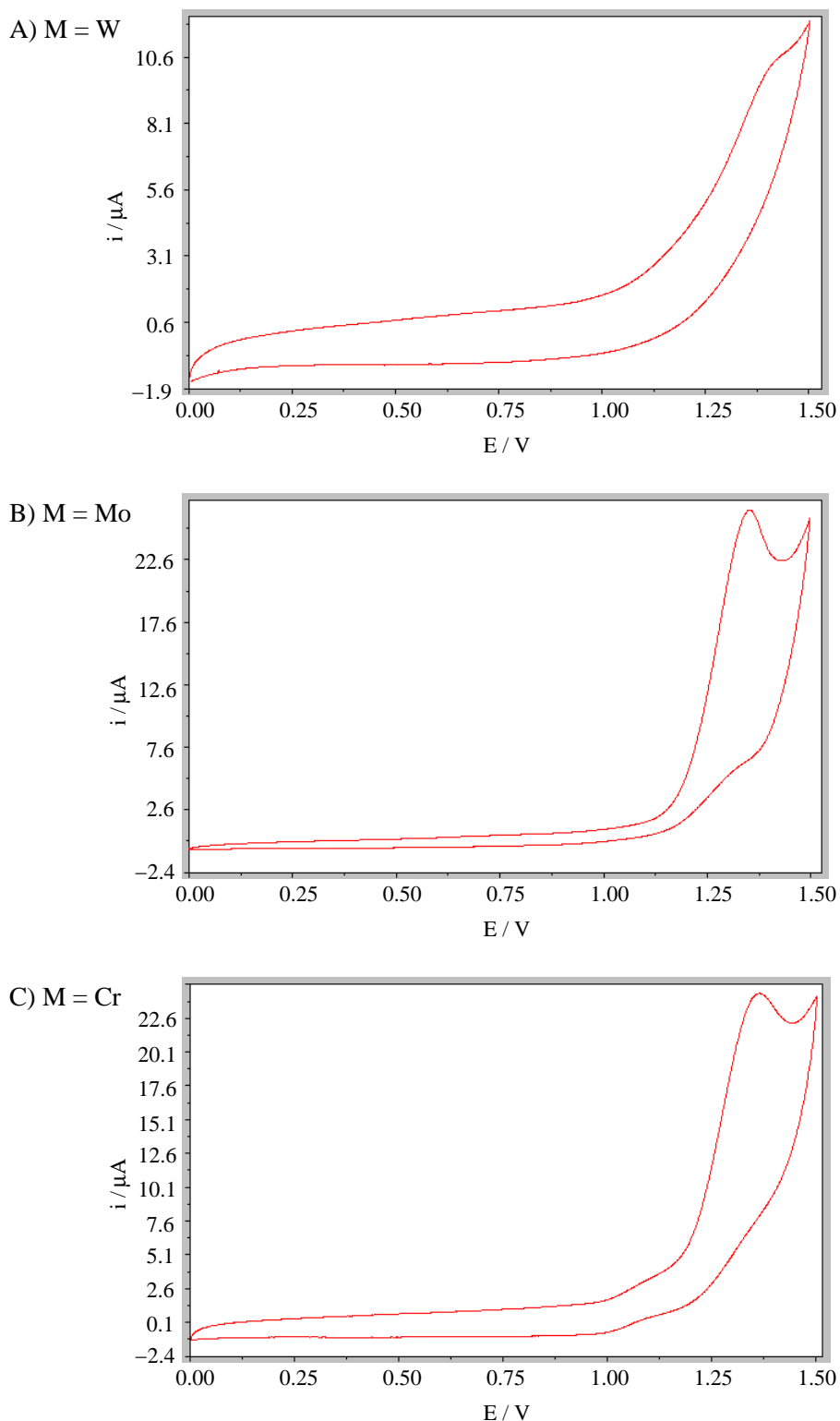
Figure 3.14: Cyclic voltammograms of 2H-azaphosphirene complexes **35** (A), **70** (B), and **71** (C) in CH$_2$Cl$_2$ ($3 \cdot 10^{-3}$ M) at a glassy carbon electrode (GCE) with 0.1 M [^{n}Bu$_4$N][PF$_6$] as supporting electrolyte between 0.00 and 1.50 V vs. AgCl/Ag/2 M LiCl in EtOH (Pt-wire as counter electrode; scan rate 0.1 V$\cdot$s^{-1}; T = 25 °C).

Table 3.7: Anodic peak potentials (E_{pa}) of $2H$-azaphosphirene complexes **35**, **70**, **71** (Fig. 3.13) and $2H$-1,4,2-diazaphosphole complexes **41b,g,m**, **126g**, and half cell potentials ($E_{1/2}$) of ferrocenyl derivatives **67**[128] and **69l**.

No.	$E_{pa}^{\dagger}$/V	$E_{pa}^{\ddagger}$/mV	No.	$E_{pa}^{\dagger}$/V	$E_{pa}^{\ddagger}$/mV	No.	$E_{1/2}^{\dagger}$/V	$E_{1/2}^{\ddagger}$/mV
35	+1.42	+910	**41b**	+1.19	+680	**67**[128]	*	+406
70	+1.36	+850	**41g**	+1.35	+840	**69l**	+0.717	+206
71	+1.33	+820	**41m**	+1.37	+860		+0.799	+288
			126g	+1.34	+830			

[†]Vs. AgCl/Ag. [‡]Calcd. vs. $E_{1/2}([FeCp_2]^+/[FeCp_2])$. [*]Value not reported.

If the anodic peak potentials of complexes **35**, **70**, and **71** are regarded as estimates[165] for their real half-wave potentials (which are accurately evaluable only from reversible redox processes[204]), oxidation of **35**, **70**, **71** by the ferrocinium cation[36] (reaction step i, Scheme 3.2, Section 3.1) is predicted to be endergonic with $\Delta_R G = +88$ (**35**), $+82$ (**70**), and $+79$ kJ·mol^{-1} (**71**) by applying Eq. (3.7) (z: number of transferred electrons per formula unit $= 1$; F: Faraday constant $= 96484.56$ C·mol^{-1}).[198]

$$\Delta_R G = -z \cdot F \cdot \Delta E. \tag{3.7}$$

A completely different redox behavior was observed by M. Beckmann (née Schlenker) for 3-ferrocenyl-$2H$-azaphosphirene complex **67**, which showed a *reversible* oxidation wave at $E_{1/2} = +406$ mV (vs. $E_{1/2}([FeCp_2]^+/[FeCp_2])$).[128] The reversibility of this process together with its comparatively low $E_{1/2}$ value strongly suggest that oxidation of complex **67** occurs at the ferrocenyl moiety rather than the pentacarbonyl metal fragment.

As in the cases of $2H$-azaphosphirene complexes **35**, **70**, **71** the oxidations of $2H$-1,4,2-diazaphosphole complexes **41b,g,m**, and **126g** were irreversible (Fig. 3.15),[37] pointing to fast following chemical reactions of the generated radical cationic $2H$-1,4,2-diazaphosphole complexes (presumably reaction with PF$_6^-$ and/or decomplexation). The anodic peak potentials of derivatives **41g,m**, **126g** (Tab. 3.7) are in the same range as those of **35**, **70**, **71**, and for the same reasons it is assumed that the oxidation occurs at the transition metal center.

---

[36]The half-wave potential ($E_{1/2}$) of the system $[FeCp_2]^+/[FeCp_2]$ was determined as $+511$ mV vs. AgCl/Ag with the same experimental setup.

[37]The oxidation waves are partially overlapped by a second oxidation step.
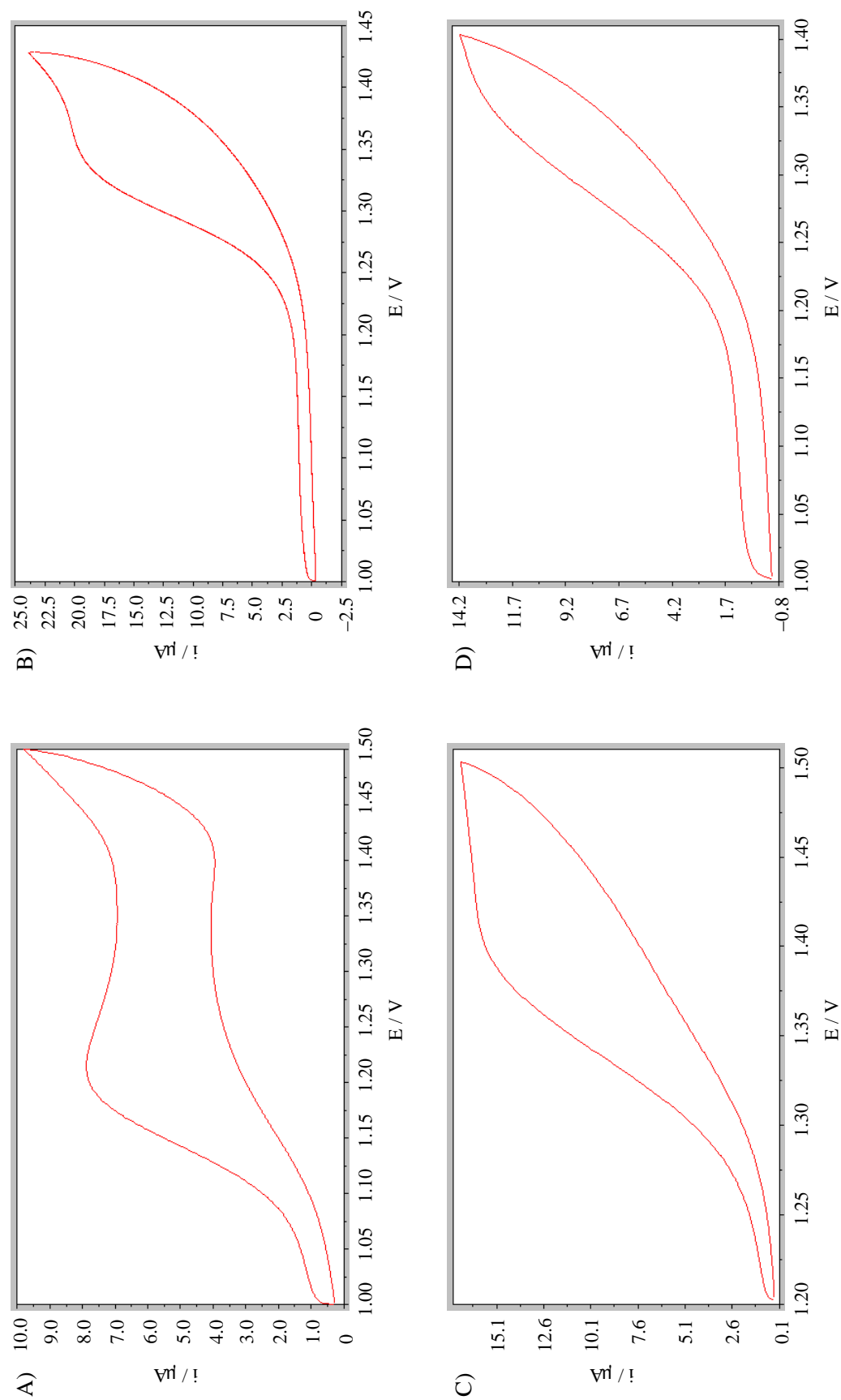
Figure 3.15: Cyclic voltammograms of 2*H*-1,4,2-diazaphosphole complexes **41b** (A), **41g** (B), **41m** (C), and **126g** (D) in CH$_2$Cl$_2$ (3 · 10^{-3} M) at a glassy carbon electrode (GCE) with 0.1 M [^{n}Bu$_4$N][PF$_6$] as supporting electrolyte between 1.00 and 1.50 V vs. AgCl/Ag/2 M LiCl in EtOH (Pt-wire as counter electrode; scan rate 0.1 V · s^{-1}; T = 25 °C).

The highest peak potential was observed for complex **41m**, which features only one aryl substituent that can interact electronically with the $2H$-1,4,2-diazaphosphole ring. Complex **41b** was oxidized at considerably lower potential. Here, the process approaches the situation of a *quasi-reversible* oxidation (Fig. 3.15, A), which may be attributed to the electron-releasing nature of the dimethylamino substituent. The comparatively electron-rich $2H$-1,4,2-diazaphosphole ligand of **41b** should cause a higher electron density at the tungsten center, thus yielding a lowering of the oxidation potential compared to **41g,m**, and **126g**.

The electrochemical data reveal that redox step iii (Scheme 3.2, Section 3.1), in principle, could constitute a balanced chemical equilibrium that, however, is shifted towards the products through fast follow-up reactions of radical cations $35^{\bullet+}$, $70^{\bullet+}$, $71^{\bullet+}$ with a nitrile.

Complexes **41b,g,m**, **126g** additionally show each a *reversible* reduction wave (Fig. 3.16 and Tab. 3.8). The absolute ratio of anodic and cathodic peak currents ($|i_{pc}/i_{pa}|$) is close to 1 in each case, which is a prerequisite for reversibility. Within this series 3,5-di(2-thienyl)-$2H$-1,4,2-diazaphosphole complex **126g** had the lowest magnitude of the reduction potential, while the largest negative value was found for electron-rich derivative **41b**.

Table 3.8: Electrochemical data for complexes **41b,g,m** and **126g** corresponding to reduction waves shown in Figure 3.16.

No.	E_{pa}/V	E_{pc}/V	ΔE_p/mV	i_{pa}/μA	i_{pc}/μA	$|i_{pc}/i_{pa}|$	$E_{1/2}$/V	$E_{1/2}^{\ddagger}$/V
41b	−1.426	−1.553	127	12.70	−13.13	1.03	−1.490	−2.001
41g	−1.131	−1.191	60	7.72	−8.81	1.14	−1.161	−1.672
41m	−1.266	−1.295	29	4.88	−7.43	1.52	−1.281	−1.792
126g	−1.109	−1.138	29	13.80	−13.89	1.01	−1.124	−1.635

Potentials vs. AgCl/Ag, or ‡calcd. vs. $E_{1/2}([FeCp_2]^+/[FeCp_2])$.

3,5-Diferrocenyl-$2H$-1,4,2-diazaphosphole complex **69l** showed two closely spaced reversible one-electron oxidations (Fig. 3.17, and Tab. 3.7) at $E_{1/2} = +206$, and $+288$ mV (vs. $E_{1/2}([FeCp_2]^+/[FeCp_2])$), which are not attributable to oxidations of the pentacarbonyl metal fragment but to oxidations of the two ferrocenyl units. The small difference between the half-wave potentials ($\Delta E_{1/2} = 82$ mV) must be ascribed to the asymmetric bonding of the bridge linking both ferrocenyl groups.
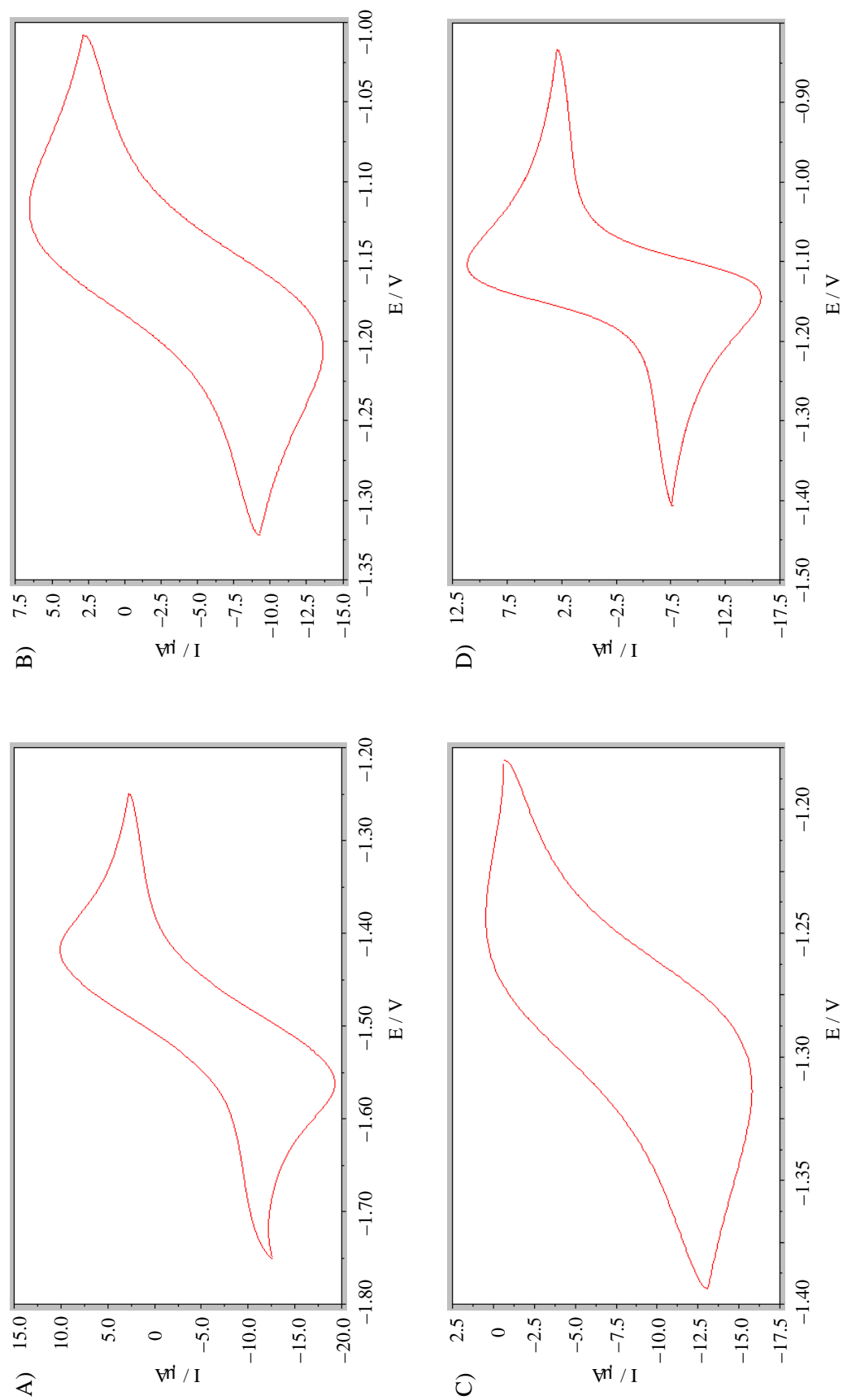
Figure 3.16: Cyclic voltammograms of 2*H*-1,4,2-diazaphosphole complexes **41b** (A) (between -1.75 and -1.25 V), **41g** (B) (between -1.35 and -1.00 V), **41m** (C) (between -1.40 and -1.18 V), and **126g** (D) (between -1.40 and -0.82 V) in CH_2Cl_2 ($3 \cdot 10^{-3}$ M) at a glassy carbon electrode (GCE) with 0.1 M [$^nBu_4N$][PF_6] as supporting electrolyte, vs. AgCl/Ag/2 M LiCl in EtOH (Pt-wire as counter electrode; scan rate 0.1 V$\cdot$s^{-1}; T = 25 °C).

It should be mentioned that ferrocenecarbonitrile shows a reversible oxidation wave $E_{1/2} = +317$ mV (vs. $E_{1/2}([FeCp_2]^+/[FeCp_2])$) under the same experimental conditions.[38] Consequently, a classification of the electronic nature of the different moieties at the ferrocenyl group in complexes **67**, **69l**, and FcCN can be provided on the basis of the obtained redox potentials: the $2H$-azaphosphiren-3-yl tungsten complex moiety can be classified as more electron-withdrawing, while the $2H$-1,4,2-diazaphosphol-3/5-yl tungsten complex moiety has a less electron-withdrawing effect than the cyano group.
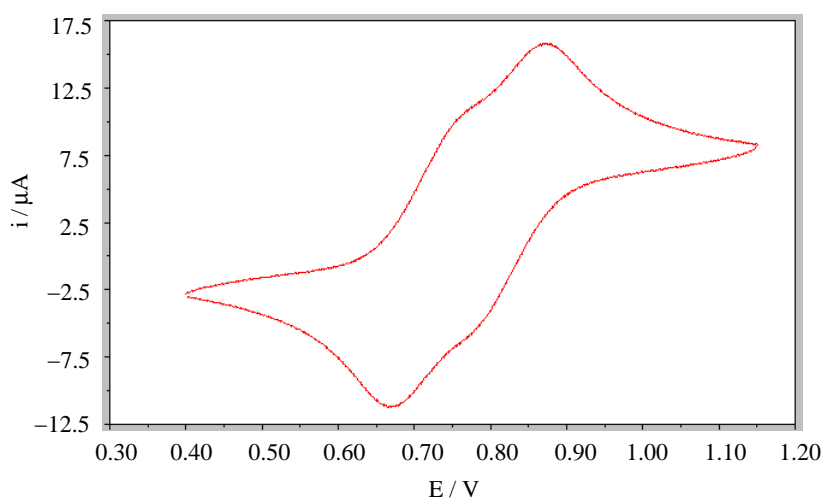
Figure 3.17: Cyclic voltammogram of $2H$-1,4,2-diazaphosphole complex **69l** in CH_2Cl_2 $(3 \cdot 10^{-3}$ M) at a glassy carbon electrode (GCE) with 0.1 M [$^nBu_4N$][PF_6] as supporting electrolyte, between 0.40 and 1.15 V vs. AgCl/Ag/2 M LiCl in EtOH (Pt-wire as counter electrode; scan rate 0.1 V$\cdot$s^{-1}; T = 25 °C).

Complex **69l** was additionally subjected to spectroelectrochemistry[39] by A. Espinosa Ferao (Murcia, Spain). The spectra of mono-oxidized species **69l**$^{•+}$ showed three absorption bands, one in the UV region at $\lambda_{max} = 285$ nm with high intensity (lgϵ = 4.39), and two at $\lambda_{max} = 341$ and 622 nm having lower intensity. The latter increased during the titration at the expense of the bands at $\lambda_{max} = 404$ and 539 nm of neutral **69l** (cf. Section 3.2.1). Two titration isosbestic points were found at $\lambda = 591$ and 490 nm. The absorption in the UV region increased during the titration experiment and showed comparable intensities to the UV bands exhibited by the corresponding neutral

---

[38]Ferrocenecarbonitrile is assumed to be formed intermediately from complex **67** in its reaction with [FeCp_2][PF_6] in the absence of further nitriles to yield complex **69l** (see Section 3.6).

[39]The generation of the oxidized species derived from **69l** was performed by constant potential electrolysis 0.15 V above $E_{1/2}$ of the second ferrocenyl wave and monitored by UV/Vis/NIR absorption spectroscopy. Stepwise coulommetric titration was performed on a ca. 10^{-3} mol$\cdot$L^{-1} solution of complex **69l** in CH_2Cl_2 with 0.15 M [$^nBu_4N$][PF_6] as supporting electrolyte, and the absorption spectra were regularly recorded for different average numbers of removed electrons (n).

complex **69l** (cf. Section 3.2.1).[40] The absorptions appearing in the visible region are comparable to bands in the same range shown by other oxidized ferrocenyl derivatives and are assigned to $Cp \rightarrow$ Fe(III) ligand–metal charge transfer (LMCT) transitions.[205] No additional bands were observed, neither in the low-energy (LE) visible region nor in the near-IR, thus excluding the occurrence of intervalence transitions and allowing the classification of **69l**$^{\bullet+}$ to as a Robin-Day Class I (negligible electronic coupling) mixed-valence compound. This result is in agreement with the rather small difference between the redox waves ($\Delta E_{1/2}$), mainly attributable to the unequal environment of the two ferrocenyl units.

On removing more electrons ($1 \leq n \leq 2$) to generate the dicationic species **69l**$^{2+}$ the intensities of the bands continued increasing, and a new band centered at λ_{max} = 734 nm appeared. The latter can be attributed to a bridge to Fe(III) transition; a titration isosbestic point was observed at $\lambda = 588$ nm.

---

[40]Transitions below 240 nm were not covered by these experiments.

3.6 Computational Studies

To get more insight into the mechanism of the SET-induced ring expansion of 2*H*-azaphosphirene complexes with nitriles, DFT calculations were carried out on model systems **91**–**94** (Scheme 3.8). Different conceivable pathways were calculated on reactions of **91** (R' = R" = CH$_3$) with the ferrocinium cation and acetonitrile (**36m**; R = CH$_3$). The influence of the nucleophilicity of the nitrile was taken into account by using cyanamide (**36p**; R = NH$_2$) as a strong nucleophilic and dicyane (**36q**; R = CN) as a weak nucleophilic nitrile derivative; **36m** may be regarded as a derivative of moderate nucleophilicity.

91, **91**$^{•+}$: R' = R" = CH$_3$ **36c**: R = Ph; **36l**: R = Fc;

92, **92**$^{•+}$: R' = CH(SiH$_3$)$_3$, R" = CH$_3$ **36m**: R = CH$_3$; **36p**: R = NH$_2$; **36q**: R = CN

93, **93**$^{•+}$: R' = CH$_3$, R" = Ph

94, **94**$^{•+}$: R' = CH$_3$, R" = Fc

Scheme 3.8: Calculated model reactions of 2*H*-azaphosphirene complexes with the ferrocinium cation and nitriles.

The competing reaction path leading to symmetrically 3,5-disubstituted 2*H*-1,4,2-diazaphosphole complexes such as **41c**, **69l**, **74c**, **75c**, **76l**, **77l** (see Section 3.3) was investigated for model systems with R' = R" = CH$_3$. In order to get an estimate for the influence of the *P*- and *C*-substituents at the 2*H*-azaphosphirene ring, calulations on complexes **92** (R' = CH(SiH$_3$)$_2$, R" = CH$_3$), **93** (R' = CH$_3$, R" = Ph), and **94** (R' = CH$_3$, R" = Fc), which are closer to the full systems, were carried out in cooperation with A. Espinosa Ferao (Murcia, Spain); the calculations on ferrocenyl-containing systems as well as on reactions leading to difluorophosphane complexes (cf. Section 3.3) were done by A. Espinosa Ferao.

3.6.1 Methodical Aspects

For the reactions of complex **91** with [FeCp$_2$]$^{•+}$ and nitriles **36m,p,q** or in the absence of nitriles calculations were carried out with the TURBOMOLE V5.9.1 program package.[206] Optimizations were done with the local Slater-Dirac exchange[207]

and the correlation energy density functional (No. V) by Vosko, Wilk, and Nusair (VWN (V))[208] together with Becke's gradient corrected exchange functional B88[209] in combination with the gradient corrected correlation functional by Perdew (P86)[210] within the RI (Resolution of the Identity) approximation[211] (hereafter referred to as RI-BP86). The split valence shell basis set SV(P)[212] was used for all atoms, and the inner shell electrons of tungsten were substituted by the scalar-relativistic effective core potential ECP-60-MWB derived from the Stuttgart-Dresden group.[213] If not otherwise denoted, the influence of the polar solvent was taken into account by employing the COSMO (Conductor-like Screening Model) approach;[214] the relative permittivity was set to $\varepsilon = 8.93$ to mimic dichloromethane. For cavity construction the atomic radii of Bondi were used, which were obtained from crystallographic data;[215] the radius for tungsten was set to 2.2230 Å. Transition states were located by using a TRIM (Trust Radius Image Minimization) algorithm.[216] Excellent initial guesses were obtained through relaxed surface scans along the bonds being formed and/or broken or torsion angles, respectively. Open-shell systems were treated in the spin-unrestricted formalism. Stationary points were characterized as minima (number of imaginary frequencies NImag = 0) or first-order saddle points (NImag = 1) by numerical or analytical vibrational frequencies calculations[217] (in the cases of gas phase calculations). Single point calculations on the geometries obtained were carried out with the same method as specified above but using the valence-triple-ζ basis set TZVP.[218] Zero point and thermal corrections to free energies were adopted from optimized structures obtained on the RI-BP86/SV(P)/ECP-60-MWB(W) + COSMO level. If not otherwise denoted, the results discussed in the following refer to these single point calculations. In addition, *Natural Bond Orbital* (NBO) population analyses were carried out as single point calculations with the GAUSSIAN 03 program package[219] on the BP86/TZVP/ECP-60-MWB(W) + COSMO[214, 220] ($\varepsilon = 8.93$) level using NBO version 3.[221]

In order to test if it is sufficient to account for only scalar-relativistic effects by using ECP-60-MWB for tungsten in the cases of both neutral and positively charged complexes, model system **91**, ferrocene, [W(CO)$_6$], and their respective radical cations were optimized within the *Zeroth Order Regular Approximation* (ZORA)[222] to the Dirac equation including spin-orbit coupling.[223] These calcultions were performed by G. von Frantzius with the ADF suite of programs[224] using the BP86 density functional in combination with the valence-triple-ζ basis set TZ2P.[225] The adiabatic ionization potentials obtained with both methods (gas phase) are in excellent agreement, and furthermore, in very good agreement with experimental data available for ferrocene[226] and [W(CO)$_6$][199–201] (Tab. 3.9).

Table 3.9: Calculated adiabatic and experimental ionization potentials (IP) of ferrocene and tungsten hexacarbonyl, and calculated adiabatic ionization potential of complex **91**.

	ZORA-BP86/TZ2P IP [kJ·mol^{-1}] / [eV]	RI-BP86/TZVP/ECP(W)[♯] IP [kJ·mol^{-1}] / [eV]	Exp. IP [eV]
Complex **91**	744.4 / 7.72	741.4 / 7.68	–
[FeCp$_2$]	654.8 / 6.78	648.8 / 6.72	6.858[a]
			6.72[b]
[W(CO)$_6$]	853.3 / 8.84	849.8 / 8.81	8.56 ± 0.13[c]
			8.60 ± 0.03[d]
			8.242 ± 0.006[e]
			8.56 ± 0.02[f]
			8.6[g]

[♯]ECP-60-MWB; geometry optimization on the RI-BP86/SV(P)/ECP-60-MWB(W) level.
[a]Vertical and [b]adiabatic IP (by electron spectroscopy).[226] [c]Vertical IP (by EI-MS).[199] [d]Vertical and [e]adiabatic IP (by photoionization).[200] [f]Determined by UV and [g]X-ray photoelectron spectroscopy.[201]

Regarding structural parameters, the relevant bond lengths and angles of complex **35** in the crystal[122] are reproduced very well by the ZORA-BP86/TZ2P calculations (gas phase) on model **91** (Tab. 3.10); the maximum deviation is below 2 %. Comparably good results are obtained with RI-BP86/SVP/ECP-60-MWB(W), whereas all distances are slightly overestimated. Nevertheless, between both methods the largest difference in calculated bond lengths is 1.3 %.

Upon oxidation of **91** the resulting radical cation **91**$^{•+}$ is predicted to have a closed-ring structure; an acyclic isomer with a broken P,N bond could not be located as energy minimum. Electron transfer to the ferrocinium cation (Scheme 3.8, i) is a highly endergonic process. The free energy of reaction calculated for this model system ($\Delta_R G_{298} = +104.9$ kJ·mol^{-1})[41] is in good accordance with the estimate for complex **35** ($\Delta_R G_{298} = +88$ kJ·mol^{-1}) obtained from its anodic peak potential with respect to the half-wave potential of the system $[FeCp_2]^+/[FeCp_2]$ (cf. Section 3.5).

The effects of oxidation of **91** on its structural parameters are generally moderate, whereas identical trends were predicted for the gas phase and for the situation in solution (Tab. 3.10). The largest effect is found for the endocyclic P,C bond length, which is increased by 4.5 % upon oxidation. Elongation, albeit to a lower extent, is observed also for the P,N bond. Considering that the C,N bond is shortened at the same time the conclusion can be drawn that the description of this heterocycle as a π

---

[41]RI-BP86/TZVP/ECP-60-MWB(W)+COSMO//RI-BP86/SV(P)/ECP-60-MWB(W)+COSMO.

donor/acceptor complex of a carbonitrile and a terminal phosphanylidene complex unit (in this case cationic), according to the Dewar-Chatt-Duncanson model[129] (Fig. 3.18, resonance structure **B**), is even more pronounced for the oxidized than for the neutral system. This can be understood by assuming a reduced ability of π back-donation from the positively charged phosphorus center to the carbonitrile unit. While the W,P bond is slightly shortened, the bond of tungsten to the *trans*-carbonyl ligand is lengthened, which is associated with a decrease of the C,O distance within this ligand.

Table 3.10: Bond distances [Å] and angles [º] for complexes **91** and **91**•+ calculated with different methods, relative variations caused by oxidation, and comparison with structural data for complex **35**.[122]

	ZORA-BP86/TZ2P Gas Phase			RI-BP86/SV(P)/ECP(W)♯ Gas Phase			Exp.*
	91	**91**•+	Relative Variation [%]	**91**	**91**•+	Relative Variation [%]	**35**
W–C†	2.021	2.067	+2.3	2.038	2.095	+2.8	2.003(9)
C–O†	1.159	1.145	−1.2	1.164	1.150	−1.2	1.160(10)
W–P	2.513	2.452	−2.4	2.531	2.481	−2.0	2.470(2)
P–C‡	1.781	1.862	+4.5	1.794	1.873	+4.4	1.759(5)
P–N	1.830	1.838	+0.5	1.854	1.862	+0.4	1.795(4)
C–N	1.272	1.249	−1.9	1.277	1.255	−1.7	1.272(7)
C–P–N§	41.2	39.4	−4.4	40.9	39.3	−4.1	41.9(2)

	RI-BP86/SV(P)/ECP(W)♯ COSMO (CH₂Cl₂)		
W–C†	2.031	2.087	+2.8
C–O†	1.167	1.152	−1.3
W–P	2.545	2.473	−2.8
P–C‡	1.794	1.876	+4.6
P–N	1.853	1.860	+0.4
C–N	1.278	1.254	−1.9
C–P–N§	41.0	39.2	−4.3

♯ECP-60-MWB. *Structural data from single-crystal X-ray crystallography.[122] †*trans*-CO. ‡Endocyclic bond. §Endocyclic angle.

Interestingly, the molecular charge and the radical center within radical cationic 2*H*-azaphosphirene complex **91**•+ are spatially separated. While the charge is almost exclusively attributed to the phosphorus center ($q_N(\mathrm{PCH_3}) = +1.01$ au), the largest positive spin population is found at the transition metal ($\rho_s(\mathrm{W}) = +0.59$ au) (Fig.

3.18[42]). Due to *spin delocalization*[228] a certain fraction is spread over the oxygen atoms of the carbonyl ligands, whereas negative values are found at their carbon centers. This phenomenon is known as *spin polarization*, a result of the exchange term introduced by the Pauli principle that induces some spin density of opposite sign at the atoms directly bonded to a paramagnetic center.[228] Altogether the pentacarbonyl metal fragment holds a positive spin population about $\rho_s(W(CO)_5) = +0.68$ au.
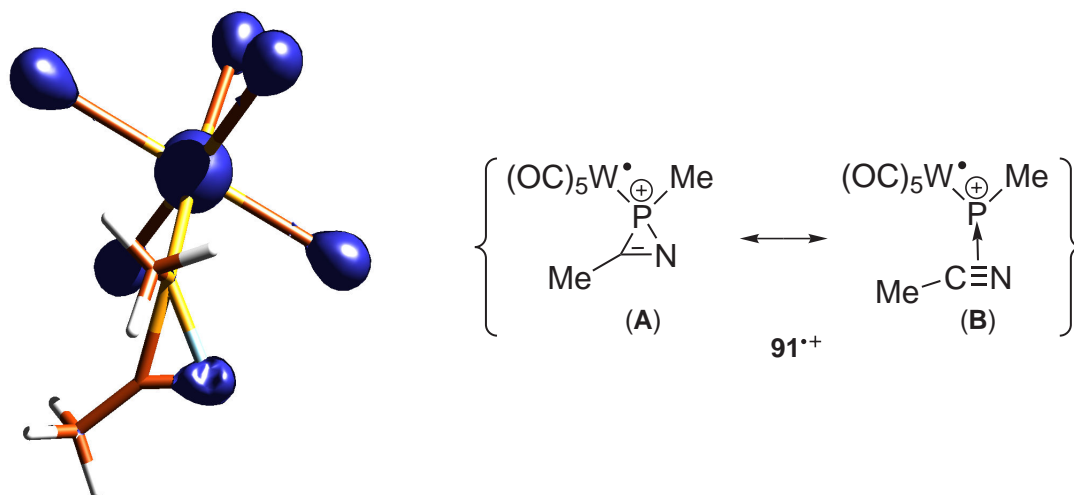
Figure 3.18: Calculated Mulliken spin density distribution (isodensity surface at 0.005 au) and canonical resonance structures of complex $91^{\bullet+}$.

The fraction of spin population at the heterocyclic ligand is mainly attributed to the nitrogen center ($\rho_s(N) = +0.15$ au), and the contribution of phosphorus is almost negligible ($\rho_s(PMe) = +0.07$ au). Thus, the radical cation $91^{\bullet+}$ is best described as 17e organometallic complex, and its valence structure can be represented by the canonical resonance forms shown in Figure 3.18.

3.6.2 Reactions with Nitriles

The computed lowest-energy pathways for the reactions of **91** with $[FeCp_2]^{\bullet+}$ and acetonitrile (**36m**) or cyanamide (**36p**) follow the same mechanistic scheme (Scheme 3.9);[43] for thermochemical data see Table 3.11.

---

[42]Plotted with the MOLDEN 4.3 program.[227]
[43]As the ring expansion steps ($91^{\bullet+} + RCN \rightarrow 96^{\bullet+}$) are subsequences of reaction ii (cf. Schemes 3.2 and 3.8), they are denoted as ii.a–c.
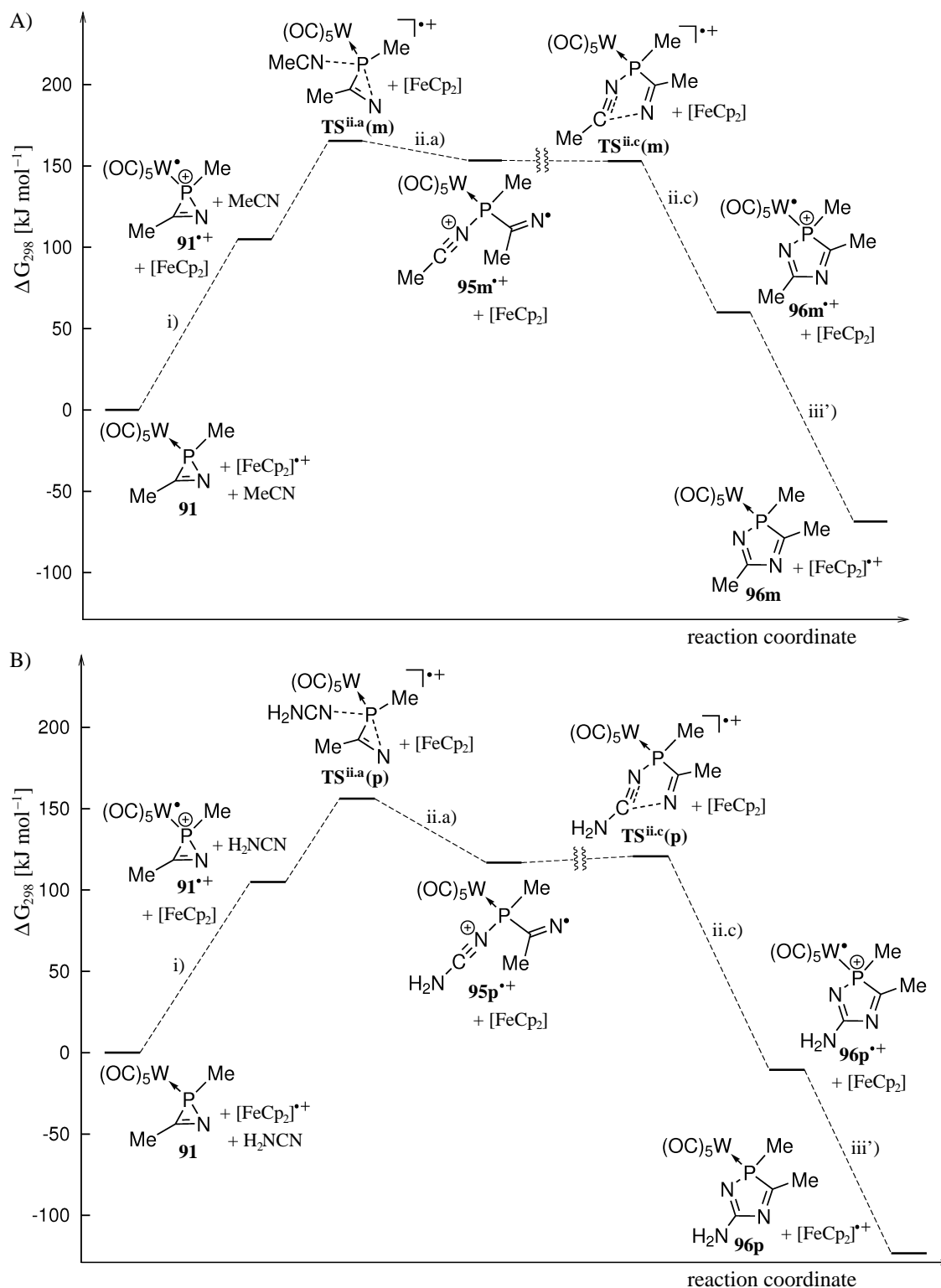
Scheme 3.9: Computed pathway for reactions of complex **91** with $[FeCp_2]^{\bullet+}$ and acetonitrile (A) or cyanamide (B) (reaction step ii.b omitted for clarity). The sum of free energies of the reactants (**91**, MeCN or H_2NCN, and $[FeCp_2]^{\bullet+}$) was arbitrarily chosen as zero-point of the ΔG_{298} scale.

Table 3.11: Calculated thermochemical data for reactions shown in Scheme 3.9 (RI-BP86/TZVP/ECP-60-MWB(W)+COSMO//RI-BP86/SV(P)/ECP-60-MWB(W) +COSMO; all values in $kJ \cdot mol^{-1}$).

	Reaction	$\Delta G_{298}^{\ddagger}$	$\Delta_R G_{298}$
i)	$91 + [FeCp_2]^{\bullet+} \rightarrow 91^{\bullet+} + [FeCp_2]$	$\sharp$	$+104.9$
ii.a)	$91^{\bullet+} + MeCN \rightarrow 95m^{\bullet+}$	$+60.5$	$+48.4$
	$91^{\bullet+} + H_2NCN \rightarrow 95p^{\bullet+}$	$+51.2$	$+11.9$
ii.b)	$95m^{\bullet+} \rightarrow 95m'^{\bullet+}$	$+7.2$	-8.8
	$95p^{\bullet+} \rightarrow 95p'^{\bullet+}$	$+7.2$	-2.5
ii.c)	$95m'^{\bullet+} \rightarrow 96m^{\bullet+}$	$+8.4$	-84.6
	$95p'^{\bullet+} \rightarrow 96p^{\bullet+}$	$+6.4$	-124.9
iii)	$96m^{\bullet+} + 91 \rightarrow 96m + 91^{\bullet+}$	$\sharp$	-23.6
	$96p^{\bullet+} + 91 \rightarrow 96p + 91^{\bullet+}$	$\sharp$	-7.9
iii')	$96m^{\bullet+} + [FeCp_2] \rightarrow 96m + [FeCp_2]^{\bullet+}$	$\sharp$	-128.5
	$96p^{\bullet+} + [FeCp_2] \rightarrow 96p + [FeCp_2]^{\bullet+}$	$\sharp$	-112.8

$\sharp$The activation barrier was not calculated; an outer sphere SET mechanism is assumed.

After oxidation of **91** (i) nitriles **36m,p** can attack at the phosphorus center of **91**$^{\bullet+}$. This yields P,N bond cleavage with formation of acyclic intermediates **95m,p**$^{\bullet+}$ (ii.a). Alternatively, taking into account the transition metal as electrophilic center an intermediate heptacoordinated tungsten complex bearing one of the nitriles **36m,p** as ligand could not be located as an energy minimum. Consequently, complex **91**$^{\bullet+}$ exhibits *ligand-centered reactivity*[229] although the radical center is localized at the metal fragment; nucleophilic attack of a nitrile occurs at the center of the highest charge density.

The nitrile-induced ring opening process is the crucial step of the overall pathway as it proceeds via the highest barrier (**TS**$^{\mathbf{ii.a}}$: Fig. 3.19,[44] left) and shows a clear dependance on the nucleophilicity of the nitrile. For the attack of H_2NCN the transition state lies considerably lower, and the reaction is less endergonic compared to the reaction with MeCN.

It is noteworthy that this kind of ring opening is not feasible for the non-oxidized $2H$-azaphosphirene complex **91**. As indicated in the transition state (denoted as **TS**$^{\mathbf{ii.d}}$**(m)**^{0}: Fig. 3.19, right) nucleophilic attack of acetonitrile at the phosphorus center is associated with displacement of the MeCN moiety of **91**, thus yielding a nitrilium phosphane ylide complex (cf. **XXV**, Scheme 1.11, Section 1.3). Although this pro-

---

[44]All depicted structures plotted with MOLDEN 4.3.[227]

cess is almost thermo-neutral ($\Delta_R G_{298} = -2.5$ kJ·mol^{-1}) the barrier is considerably higher ($\Delta G^{\ddagger}_{298} = +112.6$ kJ·mol^{-1}) compared to the nitrile-induced ring opening of the corresponding radical cation **91**$^{\bullet+}$ (ii.a). This explains why 2H-azaphosphirene complexes such as **35** (for which steric factors are more pronounced than for model system **91**) do not react with nitriles in the absence of single-electron oxidants (or other initiators; see Chapter 4) at ambient temperature as shown in Section 3.1.
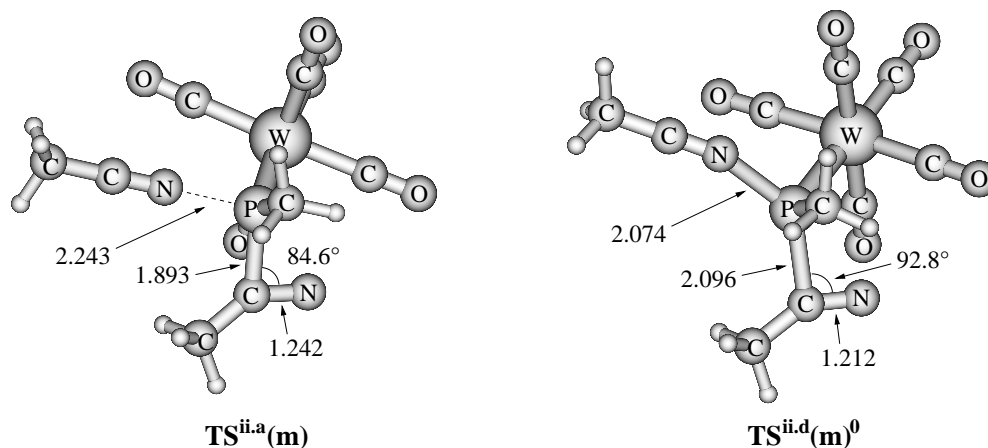
TS$^{ii.a}$(m)   **TS$^{ii.d}$(m)^0**

Figure 3.19: Calculated structures of transition states **TS$^{ii.a}$(m)** and **TS$^{ii.d}$(m)^0** for nucleophilic attack of acetonitrile at radical cation **91**$^{\bullet+}$ (left) and at neutral complex **91** (right), respectively (distances in Å).

Once acyclic intermediates **95m,p**$^{\bullet+}$ are formed, after a conformational change (rotation about the P–C(Me)N bond; reaction ii.c) to **95m,p'**$^{\bullet+}$ (Fig. 3.20) the latter can undergo facile cyclization to yield radical cationic 2H-1,4,2-diazaphosphole complexes **96m,p**$^{\bullet+}$ via a low barrier (**TS$^{ii.c}$**: Fig. 3.20) in a highly exergonic step (ii.c). Upon ring closure the reaction cycle is completed through oxidation of 2H-azaphosphirene complex **91** by **96m,p**$^{\bullet+}$ (iii), which is slightly exergonic in both cases. This yields neutral 2H-1,4,2-diazaphosphole complexes **96m,p** and complex **91**$^{\bullet+}$; the latter can restart the chain reaction. For the net ring expansion reactions the overall free energy balance is exergonic (**91** + **36m** → **96m**: $\Delta_R G_{298} = -68.7$ kJ·mol^{-1}, and **91** + **36p** → **96p**: $\Delta_R G_{298} = -123.4$ kJ·mol^{-1}).

During the successive reaction steps ii.a–c the positive charge remains mainly at phosphorus (Tab. 3.12); some amount of positive charge density is intermediately induced at the attacking nitrile. On the other hand, the spin density is almost completely shifted to the phosphane ligand in the course of the reaction.
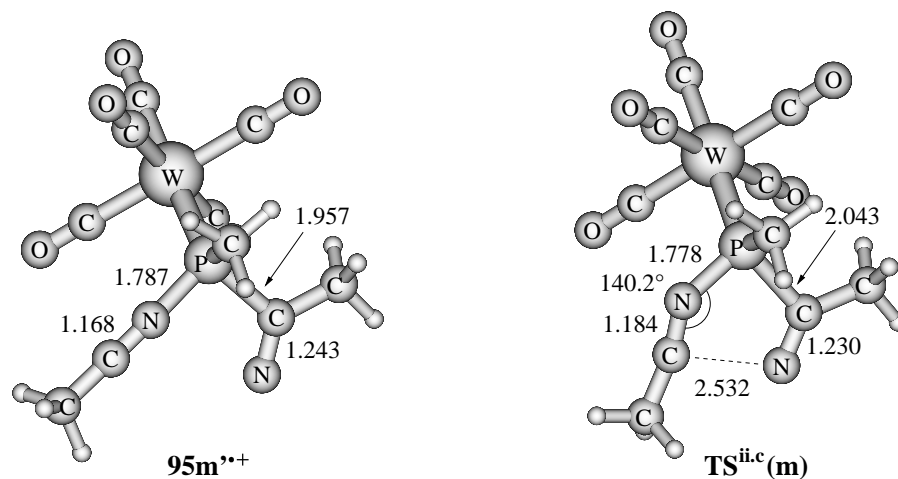
Figure 3.20: Calculated structures of acyclic intermediate **95m'**[•+] (left) and transition state **TS**[ii.c]**(m)** for its cyclization (right) (distances in Å).

Table 3.12: Evolution of calculated natural charges (q_N) and Mulliken spin populations (ρ_s) for selected molecule fragments along the reaction path shown in Scheme 3.9 (A).

	91[•+]	**TS**[ii.a]**(m)**	**95m**[•+]	**TS**[ii.c]**(m)**	**96m**[•+]
	Natural Charge (q_N) [au]				
W(CO)$_5$	+0.03	−0.17	−0.40	−0.29	+0.17
PMe	+1.01	+1.10	+1.21	+1.15	+1.15
MeCN(a)	−0.05	−0.11	−0.15	−0.17	−0.15
MeCN(b)	−	+0.19	+0.34	+0.31	−0.17
	Mulliken Spin Population (ρ_s) [au]				
W(CO)$_5$	+0.68	+0.39	+0.04	+0.24	+0.84
PMe	+0.07	+0.16	+0.16	+0.17	+0.01
N(a)	+0.15	+0.41	+0.80	+0.56	+0.12
CMe(a)	+0.10	+0.02	−0.03	−0.05	+0.03
N(b)	−	+0.01	−0.01	+0.01	+0.01
CMe(b)	−	+0.01	+0.03	+0.07	0.00

(a) MeCN unit that stems from 2H-azaphosphirene complex **91**[•+].

(b) Attacking nitrile.

In acyclic intermediate **95m$^{\bullet+}$** a spin population of only $\rho_s(\text{W(CO)}_5) = +0.04$ au remains at the metal fragment while the largest value ($\rho_s(\text{N}) = +0.80$ au) is attributed to the nitrogen atom of the former 2*H*-azaphosphirene ligand.[45] This legitimates the localization of the radical center in the canonical Lewis structures of **95m,p$^{\bullet+}$** shown in Scheme 3.9. Towards the end of the reaction path the spin center is back-transferred to the pentacarbonyl metal fragment. Hence, radical cationic 2*H*-1,4,2-diazaphosphole complexes **96m,p$^{\bullet+}$** are characterized as 17e organometallic complexes (like reactant **91$^{\bullet+}$**).

The model reaction using **91**, [FeCp$_2$]$^{\bullet+}$, and H$_2$NCN (**36p**) may be representative for the reaction of **35** with Me$_2$NCN (**36b**) in the presence of ferrocinium salts and also for the reactions of **35** with electron-rich five-membered heterocyclic nitrile derivatives **36d–g** (Section 3.1). A different situation was found for the model reaction of complex **91** with [FeCp$_2$]$^{\bullet+}$ and the electron-poor nitrile NCCN (**36q**) (Scheme 3.10 and Tab. 3.13). An attack of NCCN at the phosphorus center of **91$^{\bullet+}$** causes displacement of the MeCN moiety from the latter (**TS$^{\text{ii.d}}$(q)**: Fig. 3.21) with formation of complex **97q$^{\bullet+}$** (ii.d), analogous to the reaction of neutral complex **91** with acetonitrile. The barrier of this process is significantly higher than for the ring opening reactions of **91$^{\bullet+}$** with MeCN or H$_2$NCN (ii.a). Therefore, a ferrocinium salt-induced ring expansion of 2*H*-azaphosphirene complexes with electron-poor nitriles is not supported by the calculations.
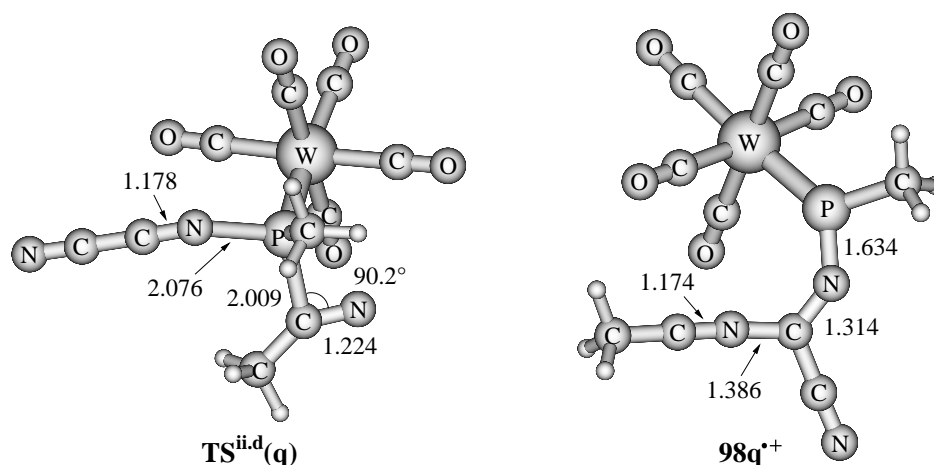
Figure 3.21: Calculated structure of transition state **TS$^{\text{ii.d}}$(q)** for the nucleophilic attack of dicyane at **91$^{\bullet+}$** (left) and calculated structure of acyclic intermediate **98q$^{\bullet+}$** of the reaction of acetonitrile with radical cationic nitrilium phosphane ylide complex **97q$^{\bullet+}$** (right) (distances in Å).

---

[45]Due to spin polarization, starting from N(a), regions of spin densities of alternating sign propagate through the phosphane ligand of **95m$^{\bullet+}$**.
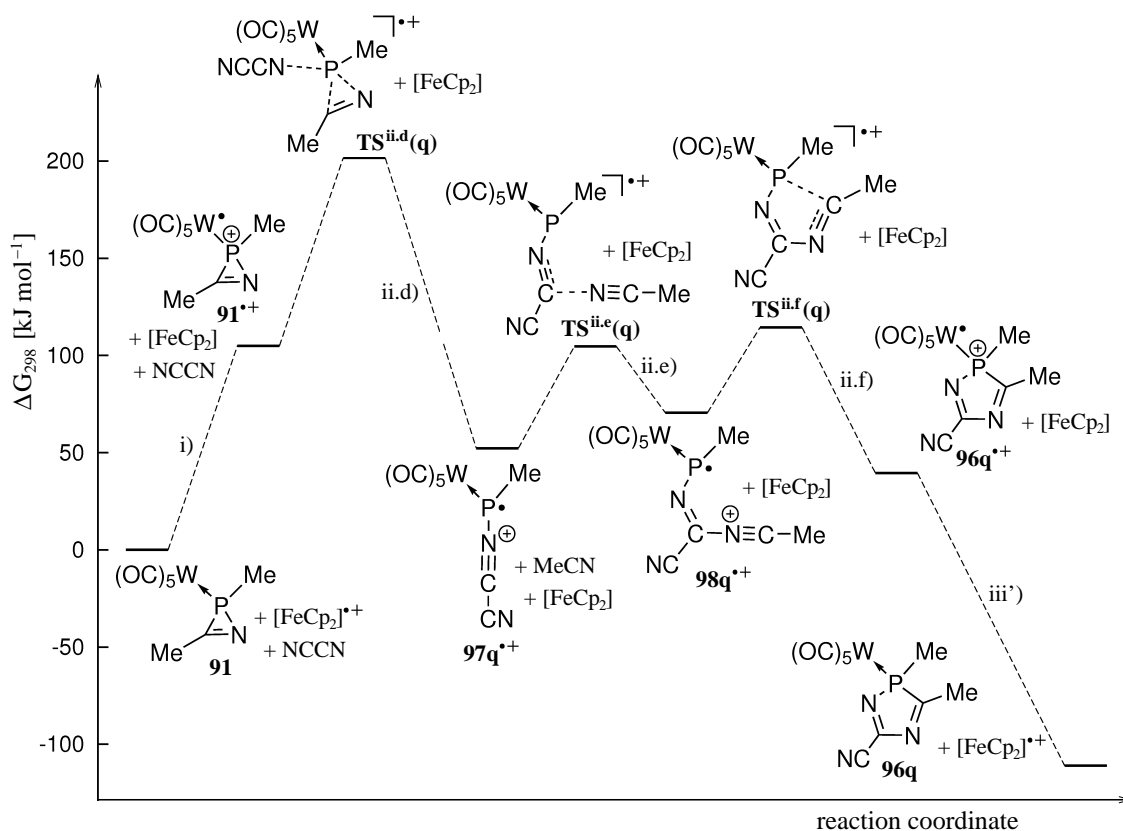
Scheme 3.10: Computed pathway for the reaction of complex **91** with the ferrocinium cation and dicyane (**36q**). The sum of free energies of the reactants (**91**, NCCN, and $[FeCp_2]^{\bullet+}$) was arbitrarily chosen as zero-point of the ΔG_{298} scale.

Table 3.13: Calculated thermochemical data for reactions shown in Scheme 3.10 (RI-BP86/TZVP/ECP-60-MWB(W)+COSMO//RI-BP86/SV(P)/ECP-60-MWB(W) +COSMO; all values in $kJ \cdot mol^{-1}$).

Reaction		$\Delta G^{\ddagger}_{298}$	$\Delta_R G_{298}$
i)	$\mathbf{91} + [FeCp_2]^{\bullet+} \rightarrow \mathbf{91}^{\bullet+} + [FeCp_2]$	$\sharp$	$+104.9$
ii.d)	$\mathbf{91}^{\bullet+} + NCCN \rightarrow \mathbf{97q}^{\bullet+} + MeCN$	$+96.7$	-52.7
ii.e)	$\mathbf{97q}^{\bullet+} + MeCN \rightarrow \mathbf{98q}^{\bullet+}$	$+52.4$	$+18.3$
ii.f)	$\mathbf{98q}^{\bullet+} \rightarrow \mathbf{96q}^{\bullet+}$	$+43.9$	-31.1
iii)	$\mathbf{96q}^{\bullet+} + \mathbf{91} \rightarrow \mathbf{96q} + \mathbf{91}^{\bullet+}$	$\sharp$	-45.6
iii')	$\mathbf{96q}^{\bullet+} + [FeCp_2] \rightarrow \mathbf{96q} + [FeCp_2]^{\bullet+}$	$\sharp$	-150.5

$\sharp$The activation barrier was not calculated; an outer sphere SET mechanism is assumed.

However, proceeding from radical cationic nitrilium phosphane ylide complex **97q•⁺**
a feasible path for the formation of 2*H*-1,4,2-diazaphosphole complex **96q** was found,
too (Scheme 3.10). Once complex **97q•⁺** is formed it can easily be attacked by the
MeCN unit that was previously released from **91•⁺** (ii.e). Acyclic intermediate **98q•⁺**
(Fig. 3.21) can subsequently undergo cyclization via a low barrier (ii.f). Finally, the
radical cation reaction cycle is closed through reduction of **96q•⁺** by the reactant
91 (iii). Also here, the overall ring expansion process is thermodynamically clearly
favored (**91** + **36q** → **96q**: $\Delta_R G_{298} = -111.0 \text{ kJ} \cdot \text{mol}^{-1}$).

3.6.3   Reactions in the Absence of Nitriles

In the absence of nitriles the MeCN fragment of **91•⁺** can be released from the oxidized
complex via a two-step mechanism (Scheme 3.11; Tab. 3.14). In the first step the P,C
bond is broken (ii.g) leading to the formation of radical cationic nitrilium phosphane
ylide complex **97m•⁺** via a low barrier (**TS^{ii.g}(m)**: Fig. 3.22, left). This process is
highly exergonic ($\Delta_R G_{298} = -77.5 \text{ kJ} \cdot \text{mol}^{-1}$), hence, complex **97m•⁺** can be regarded
as a thermodynamically favored valence isomer of radical cationic 2*H*-azaphosphirene
complex **91•⁺**.
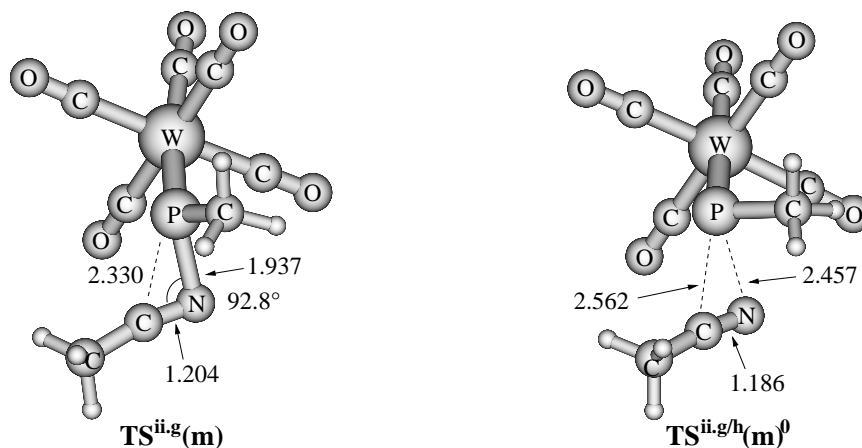
Figure 3.22: Calculated structures of transition state **TS^{ii.g}(m)** for the rearrangement
of complex **91•⁺** to radical cationic nitrilium phosphane ylide complex **97m•⁺** (left)
and of **TS^{ii.g/h}(m)⁰** for the dissociation of acetonitrile from neutral complex **91** (right)
(distances in Å).

In the second step **97m•⁺** can dissociate into a nitrile (MeCN) and a radical cationic
phosphanylidene complex fragment, **99•⁺** (ii.h).[46] This process is predicted to be

---

[46]It was confirmed that the positive charge remains at the phosphanylidene complex fragment

endergonic although it is accociated with a large increase of entropy. Even in a constrained search no transition state could be located, which points to a flat barrier.

Table 3.14: Calculated thermochemical data for reactions shown in Schemes 3.11 (R' = R" = CH$_3$) and 3.12 (RI-BP86/TZVP/ECP-60-MWB(W)+COSMO//RI-BP86/SV(P)/ ECP-60-MWB(W)+COSMO; all values in kJ·mol^{-1}).

Reaction		$\Delta G^{\ddagger}_{298}$	$\Delta_R G_{298}$
ii.g)	**91$^{\bullet+}$ → 97m$^{\bullet+}$**	+15.2	−77.5
ii.h)	**97m$^{\bullet+}$ → 99$^{\bullet+}$ + MeCN**	†	+50.9
ii.a)	**91$^{\bullet+}$ + MeCN → 95m$^{\bullet+}$**	+60.5	+48.4
ii.b)	**95m$^{\bullet+}$ → 95m'$^{\bullet+}$**	+7.2	−8.8
ii.c)	**95m'$^{\bullet+}$ → 96m$^{\bullet+}$**	+8.4	−84.6
ii.e)	**97m$^{\bullet+}$ + MeCN → 98m$^{\bullet+}$**	+88.4	+77.2
ii.f)	**98m$^{\bullet+}$ → 96m$^{\bullet+}$**	+17.0	−44.8
iii)	**96m$^{\bullet+}$ + 91 → 96m + 91$^{\bullet+}$**	♯	−23.6
iv)	**97m$^{\bullet+}$ + MeCN → 100m$^{\bullet+}$**	+91.2	+9.2
v)	**100m$^{\bullet+}$ + 91 → 100m + 91$^{\bullet+}$**	♯	−22.6
ii.i)	**97m$^{\bullet+}$ + MeCN → 95m'$^{\bullet+}$**	+113.8	+117.1
vi)	**97m$^{\bullet+}$ + MeCN → 101m$^{\bullet+}$**	+112.8	+107.3
vii)	**101m$^{\bullet+}$ → 100m$^{\bullet+}$**	*	−98.1
viii)	**97m$^{\bullet+}$ + MeCN → 102m$^{\bullet+}$**	+151.9	+126.4
ix)	**102m$^{\bullet+}$ → 100m$^{\bullet+}$**	*	−117.3

†No transition state could be located. ♯The activation barrier was not calculated; an outer sphere SET mechanism is assumed. *Not calculated.

Interestingly, the situation is different for neutral 2H-azaphosphirene complex **91**. In this case a cheletropic extrusion of acetonitrile was found, which is only slightly endergonic ($\Delta_R G_{298}$ = +12.2 kJ·mol^{-1}), but it proceeds via a higher barrier (**TS$^{\text{ii.g/h}}$(m)^0**: Fig. 3.22, right; $\Delta G^{\ddagger}_{298}$ = +70.5 kJ·mol^{-1}) compared to the ring opening process of radical cation **91$^{\bullet+}$**. For **91** the calculations did not support the possibility of a rearrangement to a nitrilium phosphane ylide complex in one step.[47]

rather than at the nitrile through calculation of the thermodynamics of the hypothetical electron transfer reaction **99$^{\bullet+}$ + 36m → 99 + 36m$^{\bullet+}$**: $\Delta_R G_{298}$ = +352.3 kJ·mol^{-1}.

[47]As outlined in the introduction neutral 2H-azaphosphirene complexes showed reactivities derived from either phosphanylidene[118,138–146] or nitrilium phosphane ylide complexes[114,126,139,146–160] as transient intermediates at higher temperatures (Section 1.3). Further calcluations on neutral model systems revealed that the latter intermediates may be formed by subsequent *end-on* attachment of a previously eliminated nitrile fragment to the phosphanylidene complex, which is predicted to be thermodynamically favored (for R' = R" = CH$_3$: $\Delta_R G_{298}$ = −14.7 kJ·mol^{-1}).

Scheme 3.11: Computed pathways for reactions of radical cationic 2*H*-azaphosphirene complexes $91^{\bullet+}$–$94^{\bullet+}$ in the absence of nitriles.

In the course of the rearrangement of radical cation $91^{\bullet+}$ the spin center, to a large extent, is shifted from the metal fragment to the phosphane ligand (Tab. 3.15). In complex $97m^{\bullet+}$ the largest positive spin population is found at phosphorus, while a minor fraction is delocalized to the carbon center. Thus, the electronic structure of $97m^{\bullet+}$ is best represented by the Lewis structure displayed in Scheme 3.11. However, the positive molecular charge is mainly attributed to phosphorus; only a minor amount of positive charge density is induced at the MeCN moiety ($q_N = +0.28$ au).

For the formation of symmetrically 3,5-disubstituted 2*H*-1,4,2-diazaphosphole complex $96m$ two conceivable pathways were found (**A** and **B**; Scheme 3.11). Alternative **A** involves nucleophilic ring opening of complex $91^{\bullet+}$ by the precedently eliminated

nitrile and subsequent cyclization of **95m'**$^{\bullet+}$. This reaction sequence (ii.a → ii.b → ii.c → iii) has already been discussed in the previous section. In pathway **B** the nitrile attacks at radical cationic nitrilium phosphane ylide complex **97m**$^{\bullet+}$ leading to acyclic intermediate **98m**$^{\bullet+}$ (ii.e), which can undergo facile cyclization in a subsequent step as well (ii.f). According to the thermochemical data for both competing reactions (Tab. 3.14) the former alternative (**A**) should be preferred because the attack of the nitrile, the crucial step in both cases, proceeds via a lower lying transition state if it occurs at complex **91**$^{\bullet+}$. These results may raise the conclusion that rearrangement ii.g is only required as a source of a nitrile and path **B** is not further followed on the way to the final product. However, it must be taken into account that the dominance of either of both pathways should depend mainly on the availability of the respective reactant. Comparing the facile rearrangement of **91**$^{\bullet+}$ to its acyclic isomer **97m**$^{\bullet+}$ with the effort that is required to liberate acetonitrile from the latter suggests that the formation of **97m**$^{\bullet+}$ may be complete prior to ring expansion.

Table 3.15: Evolution of calculated natural charges (q_N) and Mulliken spin populations (ρ_s) for selected molecule fragments along reaction path **B** shown in Scheme 3.11.

	91$^{\bullet+}$	**TS**$^{\text{ii.g}}$(m)	**97m**$^{\bullet+}$	**TS**$^{\text{ii.e}}$(m)	**98m**$^{\bullet+}$	**TS**$^{\text{ii.f}}$(m)	**96m**$^{\bullet+}$
	Natural Charge (q_N) [au]						
W(CO)$_5$	+0.03	−0.19	−0.28	−0.39	−0.44	−0.35	+0.17
PMe	+1.01	+0.93	+1.00	+1.02	+1.16	+0.97	+1.15
MeCN(a)	−0.05	+0.27	+0.28	+0.08	−0.24	−0.07	−0.17
MeCN(b)	−	−	−	+0.29	+0.52	+0.44	−0.15
	Mulliken Spin Population (ρ_s) [au]						
W(CO)$_5$	+0.68	+0.39	+0.38	+0.28	+0.18	+0.29	+0.84
PMe	+0.07	+0.48	+0.52	+0.57	+0.38	+0.45	+0.01
N(a)	+0.15	+0.10	−0.05	−0.06	−0.04	0.00	+0.01
CMe(a)	+0.10	+0.04	+0.15	+0.18	+0.32	+0.05	0.00
N(b)	−	−	−	0.00	−0.06	+0.04	+0.12
CMe(b)	−	−	−	+0.03	+0.22	+0.16	+0.03

(a) MeCN unit that remains at complex **97m**$^{\bullet+}$. (b) Attacking nitrile.

During the entire reaction sequence of path **B** (ii.g → ii.e → ii.f) the electric charge at phosphorus is approximately +1 au (Tab. 3.15), although in intermediate **98m**$^{\bullet+}$ a considerable positive charge density is found at the MeCN(b) fragment[48] that stems

[48]Note that the substituent of the attacking nitrile is attached to C^3 in the final product **96m**$^{\bullet+}$, while it is attached to C^5 if the reaction proceeds via pathway **A**. As a consequence, for complex **96m**$^{\bullet+}$ the indices (a) and (b) are transposed in Table 3.15 with respect to Table 3.12.

from the nitrile that has attacked at **97m**$^{\bullet+}$; a low negative charge is attributed to the other MeCN unit (MeCN(a)). During the reaction the spin center, to a large extent, is intermediately transferred from the transition metal to the phosphane ligand. The spin population remaining at the W(CO)$_5$ fragment reaches a minimum in acyclic complex **98m**$^{\bullet+}$ (ρ_s(W(CO)$_5$) = +0.18 au). Here, it is shared between phosphorus and the carbon center of MeCN(a). Towards the end of the reaction sequence the radical center is then back-transferred via phosphorus (in **TS$^{\text{ii.f}}$(m)**) to the pentacarbonyl tungsten fragment.

In principle, several other reaction types could be envisaged for the combination of radical cationic nitrilium phosphane ylide complex **97m**$^{\bullet+}$ with a nitrile (Scheme 3.12; Tab. 3.14). Nevertheless, all alternatives considered are less likely for the following reasons.
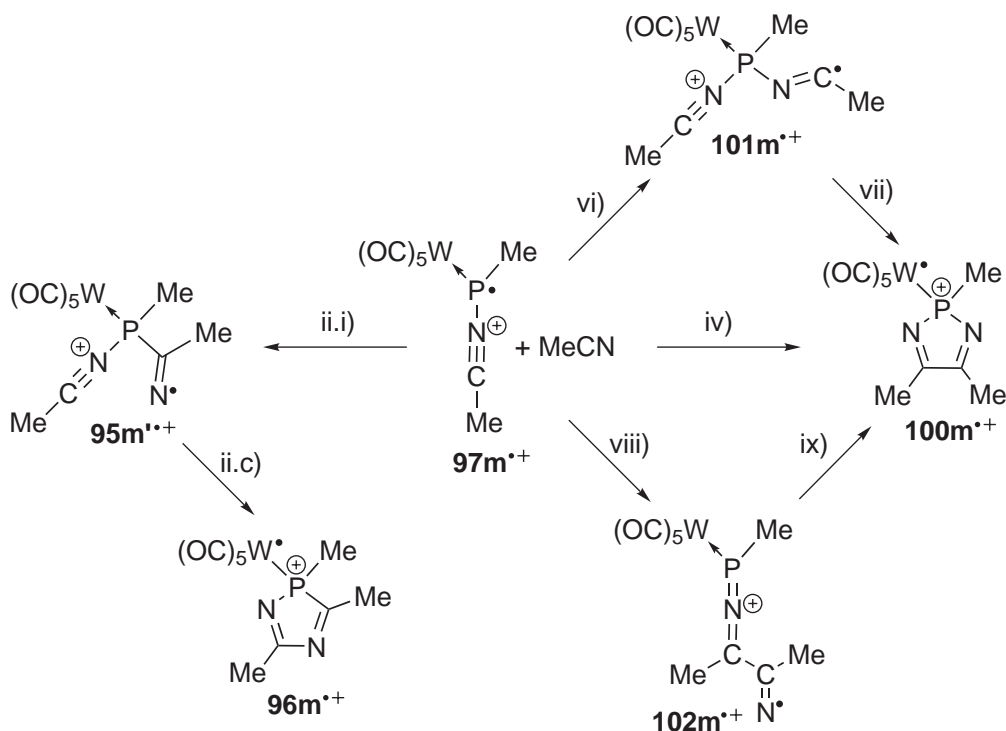
Scheme 3.12: Computed alternative pathways for the reaction of radical cationic nitrilium phosphane ylide complex **97m**$^{\bullet+}$ with acetonitrile.

Preceding P,C bond formation (reaction ii.i) is characterized as a radical addition of complex **97m**$^{\bullet+}$ to the C,N π bond of the nitrile. It leads to intermediate **95m'**$^{\bullet+}$, but it proceeds via a significantly higher barrier than the previous C,N bond formation (reaction ii.e, Scheme 3.11). Furthermore, two regiochemically different [3+2] cycloaddition reactions could be envisaged. Interestingly, for the formation of complex **96m**$^{\bullet+}$

this reaction type was not supported but for the different regiochemistry yielding radical cationic $2H$-1,3,2-diazaphosphole complex **100m**[•+] (reaction iv).[49] In this case the concerted mechanism is clearly preferred over the two alternative stepwise additions (reactions vi → vii and viii → ix), which have considerably higher barriers. It should be noted that for the chosen model system the transition state for this cycloaddition is not much higher in energy than the barrier for C,N bond formation via reaction step ii.e. However, $2H$-1,3,2-diazaphosphole complexes have never been observed in ferrocinium salt-induced reactions of $2H$-azaphosphirene complexes, and it is shown in the next section that these reactions are largely influenced by steric effects, so that substituents of the full systems should discriminate the cycloaddition pathway further with respect to the stepwise formation of $2H$-1,4,2-diazaphosphole complexes.

3.6.4 Substituent Effects

To investigate the influence of substituents at the $2H$-azaphosphirene ring, calculations were carried out on model reactions of complexes **92**–**94** (Scheme 3.11). Since these were done with a calculation method different from the one presented in the previous sections, corresponding reactions of **91** were calculated on the same level of theory for comparison. Here, only ring expansions with nitriles released from the respective $2H$-azaphosphirene complexes are considered (i.e., R = R").

All computations were performed with the GAUSSIAN 03 program package.[219] For optimizations the *Three Parameter Hybrid Functional Becke3* (B3)[230] in combination with the gradient corrected correlation functional by Lee, Yang, and Parr (LYP)[231, 232] and the valence-double-ζ basis set 6-31G(d)[233] augmented[234] with diffuse basis functions for nitrogen and fluorine atoms, and for tungsten the Los Alamos ECP plus DZ basis set (LanL2DZ)[235] was employed. Stationary points were characterized as minima or transition states by analytical vibrational frequencies calculations. Single point calculations were carried out using the Three Parameter Hybrid Functional Becke3 (B3)[230] in combination with the LYP correlation functional[231, 232] and the valence-triple-ζ basis set 6-311G(d,p)[236] with diffuse basis functions at N and F. The influence

---

[49]Comparative computational studies on neutral complex **97m** revealed that in this case two regiochemically different 1,3-dipolar cycloaddition reactions with acetonitrile are possible. The reaction that leads to $2H$-1,3,2-diazaphosphole complex **100m** proceeds via a higher barrier ($\Delta G^{\ddagger}_{298} = +120.8$ kJ·mol^{-1}), but it is thermodynamically preferred ($\Delta_R G_{298} = -88.5$ kJ·mol^{-1}) over the reaction leading to $2H$-1,4,2-diazaphosphole complex **96m** ($\Delta G^{\ddagger}_{298} = +93.6$ kJ·mol^{-1}; $\Delta_R G_{298} = -66.2$ kJ·mol^{-1}). These results are in agreement with experiments, which revealed that thermal generation of nitrilium phosphane ylide complexes in the presence of nitriles resulted in the formation of either $2H$-1,3,2-diazaphosphole[146, 155–159] or $2H$-1,4,2-diazaphosphole complexes[146, 155] or a mixture of both[146, 155] depending on the substituents and the specific reaction conditions (cf. Section 1.3).

of the solvent was taken into account by employing the COSMO approach[214, 220] with $\varepsilon = 8.93$. Zero point and thermal corrections to free energies were adopted from optimizations on the B3LYP/aug-6-31G(d)/LanL2DZ(W) level. Natural Bond Orbital population analyses using NBO version 3[221] were carried out as single point calculations on the B3LYP/aug-6-311G(d,p)/LanL2DZ(W) level of theory for the gas phase.

With this approach all activation barriers calculated for the reactions of complex **91** are somewhat higher (Tab. 3.16) compared to the method applied in the previous sections (cf. Tab. 3.14). Nevertheless, the same trends such as the preference of pathway **A** over **B** are predicted.

Table 3.16: Calculated thermochemical data for reactions shown in Schemes 3.11 and 3.13 and for redox step i in Scheme 3.8 (B3LYP/aug-6-311G(d,p)/LanL2DZ(W)+COSMO// B3LYP/aug-6-31G(d)/LanL2DZ(W); all values in $kJ \cdot mol^{-1}$).

	R' = CH$_3$ R" = CH$_3$		R' = CH(SiH$_3$)$_2$ R" = CH$_3$		R' = CH$_3$ R" = Ph		R' = CH$_3$ R" = Fc	
Rct.	$\Delta G^{\ddagger}_{298}$	$\Delta_R G_{298}$	$\Delta G^{\ddagger}_{298}$	$\Delta_R G_{298}$	$\Delta G^{\ddagger}_{298}$	$\Delta_R G_{298}$	$\Delta G^{\ddagger}_{298}$	$\Delta_R G_{298}$
i)	$\sharp$	+87.9	$\sharp$	+78.9	$\sharp$	+82.5	$\sharp$	−8.2
ii.g)	+24.0	−76.1	+22.4	−75.7	+29.5	−78.7	+86.4	−4.4
ii.h)	$\dagger$	+28.2	$\dagger$	+5.6	$\dagger$	+35.4	$\dagger$	+48.5
ii.a)§	+71.6	+49.7	+73.0	+63.0	+100.4	+73.1	+145.9	+136.1
ii.c)	+16.6	−100.8	+22.7	−106.0	+23.3	−116.8	$\dagger$	−217.7
ii.e)	+103.9	+88.6	+103.4	+85.7	+119.9	+85.9	+118.5	+70.2
ii.f)	+28.4	−63.7	+49.9	−53.0	+30.1	−50.9	+29.1	−147.5
iii)	$\sharp$	−12.6	$\sharp$	−19.1	$\sharp$	−11.3	$\sharp$	+11.8
iv)	+121.7	−8.8	+134.9	+5.2	*	*	*	*
v)	$\sharp$	+2.8	$\sharp$	−14.7	*	*	*	*
ii.j)	+37.1	−60.0	+49.4	−40.6	*	*	*	*
ii.k)	+122.4	−25.4	+132.3	−20.9	*	*	*	*

$\sharp$The activation barrier was not calculated; an outer sphere SET mechanism is assumed.

$\dagger$No transition state could be located. $^{\S}\Delta_R G_{298}$ values refer to the reaction sequence ii.a + ii.b.

$*$Not calculated.

Noteworthy is that the increase in the barrier is significantly more pronounced for the dipolar cycloaddition reaction (iv) than for the stepwise mechanism via **98m$^{\bullet+}$** (ii.e → ii.f). This effect is further increased if the methyl group at phosphorus is replaced by the sterically more demanding CH(SiH$_3$)$_2$ group, which is closer to the full system. On the other hand, the presence of this substituent has almost no influence on the barrier for the attack of the nitrile at the carbon center of radical cationic

nitrilium phosphane ylide complex **103**[•+] (ii.e). Interestingly, the same is true for the nucleophilic ring opening of radical cationic $2H$-azaphosphirene complex **91**[•+] (ii.a). It is noteworthy that a more facile oxidation is predicted for complex **92** (i), and the dissociation of **103**[•+] into **104**[•+] and acetonitrile is only slightly endergonic (ii.h).

Introduction of a C-phenyl group causes an increase in the free energy of activation for the attack of the respective nitrile (here PhCN) at the carbon center of **97c**[•+] (ii.e) as well as at phosphorus of complex **93**[•+] (ii.a; see also Fig. 3.24). Nevertheless, in the absence of external nitriles for both model systems ring expansion via pathway **A** is kinetically preferred. Altogether, the effects of P-CH(SiH$_3$)$_2$ and C-phenyl substitution are generally rather low, hence, complex **91** serves as an appropriate model for $2H$-azaphosphirene complex **35**.

Inspection of the bond lengths given in Table 3.17 reveals that the results obtained for model systems **91**–**93** are very similar, and in good accordance with the experimental data for complex **35**[122] (cf. Tab. 3.10, Section 3.6.1). Moreover, largely consistent percentual increments upon oxidation were found for all complexes **91**–**93**.

Table 3.17: Bond distances [Å] for complexes **91**–**94** and their respective radical cations **91**[•+]–**94**[•+], and relative variations caused by oxidation.

	B3LYP/aug-6-31G(d)/LanL2DZ(W)			B3LYP/aug-6-31G(d)/LanL2DZ(W)		
	91	**91**[•+]	Relative Variation [%]	**92**	**92**[•+]	Relative Variation [%]
W–C[†]	2.025	2.088	+3.1	2.024	2.085	+3.0
C–O[†]	1.157	1.142	−1.2	1.156	1.143	−1.2
W–P	2.518	2.499	−0.7	2.524	2.495	−1.2
P–C[‡]	1.782	1.835	+3.0	1.783	1.845	+3.5
P–N	1.832	1.847	+0.8	1.829	1.850	+1.2
C–N	1.268	1.249	−1.5	1.269	1.249	−1.6
	B3LYP/aug-6-31G(d)/LanL2DZ(W)			B3LYP/aug-6-31G(d)/LanL2DZ(W)		
	93	**93**[•+]	Relative Variation [%]	**94**	**94**[•+]	Relative Variation [%]
W–C[†]	2.024	2.085	+3.1	2.023	2.041	+0.9
C–O[†]	1.157	1.143	−1.2	1.157	1.151	−0.5
W–P	2.521	2.497	−1.0	2.530	2.491	−1.6
P–C[‡]	1.778	1.832	+3.0	1.779	1.780	0.0
P–N	1.823	1.831	+0.4	1.817	1.838	+1.2
C–N	1.276	1.260	−1.3	1.279	1.274	−0.4

[†] *trans*-CO. [‡] Endocyclic bond.

The situation is completely changed by *C*-ferrocenyl substitution. Concerning the thermochemical data (Tab. 3.16) the most obvious difference is found for the initial redox step (i), which is significantly facilitated for ferrocenyl substituted derivative **94**. Accordingly, major deviations from the behavior of the other model systems are found in the variations of the 2*H*-azaphosphirene ring bond lengths and in the periphery of tungsten upon oxidation. Whereas the tungsten–phosphorus bond is shortened approximately to the same degree and the P,N bond is lengthened, all other bonds listed in Table 3.17—especially the endocyclic P,C bond—are almost unaffected by oxidation.

These observations point to the fact that oxidation preferably occurrs at the ferrocenyl moiety rather than the pentacarbonyl tungsten fragment, which is further supported through the high positive charge and spin density at the ferrocenyl group of **94**$^{\bullet+}$ (Tab. 3.18 and Fig. 3.25[50]). Geometrically significant for this group is the distance between the Fe center and the centroids of the cyclopentadienyl rings. It has previously been shown[237] that this parameter is of diagnostic relevance for characterizing the degree of oxidation in ferrocene or ruthenocene complexes. It is almost insensitive to the presence of electron donating or withdrawing substituents at the Cp rings, but it is considerably increased in radical cationic metallocinium species, probably due to the removal of an electron that has slightly bonding character with respect to the metal Cp ring interaction. Thus, both Fe–Cp centroid distances are considerably elongated in complex **94**$^{\bullet+}$ compared to its neutral counterpart **94** (Fig. 3.23).

Similar results were obtained also for the pair of ferrocenyl substituted neutral and oxidized 2*H*-1,4,2-diazaphosphole complexes **110/110**$^{\bullet+}$. Likewise, but in marked contrast to methyl and phenyl derivatives **96m/96m**$^{\bullet+}$, **108/108**$^{\bullet+}$, and **109/109**$^{\bullet+}$, only small geometrical changes were found for **110/110**$^{\bullet+}$ at both the heterocycle and the tungsten pentacarbonyl center. The picture of geometrical changes at the ferrocenyl moieties is in so far more complicated as a different behavior is observed for both ferrocenyl groups present in the molecule. The Fc substituent attached to C^5 of the 2*H*-1,4,2-diazaphosphole ring experiences similar geometrical distortions as the Fc group in **94/94**$^{\bullet+}$ (Fig. 3.23), which indicates that in the oxidized species **110**$^{\bullet+}$ the radical character is localized at this center. On the other hand, the ferrocenyl substituent at C^3 remains essentially non-oxidized as evidenced by the almost unaffected Fe–Cp distances. Such kind of essentially neutral ferrocenyl unit can participate in alleviating an electron deficiency at neighboring positions by folding the Cp–Fe–Cp axis.[238] High values for $\beta_{in-plane}$ tilt angles[51] account for a tilting of the Fe d_{z^2}-type

---

[50]Plotted with the GaussView 5 program.
[51]That is the supplementary of the Cp–Fe–Cp angle, taking into account only the component in

orbital, which is involved in the σ interaction with both the a_{1g} MO of the unsubstituted Cp unit and the LUMO (π^*) of the fulvene-like structure of the substituted Cp ring (including the exocyclic bond).[238] This participation is clearly observed for the Fc group at C^3 of $\mathbf{110}^{\bullet+}$ due to the increase of $\beta_{in-plane}$, but not for the oxidized ferrocenyl moieties, the Fc group at C^3 of complex $\mathbf{110}^{\bullet+}$, or the ferrocenyl substituent of $\mathbf{94}^{\bullet+}$ whose $\beta_{in-plane}$ values decrease (Fig. 3.23).
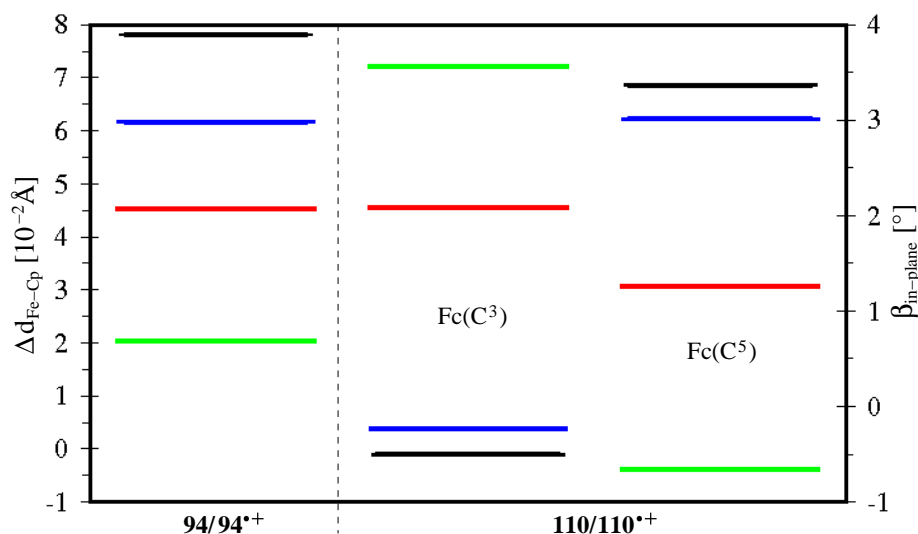
Figure 3.23: Relevant geometrical distortion parameters for ferrocenyl groups in $\mathbf{94/94}^{\bullet+}$ and $\mathbf{110/110}^{\bullet+}$ (Fc at C^3 or C^5) upon oxidation: change in Fc–Cp centroid distances (black: mono-substituted Cp ring; blue: unsubstituted Cp ring; left vertical axis), and $\beta_{in-plane}$ tilt angles in neutral (red) and oxidized (green) species (right vertical axis).

Against this background it is remarkable that the ferrocenyl substituted oxidized $2H$-azaphosphirene complex $\mathbf{94}^{\bullet+}$ shows the same reactivity patterns as methyl and phenyl derivatives $\mathbf{91}^{\bullet+}$–$\mathbf{93}^{\bullet+}$, although the spin centers are localized at different molecule fragments. However, significant differences are found in the relative preferences of alternative reaction pathways, mainly due to the strong stabilization of the oxidized form of $\mathbf{94}^{\bullet+}$, as it is discussed below.

During the ring opening process (ii.g) the radical center is almost completely transferred from the ferrocenyl moiety to phosphorus and the pentacarbonyl tungsten fragment (Tab. 3.18; Fig. 3.25). Thus, the electronic situation of $\mathbf{97l}^{\bullet+}$ resembles the observations made for complexes $\mathbf{97m,c}^{\bullet+}$ and $\mathbf{103}^{\bullet+}$ ($\mathbf{97m}^{\bullet+}$: cf. Tab. 3.15, Section 3.6.3), although a high positive charge density is accepted by the ferrocenyl substituent. Upon dissociation of ferrocenecarbonitrile ($\mathbf{36l}$) from $\mathbf{97l}^{\bullet+}$ (reaction ii.h) the positive

the plane formed by the Fe atom and the C^1-centroid axis at the substituted Cp ring.

charge and the spin center remain at the phosphanylidene complex fragment, which was supported by calculation of the thermochemical data for the hypothetical electron transfer reaction $\mathbf{99^{\bullet+}} + \mathbf{36l} \rightarrow \mathbf{99} + \mathbf{36l^{\bullet+}}$ ($\Delta_R G_{298} = +34.5$ kJ$\cdot$mol^{-1}).

Table 3.18: Evolution of calculated natural charges (q_N) and Mulliken spin populations (ρ_s) for selected fragments of molecules with R' = CH$_3$ and R'' = Fc along reaction path **B** shown in Scheme 3.11.

	$\mathbf{94^{\bullet+}}$	$\mathbf{TS^{ii.g}}$	$\mathbf{97l^{\bullet+}}$	$\mathbf{TS^{ii.e}}$	$\mathbf{113^{\bullet+}}$	$\mathbf{TS^{ii.f}}$	$\mathbf{110^{\bullet+}}$
	Natural Charge (q_N) [au]						
W(CO)$_5$	-0.31	$+0.01$	-0.03	-0.17	-0.30	-0.27	-0.34
PMe	$+0.89$	$+0.76$	$+0.26$	$+0.77$	$+0.96$	$+0.74$	$+0.49$
FcCN(a)	$+0.42$	$+0.23$	$+0.77$	$+0.09$	-0.12	$+0.15$	$+0.51$
FcCN(b)	$-$	$-$	$-$	$+0.31$	$+0.46$	$+0.38$	$+0.34$
	Mulliken Spin Population (ρ_s) [au]						
W(CO)$_5$	0.00	$+0.39$	$+0.44$	$+0.28$	$+0.04$	$+0.11$	0.00
PMe	0.00	$+0.38$	$+0.50$	$+0.61$	$+0.16$	$+0.24$	$+0.00$
N(a)	0.00	$+0.09$	-0.07	-0.07	-0.07	-0.08	-0.01
CFc(a)	$+1.00$	$+0.14$	$+0.14$	$+0.12$	$+0.76$	$+0.66$	$+1.00$
N(b)	$-$	$-$	$-$	$+0.03$	$+0.13$	$+0.07$	0.00
CFc(b)	$-$	$-$	$-$	$+0.05$	$+0.13$	$+0.07$	0.00

(a) FcCN unit that remains at complex $\mathbf{97l^{\bullet+}}$. (b) Attacking nitrile.

Contrary to the methyl and phenyl derivatives, for the further reaction with FcCN pathway **B** is preferred according to the activation barriers of the crucial reaction steps (Tab. 3.16). The barriers for the attack of FcCN at $\mathbf{97l^{\bullet+}}$ (ii.e) and for the subsequent cyclization (ii.f) are not higher than in the case of the phenyl derivative, but a pronounced increase in the activation energy corresponding to the nitrile-promoted 2H-azaphosphirene ring opening (ii.a) yielding acyclic intermediate $\mathbf{107^{\bullet+}}$ is observed. In this case path **A** is kinetically disfavored, and path **B** works not only as a source for the (required) free nitrile but also affords the electrophilic species $\mathbf{97l^{\bullet+}}$ as precursor for the open-chain intermediate $\mathbf{113^{\bullet+}}$.

The origin of this change in the preferred mechanistic pathway is mainly attributed to the very different extent to which the ferrocenyl groups effect the stability of the involved intermediates. Inspection of Figure 3.24 reveals that all Fc-containing cationic species are slightly stabilized by comparison to the Me- or Ph-substituted derivatives, but the first oxidized species, $\mathbf{94^{\bullet+}}$, and the very last one, $\mathbf{110^{\bullet+}}$, are stabilized to a large extent.
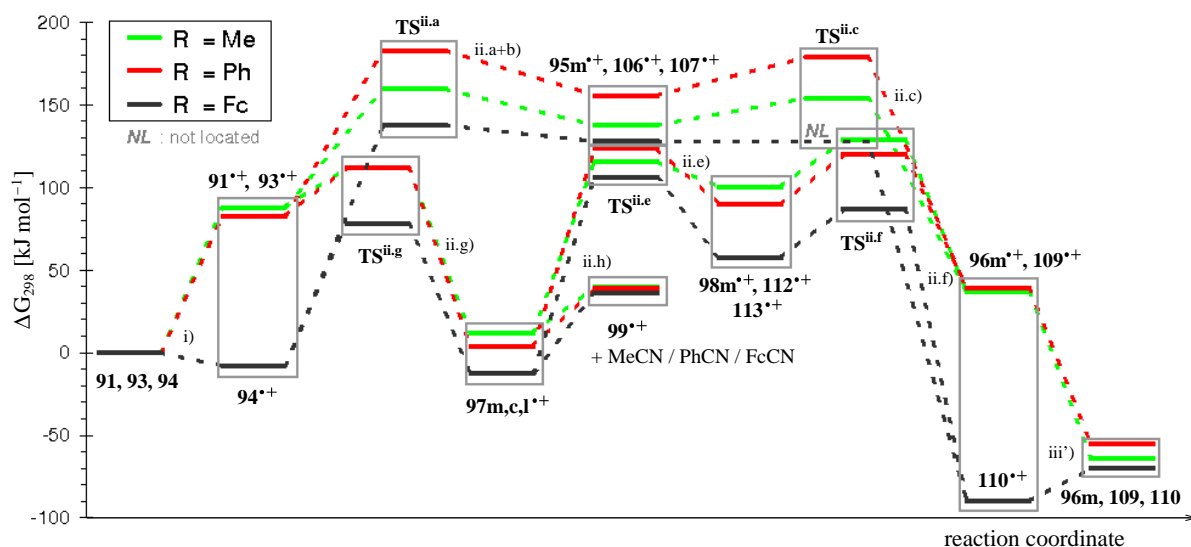
Figure 3.24: Calculated free energy niveaus for reaction steps along pathways **A** and **B** for R' = CH$_3$ and R" = Me (green), Ph (red), and Fc (black) shown in Scheme 3.11 and redox steps i (Scheme 3.8) and iii'. The sum of free energies of the reactants (**91**, **93**, or **94**, and [FeCp$_2$]$^{\bullet+}$) was arbitrarily chosen as zero-point of the ΔG_{298} scale. Each step is appropriately counterbalanced both in matter (added reagents or lost units) and charge (by means of the $[FeCp_2]^+/[FeCp_2]$ redox couple (i, iii')).

The reason for that should come from the different stabilization of the unpaired electron and the positive charge. In the course of pathway **B** the spin center, which was previously shifted towards phosphorus and the W(CO)$_5$ fragment in **97l**$^{\bullet+}$ (Tab. 3.18 and Fig. 3.25), is back-transferred to the ferrocenyl group Fc(a) upon attachment of the second ferrocenecarbonitrile (ii.e), thus reaching a positive spin population of $\rho_s(\mathrm{CFc(a)}) = +0.76$ au at this moiety[52] in acyclic intermediate **113**$^{\bullet+}$. After cyclization the spin density is completely shifted to this group, and the positive charge is shared between both ferrocenyl substituents and the phosphorus center.

On the other hand, in acyclic intermediate **107**$^{\bullet+}$ (Fig. 3.25), which is formed via pathway **A** (ii.a), almost no spin population is delocalized towards the Fc moieties ($\rho_s = +0.06$ (Fc(a)) and $+0.02$ au (Fc(b))); here the spin center is (as in the cases of Me- and Ph-derivatives) mainly localized at the nitrogen center of the former 2H-azaphosphirene ring ($\rho_s = +0.88$ au).

---

[52]Thereof only a population of $\rho_s = +0.16$ au is localized at the carbon center that carries the Fc substituent.
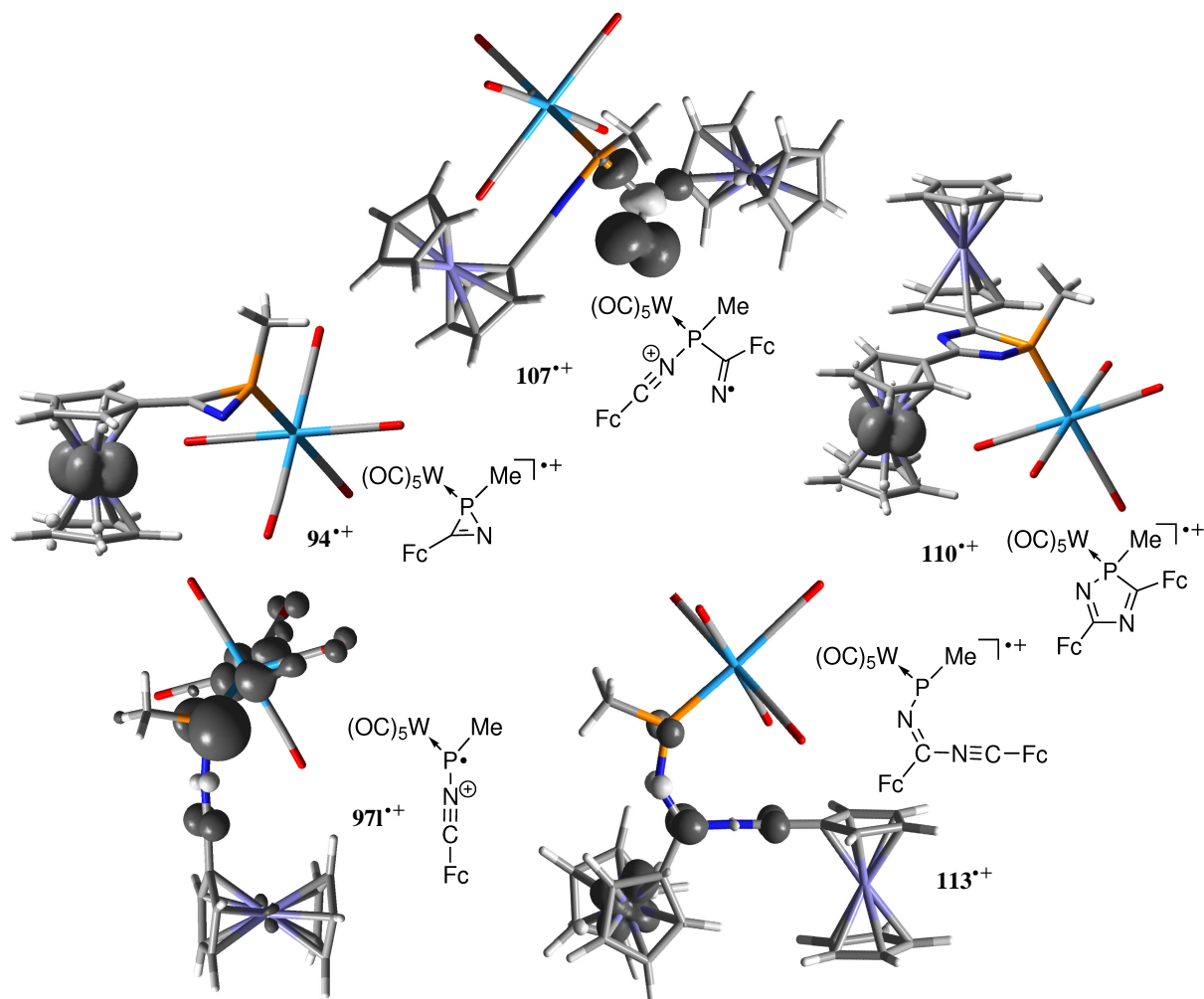
Figure 3.25: Calculated Mulliken spin density distributions (isodensity surface at 0.005 au) for ferrocenyl substituted complexes **94•+**, **97l•+**, **107•+**, **110•+**, **113•+**.

In summary, by ferrocenyl substitution a significant amount of spin density is shifted to a Fc group both in **94•+** and **110•+** as well as in intermediate **113•+**, but it has almost no effect in delocalizing the spin density in radical cationic nitrilium phosphane ylide complex **97l•+** or in **107•+**. This selective Fc-mediated spreading of the unpaired electron and the resulting stabilization of complex **94•+** in relation to **107•+** hamper the formation of **107•+** through path **A**. Thereby, path **B** is indirectly favored, as **113•+** shows enhanced stability through Fc dispersion of the unpaired electron density in relation to **97l•+**.

Finally, the endergonic character of the formation of a radical cationic phosphanyli-dene complex fragment (**99•+**, **104•+**) can largely be compensated by the highly ex-ergonic reaction with PF_6^- leading to difluorophosphane complexes **119**, **120** as final

products (Tab. 3.16). This reaction could proceed via radical intermediates $117^{\bullet}$, $118^{\bullet}$ in two sequential fluorination steps (Scheme 3.13).[53]
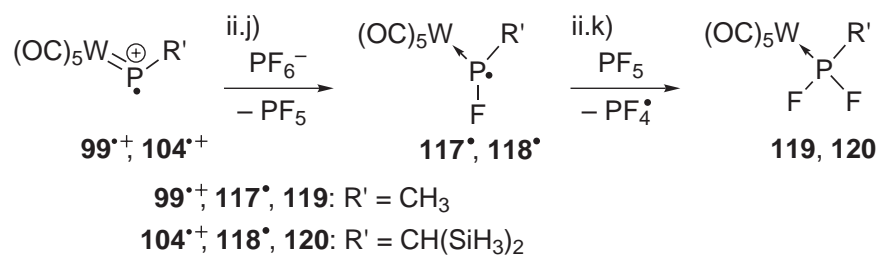
Scheme 3.13: Calculated model reactions of radical cationic phosphanylidene complexes $99^{\bullet+}$, $104^{\bullet+}$ with the hexafluorophosphate anion.

---

[53]Note that this reaction sequence is just one of several conceivable alternatives leading from $99^{\bullet+}$, $104^{\bullet+}$ to **119**, **120**; intermediately occurring redox subsequences could also be envisaged.

3.7 Conclusions

Experimental investigations on the *oxidative SET protocol* revealed that the capability of ferrocinium salts to induce ring expansion of 2H-azaphosphirene complexes with nitriles depends strongly on the amount of ferrocinium salt, the nature of the nitrile, and on the nature of the 2H-azaphosphirene complex employed (Section 3.1). Good results were obtained with comparatively electron-rich nitrile derivatives such as dimethyl cyanamide (**36b**) and hetaryl carbonitriles **36d–g**. Reactions of **35** with **36d–g** in the presence of 0.05 equivalents of [FeCp$_2$][PF$_6$] were complete within short reaction times, and it was demonstrated that 0.025 equivalents of [FeCp$_2$][PF$_6$] are sufficient to induce complete conversion of **35** in the reaction with nitrile **36g**; silver(I) and copper(II) triflate could be applied as well. Studies using varying amounts of [FeCp$_2$][PF$_6$] supported a radical cation chain reaction mechanism (see Scheme 3.2).

Weak nucleophilic nitriles did not react with 2H-azaphosphirene complexes **35** and **67** under these conditions: complex **35** showed no reaction with very electron-deficient nitrile derivatives C$_6$F$_5$CN and EtO$_2$CCN (Section 3.2), the reaction with HCN remained incomplete, and 3-ferrocenyl-2H-azaphosphirene complex **67** did not react with dinitrile NCCH$_2$CH$_2$CN (Section 3.2.1). In these cases side-reactions occurred with PF$_6^-$ from the ferrocinium salt, which points to the formation of highly electrophilic intermediates. Such side-reactions could be suppressed by using ferrocinium tetraphenylborate (instead of [FeCp$_2$][PF$_6$]), but even in the *absence of nitriles* symmetrically 3,5-disubstituted 2H-1,4,2-diazaphosphole complexes were formed (Section 3.3); the structure of 3,5-diferrocenyl-2H-1,4,2-diazaphosphole complex **69l** was determined by X-ray crystallography. Here, the nitrile that is required for the formation of these products stems from another equivalent of the 2H-azaphosphirene complex.

The applicability of the ferrocinium salt-induced ring expansion methodology to 2H-azaphosphirene molybdenum and chromium complexes seems to be limited (Section 3.4). Compared to the reaction of tungsten complex **35**, reactions of complexes **70** and **71** with benzonitrile were significantly slower, and the products suffered from decomplexation during the reactions.

Cyclic voltammetric investigations on some selected 2H-azaphosphirene and 2H-1,4,2-diazaphosphole complexes revealed irreversible oxidations for each 3-phenyl substituted derivative investigated (Section 3.5), which points to oxidation at the M(CO)$_5$ center. This is contrary to the situation of 3-ferrocenyl-2H-azaphosphirene complex **67** where the oxiation takes place at the ferrocenyl moiety.[128] Complex **69l** showed two reversible redox waves according to consecutive one-electron oxidations of both ferrocenyl units. For each 2H-1,4,2-diazaphosphole complex investigated a reversible

one-electron reduction wave was found, in addition.

DFT calculations revealed that 3-methyl- and 3-phenyl-2H-azaphosphirene model complexes **91**–**93** are oxidized at the pentacarbonyl metal fragment, while in the case of 3-ferrocenyl substituted complex **94** the oxidation of takes place at the ferrocenyl moiety (Section 3.6). The primary products **91**$^{\bullet+}$–**94**$^{\bullet+}$ in each case have a retained cyclic structure, and the positive charge is attributed to phosphorus. Nucleophilic attack of strongly or moderately nucleophilic model nitriles (H$_2$NCN, MeCN, PhCN, FcCN) at the phosphorus center of **91**$^{\bullet+}$–**94**$^{\bullet+}$ leads to acyclic intermediates **95m,p**$^{\bullet+}$, **105**$^{\bullet+}$–**107**$^{\bullet+}$, which can subsequently undergo facile cyclization to give radical cationic 2H-1,4,2-diazaphosphole complexes **96m,p**$^{\bullet+}$, **108**$^{\bullet+}$–**110**$^{\bullet+}$. The latter are reduced by reactants **91**–**94** with formation of neutral products **96m,p**, **108**–**110** and the reactive species **91**$^{\bullet+}$–**94**$^{\bullet+}$, which then can restart the chain reaction.

On the other hand, reactions with very electron-poor nitrile derivatives were not supported by the calculations, since nucleophilic attack of NCCN at the phosphorus center of **91**$^{\bullet+}$ proceeds via a high barrier and leads to displacement of the MeCN moiety from the latter (Section 3.6.2).

In the absence of nitriles complexes **91**$^{\bullet+}$–**94**$^{\bullet+}$ can rearrange to radical cationic nitrilium phosphane ylide complexes **97c,l,m**$^{\bullet+}$, **103**$^{\bullet+}$ in one step (Sections 3.6.3 and 3.6.4). Subsequent dissociation provides a nitrile, which can react either with another equivalent of **91**$^{\bullet+}$–**94**$^{\bullet+}$ or with **97c,l,m**$^{\bullet+}$, **103**$^{\bullet+}$ to give symmetrically 3,5-disubstituted complexes **96m**$^{\bullet+}$, **108**$^{\bullet+}$–**110**$^{\bullet+}$ and after reduction **96m**, **108**–**110**. The latter alternative is formally a cycloaddition reaction; it is the preferred pathway when Ar = Fc.

It should be noted that the oxidative SET protocol is in multiple senses complementary to the thermally or photochemically induced ring expansions of 2H-azaphosphirene complexes with nitriles described in the introduction (cf. Section 1.3). The most obvious differences being bond- and regio-selectivities. While under the latter conditions the P,C bond of the 2H-azaphosphirene complex is broken, and preferentially 2H-1,3,2-diazaphosphole complexes or mixtures thereof with 2H-1,4,2-diazaphosphole complexes are obtained,[146, 158] the SET-induced ring expansion selectively addresses the P,N bond and is highly regioselective. Moreover, the two synthetic routes are complementary with respect to the electronic properties of the employed trapping reagent. Thermally or photochemically, nitrilium phosphane ylide complexes (**XXV**) are generated (Section 1.3, Scheme 1.11), which react preferentially with electron-poor nitrile derivatives.[114] The current investigations revealed that SET-induced ring expansion reactions require the employment of rather electron-rich nitriles.

Chapter 4

Acid-Induced Ring Expansion of $2H$-Azaphosphirene Complexes

As outlined in the introduction, in nitrogen heterocyclic chemistry the use of Lewis and Brønsted acids to achieve C,N bond activation of small, strained heterocycles such as aziridines (**I**)[3,4] and $2H$-azirenes (**XI**)[52,53] (cf. Figures 1.1 and 1.2, Chapter 1) has found widespread applicability.[20–22, 27–29, 78, 79, 82, 83, 87–94, 105, 109, 112] Surprisingly, evidence for aziridinium derivatives (**XXVII**) (Fig. 4.1) formed intermediately is typically scarce,[239] and no definitive proof for $2H$-azirenium derivatives (**XXVIII**) has been provided so far.[79, 82, 83, 91, 92]

Figure 4.1: N-Protonated three-membered heterocycles: aziridinium (**XXVII**)[239] and $2H$-azirenium derivatives (**XXVIII**).[79, 82, 83, 91, 92]

Therefore, it is remarkable that the knowledge about the synthetic use of Brønsted acids in phosphorus heterocyclic chemistry is still very limited, especially in the area of ring expansion reactions. An early example for an intramolecular ring enlargement stems from aza-$\sigma^4\lambda^5,\sigma^3\lambda^3$-diphosphiridine chemistry where trifluoromethanesulfonic acid (CF$_3$SO$_3$H) was employed to induce a rearrangement to a 1,3-diaza-2,4-diphosphetidine via selective P,P bond cleavage.[240] Other three-membered ring systems with two phosphorus centers such as diphosphiranes[241] and $1H$-diphosphirenes[242] were reacted with hydrogen chloride, but no evidence for P-protonated species was obtained; in these cases substitution reactions occurred.

Within the scope of this Thesis, the applicability of Brønsted and Lewis acids to induce ring expansion of 2*H*-azaphosphirene complexes was investigated; one focus should be to examine reaction mechanisms.

4.1 Ring Expansion Induced by Triflic Acid

First, a strong Brønsted acid, namely trifluoromethanesulfonic acid (CF_3SO_3H; hereafter referred to as triflic acid or TfOH), was chosen to react with 2*H*-azaphosphirene complex **35** in CH_2Cl_2 in the presence of nitrile derivatives **36b,g,m,r–t** (Scheme 4.1).[1] The initially pale yellow solutions immediately turned very intensely colored (**36b**: deep red, **36g**: deep green, **36m,r–t**: deep purple). Upon subsequent addition of triethylamine at ambient temperature a color change to yellow or light orange occurred, and the formation of 2*H*-1,4,2-diazaphosphole complexes **41b,g,m,r–t** was observed.

36, **41**: R = NMe₂ (**b**), 2-thienyl (**g**), CH₃ (**m**), *t*Bu (**r**), 1-adamantyl (**s**), SiMe₃ (**t**)
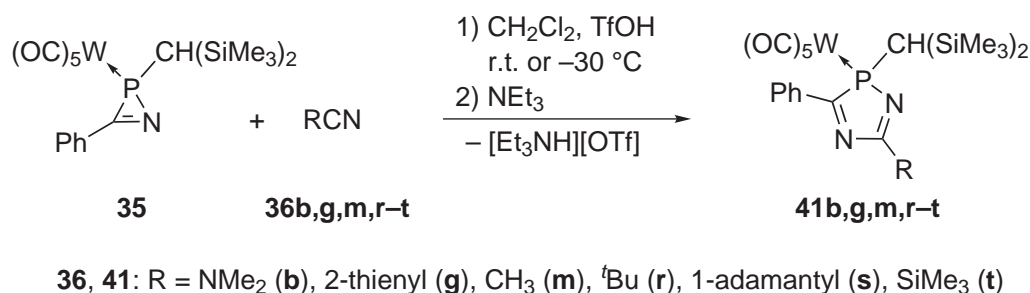
Scheme 4.1: One-pot syntheses of **41b,g,m,r–t** using 2*H*-azaphosphirene complex **35**, TfOH, nitriles **36b,g,m,r–t**, and NEt₃.

Likewise, reaction of *P*-Cp* substituted 2*H*-azaphosphirene complex **121**[125] (Cp* = 1,2,3,4,5-pentamethyl-2,4-cyclopentadien-1-yl) with **36b** and triflic acid yielded after deprotonation the selective formation of 2*H*-1,4,2-diazaphosphole complex **122b** (Scheme 4.2). The addition of TfOH was carried out at −78 °C using a more dilute solution, while performing the reaction at ambient temperature led to the formation of several by-unidentified products. It turned out that the workup was easier if pyridine was used as deprotonating reagent (instead of triethylamine).

The reaction of **35** with **36g** serves as a good case in point, as even catalytic amounts (0.1 equiv.) of TfOH were sufficient to complete the ring expansion within 24 hours. By

---

[1]In all reactions, the addition of TfOH was carried out either at room temperature or (in the presence of **36r,s**) at −30 °C.

^{31}P NMR spectroscopic reaction monitoring only the resonance of **41g** was detected, which increased at the expense of that of **35**.

The reaction of **35** with TfOH and trimethylsilyl cyanide (**36t**) yielded after deprotonation besides target product **41t** $2H$-1,4,2-diazaphosphole complex **41h** (R = H).[2] During the reaction the $^{29}Si\{^1H\}$ NMR resonance of Me_3SiOTf ($\delta = 44.2$) was detected (before addition of NEt_3), hence, partial desilylation had occurred at one stage of the reaction sequence. Nevertheless, complex **41t** could be separated from the resulting mixture via low-temperature column chromatography (8 % yield).

All other reactions were highly selective, and the products were isolated in good (**41b,g,m,r,s**: 65−93 %) or moderate yields (**122b**: 25 %) using low-temperature column chromatography. If the reactions were carried out at ambient temperature, they were complete whithin a few seconds, and in none of the reactions the formation of a by-product such as 3,5-diphenyl-$2H$-1,4,2-diazaphosphole complex **41c** was observed. This protocol offers new synthetic perspectives as even nitrile derivatives with high steric demand (**36r,s**) could successfully be employed, and the use of nitrile derivative **36t** enabled access to the first C-SiMe$_3$ ring-functionalized $2H$-1,4,2-diazaphosphole complex **41t**. However, it should be mentioned that even under these conditions an insertion of the very electron-poor nitrile pentafluorobenzonitrile (**36j**) could not be achieved (cf. Section 3.2).
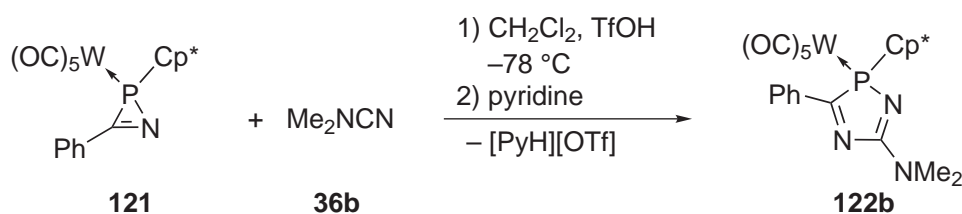
Scheme 4.2: One-pot synthesis of **122b** using $2H$-azaphosphirene complex **121**, TfOH, dimethyl cyanamide (**36b**), and pyridine.

Complexes **41b,g,m,r–t** and **122b** were characterized by multinuclear NMR experiments, mass spectrometry, IR and UV/Vis spectroscopy. The ^{31}P resonances of 5-alkyl-$2H$-1,4,2-diazaphosphole complexes **41m,r,s** appear in the same range ($\delta = 107-110$) as those of 5-hetaryl derivatives **41d–g** (cf. Tab. 3.1, Section 3.1),[3] and a common $|^1J_{WP}|$ value about 229 Hz was observed for **41m,r,s**. The resonance of P-Cp* derivative **122b** appears at significantly lower field ($\delta = 118.5$) than that of **41b** ($\delta =$

---

[2]The synthesis of complex **41h** is presented in Section 4.1.3.

[3]Note that most of the data compiled in Table 3.1 refer to measurements in CDCl$_3$. NMR data for all complexes **41b,g,m,r–t** were obtained from C$_6$D$_6$ solutions, hence, only the latter are compared in the following; $^{31}P\{^1H\}$ NMR data for **41b,g,m,r–t** are given in Table 4.2.

101.8), which seems to be a common trend within a given class of P-CH(SiMe$_3$)$_2$ and P-Cp* substituted heterocyclic compounds.[157] The smallest tungsten–phosphorus coupling constant magnitude was observed for complex **41t** (223.8 Hz).

The ^{13}C resonances of the C^3 centers of complexes **41b,g,m,r–t** and **122b** appear at $\delta = 199-202$ and have phosphorus–carbon coupling constants of $19-26$ Hz in magnitude (Tab. 4.1). While the C^5 centers of complexes **41b,g** resonate in the same range ($\delta = 165-166$), the corresponding signals of **41m,r–t** appear at somewhat lower field ($\delta = 174-183$). The largest $|^{2+3}J_{PC}|$ value was found for complex **41t** (15.2 Hz). An interesting feature of the NMR data for **41t** is the order, with respect to chemical shifts, of resonances corresponding to the three trimethylsilyl groups. While the ^{1}H and ^{29}Si NMR signals of the C^5-SiMe$_3$ group are between those of the two distinct SiMe$_3$ groups of the CH(SiMe$_3$)$_2$ moiety, its ^{13}C resonance is upfield from both trimethylsilyl carbon resonances of the latter.

Table 4.1: ^{13}C{^{1}H} NMR spectroscopic data for ring carbon centers of neutral complexes **41b,g,m,r–t**, **122b** and protonated complexes **123b**, **124b** (see Section 4.1.1).

No.	R	R'	$\delta(^{13}\text{C}^3)$	$|^{1+4}J_{PC^3}|$ [Hz]	$\delta(^{13}\text{C}^5)$	$|^{2+3}J_{PC^5}|$ [Hz]
41b$^\sharp$	NMe$_2$	CH(SiMe$_3$)$_2$	200.3	25.5	165.0	–
41g$^\sharp$	2-thienyl	CH(SiMe$_3$)$_2$	202.3	23.3	165.2	4.2
41m$^\sharp$	CH$_3$	CH(SiMe$_3$)$_2$	202.1	22.6	174.0	7.1
41r$^\sharp$	^{t}Bu	CH(SiMe$_3$)$_2$	201.2	22.3	182.9	8.4
41s$^\sharp$	1-adamantyl	CH(SiMe$_3$)$_2$	201.0	22.3	182.2	8.4
41t$^\sharp$	SiMe$_3$	CH(SiMe$_3$)$_2$	199.4	19.1	188.5	15.2
122b$^\sharp$	NMe$_2$	Cp*	199.3	24.6	166.3	3.6
123b†	NMe$_2$	CH(SiMe$_3$)$_2$	196.9	3.2	162.4	10.3
124b†	NMe$_2$	Cp*	193.6	1.3	161.0	8.1

$^\sharp$In C$_6$D$_6$. †In CD$_2$Cl$_2$.

The ^{15}N NMR resonances of the ring nitrogen atoms of complex **41m** were detected at $\delta = -116$ ($|^{1+4}J_{PN}| = 55$ Hz; N^1) and $\delta = -52$ (N^4) in an ^{1}H,^{15}N HMQC experiment via correlations with the protons of the 5-methyl group; a further long-range correlation with the CH-proton of the bis(trimethylsilyl)methyl moiety was observed for the N^1

center. Also the N^1 center of complex **41g** displays a resonance at $\delta = -116$, and for **41b** the N^1 resonance was detected at $\delta = -200$ ($|^{1+4}J_{PN}| = 55\,\text{Hz}$); the dimethylamino nitrogen resonates at $\delta = -299$.

The molecular structure of complex **41s** was determined by a single-crystal X-ray diffraction study (Fig. 4.2).[4] Its $2H$-1,4,2-diazaphosphole ring has similar structural features as observed for complexes **41b,g** (cf. Section 3.1): a comparatively long endocyclic P,C bond, a long W,P bond, and an acute endocyclic angle at phosphorus. Likewise, the phosphorus heterocycle of **41s** is almost planar[5] and adopts a largely coplanar arrangement with the phenyl substituent.[6]
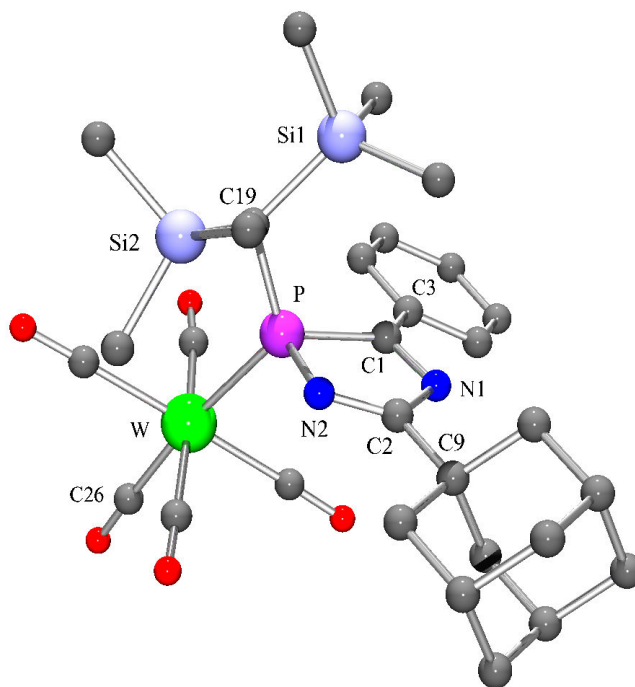
Figure 4.2: Molecular structure of complex **41s** in the crystal (hydrogen atoms omitted for clarity). Selected bond lengths [Å] and angles [º]: W–C(26) 1.997(4), W–P 2.5296(15), P–N(2) 1.704(4), P–C(1) 1.875(4), C(1)–N(1) 1.295(5), C(2)–N(2) 1.281(4), C(2)–C(9) 1.500(5), C(1)–C(3) 1.462(5), N(2)–P–C(1) 90.51(17), P–C(1)–N(1) 108.8(3), C(1)–N(1)–C(2) 110.9(3), N(1)–C(2)–N(2) 119.8(4), C(2)–N(2)–P 109.7(3).

FAB-mass spectra (positive mode) of complexes **41b,g,m,r–t** revealed consecutive losses of the CO ligands as the major fragmentation pathway. A remarkable feature of the spectra is that the signals of the protonated liberated heterocyclic ligand systems $[\mathbf{50b,g,m,r\text{–}t} + \text{H}]^+$ (m/z 364, 403, 335, 377, 455, and 393) have the highest intensity

---

[4]Monoclinic space group P $2_1/a$.

[5]Mean deviation from least-squares plane: 0.023 Å.

[6]Torsion angle between least-squares planes: 12.6 º.

in each case (cf. Section 3.1, Fig. 3.7), which demonstrates the lability of the W,P bond of 2*H*-1,4,2-diazaphospholium complexes.

4.1.1   First Investigations on the Reaction Course

The first step of investigations on the reaction course was to carry out reactions of **35** and **121** with dimethyl cyanamide (**36b**) and TfOH but without subsequently adding a base (Scheme 4.3). After workup the triflate salts **123b** and **124b** having N^1-protonated 2*H*-1,4,2-diazaphosphole complexes as cations were obtained as red powders in good yields (88 and 94 %). The constitutions of **123b** and **124b** were unambiguously identified by multinuclear NMR experiments and mass spectrometry. Recrystallization of **123b** gave single crystals suitable for an X-ray diffraction study (Fig. 4.4). Complex **123b** was independently synthesized through the reaction of pure complex **41b** with triflic acid (Scheme 4.3), which corroborates the assumption that **123b** is thermodynamically favored over its N^4- and NMe$_2$-protonated tautomers and does not neccessarily correspond with the primarily[243] formed tautomer in the reaction of **35** with TfOH and **36b**.

35, 121   **36b**   **123b, 124b**   **41b**

35, 41b, 123b: R' = CH(SiMe$_3$)$_2$
          121, 124b: R' = Cp*
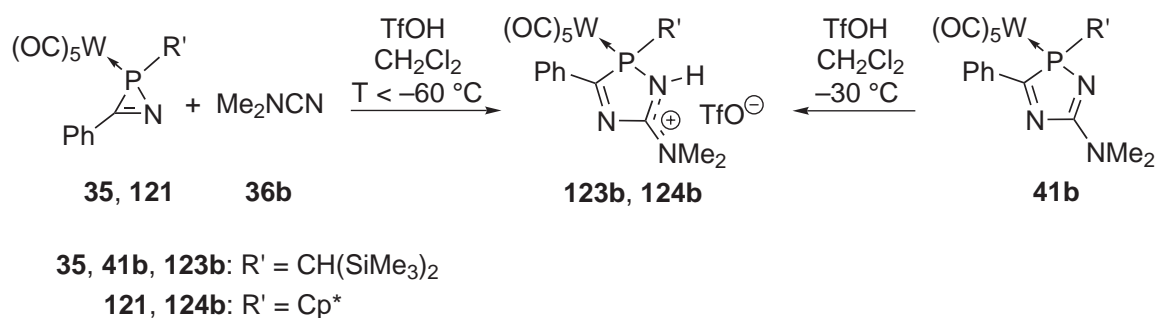
Scheme 4.3: Reactions of 2*H*-azaphosphirene complexes **35** and **121** with dimethyl cyanamide (**36b**) and TfOH, and reaction of 2*H*-1,4,2-diazaphosphole complex **41b** with TfOH.

The ^{1}H NMR spectra of **123b** and **124b** show each a broad doublet at low field corresponding to the *N*-bonded proton (**123b**: $\delta = 10.09$, $h_{1/2} = 7.8$ Hz, $|^2J_{PH}| = 22.9$ Hz; **124b**: $\delta = 10.35$, $h_{1/2} = 6.4$ Hz, $|^2J_{PH}| = 23.2$ Hz). The protonated nitrogen atom further shows a long-range correlation with the CH-proton of the bis(trimethylsilyl)-methyl moiety as estimated from ^{1}H,^{15}N HMQC experiments (**123b**: $\delta(^{15}$N$) = -264$, $|^{1+4}J_{PN}| = 22$ Hz, $|^1J_{NH}| = 92$ Hz; **124b**: $\delta(^{15}$N$) = -273$, $|^{1+4}J_{PN}| = 35$ Hz, $|^1J_{NH}| = 93$ Hz), which confirms the assignment to N^1 (Fig. 4.3). Accordingly, protonation of **41b** causes a high field shift of the N^1 resonance by 64 ppm, and the phosphorus–nitrogen coupling constant magnitude of this N center is decreased by 23 Hz (**41b**:

$|^{1+4}J_{PN}| = 55$ Hz). On the other hand, the resonance of the dimethylamino nitrogen is 30 ppm shifted to lower field. Both trends are in accordance with observations made for protonated amidines,[244, 245] guanidines,[244, 245] and imidazoles.[244, 246] For instance, protonation of 1-methylimidazole, which occurs at N^3 (the pyridine-like N atom), causes a high field shift for this nitrogen center by 73.0 ± 0.2 ppm, while a low field shift by 8.0 ± 0.2 ppm was observed for the ^{15}N resonance of N^1 (pyrrole-like N atom).[246] It should be noted that a clear assignment of the protonated nitrogen of **123b** and **124b** to N^1 (rather than N^4) was only possible on the basis of the ^{15}N NMR spectroscopic data. Concerning this distinction $^1H,^{13}C$ HMBC NMR measurements did not yield conclusive results, since the NH proton showed correlations with both ring carbon atoms.
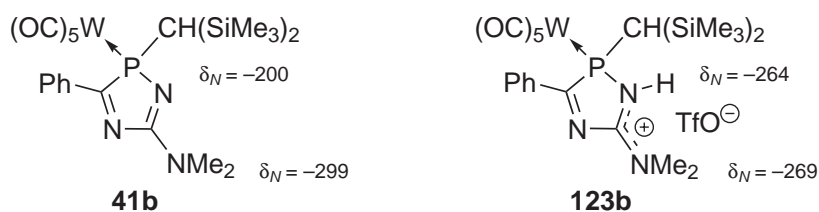
Figure 4.3: Assignment of ^{15}N NMR chemical shifts (δ_N vs. MeNO$_2$) for complexes **41b** (C$_6$D$_6$) and **123b** (CD$_2$Cl$_2$).

Comparison of the $^{13}C\{^1H\}$ NMR spectroscopic data for complexes **123b**, **124b** and their neutral congeners **41b** and **122b** reveals that the chemical shifts of the ring carbons are almost unaffected by protonation (Tab. 4.1). For both C^3 and C^5 a net high field shift around $3-6$ ppm is observed. More pronounced is the effect on the phosphorus–carbon coupling constant magnitudes of these centers. While the $|^{1+4}J_{PC}|$ values of the C^3 centers are significantly decreased (by $22-23$ Hz), for the C^5 centers an increase of $|^{2+3}J_{PC}|$ values is observed (by $5-10$ Hz). The carbon resonances of the CO groups *trans* with respect to the heterocyclic ligands are shifted to slightly higher field (by $2-3$ ppm), and their phosphorus–carbon coupling constant magnitudes are about 5 Hz increased upon protonation. As estimated for the pair **41b**/**123b** the tungsten–carbon coupling constant magnitude of the *trans*-CO ligand decreases slightly (by 1.2 Hz), thus indicating a stronger *trans* influence of the cationic compared to the neutral heterocyclic ligand.

The ^{31}P NMR chemical shifts of the P-CH(SiMe$_3$)$_2$ and the P-Cp* substituted derivative are affected in different ways through N-protonation (Tab. 4.2): while in the former case a low field shift is observed ($\Delta\delta = +3.9$ (**123b** vs. **41b**)), the latter experiences a high field shift ($\Delta\delta = -3.6$ (**124b** vs. **122b**)). In both cases an increase of the tungsten–phosphorus coupling constant magnitude is observed ($\Delta|^1J_{WP}| = 10.2$ Hz (**123b** vs. **41b**) and 7.7 Hz (**124b** vs. **122b**)).

The solid state structure of complex **123b** (Fig. 4.4) shows that the five-membered ring is not distorted from planarity due to protonation (mean deviation from least-squares plane: 0.024 Å; cf. complex **41b**: 0.031 Å), and it adopts a largely coplanar arrangement with the phenyl substituent (torsion angle between least-squares planes: 9.2 °).
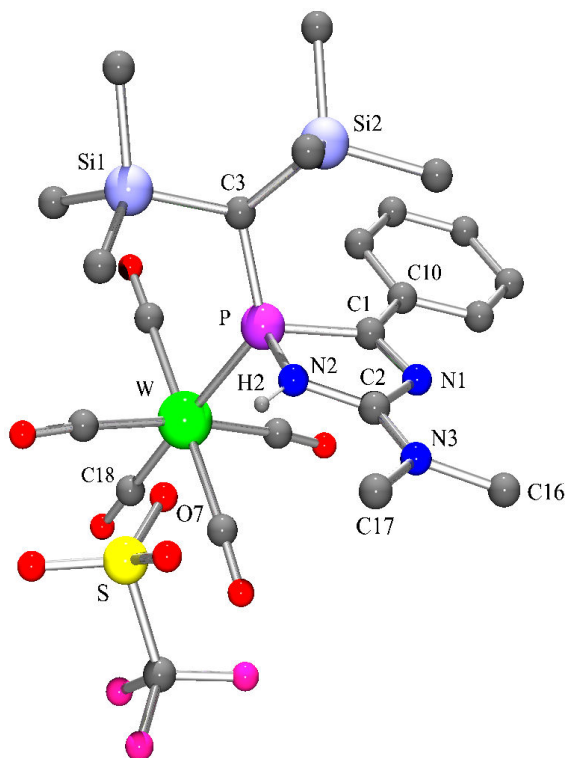
Figure 4.4: Molecular structure of complex **123b** in the crystal (except for H2 all hydrogen atoms omitted for clarity). Selected bond lengths [Å] and angles [°]: W–C(18) 2.011(7), W–P 2.5077(15), P–N(2) 1.740(5), P–C(1) 1.844(6), C(1)–N(1) 1.299(7), C(2)–N(2) 1.345(7), C(2)–N(3) 1.319(7), C(1)–C(10) 1.466(7), N(2)···O(7) 2.821(6), N(2)–P–C(1) 86.5(2), P–C(1)–N(1) 113.6(4), C(1)–N(1)–C(2) 110.8(5), N(1)–C(2)–N(2) 116.4(5), C(2)–N(2)–P 112.0(4), N(2)–C(2)–N(3) 125.5(5).

Comparison of the structure of **123b** with that of **41b** (Fig. 3.3) reveals that the exocyclic C(2),N(3) bond is further shortened (by 0.014 Å) and the endocyclic C(2),N(2) bond is lengthened upon protonation (by 0.033 Å), although the effect is not very large. However, it is conceivable that π-electron delocalization within the amidinium moiety of **123b** (and likewise **124b**) is responsible for favoring N[1]-protonated complexes over their N[4]-protonated tautomers, as it should provide strong thermodynamic stabilization. It is noteworthy that protonation of the N(2) atom[7] causes a significant

---

[7]H(2) at N(2) was located in the Fourier difference electron density.

elongation of the P,N(2) bond (by 0.058 Å), while the endocyclic P,C(1) bond is shortened by 0.040 Å. Furthermore, *N*-protonated complex **123b** exhibits smaller endocyclic angles at C(2) and P than complex **41b**, and the W,P bond is significantly shortened upon protonation (by 0.026 Å).[8]

All C,O stretch vibration bands in the IR and Raman spectra of cationic complexes **123b** and **124b** appear at larger wavenumbers than those of their neutral counterparts **41b** and **122b** (cf. spectra of **41b** and **123b**: Fig. 4.5; corresponding data are compiled in Table C.2, Appendix C). Because all spectra show several overlapping bands in the region about $1900-1960$ cm^{-1} that do not permit a clear assignment, an estimation of force constants according to the procedure described by Cotton and Kraihanzel[247] did not yield conclusive results. These bands are assigned to vibrations of local A_1 and E symmetry. Presumably due to symmetry reduction in the solid state, complexes **41b,g,m,r–t**, **122b**, **123b**, and **124b** deviate from the C_{4v} point group. As a consequence, in most cases more than two bands are found in this region. In a CH$_2$Cl$_2$ solution IR experiment carried out on complex **123b** as a good case in point (Fig. 4.5, C) in this region only one broad band with high intensity was detected.

Comparison of IR and Raman spectra allowed the assignment of one separated band at higher wavenumbers ($1976-2009$ cm^{-1}) that exhibits a low intensity in the IR but the highest intensity in the Raman spectra to a vibration of local B_1 symmetry. According to selection rules this band should be *IR inactive* within the C_{4v} point group. In fact, it emerges in the spectra of all neutral and protonated $2H$-1,4,2-diazaphosphole complexes (cf. Tab. C.2), but its intensity is always low, thus indicating a low transition probability of the corresponding normal mode. Even in solution this band does not vanish, although its intensity is significantly decreased as shown for complex **123b** in Figure 4.5 (C).

A single, isolated band >2060 cm^{-1} could be assigned to an A_1-mode that is regarded as indicative for the strength of the C,O bond *trans* to the heterocyclic ligand.[247,248] Protonation causes a shift of this band by 11 (**123b** vs. **41b**) and 13 cm^{-1} (**124b** vs. **122b**), which corroborates the idea of a stronger *trans* influence of the cationic heterocyclic ligand as indicated by the structural data for the pair **41b/123b**.

---

[8]This is accompanied with a slight lengthening of the tungsten bond to the *trans*-CO ligand (by 0.022 Å), while the C,O bond of this ligand shows a slight shortening (by 0.022 Å). Although both effects are not very pronounced, they imply a stronger *trans* influence of the cationic compared to the neutral heterocyclic ligand. This interpretation is further supported by the comparison of the NMR data for **41b** and **123b** as well as their IR spectroscopic data (vide infra).
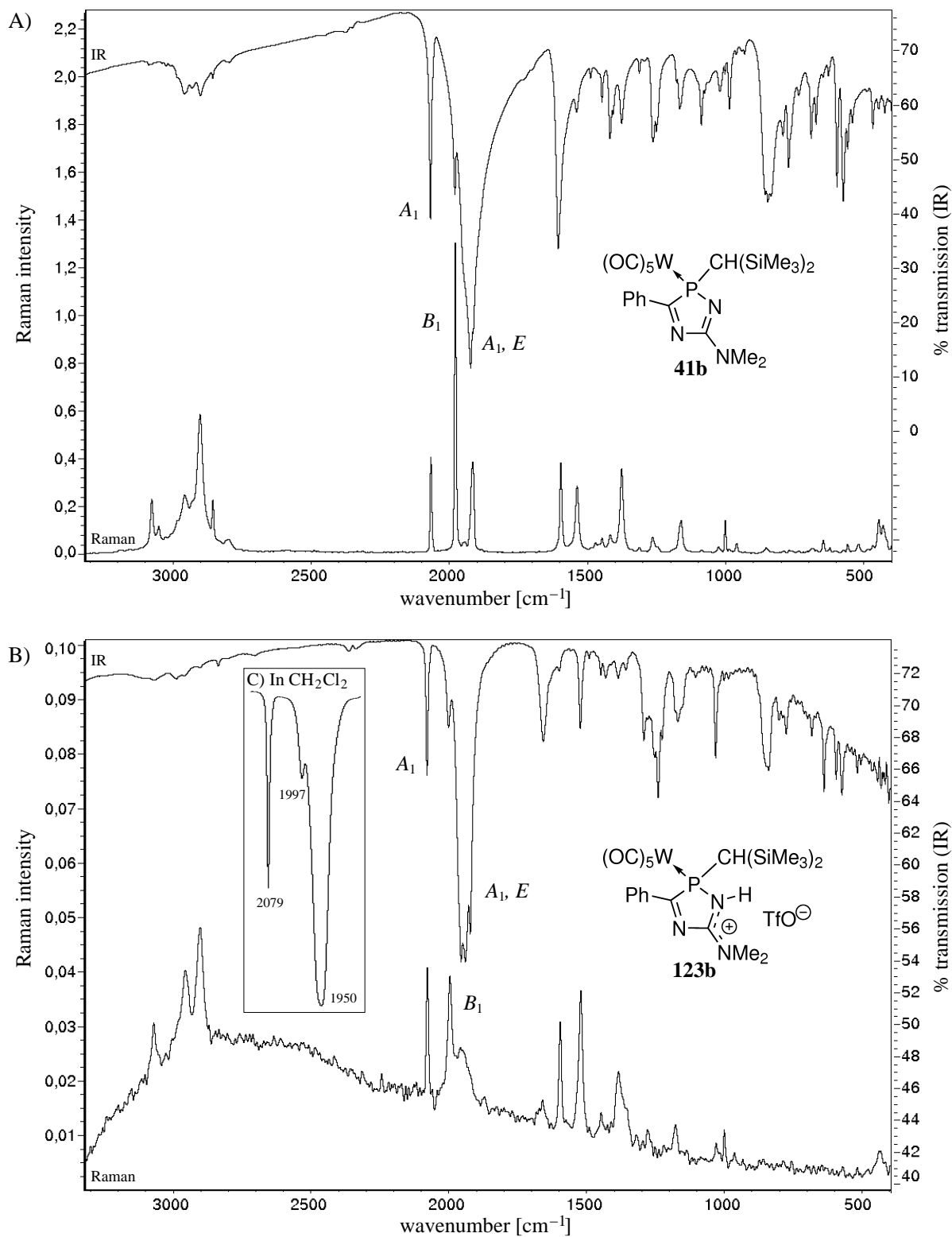
Figure 4.5: IR (KBr; right vertical axis) and Raman spectra (left vertical axis) of A) complex **41b** and B) complex **123b**. C) C,O stretch vibration bands of a spectrum of **123b** recorded in CH_2Cl_2 solution (wavenumbers in cm^{-1}).

Monitoring of reactions of **35** with nitrile derivatives **36g,m,r–t** and TfOH (before adding the base) by ^{31}P NMR spectroscopy revealed evidence for the formation of 2H-1,4,2-diazaphospholium complexes **123g,m,r–t** (Scheme 4.4; Tab. 4.2).

36, 123: R = 2-thienyl (**g**), CH$_3$ (**m**), ^{t}Bu (**r**), 1-adamantyl (**s**), SiMe$_3$ (**t**)

Scheme 4.4: Reactions of 2H-azaphosphirene complex **35** with nitriles **36g,m,r–t** and TfOH.

The ^{31}P NMR resonances of all N-protonated complexes **123g,m,r–t** are shifted to lower field compared with their neutral counterparts **41g,m,r–t** (by 4−13 ppm), and each derivative shows a phosphorus–proton coupling constant about 17−24 Hz in magnitude. Protonation further causes a systematic increase of the tungsten–phosphorus coupling constant magnitudes by 8−15 Hz. It should be noted that the cationic species **123g,m,r–t** undergo fast decomposition in solution (significantly more pronounced than the NMe$_2$ substituted derivatives **123b** and **124b**), which prevented their further characterization.

Table 4.2: ^{31}P NMR spectroscopic data for neutral complexes **41b,g,m,r–t**, **122b** and protonated complexes **123b,g,m,r–t**, and **124b**.

R	No.	$\delta(^{31}P)$	$|^1J_{WP}|$ [Hz]	No.	$\delta(^{31}P)$	$|^1J_{WP}|$ [Hz]	$|J_{PH}|$ [Hz]
NMe$_2$	**41b**$^\sharp$	101.8	241.6	**123b**†	105.7	251.8	23.0
2-thienyl	**41g**$^\sharp$	110.1	231.4	**123g**†	115.6	245.4	24.2
CH$_3$	**41m**$^\sharp$	108.7	228.9	**123m**†	118.0	239.1	16.5
^{t}Bu	**41r**$^\sharp$	108.3	228.9	**123r**‡	116.2	244.1	19.1
1-adamantyl	**41s**$^\sharp$	107.0	228.9	**123s**†	115.8	241.6	19.1
SiMe$_3$	**41t**$^\sharp$	109.4	223.8	**123t**‡	122.7	232.7	16.5
NMe$_2$	**122b**$^\sharp$	118.5	244.1	**124b**†	114.9	251.8	23.2*

$^\sharp$In C$_6$D$_6$. †In CD$_2$Cl$_2$. ‡In CH$_2$Cl$_2$. *From ^{1}H NMR spectrum.

Nevertheless, additional information about **123g,m,s** was obtained by subjecting the solutions of the reactions of **35** with nitrile derivatives **36g,m,s** and TfOH to ^{1}H and

2D ^{1}H,^{31}P HMQC NMR experiments. The spectra showed in each case a correlation of the ^{31}P signal with proton resonances of a phenyl and a CH(SiMe$_3$)$_2$ group. A broad ^{1}H resonance at low field (in the cases of **123g,s** with resolved coupling with phosphorus) confirmed the N-bonded proton. However, no conclusive evidence as to whether N^1- and N^4-protonated 2H-1,4,2-diazaphosphole complexes were formed could be deduced from these data. It should be noted that quantum chemical calculations on different model systems predict a slight preference of N^{1}H tautomers (see Section 4.4).

The reaction of **35** with acetonitrile (**36m**) and TfOH was carried out on a larger scale, and after workup a deep purple powderish solid was obtained, but due to the extreme instability of this compound in solution its characterization via ^{13}C{^{1}H} and ^{15}N{^{1}H} NMR spectroscopy could not be achieved.[9] A high resolution (HR) ESI-MS experiment revealed a signal assigned to 2H-1,4,2-diazaphospholium complex [**41m** + H]$^+$ (m/z 659.0872). The IR and Raman spectra of **123m** showed similar trends with respect to neutral complex **41m** as found for the pairs **41b**/**123b** and **122b**/**124b**. All C,O stretch vibration bands are shifted to larger wavenumbers (e.g., $\Delta\tilde{\nu}(A_1)^{[10]} = 7$ cm^{-1} and $\Delta\tilde{\nu}(B_1) = 22$ cm^{-1}).

---

[9]Here, the ^{31}P NMR spectrum showed a second resonance in the expected range for 2H-1,4,2-diazaphospholium complexes, but no ^{1}H,^{31}P correlations could be detected for this signal. Therefore, only the data for the other resonance are given in Table 4.2.

[10]Here, A_1 refers to the A_1-symmetric carbonyl stretch vibration with the largest wavenumber.

4.1.2 Variation of the *C*-Substituent

In order to exploit the newly developed ring enlargement protocol using 2*H*-azaphosphirene complexes and consecutive addition of a nitrile, triflic acid, and a base, *C*-ferrocenyl and the *C*-(2-thienyl) substituted complexes **67**[128] and **125**[124] were investigated. Reactions of **67** with **36b,l** (Scheme 4.5) and of **125** with **36b,g** (Scheme 4.6) using this method yielded selective formation of 2*H*-1,4,2-diazaphosphole complexes **69b,l** and **126b,g**.
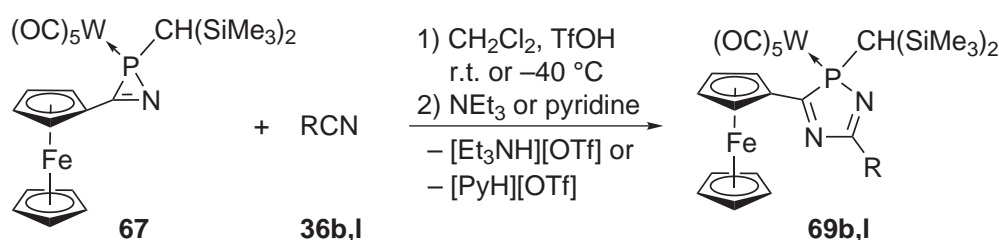
36, **69**: R = NMe$_2$ (**b**), ferrocenyl (**l**)

Scheme 4.5: One-pot syntheses of 3-ferrocenyl-2*H*-1,4,2-diazaphosphole complexes **69b,l** using 2*H*-azaphosphirene complex **67**, TfOH, nitriles **36b,l**, and NEt$_3$ or pyridine.

Also here, intensely colored solutions were formed upon addition of TfOH (i.e., **67**/**36b**: deep blue, **67**/**36l**: deep turquois, **125**/**36b**: deep red, and **125**/**36g**: deep green). Upon addition of the base the reaction mixtures underwent a second color change to result in the colors of solutions of the respective final products (**69b**: red; **69l**: deep purple; **126b,g**: light orange).
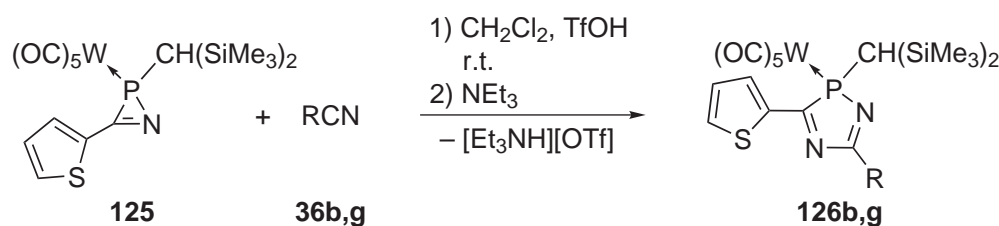
36, **126**: R = NMe$_2$ (**b**), 2-thienyl (**g**)

Scheme 4.6: One-pot syntheses of 3-(2-thienyl)-2*H*-1,4,2-diazaphosphole complexes **126b,g** using 2*H*-azaphosphirene complex **125**, TfOH, nitriles **36b,g**, and NEt$_3$.

Complexes **69b,l** and **126b,g** were purified via low-temperature column chromatography and characterized by multinuclear NMR experiments, mass spectrometry, IR

and UV/Vis spectroscopy, and single-crystal X-ray diffraction studies (Figures 4.6–4.8; **69l**: Fig. 3.8, Section 3.2.1); the purities were examined by elemental analyses.

Table 4.3: ^{31}P NMR spectroscopic data for complexes **69b,l**, **126b,g**, **127b**, and **128b**.

No.	Ar (C^3)	R (C^5)	$\delta(^{31}\text{P})$	$\|^1 J_{WP}\|$ [Hz]	$\|^{2+5} J_{PH}\|$ [Hz]
69b$^\sharp$	Fc	NMe$_2$	106.5	241.6	—
69l$^\sharp$	Fc	Fc	114.4	234.0	—
126b$^\sharp$	2-thienyl	NMe$_2$	104.0	245.4	—
126g$^\sharp$	2-thienyl	2-thienyl	110.4	235.2	—
127b†	Fc	NMe$_2$	102.6	253.0	22.9
128b†	2-thienyl	NMe$_2$	103.0	256.9	22.9

$^\sharp$In C$_6$D$_6$. †In CH$_2$Cl$_2$.

Variation of the C^3-substituent by phenyl, thienyl, and ferrocenyl has only marginal effects on the ^{31}P NMR spectroscopic data (Tab. 4.3). Complexes **69b,l** and **126b,g** show similar trends upon variation of the C^5-substituent as the 3-phenyl derivatives (cf. Tab. 4.2, Section 4.1). Noteworthy is that the resonances of complexes **69b** and **126b** appear upfield from those of their 5-aryl substituted congeners **69l** and **126g** ($\Delta\delta$ = 6−8) and have 8−10 Hz larger tungsten–phosphorus coupling constant magnitudes.

Table 4.4: ^{13}C{^{1}H} NMR spectroscopic data for ring carbon centers of complexes **69b,l** and **126b,g** (in C$_6$D$_6$).

No.	Ar (C^3)	R (C^5)	$\delta(^{13}\text{C}^3)$	$\|^{1+4} J_{PC^3}\|$ [Hz]	$\delta(^{13}\text{C}^5)$	$\|^{2+3} J_{PC^5}\|$ [Hz]
69b	Fc	NMe$_2$	206.5	26.8	165.0	—
69l	Fc	Fc	206.6	27.5	175.1	5.8
126b	2-thienyl	NMe$_2$	199.7	22.3	165.1	0.6
126g	2-thienyl	2-thienyl	195.2	22.3	165.5	5.5

The ^{13}C resonances of the C^3 centers of **69b,l**, **126b,g** appear at very low field (Tab. 4.4), whereas replacement of phenyl at this position by a ferrocenyl group further causes a low field shift by 4−6 ppm. A common feature of 5-NMe$_2$ substituted derivatives is a small $^{2+3} J_{PC}$ magnitude; as for complex **41b** this coupling could not be resolved for **69b**. Another common feature of complexes **41b**, **69b**, and **126b** is

that they show two distinct ^{1}H and ^{13}C resonances corresponding to the NMe$_2$ group, thus indicating a hindered rotation about the exocyclic C,N bond.

The molecular structures in the crystal of each complex show an essentially planar 2H-1,4,2-diazaphosphole ring[11] that is largely coplanar arranged with the aryl substituent at C^3. This also holds true for complex **69b** (Fig. 4.6). The torsion angle with respect to least-squares planes between the heterocycle and the adjacent Cp ring is 18.1°, and C^1 of this substituent (i.e., C(12)) deviates only 0.007 Å from the regression plane of the heterocyclic system. This is contrary to the situation of the 3-Fc group in complex **69l** (cf. Section 3.2.1). As in the structure of the latter the 3-ferrocenyl substituent of **69b** is transoid orientated with respect to the W(CO)$_5$ fragment.
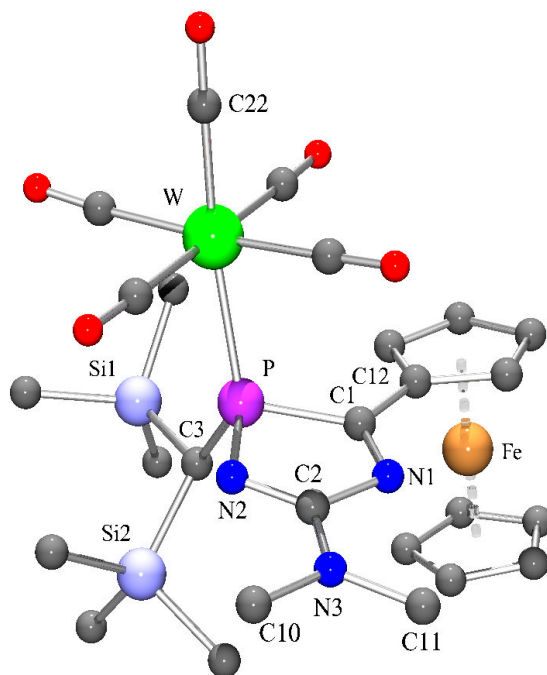
Figure 4.6: Molecular structure of complex **69b** in the crystal (hydrogen atoms omitted for clarity). Selected bond lengths [Å] and angles [°]: W–C(22) 2.000(4), W–P 2.5359(8), P–N(2) 1.683(3), P–C(1) 1.859(3), C(1)–N(1) 1.292(4), C(2)–N(2) 1.307(4), C(2)–N(3) 1.337(4), C(1)–C(12) 1.452(4), N(2)–P–C(1) 90.74(13), P–C(1)–N(1) 110.7(2), C(1)–N(1)–C(2) 108.7(3), N(1)–C(2)–N(2) 120.5(3), C(2)–N(2)–P 109.0(2), N(2)–C(2)–N(3) 123.4(3).

In all structurally characterized 5-NMe$_2$ substituted 2H-1,4,2-diazaphosphole complexes the dimethylamino nitrogen atom is trigonal planar coordinated ($\Sigma\angle$(N$_{NR_3}$): 360.0° (**41b**), 360.0° (**69b**), and 360.5° (**126b**)), and the nitrogen and carbon centers

---

[11]Mean deviations from least-squares planes: 0.023 (**69b**), 0.038 (**69l**), 0.022 (**126b**), and 0.044 Å (**126g**).

of this group deviate only slightly from the regression plane of the heterocycle (**69b**: 0.015, 0.058, and 0.032 Å; **126b**: −0.037, 0.058, and −0.080 Å). At the same time, the exocyclic C^5,N bond is rather short, thus being in the same range as the endocyclic C^5,N^1 bond. The P,N^1 bond of (uncharged) 5-dimethylamino-2*H*-1,4,2-diazaphosphole complexes is generally slightly shorter (ca. 1.68 Å) compared to 5-alkyl or 5-aryl substituted derivatives (1.70–1.71 Å).[12]
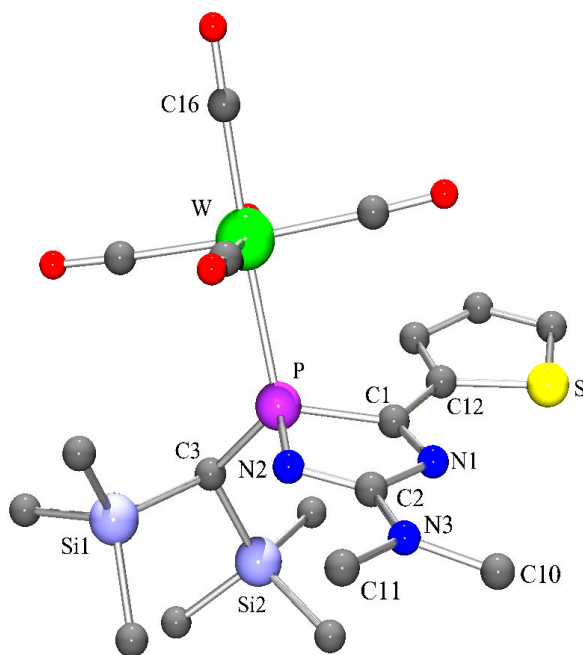
Figure 4.7: Molecular structure of complex **126b** in the crystal (hydrogen atoms omitted for clarity). Selected bond lengths [Å] and angles [º]: W–C(16) 2.005(4), W–P 2.5266(8), P–N(2) 1.683(2), P–C(1) 1.879(3), C(1)–N(1) 1.295(4), C(2)–N(2) 1.305(4), C(2)–N(3) 1.343(4), C(1)–C(12) 1.448(4), N(2)–P–C(1) 90.14(13), P–C(1)–N(1) 110.0(2), C(1)–N(1)– C(2) 109.4(3), N(1)–C(2)–N(2) 120.7(3), C(2)–N(2)–P 109.5(2), N(2)–C(2)–N(3) 123.6(3).

The structure of complex **126g** (Fig. 4.8) is best compared with that of **41g** (Fig. 3.4, Section 3.1). It features a coplanar arrangement of all three heterocyclic systems (torsion angles:[13] 6.1 º (C^3-thienyl−diazaphosphole), 8.5 º / 9.6 º (C^5-thienyl−diazaphosphole), and 9.0 º / 12.4 º (C^3-thienyl−C^5-thienyl)). The thienyl ring at C^5 is disordered. Here, the site occupation factors are almost equal (C^3-*anti*, C^5-*syn*/C^3-*anti*, C^5-*anti* arrangement[14] 59 : 41).

---

[12]An overview of structural parameters for all determined 2*H*-1,4,2-diazaphosphole complexes is given in Appendix D.

[13]Values are given for both conformations of the disordered thienyl ring.

[14]Arrangement of the thienyl rings with the 2*H*-1,4,2-diazaphosphole ring with respect to phosphorus and sulfur.
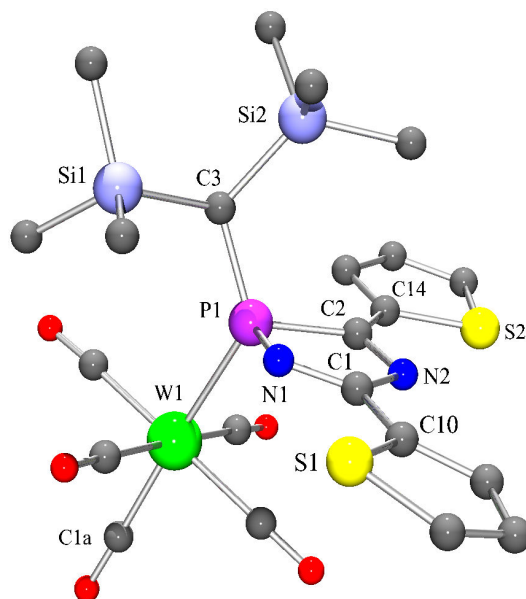
Figure 4.8: Molecular structure of complex **126g** in the crystal (hydrogen atoms omitted for clarity; only the prevailing conformation shown). Selected bond lengths [Å] and angles [°]: W(1)–C(1a) 2.009(4), W(1)–P(1) 2.5377(9), P(1)–N(1) 1.705(3), P(1)–C(2) 1.858(4), C(2)–N(2) 1.296(5), C(1)–N(1) 1.294(5), C(1)–C(10) 1.445(5), C(2)–C(14) 1.441(5), N(1)–P(1)–C(2) 90.55(16), P(1)–C(2)–N(2) 109.7(2), C(2)–N(2)–C(1) 109.5(3), N(2)–C(1)–N(1) 121.4(3), C(1)–N(1)–P(1) 108.0(2).

The IR spectra of complexes **69b,l**, **126b,g** revealed similar results as those of **41b,g,m,r–t** and **122b**.[15] The C,O stretch vibration bands reflect the slightly perturbed C_{4v} symmetry of these complexes. They show each a single, well separated band at $2066-2071$ cm^{-1} and another band with low intensity at $1976-1991$ cm^{-1}, which can be assigned to normal modes of local A_1 and B_1 symmetry, respectively. In the range of $1900-1950$ cm^{-1} three very intense and partially overlapping bands appear, which are attributable to vibrations of local A_1 and E symmetry. Two bands at $1500-1600$ cm^{-1} according to C,N stretch vibrations were observed in each case, whereas in the cases of the 5-NMe$_2$ substituted derivatives (**69b**, **126b**, as well as **41b**) one of them appears slightly above 1600 cm^{-1} and shows a higher intensity.

In the FAB-mass spectra of complexes **69b**, **126b**, and **126g** the protonated liberated ligands represented the base peaks,[16] as it was observed also for complexes **41b,g,m,r,s**.

---

[15]IR data for all 2*H*-1,4,2-diazaphosphole complexes investigated are compiled in Table C.2 (Appendix C).

[16]In the spectrum of complex **69l** the peak corresponding to [**78l** + H]$^+$ (*m/z* 613.0) was found with 85 % intensity; in this case the base peak is represented by the radical cationic heterocycle **78l**$^{•+}$.

By ^{31}P NMR spectroscopic monitoring of reactions of **67** and **125** with dimethyl cyanamide (**36b**) and TfOH before adding the base (Scheme 4.7) the resonances of 2H-1,4,2-diazaphospholium complexes **127b** and **128b** were detected (Tab. 4.3). They resonate in the same range as neutral complexes **69b** and **126b**. Generally, the trend of the chemical shift caused by protonation is not easily predictable. While low field shifts were observed in the cases of all 2-CH(SiMe$_3$)$_2$-3-phenyl substituted derivatives (**123b,g,m,r–t** vs. **41b,g,m,r–t**: $\Delta\delta = 4-13$; cf. Tab. 4.2), the resonances of **127b** and **128b** are slightly upfield from their neutral congeners ($\Delta\delta = -3.9$ (**127b** vs. **69b**) and -1.0 (**128b** vs. **126b**)), hence, they show the same trend as 2-Cp*-3-phenyl substituted derivative **124b** vs. **122b** ($\Delta\delta = -3.6$).

67, 127b: Ar = ferrocenyl
125, 128b: Ar = 2-thienyl
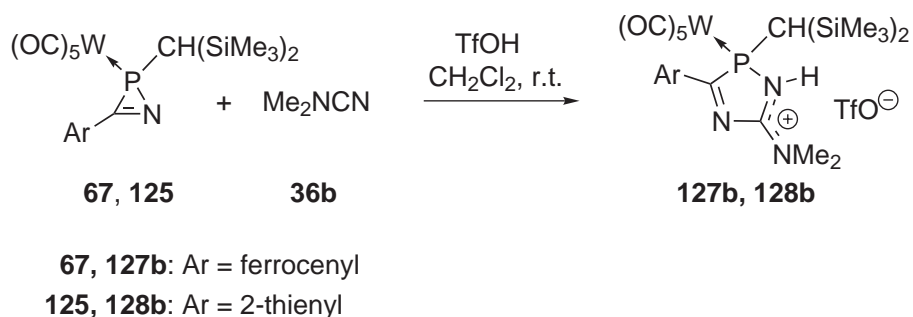
Scheme 4.7: Reactions of 2H-azaphosphirene complexes **67** and **125** with dimethyl cyanamide (**36b**) and TfOH.

On the other hand, the change of the tungsten–phosphorus coupling constant magnitude upon protonation turned out to be a characteristic feature (cf. Tab. 4.2): in each case an increase was observed ($\Delta|^1J_{WP}| = +11.4$ Hz (**127b** vs. **69b**) and $+11.5$ Hz (**128b** vs. **126b**)). The similarity of the ^{31}P NMR spectroscopic data for complexes **127b**, **128b** with those for **123b** and **124b** strongly suggests that also here N^1-protonated tautomers were formed.[17] The phosphorus–proton coupling constant of each 5-dimethylamino-2H-1,4,2-diazaphospholium complex (**123b**, **124b**, **127b**, and **128b**) is approximately 23 Hz in magnitude.

---

[17]Note that stabilization through π-electron delocalization in the amidinium moiety is not operative in hypothetical N^4- and NMe$_2$-protonated tautomers of **127b** and **128b**.

4.1.3 Reactions with HCN: An Unexpected Haptotropic Shift

Successful reactions of complexes **35**, **67**, and **125** with HCN using the TfOH/base protocol required substantially lower temperatures ($-78\,^{\circ}$C) and employment of more dilute reaction solutions (Scheme 4.8). Here, it turned out to be favorable to add the triflic acid dissolved in CH_2Cl_2 dropwise; pyridine was used as deprotonating reagent to facilitate the workup. Surprisingly, these reactions afforded mixtures of two coordination isomers: **41h** and **129h** (ratio $5:1$), **69h** and **130h** (ratio $1:2$), and **126h** and **131h** (ratio $24:1$). Complexes **129h**, **130h**, and **131h** constitute first examples of κN-bonded $2H$-1,4,2-diazaphosphole complexes.

35, **41h**, **129h**:	Ar = phenyl
67, **69h**, **130h**:	Ar = ferrocenyl
125, **126h**, **131h**:	Ar = 2-thienyl

Scheme 4.8: Reactions of $2H$-azaphosphirene complexes **35**, **67**, and **125** with HCN (**36h**), TfOH, and subsequently with pyridine.

The isomeric complexes could not be separated, and for the mixtures of **41h** and **129h** and of **126h** and **131h** NMR spectra revealed the signals of both complexes with unchanged ratios after several purification steps—even after recrystallizing and re-dissolving. Nevertheless, elemental analyses of the purified mixtures yielded satisfactory results, and the products were characterized by various analytical methods (multinuclear NMR experiments, mass spectrometry, IR and UV/Vis spectroscopy); the structures of complexes **41h** and **126h** were determined by single-crystal X-ray diffraction studies (Figures 4.12 and 4.13). Noteworthy is that the synthesis of **41h** could not be achieved via the SET protocol using ferrocinium salts (Section 3.2).

Products **69h** and **130h** decomposed during column chromatography ($-50\,^{\circ}$C, neutral Al_2O_3), but repeating the reaction, evaporating all volatiles in vacuo, dissolving the residue in diethylether, and filtering off the pyridinium triflate yielded a crude product that revealed all relevant NMR spectroscopic information.

The ^{1}H, ^{13}C{^{1}H}, ^{31}P{^{1}H}, and ^{29}Si{^{1}H} NMR spectra of each mixture showed two sets of resonance signals according to the isomeric compounds, and the data for each

complex could unambiguously be assigned by means of various shift-correlated 2D NMR experiments (Tab. 4.5).

By comparison with complexes **41b,g,m,r–t**, **69b,l**, **126b,g** the data for **41h**, **69h**, **126h** were easily identified. Their ^{31}P NMR chemical shifts are between those of their 5-NMe$_2$ substituted and 5-alkyl or -aryl substituted congeners, and their tungsten–phosphorus coupling constant magnitudes are almost as small as that of 5-silyl substituted derivative **41t**. The ^{13}C{^{1}H} NMR spectra revealed the characteristic resonances of the ring carbon centers at low field. The proton at C^5 resonates at 7.9−8.3 ppm showing a common magnitude about 34 Hz of the phosphorus–proton coupling constant for **41h**, **69h**, and **126h**.

The C^{5}H proton of κN-coordinated heterocycles **129h**, **130h**, and **131h** resonates at slightly lower field, and the corresponding phosphorus–proton coupling constant magnitudes are only about 7 Hz. The ^{31}P{^{1}H} resonances appear downfield from those of **41h**, **69h**, **126h**. They were slightly broadened with no resolved W,P couplings; in their ^{31}P NMR spectra the couplings with the proton at C^5 could not be resolved.

The ring carbon atoms show ^{13}C resonances downfield from those of complexes **41h**, **69h**, and **126h** with significantly larger phosphorus–carbon coupling constant magnitudes. Also the CO carbon centers resonate at slightly lower field. Both signals appear as doublets, and the magnitudes of the phosphorus–carbon coupling constants of *cis*- and *trans*-CO carbons are virtually identical (2−3 Hz), which is different from the typical coupling constant pattern observed for κP-complexes such as **41h**, **69h**, **126h** where the *trans*-CO carbons exhibit $|^2J_{PC}|$ values of 22−23 Hz. The *P*-bound CH functionality resonates in the same range as that of complexes **41h**, **69h**, **126h** (17−18 ppm), but the magnitude of its phosphorus–carbon coupling constant is considerably larger (55−57 Hz). An increase of $|^1J_{PC}|$ values is generally observed upon removal of a κP-bonded W(CO)$_5$ fragment as an effect of the formation of a lone pair of electrons at phosphorus.[175]

An interesting aspect of the spectra of **129h**, **130h**, and **131h** is that only one proton signal was observed for the two trimethylsilyl groups; the same phenomenon was found also in the ^{13}C{^{1}H} and ^{29}Si{^{1}H} NMR spectra. This observation points to a fast inversion of the phosphorus center.

The distinction which of the two nitrogen centers donates to the transition metal in complexes **129h**, **130h**, and **131h** could be made on the basis of 2D ^{1}H,^{15}N HMBC NMR experiments (Figures 4.9 and 4.11). The spectrum of a mixture of **41h** and **129h** displays two sets of correlation signals (Fig. 4.9), which allow the assignment of the ^{15}N NMR data to the N^1 and N^4 centers of both complexes (Tab. 4.5).

Table 4.5: Selected NMR spectroscopic data for complexes **41h**, **69h**, **126h**, **129h**, **130h**, and **131h** (all data recorded in C_6D_6 solution except for ^{15}N NMR data for complexes **41h** and **129h** in $CDCl_3$ and for **126h**, **130h**, and **131h** in CD_2Cl_2).

	41h	**129h**	**69h**	**130h**	**126h**	**131h**
$\delta(^{31}P)$	105.6	121.2	107.6	116.3	105.4	118.6
$\lvert^1 J_{WP}\rvert$/Hz	227.6	–	226.3	–	232.3	–
$CH(SiMe_3)_2$						
$\delta(^1H)$	0.98	1.77	1.25	1.58	0.97	1.70
$\lvert^2 J_{PH}\rvert$/Hz	4.0	13.9	9.8	12.7	4.1	13.2
$\delta(^{13}C)$	17.3	17.9	17.9	16.9	18.1	17.9
$\lvert^1 J_{PC}\rvert$/Hz	3.9	55.0	9.4	56.3	3.4	56.6
C^3						
$\delta(^{13}C)$	203.0	208.5	210.1	215.4	195.7	199.5
$\lvert^{1+4} J_{PC}\rvert$/Hz	22.0	35.5	22.3	38.5	21.1	35.9
C^5H						
$\delta(^1H)$	8.03	8.41	8.28	8.57	7.87	8.26
$\lvert^{3+4} J_{PH}\rvert$/Hz	33.6	6.6	33.5	7.2	34.2	7.1
$\delta(^{13}C)$	162.7	170.3	161.7	171.4	162.9	171.0
$\lvert^{2+3} J_{PC}\rvert$/Hz	7.8	14.2	8.1	12.0	9.2	12.0
CO_{cis}						
$\delta(^{13}C)$	197.5	198.4	197.2	198.2	197.4	198.3
$\lvert^{2/3} J_{PC}\rvert$/Hz	5.8	2.7	6.1	3.2	6.1	2.9
$\lvert^1 J_{WC}\rvert$/Hz	126.6	129.8	126.7	130.0	126.9	*
CO_{trans}						
$\delta(^{13}C)$	197.7	201.0	198.1	201.4	197.8	201.0
$\lvert^{2/3} J_{PC}\rvert$/Hz	22.6	1.7	22.3	1.9	23.0	1.9
$\lvert^1 J_{WC}\rvert$/Hz	144.7	*	*	149.5	144.2	*
N^1						
$\delta(^{15}N)$	−86	−165	*	−170	−88	*
$\lvert^{1+4} J_{PN}\rvert$/Hz	54	68	*	65	60	*
N^4						
$\delta(^{15}N)$	−64	−53	*	−60	−66	−56
$\lvert^{2+3} J_{PN}\rvert$/Hz	9	24	*	6	8	*

*Not resolved.

Both nitrogen atoms of **41h** show correlations with the C^{5}H proton at $\delta_H = 8.03$, and the nitrogen that resonates at $\delta_N = -86$ shows a second correlation signal with the CH-proton of the CH(SiMe$_3$)$_2$ group at $\delta_H = 0.98$ (blue boxes). This nitrogen, which features a large phosphorus–nitrogen coupling constant magnitude (54 Hz), is clearly assigned to the N^1 center.[18] Thus, the two N atoms of complex **41h** resonate in the same range as those of complex **41m** ($\delta(N^1) = -116$; $\delta(N^4) = -52$); obviously, the nature of the C^5-substituent has a slightly larger effect on N^1 ($\Delta\delta(N^1) = 30$ and $\Delta\delta(N^4) = 12$ (**41h** vs. **41m**)).
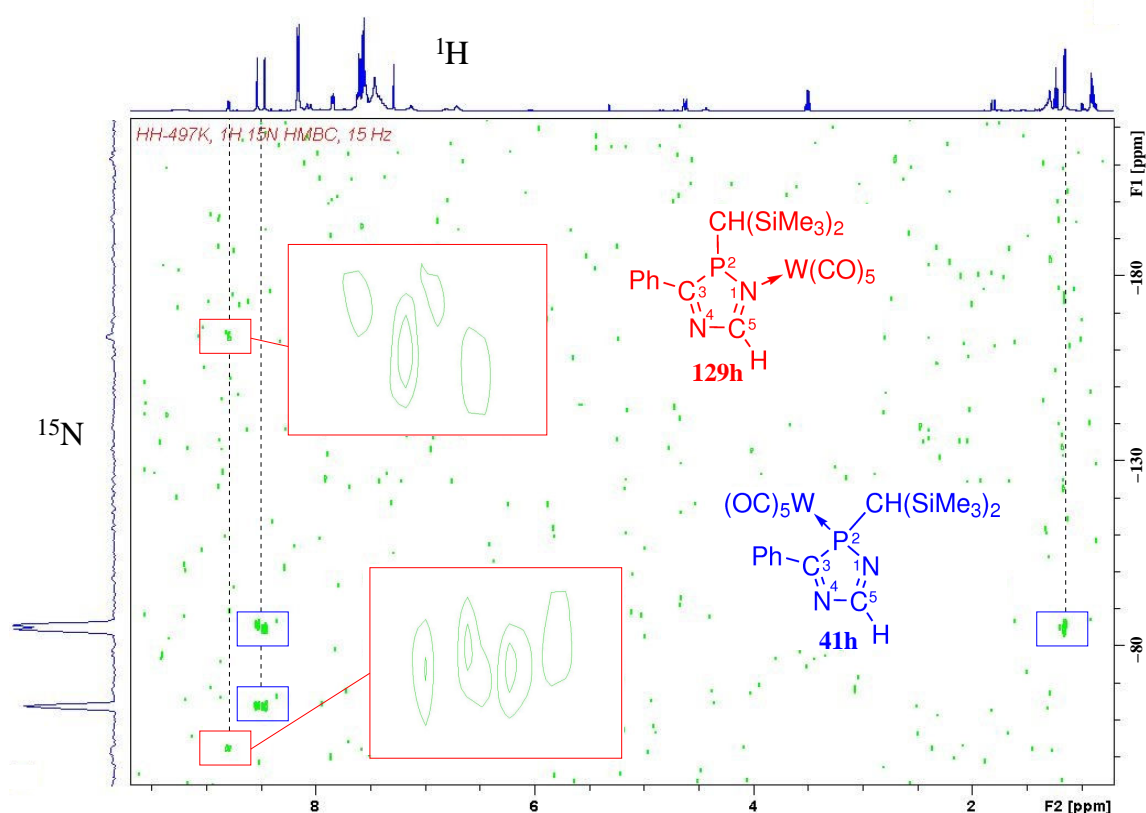
Figure 4.9: 2D ^{1}H,^{15}N HMBC NMR spectrum of a mixture of complexes **41h** and **129h** in CDCl$_3$ (horizontal axis: ^{1}H NMR spectrum; vertical axis: projection onto ^{15}N dimension; red boxes: signal extensions for complex **129h**).

The nitrogen centers of complex **129h** show correlations with the C^{5}H proton at $\delta_H = 8.41$ (zoomed in and highlighted in red boxes). While the N^4 resonance ($\delta_N = -53$, $|^{2+3}J_{PN}| = 24$ Hz) is only marginally downfield shifted with respect to **41h** ($\Delta\delta_N = 11$), the N^1 center resonates at significantly higher field ($\delta_N = -165$, $|^{1+4}J_{PN}| = 68$

---

[18]The given assignment is consistent with observations made for the N^1-protonated 2H-1,4,2-diazaphosphole complex **123b** (Section 4.1.1). In that case only the protonated nitrogen atom showed a correlation with the exocyclic CH proton, while for N^4 no such cross-peak was detected.

Hz). From this follows that the $2H$-1,4,2-diazaphosphole ligand of **129h** donates to the pentacarbonyl tungsten fragment via N^1; a metal shift ($P \rightarrow N^1$) causes a shielding of this nitrogen center by $\Delta\delta_N = -79$.

Negative ^{15}N NMR coordination shifts are generally observed for transition metal-coordinated N-donors.[244, 249–257] For instance, when forming the platinum complex **132** (Fig. 4.10) the ^{15}N resonance of ammonia experiences a high field shift by $\Delta\delta_N = -46.4$, and the resonance of the N^3 center of the 1-methylimidazole ligand is high field shifted by even $\Delta\delta_N = -91.9$.[250] On the other hand, the signal of the non-ligated N^1 center is slightly low field shifted with respect to the uncomplexed heterocycle ($\Delta\delta_N = +4.7$).[250]
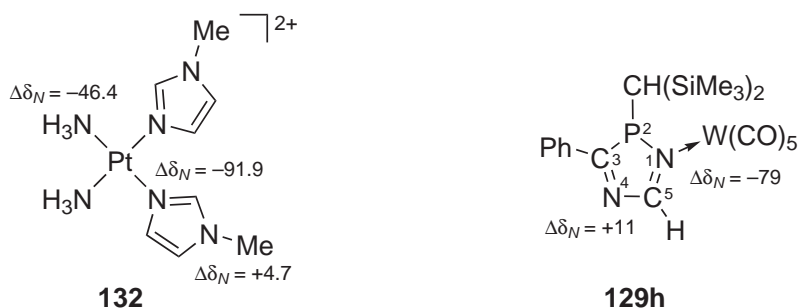
Figure 4.10: N-Donor complexes **132**[250] and **129h** and their ^{15}N NMR coordination shifts (**132**: $\Delta\delta_N = \delta_N(\text{complex}) - \delta_N(\text{ligand})$, in H_2O; **129h**: $\Delta\delta_N = \delta_N(\kappa N\text{-complex}) - \delta_N(\kappa P\text{-complex})$, in $CDCl_3$).

The 2D ^1H,^{15}N HMBC NMR spectrum of the mixture of **69h** and **130h** revealed the ^{15}N NMR spectroscopic data for κN-coordinated derivative **130h**, which is in this case the major isomer (Fig. 4.11, A).[19] Correlations of N^4 and N^1 with the C^5H proton as well as a correlation of the N^1 center with the CH-proton of the $CH(SiMe_3)_2$ moiety are well resolved. The ^{15}N data thus obtained for **130h** are very similar to those for complex **129h** (Tab. 4.5).

Complementary to this result, in the case of the mixture of **126h** and **131h** correlation signals of both nitrogen centers were detected for κP-complex **126h**, as it is present in large excess here. The ^{15}N NMR spectroscopic data for **126h** are almost identical to those for complex **41h**; the differences in their chemical shifts are below 2 ppm. For the haptomeric complex **131h** only a signal was detected arising from correlation N^4 with the C^5H proton (which is not visible in Figure 4.11 (B) due to its low intensity).

---

[19]It should be noted that the samples were not ^{15}N-enriched and that the absolute sensitivity of the ^{15}N nucleus at the 0.37 % natural abundance level is only $3.85 \cdot 10^{-6}$ (in respect to ^1H).[244]
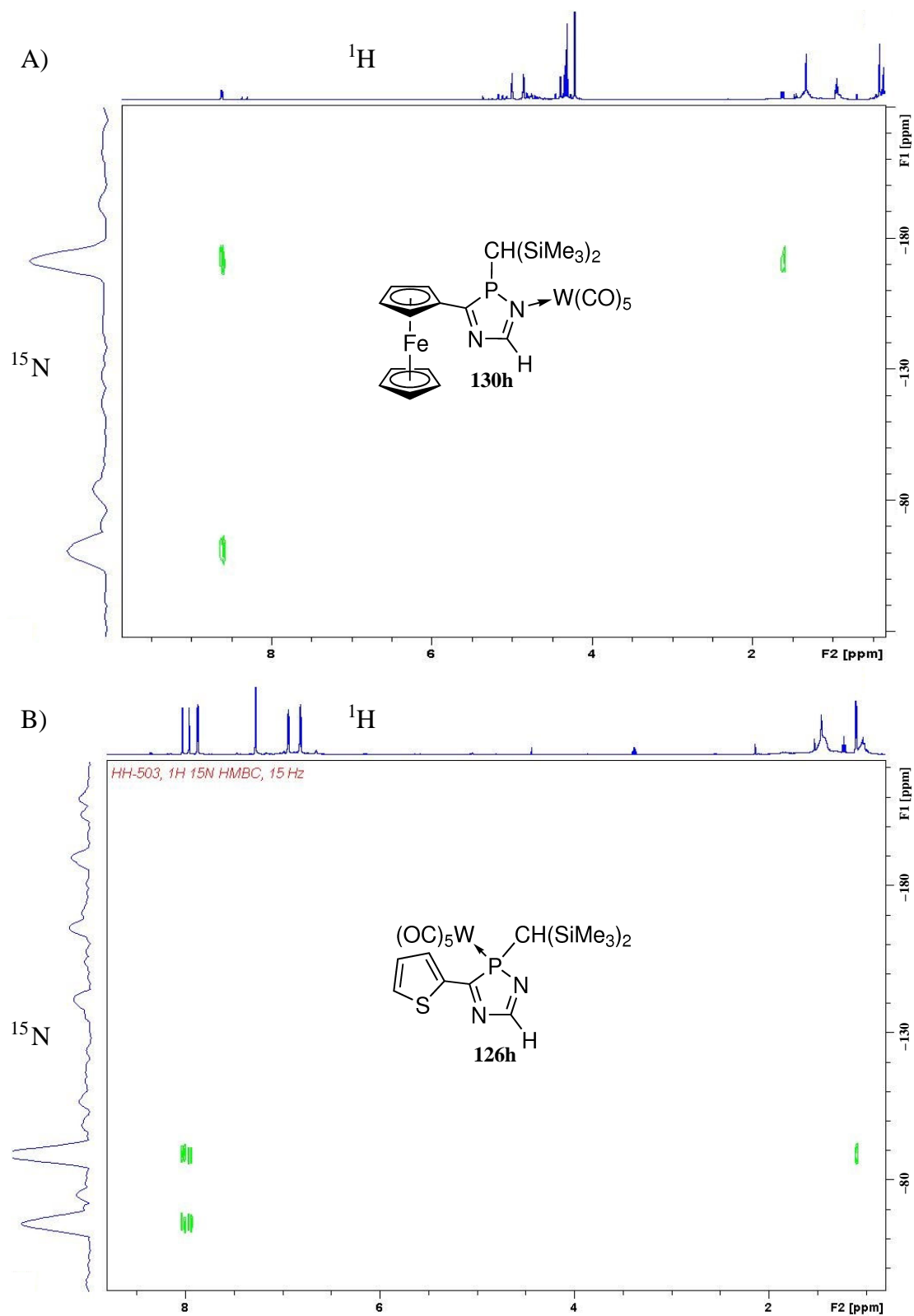
Figure 4.11: 2D ^{1}H,^{15}N HMBC NMR spectra of complexes **130** (A) and **126h** (B) in CD$_2$Cl$_2$ (horizontal axes: ^{1}H NMR spectra; vertical axes: projections onto ^{15}N dimension).

Complexes **41h** and **126h**[20] crystallize in the monoclinic space groups P $2_1/c$ and C $2/c$, respectively (Figures 4.12 and 4.13), and their molecular structures exhibit similar features as those of other $2H$-1,4,2-diazaphosphole complexes presented so far.
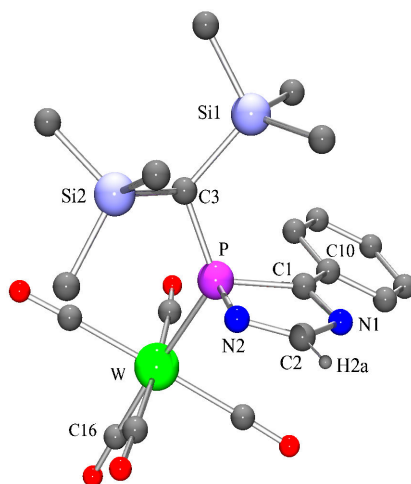
Figure 4.12: Molecular structure of complex **41h** in the crystal (except for H2a all hydrogen atoms omitted for clarity). Selected bond lengths [Å] and angles [°]: W–C(16) 1.996(5), W–P 2.5362(10), P–N(2) 1.715(3), P–C(1) 1.861(4), C(1)–N(1) 1.296(4), C(2)–N(2) 1.280(5), C(1)–C(10) 1.472(5), N(2)–P–C(1) 90.53(16), P–C(1)–N(1) 109.1(3), C(1)–N(1)–C(2) 109.7(3), N(1)–C(2)–N(2) 122.7(3), C(2)–N(2)–P 107.4(3).
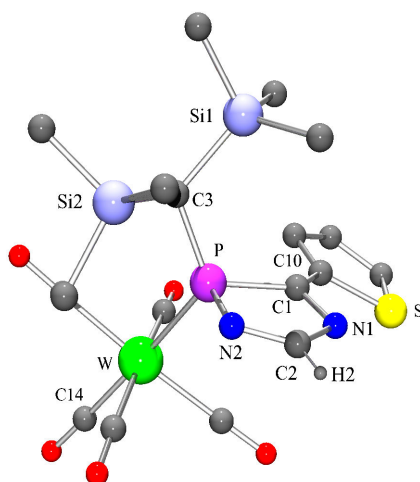
Figure 4.13: Molecular structure of complex **126h** in the crystal (except for H2 all hydrogen atoms omitted for clarity). Selected bond lengths [Å] and angles [°]: W–C(14) 2.000(3), W–P 2.5252(8), P–N(2) 1.708(3), P–C(1) 1.869(3), C(1)–N(1) 1.309(4), C(2)–N(2) 1.281(4), C(1)–C(10) 1.445(4), N(2)–P–C(1) 90.17(14), P–C(1)–N(1) 109.2(2), C(1)–N(1)–C(2) 109.5(3), N(1)–C(2)–N(2) 122.1(3), C(2)–N(2)–P 108.6(2).

---

[20]H(2) at C(2) was located in the Fourier difference electron density.

Also from mass spectra of complexes **41h** and **129h** and of **126h** and **131h** similar information was obtained as for other 2*H*-1,4,2-diazaphosphole complexes. The IR spectra (KBr) showed one set of C,O stretch vibration bands for each mixture, most likely assigned to the major haptomers **41h** and **126h**. The bands of κN-complexes **129h** and **131h** presumably are overlapped by the former and/or have too low intensities for being observed.[21]

Interestingly, the ratio of the two haptomeric complexes **41h** and **129h** in solution varied slightly with the temperature. The ^{31}P{^{1}H} NMR spectra shown in Figure 4.14 (in toluene) revealed that the relative amount of κN-complex **129h** constituted only 8 % (estimated by signal integration) at $-10\,°$C and increased with increasing temperature to 16 % at $+30\,°$C and further to 21 % at $+60\,°$C.[22]
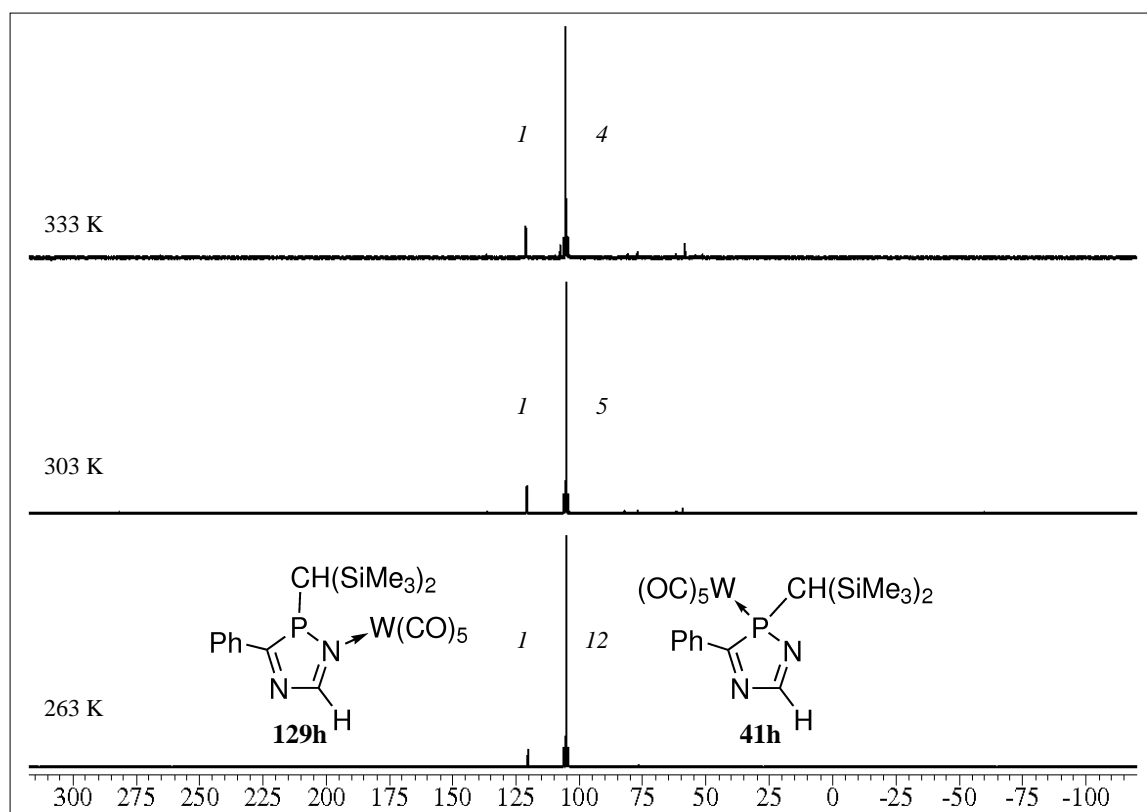
Figure 4.14: ^{31}P{^{1}H} NMR spectra with signal integrals of a mixture of complexes **41h** and **129h** in toluene at different temperatures.

This observation evidences an interconversion of both species, and thus, the constitution of a chemical equilibrium between the two haptomeric 2*H*-1,4,2-diazaphosphole

[21]UV/Vis absorption spectra are discussed in Chapter 5.

[22]It should be mentioned that some degree of decomposition of **41h** and/or **129h** occurred with increasing temperature; resonances appeared at 58.2, 77.0, 80.9, and 107.5 ppm.

complexes in solution (Scheme 4.9). Similar results were obtained also for the mixtures of **69h** and **130h** and of **126h** and **131h**.

41h, **69h**, **126h**   **129h**, **130h**, **131h**
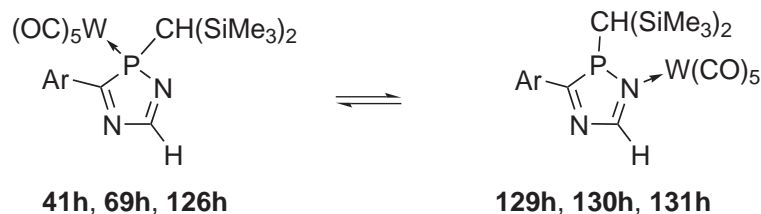
Scheme 4.9: Chemical equilibrium between haptomeric $2H$-1,4,2-diazaphosphole tungsten complexes **41h** and **129h** (Ar = phenyl), **69h** and **130h** (Ar = ferrocenyl), and **126h** and **131h** (Ar = 2-thienyl).

Since the introduction of the concept of *hemilability* in ligand design by Jeffrey and Rauchfuss,[258] there has been an increasing interest in synthesis and use of hemilabile ligands, as the different features associated with each donor atom confer unique reactivity to their metal complexes.[259] Stalke and coworkers have established so-called *Janus Head* ligands, which combine both hard and soft coordination sites. Such ligands are able to donate either via nitrogen, phosphorus, carbon, or more than one center to one metal[260, 261] or they form heterobimetallic complexes with different metal fragments.[261, 262] Equilibria between N and P as well as N,P coordination modes of chelating ligands have also been reported.[263] However, the observations made for complexes **41h**, **129h**, **69h**, **130h**, **126h**, and **131h** are unprecedented examples where equilibria were evidenced between coordination isomers involving both nitrogen and phosphorus donor centers that belong to one ring system and donate to the same metal fragment.

A reasonable explanation for the observed haptotropic (P→N)-metal shift is the steric congestion at phosphorus in the κP-complexes due to repulsion between the $W(CO)_5$ fragment and the aryl substituent at C^3, being most pronounced with the bulky ferrocenyl group in **69h**. This interpretation is in agreement with the thermal behavior of the state of the equilibrium, since an increase of internal movement should cause further destabilization of the κP-complexes with increasing temperature. The reason why a haptotropic (P→N)-metal shift was not observed in the cases of other $2H$-1,4,2-diazaphosphole tungsten complexes such as **41b,g,m,r–t**, **122b**, **69b,l**, and **126b,g** presumably is the presence of a substituent at C^5, which makes the formation of a κN-complex less favorable for steric reasons.

In order to learn more about the structures and relative energies of the isomeric species, DFT calculations[23] on **96h** and **133h** (methyl at P and C^3) were carried out

[23]RI-BP86/TZVP/ECP-60-MWB(W)+COSMO(ε = 8.93)//RI-BP86/SV(P)/ECP-60-MWB(W)

(Fig. 4.15), which may serve as model systems for complexes **41h**, **69h**, **126h** and
129h, **130h**, **131h**, respectively. Metal shift from P to N^1 (**96h** → **133h**) causes
only marginal geometrical changes within the heterocyclic system: both C,N double
bonds are slightly lengthened (C^5,N^1 +1.5 %; C^3,N^4 +1.0 %), while the C^5,N^4 bond is
shortened (−2.5 %). Nevertheless, the bond distances of **133h** are still in the range of
isolated C,N single and double bonds, and the phosphorus center shows no tendency
for planarization ($\Sigma\angle(\mathrm{P}_{PR_3})$ 296.0°). The P,N^1 bond is slightly elongated (+1.4 %),
and at the same time a decrease of the P,C^3 bond length (−1.7 %) is observed; the
endocyclic angle at P decreases marginally (to < 90°). It should be noted that upon
shift of the metal to N^1 by trend the same geometrical changes are induced as upon
protonation of this nitrogen atom (**123b** vs. **41b**; cf. Figure 3.3, Section 3.1 and Figure
4.4, Section 4.1.1).
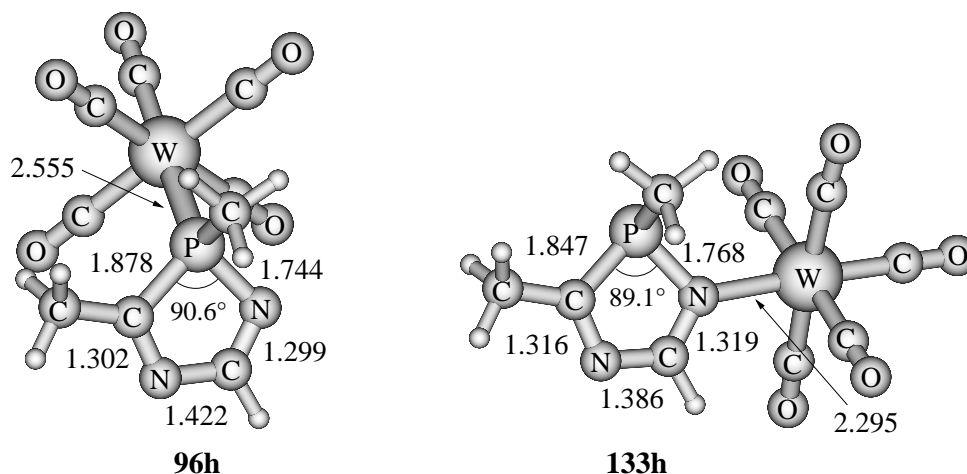
Figure 4.15: Calculated structures of haptomeric 2H-1,4,2-diazaphosphole tungsten com-
plexes **96h** and **133h**.

It is remarkable that the difference in calculated free energies for the two haptomeric
complexes is rather low; only a slight preference of the κP-coordinated isomer is pre-
dicted ($\Delta G_{298} = 2.6\,\mathrm{kJ\cdot mol^{-1}}$). A further hypothetical haptomer where the 2H-1,4,2-
diazaphosphole ligand is bound to tungsten via N^4 (not displayed) is somewhat higher
in energy (vs. **133h**: $\Delta G_{298} = +10.3\,\mathrm{kJ\cdot mol^{-1}}$).

+COSMO($\varepsilon = 8.93$).

4.1.4 Variation of the Metal Center

In order to explore the applicability of the TfOH/NEt$_3$ ring expansion protocol for molybdenum and chromium complexes, 2H-azaphosphirene complexes **70**[123] and **71**[123] were chosen to react with dimethyl cyanamide **36b** (Scheme 4.10).
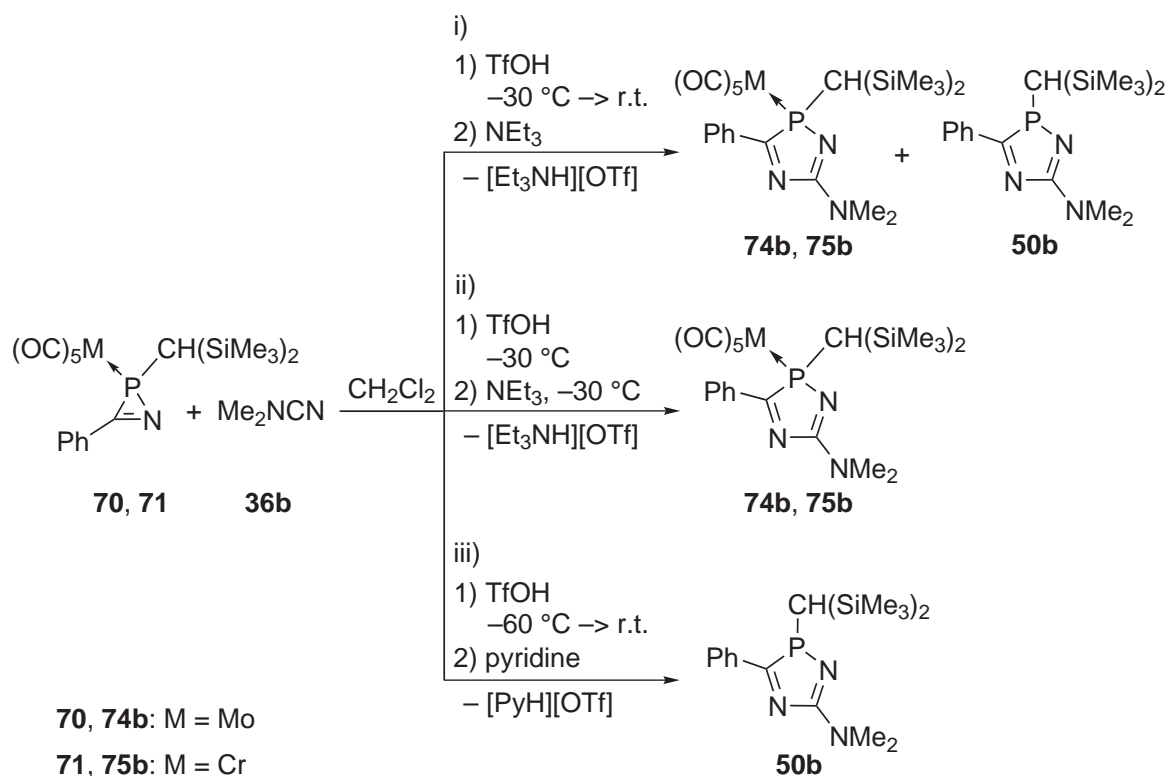
Scheme 4.10: Syntheses of 2H-1,4,2-diazaphosphole molybdenum and chromium complexes **74b**, **75b** and of 2H-1,4,2-diazaphosphole **50b**.

Test reactions revealed that the reaction conditions used for ring enlargement of tungsten complex **35** could not be adopted to complexes **70** and **71**. When triflic acid was added either at room temperature or at −30 °C and the reaction mixtures were then warmed up (i), after addition of NEt$_3$ besides the desired products **74b**, **75b** the ^{31}P{^{1}H} resonance of free 2H-1,4,2-diazaphosphole ligand **50b** was observed. Also here, initially intensely red colored solutions were formed during addition of TfOH, but upon warming up, the solutions turned greenish brown, which also served as visual indication for the onset of decomplexation.

Careful control of the reaction conditions prevented the decomplexation completely. If the addition of TfOH was carried out at about −30 °C and deprotonation with triethylamine was performed within few minutes, 2H-1,4,2-diazaphosphole complexes

74b and **75b** were the only reaction products observed by ^{31}P{^{1}H} NMR spectroscopy (ii, Scheme 4.10). Complexes **74b** and **75b** were purified by low-temperature column chromatography and obtained in good yields (**74b**: 89 %; **75b**: 85 %). They were characterized by multinuclear NMR experiments, mass spectrometry, IR and UV/Vis spectroscopy, and single-crystal X-ray diffraction studies (Figures 4.16 and 4.17).
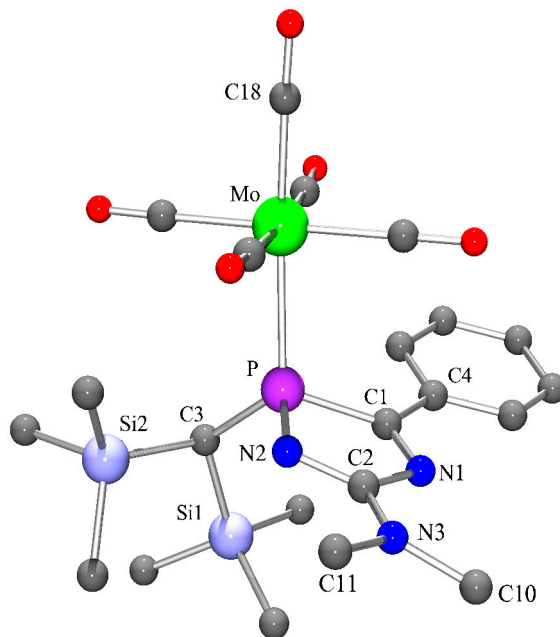
Figure 4.16: Molecular structure of complex **74b** in the crystal (hydrogen atoms omitted for clarity). Selected bond lengths [Å] and angles [°]: Mo–C(18) 2.003(4), Mo–P 2.5487(10), P–N(2) 1.673(3), P–C(1) 1.877(4), C(1)–N(1) 1.293(5), C(2)–N(2) 1.315(5), C(2)–N(3) 1.341(6), C(1)–C(4) 1.462(6), N(2)–P–C(1) 90.91(17), P–C(1)–N(1) 109.2(3), C(1)–N(1)–C(2) 110.0(3), N(1)–C(2)–N(2) 120.8(4), C(2)–N(2)–P 108.7(3), N(2)–C(2)–N(3) 123.0(4).

The ^{31}P{^{1}H} resonance of **74b** appears about 21 ppm downfield from that of complex **41b**, and complex **75b** resonates further 24 ppm at lower field (Tab. 4.7), which is a common trend for tungsten, molybdenum, and chromium complexes of a given class of ligands.[148, 163] The ^{13}C{^{1}H} NMR spectroscopic data for the heterocyclic ligand are almost unaffected by variation of the metal fragment (Tab. 4.7); compared to **41b** the magnitudes of the phosphorus–carbon coupling constants of complexes **74b** and **75b** are somewhat larger. As anticipated, the carbonyl carbon resonances show a stronger dependance on variation of the transition metal: the δ values continuously increase within the series M = W < Mo < Cr for both the *cis*- and the *trans*-CO carbon centers. In **75b** the *trans*-CO carbon has a smaller phosphorus–carbon coupling constant magnitude than the *cis*-CO groups, which is also a common feature of pentacarbonyl phosphane chromium complexes.[148, 163]

The IR spectra of **74b** and **75b** show qualitatively the same features as those of complexes **41b,g,h,m,r–t**, **122b**, **69b,l**, **126b,g,h**, thus, they shall not further be discussed (cf. Appendix C, Tab. C.2). Also the UV/Vis absorbance spectra of **74b** and **75b** revealed similar results as the spectrum of their tungsten congener **41b**, which is discussed in Chapter 5 in detail. It is noteworthy that the visible absorption band of chromium complex **75b** as well as its optical end absorption appear at longer wavelengths (λ_{max} = 439 nm; λ_{onset} = 554) compared to **41b** (λ_{max} = 407 nm; λ_{onset} = 505) and **74b** (λ_{max} = 396 nm; λ_{onset} = 508).

Complexes **74b** and **75b** (and also **41b**; Section 3.1) crystallize in the monoclinic space group P2$_1$ (No.4) and are isotypic; apart from their pentacarbonyl metal fragments they exhibit almost identical bond lengths and angles. The mean deviations from least-squares planes of the 2H-1,4,2-diazaphosphole rings are 0.027 (**74b**) and 0.033 Å (**75b**).
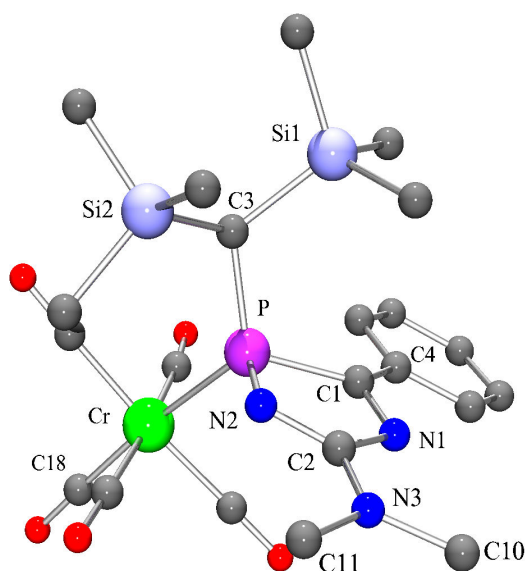
Figure 4.17: Molecular structure of complex **75b** in the crystal (hydrogen atoms omitted for clarity). Selected bond lengths [Å] and angles [°]: Cr–C(18) 1.870(2), Cr–P 2.4208(6), P–N(2) 1.682(2), P–C(1) 1.887(2), C(1)–N(1) 1.292(3), C(2)–N(2) 1.311(2), C(2)–N(3) 1.337(3), C(1)–C(4) 1.465(3), N(2)–P–C(1) 90.35(10), P–C(1)–N(1) 109.18(18), C(1)–N(1)–C(2) 110.16(18), N(1)–C(2)–N(2) 120.8(2), C(2)–N(2)–P 108.93(18), N(2)–C(2)–N(3) 122.1(2).

Insight into metal–phosphorus bond strengths of 2H-1,4,2-diazaphosphole complexes was obtained from FAB- (positive mode) and EI-mass spectra. While in the case of chromium complex **75b** m/z 415 assigned to [**75b** – 5 CO]$^{•+}$ represented the base peak of the FAB spectrum, the signal of protonated heterocycle [**50b** + H]$^+$ (m/z 364) was the base peak of the spectrum of molybdenum complex **74b**. Similar results were

obtained also for tungsten complexes (cf. previous sections), but for complex **74b** this signal clearly dominated the spectrum while the abundance of the molecular ion ([**74b** + H]$^+$: m/z 602) was only 3 %; for chromium complex **75b** the molecular cation was not even detected by FAB-MS. Under EI conditions losses of SiMe$_3$ and methyl groups as well as ring fragmentations similar to those described for complexes **41b,g** in Section 3.1 were observed also for **74b** and **75b**. Furthermore, the radical cationic heterocycle **50b**$^{\bullet+}$ was detected (m/z 363), in the spectrum of complex **75b** as base peak.

It can be concluded that the Mo,P and Cr,P bonds of **74b** and **75b** are more labile than the W,P bond of **41b**, and—more important—the metal–phosphorus bonds become significantly weakened through protonation of the heterocyclic ligand. This may serve as an explanation why fast decomplexation was observed in reactions of **70** and **71** with **36b** and TfOH (i, Scheme 4.10); obviously, it occurred at protonated 2H-1,4,2-diazaphosphole complexes, which were formed intermediately.

To investigate the influence of the triflate anion on the decomplexation reaction in the absence of any Brønsted acid, complex **74b** was reacted in methylene chloride with [^{n}Bu$_4$N][OTf]. Also here, the resonance of the liberated ligand **50b** was detected, but the decomplexation was significantly slower than in the presence of the acid; after 24 hours the reaction mixture contained approximately 19 % of **50b**.
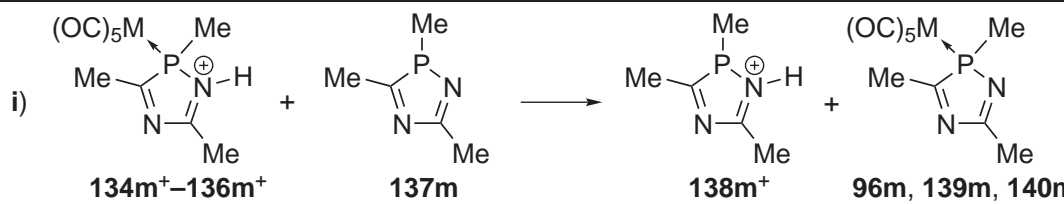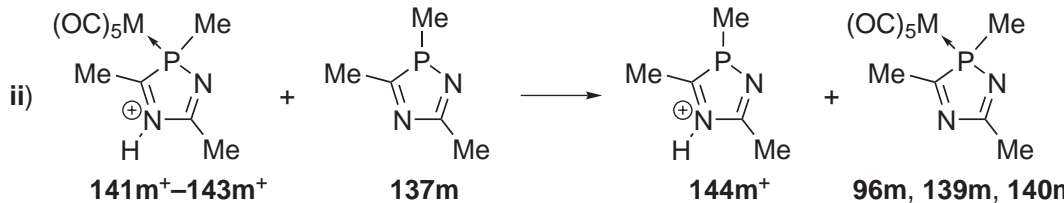
In order to get more insight into the effects of protonation of 2H-1,4,2-diazaphosphole complexes, isodesmic reactions **i** and **ii** were calculated using DFT methods (Tab. 4.6). These model reactions provide information on the change in the metal–phosphorus bond strengths induced by N-protonation of 2H-1,4,2-diazaphosphole complexes, as they describe the transfer of a pentacarbonyl metal fragment from a cationic to a neutral ligand system.[24] Here, cationic complexes **134m$^+$**–**136m$^+$** (**i**) were used as models for N^1-protonated complexes; reactions of **141m$^+$**–**143m$^+$** (**ii**) were calculated to estimate the effect of (hypothetical) N^4-protonation.

The main result is: all metal–phosphorus bonds are considerably weakened upon protonation, whereas N^1-protonation has a slightly larger effect than protonation at N^4. Against the background that 2H-1,4,2-diazaphospholium ligands showed enhanced π acidity (see Section 4.1.1) it can be concluded that the M,P bond weakening relies mainly on weakening of the σ-type phosphorus→metal donor bond upon N-protonation.

---

[24]Note that the values do not provide information on absolute magnitudes of the metal–phosphorus bond strengths. It should be mentioned that bond strengths, in general, can be estimated from vibrational spectra or calculations by evaluating *Compliance Constants*, which are available through inversion of the Hessian matrix in nonredundant internal coordinates.[264]

Table 4.6: Calculated thermochemical data for isodesmic $W(CO)_5$ exchange reactions (RI-BP86/TZVP/ECP-60-MWB(W)/ECP-28-MWB(Mo) + COSMO ($\varepsilon = 8.93$) // RI-BP86/SV(P)/ECP-60-MWB(W)/ECP-28-MWB(Mo) + COSMO ($\varepsilon = 8.93$); all values in $kJ \cdot mol^{-1}$).

M	i			ii		
	$\Delta_R E_0$	$\Delta_R H_{298}$	$\Delta_R G_{298}$	$\Delta_R E_0$	$\Delta_R H_{298}$	$\Delta_R G_{298}$
W	−36.3	−35.7	−37.3	−33.4	−32.7	−34.4
Mo	−35.0	−34.4	−35.3	−32.0	−31.2	−32.2
Cr	−37.4	−36.4	−37.9	−34.0	−33.0	−35.6

By taking advantage of this effect $2H$-1,4,2-diazaphosphole **50b** was synthesized in a one-pot reaction from complex **70** and nitrile **36b** via treatment with triflic acid in methylene chloride. When pyridine was added after several hours heterocycle **50b** was obtained as the only phosphorus-containing product (Scheme 4.10, iii), but, unfortunately, it decomposed during column chromatography (silanized silicagel, −50 °C). After repeating the reaction and workup procedures an oily crude product was obtained that revealed NMR spectroscopic information via multinuclear and various shift-correlated 2D NMR experiments (Tab. 4.7).

The ^{31}P resonance of **50b** appears only slightly upfield from that of its tungsten complex (**41b**: $\delta = 101.8$), which is consistent with the trend found for ligand **50c** versus tungsten complex **41c**[155] as well as for **78l** versus **69l** (Section 3.3). The ^{13}C NMR chemical shifts of the $2H$-1,4,2-diazaphosphole carbons are almost unaffected by decomplexation. On the other hand, all phosphorus–carbon coupling constant magnitudes are significantly increased, except for $|^{2+3}J_{PC}|$ of C^5 where the effect is negligible. Interestingly, **50b** shows only one resonance corresponding to the trimethylsilyl groups in ^1H and $^{13}C\{^1H\}$ NMR spectra, which was observed also for $2H$-1,4,2-diazaphosphole κN-complexes **129h**, **130h**, and **131h** (cf. Section 4.1.3), but in the case of **50b** the

resonances were slightly broadened, which may point to starting decoalescence. Note-worthy is that the NMe$_2$ moiety shows only one resonance for both methyl groups, thus pointing to a fast rotation about the exocyclic C^5,N bond in solution. This is in marked contrast to complexes of **50b**.

Table 4.7: Selected NMR spectroscopic data for molybdenum and chromium complexes **74b**, **75b**, protonated complexes **145b**, **146b**, protonated ligand **147b**, and neutral ligand **50b**.

	74b†	75b†	145b‡	146b‡	147b$^\sharp$	50b†
$\delta(^{31}\text{P})$	122.7	146.3	130.6	157.7	100.7	95.4
$|^{2+5}J_{PH}|$/Hz	–	–	22.9	22.9	28.0	–
$CH(\text{SiMe}_3)_2$						
$\delta(^{13}\text{C})$	21.4	22.5	×	×	21.1	18.6
$|^{1}J_{PC}|$/Hz	11.6	9.7	×	×	63.7	56.9
C^3						
$\delta(^{13}\text{C})$	201.3	200.5	×	×	211.8	210.6
$|^{1+4}J_{PC}|$/Hz	29.7	31.7	×	×	40.4	52.4
C^5						
$\delta(^{13}\text{C})$	164.7	163.7	×	×	165.9	167.4
$|^{2+3}J_{PC}|$/Hz	0.7	0.8	×	×	0.4	1.1

†In C$_6$D$_6$. ‡In CH$_2$Cl$_2$. $^\sharp$In CD$_2$Cl$_2$. $^\times$Not determined.

By ^{31}P NMR spectroscopic monitoring of reactions of **70** and **71** with TfOH and **36b** evidence was obtained for the formation of N^1-protonated 2H-1,4,2-diazaphos-phole complexes **145b** and **146b** in the primary reaction step (Scheme 4.11, Fig. 4.18, and Tab. 4.7). Their resonances are slightly downfield from those of respective neutral complexes **74b** and **75b** and show large phosphorus–proton couplings about 23 Hz in magnitude as observed for N^1-protonated complexes **123b**, **124b** (Section 4.1.1), **127b**, and **128b** (Section 4.1.2). During the reactions both signals decreased in favor of a resonance at $\delta = 100.7$ ($|^2J_{PH}| = 28.0$ Hz) that is assigned to the noncoordinated N^1-protonated ligand **147b**.

Adding of cold n-pentane to a solution of **147b** yielded a brownish-green precipitate that was, after workup, subjected to multinuclear NMR and diverse shift-correlated 2D NMR experiments, which revealed all relevant NMR spectroscopic information on N^1-protonated 2H-1,4,2-diazaphosphole **147b** (Tab. 4.7).

Scheme 4.11: *Consecutive* reactions of $2H$-azaphosphirene molybdenum and chromium complexes **70**, **71** with dimethyl cyanamide (**36b**), TfOH, and pyridine.

Figure 4.18: ^{31}P{^{1}H} NMR spectra recorded during the reaction of molybdenum complex **70** with nitrile **36b** and TfOH (Scheme 4.11). Extensions of the resonances from proton-coupled ^{31}P NMR spectra show signal splitting due to ^{31}P,^{1}H coupling.

Comparison of the NMR data for **147b** and its neutral congener **50b** revealed that the ^{31}P NMR chemical shift is slightly increased (by 5.3 ppm), while the ^{13}C{^{1}H} NMR spectroscopic data are almost unaffected by protonation. Unlike **50b**, the protonated heterocycle **147b** shows two sets of resonances corresponding to the SiMe$_3$ groups in ^{1}H, ^{13}C{^{1}H}, and ^{29}Si{^{1}H} NMR spectra. Furthermore, two sets of ^{1}H and ^{13}C resonances were detected for the NMe$_2$ substituent. The latter observation is easily understood, since rotation about the exocyclic C^5,N bond should be restricted through formation of a more pronounced π interaction between the dimethylamino nitrogen and C^5 due to protonation at N^1.

The constitution of **147b** was further supported by ^{1}H,^{15}N HMQC NMR experiments; the assinment of the ^{15}N NMR data is shown in Figure 4.19. The data for **147b** are comparable to those for N^1-protonated tungsten complex **123b** (δ(N^1) = −264, $|^{1+4}J_{PN}|$ = 15 Hz; δ(NMe$_2$) = −269), and also here, the protonated nitrogen atom showed a long-range correlation with the CH proton of the bis(trimethylsilyl)methyl group.
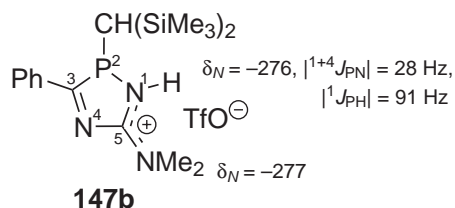
Figure 4.19: Assignment of ^{15}N NMR spectroscopic data for N^1-protonated 2H-1,4,2-diazaphosphole **147b** (CD$_2$Cl$_2$).

4.1.5   Insertion of an Isonitrile: Access to a Novel Heterocycle Complex

Selective ring expansion of $2H$-azaphosphirene complex **35** with cyclohexyl isocyanide (**148**) was achieved at low temperature ($-30\,^{\circ}$C). Addition of triflic acid, warming to ambient temperature, and subsequent addition of triethylamine yielded the novel 2,3-dihydro-1,3-azaphosphete complex **149** (Scheme 4.12). The product was isolated, purified by low-temperature column chromatography, and its constitution was unambiguously identified by multinuclear NMR experiments, mass spectrometry, IR and UV/Vis spectroscopy, and a single-crystal X-ray diffraction study (Fig. 4.21); the purity was examined by elemental analysis.
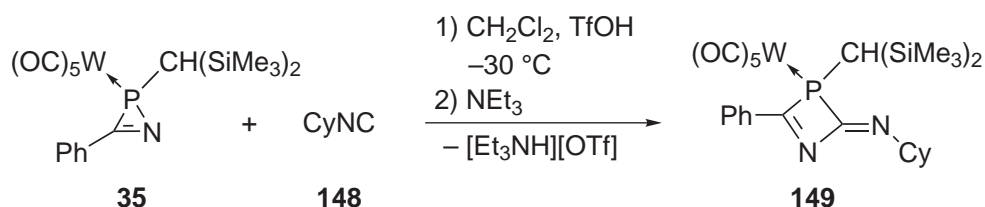
Scheme 4.12: Synthesis of 2,3-dihydro-1,3-azaphosphete complex **149** using $2H$-azaphosphirene complex **35**, TfOH, isonitrile **148** (Cy = cyclohexyl), and NEt$_3$.

Complex **149** is the first derivative of this class of compounds having a 2,3-dihydro-1,3-azaphosphete ligand; it shows a ^{31}P NMR resonance at $\delta = 104.0$ ($|^1J_{WP}| = 220.0$ Hz). So far, only cationic N-alkyl 2,3-dihydro-1,3-azaphosphetium derivatives **150a–f** are known, synthesized from phosphenium salts and isonitriles by Majoral and coworkers (Scheme 4.13), which display ^{31}P resonances at about $109-129$ ppm.[265]

Interestingly, the ^{31}P NMR spectroscopic data for complex **149** are very close to those for $2H$-1,4,2-diazaphosphole complexes (Fig. 4.20). Noteworthy is that the C^2 resonance[25] appears at comparatively high field ($\delta = 156.6$) and has a large coupling constant magnitude ($|^{1+3}J_{PC}| = 67.2$ Hz), while the C^4 center resonates at very low field ($\delta = 198.5$) showing a coupling constant with significantly smaller magnitude ($|^{1+3}J_{PC}| = 8.4$ Hz).[26] In contrast, both ring carbon centers of **150a–f** resonate in the same range ($\delta = 159-165$) and have phosphorus–carbon coupling constant magnitudes about $4-19$ Hz.[265]

---

[25]For atom numbering see Fig. 4.20.

[26]Note that the hybridisation of both carbon centers (sp^2) as well as their sum of scalar couplings to phosphorus (^{1+3}J) are identical.
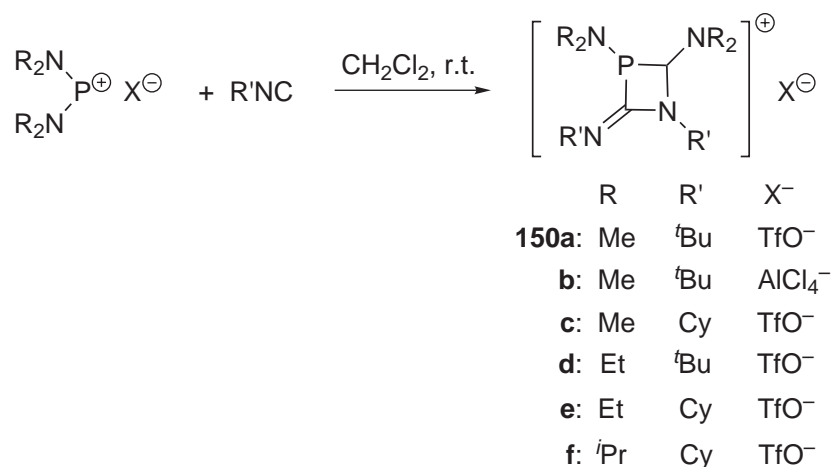
Scheme 4.13: Syntheses of *N*-alkyl 2,3-dihydro-1,3-azaphosphetium salts **150a–f** presented by Majoral and coworkers.[265]

A comparison of the $^{13}C\{^1H\}$ NMR resonances observed for the PCN units of the three-, four-, and five-membered rings shown in Figure 4.20 reveals that both the chemical shifts and—more pronounced—the phosphorus–carbon coupling constant magnitudes continuously increase with the ring size.
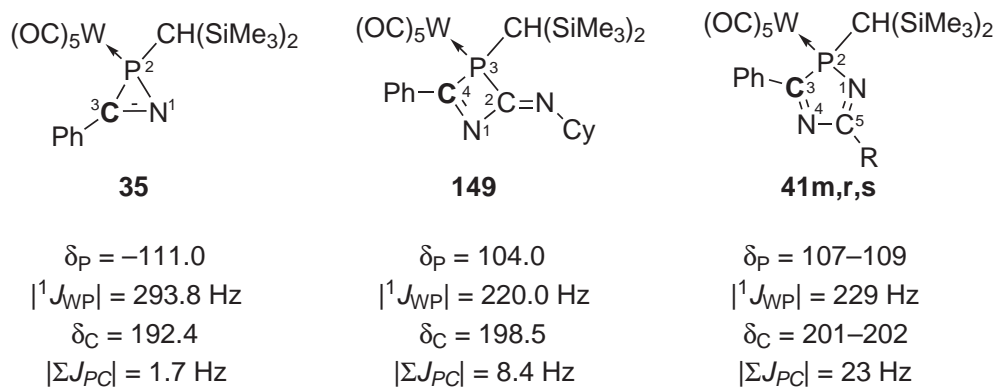
Figure 4.20: $^{31}P\{^1H\}$ and $^{13}C\{^1H\}$ NMR spectroscopic data (ring carbon at the PCN moiety; bold face marked) for complexes **35**,[266] **149**, and **41m,r,s** (R = CH$_3$ (**m**), 1-adamantyl (**r**), ^{t}Bu (**s**)) (all data from C$_6$D$_6$ solution).

Complex **149** crystallizes in the triclinic space group P$\bar{1}$ with two independent molecules in the asymmetric unit, which show no significant differences in their structural parameters (see Appendix E, Fig. E.13). Therefore, only one molecule is displayed here (Fig. 4.21). The four-membered heterocycle is almost planar (mean deviation from least-squares plane: 0.018 Å), and adopts an almost coplanar arrangement with the phenyl substituent (twist angle with respect to least-sqares planes: 19.0°).

The endocyclic angle at P is very small (C(1)–P–C(2) 68.0°(3)); the same holds true for the sum of the angles at phosphorus ($\Sigma\angle(P_{PR_3})$ 293.3°). Complex **149** features two comparatively long endocyclic P,C bonds, and the W,P distance is slightly shorter as in $2H$-1,4,2-diazaphosphole complexes.
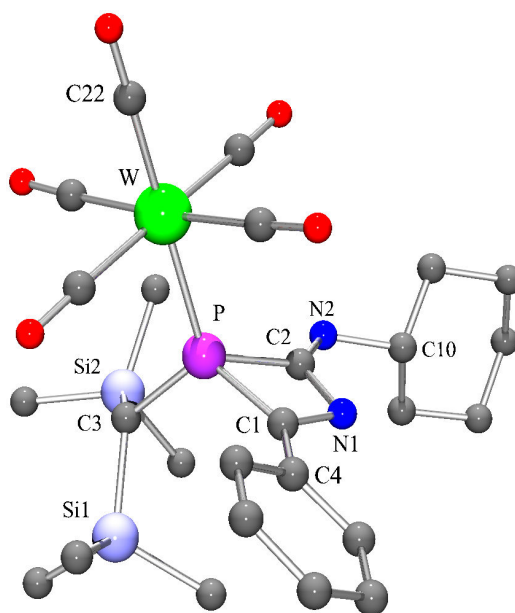
Figure 4.21: Molecular structure of complex **149** in the crystal (hydrogen atoms omitted for clarity). Selected bond lengths [Å] and angles [°]: W–C(22) 2.005(6), W–P 2.4987(13), P–C(1) 1.878(6), P–C(2) 1.874(6), C(1)–N(1) 1.312(7), N(1)–C(2) 1.436(7), C(2)–N(2) 1.239(7), C(1)–C(4) 1.443(8), C(1)–P–C(2) 68.0(3), P–C(1)–N(1) 98.4(4), C(1)–N(1)–C(2) 99.4(5), N(1)–C(2)–P 94.2(4), P–C(2)–N(2) 135.3(4).

The IR spectrum showed the characteristic bands for C,O stretch vibrations of a pentacarbonyl phosphane tungsten complex having a slightly perturbed C_{4v} symmetry. They appear in the same range as those of $2H$-1,4,2-diazaphosphole tungsten complexes. The well separated A_1 band was found at 2071 cm^{-1}, and the B_1 vibration resonates at 1987 cm^{-1} showing a lower intensity. Three very intense bands were detected at 1947, 1930, and 1906 cm^{-1} according to vibrations of local A_1 and E symmetry.

In the UV/Vis spectrum the longest-wavelength absorption was centered at λ_{max} = 397 nm, and optical end absorption was recorded at λ_{onset} = 472 nm, which is at significantly shorter wavelength compared to $2H$-1,4,2-diazaphosphole complexes. The $\pi-\pi^*$ transition was detected at λ_{max} = 290 nm, thus, in the same range as in the cases of complexes **41m,r,s**.

Under EI-MS conditions complex **149** showed no ring fragmentation; successive expulsion of all five CO ligands constituted the major fragmentation pathway.

It is noteworthy that complex **149** could not be obtained directly from 2*H*-azaphosphirene complex **35** and cyclohexyl isocyanide (**148**) in the absence of TfOH.[267, 268] E. Ionescu carried out reactions of **35** with cyclohexyl and *tert*-butyl isocyanide under thermal and photochemical conditions (Scheme 4.14). In these cases displacement of the PhCN moiety from the phosphorus center of **35** was observed, thus yielding mono-phosphacarbodiimide complexes **152a,b**.[27] It should be noted that the synthesis of complex **149** could also not be achieved via the oxidative SET protocol using ferrocinium hexafluorophosphate (Chapter 3).
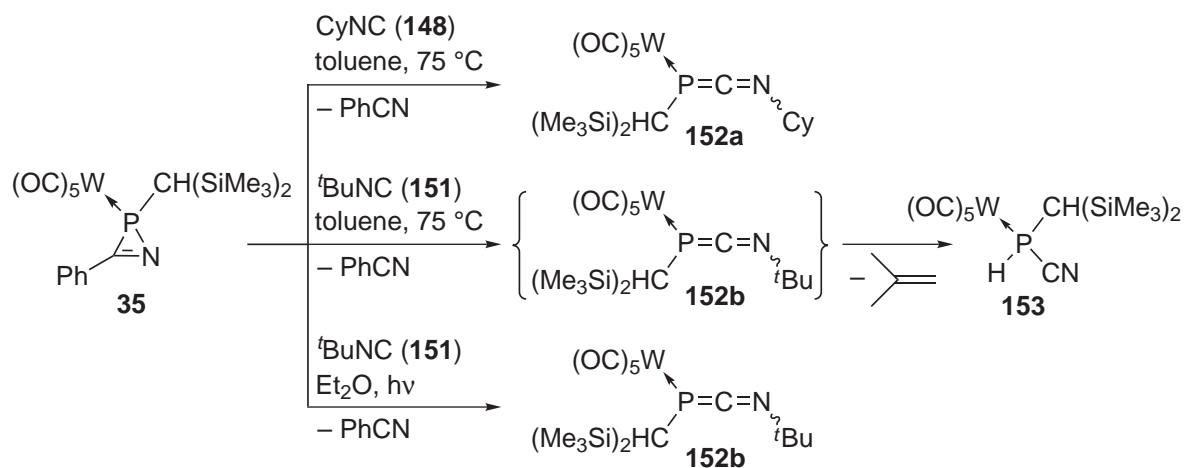
Scheme 4.14: Thermal and photochemical reactions of 2*H*-azaphosphirene complex **35** with isonitriles **148** and **151**.[267, 268]

In order to get more insight into the triflic acid-induced formation of complex **149**, the reaction of **35** with **148** and TfOH was carried out without subsequently adding a base (Scheme 4.15). Upon addition of the acid the reaction mixture immediately turned deep red,[28] and after workup the triflate salt **154** of the *N*-protonated 2,3-dihydro-1,3-azaphosphete complex was obtained. Although multinuclear (^{1}H, ^{13}C, ^{29}Si, ^{31}P) one- and two-dimensional NMR experiments were performed, the position of the *N*-bonded proton could not unambiguously be established.

The ^{31}P NMR resonance of complex **154** at $\delta = 106.9$ ($|^1J_{WP}| = 240.3$ Hz) is only 2.9 ppm downfield from that of its neutral congener **149**, but its tungsten–phosphorus

---

[27]Under thermal conditions complex **152b** immediately reacted further to cyanophosphane complex **153** via ω-H activation and elimination of isobutene, but it could be isolated from the photochemical reaction.

[28]By ^{31}P NMR reaction monitoring only the resonance of complex **154** was detected; no further intermediates were observed.

coupling constant is significantly larger ($\Delta |^1 J_{WP}| = 20.3$ Hz). The signal shows a coupling with the NH proton being 6.4 Hz in magnitude, and the ^{1}H resonance of this proton was found at very low field ($\delta = 12.07$, $h_{1/2} = 40$ Hz).

Scheme 4.15: Reaction of 2H-azaphosphirene complex **35** with isonitrile **148** and TfOH.

The ^{13}C{^{1}H} NMR resonances of the ring carbons were detected at $\delta(C^2) = 179.8$ ($|^{1+3}J_{PC}| = 24.2$ Hz) and $\delta(C^4) = 211.9$ ($|^{1+3}J_{PC}| = 14.9$ Hz), thus, both nuclei have experienced a significant low field shift through N-protonation ($\Delta\delta = 23.2$ (C^2) and 13.4 (C^4)). The phosphorus–carbon coupling constants are affected in different ways: while the $^{1+3}J_{PC}$ magnitude of C^2 is 43.0 Hz decreased, an increase by 11.6 Hz was observed for the coupling constant of the C^4 center. The C^4 resonances of both **149** and **154** showed satellites arising from $^{2+4}J_{WC}$ couplings (~ 3 Hz). Noteworthy is that the phosphorus–carbon coupling constant magnitude of the *trans*-CO carbon is increased by 3.9 Hz upon protonation.

4.2 Investigations on the Applicability of Several Brønsted and Lewis Acids

To examine effectiveness and dependance of ring expansion reactions from Brønsted acid strengths, studies were carried out using 2H-azaphosphirene complex **35**, dimethyl cyanamide (**36b**), and different acids in methylene chloride. The following acids were chosen: triflic acid, tetrafluoroboric acid diethyl ether complex, fuming and concentrated sulfuric acid, trifluoroacetic acid (TFA), trichloroacetic acid (TCA), triethylammonium triflate, and acetic acid (Scheme 4.16).[29] In those reactions that yielded a characteristic color change from yellow to red, indicating the protonation of complex **35** and/or its reaction with dimethyl cyanamide (i.e., the formation of complex **123b**), a base was subsequently added (pyridine or NEt$_3$), and the reaction mixture was then analyzed by ^{31}P$\{^1$H$\}$ NMR spectroscopy. In the cases of [Et$_3$NH][OTf] and CH$_3$CO$_2$H the analyses were carried out without previous addition of a base; results are given in Table 4.8.[30]
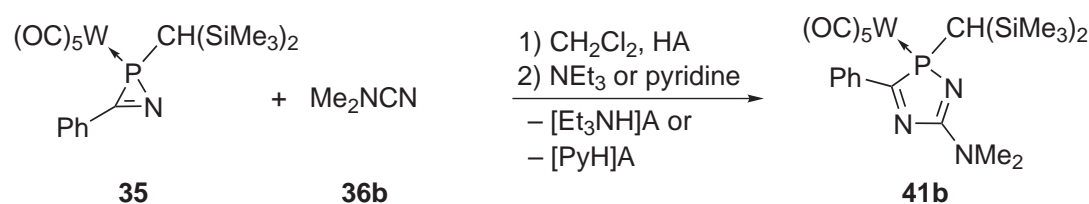
HA = TfOH, HBF$_4$·Et$_2$O, H$_2$SO$_4$·(SO$_3$)$_x$, H$_2$SO$_4$, CF$_3$CO$_2$H, CCl$_3$CO$_2$H, [Et$_3$NH][OTf], CH$_3$CO$_2$H

Scheme 4.16: Ring expansion reactions of 2H-azaphosphirene complex **35** with dimethyl cyanamide (**36b**) induced by several Brønsted acids, and optional subsequent reaction with a base (if an occurring reaction was visually indicated).

Complete conversion of **35** and formation of the expected ring expansion product **41b** was achieved only with triflic acid and TFA. The reaction with HBF$_4$·Et$_2$O gave approximately 9 % of complex **79a**, which was observed before (cf. Section 3.3 and Section 4.3.2), showing that BF$_4^-$ had taken part in the reaction course. Although the reaction with sulfuric acid yielded complete consumption of **35**, it was unselective; the amount of **41b** was only 34 % besides several unidentified by-products. By employment of fuming sulfuric acid ("oleum", H$_2$SO$_4$·(SO$_3$)$_x$) the amount of **41b** was increased to 45 %. When TCA was used about 62 % **41b** was formed; the major

---

[29]Values of Hammett acidity functions H_0[269] were reported for the neat acids in the cases of triflic acid (-13.7),[270] sulfuric acid (-10.6),[269] and trifluoroacetic acid (-2.7).[270]

[30]Most reactions were carried out at various temperatures and concentrations; only the "best" results are given.

by-product displayed a ^{31}P resonance at $\delta = 59.9$ and was not further characterized. Almost no reaction occurred between **35** and **36b** in the presence of triethylammonium triflate[31] or acetic acid. In conclusion, within this series the weakest Brønsted acid that is sufficient to initiate ring expansion of 2H-azaphosphirene complex **35** is trichloroacetic acid.

Table 4.8: Ratio of complex **41b** (by ^{31}P{^{1}H} NMR signal integration) in Brønsted and Lewis acid-induced ring expansion reactions shown in Schemes 4.16–4.19.

Brønsted Acid	Ratio of **41b** [%]	Lewis Acid	Ratio of **41b** [%]
TfOH	100	$BF_3 \cdot Et_2O$	62
$HBF_4 \cdot Et_2O$	84	$B(C_6F_5)_3$	97
$H_2SO_4 \cdot (SO_3)_x$	45	$Li[PF_6]$	44
H_2SO_4	34	$Li[OTf]/CH_2Cl_2$	19
CF_3CO_2H	100	$Li[OTf]/THF$	0
CCl_3CO_2H	62	$Li[OTf]/12$-cr-4	0
$[Et_3NH][OTf]$	0	$Li[B(C_6F_5)_4]$	85
CH_3CO_2H	0	CuCl	0
		$[Cu(MeCN)_4][OTf]$	14

To complete this study, the same model system as before was examined together with the following Lewis acids (LA): boron trifluoride diethyl etherate and tris(pentafluorophenyl)borane as well as lithium hexafluorophosphate, lithium triflate, lithium tetrakis(pentafluorophenyl)borate (Scheme 4.17), copper(I) chloride (Scheme 4.18), and tetrakisacetonitrile copper(I) triflate (Scheme 4.19); results are given in Table 4.8. The reaction with $BF_3 \cdot Et_2O$ yielded complete conversion of **35** and 62 % of **41b** was formed. Reaction monitoring by ^{31}P{^{1}H} NMR spectroscopy revealed the formation of by-products with large phosphorus–fluorine couplings, one of which could be assigned to complex **174**, which was observed also in the reaction of **35** with $BF_3 \cdot Et_2O$ in the absence of nitriles (see Section 4.3.2). Obviously, a fluoride source was being generated from $BF_3 \cdot Et_2O$ in the presence of 2H-azaphosphirene complex **35**. Such side-reactions were avoided by using tris(pentafluorophenyl)borane, which yielded a selective reaction; after 6 days complex **35** was completely converted, and 97 % of **41b** was formed.

The ^{31}P{^{1}H} NMR spectrum recorded during the reaction of **35** with **36b** in the presence of $Li[PF_6]$ showed a resonance in the range of the expected product **41b** centered at $\delta \approx 102$ (ca. 53 %). Interestingly, the signal was significantly broadened

---

[31]After one week a ^{31}P resonance at $\delta = 97.0$ (3 %) was detected, which may be assigned to free ligand **50b** presumably formed via complex **41b**.

($h_{1/2}$ = 70 Hz) presumably arising from an adduct [**LA–41b**] of complex **41b** and the lithium cation (Scheme 4.17); the broadening could result from ^{31}P,^{7}Li and ^{31}P,^{6}Li couplings. Also here, several by-products with large phosphorus–fluorine couplings were observed, among them were fluorophosphane complexes **79a,b**. After 3 days the broad ^{31}P resonance of adduct [**LA–41b**] had vanished, and a sharp signal assigned to **41b** was detected; complex **35** was completely consumed.

LA = BF$_3$·Et$_2$O, B(C$_6$F$_5$)$_3$, Li[PF$_6$], Li[OTf], Li[OTf]/THF, Li[OTf]/12-cr-4, Li[B(C$_6$F$_5$)$_4$]
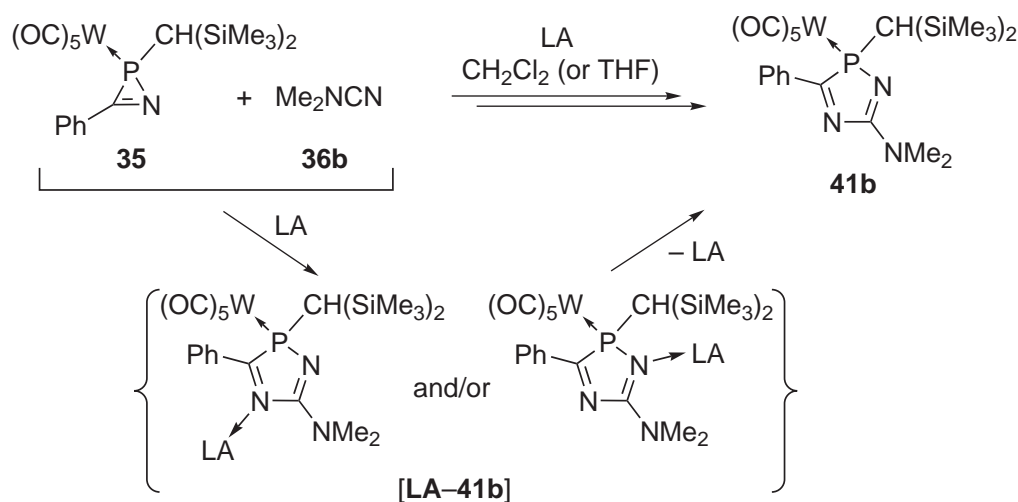
Scheme 4.17: Ring expansion reactions of 2H-azaphosphirene complex **35** with dimethyl cyanamide (**36b**) induced by Lewis acids.

The reaction with Li[OTf] was very slow. After one day the mixture contained approximately 19 % of **41b**, but no further conversion was observed. So as to achieve a higher degree of solvation of the lithium salt, the reaction was carried out a) in THF and b) in the presence of an equimolar amount of 12-crown-4 in CH$_2$Cl$_2$. Both approaches turned out to be counterproductive; no conversion of **35** was observed in both reactions. Obviously, 2H-azaphosphirene complex **35** cannot compete with THF or 12-crown-4 for coordination of the lithium cation. Lithium tetrakis(pentafluorophenyl)-borate, which has a rather weak nucleophilic anion and is sufficiently soluble in methylene chloride, turned out to be an appropriate choice: about 85 % of **41b** was formed within less than two days.

In the reaction with CuCl complete conversion of **35** was observed but no formation of **41b**. Instead, two products were formed that were identified as 2H-1,3,2-diazaphosphole complexes **46**[146] (δ = 149.7, $|^1J_{WP}|$ = 259.4 Hz; 70 %) and **155**[146] (δ = 132.9, $|^1J_{WP}|$ = 263.2 Hz; 30 %). Both complexes have been observed only in thermal reactions of **35** via nitrilium phosphane ylide complexes, so far.[146] (see Section 1.3).
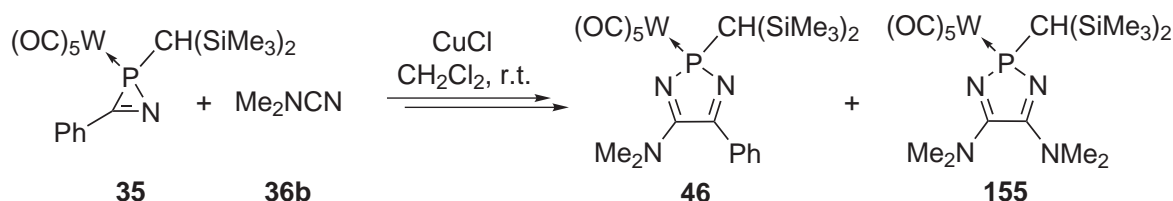
Scheme 4.18: Reaction of 2H-azaphosphirene complex **35** with dimethyl cyanamide
(**36b**) in the presence of copper(I) chloride.

Complexes **46** and **155** were observed also in the reaction of **35** with **36b** in the
presence of [Cu(MeCN)$_4$][OTf] (after 12 h: 11 % (**46**) and 27 % (**155**)), but here, some
amount of target complex **41b** (ca. 14 %) and around 3 % of **41m** was formed, in
addition (Scheme 4.19). The formation of the latter is easily understood as acetonitrile
is released from [Cu(MeCN)$_4$][OTf] during the reaction and competes with Me$_2$NCN
for ring expansion.
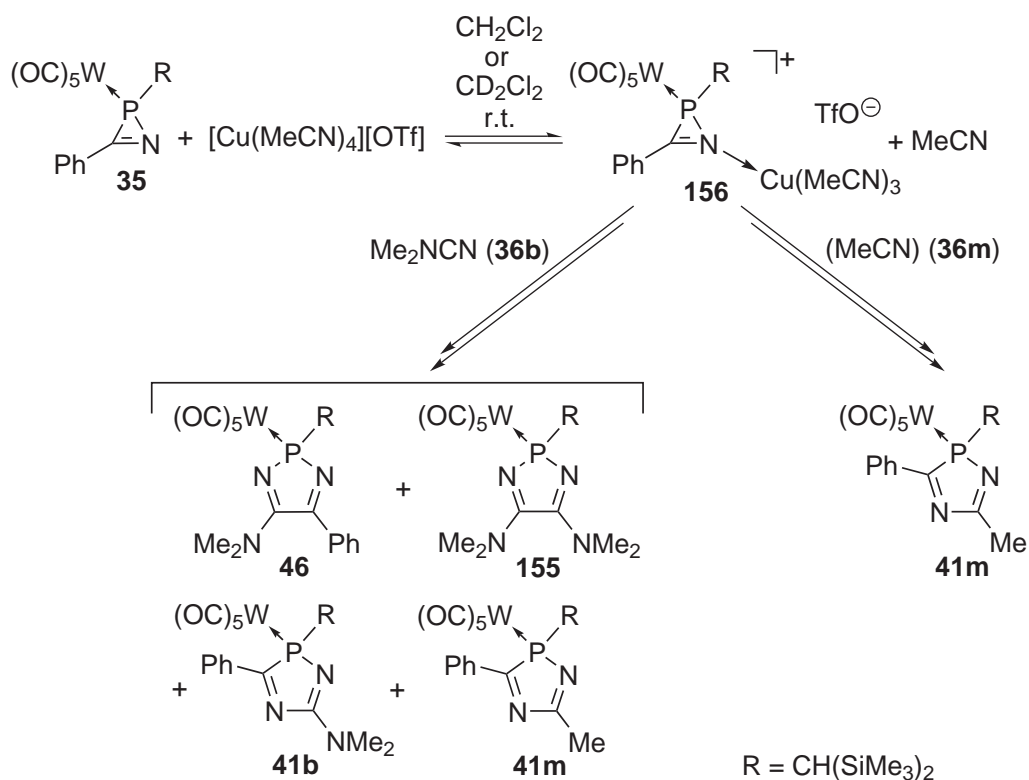
Scheme 4.19: Reaction of 2H-azaphosphirene complex **35** with [Cu(MeCN)$_4$][OTf] and
dimethyl cyanamide (**36b**) or acetonitrile (**36m**) or without addition of a nitrile.

Interestingly, the resonance of reactant **35** was no longer detected during the re-
action, but the resonances of the four products mentioned beforehand increased at

the expense of a signal at $\delta = -92.3$ ($|^1J_{PW}| = 294.5$ Hz). This is about 17 ppm downfield from 2H-azaphosphirene complex **35**, but its tungsten–phosphorus coupling constant magnitude is virtually identical. In order to obtain more information about this reactive intermediate, the reaction of **35** with [Cu(MeCN)$_4$][OTf] was carried out without adding dimethyl cyanamide, and the mixture was analyzed by one- and two-dimensional ^{1}H and ^{31}P NMR spectroscopy. After 25 min already 27 % of ring expansion product **41m** was formed (Fig. 4.22), and the high field resonance was in this case detected at $\delta = -84.2$, thus, about 25 ppm downfield from **35**, whereas the tungsten–phosphorus coupling constant magnitude was almost unaffected ($|^1J_{PW}| = 297.5$ Hz).[32]
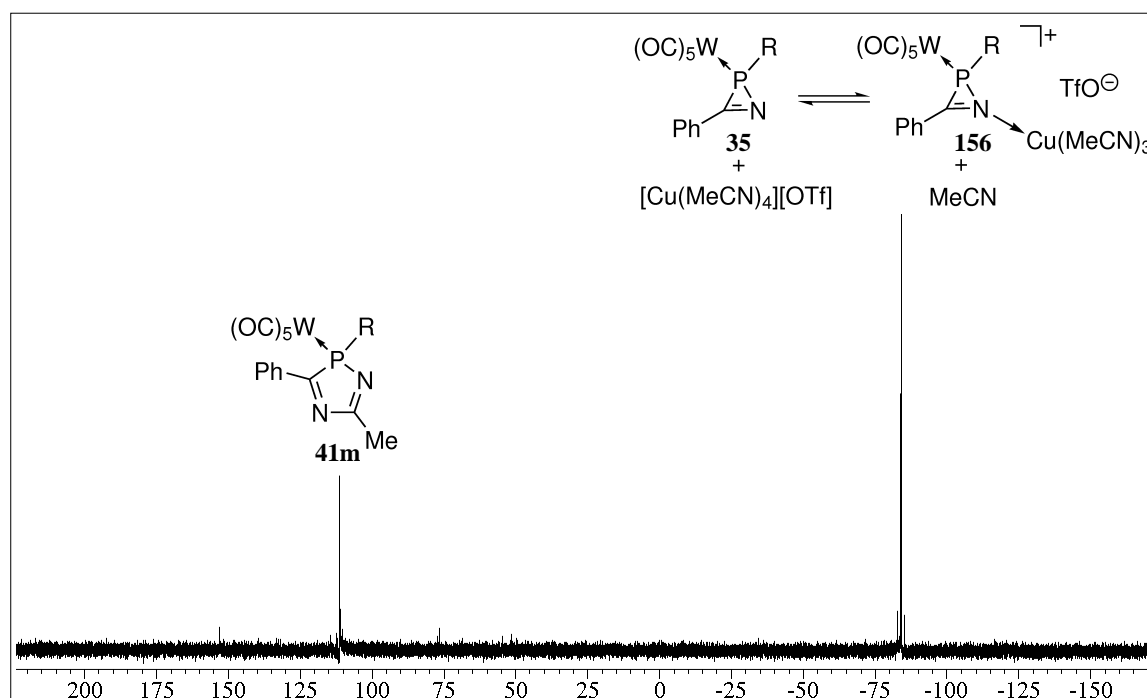
Figure 4.22: ^{31}P{^{1}H} NMR spectrum recorded during the reaction of 2H-azaphosphirene complex **35** with [Cu(MeCN)$_4$][OTf] after 25 min (Scheme 4.19; R = CH(SiMe$_3$)$_2$).

The ^{1}H NMR spectrum revealed resonances of a bis(trimethylsilyl)methyl and a phenyl group attributable to a 2H-azaphosphirene complex, and only one methyl resonance for CH$_3$CN was detected ($\delta = 2.14$).[33] When [Cu(MeCN)$_4$][OTf] was reacted with two equivalents of **35** a broad ^{31}P{^{1}H} resonance at $\delta = -99.0$ ($h_{1/2} = 57$ Hz) was observed; the $|^1J_{PW}|$ value can only roughly be estimated as 290 Hz. Also here,

---

[32]Here, the reaction was carried out using a higher molar concentration of reactants as before.

[33]This is 0.17 ppm downfield from pure acetonitrile (under the same measuring conditions) and only 0.03 ppm upfield from the methyl resonance of complex [Cu(MeCN)$_4$][OTf] in CD$_2$Cl$_2$ solution at the same concentration.

no further signals appeared in this region. Putting all this information together the conclusion is drawn that complexes **35** and $[\text{Cu(MeCN)}_4]^+$ form an equilibrium with heterobimetallic complex **156** where at least one MeCN ligand of $[\text{Cu(MeCN)}_4]^+$ is replaced by **35** and the ligand exchange at the copper(I) center occurs fast on the NMR time scale, thus giving rise to averaged signals.

The distribution of ring expansion products obtained with $[\text{Cu(MeCN)}_4][\text{OTf}]$ showed a strong dependance on the nitrile derivative employed (Scheme 4.19). While the reaction with dimethyl cyanamide yielded some amount of complexes **46** and **155**, reaction of **35** with $[\text{Cu(MeCN)}_4][\text{OTf}]$ in the absence of Me_2NCN revealed no evidence for the formation of $2H$-1,3,2-diazaphosphole complexes. When one equivalent of acetonitrile was added to a mixture of **35** and $[\text{Cu(MeCN)}_4][\text{OTf}]$ about 86 % of **41m** was formed.

4.3   Experimental Investigations on the Reaction Course

To get further insight into the course of the ring enlargement reaction of 2*H*-azaphosphirene complexes with nitriles using Brønsted acids, reaction of complex **35** with nitrile **36g** and TfOH was carried out at low temperature ($-80\,°C$) and was monitored by $^{31}P\{^1H\}$ NMR spectroscopy between -80 and $-20\,°C$ (Fig. 4.23).
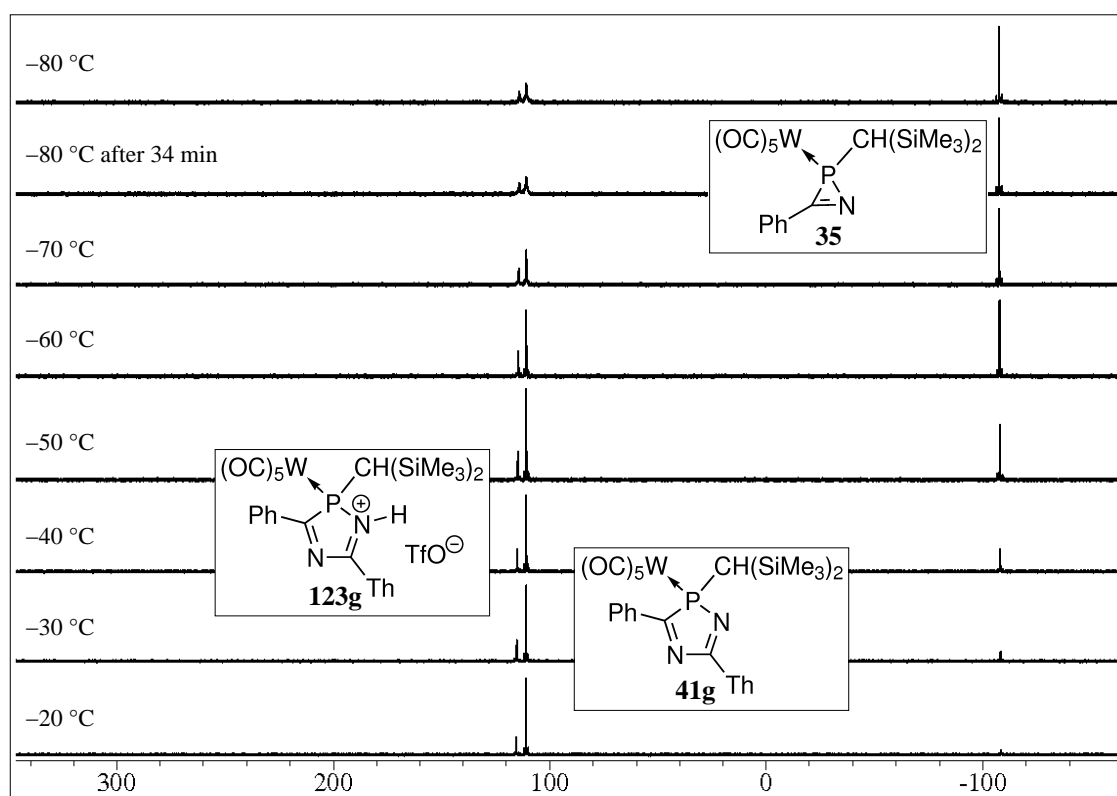
Figure 4.23: $^{31}P\{^1H\}$ NMR spectra recorded during the reaction of 2*H*-azaphosphirene complex **35** with 2-thiophenecarbonitrile (**36g**) and TfOH between -80 and $-20\,°C$ (Th = 2-thienyl).

During the reaction 2*H*-1,4,2-diazaphospholium complex **123g** was the only intermediate that could be observed. The resonances of **123g** and neutral complex **41g** increased slowly at the expense of that of **35**. No other species were observed such as 2*H*-azaphosphirenium complex [**H**−**35**]$^{+}$, which might be formed in the primary reaction step.[34] In this section further studies on the reaction mechanism are presented.

---

[34]Alternatively, it could be envisaged that instead of **35** the nitrile is protonated in the first step. As a good case in point, the reaction of complex **35**, acetonitrile, and TfOH was carried out in a

4.3.1 Mass Spectrometric Studies

Turning to mass spectrometry gas phase conditions, protonated $2H$-azaphosphirene complexes were generated via electrospray ionization (ESI) of complexes **35** and **121**. When methanol was used as spray solvent fragmentation via loss of CO dominated the spectra, but from acetonitrile solutions protonated complexes $[M + H]^+$ (**35**: m/z 618; **121**: m/z 594) were obtained in high abundances. Furthermore, metallated species $[M + Na]^+$ (m/z 640 and 616) and $[M + K]^+$ (m/z 656 and 632) were observed confirming that $2H$-azaphosphirene complexes can form complexes with alkali metal ions. When the spectrometer was contamined with Cu^+ ions complex $[2\,M + Cu]^+$ containing two molecules of **35** coordinated to copper(I) was observed, in addition (m/z 1297).

Besides such metal complexes, formal solvent adducts of **35** were observed at m/z 659, 636, and 650 corresponding to $[35 + H + CH_3CN]^+$, $[35 + H + CH_3OH]^+$, and $[35 + H + H_2O]^+$, respectively. Their structures might be interpreted as either noncovalent adducts or as cyclic or acyclic complexes with the N or the O atom of the solvent molecule covalently bound to the phosphorus or the carbon center of **35** (structures 159^+–164^+; Fig. 4.24). DFT calculations, which were performed on model systems,[35] confirmed these structures as minima and further revealed that acyclic structures 160^+, 163^+, and 164^+ should be thermodynamically favored over their cyclic isomers 159^+, 161^+, and 162^+;[36] O-protonated tautomers of 161^+–164^+ were not confirmed as minima. According to computational studies on the mechanism of the acid-induced ring expansion (Section 4.4) the acyclic acetonitrile adduct 160^+ is a plausible intermediate of this reaction. On the other hand, $[35 + H + CH_3CN]^+$ might not correspond to an intermediate but to the N^1- or N^4-protonated product $[41m + H]^+$ of the ring expansion reaction with acetonitrile proceeding either in solution or during the ESI process.[37]

---

different order and each step was monitored by ^1H and $^{31}P\{^1H\}$ NMR spectroscopy. Here, MeCN was reacted first with TfOH in CD_2Cl_2, and then a solution of **35** was added. After subsequent addition of NEt_3 the formation of complex **41m** was observed, hence, the alternative mechanism mentioned beforehand cannot be ruled out on an experimental basis. However, it is largely excluded on the basis of computational results (see Section 4.4.1).

[35]B3LYP/aug-TZVP/ECP-60-MWB(W)//RI-BLYP/aug-SVP/ECP-60-MWB(W); model system: CH_3 at P (instead of $CH(SiMe_3)_2$ or Cp^*) and CH_3 in place of phenyl.

[36]The model system for 160^+ is 105.4 $kJ \cdot mol^{-1}$ lower in energy than that for its cyclic structural isomer 159^+, and the model for 163^+ is by 118.1 $kJ \cdot mol^{-1}$ more stable than that for complex 161^+.

[37]The gas phase calculations revealed that the model system for the N^1-protonated complex is the most stable isomer. Its N^4-protonated tautomer is 22.4 $kJ \cdot mol^{-1}$ higher in energy, and the model system for acyclic structure 160^+ is by 98.3 $kJ \cdot mol^{-1}$ less stable.
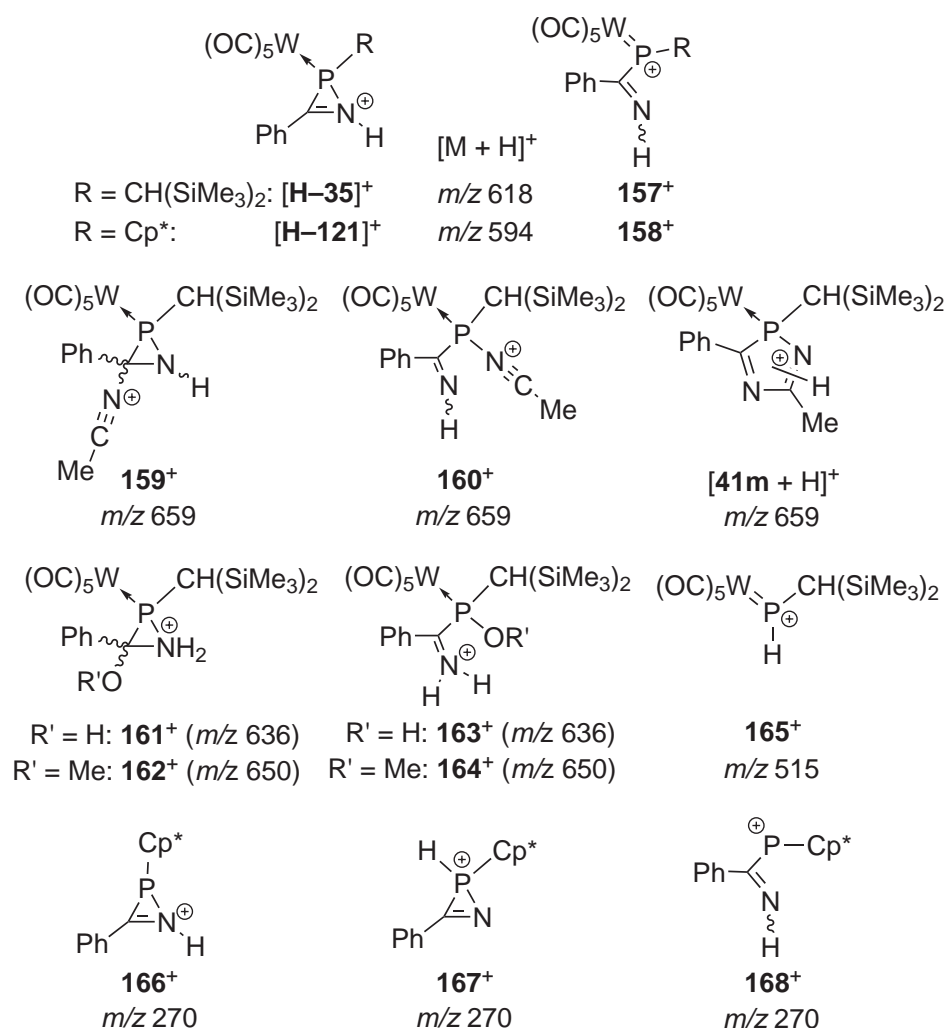
Figure 4.24: Protonation of 2H-azaphosphirene complexes **35** and **121** by ESI-MS and possible cation structures.

To gain more information about the structures of the detected species, the ions were mass-selected and fragmented by collisions with argon (CID-MS/MS). Exemplarily, MS/MS studies were carried out on derivatives with R(P) = CH(SiMe$_3$)$_2$. The main gas phase fragmentation of [**35** + H]$^+$ was a successive expulsion of all five CO ligands. In addition, loss of benzonitrile yielded a signal at m/z 515.0, which can be assigned to H-functionalized phosphenium complex **165**$^+$ (Fig. 4.24). In contrast, the water adduct [**35** + H + H$_2$O]$^+$ fragmented via two pathways: i) loss of the whole W(CO)$_5$ moiety and ii) consecutive losses of single CO ligands. Thus, the assignment of [**35** + H + H$_2$O]$^+$ to a noncovalent (i.e., hydrogen bonded) water adduct can be ruled out due to the distinct difference with the fragmentation pattern of [**35** + H]$^+$. Unfortunately, [**35** + H + CH$_3$CN]$^+$ was not obtained in abundances high enough for reasonable MS/MS spectra. Yet, the results for the water adduct already suggest

that an acyclic acetonitrile adduct 160^+ should not be distinguishable from the cyclic structure $[41m + H]^+$ by CID-MS/MS due to very similar fragmentation patterns: $[41m + H]^+$ was obtained in the gas phase by ESI of an acetonitrile solution of isolated complex $41m$. Also in this case loss of $W(CO)_5$ dominated the spectra, and consecutive losses of single CO ligands were observed in much lower intensities as the only alternative fragmentation pathway.

Interestingly, the protonated P-Cp* derivative $[121 + H]^+$ showed cleavage of the $W(CO)_5$ group as main gas phase fragmentation. Three different structures for m/z 270 are conceivable, a priori: $2H$-azaphosphirenium structure 166^+, cyclic phosphonium structure 167^+, and acyclic phosphenium structure 168^+ (Fig. 4.24). DFT calculations on the all-methyl substituted model system predict a thermodynamic preference of structure 166^+ over 167^+ and 168^+.[38] In the CID-MS/MS spectra of $[121 + H]^+$, additionally, a peak was detected that can be assigned to complex $[W(CO)_5(PNH)]^+$ (m/z 369.9) resulting from elimination of $C_{17}H_{20}$ from $[121 + H]^+$; the corresponding protonated organic fragment $C_{17}H_{21}^+$ was detected as well (m/z 225.2). A similar fragmentation was neither observed for $[35 + H]^+$ nor for the unprotonated radical cation $121^{\bullet+}$ in EI-mass spectra of 121.

4.3.2 Reactions of $2H$-Azaphosphirene Complexes with Brønsted and Lewis Acids in the Absence of Trapping Reagents

To gain additional insight into the course of the ring expansion reactions in solution, the reaction of $2H$-azaphosphirene complex 35 with triflic acid was examined at low temperature *in the absence* of any trapping reagents such as nitriles or isonitriles (Scheme 4.20). Upon addition of TfOH to a methylene chloride solution of 35 the mixture turned deep wine-red, and the ^{31}P NMR spectrum showed besides the resonance of unreacted 35 two intense signals (Fig. 4.25): one at 223.3 ppm ($|^1J_{WP}| =$ 293.0 Hz; $\mathbf{A}$) and one at -50.6 ppm with a very small tungsten–phosphorus coupling constant magnitude ($|J_{WP}| = 21.4$ Hz; $\mathbf{B}$) and a phosphorus–proton coupling constant of 14.0 Hz in magnitude; the ratio of $\mathbf{A} : \mathbf{B} : 35$ was approximately $5 : 1 : 4.5$ (estimated by signal integration). As all attempts to isolate and purify these products were prevented by their extreme instability, their characterization was achieved by recording multinuclear (^{1}H, ^{13}C, ^{15}N, ^{29}Si, ^{31}P) one- and two-dimensional NMR spectra at low temperature from the reaction mixture.

---

[38]The model system for 166^+ is 51.7 kJ·mol^{-1} lower in energy than that for 167^+ and by 119.2 kJ·mol^{-1} favored over the model for 168^+.
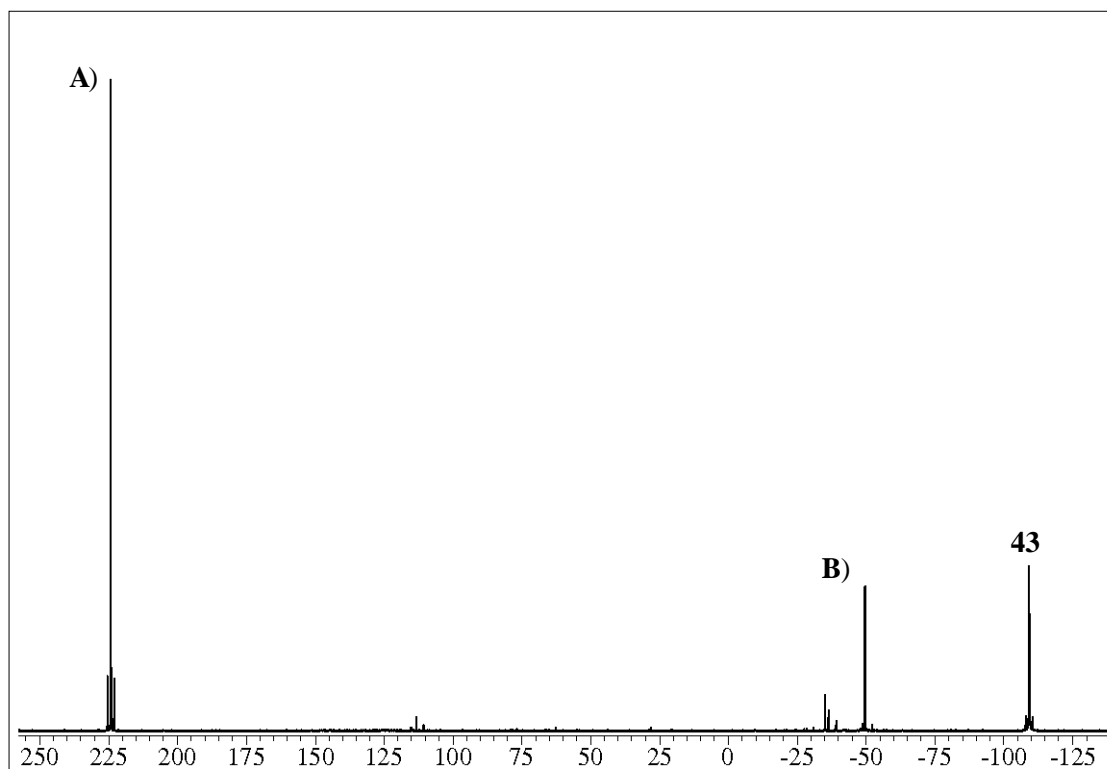
Figure 4.25: ^{31}P$\{^{1}$H$\}$ NMR spectrum recorded during the reaction of 2*H*-azaphosphirene complex **35** with TfOH after 30 minutes at $-17\,^{\circ}$C (Scheme 4.20).

The 2D NMR experiments allowed to establish correlations between the signal **A** and the *ortho*-protons of a phenyl group, a trimethylsilyl moiety, an isolated olefinic proton ($\delta = 8.52$, $|^{2}J_{PH}| = 2.3$ Hz), and an NH proton that is according to a ^{1}H,^{15}N HSQC experiment part of an NH$_2$ moiety. The olefinic proton is bound to a carbon atom that gives rise to a doublet ($|^{1}J_{PC}| = 26.8$ Hz) with a chemical shift of 175.0 ppm and further exhibits a long-range correlation with the silicon atom of a trimethylsilyl moiety. Both the phenyl and the olefinic protons display another long-range correlation with a ^{13}C signal that appeared as a doublet at very low field ($\delta = 190.2$, $|^{1}J_{PC}| = 22.6$ Hz) and was assigned to the carbon atom of an iminium moiety directly attached to phosphorus. Putting all available pieces of information together strongly suggested to formulate the constitution of this product as *N*-protonated 1-aza-3-phosphabutadiene complex **169** (Scheme 4.20). The assignment of the *Z*-configuration at the P,C double bond was derived from the analysis of a 2D ^{1}H NOESY spectrum, which revealed that one of the NH protons displayed a NOE correlation with the SiMe$_3$ moiety but not with the CH proton at the same carbon atom. Even if similar correlations as for **A** were likewise established for the ^{31}P NMR signal **B** (see Experimental Part), a significant difference between both compounds immediately became evident in the substantially

increased shielding for both the proton ($\delta = 3.81$) and the carbon atom ($\delta = 38.2$) of the phosphaalkene moiety. In combination with the strong decrease in $\delta(^{31}\mathrm{P})$ as well as $|J_{WP}|$, these data can be considered as characteristic for the presence of a phosphaalkene π complex[271] being in good agreement with the structure of **170**. As the ^{1}H NOESY spectrum showed a correlation between the signals of the olefinic CH and one of the NH protons whereas at the same time the corresponding NH$\cdots$SiMe$_3$ correlation was absent, it was concluded that the P,C double bond in **170** exhibits E-configuration. Complexes **169** and **170** are thus not only coordination isomers but also exhibit different configurations at the P,C double bond.
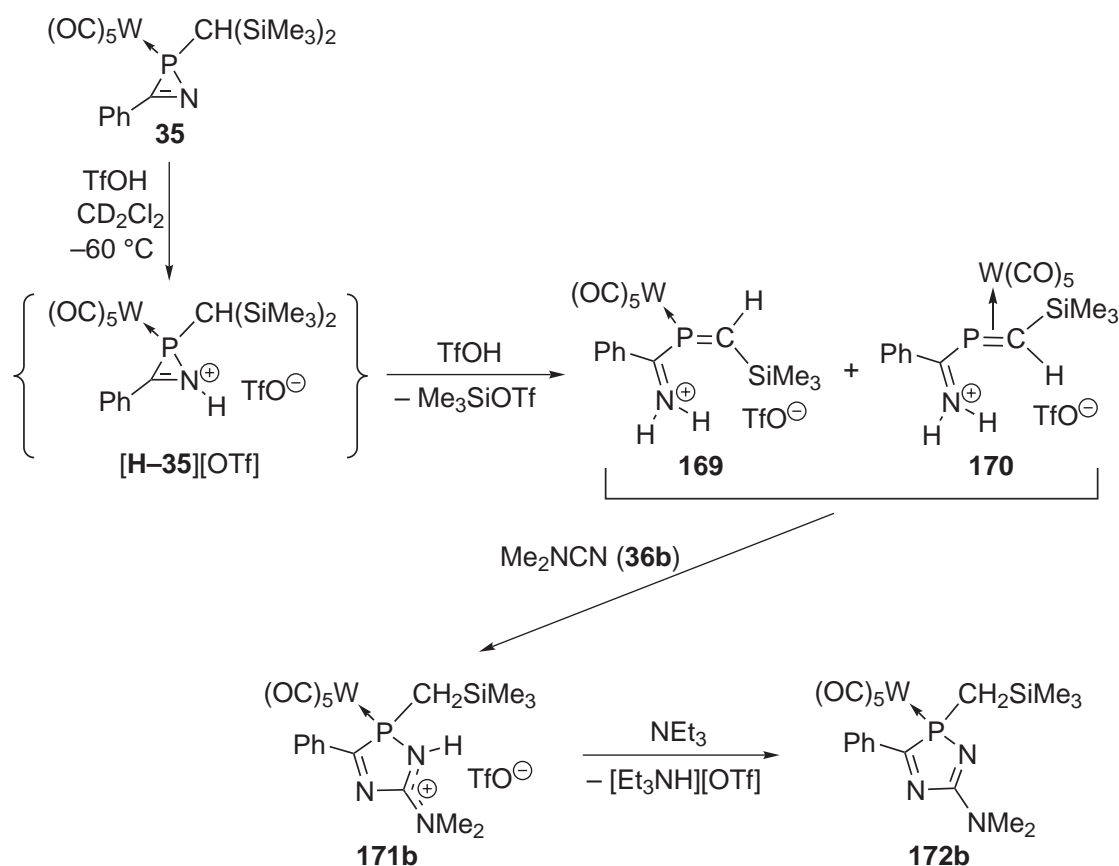
Scheme 4.20: *Consecutive* reaction of 2H-azaphosphirene complex **35** with TfOH, nitrile **36b**, and NEt$_3$.

The formation of **169** and **170** can be explained as follows: reaction of **35** with one equivalent of triflic acid transiently yields [**H–35**][OTf] in the first protonation step. Subsequent desilylation combined with ring opening and a second protonation step affords a mixture of the 1-aza-3-phosphabutadiene complexes **169** and **170**. This hypothesis is corroborated by the identification of the NMR signals of Me$_3$SiOTf in the reaction mixture ($\delta(^1\mathrm{H}) = 0.48$, $|^2J_{SiH}| = 7$ Hz; $\delta(^{13}\mathrm{C}) = -0.3$; $\delta(^{29}\mathrm{Si}) = 44.2$). The

formation of two geometrical isomers can be rationalized assuming that the elimination of Me$_3$SiOTf is not stereospecific. The different coordination mode in both products presumably is attributable to steric effects as in a η^1-coordination isomer of **170** the attachment of the bulky SiMe$_3$ and W(CO)$_5$ groups on the same side of the double bond would imply substantially increased steric congestion.

Reacting a mixture of in situ generated **169** and **170** with nitrile derivative **36b** (Scheme 4.20) resulted in the formation of a product with a resonance at $\delta(^{31}\text{P}) = 102.9$. The recorded NMR data were similar to those for 2H-1,4,2-diazaphospholium complex **123b** with the major difference that the spectra revealed the presence of one instead of two SiMe$_3$ groups and two diastereotopic methylene protons. A broad doublet at low field indicated a proton bonded to a nitrogen atom that in turn showed a direct phosphorus–nitrogen coupling and a long-range correlation with the diastereotopic methylene protons as estimated from ^{1}H,^{15}N HMQC experiments ($\delta(^{15}\text{N}) = -269$, $|^{1+4}J_{PN}| = 19$ Hz, $|^1J_{NH}| = 93$ Hz). These data are in agreement with the structure of N^1-protonated 2H-1,4,2-diazaphosphole complex **171b**. Upon addition of triethylamine **171b** was transformed into complex **172b**, which was isolated and purified. The structure of **172b** was unambiguously confirmed by multinuclear NMR experiments, mass spectrometry, IR and UV/Vis spectroscopy, and a single-crystal X-ray diffraction study (Fig. 4.26); the purity was examined by elemental analysis.

Protonation of P-CH$_2$SiMe$_3$ substituted complex **172b** obviously has a larger effect on the ^{31}P NMR spectroscopic parameters than in the case of **41b** by inducing both a more pronounced deshielding of the ^{31}P NMR signal ($\Delta\delta = 7.1$ (**172b**/**171b**) vs. 3.9 (**41b**/**123b**)) and a larger increase in the tungsten–phosphorus coupling constant magnitude ($\Delta|^1J_{WP}| = 24.1$ Hz (**172b**/**171b**) vs. 10.2 Hz (**41b**/**123b**)). The effect on the NMR data for the nitrogen and carbon atoms resembles the trend found for the pair **41b**/**123b**: the ^{15}N resonance of N^1 is 66 ppm high field shifted along with a decrease of the phosphorus–nitrogen coupling constant magnitude by 30 Hz, while the resonance of the dimethylamino nitrogen is slightly shifted to lower field ($\Delta\delta = +28$ (**172b**/**171b**)); the ^{13}C resonances of the ring carbons are almost unaffected upon protonation of **172b** ($\Delta\delta = -3.6$ (C^3) and -3.5 (C^5) **171b** vs. **172b**).

Comparison of the structure of complex **172b** with that of **41b** reveals that the endocyclic N(3)–P–C(1) angle is only slightly widened due to the presence of a substituent with lower steric demand at phosphorus (cf. **41b**: 90.7°; Fig. 3.3, Section 3.1). The effect is more pronounced for the sum of the angles at the P center, which is somewhat smaller ($\Sigma\angle(\text{P}_{PR_3})$ 303.5°) than in the case of complex **41b** ($\Sigma\angle(\text{P}_{PR_3})$ 307.8°), being primarily a result of a decrease of the C(3)–P–C(1) angle by 8.0° (**41b**/**172b**). Presumably for the same reason the P,W bond in **172b** is significantly shortened (by 0.029 Å).
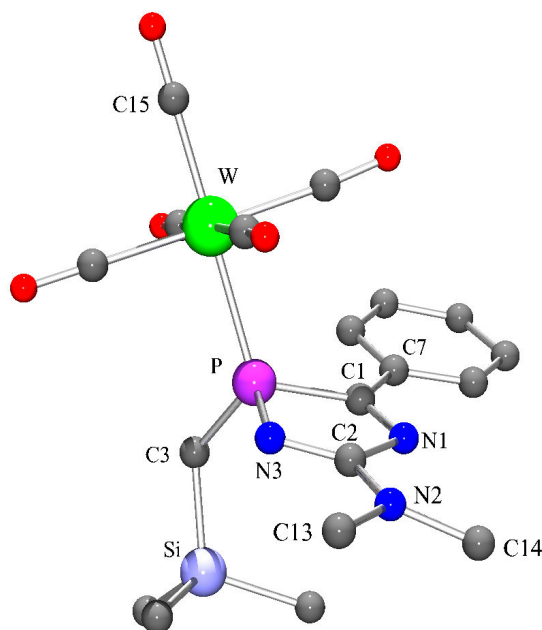
Figure 4.26: Molecular structure of complex **172b** in the crystal (hydrogen atoms omitted for clarity). Selected bond lengths [Å] and angles [°]: W–C(15) 2.027(12), W–P 2.505(3), P–N(3) 1.663(8), P–C(1) 1.853(10), C(1)–N(1) 1.300(12), C(2)–N(3) 1.305(13), C(2)–N(2) 1.334(12), C(1)–C(7) 1.454(13), N(3)–P–C(1) 92.0(4), P–C(1)–N(1) 109.8(7), C(1)–N(1)–C(2) 108.9(8), N(1)–C(2)–N(3) 119.7(9), C(2)–N(3)–P 109.3(7), N(3)–C(2)–N(2) 125.9(10).

In order to avoid the side-reactions discussed beforehand, the reaction of P-Cp* substituted $2H$-azaphosphirene complex **121** with TfOH was examined in the absence of trapping reagents. Here, the observation and characterization of $2H$-azaphosphir-enium complex [**H–121**][OTf] was achieved by multinuclear (^{1}H, ^{13}C, ^{31}P) one- and two-dimensional NMR experiments at low temperature (Scheme 4.21).
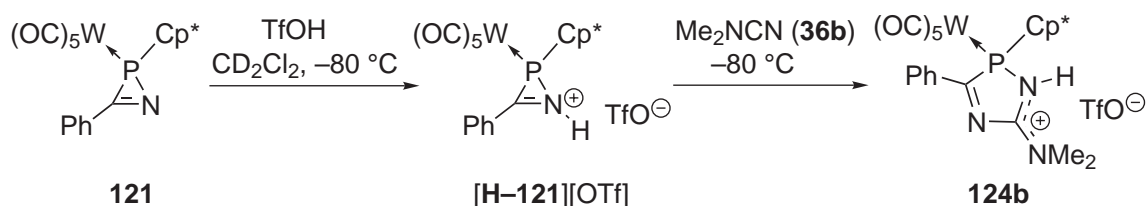
Scheme 4.21: *Consecutive* reaction of $2H$-azaphosphirene complex **121** with TfOH and nitrile **36b**.

Compared with complex **121** the ^{31}P resonance of [**H–121**][OTf] ($\delta = -61.4$, $|^1J_{WP}|$ = 263.2 Hz) is 45.0 ppm downfield shifted while the tungsten–phosphorus coupling constant magnitude is 23.3 Hz smaller. In the ^{1}H NMR spectrum complex [**H–121**][OTf] gives rise to a slightly broadened resonance at low field with a well resolved coupling

with phosphorus (δ = 12.8, $h_{1/2}$ = 8 Hz, $|^{2+3}J_{PH}|$ = 15 Hz). It showed no ^{1}H,^{13}C correlation in an HSQC experiment thus confirming the N-bonded proton. As complex [**H**–**121**][OTf] exhibited a moderate stability only in dilute solutions and at low temperature, not all ^{13}C NMR resonances could unambiguously be assigned. The characteristic ring carbon resonance of [**H**–**121**][OTf] was detected at 184.1 ppm ($|^1J_{PC}|$ = 13.4 Hz) showing that the chemical shift is almost unaffected by protonation ($\Delta\delta$ = −5.2), while the magnitude of the phosphorus–carbon coupling constant is significantly increased (by 12.1 Hz compared to **121**). Upon addition of nitrile derivative **36b** to a solution of [**H**–**121**][OTf] it underwent ring expansion yielding complex **124b** as evidenced by NMR spectroscopy (Scheme 4.21).

It was demonstrated that the protonation of **121** can be reversed by adding NEt$_3$ to a solution of freshly prepared [**H**–**121**][OTf] (Scheme 4.22). The mixture turned from wine-red to light yellow, and the regeneration of complex **121** was evidenced by ^{31}P NMR spectroscopy.
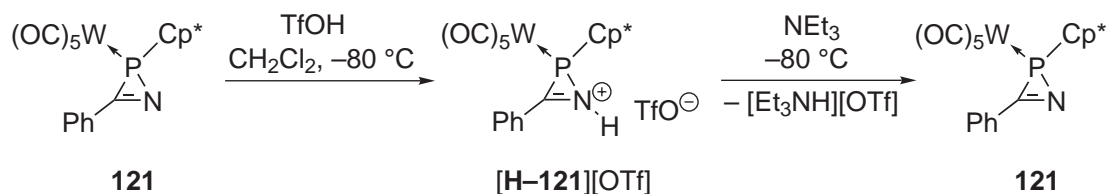
Scheme 4.22: *Reversible* protonation of 2H-azaphosphirene complex **121**.

Reaction of 2H-azaphosphirene complex **35** in CH$_2$Cl$_2$ with HBF$_4 \cdot$ Et$_2$O at −65 °C also yielded a color change from yellow to red (Scheme 4.23), but the ^{31}P{^{1}H} NMR spectrum showed two resonances at low field with large phosphorus–fluorine coupling constant magnitudes (δ = 189.6, $|^1J_{WP}|$ = 314.1 Hz, $|^1J_{PF}|$ = 887.6 Hz; δ = 193.3, $|^1J_{WP}|$ = 281.0 Hz, $|^1J_{PF}|$ = 857.0 Hz; ratio ca. 2.2 : 1); the former signal was significantly broadened ($h_{1/2}$ = 22 Hz). After washing the crude product mixture with n-pentane a red powderish solid was obtained, which was highly hygroscopic[39] and was characterized by NMR, IR, and UV/Vis spectroscopy as a mixture of complexes **173** and **79b**; a HR-ESI-MS experiment revealed a signal corresponding to [**79b** + H]$^+$ (m/z 638.0665). Obviously, protonation of the N-center of **35** causes ring opening combined with abstraction of fluoride from the tetrafluoroborate ion; the generated BF$_3$ is then (partly) coordinated by the evolving nitrogen lone pair.

The P-bonded fluorine atoms resonated at δ = −120.3 (**173**) and −113.3 (**79b**), and the BF$_3$ fragment of complex **173** was confirmed by its ^{19}F resonance at δ = −147.2 as well as its ^{11}B resonance at δ = 0.5. The ^{1}H NMR spectrum displayed a very broad

---

[39]Upon exposure of a sample to air atmosphere it turned brownish and adopted an oily consistency.

signal at low field ($\delta = 10.6$) that presumably arises from superposition of the NH proton resonances of both complexes. The imine carbon centers of **173** and **79b** give rise to distinctly different ^{13}C resonances. While complex **173** shows a broad signal at $\delta = 190.7$, the resonance of **79b** appears at even lower field ($\delta = 207.8$) and displays resolved $^1J_{PC}$ and $^2J_{FC}$ couplings each being 14.4 Hz in magnitude.
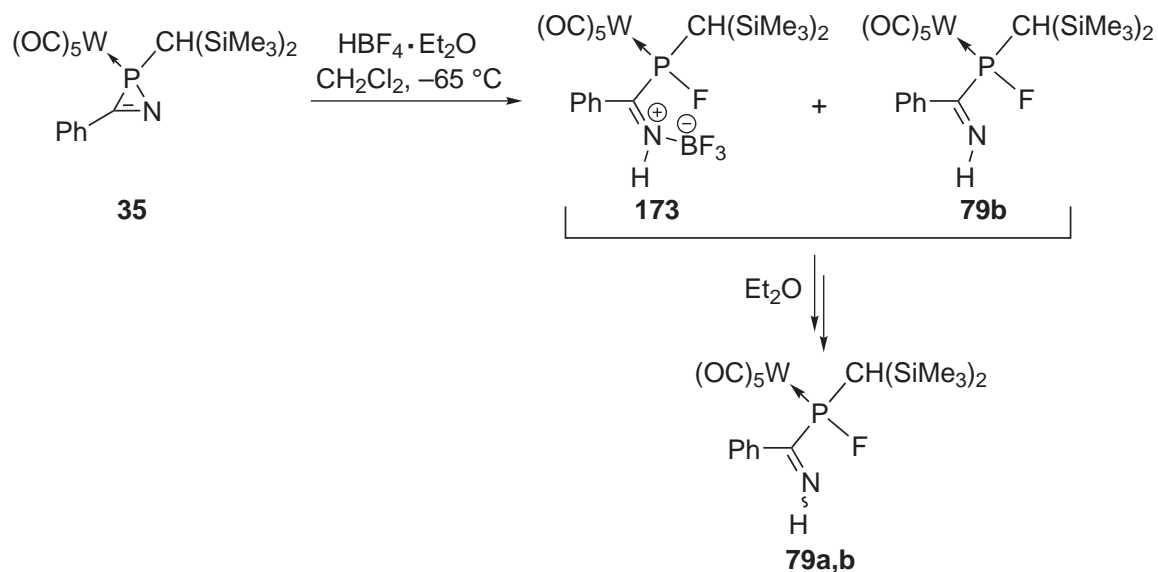
Scheme 4.23: Reaction of 2H-azaphosphirene complex **35** with HBF$_4$ · Et$_2$O.

The IR spectrum revealed two NH stretch vibration bands arising from an isolated ($\tilde{\nu} = 3325$ cm^{-1}) and a hydrogen bonded NH group ($\tilde{\nu} = 3108$ cm^{-1}). Furthermore, a NH deformation band (δ_{NH}) at $\tilde{\nu} = 1083$ cm^{-1} was detected, which is characteristic for hydrogen bonds.[272] While the ν_{A_1}(CO) bands of the two complexes were detected at $\tilde{\nu} = 2085$ and 2077 cm^{-1}, the second ν_{A_1}(CO) and the ν_E(CO) bands of complexes **173** and **79b** overlap to give an intense absorption maximum centered at $\tilde{\nu} = 1943$ cm^{-1}.

In order to separate complexes **173** and **79b**, their mixture was subjected to column chromatography at $-30\,^{\circ}$C, and when the polarity of the eluent (petroleum ether at the start) was increased through addition of 10 % diethyl ether a color change from red to yellow was observed on the column. Finally, a 2.4 : 1 mixture of **79b** and another complex was obtained that displayed a ^{31}P resonance at $\delta = 197.5$, $|^1J_{WP}| = 289.3$ Hz, $|^1J_{PF}| = 824.0$ Hz, $|^3J_{PH}| = 50.9$ Hz). The latter could be assigned to complex **79a**, which differs from **79b** by the configuration at the C,N double bond (Scheme 4.23).[40] A mixture with the same composition was obtained when a mixture of complexes **173**

---

[40]No resonance was detected by ^{11}B{^{1}H} NMR spectroscopy, and the ^{19}F{^{1}H} NMR spectrum did not reveal the presence of a BF$_3$ group.

and **79b** was dissolved in diethyl ether, thus showing that the ether can displace the
BF$_3$ group from **173** in solution.

When a methylene chloride solution of 2H-azaphosphirene complex **35** was treated
with BF$_3 \cdot$ Et$_2$O in the absence of trapping reagents at $-65\,^{\circ}$C (Scheme 4.24), initially,
a color change from yellow to orange was observed, and also here, a ^{31}P$\{^1$H$\}$ resonance
with a large phosphorus–fluorine coupling constant magnitude was detected at low
field, which was slightly broadened ($\delta = 202.5$, $h_{1/2} = 13.1$ Hz, $|^1J_{WP}| = 315.3$ Hz,
$|^1J_{PF}| = 845.6$ Hz). While warming to ambient temperature the reaction mixture
turned brownish and very broad ^{31}P$\{^1$H$\}$ signals (or sets of signals) were detected
between -115 and -99 ppm and between -40 and -26 ppm, which might indicate
starting oligomer/polymer formation.
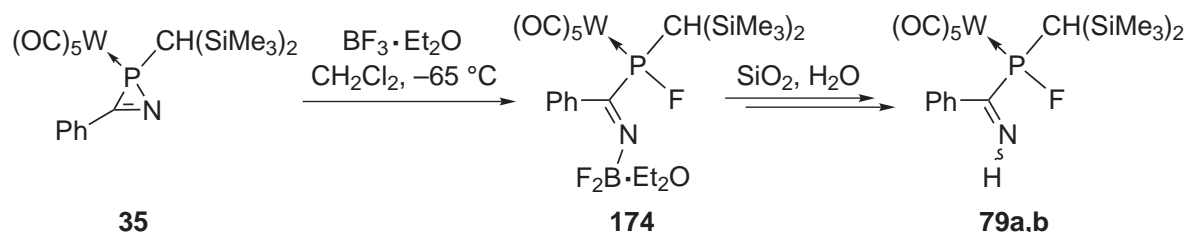
Scheme 4.24: Reaction of 2H-azaphosphirene complex **35** with BF$_3 \cdot$ Et$_2$O.

In order to suppress follow-up reactions and to obtain the primarily formed product,
all volatiles were removed in vacuo at low temperature immediately after addition of
BF$_3 \cdot$ Et$_2$O. This yielded a yellow solid containing mainly the primarily formed fluo-
rophosphane complex. Analysis by multinuclear (^{1}H, ^{11}B, ^{19}F, ^{31}P) NMR experiments
revealed a bis(trimethylsilyl)methyl, a phenyl, and a BF$_2$ group; a methyl as well
as a methlyene resonance in the ^{1}H NMR spectrum evidenced the presence of one
equivalent of coordinated diethyl ether. The data obtained are in good agreement
with the structure of complex **174**. Consequently, electrophilic attack of BF$_3 \cdot$ Et$_2$O
at the nitrogen center of **35** causes ring opening and fluoride transfer from boron to
phosphorus.

An attempt to purify **174** by low-temperature column chromatography yielded com-
plexes **79a,b**, which presumably were formed via reaction of **174** with traces of water
present in the employed silica gel (Scheme 4.24). Complex **79a** was isolated in pure
form (ca. 23 %) and unambiguously characterized by multinuclear NMR experiments
and mass spectrometry. Its ^{31}P$\{^1$H$\}$ resonance was detected at $\delta = 196.7$ ($|^1J_{WP}| =$
288.6 Hz, $|^1J_{PF}| = 824.0$ Hz), and the corresponding ^{19}F$\{^1$H$\}$ resonance was found at δ
$= -116.0$. The imine carbon resonates at $\delta = 184.7$ and shows couplings with phospho-
rus and fluorine. A ^{1}H resonance at $\delta = 10.15$ with a large phosphorus–proton coupling

constant magnitude (51.5 Hz) evidenced the N-bonded proton; no ^{11}B resonance was detected.

Under FAB-mass spectrometric conditions complex **79a** undergoes successive expulsion of CO ligands as major fragmentation pathway. Furthermore, loss of the whole $W(CO)_5$ group was observed (m/z 314).

4.4 Computational Studies

In order to elucidate the mechanism of the ring expansion of 2*H*-azaphosphirene complexes with nitriles induced by triflic acid, several conceivable pathways were examined in a theoretical study by means of DFT calculations. All calculations were carried out with the TURBOMOLE V5.9.1 program package[206] using the same methods as employed for the SET-induced reactions (cf. Section 3.6.1), but with the following modifications: diffuse basis functions were added to the basis sets of atoms that potentially might accept a considerable amount of negative charge, these are, oxygen, sulfur, carbon, and fluorine belonging to triflate (or triflic acid). Therefore, uncontracted gaussian functions (one of *s*- and *p*-type each) with exponents of 0.0845 for O, 0.0405 for S, 0.0438 for C, and 0.1076 for F were added to the SV(P) basis set, which was used for optimizations (here denoted as aug-SV(P)). The same augmentations were done for the TZVP basis (denoted as aug-TZVP), which was used for single point energy calculations. For optimizations an additional set of polarization functions was added to the basis of the hydrogen atom that stems from triflic acid (i.e., the SVP basis set was employed for this atom).

First, different conceivable pathways were calculated on reactions of *C,P*-dimethyl substituted 2*H*-azaphosphirene complex **91** with acetonitrile (**36m**). Then, the influence of the nucleophilicity of the nitrile was taken into accout by using cyanamide (**36p**) as a strong and dicyane (**36q**) as a weak nucleophilic nitrile derivative. Finally, the ring expansion reaction with an isonitrile, methyl isocyanide, was investigated.

4.4.1 Reactions with Nitriles

As the experimental investigations revealed that the first reaction step most likely is protonation of the *N*-center of the 2*H*-azaphosphirene complex by TfOH, this was simulated computationally first for the gas phase. When a triflic acid molecule was approached to the *N*-center of **91** electrostatic complex **91**···HOTf was formed with an O–H···N hydrogen bond to the 2*H*-azaphosphirene nitrogen (Fig. 4.27, left). This is not surprising since a proton transfer, which is associated with charge separation, is generally disfavored if no stabilization effects are operative by a surrounding medium. On the other hand, when protonation of **91** was enforced in the gas phase by omitting the triflate anion P,N bond cleavage occurred (during geometry optimization), and phosphenium complex **175**$^+$ was obtained (Fig. 4.27, middle).
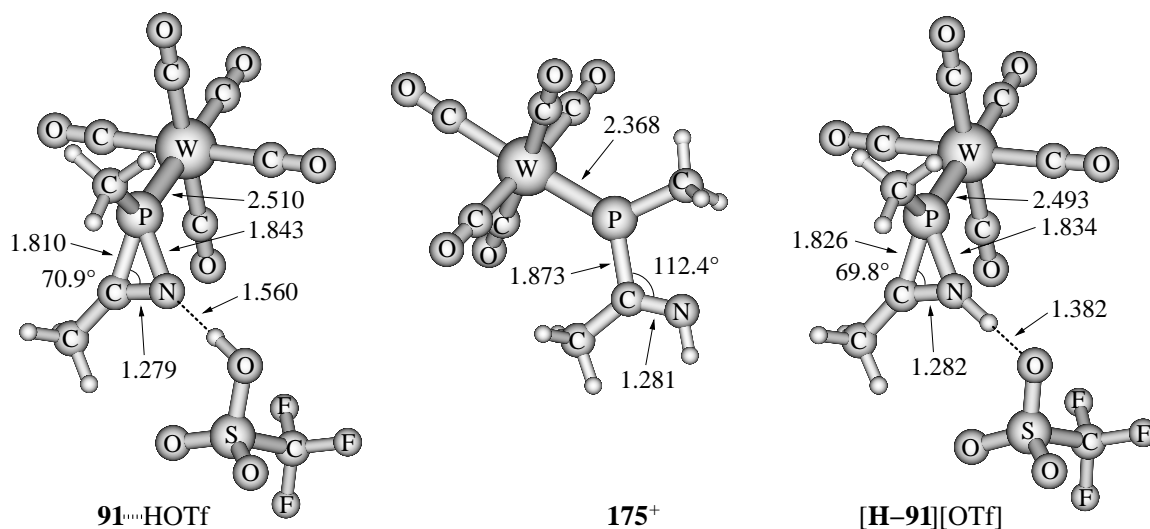
Figure 4.27: Calculated structures of **91**$\cdots$HOTf in the gas phase (left), phosphenium complex **175**$^+$ (middle), and 2*H*-azaphosphirenium complex [**H–91**][OTf] (right; solution simulated with the COSMO approach) (distances in Å).

A protonated 2*H*-azaphosphirene complex with retained cyclic structure (with or without the triflate attached) could be calculated by modeling the polar environment using the COSMO approach[214] with $\varepsilon = 8.93$ to mimic methylene chloride as solvent. Since complex [**H–91**][OTf] (Fig. 4.27, right), where the triflate anion remains attached via a hydrogen bond (d(N–O) 2.538 Å), is significantly lower in free energy than the respective solvent-separated ions (by 44.5 kJ·mol^{-1}), [**H–91**][OTf] was taken as starting point of pathways **A** and **B** shown in Schemes 4.25 and 4.26; corresponding thermochemical data are given in Table 4.9.

Pathway A: The formation of [**H–91**][OTf] from **91** and TfOH is exothermic ($\Delta_R H_{298} = -35.1$ kJ·mol^{-1}) with respect to separated reactants but slightly endergonic ($\Delta_R G_{298} = +11.0$ kJ·mol^{-1}; Scheme 4.25, reaction i). However, it becomes favored on decreasing the temperature (e.g., at $-80\,^{\circ}$C: $\Delta_R G_{193} = -5.4$ kJ·mol^{-1}). Nucleophilic attack of acetonitrile at the phosphorus center of [**H–91**][OTf] induces cleavage of the P,N bond (ii), thus, ring opening in an S$_N$2-type fashion via transition state **TS$^{\mathbf{ii}}$(m)** (Fig. 4.28, left). This leads to *P*-nitrilium substituted phosphane complex [**176m**][OTf]. After rotation about the P–C(Me)N bond (reaction iii; not shown) to conformer [**176m'**][OTf] (Fig. 4.28, right)[41] the latter can undergo cyclization (iv) to give N^4-protonated 2*H*-1,4,2-diazaphosphole complex [**141m**][OTf]. This step is predicted to be highly exergonic, and its barrier is very flat (**TS$^{\mathbf{iv}}$(m)**: Fig. 4.29, left).

---

[41]In this case the formation of solvent-separated ions is thermodynamically slightly favored over an attachment of triflate to the NH functionality of **176**$^+$ or **176'**$^+$ via a hydrogen bond.

Table 4.9:   Calculated thermochemical data for reactions shown in Schemes
4.25–4.27 (R = CH$_3$) and for deprotonation of complex **[134m]**[OTf] by
NMe$_3$ (RI-BP86/aug-TZVP/ECP-60-MWB(W)+COSMO//RI-BP86/aug-SV(P)/ECP-
60-MWB(W)+COSMO; all values in kJ·mol^{-1}).

Reaction		$\Delta G^{\ddagger}_{298}$	$\Delta_R G_{298}$
i)	**91** + TfOH → **[H–91]**[OTf]	♯	+11.0
ii)	**[H–91]**[OTf] + MeCN → **[176m]**[OTf]	+69.7	+33.9
iii)	**[176m]**[OTf] → **[176m']**[OTf]	+3.1	+0.2
iv)	**[176m']**[OTf] → **[141m]**[OTf]	+4.4	−134.2
v)	**[141m]**[OTf] → **[134m]**[OTf]	♯	−11.1
vi)	**[134m]**[OTf] + NMe$_3$ → **96m** + [Me$_3$NH][OTf]	♯	−48.5
vii)	**[H–91]**[OTf] → **[175]**[OTf]	+46.5	+44.9
viii)	**[175]**[OTf] + MeCN → **[176m']**[OTf]	*	−10.8
ix)	**[175]**[OTf] → **175**$^+$ + TfO$^-$	♯	+4.3
x)	**175**$^+$ + TfO$^-$ → **177**	♯	−87.9
xi)	**177** + MeCN → **[176m]**[OTf]	+82.1	+72.8

♯Not calculated. *Not located.
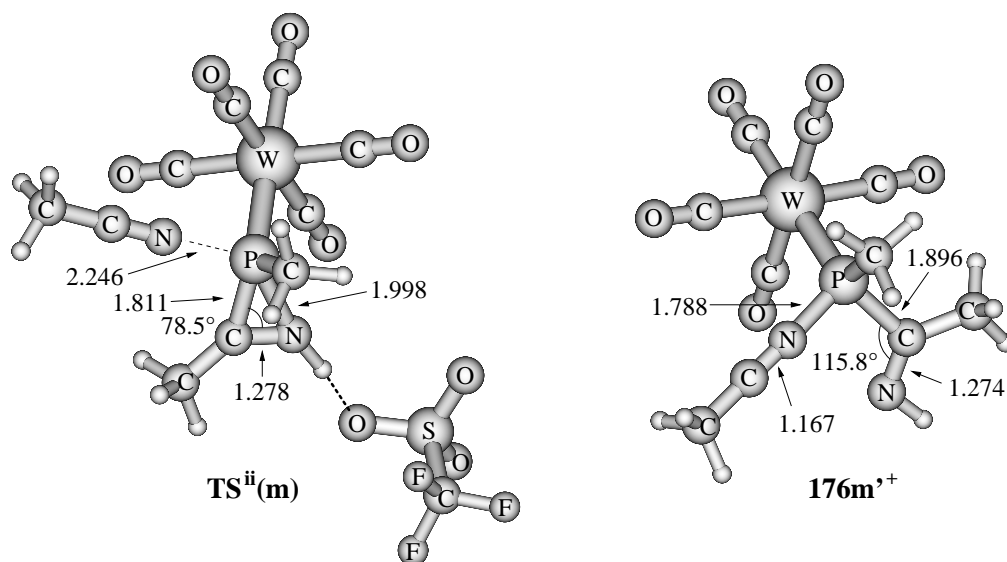
Figure 4.28: Calculated structure of transition state **TS^{ii}(m)** for the nucleophilic ring
opening of **[H–91]**[OTf] by acetonitrile (left) and calculated structure of acyclic inter-
mediate **176'$^+$** (right) (distances in Å).

For the chosen model system, N^1-protonated $2H$-1,4,2-diazaphosphole complex [**134m**]-[OTf] is thermodynamically favored over [**141m**][OTf] by 11.1 kJ·mol^{-1} (v). The final deprotonation of [**134m**][OTf] with trimethylamine as model for the base yields neutral $2H$-1,4,2-diazaphosphole complex **96m** (vi; not displayed).
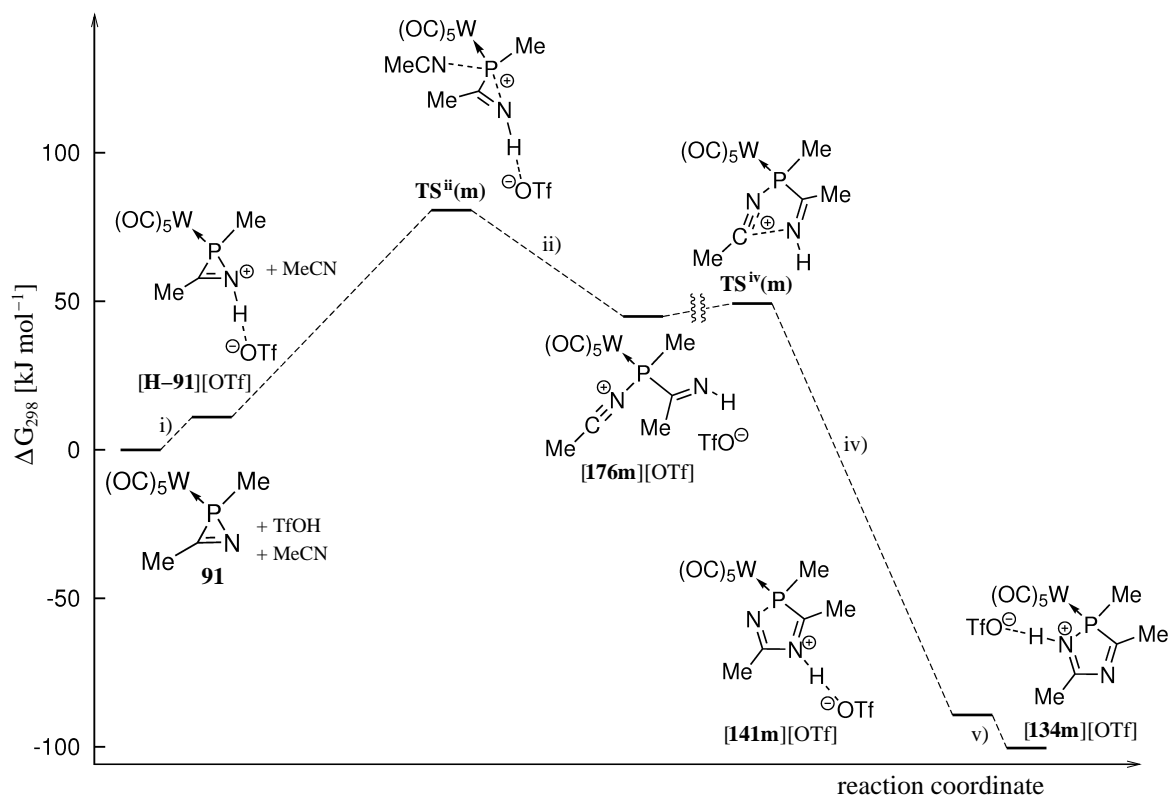
Scheme 4.25: Computed pathway **A** for the reaction of complex **91** with TfOH and acetonitrile starting with formation and ring opening of [**H–91**][OTf] induced by nucleophilic attack of acetonitrile (reaction step iii omitted for clarity). The sum of free energies of the reactants (**91**, TfOH, and MeCN) was arbitrarily chosen as zero-point of the ΔG_{298} scale.

Pathway B: As indicated by the calculations for the gas phase, N-protonation induces an activation of the P,N bond of **91**. Also in solution $2H$-azaphosphirenium complex [**H–91**][OTf] is prone to undergo facile spontaneous ring opening (Scheme 4.26, vii) with formation of phosphenium complex [**175**][OTf] (Fig. 4.29, right). The latter exhibits a short P,W bond (2.367 Å), which is typical for phosphenium tungsten complexes.[273] It can easily be attacked by acetonitrile (viii) resulting in the formation of complex [**176m'**][OTf]. For this reaction step—even in a constrained search—no transition state could be located, and due to the high electrophilicity of phosphenium complexes[273] the barrier for nucleophilic attack at the phosphorus center can be expected to be very flat. The following reaction sequence corresponds to steps iv–vi, which have already been discussed above (for pathway **A**).

Scheme 4.26: Computed pathway **B** for the reaction of complex **91** with TfOH and acetonitrile starting with formation and spontaneous ring opening of [**H–91**][OTf]. The sum of free energies of the reactants (**91**, TfOH, and MeCN) was arbitrarily chosen as zero-point of the ΔG_{298} scale.
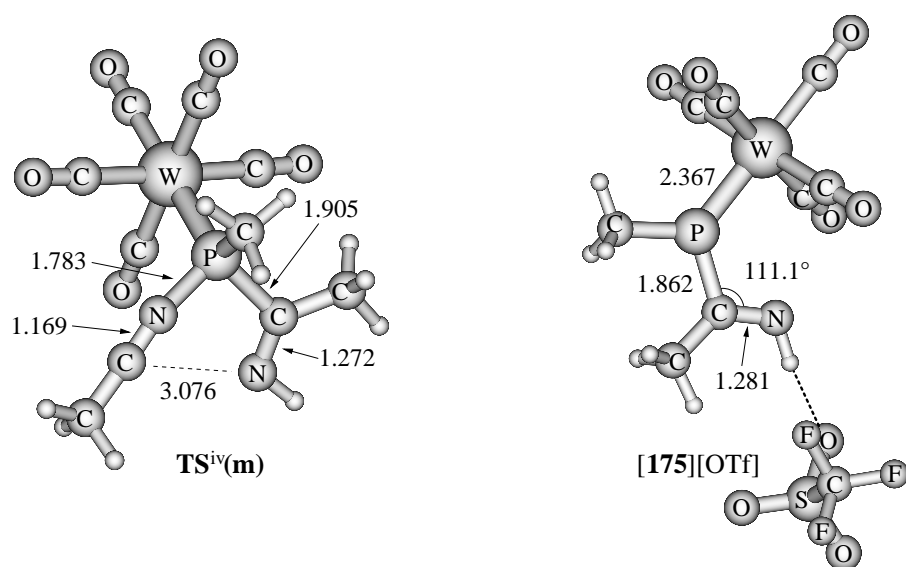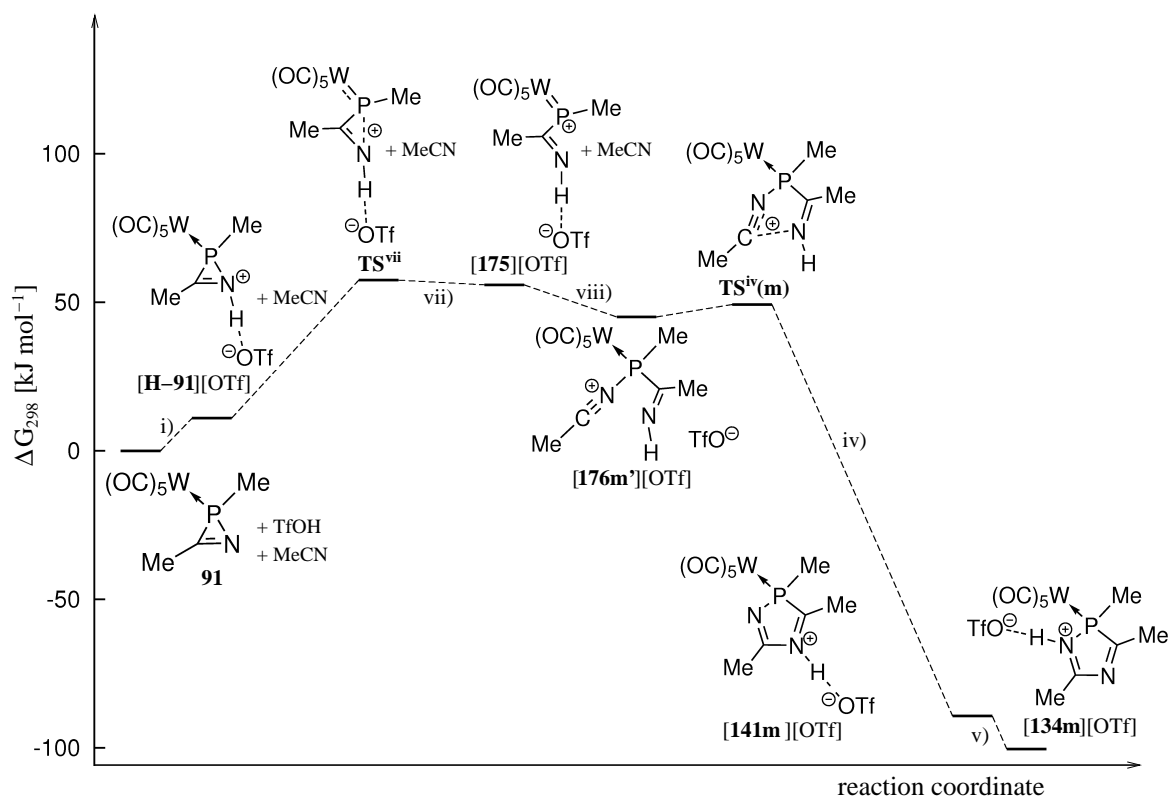
Figure 4.29: Calculated structure of transition state $\mathbf{TS^{iv}(m)}$ for the cyclization of **176m'**$^{+}$ (left) and calculated structure of phosphenium complex [**175**][OTf] (right) (distances in Å).

Additionally, pathway **C** was considered (Scheme 4.27; for thermochemical data see Table 4.9). After generation of complex [**175**][OTf] (via i, vii, Scheme 4.26) an attachment of triflate to the phosphenium center (x) with formation of *P*-OTf substituted phosphane complex **177** (Fig. 4.30, left) is thermodynamically favored. In a subsequent reaction step (xi) the triflate, in principle, can be displaced by acetonitrile to give [**176m**][OTf], but this has to proceed over a comparatively high barrier (**TS^{xi}(m)**: Fig. 4.30, right) and is endergonic.
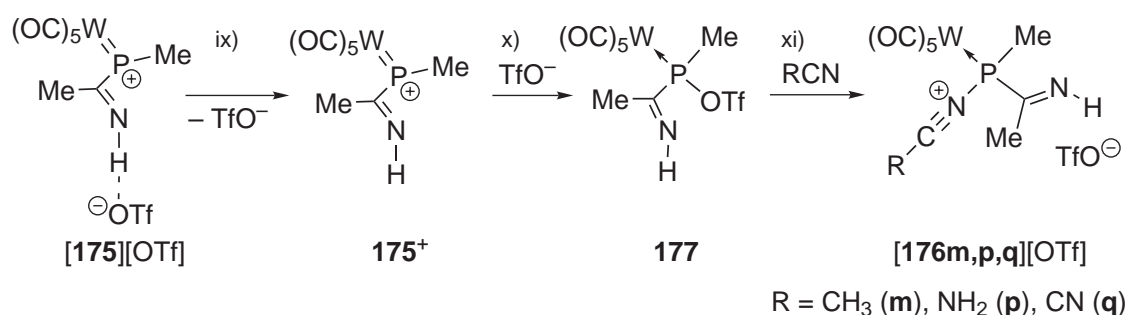
Scheme 4.27: Computed alternative pathway **C** for the formation of intermediates [**176m,p,q**][OTf] in reactions of **91** with TfOH and nitriles.
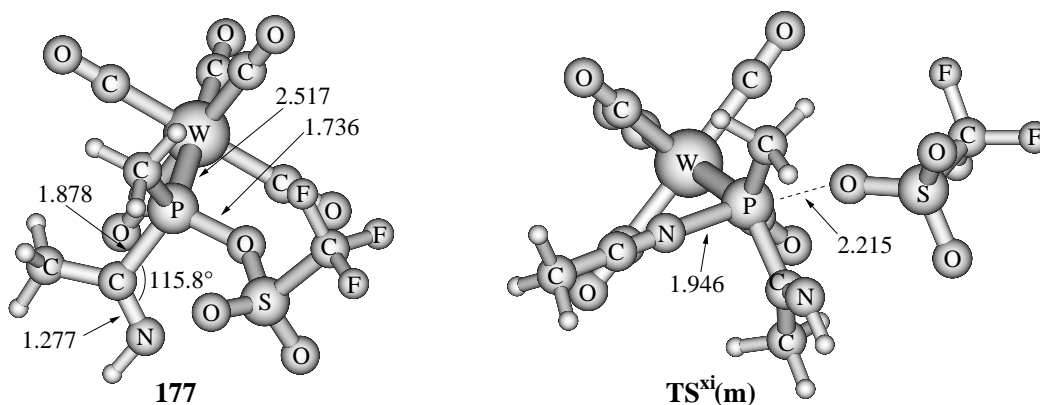
Figure 4.30: Calculated structures of *P*-OTf substituted phosphane complex **177** (left) and transition state **TS^{xi}(m)** for the nucleophilic displacement of triflate from **177** by acetonitrile (right) (distances in Å).

As experimental investigations on the reaction course have not provided any evidence for the intermediacy of a *P*-OTf substituted phosphane complex (Section 4.3), the conclusion is drawn that its formation is suppressed by competing reactions. These are, binding of a nitrile or an isonitrile followed by irreversible cyclization or (in the absence of such trapping reagents) elimination of a trimethylsilyl moiety in the case

of complex **35** (see Section 4.3.2). It should be noted that the attachment of triflate to the P-center of [**175**][OTf] must be preceded by breaking of the H-bond that binds the triflate to its counterion (reaction ix), as the hydrogen atom and the phosphorus substituent at the C,N double bond of [**175**][OTf] are *trans*-orientated; formation of **177** via nucleophilic ring opening of [**H–91**][OTf] by TfOH was not supported by the calculations.

Cleavage of the C,N double bond of [**H–91**][OTf] did not lead to a reasonable intermediate. Though, if the attack of MeCN (via N) takes place at the ring carbon of [**H–91**][OTf], cyclic adduct [**178**][OTf] is formed, which was computed as a local energy minimum (Fig. 4.31, left).[42]
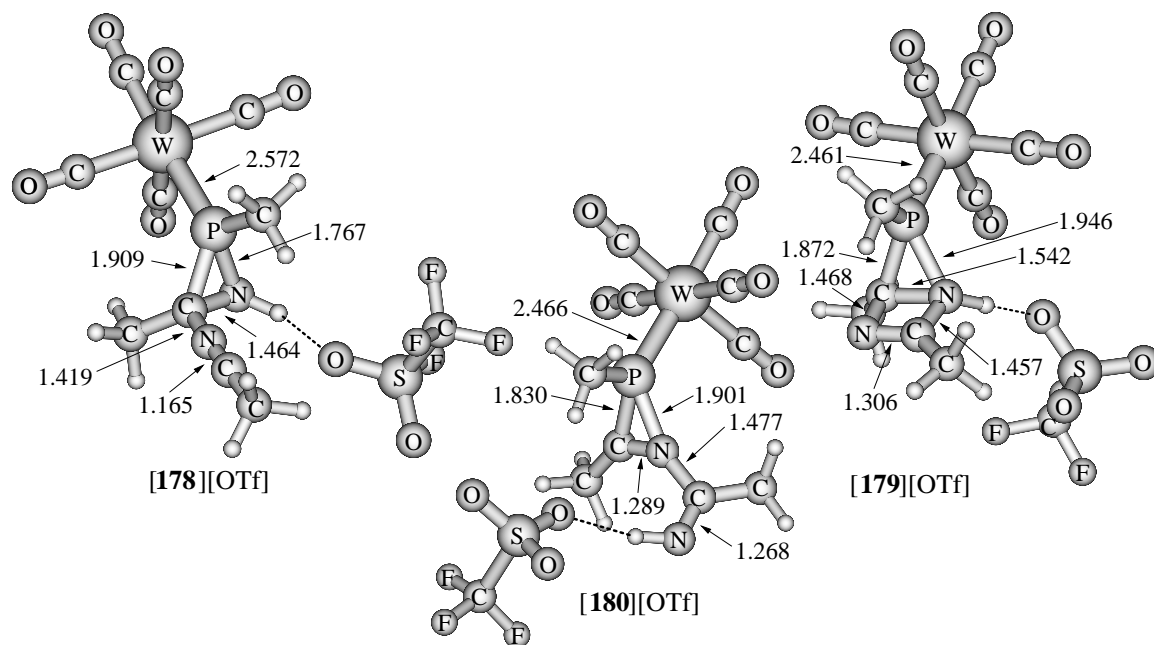
Figure 4.31: Calculated structures of the primary product [**178**][OTf] of the nucleophilic attack of acetonitrile at the carbon center of [**H–91**][OTf] (left), of its bicyclic valence isomer [**179**][OTf] (right), and of the primary product [**180**][OTf] of the nucleophilic attack of **91** at **36m**···HOTf (middle) (distances in Å).

However, the formation of [**178**][OTf] from [**H–91**][OTf] and acetonitrile is unfavored ($\Delta_R G_{298} = +82.0$ kJ·mol^{-1}). In comparison with [**176m**][OTf], the primary product of the attack of MeCN at the phosphorus center of either [**H–91**][OTf] or [**175**][OTf] (cf. ii and viii, Tab. 4.9), complex [**178**][OTf] is by 48.1 kJ·mol^{-1} higher in free energy.

---

[42]Cf. the adduct **25** that was obtained by Leonard and Zwanenburg upon reaction of 2H-azirene **20** with pyridinium perchlorate (Section 1.2, Scheme 1.8).[79]

Furthermore, complex [**179**][OTf] was found as an energy minimum structure (Fig. 4.31, middle). It could result from intramolecular nucleophilic attack of the azaphosphiridine nitrogen of [**178**][OTf] at the carbon center of its nitrilium moiety. Complex [**179**][OTf] is a bicyclic valence isomer of N^1-protonated $2H$-1,4,2-diazaphosphole complex [**134m**][OTf], but obviously, it is highly strained so that its free energy content exceeds that of [**134m**][OTf] by 225.2 kJ·mol^{-1}, and the formation from [**178**][OTf] is endergonic with 32.0 kJ·mol^{-1}. According to the thermochemical data the occurrence of structures such as [**178**][OTf] and/or [**179**][OTf] in the reaction of $2H$-azaphosphirene complexes with triflic acid and nitriles is largely excluded.

A further pathway that could not be ruled out alone on the basis of the experimental observations (Section 4.3) starts with protonation of the nitrile (instead of the $2H$-azaphosphirene complex) by triflic acid. Then the $2H$-azaphosphirene complex could attack via nitrogen at the carbon center of the protonated nitrile. According to the calculations in the first step of this pathway the proton of triflic acid is not transferred to acetonitrile, but an electrostatic complex **36m**···HOTf is formed where the acid is bound to MeCN via an O–H···N hydrogen bond.[43] Its formation is predicted to be slightly endergonic with $\Delta_R G_{298} = +6.6$ kJ·mol^{-1}, which is in the same range as for protonation of $2H$-azaphosphirene complex **91** (cf. Tab. 4.9). However, the further reaction to the primary product [**180**][OTf] of the attack of **91** at **36m**···HOTf (Fig. 4.31) is clearly unfavored ($\Delta_R G_{298} = +97.2$ kJ·mol^{-1}), therefore, this alternative pathway is largely ruled out.

In summary, pathway **B** should be the most preferred reaction sequence due to the facile formation of phosphenium complex [**175**][OTf] (vii) and its barrierless reaction with acetonitrile (viii). Noteworthy is that also the barrier for the crucial step (ii) of pathway **A** is not significantly higher than the analogous nitrile-promoted ring opening reaction of radical cationic $2H$-azaphosphirene complex **91**$^{\bullet+}$ (cf. Section 3.6.2).

Looking at the facile P,N bond cleavage of [**H–91**][OTf] it should be pointed out that weakening of this bond is not evident from the structural parameters of [**H–91**][OTf] or from the change in structural parameters due to N-protonation of **91**, respectively (Tab. 4.10). Interestingly, the P,N bond is not lengthened, but somewhat shortened upon protonation. This is contrary to the effect induced by single-electron oxidation (cf. Section 3.6.1, Tab. 3.10). On the other hand, as observed upon oxidation, the endocyclic P,C distance is increased upon N-protonation. As a consequence, the endocyclic P–C–N angle, which is the major reaction coordinate of the ring opening

---

[43]According to the calculations protonation of acetonitrile combined with dissociation of triflate (in CH_2Cl_2 solution) as well as addition of the OH functionality of TfOH to the triple bond of MeCN are highly disfavored: $MeCN + TfOH \rightarrow MeCNH^+ + TfO^-$ ($\Delta_R G_{298} = +97.0$ kJ·mol^{-1}) and $MeCN + TfOH \rightarrow MeC(OTf)NH$ ($\Delta_R G_{298} = +73.1$ kJ·mol^{-1}).

process, is not widened. Shortening of the W,P bond along with elongation of the distance of tungsten to the *trans*-CO ligand and shortening of the C,O bond length of this ligand indicate that the cationic ligand of [**H**–**91**][OTf] exhibits a stronger *trans* influence than the neutral heterocyclic ligand in **91**.

Table 4.10: Calculated bond distances [Å] and angles [º] for neutral complex **91** and protonated complex [**H**–**91**][OTf] and relative variations caused by protonation.

	91	[**H**–**91**][OTf]	Relative Variation [%]
W–C[†]	2.031	2.044	+0.6
C–O[†]	1.167	1.162	−0.4
W–P	2.545	2.493	−2.0
P–C[‡]	1.794	1.826	+1.8
P–N	1.853	1.834	−1.0
C–N	1.278	1.282	−0.3
C–P–N	41.0	41.0	0.0
P–C–N	72.0	69.8	−3.0

[†]*trans*-CO. [‡]Endocyclic bond.

Against this background, it should be pointed to the divergent reactivities of radical cationic and protonated 2H-azaphosphirene complexes: while the former undergo P,C bond breaking in the absence of trapping reagents, no experimental or computational evidence for such reaction mode was found for the latter; a primary product that might result from [**H**–**91**][OTf] through P,C bond cleavage was not located computationally. Here, spontaneous break of the P,N bond can occur, while the calculations did not support an analogous reaction mode for the radical cationic system (cf. Section 3.6).

Calculations of compliance constants, which are diagonal elements of the inverse force field, thus, a measure of bond strengths[264] were performed[44] by G. von Frantzius on **91**^{Cr} and [**H**–**91**^{Cr}]$^+$ (chromium instead of tungsten).[277] These calculations revealed that the P,N bond is weakened by 9 % and the P,C bond by even 24 %, while the Cr,P bond is strengthened by 14 % upon *N*-protonation. Nevertheless, the P,N bond constitutes the position of largest compliance, that is, the weakest bond of both the neutral and the protonated 2H-azaphosphirene complex models. A further result was that the positive charge (Hirshfeld[278]) in 2H-azaphosphirenium complex [**H**–**91**^{Cr}]$^+$ is spread over phosphorus (+0.29 au), chromium (+0.21 au), and carbon (+0.15 au).

[44]Calculations were carried out with the GAUSSIAN 03 program package[219] using the density functional BP86[208–210] in combination with the basis set TZVP.[218] The IEF-PCM[274–276] solvent model was used with $\varepsilon = 8.93$ to mimic methylene chloride.

For reactions of [**H**–**91**][OTf] with cyanamide or dicyane only the most plausible pathways **A** and **B** (Schemes 4.28 and 4.29) and additionally pathway **C** were considered; for thermochemical data see Table 4.11. The transition state for nucleophilic ring opening of [**H**–**91**][OTf] by H_2NCN (ii) is 17.1 $kJ \cdot mol^{-1}$ lower in free energy than for the analogous reaction with MeCN. The resulting formation of acyclic intermediate [**176p**][OTf][45] is only slightly endergonic in this case, and with respect to phosphenium complex [**175**][OTf] its formation is exergonic (viii).

Table 4.11: Calculated thermochemical data for reactions shown in Schemes 4.28 (R = NH_2) and 4.29 (R = CN) and for deprotonation of complexes [**134p,q**][OTf] (vi) and [**141q**][OTf] (vi') by NMe_3 (RI-BP86/aug-TZVP/ECP-60-MWB(W)+COSMO//RI-BP86/ aug-SV(P)/ECP-60-MWB(W)+COSMO; all values in $kJ \cdot mol^{-1}$).

Reaction		$\Delta G^{\ddagger}_{298}$	$\Delta_R G_{298}$
i)	**91** + TfOH → [**H**–**91**][OTf]	$\sharp$	+11.0
ii)	[**H**–**91**][OTf] + H_2NCN → [**176p**][OTf]	+52.6	+8.7
	[**H**–**91**][OTf] + NCCN → [**176q**][OTf]	+103.6	+96.6
iii)	[**176p**][OTf] → [**176p'**][OTf]	+4.7	$\dagger$
	[**176q**][OTf] → [**176q'**][OTf]	−3.7	$\dagger$
iv)	[**176p**][OTf] → [**141p**][OTf]	−	−156.8
	[**176q**][OTf] → [**141q**][OTf]	−	−198.3
v)	[**141p**][OTf] → [**134p**][OTf]	$\sharp$	−35.1
	[**141q**][OTf] → [**134q**][OTf]	$\sharp$	+8.3
vi)	[**134p**][OTf] + NMe_3 → **96p** + [Me_3NH][OTf]	$\sharp$	−31.2
	[**134q**][OTf] + NMe_3 → **96q** + [Me_3NH][OTf]	$\sharp$	−108.7
vi')	[**141q**][OTf] + NMe_3 → **96q** + [Me_3NH][OTf]	$\sharp$	−117.0
vii)	[**H**–**91**][OTf] → [**175**][OTf]	+46.5	+44.9
viii)	[**175**][OTf] + H_2NCN → [**176p**][OTf]	$*$	−36.1
	[**175**][OTf] + NCCN → [**176q**][OTf]	$*$	+51.8
xi)	**177** + H_2NCN → [**176p**][OTf]	+68.0	+47.4
	177 + NCCN → [**176q**][OTf]	$*$	+135.3

$\sharp$Not calculated. $\dagger$Conformers [**176p,q**][OTf] could not be located. $*$Not located.

If the reaction would proceed via *P*-OTf substituted phosphane complex **177** (pathway **C**), the barrier **TS**[**xi**] for the subsequent displacement of triflate by cyanamide is 14.1 $kJ \cdot mol^{-1}$ lower than in the case of acetonitrile. However, this pathway is not regarded as a reasonable alternative, since reactions of [**H**–**91**][OTf] (ii) or [**175**][OTf]

---

[45]In the cases of R = NH_2 and CN rotamers [**176p,q'**][OTf], and, accordingly, the transition states **TS**[**iv**](**p,q**), could not be located. Immediate cyclization to give N^4-protonated $2H$-1,4,2-diazaphosphole complexes [**141p,q**][OTf] occurred during geometry optimization, which indicates that the cyclization barriers—if they exist—should be very low.

with H$_2$NCN (viii) are expected to be faster than the formation of complex **177** through competing binding of triflate (x). With dicyane as nucleophile the barrier for the attack at phosphorus of [**H–91**][OTf] (ii) increases significantly, and the formation of [**176q**][OTf]—even from phosphenium complex [**175**][OTf] (viii)—becomes thermodynamically unfavored.

For all model systems employed the cyclization reaction (iv) is highly exergonic. Revealing is a comparison of N^{1}H and N^{4}H tautomers (reaction v). When R = NH$_2$ the stabilization of N^1-protonated isomer [**134p**][OTf] over [**141p**][OTf] is 35.1 kJ·mol^{-1}, which can be attributed to the formation of the conjugated amidinium moiety in [**134p**][OTf]. On the other hand, when R = CN the N^{4}H tautomer [**141q**][OTf] is slightly favored. Finally, the deprotonation reaction with NMe$_3$ (as model for NEt$_3$ or pyridine) is exergonic in each case (reaction vi), and it is not surprising that this effect is most pronounced for the deprotonation of complex [**134q**][OTf] (R = CN), or directly of [**141q**][OTf] (reaction vi'), which are the electron poorest, thus, the most acidic protonated heterocycle complexes within this series.

It is concluded that the electronic nature of the nitrile has a strong influence on the course. Electron rich derivatives such as cyanamides should facilitate the reaction at each point. It is noteworthy that, in principle, the same reaction pathways are possible (computationally) for the acid-induced ring expansion with the electron poor nitrile derivative dicyane. This is in marked contrast to the SET-induced reactions (cf. Section 3.6.2). Nevertheless, from inspection of the thermochemical data (Tab. 4.11) it must be concluded that acid-induced ring expansions with very electron poor nitrile derivatives such as dicyane are also not supported.
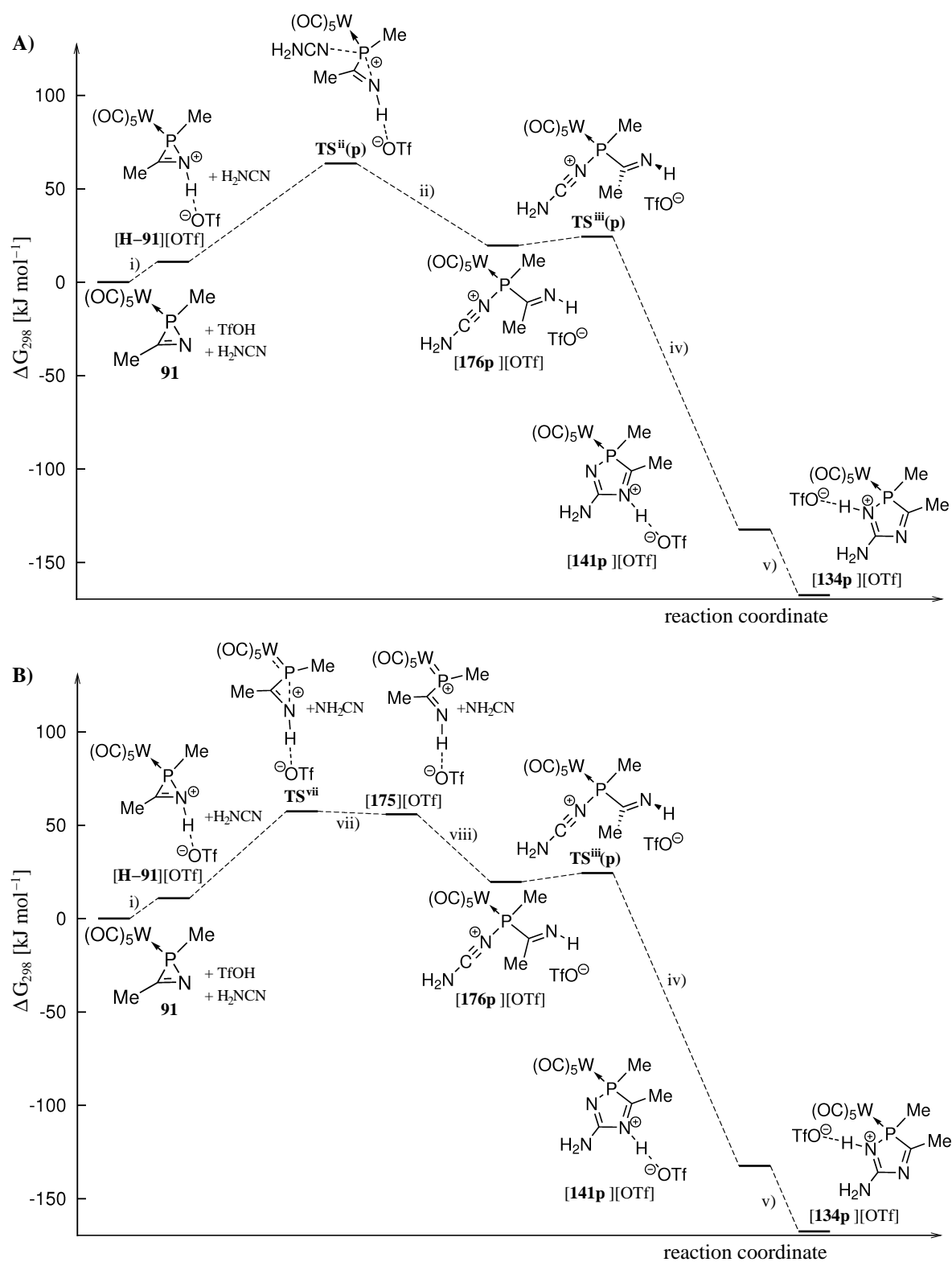
Scheme 4.28: Computed pathways **A** and **B** for the reaction of complex **91** with TfOH and cyanamide. The sum of free energies of the reactants (**91**, TfOH, and H₂NCN) was arbitrarily chosen as zero-point of the ΔG_{298} scale.
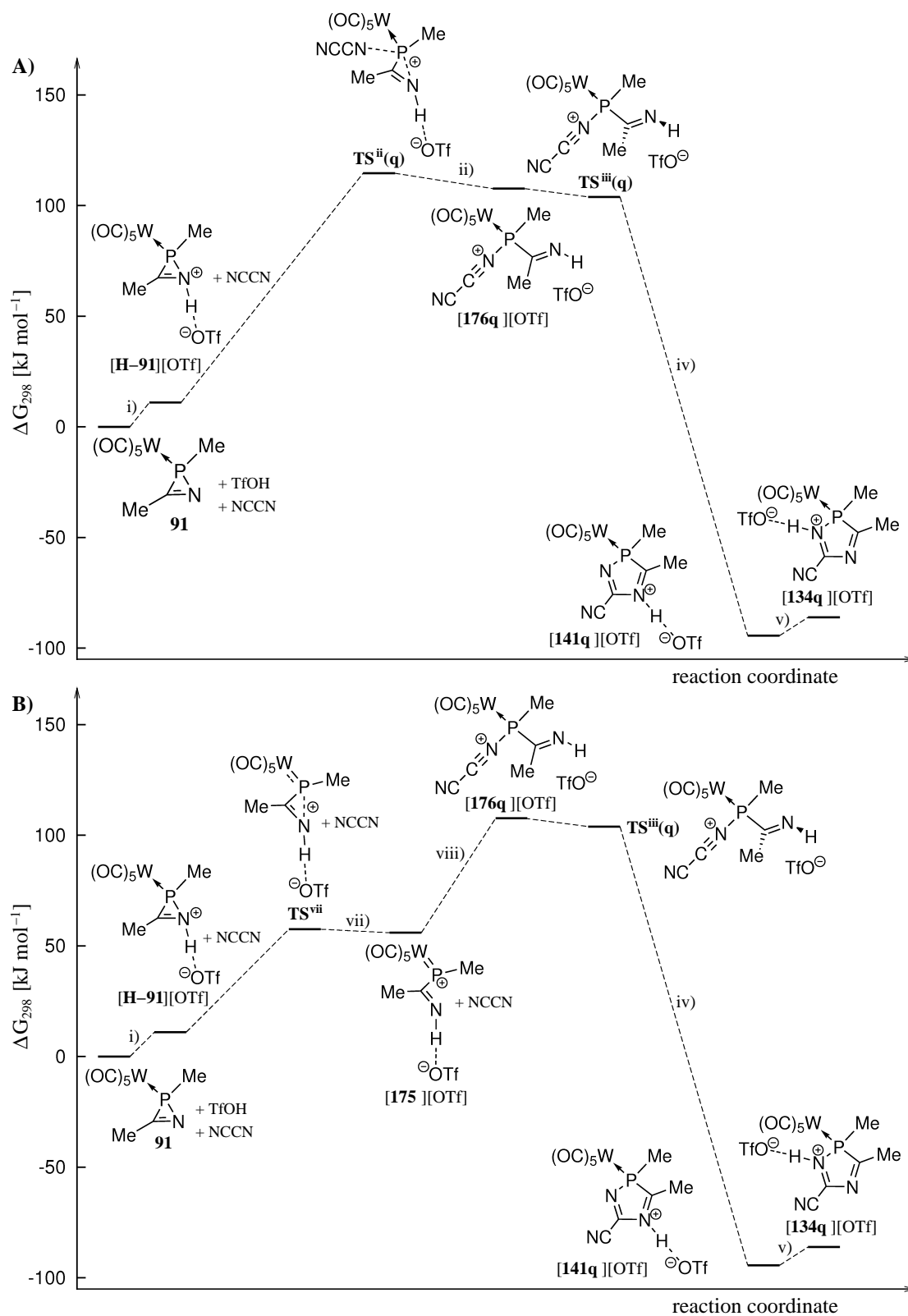
Scheme 4.29: Computed pathways **A** and **B** for the reaction of complex **91** with TfOH and dicyane. The sum of free energies of the reactants (**91**, TfOH, and NCCN) was arbitrarily chosen as zero-point of the ΔG_{298} scale.

4.4.2 Reaction with an Isonitrile

N-Protonation of $2H$-azaphosphirene complex **35** most likely is the first reaction step also in the formation of 2,3-dihydro-1,3-azaphosphete complex **149** from **35** and cyclohexyl isocyanide (**148**) (Section 4.1.5).
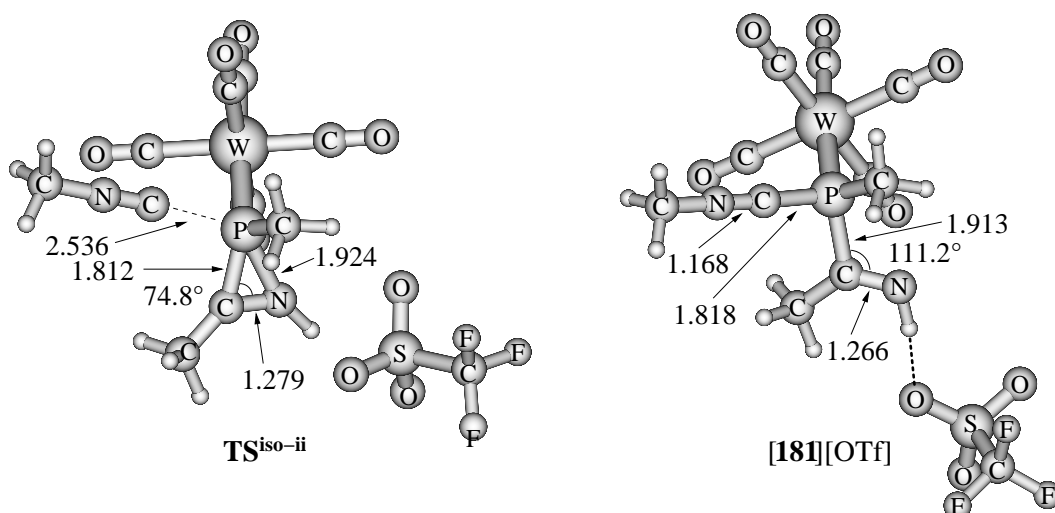
Figure 4.32: Calculated structure of transition state **TS^{iso-ii}** for the nucleophilic ring opening of [**H**–**91**][OTf] by methyl isocyanide (left) and calculated structure of acyclic intermediate [**181**][OTf] (right) (distances in Å).

Calculations on C,P-dimethyl substituted model system **91** using methyl isocyanide as model for isonitrile **148** revealed that an acyclic intermediate, [**181**][OTf] (Fig. 4.32, right), having an almost linear arrangement of the PCNC moiety (P–C–N 175.3°; C–N–C 179.1°), can be formed either from $2H$-azaphosphirenium complex [**H**–**91**][OTf] or via phosphenium complex [**175**][OTf]: [**H**–**91**][OTf] + MeNC → [**181**][OTf] ($\Delta_R G_{298}$ = -21.0 kJ·mol^{-1}); [**175**][OTf] + MeNC → [**181**][OTf] ($\Delta_R G_{298}$ = -65.9 kJ·mol^{-1}). Both reactions are thermodynamically more favored than the formation of intermediate [**176m**][OTf] (or [**176m'**][OTf]) from the reaction of $2H$-azaphosphirene complex **91** with TfOH and acetonitrile (Section 4.4.1).

The barrier for nucleophilic ring opening of [**H**–**91**][OTf] by MeNC (**TS^{iso-ii}**: Fig. 4.32, left) was estimated as $\Delta G^{\ddagger}_{298}$ = $+48.3$ kJ·mol^{-1}, hence, it is 21.4 kJ·mol^{-1} lower in free energy than the barrier for the analogous reaction with acetonitrile and even slightly lower than for the reaction with cyanamide (by 4.3 kJ·mol^{-1}). Also in this case in a constrained search no transition state could be located for the attack of MeNC at the phosphenium center of [**175**][OTf].

4.5   Conclusions

In this chapter it was demonstrated that highly selective ring enlargement reactions of 2H-azaphosphirene complexes can be induced by strong Brønsted and Lewis acids.

The newly developed protocol using consecutive reaction with triflic acid and a base (NEt$_3$ or pyridine) could successfully be applied to 2H-azaphosphirene complexes with different C- and P-substituents in the presence of nitriles leading to 2H-1,4,2-diazaphosphole complexes, which were isolated in good or moderate yields (Section 4.1). During the reactions (before adding the base) 2H-1,4,2-diazaphospholium complexes were observed, which turned out to be very unstable in solution. Nevertheless, complexes **123b,m** and **124b** could be isolated, and the structure of **123b** was determined by a single-crystal X-ray diffraction study thus confirming the location of the proton at N^1; for **123b** and **124b** this was evidenced also by ^{1}H,^{15}N HMQC NMR experiments.

Using this methodology even nitriles with high steric demand (**36r,s**) could successfully be employed, and apart from the reaction of **35** with trimethylsilyl cyanide (**36t**) in which partial desilylation occurred during the reaction no by-products were observed such as symmetrically 3,5-disubstituted 2H-1,4,2-diazaphosphole complexes (cf. Chapter 3). It is noteworthy that ring expansion reactions with the parent nitrile HCN (**36h**) could be achieved (Section 4.1.3), which was not successful when using the oxidative SET protocol (cf. Section 3.2). Here, an unexpected haptotropic (P→N)-metal shift was observed as the products **41h**, **69h**, and **126h** were obtained in mixtures with complexes **129h**, **130h**, and **131h**, which constitute first examples of κN-bonded 2H-1,4,2-diazaphosphole complexes.

Also contrasting the SET protocol, the TfOH/NEt$_3$ ring expansion methodology could successfully be applied to molybdenum and chromium complexes **70** and **71** (Section 4.1.4). During the reactions partial decomplexation was observed, but this could completely be prevented by performing the reactions at low temperature and adding the base after short periods. On the other hand, after prolonged reaction times complete decomplexation occurred. N^1-Protonated 2H-1,4,2-diazaphosphole **147b** was characterized by multinuclear NMR experiments, and after deprotonation neutral heterocycle **50b** was obtained. Although it suffered from decomposition during column chromatography all relevant NMR spectroscopic information about **50b** was obtained from the crude product.

Reaction of 2H-azaphosphirene complex **35** with an isonitrile enabled access to the novel 2,3-dihydro-1,3-azaphosphete complex **149**, which was isolated and structurally confirmed (Section 4.1.5). Also here, an N-protonated heterocyclic intermediate, **154**,

was observed before the addition of the base.

Investigations on various Brønsted acids to induce ring expansion of $2H$-azaphosphirene complex **35** with nitrile **36b** revealed that best performances are obtained if acids are employed that form weak nucleophilic corresponding anions (Section 4.2). Also Lewis acids such as $B(C_6F_5)_3$ and $Li[B(C_6F_5)_4]$ yielded good results. Reactions with copper(I) salts gave additionally $2H$-1,3,2-diazaphosphole complexes **46** and **155**, and in the reaction of **35** with $[Cu(MeCN)_4][OTf]$ evidence for heterobimetallic complex **156** was obtained, which is in equilibrium with the reactants.

Reaction of **35** with TfOH in the absence of trapping reagents gave coordination-isomeric 1-aza-3-phosphabutadiene complexes **169** and **170** (Section 4.3.2). Upon reaction of in situ generated **169** and **170** with nitrile **36b** N^1-protonated $2H$-1,4,2-diazaphosphole complex **171b** was formed, which features a CH_2SiMe_3 group at phosphorus; after deprotonation neutral complex **172b** was obtained. In reactions of **35** with $HBF_4 \cdot Et_2O$ and $BF_3 \cdot Et_2O$ ring opening and P,F bond formation occurred.

The first $2H$-azaphosphirenium complex $[\mathbf{H}–\mathbf{121}][OTf]$ was observed and characterized by multinuclear NMR spectroscopy at low temperature upon reaction of P-Cp* substituted complex **121** with TfOH. It was shown that protonation of **121** can be reversed, and when a nitrile (**36b**) was added to a solution of $[\mathbf{H}–\mathbf{121}][OTf]$ ring expansion occurred with formation of complex **124b**.

DFT calculations revealed that $2H$-azaphosphirenium complex $[\mathbf{H}–\mathbf{91}][OTf]$, formed upon N-protonation of $2H$-azaphosphirene complex model **91**, is prone to undergo spontaneous ring opening with formation of phosphenium complex $[\mathbf{175}][OTf]$ (Section 4.4). The latter can easily be attacked by a nitrile, and the resulting intermediates $[\mathbf{176m,p,q'}][OTf]$ can subsequently undergo facile cyclization. Overall, the calculated barriers are not higher than those occurring on the pathway of the SET-induced ring expansion. It should be noted that, in principle, the same reaction pathways are possible for acid-induced ring expansion with the electron-poor nitrile derivative NCCN as for MeCN and H_2NCN, though the barriers for NCCN are significantly higher. Reactions with isonitriles are predicted to proceed in a similar way via acyclic intermediates such as $[\mathbf{181}][OTf]$.

Chapter 5

Investigations on the Photophysical Properties of $2H$-1,4,2-Diazaphosphole Complexes

Linear π-conjugated oligomers and polymers based on a planar backbone of sp^2-bonded atoms have attracted increasing interest in recent years owing to their potential application in electronic devices, for example, in organic light-emitting diodes (OLEDs), thin-film transistors, or photovoltaic cells.[279–285] The optical and electronic properties of these macromolecules depend mainly on their HOMO−LUMO gap and the electron density of the backbone. Several strategies have been developed to vary these parameters with the aim of preparing novel conjugated frameworks with enhanced performance. One successful approach was to incorporate heterocyclic building blocks with different aromatic character and electronic nature in the backbone of π-conjugated systems.[280–285] It turned out that low aromaticity favors electron delocalization along the main chain, while maximum conjugation was obtained in copolymers with alternating electron-rich and electron-deficient subunits due to intramolecular charge transfer (ICT).[281] Heterocyclopentadienes have been extensively used for such purposes, since their electronic properties depend significantly on the nature of the heteroatoms. For example, 2,5-diarylsiloles have found applications as electron-transporting materials in organic light-emitting diodes.[285, 286] The reason for the observed lowering in $\pi-\pi^*$ transition energies of group 14 heterocyclopentadienes compared to their parent carbocycles (e.g., **182b** vs. **182a**; Fig. 5.1) is believed to rely on $\sigma^*-\pi^*$ conjugation in the central ring, that is, the interaction of σ^* orbitals of the two exocyclic σ bonds at the

ring silicon with a π^* orbital of the butadiene moiety;[282] similar results were obtained also for Ge and Sn analogs of **182a,b**.[282] By dibromination of a derivative of **182b** and cross-coupling with a silole-2,5-diboronic acid (Suzuki-Miyaura cross-coupling) a silole-thiophene alternating copolymer was synthesized, which exhibited an extremely narrow optical band gap (1.55 eV).[283]

182a: E = C
    λ_{max} = 368 nm
182b: E = Si
    λ_{max} = 418 nm

183a: Ar = 2-pyridyl
    λ_{max} = 390 nm
183b: Ar = 2-thienyl
    λ_{max} = 412 nm
183c: Ar = phenyl
    λ_{max} = 354 nm

184a: R = H
    λ_{max} = 338 nm
184b: R = SiMe$_3$
    λ_{max} = 344 nm
184c: R = SiMe$_2{}^t$Bu
    λ_{max} = 364 nm

126g: λ_{max} = 341 nm,
    444 nm

49: λ_{max} = 408 nm

185: λ_{max} = 391 nm
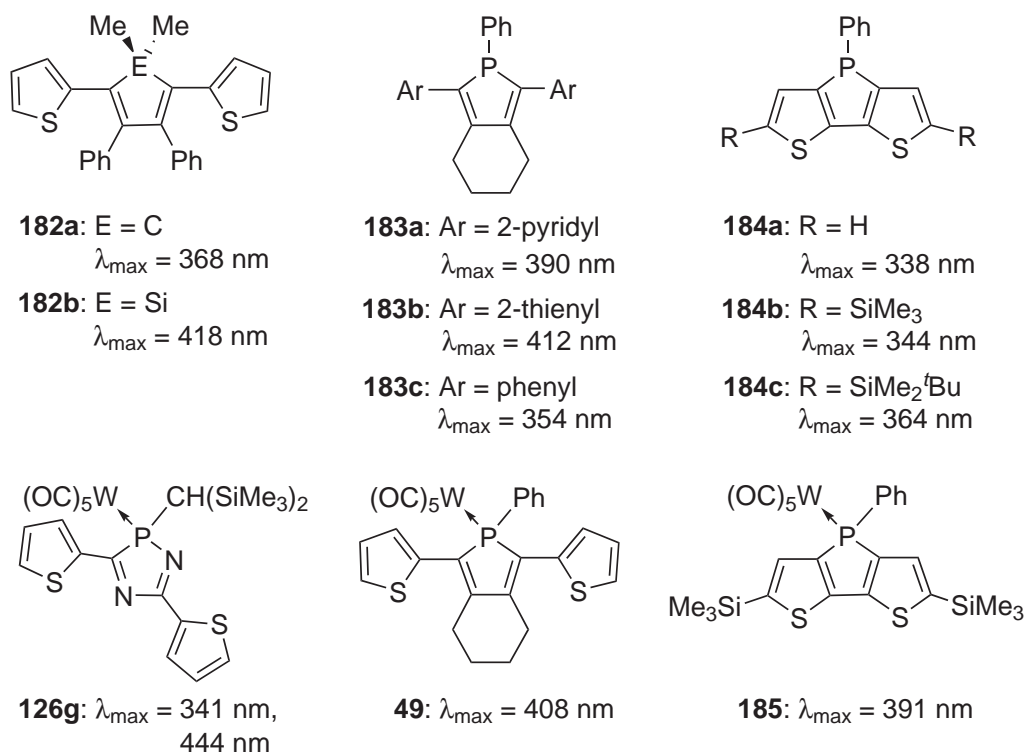
Figure 5.1: 1,4-Diarylcyclopentadiene **182a**,[282] 2,5-diarylsilole **182b**,[282] 2,5-diaryl-phospholes **183a–c**,[183] dithieno[3,2-b:2',3'-d]phospholes **184a–c**,[287] 3,5-di(2-thienyl)-2H-1,4,2-diazaphosphole complex **126g**, 2,5-di(2-thienyl)phosphole complex **49**,[183] and dithieno[3,2-b:2',3'-d]phosphole complex **185**.[288] Absorption maxima recorded in CHCl$_3$ (**182a,b**),[282] THF (**183a–c**, **49**),[183] CH$_2$Cl$_2$ (**184a–c**,[287] **185**[288]), or n-pentane (**126g**).

The first polymer containing phosphole rings in the backbone was reported by Tilley and coworkers.[289, 290] Réau and coworkers have established 2,5-diaryl- and 2,5-dihetarylphospholes such as **183a–c**[183, 290] (Fig. 5.1). Investigations on their optical and electrochemical properties revealed that delocalization of the π-system reaches a maximum with two 2-thienyl substituents being attached to the phosphole ring.[183] It was further supported by calculations that this effect is due to a low lying LUMO—mainly localized at the phosphole moiety—in combination with a high HOMO energy caused by the electron-rich 2-thienyl substituents. Phosphole derivative **183b** was employed in an electropolymerization process, which gave an electroactive film on a

platinum surface showing a low optical band gap.

Baumgartner and coworkers have developed a different strategy making use of fused tricyclic dithieno[3,2-*b*:2',3'-*d*]phospholes[287, 288, 290–293] such as **184a–c**[287] (Fig. 5.1). Their photophysical properties can effectively be tuned through variation of the substituents R at the thiophene rings or by modification at phosphorus. Polymeric materials based on these systems have also been described.[291, 292] Complexation of the phosphorus center of **184a–c** with transition metal fragments such as AuCl or W(CO)$_5$ (e.g., complex **185**: Fig. 5.1) causes a red shift of the $\pi-\pi^*$ absorption by $20-50$ nm,[288] whereas in the cases of 2,5-diarylphospholes **183a–c** the effect of transition metal complexation on their photophysical properties is rather low (e.g., complex **49**,[183] Fig. 5.1).

5.1   Neutral 2*H*-1,4,2-Diazaphosphole Complexes

2*H*-1,4,2-Diazaphosphole complexes revealed interesting photophysical properties: by UV/Vis spectroscopy for each complex a band was detected at very long wavelength (in most cases at $\lambda_{max} > 400$ nm), and one or two absorption maxima with higher intensity were found at about $280-350$ nm (Tab. 5.1).

Of all neutral 2*H*-1,4,2-diazaphosphole complexes presented in this work 3,5-di(2-thienyl) substituted complex **126g** (Fig. 5.1) shows the lowest-lying absorption maximum (apart from ferrocenyl-containing derivatives **69b,l**[1]). It is centered at even longer wavelength ($\lambda_{max} = 444$ nm, lg$\epsilon = 3.41$) than the longest-wavelength absorption maxima of cyclopentadiene, silole, and phosphole derivatives displayed in Figure 5.1. The largely coplanar arrangement of the three adjacent ring systems of **126g** in the crystal state (see Fig. 4.8, Section 4.1.2) may allow an extended π conjugation over the three heterocycles. Since the 2*H*-1,4,2-diazaphosphole ring can be devised from the phosphole ring by replacement of two CR units by nitrogen atoms, an even lower LUMO energy may be expected for 2*H*-1,4,2-diazaphosphole complexes compared to complexes of phospholes. This was evidenced from cyclovoltammetric investigations (Section 3.5), which revealed that complex **126g** is reversibly reduced at $E_{1/2} = -1.635$ V vs. $E_{1/2}(FeCp_2^+/FeCp_2)$. For comparison, complex **49** shows an irreversible reduction wave at $E_{pc} = -2.20$ V vs. $E_{1/2}(FeCp_2^+/FeCp_2)$.[183] On the other hand, complex **49** exhibits a slightly lower anodic peak potential ($E_{pa} = +0.70$ V) than **126g** ($E_{pa} = +0.83$ V), which points to a higher HOMO energy in the former case; for both complexes the oxidations were irreversible under the applied measuring conditions.

---

[1]Complexes **69b,l** exhibit another low-energy band, which is due to the presence of a ferrocenyl group. This was discussed for complex **69l** in Section 3.2.1.

Table 5.1: Selected UV/Vis spectroscopic data for 2*H*-1,4,2-diazaphosphole complexes presented in this work (assignment on the basis of TD-DFT calculations; HE: High-energy band; MLCT: metal−ligand charge transfer; L: 2*H*-1,4,2-diazaphosphole ligand; M = W, Mo, Cr).

No.	λ_{max} HE [nm]	λ_{max} L$_{\pi-\pi^*}$ [nm]	λ_{max} MLCT [nm]	λ_{max} Fc$_{d-d/d_\pi-\pi^*}$ [nm]	λ_{onset} [nm]
41b	227	288*, 350	407	−	505
41g	232	317	435	−	560
41h/129h	229	296, 312	398, 433	−	619
41m	228	289	425	−	554
41r	230	292	419	−	551
41s	230	292	418	−	542
41t	231	284	432	−	553
69b	205, 231	299*, 352	385	520	631
69l	205, 227	296	404	539	718
74b	228, 234	286*, 348	396	−	508
75b	225	286*, 351	439	−	554
122b	226	284*, 348	400	−	504
123b[†]	234	306	463	−	649
124b[†]	238	301	445	−	630
126b	232	292, 325*	413	−	525
126g	232	341	444	−	584
126h/131h	233	293, 347*	438	−	601
172b	232	287*, 345	411	−	506
190[§]	233	295, 345*	422	−	546

All data recorded in *n*-pentane solution, except for [†]recorded in CH$_2$Cl$_2$.

[§]Presented in Chapter 6. *Refers to the most intense maximum in this region.

In order to provide an interpretation of the UV/Vis spectra of 2*H*-1,4,2-diazaphosphole complexes, vertical singlet excitations were calculated by means of *Time-Dependent Density Functional Theory* (TD-DFT).[294, 295] This was performed with the TURBOMOLE V5.9.1 program package[206] using the Three Parameter Hybrid Functional Becke3 (B3)[230] in combination with the gradient corrected correlation functional by Lee, Yang, and Parr (LYP).[231] Ahlrichs and coworkers showed that this combination gave the best results among several tested density functionals; the calculated excitation energies were approximately 0.4 eV too low, but the right ordering of states was predicted for several molecules of different sizes.[295] For the current study on 2*H*-1,4,2-diazaphosphole complexes the valence-double-ζ basis set SV(P)[212] was used for all atoms, and the core electrons of tungsten were substituted by the ef-

fective core potential ECP-60-MWB.[213] Optimizations were done with the gradient corrected exchange functional by Becke (B88)[209] in combination with the correlation functional LYP[231] with the RI approximation[211] and the basis set SV(P).[212] The stationary points were characterized as minima by analytical vibrational frequencies calculations.[217] In Appendix B it is demonstrated that the results obtained with this approach are reliable in so far as they do not significantly differ from the results obtained with a larger basis set (TZVP[218]). Furthermore, it is shown that using different methods for geometry optimizations and single point calculations does not have a severe impact on the calculated excitation energies, either.

The electronic transitions calculated for complex **126g** that have considerable oscillator strengths are given in Table 5.2, and the orbitals with major contributions are displayed in Figure 5.2. In Figure 5.3 the computed data are plotted in comparison to the experimentally recorded UV/Vis absorption spectrum (in wavenumbers).[2]

Table 5.2: Calculated vertical singlet excitations for complex **126g** (TD-B3LYP/SV(P)/ECP-60-MWB(W)//RI-BLYP/SV(P)/ECP-60-MWB(W)). Only the major orbital contributions are given.

No.	$\tilde{\nu}$ [cm^{-1}]	λ [nm]	Oscillator strength	Orbital contributions			$\|c\|^2$ [%]
1	18930	528	0.0019	**HOMO**	$\rightarrow$	**LUMO**	98
2	19870	503	0.0241	**HOMO−1**	$\rightarrow$	**LUMO**	98
4	24912	401	0.0978	**HOMO−3**	$\rightarrow$	**LUMO**	88
6	27721	361	0.1144	**HOMO−6**	$\rightarrow$	**LUMO**	47
				HOMO−4	$\rightarrow$	**LUMO**	35
8	27928	358	0.1886	**HOMO−4**	$\rightarrow$	**LUMO**	51
				HOMO−6	$\rightarrow$	**LUMO**	24

The three highest occupied molecular orbitals (HOMO, HOMO−1, HOMO−2; the latter is not displayed) are metal *d* orbitals of π type with respect to the metal−diazaphosphole ligand bond axes. The LUMO is characterized as a π^* orbital of the heterocyclic system extended over all three rings, whereas the major contribution is given by the carbon and nitrogen atoms of the 2*H*-1,4,2-diazaphosphole ring. The contribution of phosphorus is negligible, and a possible $\sigma^*-\pi^*$ conjugation (as in the cases of silole, germole, or stannole derivatives[282]) is not supported, here.

---

[2]It is switched to wavenumbers because of the direct proportionality to excitation energies. In the tables calculated transitions are numbered according to increasing wavenumbers.
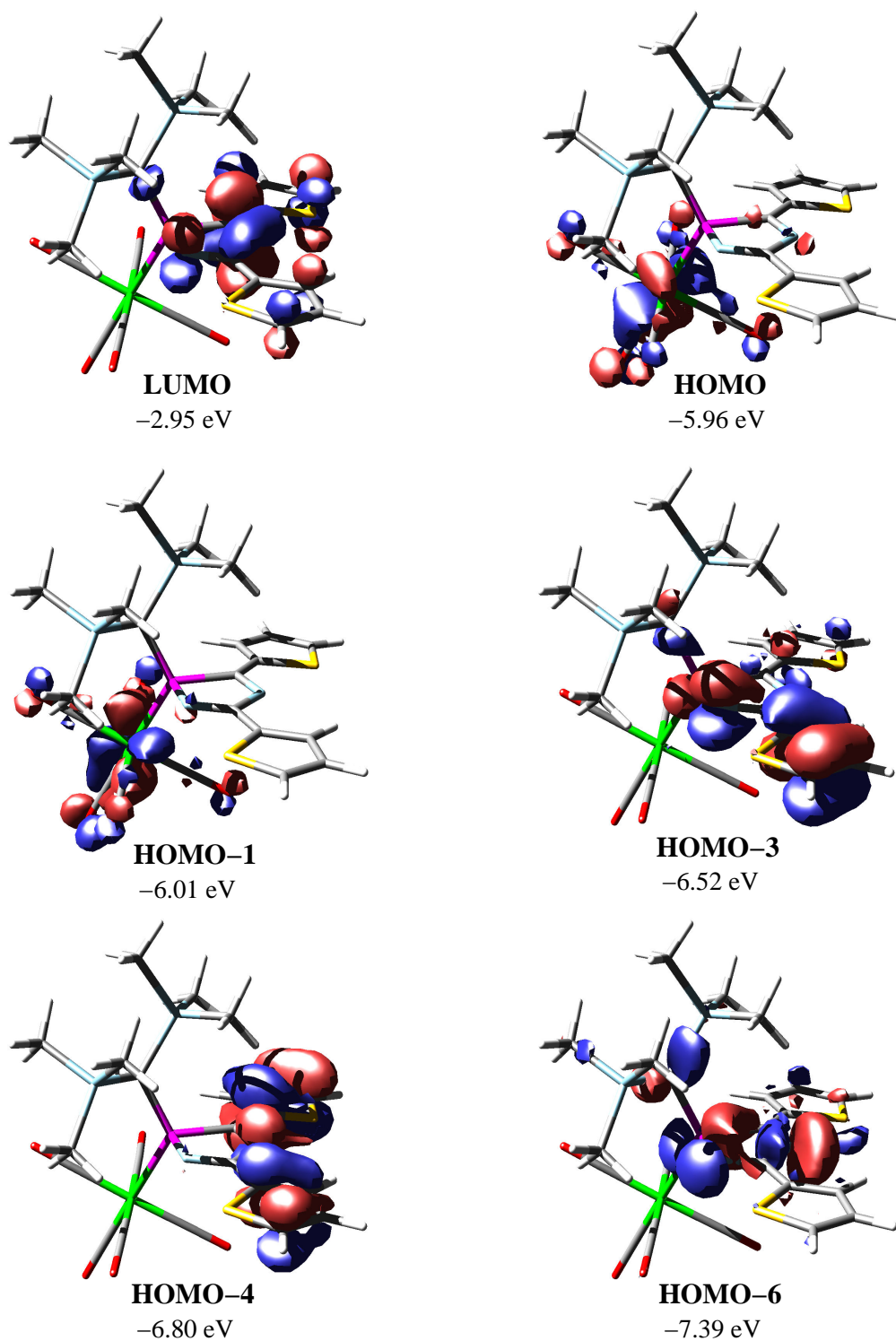
Figure 5.2: Visualization of selected molecular orbitals calculated for complex **126g** (B3LYP/ SV(P)/ECP-60-MWB(W)//RI-BLYP/SV(P)/ECP-60-MWB(W); isovalue 0.04 au).
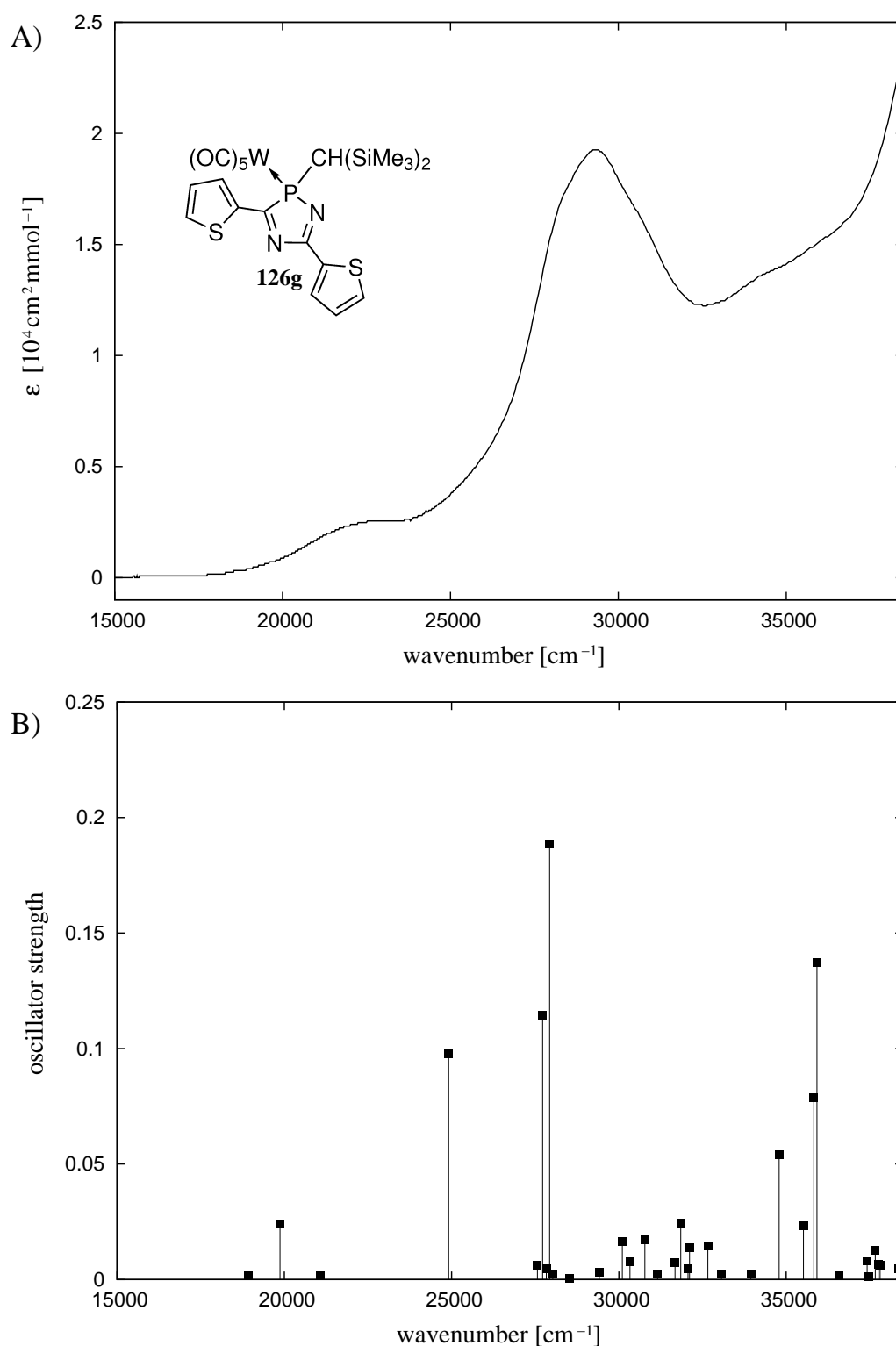
Figure 5.3: A) UV/Vis spectrum of complex **126g** (*n*-pentane). B) Calculated vertical singlet excitations for complex **126g** (TD-B3LYP/SV(P)/ECP-60-MWB(W)//RI-BLYP/SV(P)/ECP-60-MWB(W)).

All low-energy excitations considered occur into the LUMO ($\varepsilon = -2.95$ eV). The second lowest unoccupied orbital (LUMO+1; not shown), a metal d orbital of σ type with respect to the *cis*-carbonyl ligands (i.e., $d_{x^2-y^2}$), is significantly higher in energy ($\varepsilon = -1.64$ eV). While the HOMO→LUMO transition probability is almost zero, the first two excitations having considerable oscillator strengths are predicted at 19870 cm^{-1} (No. 2) and 24912 cm^{-1} (No. 4). Both transitions have distinctly different origins. While the former is characterized as a metal−ligand charge transfer (MLCT) process, since it occurs from HOMO−1 to the LUMO, the latter can unambiguously be assigned to a $\pi-\pi^*$ transition. Here, the electron is excited from HOMO−3, which is an almost pure π orbital where the dominance of the thienyl ring at C^5 is clearly evident; the contribution of the thienyl substituent at C^5 is rather low.

Bearing in mind that the applied calculation method yields excitation energies that might by trend be somewhat too low,[295] an assignment of the low-energy band detected at 22500 cm^{-1} ($\lambda = 444$ nm) to the MLCT process is plausible. The more intense absorption band centered at 29400 cm^{-1} ($\lambda_{max} = 341$ nm) might arise from superposition[3] of the $\pi-\pi^*$ transition (No. 4) and two further nearly degenerate excitations, No. 6 and No. 8. The latter two occur from HOMO−4 and HOMO−6 into the LUMO. To excitation No. 8, which is predicted to have higher intensity, the contribution of HOMO−4 prevails. This orbital exhibits distinct π characteristics and is uniformly distributed over all three heterocycles, hence, the corresponding excitation is best described as a $\pi-\pi^*$ transition. In the case of transition No. 6 the contributions of HOMO−6 and HOMO−4 are almost balanced, with a slight dominance of HOMO−6. This orbital has the largest amplitude at the lone pairs of the 2H-1,4,2-diazaphosphole ring nitrogen atoms. Therefore, the corresponding excitation is tentatively ascribed to an $n-\pi^*$ transition.

Looking at the optical end absorptions (λ_{onset}) of 2H-1,4,2-diazaphosphole complexes it is remarkable that the largest value was obtained for the mixture of **41h** and **129h** (Tab. 5.1)[4] although these complexes feature only two conjugated cyclic π systems. In the spectrum of **41h** and **129h** (Fig. 5.4) two flat low-energy absorption maxima were found at $\tilde{\nu}_{max} = 23100$ cm^{-1} and $\tilde{\nu}_{max} = 25100$ cm^{-1}. Furthermore, two partially overlapping bands having almost equal intensities were detected at $\tilde{\nu}_{max} = 32100$ cm^{-1} and $\tilde{\nu}_{max} = 33800$ cm^{-1}. A large λ_{onset} value was found also for the mixture of 3-(2-thienyl) substituted derivatives **126h** and **131h** ($\lambda_{onset} = 601$ nm), but it is noteworthy that this feature is less pronounced here.[5] Against the background that the mixture

---

[3]The shape of the experimental spectrum in this region suggests that more than one transition might contribute to this band, thus giving rise to shoulders near the absorption maximum.

[4]Besides ferrocenyl-containing derivatives **69b,l** and protonated complexes **123b** and **124b**; the latter are discussed in Section 5.2.

[5]Note that for analogous 3-phenyl and 3-(2-thienyl) substituted derivatives **41b** vs. **126b** and **41g**

of **41h** and **129h** contains a larger amount of the κN-coordinated complex than the mixture of **126h** and **131h**, the assumption is strongly suggested that the observations mentioned beforehand may be caused by this isomer.
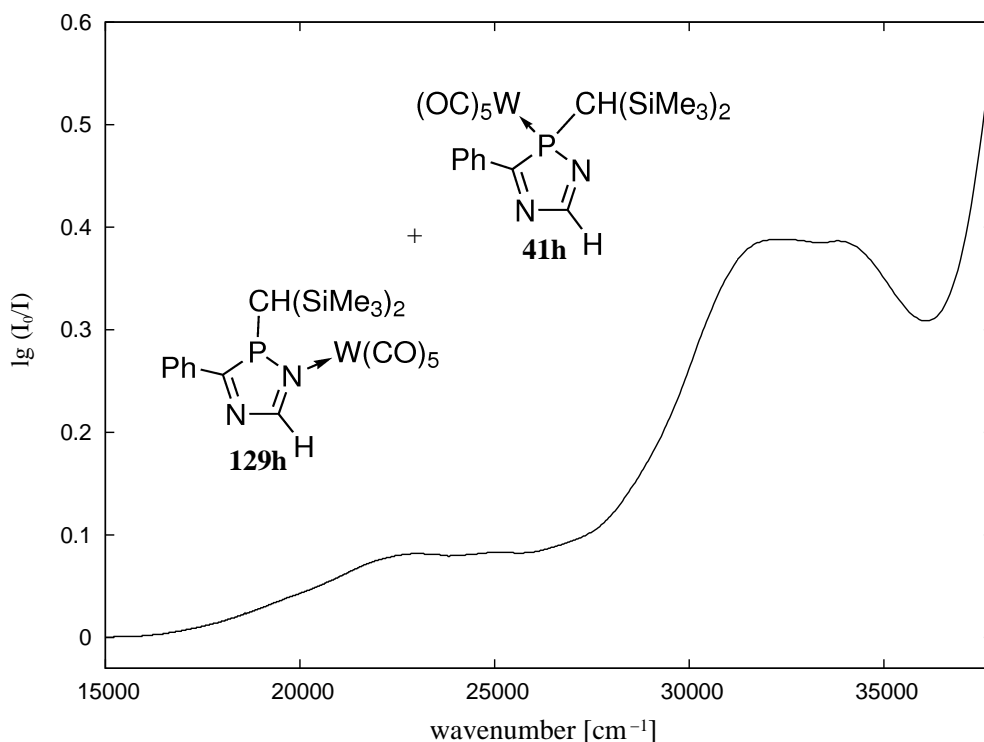
Figure 5.4: UV/Vis spectrum of a of mixture of complexes **41h** and **129h** (*n*-pentane).

In order to prove this hypothesis, vertical excitations were calculated for complexes **41h**, **129h**, **126h**, and **131h**. The calculations on the κP-bonded complexes **41h** and **126h** revealed similar results as obtained for complex **126g** (see Appendix B for details); as a good case in point, the data calculated for **41h** are displayed in Figure 5.5 (A).

Noteworthy are three major points: 1) The low-energy MLCT absorptions of **41h** ($\tilde{\nu} = 20295$ cm^{-1}) and **126h** ($\tilde{\nu} = 20015$ cm^{-1}) are not lower than that of **126g** ($\tilde{\nu} = 19870$ cm^{-1}). 2) An analog of the transition at 24912 cm^{-1} of complex **126g** is missing; for the latter this involved a π orbital with major contribution from the thienyl ring at C^5 (HOMO-3; cf. Fig. 5.2). 3) All excitations of thienyl substituted derivative **126h** have slightly smaller wavenumbers than analogous excitations of complex **41h**.

vs. **126g** the larger λ_{onset} values were detected for the latter.
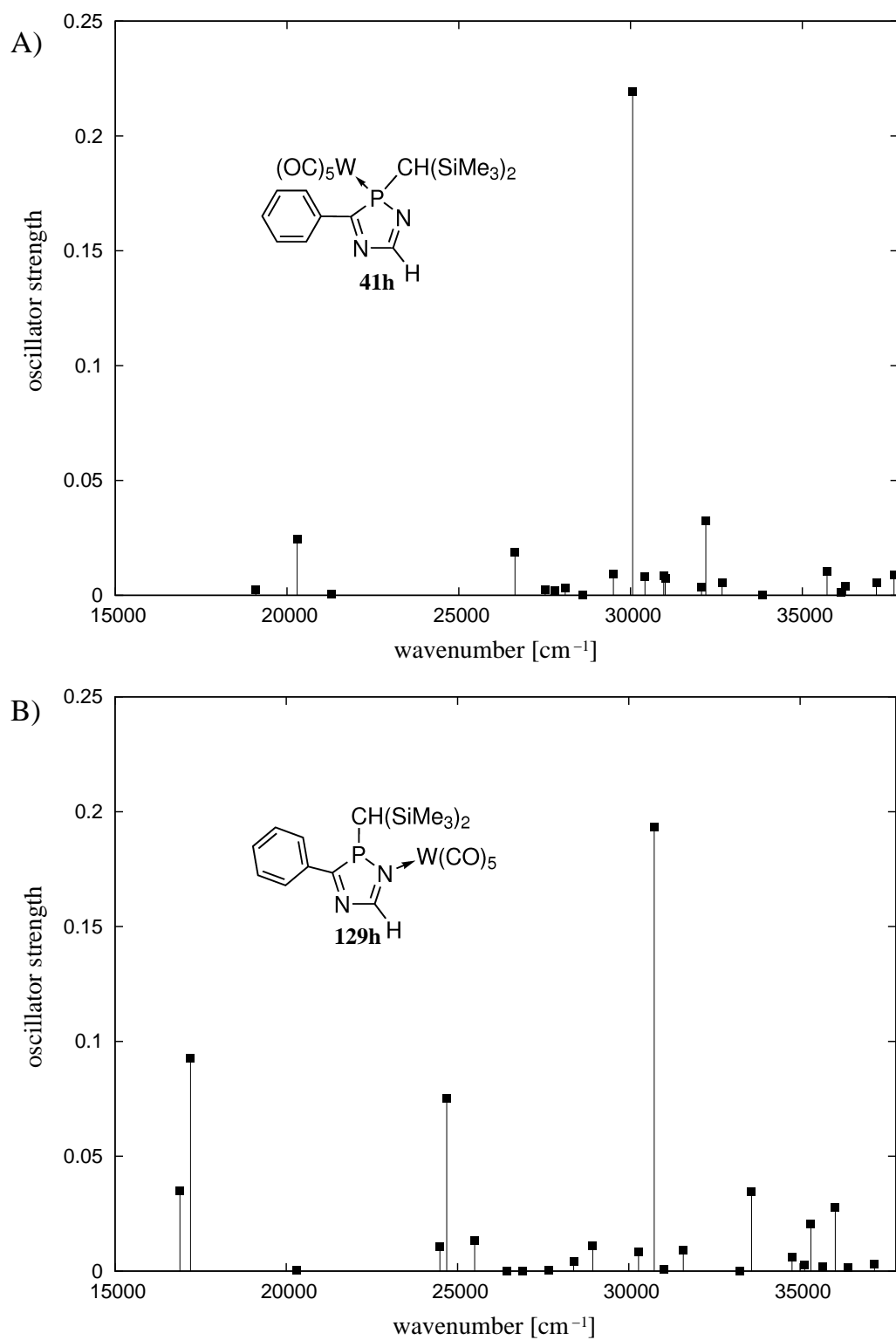
Figure 5.5: Calculated vertical singlet excitations for complexes **41h** (A) and **129h** (B) (TD-B3LYP/SV(P)/ECP-60-MWB(W)//RI-BLYP/SV(P)/ECP-60-MWB(W)).

The κN-complexes **129h** and **131h** exhibit two very low lying transitions with comparatively high intensities (No. 1 and No. 2, Tab. 5.3). Both correspond to excitations from HOMO and HOMO−1 into the lowest virtual orbital (LUMO). As a good case in point, the data calculated for complex **129h** are visualized in Figure 5.5 (B), and relevant orbitals are displayed in Figure 5.6.

Table 5.3: Calculated vertical singlet excitations for complexes **129h** and **131h** (TD-B3LYP/SV(P)/ECP-60-MWB(W)//RI-BLYP/SV(P)/ECP-60-MWB(W)). Only the major orbital contributions are given.

No.	$\tilde{\nu}$ [cm^{-1}]	λ [nm]	Oscillator strength	Orbital contributions			$|c|^2$ [%]
129h							
1	16894	591.9	0.0348	**HOMO−1**	$\rightarrow$	**LUMO**	62
				HOMO	$\rightarrow$	**LUMO**	37
2	17203	581.3	0.0925	**HOMO**	$\rightarrow$	**LUMO**	62
				HOMO−1	$\rightarrow$	**LUMO**	37
5	24682	405.1	0.0751	**HOMO−3**	$\rightarrow$	**LUMO**	86
13	30741	325.3	0.1933	**HOMO−4**	$\rightarrow$	**LUMO**	70
131h							
1	16289	613.9	0.0409	**HOMO−1**	$\rightarrow$	**LUMO**	59
				HOMO	$\rightarrow$	**LUMO**	40
2	16608	602.1	0.0929	**HOMO**	$\rightarrow$	**LUMO**	59
				HOMO−1	$\rightarrow$	**LUMO**	40
4	24172	413.7	0.1030	**HOMO−3**	$\rightarrow$	**LUMO**	83
12	29095	343.7	0.1223	**HOMO−4**	$\rightarrow$	**LUMO**	54

The LUMO is a π^* orbital extended over the two ring systems. Here, a certain participation of the phosphorus lone pair becomes obvious, although the phosphorus center is significantly pyramidalized in both the calculated structures ($\Sigma\angle(PR_3)$ 311.2$\,^\circ$ (**129h**) and 308.4$\,^\circ$ (**131h**)). Both HOMO and HOMO−1 constitute metal d orbitals, hence, the two lowest-lying absorptions are assigned to MLCT processes. The HOMO has a larger contribution to the second, more intense transition. The lobes of this orbital are orientated in such way that π interaction with the heterocyclic ligand is maximized, that is, perpendicular to the heterocycle ring plane.

Different from the situation in the κP-coordinated derivatives **41h** and **126h**, the transition metal center of **129h** and **131h** is located in the heterocycle ring plane. The result is a more pronounced overlap of appropriately orientated d orbitals with

the heterocyclic π system, which may serve as an explanation why an optically induced MLCT is more likely in these cases.

Considerable oscillator strengths were predicted also for HOMO$-3\rightarrow$LUMO and HOMO$-4\rightarrow$LUMO excitations, whereas the latter can unambiguously be assigned to a $\pi-\pi^*$ transition. The HOMO-4 is a π orbital that is significantly polarized towards the aryl substituent; certain π-type contributions are found also at the nitrogen atoms of the 2H-1,4,2-diazaphosphole ring. The HOMO-3 cannot exclusively be classified as either σ or as π orbital. By far the largest contribution is provided by the lone pair at phosphorus, which is due to the pyramidalization of the phosphorus center necessarily nonsymmetric with respect to the ring plane. Therefore, the corresponding excitation is tentatively ascribed to an $n-\pi^*$ transition.

LUMO
-3.05 eV

HOMO
-5.65 eV

HOMO-1
-5.80 eV

HOMO-3
-6.78 eV

HOMO-4
-7.47 eV
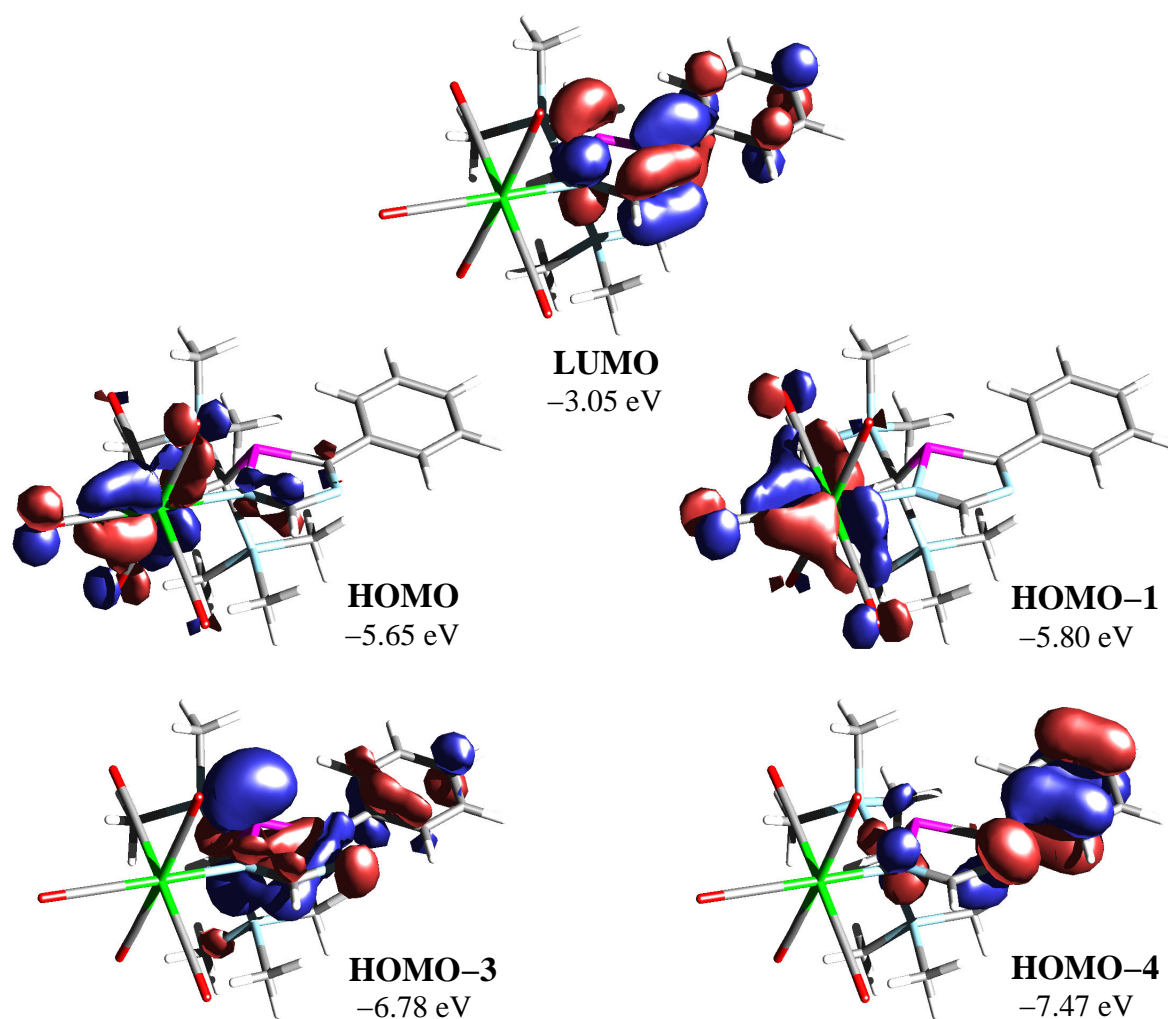
Figure 5.6: Visualization of selected molecular orbitals calculated for complex **129h** (B3LYP/ SV(P)/ECP-60-MWB(W)//RI-BLYP/SV(P)/ECP-60-MWB(W); isovalue 0.04 au).

In conclusion, the theoretical results corroborate the hypothesis that the κN-coordinated complexes **129h** and **131h** are responsible for the long-wave optical end absorptions observed in the spectra of the mixtures of **41h** and **129h** and of **126h** and **131h** due to very intense and low lying MLCT absorptions. As all excitations of 3-(2-thienyl) substituted derivative **131h** are lower in energy than those of **129h**, the assumption is strongly supported that the longer wavelength in optical end absorption observed for the mixture of **41h** and **129h** compared to **126h** and **131h** may be due to the higher ratio of the κN-coordinated isomer **129h** in the former mixture.

Comparison of the calculated data for complexes **41h** and **129h** (Fig. 5.5) with the experimental UV/Vis spectrum of their mixture (Fig. 5.4) reveals that the $\pi-\pi^*$ absorption band at $\tilde{\nu}_{max} = 32100$ cm^{-1} and the MLCT band at $\tilde{\nu}_{max} = 25100$ cm^{-1} may be caused by the κP-coordinated isomer **41h**, while the corresponding bands at $\tilde{\nu}_{max} = 33800$ cm^{-1} and $\tilde{\nu}_{max} = 23100$ cm^{-1} may arise from isomer **129h**.

5.2   The Effect of N-Protonation

Réau and coworkers presented pospholium salts with remarkable photophysical properties. For instance, derivative **186** (Fig. 5.7), obtained by P-alkylation of 2,5-di(2-thienyl)phosphole **183b** (cf. Fig. 5.1) with methyl triflate, showed a red shift of the $\pi-\pi^*$ absorption by $\Delta\lambda_{max} = 30$ nm ($\Delta\lambda_{onset} = 60$ nm), which was attributed to a lowering of the LUMO energy, and thus a lowering of the HOMO$-$LUMO gap, through introduction of a positive charge at the central phosphorus heterocycle.[183] Similar observations were made by Baumgartner and coworkers for phospholium triflate salts **187a,b**[6] (Fig. 5.1).[292] Acidichroism, that is, red shift of visual absorption bands upon protonation, has been observed also for some imine derivatives.[296]

186: λ_{max} = 442 nm
λ_{onset} = 528 nm

187a: X = H
λ_{max} = 276, 376 nm

187b: X = Br
λ_{max} = 279, 411 nm

123b: λ_{max} = 306, 463 nm
λ_{onset} = 649 nm
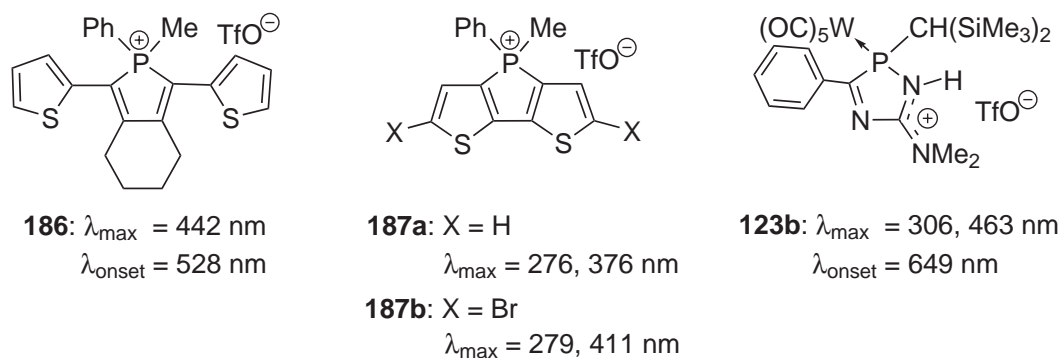
Figure 5.7: Phospholium salts **186**[183] and **187a,b**[292] and 2H-1,4,2-diazaphospholium complex salt **123b**. Absorption maxima and optical end absorptions recorded in THF (**186**)[183] or CH$_2$Cl$_2$ (**187a,b**,[292] **123b**).

It was observed that 2H-1,4,2-diazaphospholium complexes are intensely colored (Section 4.1.1), and bathochromic shifts were found for all bands of **123b** (Fig. 5.7) and **124b** compared to their neutral counterparts **41b** and **122b** (Tab. 5.1). Noteworthy are the extremely long-wave optical end absorptions of **123b**, **124b**.

Inspection of Figure 5.8 reveals a significant red shift of the longest-wavelength absorption maximum of complex **123b** with respect to the corresponding band of **41b** ($\Delta\tilde{\nu}_{max} = 3000$ cm^{-1}). Another remarkable effect of protonation derived from the spectra is a pronounced increase in the molar absorptivity of the band in the region of $\pi-\pi^*$ transitions. On the other hand, the weak band at $\tilde{\nu}_{max} = 28600$ cm^{-1} of complex **41b** is either missing in the spectrum of **123b** or it is overlapped by other bands.

---

[6]Monomer **187b** was copolymerized with a difunctionalized fluorene to give a conjugated polyelectrolyte (CPE) with intriguing photoluminiscence properties.[292]
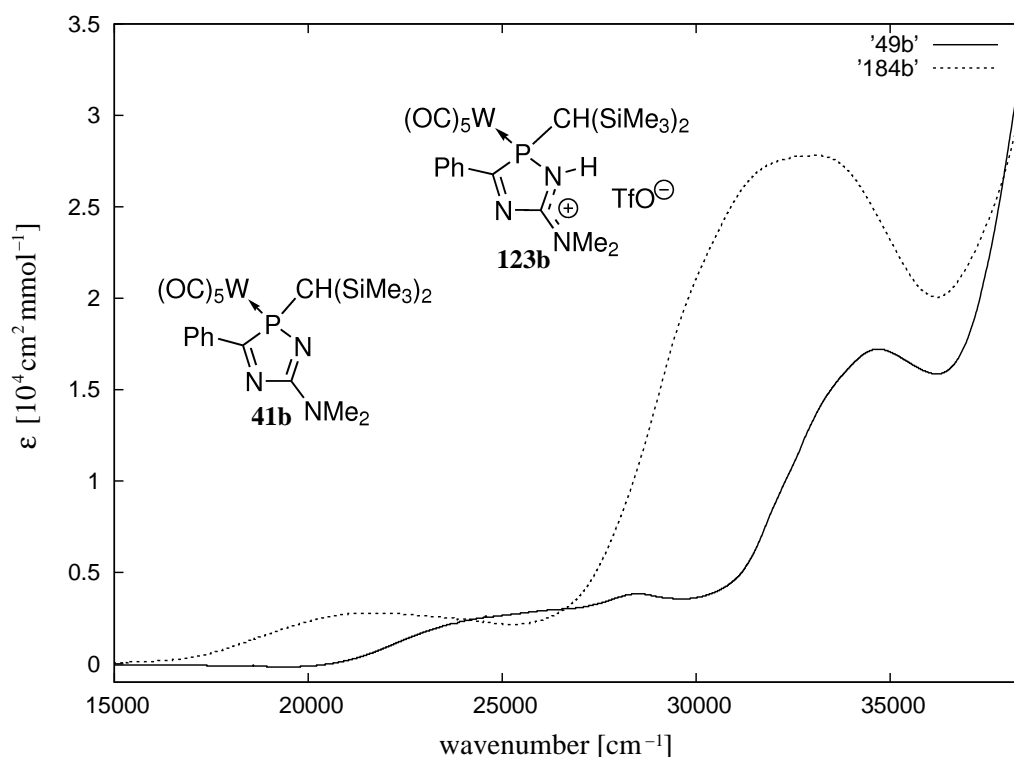
Figure 5.8: UV/Vis spectra of complexes **41b** (solid line; *n*-pentane) and **123b** (dashed line; CH$_2$Cl$_2$).

It is conceivable that *N*-protonation of 2*H*-1,4,2-diazaphosphole complexes causes a decrease of their π^* energies, thus being the reason for the bathochromic shifts observed. In order to prove this hypothesis, vertical excitations were calculated for complex **41b**, bare cation [**H–41b**]$^+$, and contact ion pair [**H–41b**][OTf], the latter having triflate bound to [**H–41b**]$^+$ via a hydrogen bond (Tab. 5.4).

As in the cases of **41h** and **126g,h** the probability of the HOMO→LUMO transition is almost negligible for complex **41b**, and the first relevant excitation, HOMO−1→ LUMO, is assigned to an MLCT process. Also here, the LUMO is a π^* orbital (Fig. 5.9). It shows contributions of both conjugated ring systems and the exocyclic dimethylamino nitrogen, whereas the contribution of the central phosphorus heterocycle clearly dominates. The second excitation having considerable oscillator strength (No. 4) is a $\pi-\pi^*$ transition occurring from HOMO−3, which is a π orbital that is largely restricted to the amidine moiety; a certain π-type contribution is provided also by the phosphorus center. An assignment to the weak band at $\tilde{\nu}_{max} = 28600$ cm^{-1} in the UV/Vis spectrum is plausible.

Table 5.4: Calculated vertical singlet excitations for complexes **41b**, [**H–41b**]$^+$, and [**H–41b**][OTf] (TD-B3LYP/SV(P)/ECP-60-MWB(W)//RI-BLYP/SV(P)/ECP-60-MWB(W)). Only the major orbital contributions are given.

No.	$\tilde{\nu}$ [cm^{-1}]	λ [nm]	Oscillator strength	Orbital contributions			$\|c\|^2$ [%]
Complex **41b**
1	20912	478	0.0032	**HOMO**	$\rightarrow$	**LUMO**	99
2	21867	457	0.0199	**HOMO−1**	$\rightarrow$	**LUMO**	99
4	25183	397	0.0456	**HOMO−3**	$\rightarrow$	**LUMO**	95
15	32992	303	0.1107	**HOMO−4**	$\rightarrow$	**LUMO**	42
				HOMO−6	$\rightarrow$	**LUMO**	28
17	33636	297	0.0850	**HOMO−7**	$\rightarrow$	**LUMO**	44
				HOMO−4	$\rightarrow$	**LUMO**	19
19	33898	295	0.1368	**HOMO−7**	$\rightarrow$	**LUMO**	35
				HOMO−4	$\rightarrow$	**LUMO**	29
Cation [**H–41b**]$^+$
1	15630	640	0.0076	**HOMO**	$\rightarrow$	**LUMO**	84
2	16661	600	0.0201	**HOMO−1**	$\rightarrow$	**LUMO**	84
5	27071	369	0.0272	**HOMO−5**	$\rightarrow$	**LUMO**	74
				HOMO−3	$\rightarrow$	**LUMO**	15
10	29317	341	0.3072	**HOMO−3**	$\rightarrow$	**LUMO**	44
				HOMO−4	$\rightarrow$	**LUMO**	28
Contact ion pair [**H–41b**][OTf]
1	17355	576	0.0096	**HOMO**	$\rightarrow$	**LUMO**	93
2	18730	534	0.0209	**HOMO−1**	$\rightarrow$	**LUMO**	90
5	26731	374	0.0132	**HOMO−4**	$\rightarrow$	**LUMO**	81
14	30950	323	0.0600	**HOMO−9**	$\rightarrow$	**LUMO**	69
				HOMO−6	$\rightarrow$	**LUMO**	25
16	32072	312	0.2089	**HOMO−7**	$\rightarrow$	**LUMO**	37
				HOMO−6	$\rightarrow$	**LUMO**	23
				HOMO−9	$\rightarrow$	**LUMO**	18
				HOMO−10	$\rightarrow$	**LUMO**	12
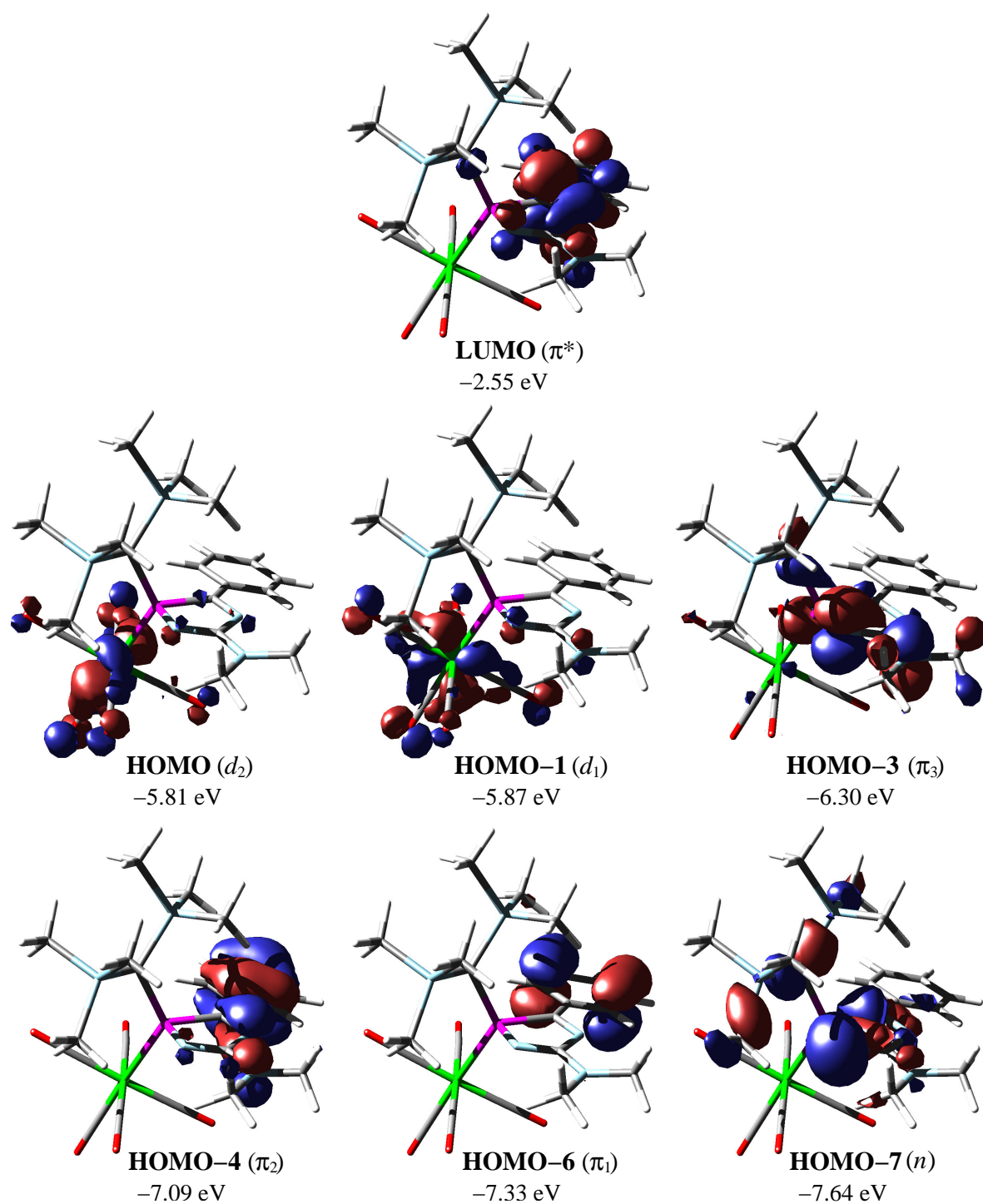
Figure 5.9: Visualization of selected molecular orbitals calculated for complex **41b** (B3LYP/ SV(P)/ECP-60-MWB(W)//RI-BLYP/SV(P)/ECP-60-MWB(W); isovalue 0.04 au). Orbitals were labeled as n, π_i, or d_i in order to provide a comparison with analogous orbitals of $[\mathbf{H}\text{–}\mathbf{41b}]^+$ and $[\mathbf{H}\text{–}\mathbf{41b}][\text{OTf}]$.
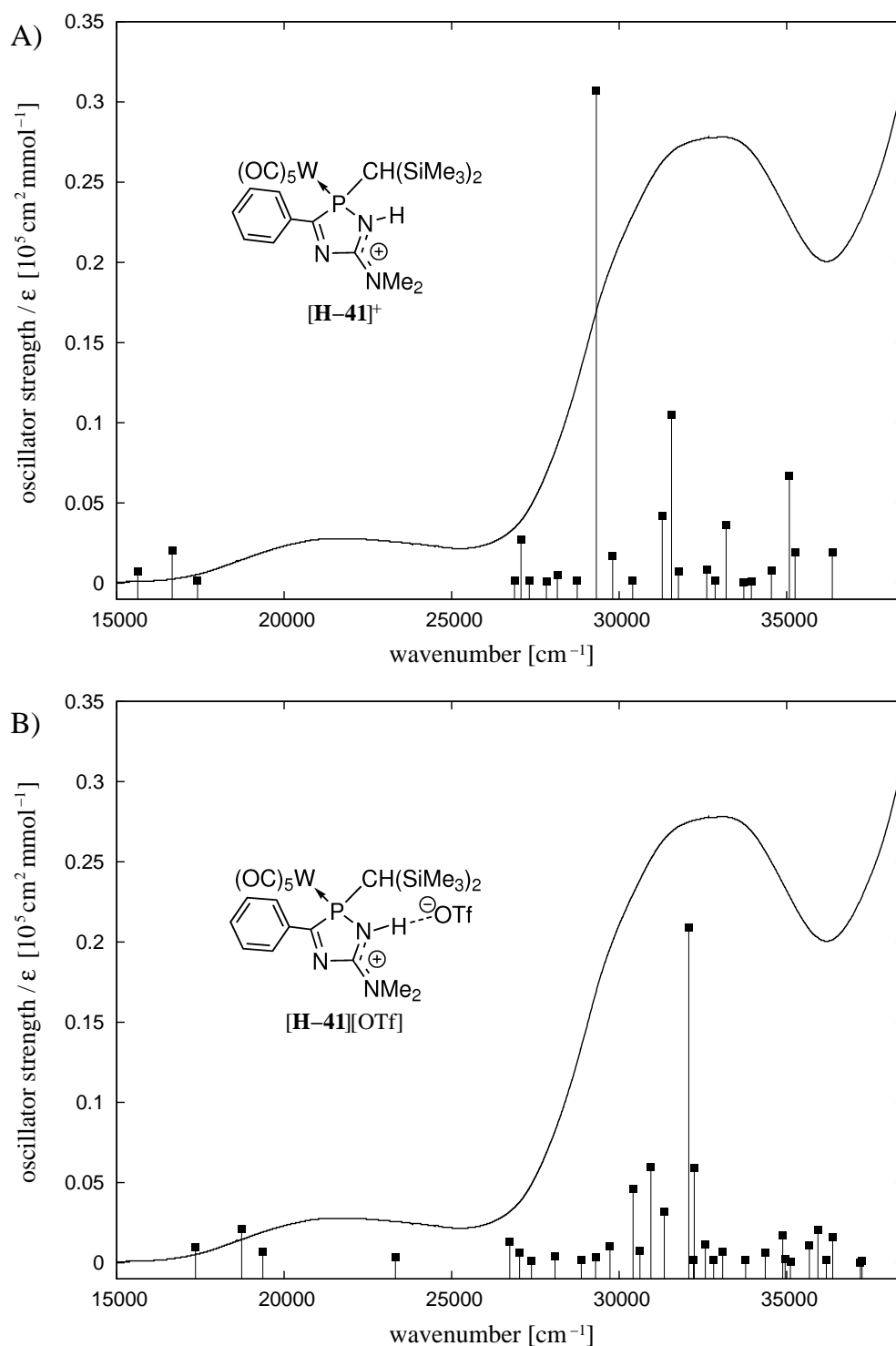
Figure 5.10: Comparison of the experimental UV/Vis spectrum of **123b** (CH$_2$Cl$_2$; solid line) with calculated vertical singlet excitations for cation [**H–41b**]$^+$ (A) and contact ion pair [**H–41b**][OTf] (B) (TD-B3LYP/SV(P)/ECP-60-MWB(W)//RI-BLYP/SV(P)/ECP-60-MWB(W)).

In the region at about $33000-34000$ cm^{-1} three very close excitations with considerable intensity are predicted for **41b**. Obviously, they superpose to give a distinct maximum at $\tilde{\nu}_{max} = 34700$ cm^{-1} in the UV/Vis spectrum (Fig. 5.8). Excitation No. 15 is characterized as a $\pi-\pi^*$ transition occurring from HOMO-4 and HOMO-6. While the former is spread over all coplanar molecule fragments (i.e., both rings and the dimethylamino group), the latter is largely localized at the phenyl ring. A contribution of HOMO-4 is predicted also for transitions No. 17 and No. 19, but in these cases another orbital, HOMO-7, plays the major role. This exhibits mainly σ character, and the largest lobe is localized at N^1 pointing outwards the ring. Therefore, a classification of these transitions as being of $n-\pi^*$ type appears more appropriate.

The major effects caused by protonation of **41b** can be summarized as follows. All orbital energies are significantly decreased (Tab. 5.5),[7] which is more pronounced for the cation $[\mathbf{H}–\mathbf{41b}]^+$ than for the contact ion pair $[\mathbf{H}–\mathbf{41b}][\mathrm{OTf}]$.

Table 5.5: Calculated orbital energies [eV] for complexes **41b**, $[\mathbf{H}–\mathbf{41b}]^+$, and $[\mathbf{H}–\mathbf{41b}][\mathrm{OTf}]$ (B3LYP/SV(P)/ECP-60-MWB(W)//RI-BLYP/SV(P)/ECP-60-MWB(W)).

Orbital[†]	**41b**	$[\mathbf{H}–\mathbf{41b}]^+$	$[\mathbf{H}–\mathbf{41b}][\mathrm{OTf}]$
π^*	-2.55 (**LUMO**)	-6.17 (**LUMO**)	-3.45 (**LUMO**)
d_2	-5.81 (**HOMO**)	-8.76 (**HOMO**)	-6.26 (**HOMO**)
d_1	-5.87 (**HOMO−1**)	-8.85 (**HOMO−1**)	-6.38 (**HOMO−1**)
π_3	-6.30 (**HOMO−3**)	-10.37 (**HOMO−5**)	-7.51 (**HOMO−4**)
π_2	-7.09 (**HOMO−4**)	-10.10 (**HOMO−3**)	-7.75 (**HOMO−6**)
π_1	-7.33 (**HOMO−6**)	-10.15 (**HOMO−4**)	-7.94 (**HOMO−9**)
n	-7.64 (**HOMO−7**)	$-$	$-$

[†]For orbital denotation see Figure 5.9.

Protonation at the $2H$-1,4,2-diazaphosphole ring has a stronger impact on those orbitals that are localized at this ring than on metal-centered orbitals. For example, the energy of the LUMO (π^*) is lowered by 3.62 ($[\mathbf{H}–\mathbf{41b}]^+$ vs. **41b**) or 0.9 eV ($[\mathbf{H}–\mathbf{41b}][\mathrm{OTf}]$ vs. **41b**), respectively. As the effect on metal-centered orbitals such as d_1 and d_2 is significantly lower ($\Delta\varepsilon(d_1) = 2.98$ ($[\mathbf{H}–\mathbf{41b}]^+$ vs. **41b**), 0.51 eV ($[\mathbf{H}–\mathbf{41b}][\mathrm{OTf}]$ vs. **41b**) and $\Delta\varepsilon(d_2) = 2.95$ ($[\mathbf{H}–\mathbf{41b}]^+$ vs. **41b**), 0.45 eV ($[\mathbf{H}–\mathbf{41b}][\mathrm{OTf}]$ vs. **41b**)), the excitation energies for all MLCT processes[8] are decreased, thus being

---

[7]For most orbitals of complex **41b** congeners can be found in complexes $[\mathbf{H}–\mathbf{41b}]^+$ and $[\mathbf{H}–\mathbf{41b}][\mathrm{OTf}]$. Because some have a different energetical order, they were labeled as n, π_i, or d_i in order to facilitate the comparison.

[8]It should be noted that also the HOMO→LUMO excitations have non-zero transition probabilities in the cases of $[\mathbf{H}–\mathbf{41b}]^+$ and $[\mathbf{H}–\mathbf{41b}][\mathrm{OTf}]$.

the reason for the bathochromic shifts of the longest-wavelength bands in the spectra of **123b** and **124b** resulting in pronounced long-wave optical end absorptions.

The π_3 orbital, which is localized at the amidine moiety, is even more affected through the perturbation induced by protonation than the LUMO; its energy is decreased by even 4.07 eV (**[H−41b]**$^+$ vs. **41b**) or 1.21 eV (**[H−41b]**[OTf] vs. **41b**). Consequently, the corresponding excitation is blue shifted (cf. No. 4 of **41b** and No. 5 of **[H−41b]**$^+$ and **[H−41b]**[OTf]). The reason why this band was not observed in the spectrum of **123b**, besides its low oscillator strength, is presumably an overlap with the very intense $\pi−\pi^*$ absorptions, which, in turn, are red shifted with respect to **41b**. The orbitals contributing to the latter process, π_1 and π_2, are somewhat less affected through protonation than the LUMO because they are polarized towards the phenyl substituent. An analog of HOMO−7 of complex **41b**, corresponding to the lone pair at N^1 (denoted as n), is missing in **[H−41b]**$^+$ and **[H−41b]**[OTf] as this lone pair is protonated. Therefore, the spectra of the latter complexes lack a counterpart to the excitation No. 19 of **41b**.

The contact ion pair **[H−41b]**[OTf] exhibits one excitation, No. 16, that has a congener neither in complex **41b** nor in the bare cation **[H−41b]**$^+$ (see Tab. 5.4 and Fig. 5.10). Four occupied orbitals contribute to this transition: π_1, π_2, and the orbitals HOMO−7 and HOMO−10 (Fig. 5.11). Since the latter two are mainly localized at the oxygen atoms of the triflate anion,[9] the corresponding transition is tentatively classified as an anion−cation charge transfer process.

HOMO−7
−7.82 eV

HOMO−10
−7.97 eV
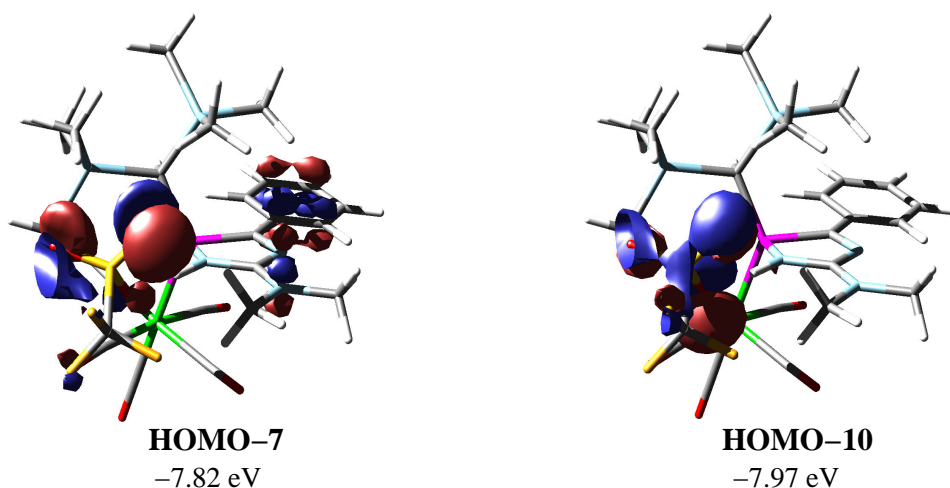
Figure 5.11: Visualization of selected molecular orbitals calculated for complex **[H−41b]**[OTf] (B3LYP/SV(P)/ECP-60-MWB(W)//RI-BLYP/SV(P)/ECP-60-MWB(W); isovalue 0.04 au).

---

[9]The highest occupied molecular orbital that is exclusivley loalized at the triflate oxygens is HOMO−3 (not shown).

Comparison of Figures 5.10 (A) and 5.10 (B)[10] reveals that the experimental UV/Vis spectrum of **123b** is better reproduced by the calculations on the contact ion pair [**H–41b**][OTf] than by the calculations on the pure cation [**H–41b**]$^+$.

---

[10]When comparing the graphs in Figure 5.10 with those of complexes **126g** and **41h** (Figures 5.3 and 5.5) it should be taken into account that the vertical axes are differently scaled.

Chapter 6

Attempted Synthesis of *N*-Heterocyclic Carbenes with Phosphorus in the Backbone

Since the first *N*-heterocyclic carbene (NHC) **XXIX** (Fig. 6.1) was synthesized and structurally confirmed by Arduengo, III et al.,[297] these heterocyles have emerged as a new class of versatile ancillary ligands in organometallic chemistry owing to their unique coordination properties (good σ-donor, poor π-acceptor). They are often a valid alternative to the widely used phosphane ligands in catalytic reactions. For instance, organometallic complexes containing NHC ligands are effectively employed in ruthenium catalyzed olefin metathesis,[298] iridium catalyzed hydrogenation and hydrogen transfer,[299] platinum catalyzed hydrosilylation,[300] and palladium catalyzed C–C coupling reactions.[301]

It is assumed that the two amino groups at the carbene center provide substantial support to the stability of NHCs such as **XXIX** and **XXX**[302] through donative π conjugation.[62] Against this background another breakthrough in the field of *N*-heterocyclic carbenes was the synthesis of carbene **XXXI**, which is stabilized by only one nitrogen atom, reported very recently by Bertrand and coworkers;[303] on a conference they further presented an amino-phosphino carbene (**XXXII**).[304] An unprecedented anionic heterocyclic carbene (**XXXIII**) having two phosphorus atoms adjacent to the carbene center was presented in 1999 by Niecke and coworkers;[305] it was demonstrated that **XXXIII** can form an adduct with trimethylalane via the carbene center.[305] Recently, Bertrand and coworkers reported the synthesis of carbene **XXXIV**,[306] a diphosphorus analogue of Enders' NHC **XXX**, and metal complexes thereof,[306] which may also have potential of application in catalysis.[307]
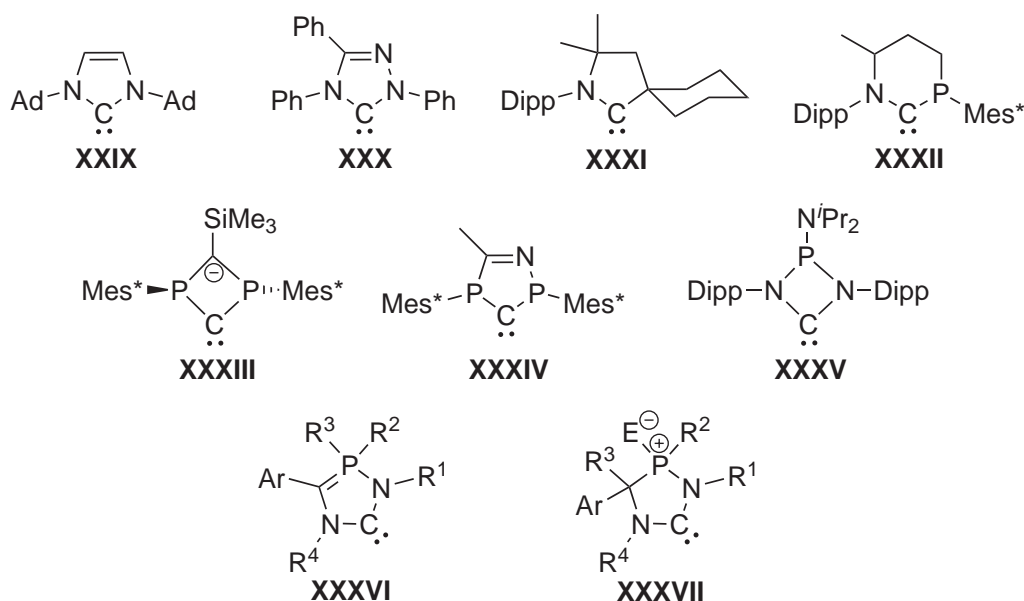
Figure 6.1: Existing *N*- and *P*-heterocyclic carbenes (**XXIX**,[297] **XXX**,[302] **XXXI**,[303] **XXXII**,[304] **XXXIII**,[305] **XXXIV**,[306] and **XXXV**[308]) and potential *N*-heterocyclic carbenes with phosphorus in the backbone (**XXXVI**, **XXXVII**: R^1−R^4: common organic substituents; **XXXVII**: E = O, S).

Grubbs and coworkers previously presented the first *N*-heterocyclic carbene **XXXV** with phosphorus in the backbone.[308] Five-membered NHCs having phosphorus in the backbone such as **XXXVI** and **XXXVII** are still unknown. Since 5-unsubstituted $2H$-1,4,2-diazaphosphole complexes **41h** and **126h** as well as the 5-SiMe$_3$ substituted derivative **41t**, which have become accessible through this work (Sections 4.1.3 and 4.1), may serve as appropriate precursors for **XXXVI** and **XXXVII**, a concept for their syntheses was devised and examined within the scope of a research project supported by the DAAD and connected with a stay in the group of A. J. Arduengo, III. Although the syntheses of **XXXVI** and **XXXVII** could not be completed in the period of this project, preliminary results are presented in the following sections.

6.1   Alkylation Reactions

The concept included *N*-alkylation of complexes **41h** and **129h** in the first step. Therefore, several established methylating reagents were tested such as MeI, [Me$_3$O][BF$_4$], MeOTf, and the combination of ^{t}BuCl and GaCl$_3$,[309] each under various reaction conditions (solvent, concentration, temperature). Unfortunately, all these attempts yielded no clean reaction (Scheme 6.1).

RX = MeI, [Me$_3$O][BF$_4$], MeOTf, ^{t}BuCl / GaCl$_3$
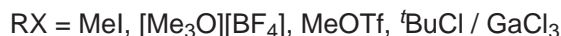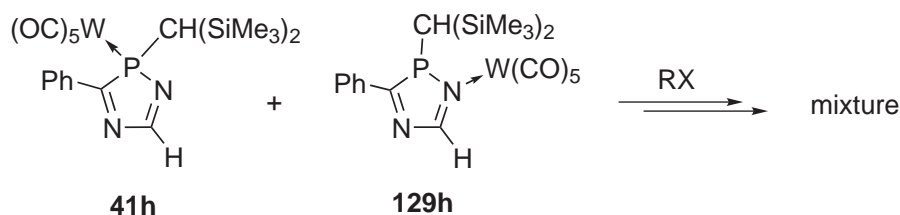
Scheme 6.1: Attempted alkylation of 2H-1,4,2-diazaphosphole complexes **41h** and **129h**.

Then, a method was chosen that uses methyl triflate in combination with catalytic amounts of triflic acid,[310] which was termed *triflic acid catalysis*.[311] First attempts to methylate complexes **41h** and **129h** with this approach (Scheme 6.2) were carried out in CD$_2$Cl$_2$ (the commercial sample of that solvent was employed as received, i.e., without prior purification). Monitoring by ^{31}P NMR spectroscopy revealed an almost clean reaction to yield a product that resonated at $\delta = 130.6$ ($|^1J_{WP}| = 253.1$ Hz, $|^{3+4}J_{PH}| = 32.3$ Hz, $|^2J_{PH}| = 21.0$ Hz). Surprisingly, this result could not be reproduced when the reaction was carried out on a larger scale in dried CH$_2$Cl$_2$ as solvent. Obviously, a certain quantity of water present in solution was necessary to account for a complete reaction.
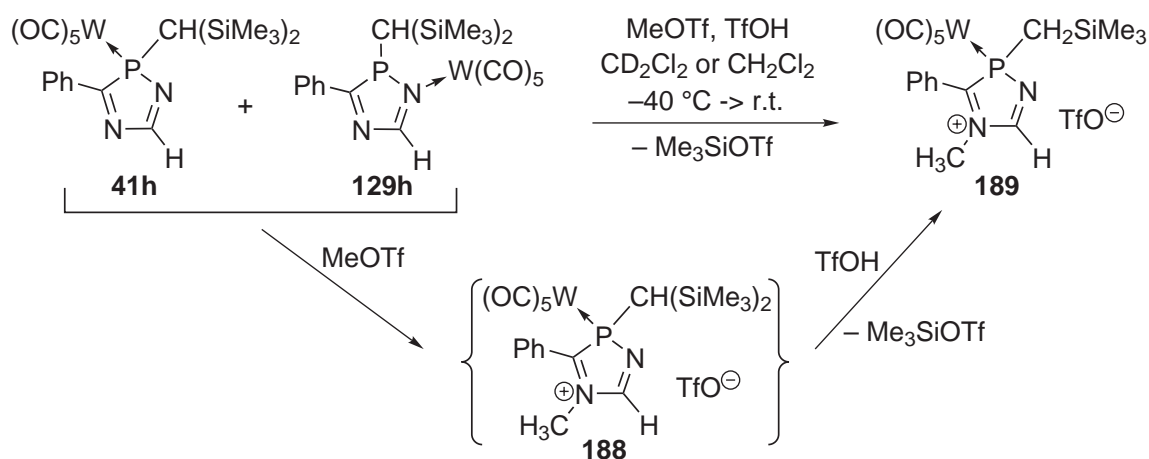
Scheme 6.2: Reaction of 2H-1,4,2-diazaphosphole complexes **41h** and **129h** with MeOTf in the presence of TfOH.

A clean reaction was observed when triflic acid was employed in at least stoichiometric amounts (Scheme 6.2). Unfortunately, the product (**189**) decomposed during evaporation of the volatiles as well as upon addition of *n*-hexane. Therefore, the structural identification of complex **189** was done by subjecting a solution of *in situ* generated **189** to multinuclear NMR experiments.

Correlation of a proton resonance at $\delta = 4.26$ with the phosphorus signal, according to a 2D ^{1}H,^{31}P HMQC NMR experiment, confirmed the *N*-methyl group; the corresponding ^{13}C resonance was detected at $\delta = 40.5$ ($|^{3+4}J_{PC}| = 2.2$ Hz). Long-range correlations were found for the methyl protons not only with both ring carbons but also with the *ortho*- and *para*-carbon centers of the phenyl group (via ^{1}H,^{13}C HMBC NMR spectroscopy). This supports the assignment to **189**, thus being an N^4- rather than an N^1-methylated complex. The quartet ^{13}C resonance of the CF$_3$ group at $\delta = 120.4$ ($|^1J_{FC}| = 318.0$ Hz) is characteristic for the presence of anionic triflate.[265]

Surprisingly, only one proton signal according to a SiMe$_3$ group was found and two diastereotopic methylene protons. The latter were bound to a carbon that resonated at $\delta(^{13}\text{C}) = 17.2$ ($|^1J_{PC}| = 11.9$ Hz), which evidenced a *P*-CH$_2$SiMe$_3$ group. Obviously, the desired product **188** was formed only intermediately and underwent subsequent desilylation in the presence of triflic acid to give **189** (Scheme 6.2). This interpretation was reinforced by the observation of the characteristic proton resonance of Me$_3$SiOTf ($\delta = 0.48$) and explains why one equivalent of triflic acid (or water, which can form triflic acid with MeOTf) is required for a complete reaction.

N-Alkylation together with desilylation has a similar effect on the NMR data for the ring atoms as *N*-protonation combined with desilylation. This is revealed by a comparison of the pair **41h/189** with the pair of **41b** and its protonated, partially desilylated congener **171b** (see Section 4.3.2). For **189** vs. **41h** the ^{13}C resonance of the C^5 center is 11.2 ppm upfield shifted associated with an increase in $|^{2+3}J_{PC}|$ by 5.9 Hz, while the $|^{1+4}J_{PC}|$ value for the C^3 center is 12.3 Hz decreased. The strongest effect is found for the ^{31}P resonance ($\Delta\delta = +25.0$, $\Delta|^1J_{WP}| = +25.5$ Hz). The increase in $|^1J_{WP}|$ is in the same range as for **171b** vs. **41b**, but the effect on the ^{31}P NMR chemical shift is significantly more pronounced.

6.2 Desilylation Reactions

Due to the result that this partial desilylation complicated the alkylation reaction of **41h** and **129h**, it was decided to remove both trimethylsilyl groups in a previous step. For such purpose tetra-*n*-butylammonium fluoride (TBAF) is widely-used, often in combination with acetic acid as a proton source.[312] This method was applied to complexes **126h** and **131h**, but the reaction was unselective, presumably due to the nucleophilicity of the acetate ion and/or the presence of water in the acid. Therefore, triethylammonium triflate (freshly prepared from NEt$_3$ and TfOH) was chosen as a mild proton donator, which forms the less nucleophilic anion TfO$^-$.
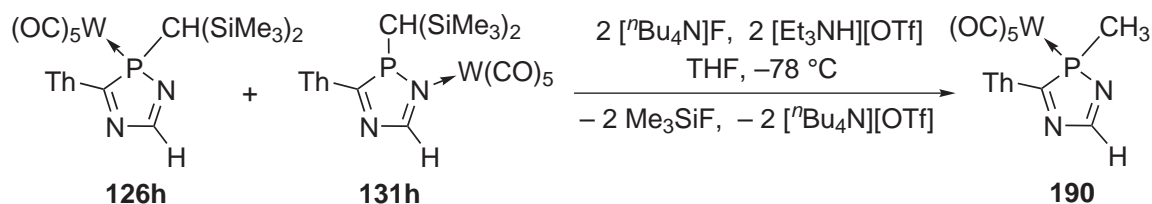
Scheme 6.3: Desilylation of $2H$-1,4,2-diazaphosphole complexes **126h** and **131h** (Th = 2-thienyl).

Consecutive addition of THF solutions of [Et$_3$NH][OTf] and TBAF to a solution of **126h** and **131h** at $-78\,^\circ$C (Scheme 6.3) yielded a clean reaction as evidenced by the ^{31}P resonance of complex **190** at $\delta = 95.7$ ($|^1J_{WP}| = 240.3$ Hz) showing the multiplicity of a doublet of a quartet ($|^{3+4}J_{PH}| = 34.4$ Hz, $|^2J_{PH}| = 7.4$ Hz). Interestingly, only complex **190** was observed, and no evidence for a κN-bonded isomer thereof was obtained, although the employed mixture contained both **126h** and **131h**. It is concluded that either the κN-haptomer **131h** (or that of **190**) had decomposed during the reaction (although no by-products were observed by ^{31}P NMR reaction monitoring), or a $N{\to}P$ shift of the W(CO)$_5$ fragment had occurred due to the lower steric demand of the exocyclic P-substituent of **190** compared to **126h** and **131h**. Complex **190** was purified via low-temperature column chromatography and was characterized by multinuclear NMR experiments, mass spectrometry, IR and UV/Vis spectroscopy. Additionally, a single-crystal X-ray diffraction study was carried out (Fig. 6.2).

The effect of desilylation (**190** vs. **126h**) on the ^{13}C NMR parameters for the ring carbons is low. Noteworthy is a decrease of the phosphorus–carbon coupling constant magnitude for the C^3 resonance by 12.4 Hz. On the other hand, the $|^1J_{PC}|$ value for the desilylated carbon center is 21.5 Hz increased. The ^{31}P resonance is 9.9 ppm high field shifted, while the tungsten–phosphorus coupling constant increases by 10.6 Hz in magnitude, which correlates with the W,P bond shortening (vide infra) through the modification of the P-substituent.

The IR spectrum of complex **190** reveals similar results as those of other $2H$-1,4,2-diazaphosphole complexes. It shows characteristic bands according to C,O stretch vibrations at $\tilde{\nu} = 2077$ cm^{-1} (A_1) and $\tilde{\nu} = 1989$ cm^{-1} (B_1) and a broad band centered at $\tilde{\nu} = 1923$ cm^{-1} resulting from an overlap of resonances according to modes of local A_1 and E symmetry.

The UV/Vis absorption spectrum of complex **190** shows a similar shape as that of the mixture of **126h** and **131h**, and the absorption maxima are found in the same range (see Tab. 5.1, Section 5.1). A pronounced difference between both spectra is found in the long-wave region: optical end absorption of **190** appears at significantly

shorter wavelength (λ_{onset} = 529 nm; cf. **126h** and **131h**: λ_{onset} = 601 nm). This observation corroborates the interpretation (given in Section 4.1.3) that the shape of the UV/Vis spectrum of the mixture of **126h** and **131h** is in the long-wave region dominated by the optical properties of κN-complex **131h**, which exhibits very low-lying transitions with considerable oscillator strengths. Since such isomeric complex is missing in the solution of complex **190**, a hypsochromic shift of the optical end absorption and the MLCT absorption maximum results.
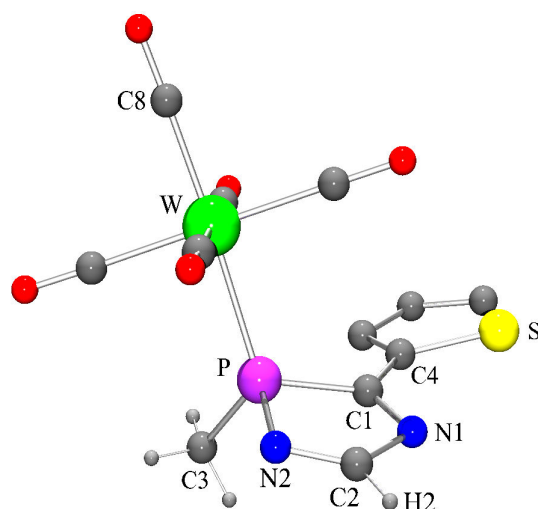
Figure 6.2: Molecular structure of complex **190** in the crystal (hydrogen atoms of the thienyl moiety omitted for clarity; only the prevailing conformation (81 %) shown). Selected bond lengths [Å] and angles [°]: W–C(8) 2.007(4), W–P 2.4763(9), P–N(2) 1.713(3), P–C(1) 1.848(4), C(1)–N(1) 1.308(4), C(2)–N(2) 1.278(5), C(1)–C(4) 1.434(5), N(2)–P–C(1) 91.04(16), P–C(1)–N(1) 109.8(3), C(1)–N(1)–C(2) 108.5(3), N(1)–C(2)–N(2) 122.6(3), C(2)–N(2)–P 107.4(3).

Under EI-mass spectrometric conditions the major fragmentation pathway of **190** constituted successive losses of all five CO ligands. Furthermore, expulsion of the thienyl substituent (together with 4 CO groups: m/z 312) was observed.

Complex **190** crystallizes in the triclinic space group P$\bar{1}$ (Fig. 6.2). The 2-thienyl ring at C^3 is statistically disordered showing an *anti* arrangement of the two heterocycles with respect to phosphorus and sulfur in the prevailing conformation (81 %). The molecular structure of **190** in the crystal is best compared with that of **126h**; within their 2*H*-1,4,2-diazaphosphole rings both complexes have almost identical bond lengths and angles. The W,P bond of **190** is 0.050 Å shortened with respect to **126h**, presumably due to the lower steric demand of the exocyclic *P*-substituent. The reduction of the size of this substituent further causes a decrease in the sum of the angles at P ($\Sigma\angle(P_{PR_3})$ 301.8°; cf. **126h**: $\Sigma\angle(P_{PR_3})$ 310.1°). No significant effect was found

for the endocyclic angle at phosphorus, but for the C(3)–P–C(1) angle, which is significantly decreased (by 10.3°) as observed also for the pair of complex **41b** and its partially desilylated congener **172b** (cf. Section 4.1.3). The phosphorus heterocycle of **190** is almost planar,[1] and the twist angle between the two heterocycles $(24.0°)^{[2]}$ is slightly larger than that of complex **126h** (16.6°).

6.3   Decomplexation Reactions

Concerning the attempted syntheses of *N*-heterocyclic carbenes **XXXVI**, **XXXVII** (Fig. 6.1) from 2*H*-1,4,2-diazaphosphole complexes, a decomplexation must be included as one synthetic step. Therefore, preliminary studies were carried out on 2*H*-1,4,2-diazaphosphole complexes **41h** and **129h**, **41g**, and **126h** and **131h**. The newly developed method presented in Section 4.1.4 that enables access to free 2*H*-1,4,2-diazaphosphole ligands directly from 2*H*-azaphosphirene complexes and nitriles could not be applied to **41h** and **129h** as well as **126h** and **131h** due to the instabilities of the occurring cationic intermediates in solution.

First, an approach devised by Mathey et al. was applied that uses the chelate ligand 1,2-bis(diphenylphosphino)ethane (DPPE) to replace the desired phosphane ligand (and one CO group) by substitution.[73, 313] The reaction was tested for complex **41g** because larger quantities of this derivative were readily available (Scheme 6.4).

41g   **50g**   **191**   **192**
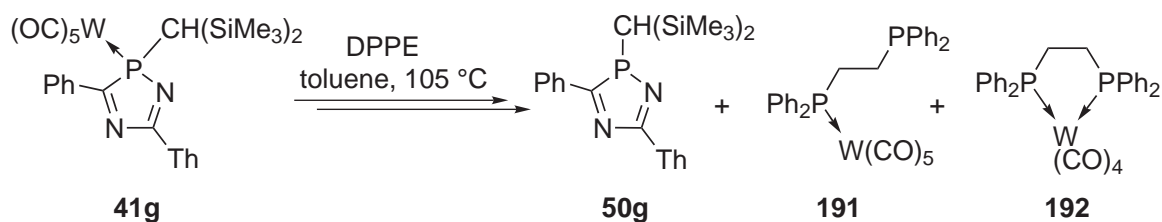
Scheme 6.4: Decomplexation of 2*H*-1,4,2-diazaphosphole complex **41g** using 1,2-bis(diphenylphosphino)ethane (DPPE) in toluene at 105 °C (Th = 2-thienyl).

During the thermolysis of **41g** in the presence of DPPE at 105 °C the reaction mixture turned brownish, and ^{31}P NMR reaction monitoring revealed complete conversion of **41g** within 3 hours; the formation of free ligand **50g** was evidenced by its ^{31}P NMR resonance at $\delta = 101.8$. The by-products $[W(CO)_4(dppe)]$ (**192**) and the primary product of ligand substitution, **191**, were identified by their characteris-

---

[1] Mean deviations from least-squares plane: 0.034 Å.
[2] Value corresponds to the prevailing conformation.

tic ^{31}P resonances. Unfortunately, all attempts to separate **50g** from the mixture by low-temperature column chromatography failed.

Therefore, another approach had to be chosen. The use of pyridinium perbromide to oxidize the tungsten center in the first step in order to facilitate a subsequent ligand substitution by 2,2'-bipyridyl according to the procedure presented by Mathey et al.[70, 314–316] was applied to complexes **41h** and **129h**, but this led to a complex mixture of products. Then, an observation made by H. Wilkens was taken up who had obtained evidence for decomplexation of a 2*H*-1,4,2-diazaphosphole complex in neat benzonitrile at higher temperature.[155] Because of the high boiling point of this solvent ($188-191$ °C), which complicated the workup, the methodology was modified by using acetonitrile instead. When acetonitrile solutions of **41h** and **129h** as well as of **126h** and **131h** were heated at 75 °C (Scheme 6.5), a color change from orange to light brownish occurred, and the resonances of the κN-coordinated complexes **129h** and **131h** were no longer detected by ^{31}P NMR reaction monitoring. Instead, the signals of the free ligands **50h** at $\delta = 97.6$ ($|^{3+4}J_{PH}| = 17.2$ Hz) and **193h** at $\delta = 96.1$ ($|^{3+4}J_{PH}| = 19.1$ Hz) emerged and increased further at the expense of those of **41h** and **126h**, respectively.

41h, **129h**, **50h**: Ar = phenyl
126h, **131h**, **193h**: Ar = 2-thienyl
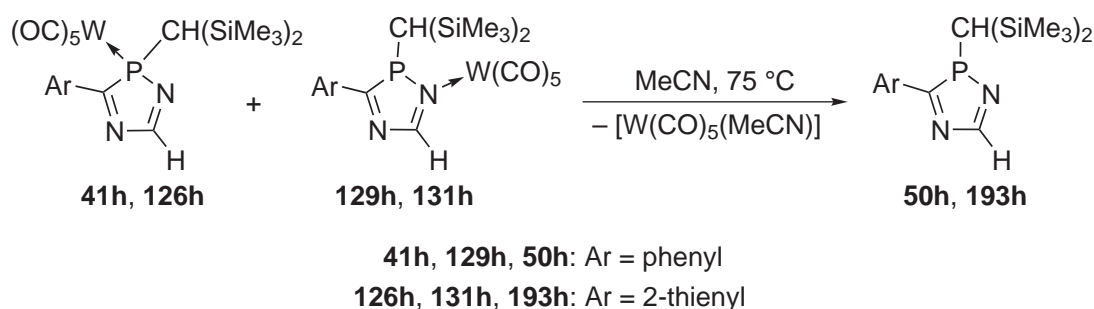
Scheme 6.5: Decomplexation of 2*H*-1,4,2-diazaphosphole complexes **41h**, **129h**, **126h**, and **131h** in acetonitrile at 75 °C.

Both reactions were complete within less than 1.5 hours. Obviously, the W,N bonds of complexes **129h** and **131h** as well as the W,P bonds of complexes **41h** and **126h** are labile enough that a rather weak ligand such as acetonitrile can displace the 2*H*-1,4,2-diazaphosphole ligands from their W(CO)$_5$ complexes (at least if it is present in large excess). Alike derivative **50b** (cf. Section 4.1.4) heterocycles **50h** and **193h** suffered from decomposition during the workup, but all relevant NMR spectroscopic information was obtained from the crude products. The data revealed similar trends upon decomplexation as observed for **50b** versus **41b** discussed in Section 4.1.4 (see also Tab. C.1, Appendix D).

Chapter 7

Synthesis of a Dinuclear Bis-2H-azaphosphirene Complex

The most general route to P–CH(SiMe$_3$)$_2$ substituted 2H-azaphosphirene complexes (**XXII**), developed by Streubel et al.,[118,119] is a triethylamine-induced condensation-rearrangement cascade reaction starting from Fischer-type aminocarbene metal complexes (**XXXVIII**)[317] and [bis(trimethylsilyl)methylene]halogenophosphanes (**194**, **195**)[318] (Scheme 7.1). This method enabled access not only to complexes **35**,[122,172] **67**,[128] **70**,[123] **71**,[123] **72**,[194] **73**,[194] and **125**[124] but also to several derivatives having *para*[122,172] or *ortho*[127] substituted phenyl groups or hetaryl groups at C^3.[124,172] Furthermore, 3-aryl-2H-azaphosphirene complexes with phosphane co-ligands in the coordination sphere of the metal have been prepared.[319]

The course of such reactions depends strongly on the steric demand of the aryl group of the carbene complex employed. 2H-Azaphosphirene complexes with 2,4-, 2,6-, or 3,5-disubstituted[320] and 2,4,6-trisubstituted[321] 3-phenyl groups showed significantly enhanced reactivity towards triethylammonium chloride, which is formed during the reaction, thus leading to chlorophosphane complexes such as **43** (see Scheme 1.15, Section 1.3); this type of follow-up reaction generally proceeds faster when methylene chloride is used as solvent (instead of diethyl ether).[119]

The proposed mechanism[118,119] starts with a base-induced condensation of the carbene complex and the halogeno(methylene)phosphane with formal hydrogen halide elimination and formation of intermediate **XL** (Scheme 7.1). This undergoes a subsequent [1,3]-H shift to give the 2-aza-1-phospha-4-metallabutadiene-type system **XLI** as a further intermediate.[1] An intramolecular nucleophilic attack of phosphorus at the

---

[1]The intermediacy of **XL** and **XLI** was evidenced by ^{31}P$\{^1$H$\}$ NMR spectroscopy.[321]

carbene center of **XLI** was suggested to explain the ring formation,[114, 119, 321] which is followed by a combined haptotropic rearrangement (C→P-metal shift) and valence isomerization to give 2*H*-azaphosphirene metal complexes **XXII** as final products.
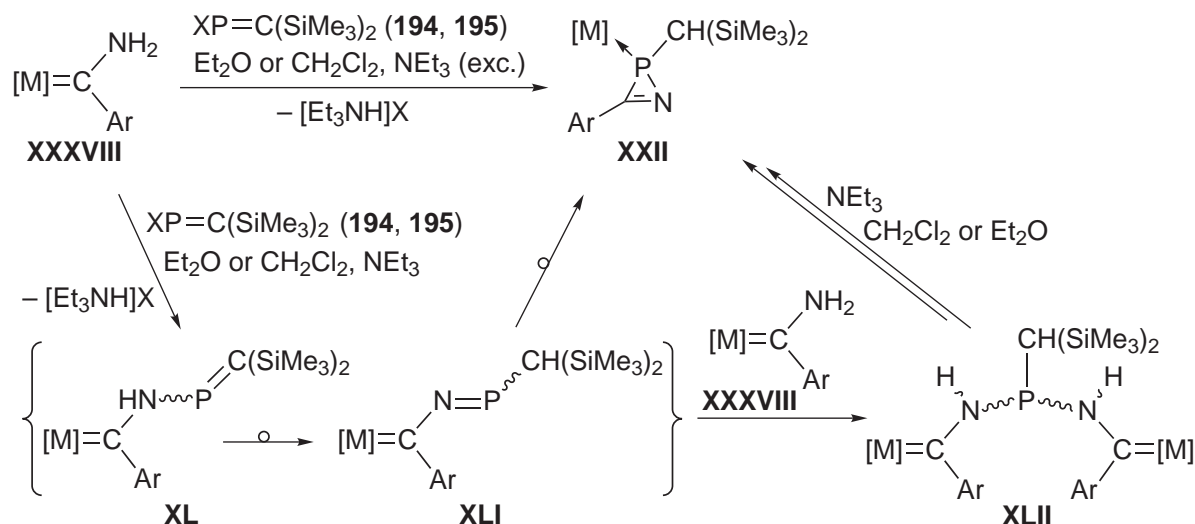
Scheme 7.1: Synthesis of 2*H*-azaphosphirene complexes (**XXII**) using metal carbene complexes (**XXXVIII**) and [bis(trimethylsilyl)methylene]halogenophosphanes **194** (X = Cl) or **195** (X = Br),[118, 119] proposed intermediates **XL**[321] and **XLI**,[321] and their trapping reaction with another equivalent of carbene complex (**XXXVIII**) yielding dinuclear *N,N'*-λ^3-P-bridged carbene metal complexes (**XLII**)[123, 127, 319, 321] ([M] = W(CO)$_5$, Mo(CO)$_5$, Cr(CO)$_5$; Ar = aryl, hetaryl, ferrocenyl).

A side-reaction that was generally favored when reactions were carried out at higher concentrations and/or at lower temperatures led to the formation of dinuclear *N,N'*-λ^3-P-bridged carbene metal complexes (**XLII**);[123, 127, 319, 321] in one case two diastereomers of **XLII** (*E,E* and *E,Z*)[2] were observed.[319] Complexes **XLII** were interpreted as trapped products of intermediates of type **XL** or **XLI**.[123, 123, 127, 319] Further investigations supported the interpretation that they result from the addition of the NH functionality of another equivalent of **XXXVIII** to the P,N double bond of **XLI**.[123] It has been shown for some derivatives of **XLII** that their formation can be reversed, as they could be transformed into the corresponding 2*H*-azaphosphirene complexes in the presence of triethylamine[123, 319, 321] (Scheme 7.1).

A dinuclear 1,1'-ferrocenediyl-bridged bis-2*H*-azaphosphirene tungsten complex was a target of particular interest. For its synthesis according to the route described above 1,1'-ferrocenediyl-bis(aminocarbene) complex **199** was required. This has first

---

[2]In general, C,N bonds of aminocarbene complexes have enhanced bond orders, thus leading to *E/Z*-isomeric forms.[317]

been synthesized by M. Schlenker within the scope of her Diploma Thesis.[192] The described method was largely adopted (Scheme 7.2), but the purification procedures were basically modified, here.
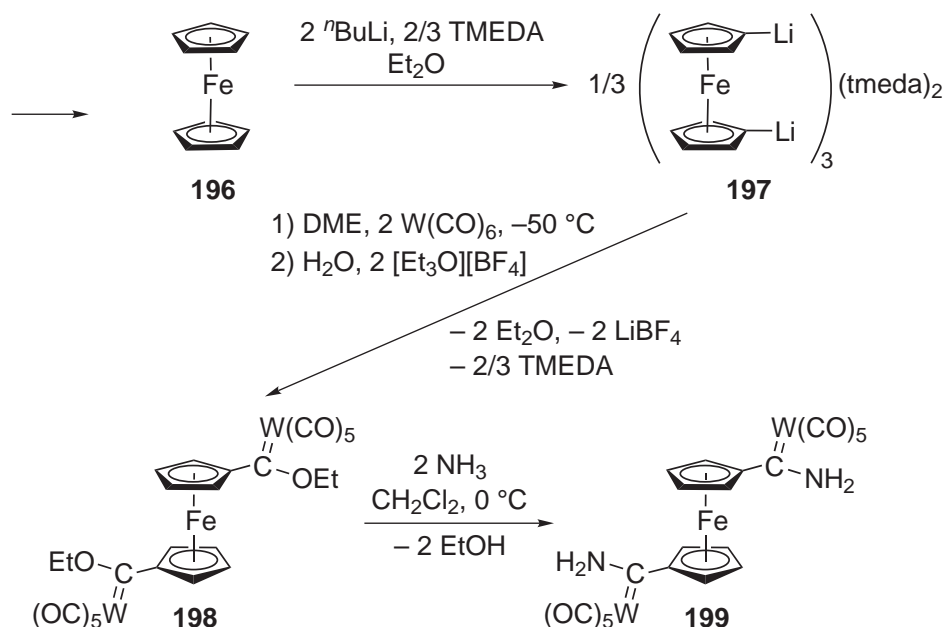
Scheme 7.2: Synthesis of dinuclear bis(aminocarbene) complex **199**.

Reaction of 1,1'-dilithioferrocene TMEDA adduct **197** with tungsten hexacarbonyl and subsequently with triethyloxonium tetrafluoroborate gave besides complex **198** the mononuclear complex [ethoxy(ferrocenyl)carbene]pentacarbonyltungsten(0) as major by-product. The latter (along with unreacted $W(CO)_6$ and ferrocene) was separated from the target product via soxhlet extraction. In this way complex **198** was isolated in 31 % yield. Subsequent ammonolysis in CH_2Cl_2 gave 1,1'-ferrocenediyl-bis(aminocarbene) complex **199**, which was purified by low-temperature column chromatography, thus obtained in 62 % yield.

Complex **199** was then reacted with [bis(trimethylsilyl)methylene]chlorophosphane **194** in the presence of triethylamine (Scheme 7.3, i), whereas several variations of the reaction conditions were examined, such as the solvent, the stoichiometry, the concentration, the temperature, and the order of addition of the reactants, but all these reactions were unselective. Likewise, either by turning to bromo(methylene)phosphane **195** (instead of **194**) or via previous dilithiation[322] of the amino functionality of **199** (ii) and subsequent reaction of **200** with **194** (iii) only complex mixtures of products were obtained. After workup of one of these reactions, when a solution of **199** in a solvent mixture of Et_2O, CH_2Cl_2, and THF was employed and slowly added to a solution of **194** in Et_2O and NEt_3 at 30 °C, single-crystals suitable for X-ray

crystallography were obtained from the $7th$ fraction of the chromatographic separation procedure. The product had the constitution of dinuclear complex **201** featuring one 2H-azaphosphirene and one aminocarbene complex unit (Fig. 7.1).
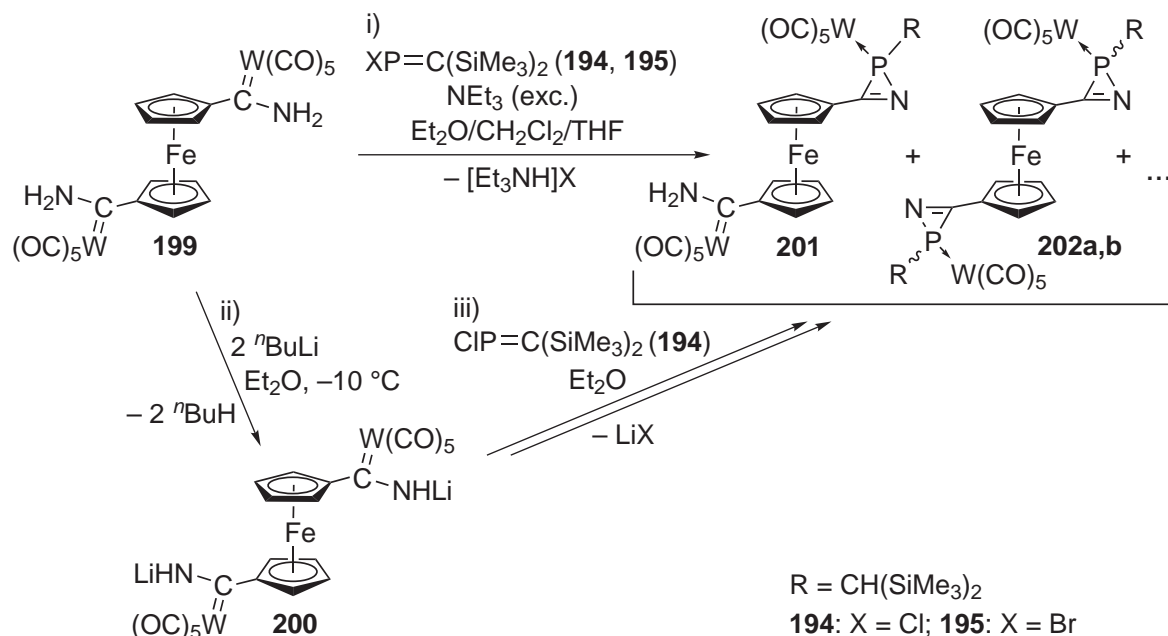
Scheme 7.3: Attempted synthesis of bis-2H-azaphosphirene complexes **202a,b** using carbene complex **199**, [bis(trimethylsilyl)methylene]chloro- or bromophosphane, and triethylamine or n-butyllithium.

Complex **201** shows a ^{31}P resonance at $\delta = -112.8$ ($|^1J_{WC}| = 296.3$ Hz), thus in the same range as 2H-azaphosphirene complex **67** ($\delta = -115.3$, $|^1J_{WC}| = 299.4$ Hz). The characteristic resonances of the NH protons of the aminocarbene moiety were detected at $\delta = 8.26$ and 7.58.

It crystallizes in the monoclinic space group P $2_1/c$ (Fig. 7.1) together with one molecule of diethyl ether per formula unit bound to the amino group of **201** via a hydrogen bond (d(N(2)–O(1S)) 2.882(5)). In this structure the two features of 3-ferrocenyl-2H-azaphosphirene **67**[128] and amino(ferrocenyl)carbene complex **203**[128] are combined (Tab. 7.1). At the 2H-azaphosphirene complex unit the typical similarity of endocyclic P,C and P,N bond lengths is found (as in complex **67**), and the three-membered ring, to a large extent, adopts a coplanar orientation with the adjacent cyclopentadienyl ring (torsion angle between least-squares planes: 15.1°).
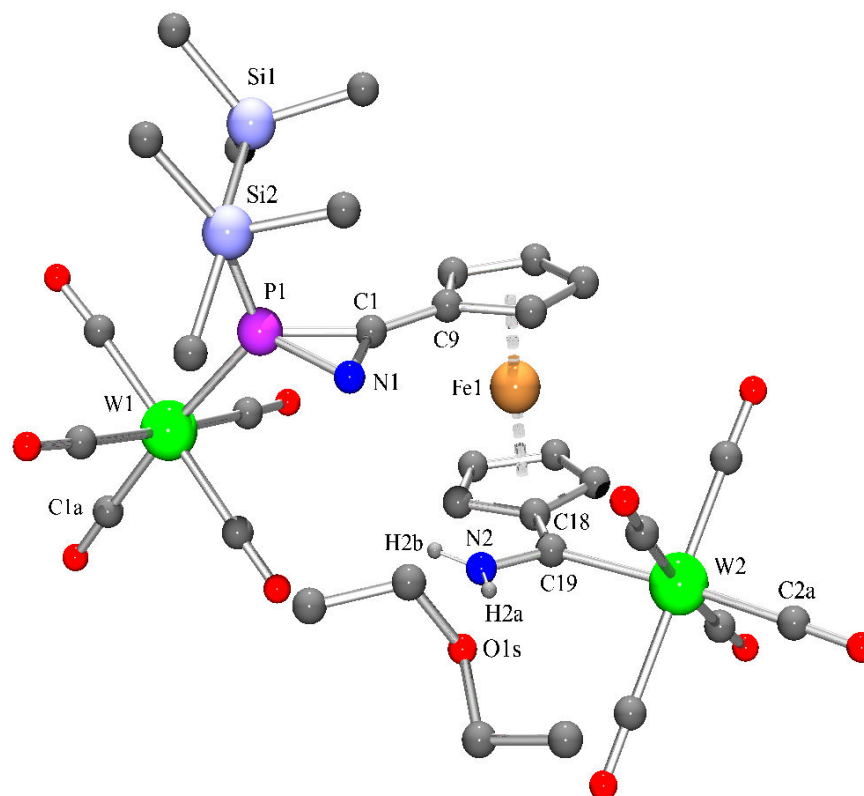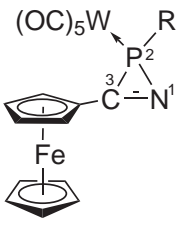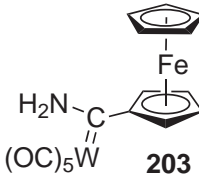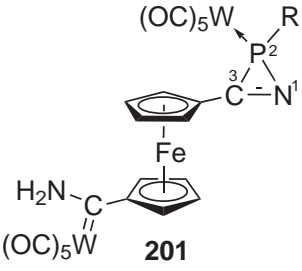
Figure 7.1: Molecular structure of complex **201** in the crystal (except for H2a and H2b all hydrogen atoms omitted for clarity). Selected bond lengths [Å] and angles [°]: W(1)–C(1a) 1.986(5), W(1)–P(1) 2.4827(11), P(1)–N(1) 1.798(4), P(1)–C(1) 1.769(4), N(1)–C(1) 1.280(5), C(1)–C(9) 1.440(6), C(18)–C(19) 1.472(6), C(19)–N(2) 1.313(5), C(19)–W(2) 2.223(4), W(2)–C(2a) 2.005(5), N(1)–P(1)–C(1) 42.05(17), P(1)–C(1)–N(1) 70.2(2), C(1)–N(1)–P(1) 67.8(2), C(18)–C(19)–N(2) 113.0(4), C(18)–C(19)–W(2) 126.4(3), N(2)–C(19)–W(2) 120.5(3).

The carbene center at the other Cp ring of **201** is (as in complex **203**) trigonal planar coordinated ($\Sigma\angle$ 359.9°) and lies together with the amino nitrogen and, to some extent, also the tungsten center in the plane of the attached cyclopentadienyl ring (deviations from least-squares plane: 0.029 ($C_{carbene}$), 0.140 (NH$_2$), −0.210 Å (W)). A comparatively long W,$C_{carbene}$ bond in combination with a rather short $C_{carbene}$,N bond point to a pronounced contribution of the iminiumacylmetallate resonance structure, which is typical for this class of compounds.[323] The two Cp rings of **201** adopt an almost eclipsed arrangement in the crystal state (rotation angle: 6.6°). The structure shows a conformation where the distance between the bulky 2H-azaphosphirene and carbene complex moieties is far from being maximized; both groups are attached to vicinal carbon centers at the two coplanar cyclopentadienyl rings (torsion angle between Cp rings: 0.7°).

Table 7.1: A) Selected bond lengths [Å] and B) angles [°] for complexes **67**,[128] **203**,[128] and **201** (R = CH(SiMe$_3$)$_2$).

		67	**203**	**201**
A)	W–P	2.487(10)	–	2.4827(11)
	P–C^3	1.763(4)	–	1.769(4)
	P–N^1	1.803(3)	–	1.798(4)
	C^3–N^1	1.285(5)	–	1.280(5)
	W–C$_{carbene}$	–	2.249(4)	2.223(4)
	C$_{carbene}$–NH$_2$	–	1.306(5)	1.313(5)
	C$_{carbene}$–C$^1_{Cp}$	–	1.489(5)	1.472(6)
B)	C^3–P–N^1	42.23(18)	–	42.05(17)
	P–N^1–C^3	67.2(2)	–	67.8(2)
	N^1–C^3–P	70.5(2)	–	70.2(2)

This result indicates that intramolecular side-reactions might complicate the attempted synthesis of **202a,b** when starting from bis(aminocarbene) complex **199**. In some of the reactions displayed in Scheme 7.3 a ^{31}P NMR resonance at $\delta = 66.0$ showing no ^{183}W satellites was detected, which is in a reasonable range for an N,N'-λ^3-P-bridged carbene complex (**XLII**; cf. Scheme 7.1).

When the reaction of **199** with **194** and NEt$_3$ was carried out in a dilute CH$_2$Cl$_2$ solution and using one equivalent of chloro(methylene)phosphane **194** quantitative formation of ferrocenophane complex **205** was observed (Scheme 7.4).

The formation of **205** can be understood as a result of the intramolecular attack of the aminocarbene complex NH functionality of intermediate **204** (analogous to **XLI**, Scheme 7.1) at its P,N double bond.[3] After optimization of the reaction and purification conditions complex **205** was isolated in 62 % yield, and its molecular structure was unambiguously identified by multinuclear NMR experiments, mass spectrometry, IR and UV/Vis spectroscopy, and a single-crystal X-ray diffraction study (Fig. 7.2); the elemental composition was examined by elemental analysis.

---

[3]Alternatively, an intramolecular attack at the P,C double bond of an intermediate of type **XL** (Scheme 7.1) is also conceivable.
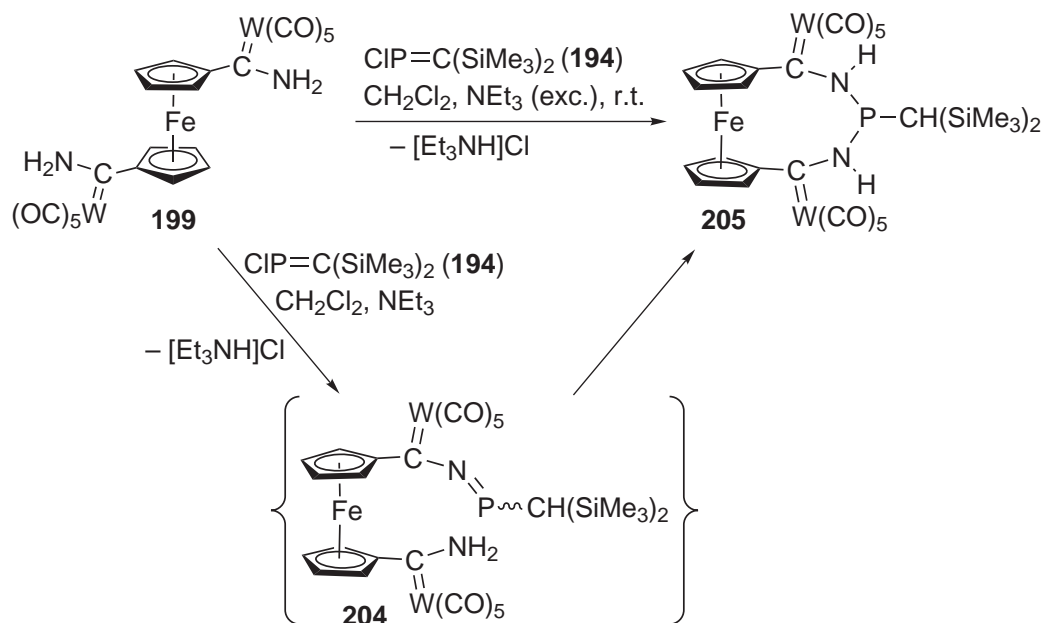
Scheme 7.4: Synthesis of ferrocenophane complex **205** using carbene complex **199**, [bis-(trimethylsilyl)methylene]chlorophosphane (**194**), and triethylamine.
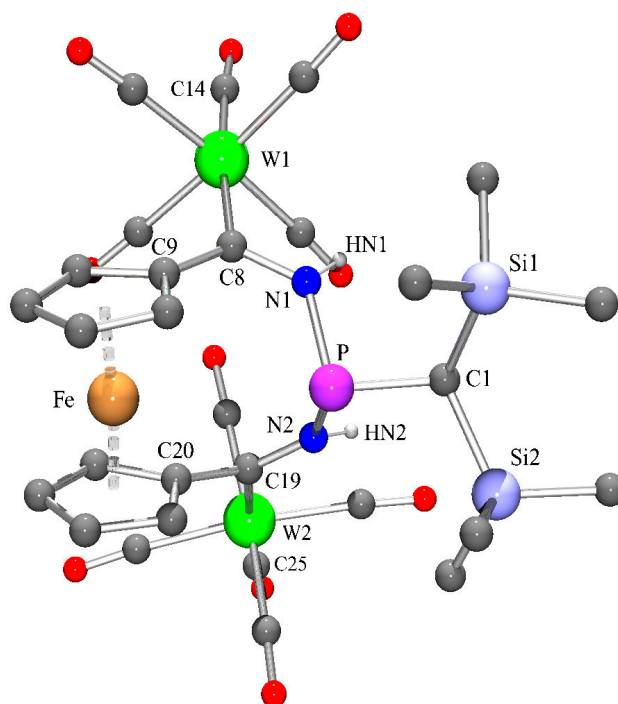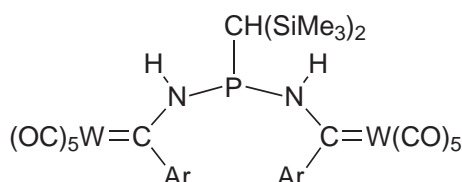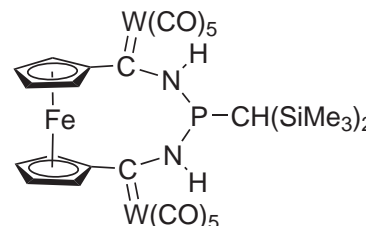
Figure 7.2: Molecular structure of complex **205** in the crystal (except for HN1 and HN2 all hydrogen atoms omitted for clarity). Selected bond lengths [Å] and angles [º]: P–C(1) 1.816(3), P–N(1) 1.769(3), N(1)–C(8) 1.362(4), C(8)–W(1) 2.207(3), C(8)–C(9) 1.462(4), W(1)–C(14) 2.024(3), C(1)–P–N(1) 99.04(13), N(1)–P–N(2) 94.25(13), P–N(1)–C(8) 129.2(2), N(1)–C(8)–C(9) 115.0(3), N(1)–C(8)–W(1) 118.4(2).

Complex **205** crystallizes in the monoclinic space group P $2_1/n$ and shows E,E configuration at the C,N bonds (Fig. 7.2). Looking at the molecular structure it appears plausible that steric reasons are responsible for the formation of exclusively this diastereomer. The Cp–Fe–Cp axis is slightly folded ($\beta_{in-plane}$ 5.4°), whereas the Cp rings are *tilted away* from the linking bridge. Different from the situation found in the structures of complexes **201** and **203** the nitrogen and tungsten centers of **205** are out of the plane of the Cp ring at the corresponding carbene unit (deviations from least-squares planes: 0.492 (N(1)), 0.633 (W(1)), 0.520 (N(2)), and 1.836 Å (W(2))), but the carbene centers are trigonal planar coordinated ($\Sigma\angle$ 359.9° (C(8)) and 359.1° (C(19))). The bond lengths within this structural unit are comparable to those of the other structurally characterized N,N'-λ^3-P-bridged carbene tungsten complexes **206a**[127] and **206b**[321] (Tab. 7.2); the phosphorus center of **205** is largely pyramidalized ($\Sigma\angle$ 292.9°).

Table 7.2: Selected bond lengths [Å] for complexes **206a**,[127] **206b**,[321] and **205**.

	206a Ar = o-anisyl	206b Ar = mesityl	205
W–C$_{carbene}$	2.167(5)	2.193(2)	2.207(3)
	2.185(5)	2.222(2)	2.206(3)
C$_{carbene}$–N	1.363(7)	1.333(3)	1.362(4)
	1.314(7)	1.322(3)	1.325(4)
P–N	1.756(5)	1.7725(19)	1.769(3)
	1.781(5)	1.795(2)	1.787(3)

In the IR spectrum (KBr) the N,H stretch vibration band was detected at $\tilde{\nu} = 3305$ cm^{-1}, and the spectrum shows more than five distinct C,O stretch vibration bands, which might be due to the different degree of rotation about the W,C$_{carbene}$ bonds in the conformation in the solid state. The C_S symmetry of complex **205** becomes apparent from its NMR spectroscopic parameters. The two halves of the molecule give rise to a common set of ^{1}H as well as ^{13}C resonances, and as the phosphorus center is achiral, for the two SiMe$_3$ groups the respective proton, carbon, and silicon centers are magnetically equivalent. The carbene carbon resonates at $\delta = 279.5$ ($|^2J_{PC}| = 1.6$

Hz), thus being significantly deshielded compared to aminocarbene complex **203** ($\delta = 254.8$)[128] but in the same range as the carbene centers of other N,N'-λ^3-P-bridged carbene tungsten complexes such as **206a** or **206b** (e.g., **206b**: $\delta = 283.1$ and 301.0, $|^2J_{PC}| = 4.2$ Hz).[321] Characteristic is also the low field resonance of the NH proton ($\delta = 9.39$, $|^2J_{PH}| = 4.5$ Hz).

The UV/Vis spectrum of **205** shows two low energy absorption bands at $\lambda_{max} = 429$ and 375 nm, which are assigned to either d–d transitions of Fe(II)[189] or metal–ligand charge transfer processes occurring from the iron center to the acceptor-substituted cyclopentadienyl rings (d_π–π^*).[190,191]

Since other N,N'-λ^3-P-bridged carbene complexes (**XLII**) could be transformed into corresponding $2H$-azaphosphirene complexes (see above; Scheme 7.1), pure complex **205** was reacted with chloro(methylene)phosphane **194** and triethylamine in methylene chloride (Scheme 7.5). After 20 hours complex **205** was completely converted, and by $^{31}P\{^1H\}$ NMR spectroscopic monitoring four resonances were detected, approximately with a $3:3:1:1$ ratio. The former two resonances belong to an AB spin system ($\delta = 77.5$, $|^1J_{WP}| = 254.3$ Hz, $|^{1+3}J_{PP}| = 115.7$ Hz and $\delta = 90.5$), while the latter two were detected at higher field ($\delta = -113.6$, $|^1J_{WP}| = 292.5$ Hz and -113.2, $|^1J_{WP}| = 302.6$ Hz) and could be assigned to complexes **202a,b**, the diastereomeric forms of the targeted bis-$2H$-azaphosphirene complex.
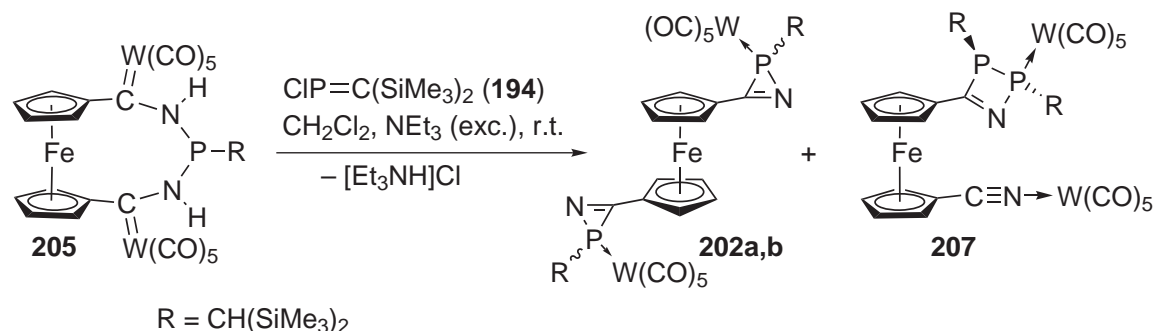
Scheme 7.5: Synthesis of bis-$2H$-azaphosphirene complexes **202a,b** and 2,3-dihydro-1,2,3-azadiphosphete complex **207** using complex **205**, [bis(trimethylsilyl)methylene]chlorophosphane, and triethylamine.

All attempts to optimize the reaction conditions by variation of temperature, concentration, or the amount of **194** or NEt$_3$ added yielded in each case a mixture of the products mentioned above with approximately the same ratio. Furthermore, the products exhibited a similar retention behavior on the chromatographic column, which prevented their separation in this way. However, it turned out that their solubilities in n-pentane differed sufficiently so that complex **207** could be separated from the mix-

ture via extraction with cold *n*-pentane. Complex **207**, which features a 2,3-dihydro-
1,2,3-azadiphosphete complex and a nitrile complex unit, was identified by multin-
uclear NMR experiments, mass spectrometry, and a single-crystal X-ray diffraction
study (Fig. 7.3).
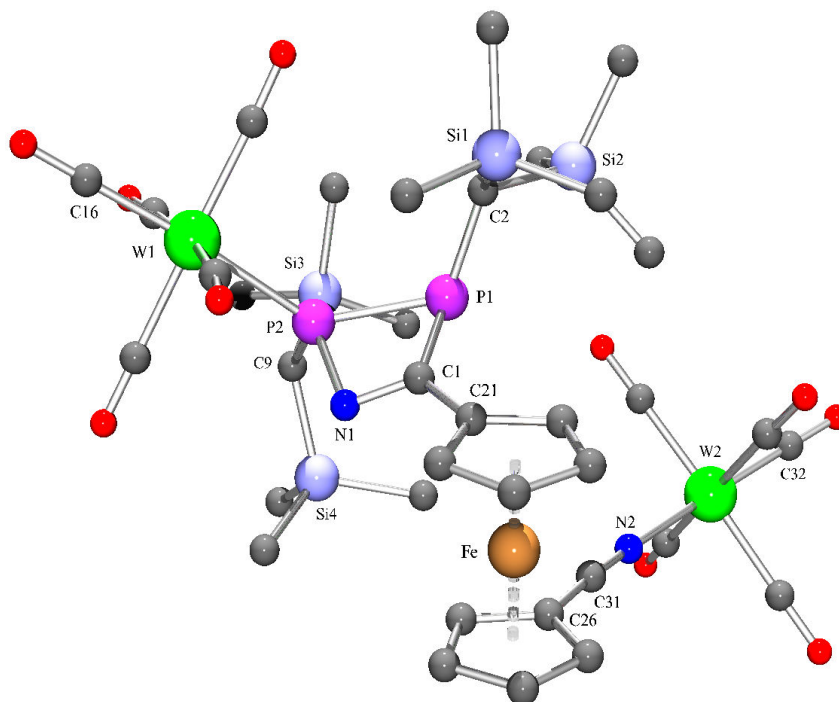
Figure 7.3: Molecular structure of complex **207** in the crystal (hydrogen atoms omit-
ted for clarity). Selected bond lengths [Å] and angles [°]: W(1)–C(16) 2.006(4), W(1)–
P(2) 2.5188(8), P(2)–P(1) 2.2543(11), P(2)–N(1) 1.751(3), P(1)–C(2) 1.861(3), P(1)–C(1)
1.841(3), C(1)–N(1) 1.305(4), C(1)–C(21) 1.458(4), C(26)–C(31) 1.416(5), C(31)–N(2)
1.153(5), N(2)–W(2) 2.177(3), W(2)–C(32) 1.970(4), P(1)–P(2)–N(1) 78.43(10), P(2)–P(1)–
C(1) 69.74(10), P(1)–C(1)–N(1) 107.8(2), C(1)–N(1)–P(2) 100.4(2).

After complete removal of **207** from the product mixture via soxhlet extraction
the residue, which contained mainly bis-2*H*-azaphosphirene complexes **202a,b** and
triethylammonium chloride, was subjected to low-temperature column chromatogra-
phy. This afforded a purified mixture of diastereomers **202a,b** in about 14 % yield.
Complexes **202a,b** were unambiguously characterized via multinuclear NMR spec-
troscopy, mass spectrometry, and UV/Vis spectroscopy; the elemental composition
was confirmed through a HR-ESI-MS experiment (m/z 1265.0165).

The high field shifted ^{31}P resonances of **202a,b** (vide supra) having large tungsten–
phosphorus coupling constant magnitudes are characteristic for 2*H*-azaphosphirene
tungsten complexes ($|^1J_{WP}|$ 290−300 Hz, in general[114]). The ^{13}C resonances of the

$2H$-azaphosphirene ring carbons were detected at very low field ($\delta = 189.5$ and 189.6), which is also a typical feature of this heterocylic system (cf. complex **67**: $\delta = 192.5$).[128] The ^{1}H and ^{13}C{^{1}H} NMR spectra of **202a,b** showed the typical patterns of equally mono-substituted Cp rings of a ferrocenediyl moiety.

Turning to the formation of complex **207**, it should be noted that Streubel and coworkers have reported on the formation of 4-phenyl-2,3-dihydro-1,2,3-azadiphosphete complex **209**[135–137, 268] upon thermolysis of $2H$-azaphosphirene complex **35** in solution.[4] (Scheme 7.6). Depending on the specific reaction conditions mixtures of products **208**–**211** were obtained in varying ratios,[268] whereas P-trimethylsilyl substituted η^1-E-phosphaalkene complex **208** was identified as the primary reaction product. It was almost quantitatively formed in dilute solutions at high(er) temperatures and after short reaction times,[136] while employment of more concentrated solutions, slightly lower temperatures, and longer reaction times favored the formation of 2,3-dihydro-1,2,3-azadiphosphete complex **209**[135–137] and 2,5-dihydro-1,3-diaza-2,5-diphosphinine complex **210**.[134, 136, 137]
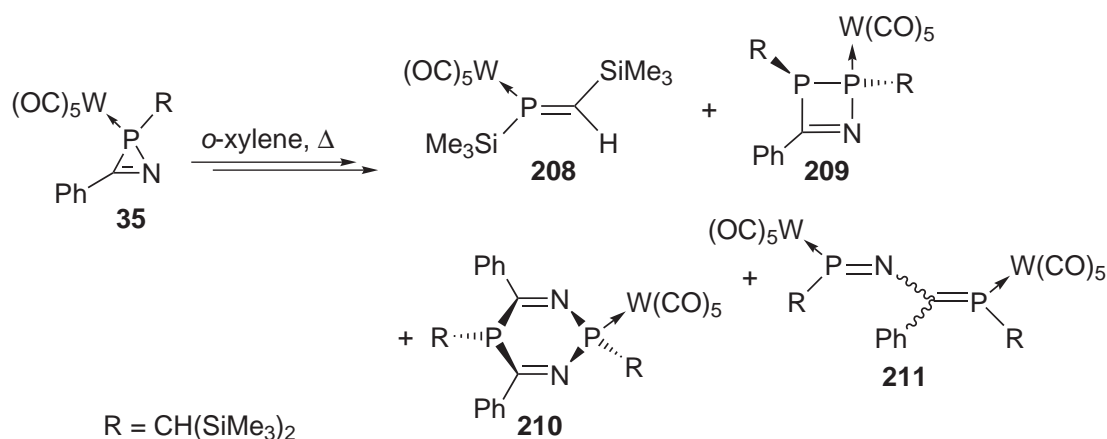
Scheme 7.6: Thermal decomposition of $2H$-azaphosphirene complex **35** in *ortho*-xylene.[268]

The formation of phosphaalkene complex **208** was explained as a result from a 1,2-(C→P)-trimethylsilyl shift occurring at transient phosphanylidene complex **212** (Scheme 7.7, ii), which is generated through loss of benzonitrile from **35** (i).[136] It was proposed that complex **209** can be formed on two different pathways.[135, 136] One competes with the formation of **208** in more concentrated solutions and proceeds via electrophilic attack of complex **212** at the nitrogen center of another equivalent of **35** with intermediate formation of adduct **213** (iii). Subsequent rearrangement and loss of W(CO)$_5$ leads to 2,3-dihydro-1,2,3-azadiphosphete complex **209** (iv).[135]

---

[4]Similarly, an analog of complex **209** having a P-Cp* substituent was obtained from thermal decomposition of $2H$-azaphosphirene complex **121**.[142]

The observation was made that **209** was formed also at the expense of phosphaalkene complex **208** in freshly prepared solutions of the latter at ambient temperature.[136] This result pointed to a benzonitrile-induced 1,2-(P→C)-trimethylsilyl shift occurring on the alternative pathway (v) for the formation of **209**.[136] However, the fate of the eliminated W(CO)$_5$ fragment was not clarified.[5]
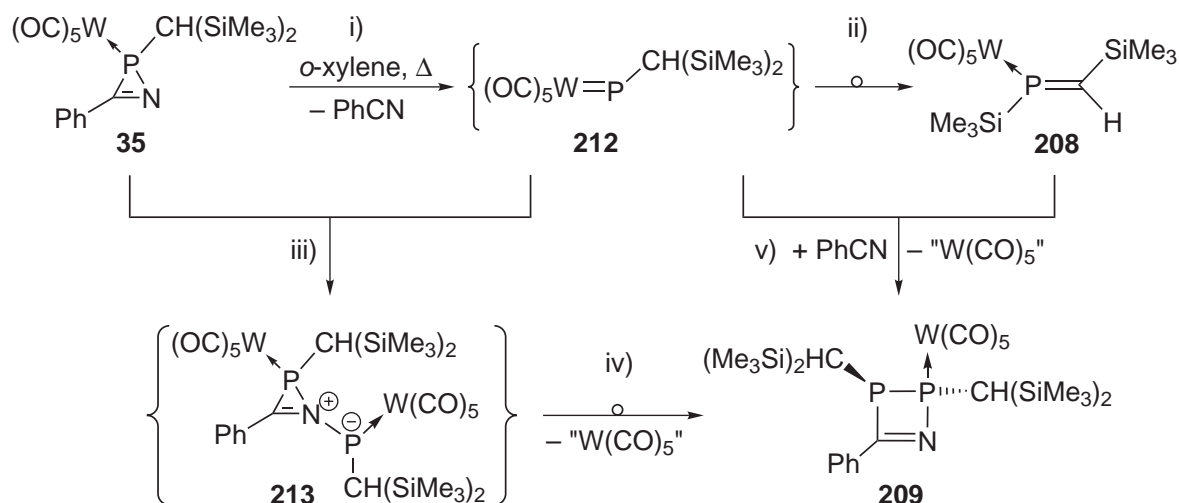
Scheme 7.7: Proposed mechanism of the formation of complexes **208** and **209** upon thermal decomposition of **35** shown in Scheme 7.6.[135, 136]

The knowledge about the formation of **209** from these thermolysis experiments might suggest that complex **207** is result from a follow-up reaction of bis-2*H*-azaphosphirene complexes **202a,b**, possibly involving phosphanylidene complex **212**. However, the purified complexes **202a,b** were found to be stable in a [D$_2$]methylene chloride solution for about 24 hours at ambient temperature in an NMR tube, and apart from hydrolysis giving the commonly observed siloxyphosphane complex **44** (cf. Scheme 1.15, Section 1.3), they showed no evidence for a follow-up reaction to yield complex **207**. Although the mechanism for the formation of **207** remains unclear, it can be concluded that complex **207** is not a follow-up product of **202a,b** but rather the product of a side-reaction.[6]
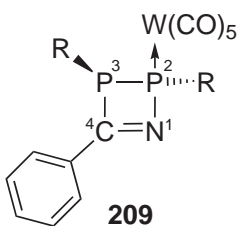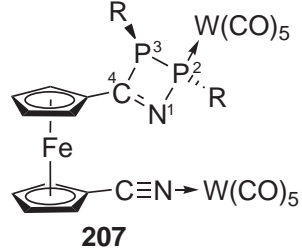
Complex **207** crystallizes in the triclinic space group P$\bar{1}$ (Fig. 7.3). Within the error margins the bond lengths and angles of its heterocycle are identical to those of complex **209** (Tab. 7.3). Likewise, the four-membered ring of **207** is slightly folded (mean

---

[5]Presumably a second equivalent of benzonitrile is involved in decomplexation in step v. This is supported by the results obtained in this work: in complex **207** the resulting nitrile complex fragment remains in the same molecule.

[6]It should be noted that the ratio of **207** and **202a,b** did not significantly change on decreasing the reaction temperature.

deviation from least-squares plane: 0.095 Å; torsion angle P^3–C^4–N^1–P^2: $-18.3\,°$; deviation of P^2 from the P^3–C^4–N^1 plane: 0.883 Å). The bis(trimethylsilyl)methyl groups adopt *trans* positions at the heterocycle; the $CH(P^2)$–P^2–P^3–$CH(P^3)$ torsion angle was determined as $132.9\,°$. Noteworthy are the two distinctly different exocyclic P,C bond lengths: in both complexes the σ^3-phosphorus center has a significantly longer distance to its exocyclic substituent than the σ^4-phosphorus center. As in the case of complex **201** (Fig. 7.1) both substituents at the ferrocene of **207** point into the same half space, as they are attached to vicinal carbon centers at the two almost eclipsed arranged (rotation angle: $8.3\,°$), coplanar cyclopentadienyl rings (torsion angle between Cp rings: $2.9\,°$). Also here the twist angle between the heterocycle and the adjacent Cp ring is rather small (with respect to least-squares planes: $23.7\,°$).

Table 7.3: A) Selected bond lengths [Å] and B) angles [°] for complexes **209**[135] and **207** (R = $CH(SiMe_3)_2$).

		209	**207**
A)	W–P^2	2.5257(6)	2.5188(8)
	P^2–P^3	2.2577(8)	2.2543(11)
	P^2–N^1	1.7473(18)	1.751(3)
	P^3–C^4	1.846(2)	1.841(3)
	C^4–N^1	1.304(3)	1.305(4)
	P^2–$CH(SiMe_3)_2$	1.829(2)	1.833(3)
	P^3–$CH(SiMe_3)_2$	1.861(2)	1.861(3)
B)	C^4–P^3–P^2	69.92(7)	69.74(10)
	P^3–P^2–N^1	78.51(6)	78.43(10)
	P^2–N^1–C^4	101.26(14)	100.4(2)
	N^1–C^4–P^3	107.80(15)	107.8(2)

The NMR spectroscopic data for the 2,3-dihydro-1,2,3-azadiphosphete complex unit of **207** are similar to those of complex **209**. It is remarkable that the ^{13}C resonance of the ring carbon center is found in the same range as that of the C^3 center of $2H$-1,4,2-diazaphosphole complexes (cf. Chapters 3–6), which is in comparison with 1,2-dihydro-1,2,4-azadiphosphete **214**[324] and 1,2-dihydro-1,2,3-triphosphete complex **215**[325] at somewhat higher field.
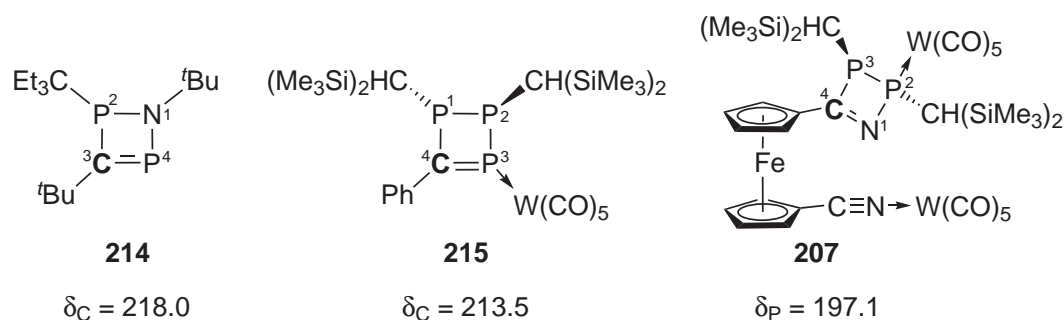
Figure 7.4: $^{13}C\{^{1}H\}$ NMR spectroscopic data for ring carbon centers of 1,2-dihydro-1,2,4-azadiphosphete **214**,[324] 1,2-dihydro-1,2,3-triphosphete complex **215**,[325] and 2,3-dihydro-1,2,3-azadiphosphete complex **207** (all data from C_6D_6 solutions).

Noteworthy is that the two methine carbons have distinctly different ^{13}C NMR chemical shifts as well as distinctly different phosphorus–carbon coupling constant magnitudes: $\delta = 16.5$ ($|J_{PC}| = 79.5$ and 7.1 Hz) and $\delta = 34.7$ ($|J_{PC}| = 20.7$ and 10.3 Hz); this feature was observed also for complex **209**. The carbon resonance of the $W(CO)_5$-coordinated cyano group ($\delta = 126.2$) is in the typical range of pentacarbonyltungsten(0) nitrile complexes.[326]

Chapter 8

Conclusions

In combined experimental and computational studies the scope of different strategies for P,N bond activation and ring expansion of $2H$-azaphosphirene complexes was investigated.

In Chapter 3 a protocol using nitriles and catalytic amounts of SET oxidants such as ferrocinium salts was explored in detail. Reactions of $2H$-azaphosphirene complex **35** with nitrile derivatives **36b,g** in the presence of [FeCp$_2$][PF$_6$] showed highly selective insertions of the nitrile into the P,N bond of **35** at ambient temperature (Scheme 8.1, i). $2H$-1,4,2-Diazaphosphole complexes **41b,g** were isolated in good yields, and their structures were confirmed by single-crystal X-ray diffractometry.

Studies on the reaction course revealed a strong dependance of the reaction rate on the nature of the nitrile and on the amount of ferrocinium hexafluorophosphate employed. The latter could be reduced to 0.05 equivalents without overall decrease in conversion for reactions of **35** with hetaryl carbonitriles **36d–g**, and the reaction with **36g** proceeded smoothly with even 0.025 equivalents of [FeCp$_2$][PF$_6$] (Scheme 8.1, i). A non-exponential reaction progression, together with the formation of ferrocene, points to a radical cation chain reaction mechanism initiated by single-electron oxidation of the $2H$-azaphosphirene complex by the ferrocinium cation.

Very electron-poor nitrile derivatives (C_6F_5CN, EtO_2CCN) did not react with complex **35** under these conditions, and the reaction of **35** with HCN remained incomplete. Also an attempt to insert a dinitrile ($NCCH_2CH_2CN$) into the P,N bond of 3-ferrocenyl-$2H$-azaphosphirene complex **67** failed. In this case $2H$-1,4,2-diazaphosphole complex **69l** having two ferrocenyl substituents was obtained, which was isolated and structurally confirmed (Fig. 8.1). Obviously, the FcCN fragment that is required for the formation of **69l** stems from the $2H$-azaphosphirene complex (**67**).

i)
RC**N** (**36b,d–g**)
[FeCp$_2$][PF$_6$] (cat.), r.t.

41b,d–g

ii)
[FeCp$_2$][PF$_6$] (cat.), r.t.
CH$_2$Cl$_2$

41c, **74c**, **75c**
69l, **76l**, **77l**

+

85–87

35, **70**, **71**
67, **72**, **73**

iii)
PhC**N** (**36c**)
[FeCp$_2$][PF$_6$] (cat.), r.t.

74c, **75c**

+

50c

35, **41c**: Ar = Ph; M = W
70, **74c**: Ar = Ph; M = Mo
71, **75c**: Ar = Ph; M = Cr
67, **69l** : Ar = Fc; M = W   **85**: M = W
72, **76l** : Ar = Fc; M = Mo   **86**: M = Mo
73, **77l** : Ar = Fc; M = Cr   **87**: M = Cr   R' = CH(SiMe$_3$)$_2$

36, **41**: R = NMe$_2$ (**b**), 1,5-dimethyl-2-pyrryl (**d**), 2-furyl (**e**), 3-thienyl (**f**), 2-thienyl (**g**)
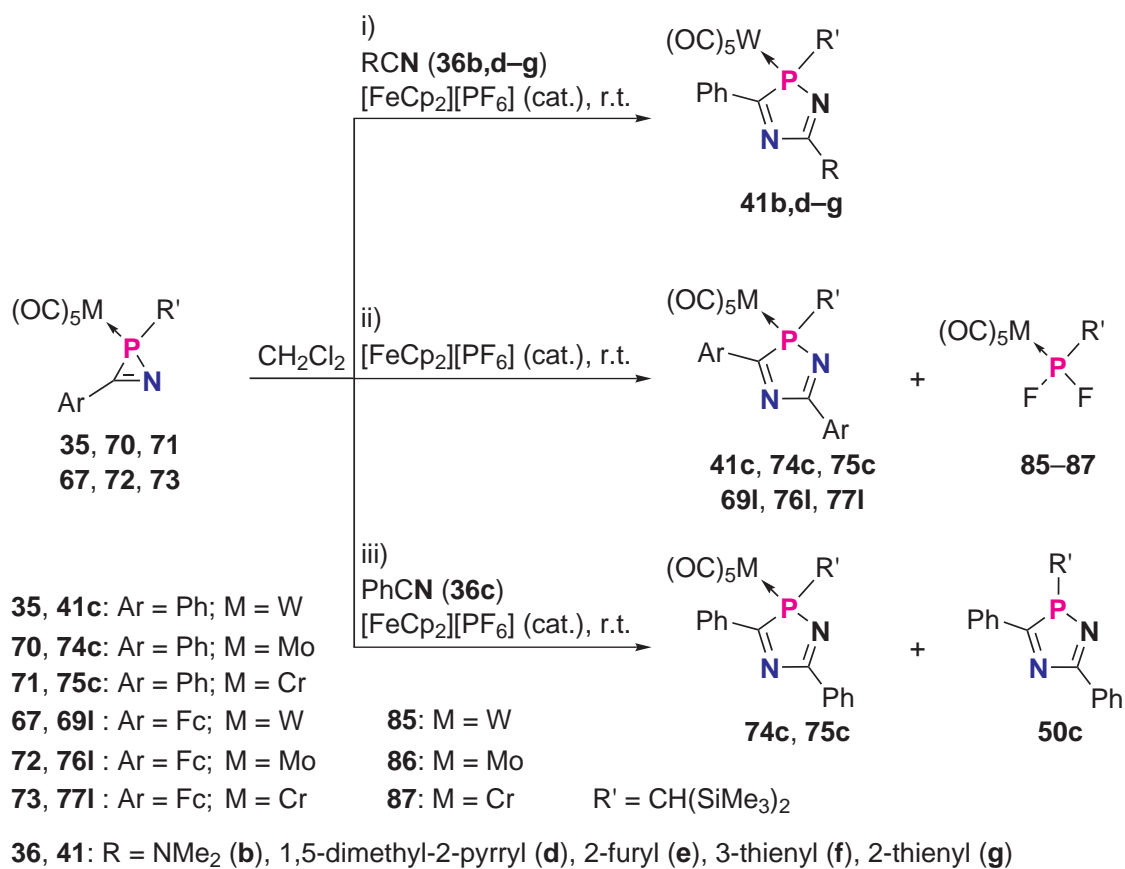
Scheme 8.1: SET-induced ring expansion reactions of 2H-azaphosphirene complexes **35**, **67**, and **70**–**73**.
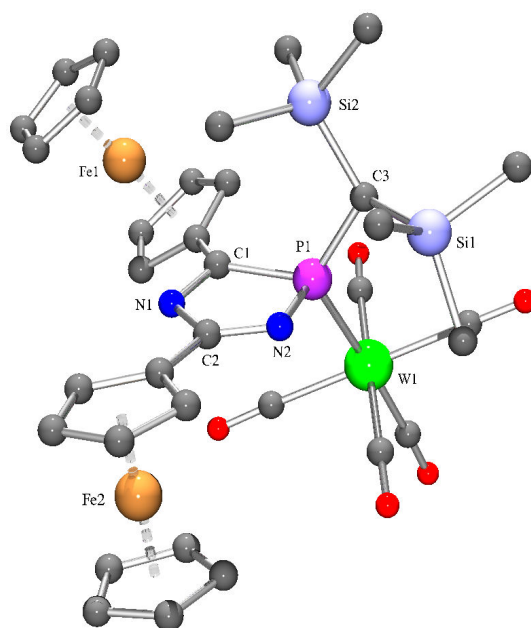
Figure 8.1: Molecular structure of **69l** in the crystal (hydrogen atoms omitted for clarity).

Reactions of 2*H*-azaphosphirene complexes **35**, **67**, and **70**–**73** with ferrocinium hexafluorophosphate were examined in the *absence of nitriles* (Scheme 8.1, ii). Here, besides several side-products bearing P,F bonds such as difluorophosphane complexes **85**–**87** symmetrically 3,5-disubstituted 2*H*-1,4,2-diazaphosphole complexes **41c**, **74c**, **75c**, **69l**, and **77l** were observed. The investigations revealed a strong dependance on the $M(CO)_5$ fragment as reactions of molybdenum and chromium complexes **70**–**73** were significantly slower; complex **76l** was not observed. During reactions of **70** and **71** with benzonitrile (**36c**) in the presence of $[FeCp_2][PF_6]$ the desired products **74c** and **75c** underwent partial decomplexation, which prevented their isolation using this synthetic methodology (Scheme 8.1, iii).

Cyclic voltammetric investigations were carried out on selected 2*H*-azaphosphirene and 2*H*-1,4,2-diazaphosphole complex derivatives. While **69l** showed two reversible oxidation waves according to consecutive one-electron oxidations of both ferrocenyl units, complexes **35**, **70**, **71**, **41g,m**, and **126g** were irreversibly oxidized at higher potential, which points to a pentacarbonyl metal-centered oxidation. Additionally, a reversible one-electron reduction wave was found for each 2*H*-1,4,2-diazaphosphole complex investigated. It is remarkable that the behavior of 2*H*-azaphosphirene complexes **35**, **70**, and **71** is contrary to the situation of 3-ferrocenyl substituted derivative **67** where oxiation takes place at the ferrocenyl moiety.

DFT calculations carried out on different model systems revealed that the primary products **91**$^{\bullet+}$–**94**$^{\bullet+}$ of the oxidation of respective 2*H*-azaphosphirene complexes have a retained cyclic structure (Scheme 8.2, i). When R" = CH_3 (R' = CH_3, $CH(SiH_3)_2$) or R" = Ph (R' = CH_3) these species are best described as 17e organometallic complexes where the radical center is localized at the pentacarbonyl metal fragment while the positive charge is attributed to phosphorus (**91**$^{\bullet+}$: Scheme 8.2, left). By *C*-ferrocenyl substitution the spin density is completely shifted to this substituent. Nevertheless, the same chemical behavior was predicted for the different model complexes. *In silico* reactions with nitriles of strong and moderate nucleophilicity resulted in the formation of acyclic species **95m,p**$^{\bullet+}$, **105**$^{\bullet+}$–**107**$^{\bullet+}$ via nucleophilic attack of the nitrile at the phosphorus center of **91**$^{\bullet+}$–**94**$^{\bullet+}$ (ii). Consequently, radical cationic 2*H*-azaphosphirene complexes constitute metal-centered radicals that show *ligand-centered reactivity*; nucleophilic attack of a nitrile occurs at the position of the highest positive charge density.

Subsequent cyclization of **95m,p**$^{\bullet+}$, **105**$^{\bullet+}$–**107**$^{\bullet+}$ giving radical cationic 2*H*-1,4,2-diazaphosphole complexes **96m,p**$^{\bullet+}$, **108**$^{\bullet+}$–**110**$^{\bullet+}$ proceeds via a low barrier (iii). The cycle is closed through oxidation of the reactants **91**–**94** by the latter (iv) with release of neutral products **96m,p**, **108**–**110** and formation of the reactive species **91**$^{\bullet+}$–**94**$^{\bullet+}$, which then can restart the chain reaction.
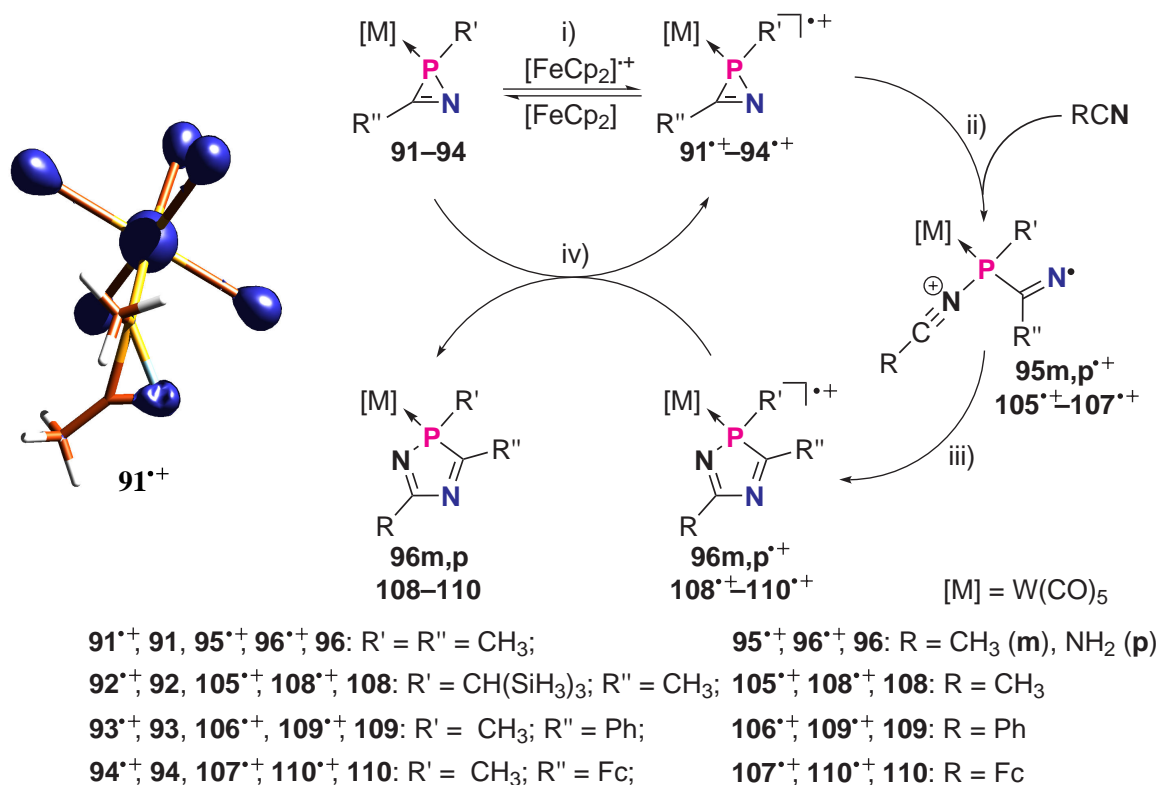
Scheme 8.2: Calculated Mulliken spin density for complex **91**$^{\bullet+}$ and mechanism of the SET-induced chain reaction of 2*H*-azaphosphirene complexes **91**–**94** with nitriles.
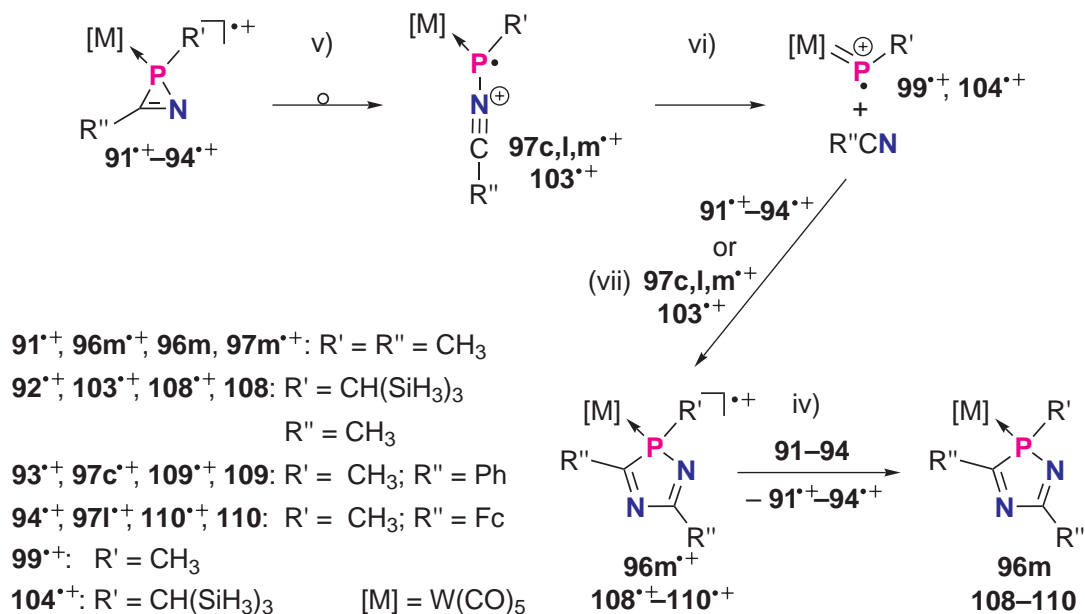
Scheme 8.3: Mechanism of the formation of symmetrically 3,5-disubstituted 2*H*-1,4,2-diazaphosphole complexes **96m**, **108**–**110** in reactions of 2*H*-azaphosphirene complexes **91**–**94** with [FeCp$_2$]$^{\bullet+}$ in the absence of nitriles.

On the other hand, nucleophilic attack of the electron-poor nitrile NCCN at $91^{\bullet+}$ proceeds via a very high barrier and leads to displacement of the MeCN moiety of $91^{\bullet+}$ (not shown). In the absence of nitriles radical cationic $2H$-azaphosphirene complexes $91^{\bullet+}$–$94^{\bullet+}$ can rearrange to their valence isomers $97c,l,m^{\bullet+}$, $103^{\bullet+}$ in one step (Scheme 8.3, v). Subsequent dissociation (vi) provides the nitrile (R"CN) that can react either with another equivalent of $91^{\bullet+}$–$94^{\bullet+}$ or with $97c,l,m^{\bullet+}$, $103^{\bullet+}$ (vii) to give symmetrically 3,5-disubstituted complexes $96m^{\bullet+}$, $108^{\bullet+}$–$110^{\bullet+}$ and after reduction $96m$, 108–110. The formal cycloaddition reaction (vii) is the preferred pathway when Ar = Fc.

In Chapter 4 a new synthetic strategy is presented: the one-pot synthesis of $2H$-1,4,2-diazaphosphole complexes from $2H$-azaphosphirene complexes and nitriles by consecutive reaction with the strong Brønsted acid TfOH and a base. This was applied to the syntheses of complexes **41b,g,m,r–t**, **69b,l**, **74b**, **75b**, **122b**, and **126b,g** (Scheme 8.4). In each case a highly selective insertion of the nitrile into the P,N bond of the $2H$-azaphosphirene complex was observed, and all products were isolated and unambiguously characterized; single-crystal X-ray diffraction studies were carried out on **41s**, **69b**, **126b,g**, **74b**, and **75b**. This protocol offers new synthetic perspectives as even nitriles with high steric demand (**36r,s**) could successfully be employed, and the use of nitrile derivative **36t** enabled access to the first C-SiMe$_3$ ring-functionalized $2H$-1,4,2-diazaphosphole complex **41t**. Furthermore, P-Cp* substituted $2H$-azaphosphirene complex **121**, C-ferrocenyl and C-(2-thienyl) substituted complexes **67** and **125**, and molybdenum and chromium complexes **70**, **71** could be employed as well.

Scheme 8.4: One-pot syntheses of **41b,g,m,r–t**, **122b**, **69b,l**, **126b,g**, **74b**, and **75b** via acid-induced ring expansion of $2H$-azaphosphirene complexes **35**, **121**, **67**, **125**, **70**, and **71** with nitriles.

By ^{31}P NMR spectroscopy evidence was obtained for the formation of $2H$-1,4,2-diazaphospholium complexes **123b,m,g,r–t**, **124b**, **127b**, **128b**, **145b**, **146b** (Scheme 8.5). Complexes **123b** and **124b** were isolated in good yields. The location of the proton at N^1 was confirmed by ^{1}H,^{15}N HMQC NMR experiments and for **123b** additionally by a single-crystal X-ray diffraction study.

35, **123**: M = W; Ar = Ph;   R' = CH(SiMe$_3$)$_2$
121, **124**: M = W; Ar = Ph;   R' = Cp*
67, **127**: M = W; Ar = Fc;   R' = CH(SiMe$_3$)$_2$
125, **128**: M = W; Ar = 2-Th; R' = CH(SiMe$_3$)$_2$
70, **145**: M = Mo; Ar = Ph;   R' = CH(SiMe$_3$)$_2$
71, **146**: M = Cr; Ar = Ph;   R' = CH(SiMe$_3$)$_2$

R = NMe$_2$ (**b**), 2-Th (**g**), CH$_3$ (**m**),
    ^{t}Bu (**r**), 1-Ad (**s**), SiMe$_3$ (**t**)

Scheme 8.5: Formation of $2H$-1,4,2-diazaphospholium complexes **123b,m,g,r–t**, **124b**, **127b**, **128b**, **145b**, and **146b**; molecular structure of complex **123b** in the crystal (hydrogen atoms omitted for clarity).

In ring expansion reactions of $2H$-azaphosphirene molybdenum and chromium complexes **70** and **71** partial decomplexation was observed, but this could completely be prevented by adding the base after short reaction times at low temperature. DFT calculations on all-methyl tungsten, molybdenum, and chromium model systems revealed

a significant metal–phosphorus bond weakening in $2H$-1,4,2-diazaphosphole complexes upon protonation. This led to the idea of a one-pot synthesis of heterocycle **50b** from **70** or **71** and nitrile **36b** without prior purification of its metal complexes **74b** or **75b**. After prolonged reaction times complete decomplexation of protonated intermediates **145b** and **146b** was observed, and the N^1-protonated liberated ligand **147b** was characterized by NMR multinuclear spectroscopy. When pyridine was added to a solution of **147b** neutral heterocycle **50b** was obtained as the only phosphorus-containing product. Although it decomposed during column chromatography, all relevant NMR spectroscopic information about **50b** was obtained from the raw product.

Ring expansion reactions of $2H$-azaphosphirene complexes **35**, **67**, and **125** with HCN afforded coordination-isomeric complexes **41h** and **129h**, **69h** and **130h**, and **126h** and **131h** each as mixture (Scheme 8.6). Complexes **129h**, **130h**, **131h** constitute first examples of κN-bonded $2H$-1,4,2-diazaphosphole complexes. The identification of the donating N atom was achieved on the basis of ^{15}N NMR spectroscopic data. The κP-bonded haptomers were the major components in the cases of Ar = phenyl and 2-thienyl, and the product mixtures could be purified by low-temperature column chromatography; single-crystal X-ray diffraction studies were carried out on **41h** and **126h**. In contrast, when Ar = ferrocenyl κN-bonded complex **130h** prevailed in the mixture with **69h**, but here, both products decomposed during column chromatography. The reason for the preference of the κN-coordination mode in this case presumably is the pronounced steric demand of the ferrocenyl group.

Scheme 8.6: Syntheses of $2H$-1,4,2-diazaphosphole-κP and -κN complexes **41h**, **69h**, **126h**, **129h**, **130h**, and **131h** (Th = 2-thienyl).

Furthermore, ^{31}P{^{1}H} NMR spectroscopic measurements at varying temperatures evidenced in each case a chemical equilibrium between the two haptomeric $2H$-1,4,2-diazaphosphole complexes in solution (Scheme 8.6). This was further supported by DFT calculations.

The novel 2,3-dihydro-1,3-azaphosphete complex **149** was obtained via ring expansion of 2*H*-azaphosphirene complex **35** using isonitrile **148** (Scheme 8.7). The molecular structure of **149** was confirmed by single-crystal X-ray diffractometry (Fig. 8.2).

Scheme 8.7: Synthesis of 2,3-dihydro-1,3-azaphosphete complex **149** using 2*H*-azaphosphirene complex **35**, TfOH, isonitrile **148** (Cy = cyclohexyl), and NEt₃.
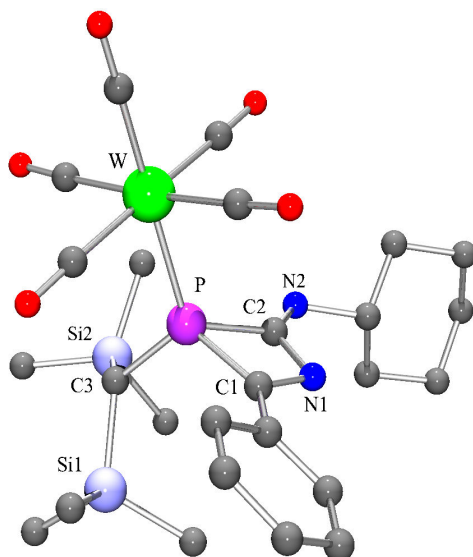
Figure 8.2: Molecular structure of complex **149** in the crystal (hydrogen atoms omitted for clarity).

In order to prove and/or expand the concept of bond activation, various Brønsted and Lewis acids were examined. This was done for the reaction of complex **35** with nitrile **36b** as a good case in point (Scheme 8.8). The best results were obtained with trifluoroacetic acid and tris(pentafluorophenyl)borane. Lithium tetrakis(pentafluorophenyl)borate was capable of inducing a selective reaction as well. When $HBF_4 \cdot Et_2O$, $BF_3 \cdot Et_2O$, or $Li[PF_6]$ was employed, besides target complex **41b** several fluorinated by-products were observed. Also reactions with sulfuric acid, oleum, and trichloroacetic acid were less selective. No ring expansion occurred in the presence of triethylammonium triflate or acetic acid, thus revealing and marking the Brønsted acid strength borderline.
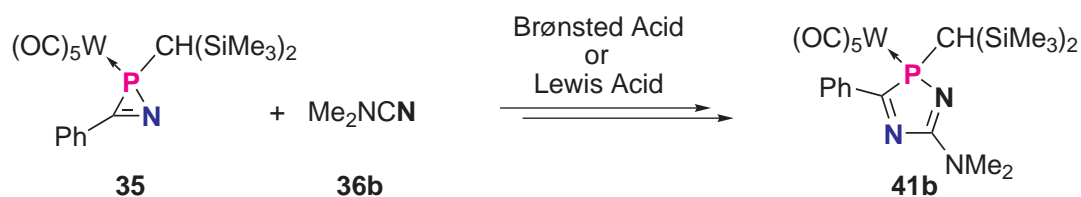
Scheme 8.8: Ring expansion of 2*H*-azaphosphirene complex **35** with dimethyl cyanamide (**36b**) induced by several Brønsted and Lewis acids.

Reaction of **35** with TfOH gave 1-aza-3-phosphabutadiene complexes **169** and **170**, which have different coordination modes and different configurations at the P,C double bond (Scheme 8.9). Their characterization was achieved by low-temperature multinuclear one- and two-dimensional NMR spectroscopy from the reaction mixture.
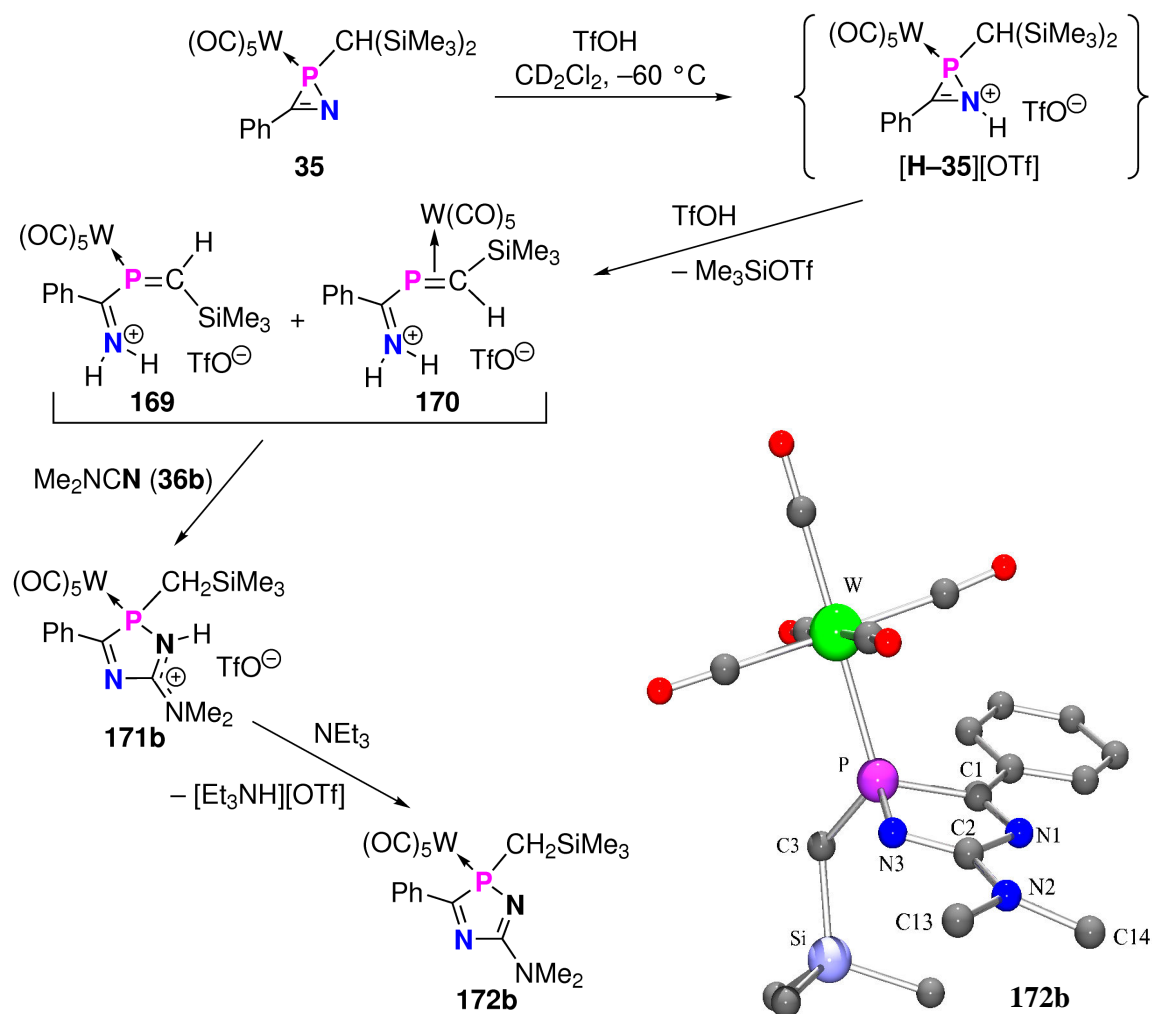
Scheme 8.9: *Consecutive* reaction of 2*H*-azaphosphirene complex **35** with TfOH, nitrile **36b**, and NEt₃; molecular structure of **172b** in the crystal (hydrogen atoms omitted for clarity).

Their formation can be explained as follows: reaction of **35** with one equivalent of triflic acid yields transiently [**H**–**35**][OTf], which undergoes subsequent desilylation combined with ring opening followed by a second protonation step. Reacting a mixture of in situ generated **169** and **170** with nitrile **36b** resulted in the formation of N^1-protonated $2H$-1,4,2-diazaphosphole complex **171b** having a CH$_2$SiMe$_3$ group at phosphorus. After deprotonation with triethylamine neutral complex **172b** was obtained, which was isolated and structurally confirmed.

The first $2H$-azaphosphirenium complex [**H**–**121**][OTf] was observed in the reaction of P-Cp* substituted complex **121** with TfOH (Scheme 8.10). It was characterized by multinuclear one- and two-dimensional NMR experiments at low temperature. Upon addition of nitrile **36b** ring expansion occurred with formation of complex **124b**. Moreover, it was demonstrated that the protonation of **121** can be reversed by adding triethylamine to a solution of [**H**–**121**][OTf] (Scheme 8.10).
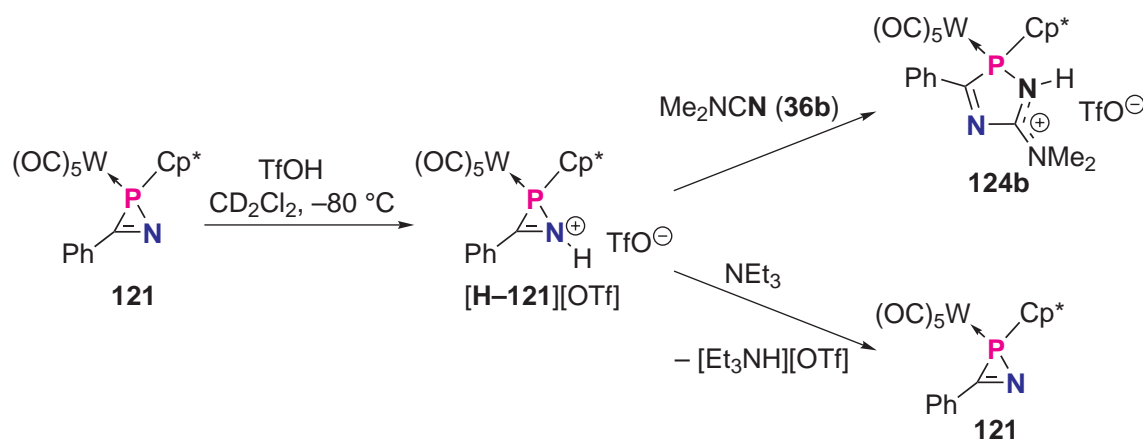
Scheme 8.10: *Consecutive* reaction of $2H$-azaphosphirene complex **121** with TfOH and nitrile **36b**, and deprotonation of complex [**H**–**121**][OTf] with NEt$_3$.

The mechanism of the acid-induced ring expansion of $2H$-azaphosphirene complexes with nitriles and isonitriles was elucidated by DFT calculations on C,P-dimethyl substituted model system **91** (Scheme 8.11). This revealed that upon N-protonation of **91** complex [**H**–**91**][OTf] is prone to undergo spontaneous ring opening with formation of phosphenium complex [**175**][OTf]. The following nucleophilic attack of nitriles **36m,p** at the phosphorus center of [**175**][OTf] is a barrierless process. Intermediates [**176m,p**][OTf] can subsequently undergo facile cyclization. In principle the same reaction pathways are possible for acid-induced ring expansion with the electron-poor nitrile derivative NCCN as for MeCN and H$_2$NCN (though the barrier is significantly higher). This is in marked contrast to the respective SET-induced reactions.
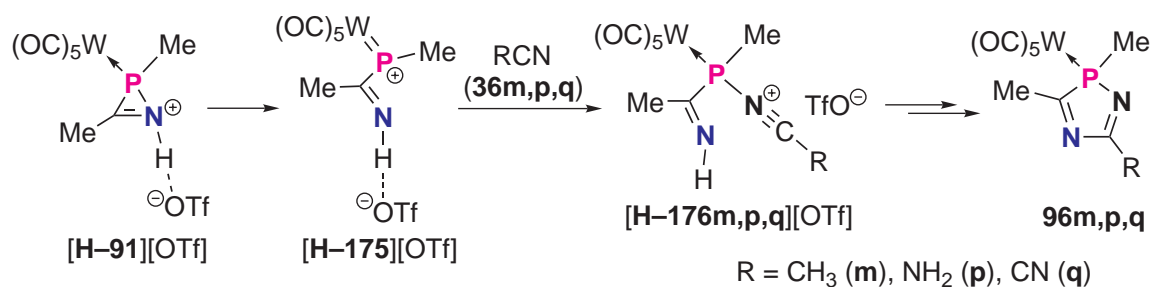
Scheme 8.11: Mechanism of the acid-induced ring expansion of 2H-azaphosphirene complexes.

In Chapter 5 investigations on the photophysical properties of neutral and protonated 2H-1,4,2-diazaphosphole complexes are presented. All derivatives show an absorption band at very long wavelength. This gives rise to remarkably long wave optical end absorptions. The experimental observations were interpreted on the basis of time-dependent DFT calclulations, which revealed that the lowest-lying transition is assigned to a metal−ligand charge transfer (MLCT) process occurring from the metal d orbital HOMO−1 into the LUMO (Fig. 8.3). The latter is a π^* orbital, which is in complex **126g** extended over all three coplanar rings. The most intense $\pi-\pi^*$ transition occurs from HOMO−4.
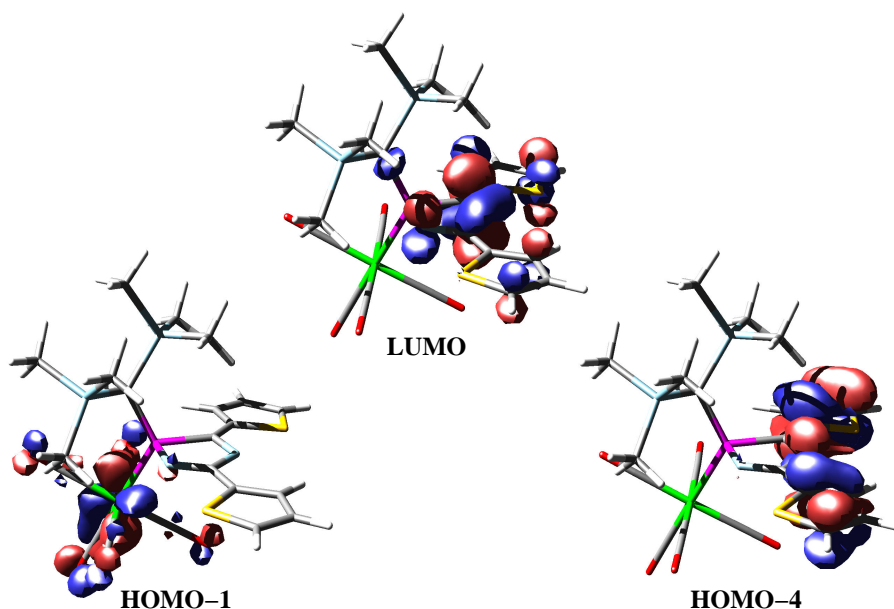
Figure 8.3: Visualization of calculated molecular orbitals of complex **126g**.

The investigations further revealed that the longest-wavelength absorption in the spectra of the mixtures of **41h** and **129h** as well as **126h** and **131h** result from MLCT excitations of the respective κN-coordinated isomers **129h**, **131h**.

The MLCT absorptions of *N*-protonated 2*H*-1,4,2-diazaphosphole complexes **123b** and **124b** are at even longer wavelengths, which causes very intense colors of their salts. TD-DFT calculations revealed that this phenomenon is a result of a pronounced decrease of the LUMO energy upon protonation, while the metal-centered orbitals are less affected.

In Chapter 6 a new strategy for the synthesis of *N*-heterocyclic carbenes with phosphorus in the backbone was outlined and examined. In the reaction of complexes **41h** and **129h** with methyl triflate and triflic acid methylation of the N^4-center was observed (Scheme 8.12, i). At the same time partial desilylation occurred at the exocyclic *P*-substituent. Both trimethylsilyl groups of complexes **126h** and **131h** could be removed via reaction with tetra-*n*-butylammonium fluoride in the presence of triethylammonium triflate (ii). This afforded *P*-methyl substituted 2*H*-1,4,2-diazaphosphole complex **190**.
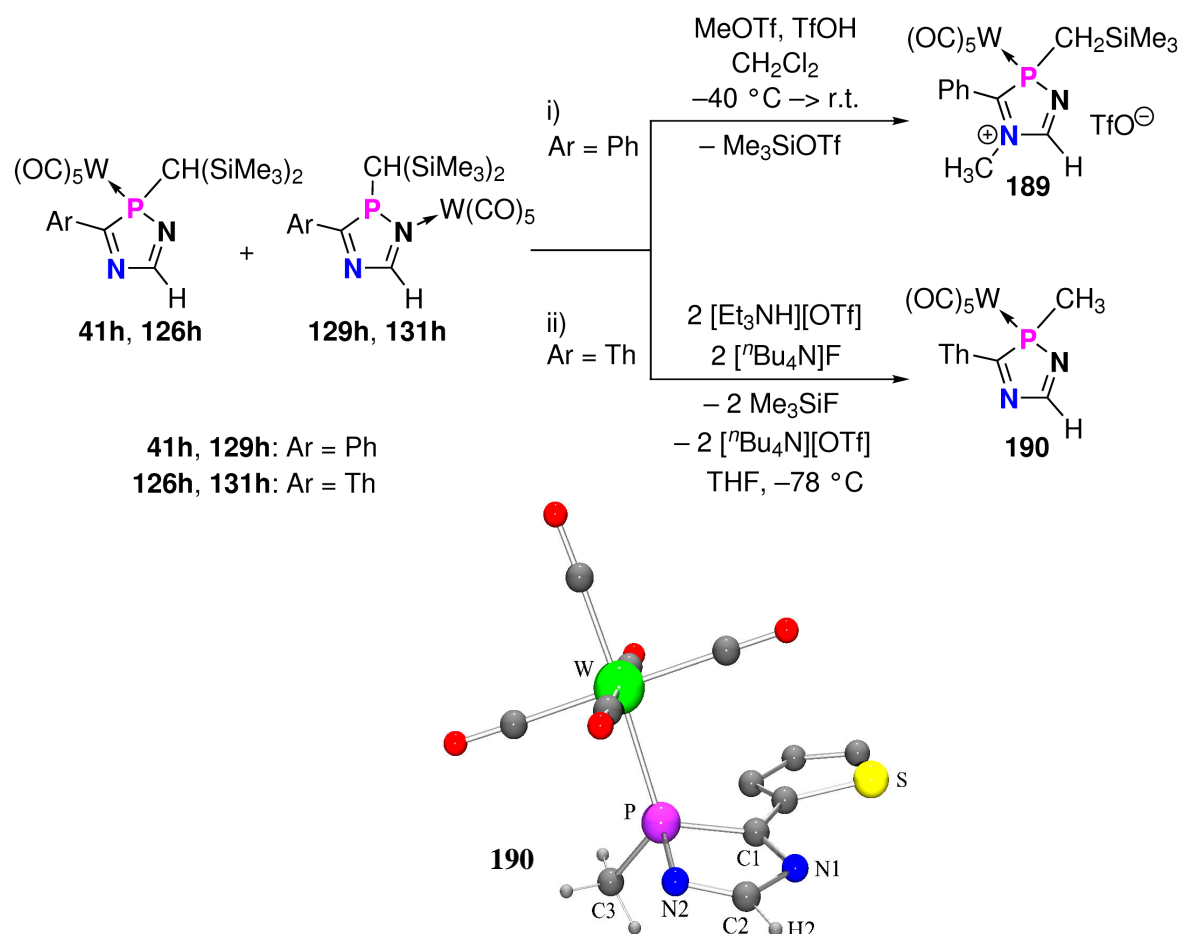
Scheme 8.12: Reaction of 2*H*-1,4,2-diazaphosphole complexes **41h**, **129h** with MeOTf in the presence of TfOH, and desilylation of complexes **126h**, **131h** (Th = 2-thienyl); molecular structure of complex **190** in the crystal (hydrogen atoms omitted for clarity).

In Chapter 7 the synthesis of 1,1'-ferrocenediyl-bridged bis-2H-azaphosphirene complexes **202a,b** is presented. From the reaction of bis(aminocarbene) complex **199** with chloro(methylene)phosphane **194** in the presence of triethylamine dinuclear complex **201** was obtained (Fig. 8.4), which features one 2H-azaphosphirene and one aminocarbene complex unit.

When complex **199** was reacted with one equivalent of **194** and NEt$_3$ in a dilute methylene chloride solution (Scheme 8.13) selective formation of ferrocenophane complex **205** was observed. Complex **205** was isolated in good yield and structurally confirmed (Fig. 8.4). Reaction of **205** with **194** and NEt$_3$ in a more concentrated solution (Scheme 8.13) yielded a mixture of **202a,b** and 2,3-dihydro-1,2,3-azadiphosphete complex **207** (Fig. 8.4). The latter could be separated via soxhlet extraction, and by subsequent low-temperature column chromatography a purified mixture of the diastereomeric 1,1'-ferrocenediyl-bridged bis-2H-azaphosphirene complexes **202a,b** was obtained, though the yield was only about 14 %.
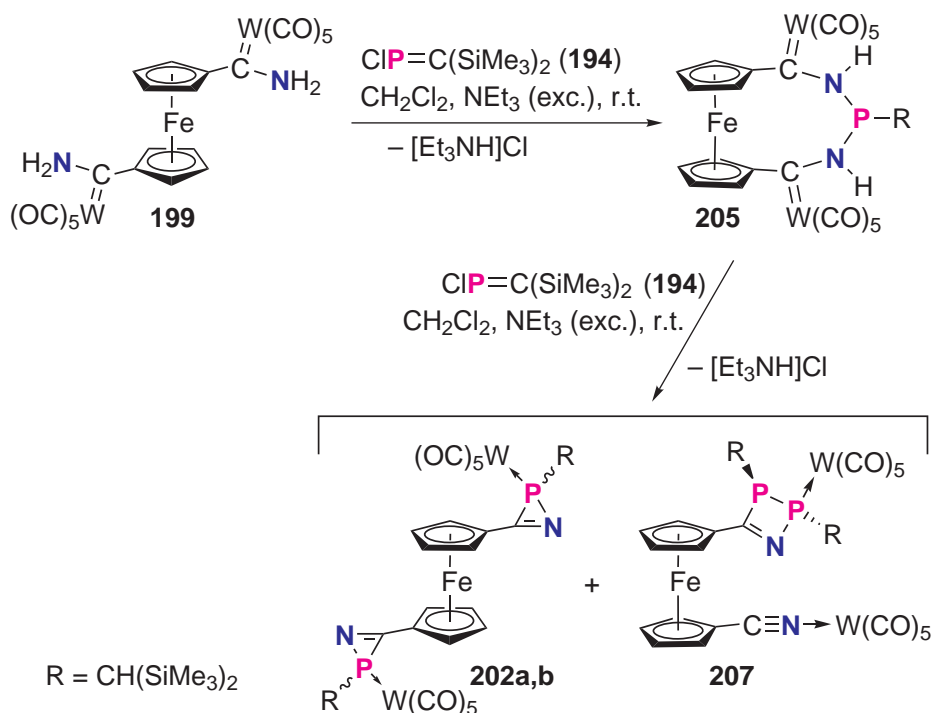
Scheme 8.13: Synthesis of ferrocenophane complex **205**, bis-2H-azaphosphirene complexes **202a,b**, and 2,3-dihydro-1,2,3-azadiphosphete complex **207**.
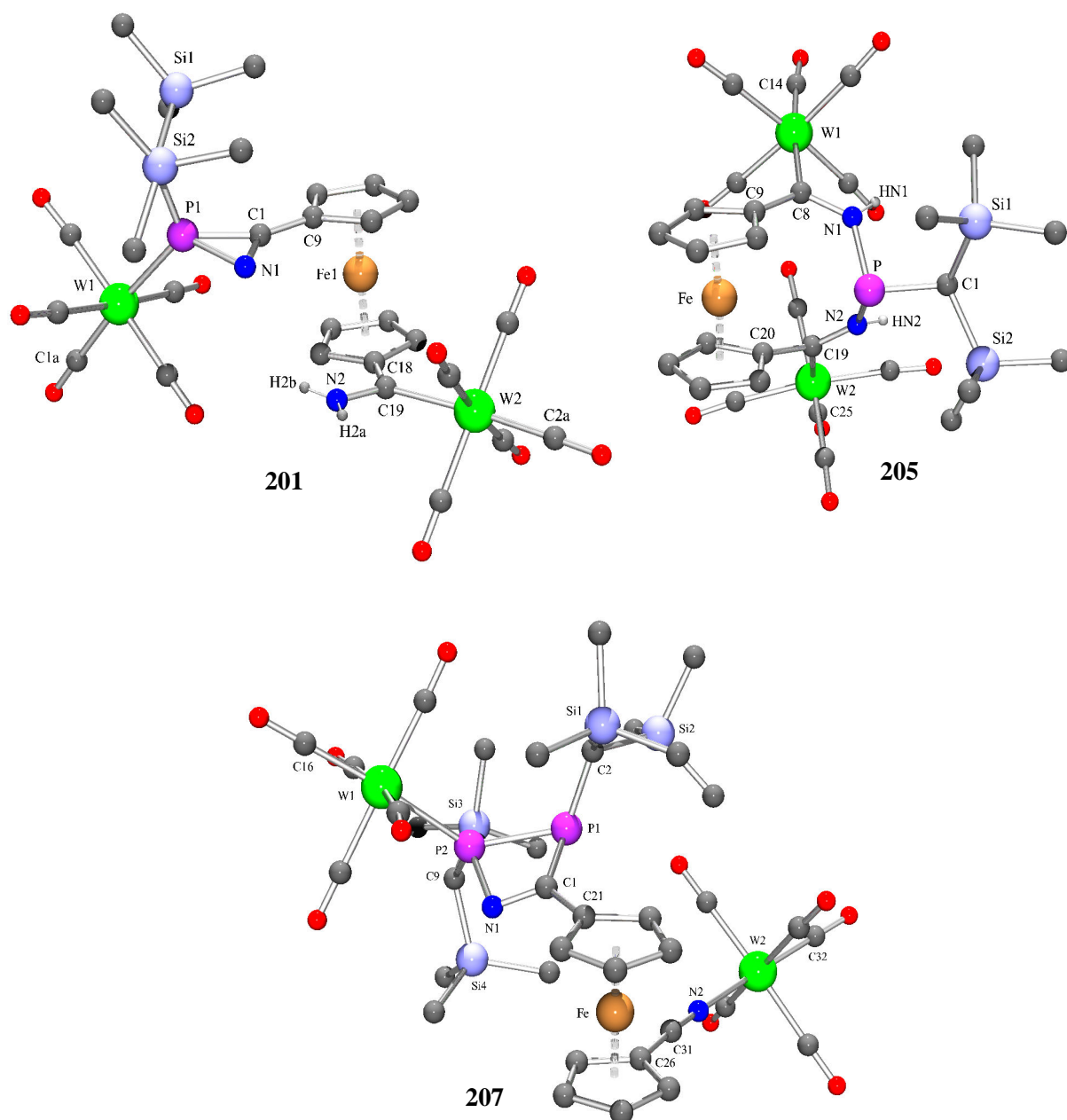
Figure 8.4: Molecular structures of complexes **201**, **205**, and **207** in the crystal (hydrogen atoms omitted for clarity).

Chapter 9

Theoretical Background of Computational Methods

9.1 Density Functional Theory

The basis for Density Functional Theory (DFT) is the *proof by Hohenberg and Kohn*[327] that there exists a one-to-one correspondence between the ground state electron density $\rho(\mathbf{r})$ of a system and the external potential of the electrons. Except for a phase factor, the wave function $\Psi(\mathbf{r})$ is completely determined by $\rho(\mathbf{r})$.

$$\Psi(\mathbf{r}) \leftrightarrow v(\mathbf{r}) \leftrightarrow \rho(\mathbf{r}). \tag{9.1}$$

Then, the external potential can be expressed as functional depending on the density:

$$v = v[\rho(\mathbf{r})]. \tag{9.2}$$

For unperturbed molecular systems the external potential corresponds to the electrostatic attraction by the nuclei. Since the potential $v[\rho(\mathbf{r})]$, which is determined by the density, can be used in the Schrödinger equation, all eigenfunctions of the Hamilton operator − ground and excited state wave functions − can be expressed as functional of the ground state density:

$$\Psi_k = \Psi_k[\rho(\mathbf{r})]. \tag{9.3}$$

Consequently, the expectation values of Hermitian operators, and hence, all observable variables, are functionals of the ground state electron density, for instance, the

electronic energy:

$$
\begin{aligned}
E_\nu^{el}[\rho(\mathbf{r})] &= \left\langle \psi_\nu^{el} \left| \hat{T}_e + \hat{V}_{ee} + \hat{V}_{Ke} \right| \psi_\nu^{el} \right\rangle \\
&= T_e^{(\nu)}[\rho(\mathbf{r})] + V_{ee}^{(\nu)}[\rho(\mathbf{r})] + \int \rho(\mathbf{r})\, v[\rho(\mathbf{r})]\, d\mathbf{r}.
\end{aligned}
\tag{9.4}
$$

On the basis of the *Kohn-Sham formalism*[328] a hypothetical system of non-interacting electrons ($V_{ee}[\rho(\mathbf{r})] = 0$) is introduced whose external potential $v_S[\rho(\mathbf{r})]$ is adjusted in such way that the same density is obtained as for the real system. The corresponding Hamilton operator is represented as sum of one-particle operators:

$$
\hat{H} = \sum_{a=1}^{n} \left(-\frac{1}{2}\hat{\Delta}_a + v_S(\mathbf{r}_a) \right) = \sum_{a=1}^{n} \hat{h}_s(\mathbf{r}_a).
\tag{9.5}
$$

The potential $v_S(\mathbf{r}_a)$ can be obtained from the ground state electron density:

$$
v_S(\mathbf{r}_a) = v_S[\rho(\mathbf{r})].
\tag{9.6}
$$

The eigenfunctions $\phi_a(\mathbf{r}_a)$ of the one-particle operators $\hat{h}_s(\mathbf{r}_a)$ (Eq. (9.7)) are the *Kohn-Sham orbitals*. Their eigenvalues have the meaning of orbital energies ϵ_a (Eq. (9.7)).

$$
\hat{h}_s(\mathbf{r}_a)\phi_a(\mathbf{r}_a) = \epsilon_a \phi_a(\mathbf{r}_a).
\tag{9.7}
$$

The total electronic energy $E_S[\rho(\mathbf{r})]$ of the non-interacting system,

$$
E_S[\rho(\mathbf{r})] = T_S[\rho(\mathbf{r})] + \int v_S[\rho(\mathbf{r})]\, \rho(\mathbf{r})\, d\mathbf{r},
\tag{9.8}
$$

with the kinetic energy functional,

$$
T_S[\rho(\mathbf{r})] = \sum_{a=1}^{n} \left\langle \phi_a[\rho(\mathbf{r})] \left| -\frac{1}{2}\Delta \right| \phi_a[\rho(\mathbf{r})] \right\rangle,
\tag{9.9}
$$

is then the sum of the n lowest orbital energies ϵ_a. Within Kohn-Sham formalism the kinetic energy is calculated under the assumption of non-interacting electrons from Eq. (9.9), and the remaining kinetic energy that arises from electron-correlation is absorbed into an *exchange-correlation term* $E_{xc}[\rho(\mathbf{r})]$ (Eq. (9.10)) together with the exchange contribution. The Coulomb part $J[\rho(\mathbf{r})]$ of the electron-electron interaction as well as the interaction with the nuclei $V_{Ke}[\rho(\mathbf{r})]$ are treated classically. Overall, the

general DFT energy expression can be written as:

$$E_{DFT}[\rho(\mathbf{r})] = T_S[\rho(\mathbf{r})] + V_{Ke}[\rho(\mathbf{r})] + J[\rho(\mathbf{r})] + E_{xc}[\rho(\mathbf{r})]. \tag{9.10}$$

If the exact $E_{xc}[\rho(\mathbf{r})]$ was known, $E_{DFT}[\rho(\mathbf{r})]$ would provide the exact total energy for any given system, including electron correlation. Since this is not the case, different approaches to parameterize $E_{DFT}[\rho(\mathbf{r})]$ have been developed, some of which are discussed in the following.

It is customary to separate $E_{xc}[\rho(\mathbf{r})]$ into two parts, a pure exchange $E_x[\rho(\mathbf{r})]$ and a correlation part $E_c[\rho(\mathbf{r})]$:

$$E_{xc}[\rho(\mathbf{r})] = E_x[\rho(\mathbf{r})] + E_c[\rho(\mathbf{r})]. \tag{9.11}$$

So, the two contributions can be treated separately, and the different approaches for each part can be combined in various ways.

The *Local Density Approximation* (LDA)[328] is based on the assumption that the density locally can be treated as a uniform electron gas, thus, it can be described by a slowly varying function. For the calculation of the exchange energy the Dirac formula[329, 330] is used, which is also implemented in the *Thomas-Fermi-Dirac* (TFD) theory.[331] A generalization of this approach is known as the *Local Spin Density Approximation* (LSDA), which can be applied also for systems with different α- and β-spin densities. The L(S)DA exchange functional is often combined with the *VWN correlation functional* by Vosko, Wilk und Nusair,[208] which bases on the results of a very accurate determination of the correlation energy of the uniform electron gas for different densities using Monte Carlo methods.[332, 333] In general, the L(S)DA approximation underestimates the exchange energy by about 10 %, and the correlation energy, which averages ca. 10 % of the exchange contribution, is overestimated, often by a factor close to 2.[334] In summary, the exchange-correlation energy is overestimated by about 7 %. Furthermore, the L(S)DA approximation cannot reproduce the correct asymptotic behavior for the exchange-correlation energy density, which decays with 1/r for large values of r. As a consequence, bond strengths are typically overestimated.

A significant improvement is provided by *General Gradient Approximation* (GGA) methods. The influence of inhomogenities in the electron density is captured by taking into account the dependance of the exchange and the correlation energy not only on the density but also on its gradient. Examples for gradient corrected exchange functionals are the *PW86 functional* by Perdew and Wang[335] and Becke's *B88 functional*,[209] which has the correct asymptotic behavior for the energy density (but not for the exchange potential).[336]

In 1986, Perdew proposed a gradient correction for the correlation contribution that is known as $P86$[210,337] and was modified by Perdew and Wang in 1991 ($PW91$).[338] Another correlation functional was developed by Lee, Yang, and Parr (LYP) that is not based on a correction to the L(S)DA but on calculations of the correlation energy in the helium atom by Colle and Salvetti.[339]

So-called *hybrid methods* are frequently employed, which use appropriate combinations of different functionals and a certain fraction of "exact" (Hartree-Fock) exchange. One example is the *Becke 3 Parameter Functional* (B3):[230,231]

$$E_{xc}^{B3} = a\,E_x^{L(S)DA} + (1-a)\,E_x^{KS} + \Delta E_x^{B88} + c\,E_c^{L(S)DA} + (1-c)\,\Delta E_c^{GGA}. \quad (9.12)$$

The term E_x^{KS} conforms to the Hartree-Fock exchange, with the difference that Kohn-Sham orbitals are employed, here.

A *double-hybrid density functional* (DHDF), termed *B2PLYP*, that adds a non-local perturbation correction for the correlation part (in addition to a non-local exchange contribution) to a standard hybrid functional was recently developed by Grimme.[340] He further proposed an empirical dispersion term (DFT-D) including damped atom-pairwise dispersion corrections of the form $C^6 \cdot R^{-6}$.[340,341] It was demonstrated[342] that B2PLYP is also applicable to electronically excited states in the framework of *Time-Dependent Density Functional Theory* (TD-DFT)[294,295] or the closely related *Tamm-Dancoff Approximation* (TDA-DFT).[343] Using this functional the *self-interaction error* (i.e., the unphysical interaction of an electron with itself) is considerably reduced compared to local GGA functionals and widely used hybrid functionals such as B3LYP.[342] Recently, Truhlar presented the so-called *M05-class* and *M06-class* functionals, whereby shortcomings such as the inaccuracy in the evaluation of medium-range correlation energies and the self-interaction error are significantly reduced.[344]

In DFT, the variational principle is used for optimization of the molecular orbitals; the variation is carried out with respect to the electron density.[345,346] For the effective potential $v_S(\mathbf{r})$ the following expression results:

$$v_S[\rho(\mathbf{r})] = v[\rho(\mathbf{r})] + \int \frac{\rho(\mathbf{r}')}{|\mathbf{r} - \mathbf{r}'|}\,d\mathbf{r}' + V_{xc}[\rho(\mathbf{r})],$$

$$\text{with} \quad V_{xc}[\rho(\mathbf{r})] := \frac{\delta}{\delta\rho(\mathbf{r})} E_{xc}[\rho(\mathbf{r})]. \quad (9.13)$$

The ground state electron density of the real system, which results from the variational

procedure, corresponds to the electron density

$$\rho(\mathbf{r}) = \sum_{a=1}^{n} |\phi_a(\mathbf{r})|^2 \tag{9.14}$$

that is obtained from the solution of Eq. (9.7) with the effective potential (Eq. (9.13)) of the interacting system. Eqs. (9.7) and (9.13) are called *Kohn-Sham equations*. Upon the introduction of a basis set of spatial molecular orbitals, the Kohn-Sham equations are transformed into a linear system of equations:

$$\mathbf{h}_{\text{KS}}\mathbf{C} = \mathbf{S}\mathbf{C}\boldsymbol{\epsilon}. \tag{9.15}$$

9.2 Resolution of the Identity

The evaluation of two-electron-four-center integrals arising in Coulomb and exchange terms is a very time consuming part of electronic structure calculations.[347] By the use of the *Resolution of the Identity* (RI) approximation these integrals can be transformed into significantly simpler three- and two-center integrals, which results in a substantial reduction of computation time. This approach was first employed in DFT for methods that use pure GGA functionals (Section 9.1), for simplification of the Coulomb integrals.[211] In such methods the exchange term is evaluated as density functional[1]. Without the use of the RI approximation the determination of the Coulomb part requires the calculation of two-electron-four-center integrals of the basis functions[2]:

$$J[\rho(\mathbf{r})] = \frac{1}{2} \int \int \frac{\rho(\mathbf{r})\rho(\mathbf{r}')}{|\mathbf{r} - \mathbf{r}'|} \, d\mathbf{r} \, d\mathbf{r}' \equiv \frac{1}{2} \sum_{\mu\nu} \sum_{\kappa\lambda} P_{\mu\nu} P_{\kappa\lambda} \left(\mu\nu|\kappa\lambda\right). \tag{9.16}$$

In the framework of the RI approximation the electron density is expanded into an atom-centered auxiliary basis set:

$$\rho(\mathbf{r}) \approx \sum_{\alpha} C_\alpha g_\alpha(\mathbf{r}) = \tilde{\rho}(\mathbf{r}). \tag{9.17}$$

Hypothetically, the exact density $\rho(\mathbf{r})$ could be captured, if a complete basis was used. In order to determine the coefficients C_α (Eq. (9.17)) of a finite basis set $\{g_\alpha\}$, according to a method by Almlöf et al.,[348] the Coulomb functional of two difference densities $(\rho(\mathbf{r}) - \tilde{\rho}(\mathbf{r}))$ are minimized using the variational principle. This procedure

---

[1]This does not hold for the use of hybrid functionals, where the exchange energy is partly determined from Kohn-Sham orbitals.

[2]The *chemists' notation* is applied.

gives the following expression for the Coulomb energy:

$$J[\tilde{\rho}(\mathbf{r})] = \frac{1}{2} \sum_{\alpha\beta} \sum_{\mu\nu} \sum_{\kappa\lambda} P_{\mu\nu} P_{\kappa\lambda} (\mu\nu|\alpha)(\alpha|\beta)^{-1}(\beta|\kappa\lambda). \qquad (9.18)$$

The computation time for the evaluation of the Coulomb energy from Eq. (9.16) scales with the $4th$ power of the number N of basis functions. By employment of the RI approximation (Eq. (9.18)) the slope goes only with N^3.[347]

The RI approximation has been implemented for other quantum chemical methods as well, for example, for Hartree Fock,[348, 349] MP2,[350, 351] MCSCF,[352] and for CCSD[353] for the calculation of both Coulomb and exchange integrals.[354]

9.3   Implicit Solvation Models

Most chemical reactions being of technical and biological relevance take place in condensed phases, especially in liquid solutions. The influence of the solvent on equilibria, reaction barriers, and mechanisms, particularly for ionic reactions as discussed in this work, plays an important role, and thus, it cannot be neglected in theoretical investigations.[355, 356]

One common approach uses an explicit treatment of some solvent molecules. Due to the strong and long-range electrostatic forces that dominate many solvation phenomena,[357] it is not sufficient to consider just a few molecules in the closest proximity of the solute, rather a large quantity must be included in the model. This causes an enormous increase of computation time. For example, the explicit treatment of 200 molecules of methylene chloride adds 3000 degrees of freedom. Observable structural and dynamical properties of a solute must be averaged over these degrees of freedom, typically by *Monte Carlo*[358] or *Molecular Dynamics* (MD) techniques.[357, 359, 360]

An approach that yields accurate results in acceptable time periods deals with an implicit treatment of the solvent. Such methods are based on the physical picture, wherein the solute $\mathcal{M}$ is embedded in a solvent cavity, surrounded by a continuous medium that is exclusively characterized by its macroscopic properties. So, the averaging of the properties of single solvent molecules becomes implicit in the properties of the continuous medium.[357] In the following section the main principles of the implicit solvent models, which were employed in this work, are described briefly.

According to the definition of Ben-Naim,[361] the solvation process for a solute $\mathcal{M}$ in a solvent $\mathcal{S}$ consists of transferring $\mathcal{M}$ from a fixed position in the ideal gaseous phase

to a fixed position in $\mathcal{S}$, at constant temperature, pressure, and chemical composition. This process is accompanied by a constraint in the solutes freedom of movement, and the Gibbs free energy of solvation reads:

$$\Delta G_{sol} = \Delta G_{MS} + RTln\left(\frac{q_{rot,g} \cdot q_{vib,g}}{q_{rot,s} \cdot q_{vib,s}}\right) - RTln\left(\frac{n_{M,g} \cdot \Lambda_{M,g}^3}{n_{M,s} \cdot \Lambda_{M,s}^3}\right) + p\Delta V. \quad (9.19)$$

Here, $q_{rot,g}, q_{vib,g}, q_{vib,s}$, and $q_{rot,s}$ denote the microscopic partition functions for rotation and vibration of $\mathcal{M}$ in gas phase and in solution, respectively, $n_{M,g}$ and $n_{M,s}$ are the numeral densities of $\mathcal{M}$ molecules, and $\Lambda_{M,s}$ and $\Lambda_{M,s}$ are the momentum partition functions in the respective phase. The third term can be reduced to a logarithm of the ratio of the volumes that are accessible in the gase phase and in solution: $RT\,ln(V_g/V_s)$.[362] The contribution of the pressure-volume work, $p\Delta V$, is usually less than 10^{-3} kcal/mol, and thus may be neglected as an appropriate approximation.[362]

The *coupling work* of $\mathcal{M}$ and $\mathcal{S}$ can be divided into four contributions:[362]

$$\Delta G_{MS} = \Delta G_{cav} + \Delta G_{el} + \Delta G_{dis} + \Delta G_{rep}. \quad (9.20)$$

ΔG_{cav} corresponds to the work spent in forming a cavity of appropriate shape and volume for the molecule inside the liquid. During this hypothetical process no solute−solvent interactions take place. In consequence, ΔG_{cav} yields a contribution to the free energy of solvation but has no effect on the total energy of the solute, hence, it cannot be included into the quantum description of $\mathcal{M}$. The stabilization of the dilution state of a system is mainly effected by electrostatic interactions (ΔG_{el}) with the solvent. This contribution can be captured by inclusion into the quantum description of $\mathcal{M}$. The two final terms of Eq. (9.20) are effected by the dynamic correlation of the electron shell of $\mathcal{M}$ and the electrons of single solvent molecules on the cavity surface. Dispersion interactions (ΔG_{dis}) contribute to energy stabilization. The origin of the repulsion term (ΔG_{rep}) is the exponential decay of the electron density at large distance to the nuclei of $\mathcal{M}$ with a finite probability distribution in the region of the continuum, yielding a repulsive interaction with the electrons of solvent molecules.

In most implicit solvent models the cavity features a sharp border between the solute $\mathcal{M}$ and the continuous medium. The methods used in this work define the cavity by atom-centered, interlocking spheres, whose size is given by their van der Waals radii, multiplied by a correction factor f. A popular set of reference atomic radii is that of Bondi,[215] obtained from crystallographic data. Miertuš, Scrocco, and Tomasi[363] have proposed a correction factor of $f = 1.2$ for neutral molecules, which was confirmed by a comparison of PCM (Polarizable Continuum Model) calculations with Monte Carlo simulations.[362]

9.3.1   Electrostatic Interactions

The electrostatic models presented in this section apply for homogenous, isotropic so-
lutions at infinite dilution. It is assumed that at every given point inside the continuum
the polarization depends linearly on the strength of an external electrical field. Ac-
cordingly, the medium is characterized by a static, scalar field of the dielectric constant
$\varepsilon(\mathbf{r})$:

$$\varepsilon(\mathbf{r}) = \begin{cases} 1, & \mathbf{r} \in \Omega_i \\ \varepsilon, & \mathbf{r} \in \Omega_e, \end{cases} \tag{9.21}$$

where Ω_i and Ω_e denote the regions inside and outside the cavity, respectively; Ω_e
extends to infinity. The charge distribution ρ_M of the solute $\mathcal{M}$ is supposed to be
confined inside the cavity. With these assumptions the total electrostatic potential Φ
is defined by the *Poisson* (Eq. (9.22)) and the *Laplace equations* (Eq. (9.23)).

$$\Delta\Phi(\mathbf{r}) = -4\pi\rho_M(\mathbf{r}), \quad \mathbf{r} \in \Omega_i. \tag{9.22}$$

$$\Delta\Phi(\mathbf{r}) = 0, \qquad\qquad \mathbf{r} \in \Omega_e. \tag{9.23}$$

The electrostatic potential must fulfill the following boundary conditions: a continuous
trend on the surface,

$$\Phi_i = \Phi_e, \tag{9.24}$$

and the normal components of the electric displacement field must coincide on the
cavity surface:

$$\frac{\partial\Phi_i}{\partial n} = \varepsilon\frac{\partial\Phi_e}{\partial n}. \tag{9.25}$$

The coordinate n is directed according to the normal of the cavity surface, $\mathbf{n}$, pointing
outwards.

The electrostatic potential $\Phi(\mathbf{r})$ around a charge distribution ρ_M differs from that in
vacuo due to polarization of the surrounding medium. In turn, the charge distribution
is effected by the reaction field created by this medium, $\Phi_\sigma(\mathbf{r})$. In a classical model
where the charge distribution is limited to the volume inside the cavity the electrostatic
interaction energy is:

$$W_{MS} = \int_{\Omega_i} \rho_M(\mathbf{r})\Phi_\sigma(\mathbf{r})\,d\mathbf{r}. \tag{9.26}$$

The reaction potential $\Phi_\sigma(\mathbf{r})$ can be described, everywhere in the space, in terms of an apparent charge distribution σ spread on the cavity surface. This method is called *Apparent Surface Charge* (ASC) approach.[362] The total potential field $\Phi(\mathbf{r})$ is composed of two contributions, one originating from the charge distribution $\rho_M(\mathbf{r})$ of the solute, and the reaction field created by the surface charges with the density $\sigma(\mathbf{s})$:

$$\Phi(\mathbf{r}) = \Phi_M(\mathbf{r}) + \Phi_\sigma(\mathbf{r}) = \int_{\Omega_{i+e}} \frac{\rho_M(\mathbf{r}')}{|\mathbf{r} - \mathbf{r}'|}\, d\mathbf{r}' + \int_\Sigma \frac{\sigma(\mathbf{s})}{|\mathbf{r} - \mathbf{s}|}\, d\mathbf{s}. \tag{9.27}$$

The surface charge distribution density can be expressed in terms of the difference of the components of the respective polarization vectors $\mathbf{P}_i$ and $\mathbf{P}_e$ perpendicular to the surface:

$$\sigma = -(\mathbf{P}_e - \mathbf{P}_i) \cdot \mathbf{n}. \tag{9.28}$$

The polarization $\mathbf{P}_j$ inside a medium j is connected with the gradient of the electrostatic potential, in other words, with the strength of the electric field inside this medium:

$$\mathbf{P}_j = -\frac{\varepsilon_j - 1}{4\pi} \vec{\nabla}\Phi = \frac{\varepsilon_j - 1}{4\pi}\,\mathbf{E}. \tag{9.29}$$

By insertion of the boundary conditions (Eqs. (9.24) and (9.25)) the surface charge density gives:

$$\sigma = \mathbf{P}_e \cdot \mathbf{n} = \frac{\varepsilon - 1}{4\pi}\vec{\nabla}\Phi_e \cdot \mathbf{n} = \frac{\varepsilon - 1}{4\pi\varepsilon}\vec{\nabla}\Phi_i \cdot \mathbf{n}. \tag{9.30}$$

A further additional condition is derived from the *Gauss theorem*, whereby the total apparent surface charge $\sigma(\mathbf{s})$ is connected to the embedded charge Q_M by the expression:

$$\int_\Sigma \sigma(\mathbf{s})\, d\mathbf{s} = -\frac{\varepsilon - 1}{\varepsilon}\, Q_M \tag{9.31}$$

Because a portion of ρ_M is generally spreading out the cavity, the surface charge density must be normalized according to Eq. (9.31).

In order to obtain a numerical solution of the implicit equations (9.30) and (9.27), the surface is divided into an appropriate number of surface elements a_k, called "*tesserae*", containing a constant charge q_k in the internal point $\boldsymbol{s}_k$:

$$q_k = a_k\sigma(\boldsymbol{s}_k), \tag{9.32}$$

so that the reaction potential is given by the sum of the contributions of each surface element:

$$\Phi_\sigma = \sum_k \frac{q_k}{|\mathbf{r} - \boldsymbol{s}_k|}. \tag{9.33}$$

This approach is called *Boundary Element Method* (BEM). There are different available methods to solve the BEM problem. The *Polarizable Continuum Model* (PCM) uses an iterative procedure,[363–366] and a different version uses a closure solution.[367] Hoshi et al. have presented a Green's function approach to the BEM problem,[367–373] which allows to express the apparent surface charge distribution $\sigma(\mathbf{s})$ as a linear function of the charge distribution $\rho_M(\mathbf{r})$. A further approach is based on the *Integral Equation Formalism* (IEF-PCM).[274–276]

The *Conductor-like Screening Model* (COSMO), which was employed in this work, is an ASC variant as well. It is based on the theory of screening in conductors.[214, 220, 374] Here, the polarizable continuum is modeled as electrical conductor. The advantage of this approach is due to the simpleness of its boundary conditions. Upon the surface Σ of an ideal conductor the electrostatic potential vanishes:

$$\Phi_\Sigma = 0. \tag{9.34}$$

The COSMO also uses a division of the cavity surface into small segments a_k with constant charges q_k. The electrostatic potential is generated by these charge elements and the charges Q_i of the solute $\mathcal{M}$:

$$\boldsymbol{\Phi}_\Sigma = \mathbf{B}\mathbf{Q} + \mathbf{A}\mathbf{q},$$

$$\text{with} \qquad B_{ik} = \frac{1}{a_k} \int_{a_k} \frac{1}{|\mathbf{r} - \mathbf{r}_i|}\, d\mathbf{r} \approx \frac{1}{|\mathbf{s}_k - \mathbf{r}_i|}\ ,$$

$$A_{kl} = \frac{1}{a_k a_l} \int_{a_k} \int_{a_l} \frac{1}{|\mathbf{r} - \mathbf{r}'|}\, d\mathbf{r}\, d\mathbf{r}' \approx \frac{1}{|\mathbf{s}_k - \mathbf{s}_l|} \qquad \text{and} \qquad A_{kk} \approx 1.07 \sqrt{\frac{4\pi}{a_k}}\ . \tag{9.35}$$

The condition (9.34) yields the conditional equation for the surface charges q_k:

$$\mathbf{q} = -\mathbf{A}^{-1}\mathbf{B}\mathbf{Q}, \tag{9.36}$$

and the total screening energy reads:

$$\Delta E = -\frac{1}{2}\mathbf{Q}^\dagger \mathbf{B}^\dagger \mathbf{A}^{-1}\mathbf{B}\mathbf{Q} = -\frac{1}{2}\mathbf{Q}^\dagger \mathbf{D}\mathbf{Q}. \tag{9.37}$$

Thus, the COSMO provides a Green's function solution to the BEM problem with rather simple expressions for the screening energy and its analytic gradient with respect to the solute coordinates, which makes geometry optimization of a solute $\mathcal{M}$ within a realistic dielectric continuum model become practicable. The expressions given above are exact for infinitely strong dielectrics ($\varepsilon = \infty$), thus, for conductors. Dielectric screening energies scale with a factor $f(\varepsilon) = (\varepsilon - 1)/(\varepsilon + x)$ (with $0 \leq x \leq 2$) that depends on the dielectric permittivity ε of the screening medium. Therefore, the COSMO scales the interaction energy (Eq. (9.37)) by the correction factor $f(\varepsilon)$.

9.3.2 The Effective Hamiltonian

If the solute $\mathcal{M}$ is calculated in terms of quantum mechanical techniques, the electrostatic interactions of $\mathcal{M}$ with the solvent can be covered by introduction of a perturbation operator, the interaction operator $\hat{V}_{int}$.[362] The electronic Hamiltonian $\hat{H}_M^{(0)}$ of $\mathcal{M}$ in vacuo is replaced by an effective Hamiltonian $\hat{H}_{eff}$ of $\mathcal{M}$ in solution:

$$\hat{H}_{eff}\,\psi(\mathbf{q}, \bar{\mathbf{Q}}) = \left(\hat{H}_M^{(0)} + \hat{V}_{int}\right)\psi(\mathbf{q}, \bar{\mathbf{Q}}) = E^{el}(\mathbf{Q})\psi(\mathbf{q}, \bar{\mathbf{Q}}), \qquad (9.38)$$

where the reaction field operator $\hat{V}_{int}$ in turn depends on the solution $\psi(\mathbf{q}, \bar{\mathbf{Q}})$ of Eq. (9.38). Its iterative solution is the so-called *Self-Consistent Reaction Field* (SCRF) procedure. Thereby, the appearance of the reaction field $\Phi_S(\mathbf{r})$ and the relaxation of the charge distribution of $\mathcal{M}$ in response to the reaction field result simultaneously upon energy optimization.

The solute$-$solvent interaction contribution to the total energy of $\mathcal{M}$ reads:

$$W_{MS} = \int_{\Omega_{i+e}} \psi^*(\mathbf{q}, \bar{\mathbf{Q}})\,\hat{V}_{int}\,\psi(\mathbf{q}, \bar{\mathbf{Q}})\,d\mathbf{q}_1 d\mathbf{q}_2 \cdots d\mathbf{q}_n = \int_{\Omega_{i+e}} \rho_M(\mathbf{r})\Phi_S(\mathbf{r})\,d\mathbf{r}. \quad (9.39)$$

The charge distribution $\rho_M(\mathbf{r})$ is composed of the discrete nuclear charge distribution $\rho_K(\mathbf{r})$ and the electron density function $\rho_e(\mathbf{r})$:

$$\rho_M(\mathbf{r}) \;=\; \rho_K(\mathbf{r}) + \rho_e(\mathbf{r}), \;\; \text{with}$$

$$\rho_K(\mathbf{r}) = \sum_{\alpha}^{N} Z_\alpha \delta(\mathbf{r} - \mathbf{Q}_\alpha) \quad \text{and} \quad \rho_e(\mathbf{r}) = -\int |\psi(\mathbf{q}, \bar{\mathbf{Q}})|^2\, d\mathbf{q}_2 \cdots d\mathbf{q}_n. \,(9.40)$$

Thus, the reaction field operator is given by:

$$\hat{V}_{int} = \sum_{\alpha}^{N} Z_\alpha \Phi_\sigma(\mathbf{Q}_\alpha) - \sum_{i}^{n} \Phi_\sigma(\mathbf{q}_i). \qquad (9.41)$$

The $\Phi_\sigma(\mathbf{Q}_\alpha)$ and $\Phi_\sigma(\mathbf{q}_i)$ are the values of the reaction potential at the location of nucleus α and electron i, respectively. The reaction potential is usually divided into two parts:

$$\Phi_S(\mathbf{r}) = \Phi_{S,K}(\mathbf{r}) + \Phi_{S,e}(\mathbf{r}). \tag{9.42}$$

Here, $\Phi_{\sigma,K}(\mathbf{r})$ is the contribution that is effected exclusively by the nuclei of $\mathcal{M}$, while $\Phi_{\sigma,e}(\mathbf{r})$ is generated by the electron distribution $\rho_e(\mathbf{r})$ of $\mathcal{M}$. The resulting expression for the interaction energy W_{MS} consists of four terms:

$$
\begin{aligned}
W_{MS} &= \int_{\Omega_{i+e}} [\rho_K(\mathbf{r}) + \rho_e(\mathbf{r})] \cdot [\Phi_{\sigma,K}(\mathbf{r}) + \Phi_{\sigma,e}(\mathbf{r})] \, d\mathbf{r} \\
&= W_{K,K} + W_{K,e} + W_{e,K} + W_{e,e} \, .
\end{aligned}
\tag{9.43}
$$

The energy $E^{el}(\mathbf{Q}) = E^{el(0)}(\mathbf{Q}) + W_{MS}$ from Eq. (9.38) corresponds to the work spent in assembling nuclei and electrons of the solute $\mathcal{M}$ in an already polarized dielectric. The electrostatic free energy that is hypothetically released through the assembly of $\mathcal{M}$ in a not pre-polarized medium is given as a functional of the wave function:[375]

$$
\begin{aligned}
\mathcal{G}[\psi] = E^{el(0)}(\mathbf{Q}) + \frac{1}{2} W_{MS} &= \left\langle \psi | \hat{H}_M^{(0)} | \psi \right\rangle + \frac{1}{2} \left\langle \psi | \hat{V}_{int} | \psi \right\rangle \\
&= E^{el}(\mathbf{Q}) - \frac{1}{2} W_{MS} \, .
\end{aligned}
\tag{9.44}
$$

Eq. (9.44) may be derived by the *charging parameter method* applied in electrostatics and statistical thermodynamics.[362,376–378] Here, an attenuated solute−solvent interaction potential is defined as the full potential $U(\mathbf{\Omega})$ multiplied by a parameter λ that ranges from 0 to 1 ($\mathbf{\Omega}$ denotes the collection of solvent coordinates), and the corresponding distribution function $g_S(\mathbf{\Omega}; \lambda)$ of solvent particles. Upon averaging over all solvent coordinates $\mathbf{\Omega}$ for W_{MS} is obtained:

$$W_{MS}(\lambda) = \int U(\mathbf{\Omega}) g_S(\mathbf{\Omega}; \lambda) \, d\mathbf{\Omega} \, . \tag{9.45}$$

This expression is equivalent to Eq. (9.43) if electrostatic interactions only are considered. The free energy change due to the building up of the solvent polarization in the presence of the solute $\mathcal{M}$ is then:

$$\Delta G_{el} = \int_0^1 W_{MS}(\lambda) \, d\lambda = \frac{1}{2} W_{MS} \tag{9.46}$$

because of the proportionality of the distribution function $g_S(\mathbf{\Omega}; \lambda)$ to the parameter λ for linear dielectrics.

Minimization of the free energy is done by applying the variational principle to the functional $\mathcal{G}[\psi]$.[368] For example, within the Hartree-Fock SCF the Fock matrix $\mathbf{F}^{(0)}$ of the system in the gaseous phase is replaced by:[220]

$$\mathbf{F}' = \mathbf{F}^{(0)} + \frac{1}{2}(\mathbf{j} + \mathbf{y}) + \mathbf{X}. \tag{9.47}$$

The one-electron terms $\mathbf{j}$ and $\mathbf{y}$ arise from the interaction of $\rho_K(\mathbf{r})$ with $\Phi_{\sigma,e}(\mathbf{r})$ and $\rho_e(\mathbf{r})$ with $\Phi_{\sigma,K}(\mathbf{r})$, respectively. Because of the interaction of $\rho_e(\mathbf{r})$ with $\Phi_{\sigma,e}(\mathbf{r})$ an additional two-electron term ($\mathbf{X}$) appears. In analogy, the SCRF method can by applied in density functional theory by modification of the Kohn-Sham operator.[220,379] The quantum mechanical treatment is not restricted to Hartree-Fock and DFT. SCRF calculations can be combined with different *ab initio*[362,380–391] and semi-empirical methods.[392]

The functional (9.44) contains only those parts of the free energy that depend on the wave function. Other contributions such as the interaction U_{KK} of $\rho_K(\mathbf{r})$ with $\Phi_{\sigma,K}(\mathbf{r})$, the repulsion of the nuclei V_{KK} as well as the sum of the non-electrostatic effects G_{nel} add to the free energy $\mathcal{G}[\psi]$. In summary, the free energy is:[220]

$$G = \left\langle \psi | \hat{H}_M^{(0)} | \psi \right\rangle + \frac{1}{2} \left\langle \psi | \hat{V}_{int} | \psi \right\rangle + \frac{1}{2} U_{KK} + V_{KK} + G_{nel}. \tag{9.48}$$

Chapter 10

Experimental Part

10.1 General Procedures

All operations were performed in an atmosphere of deoxygenated and dried argon (or nitrogen) (BTS catalyst (Merck) heated at $100-130\,°C$, phosphorus pentoxide, and silica gel) using standard Schlenk techniques with conventional glassware, which was evacuated, heated in vacuo, and filled with inert gas before usage. Solvents were dried according to procedures described in the literature[393] and stored in amber glass bottles under inert atmosphere over sodium wire or molecular sieves. Most products were purified by low-temperature column chromatography using chromatographic columns equipped with integrated cooling mantles cooled with a connected cryostat (cooling medium: ethanol, technical grade); in most cases retention factors were previously estimated by thin layer chromatography. In the description of experimental procedures the applied temperatures, the column dimensions (length $\times$ diameter), the solvent mixtures that were used as eluents, and the materials of the employed stationary phase are specified (i.e., silica gel 60, $60-200$ mesh (Merck), silanized silica gel 60, $60-200$ mesh (Merck), or neutral aluminum oxide (Merck)).

10.1.1 Analytical Methods

Melting points (or decomposition temperatures) were determined with a Büchi apparatus Type S; the values are not corrected.

  NMR data were recorded on a Bruker Avance 300 spectrometer (^{1}H: 300.13 MHz; ^{11}B: 96.3 MHz; ^{13}C: 75.5 MHz; ^{15}N: 30.4 MHz; ^{19}F: 282.4 MHz; ^{29}Si: 59.6 MHz; ^{31}P:

121.5 MHz) or a Bruker Avance 400 spectrometer (^{1}H: 400.13 MHz; ^{13}C: 100.6 MHz; ^{15}N: 40.5 MHz; ^{29}Si: 79.5 MHz; ^{31}P: 161.9 MHz) at 30 °C (if not otherwise denoted) using C_6D_6, $CDCl_3$, CD_2Cl_2, or CD_3CN as solvent and internal secondary standard; chemical shifts (δ) are referenced to external standards: tetramethylsilane (^{1}H, Ξ = 100.000000; ^{13}C, Ξ = 25.145020; ^{29}Si, Ξ = 19.867187 MHz), boron trifluoride diethyl etherate in $CDCl_3$ (^{11}B, Ξ = 132.083974 MHz), nitromethane (^{15}N, Ξ = 10.136767 MHz), trichlorofluoromethane (^{19}F, Ξ = 94.094011 MHz), and 85% H_3PO_4 (^{31}P, Ξ = 40.480742 MHz). The assignment of NMR signals was supported by ^{1}H gsCOSY as well as ^{1}H detected, pfg-selected 2D ^{1}H,X (X = ^{13}C, ^{15}N, ^{29}Si, ^{31}P) gsHSQC, gsHMQC, or gsHMBC measurements, and in the cases of complexes **169** and **170** by ^{1}H gsNOESY measurements. ^{15}N NMR data were obtained from ^{1}H detected, pfg-selected 2D ^{1}H,^{15}N gsHMQC or gsHMBC measurements. ^{31}P{^{1}H} NMR (and in some cases ^{19}F{^{1}H} or ^{1}H NMR) spectroscopic reaction monitoring was carried out to follow reaction progressions, and signal integration was used to estimate product shares (%) of reaction mixtures. Magnitudes of coupling constants are abbreviated as $|^xJ_{AB}|$, where A and B denote the coupling nuclei (nuclear number omitted; ordered by decreasing atomic number), and x denotes the number of bonds that separate A and B (for further abbreviations see Appendix A); only absolute values were determined.

FAB-mass spectra (positive mode) were recorded on a Kratos Concept 1H spectrometer using *meta*-nitrobenzyl alcohol (*m*NBA) as matrix, and EI-mass spectra were recorded on a MAT 95 XL Finnigan (70 eV) spectrometer; apart from m/z values of the molecular ions, only m/z values having intensities of at least 10 % are given.[1] A Bruker Daltonik autoflex II TOF/TOF spectrometer was used to record MALDI-mass spectra (positive mode); only m/z values of the molecular ions are given. ESI-mass spectra (positive mode) and ESI tandem mass spectra were recorded on a Bruker APEX IV Fourier transform ion cyclotron resonance (FT-ICR) mass spectrometer equipped with an Apollo ESI source (selected data given). For MS/MS, collision-induced dissociation (CID) spectra were measured after mass-selection of the respective ion; argon was used as collision gas. Furthermore, some ESI-mass spectra were recorded on a Bruker Daltonik micrOTOF-Q spectrometer (selected data given). Assignments of ionic molecule fragments based on plausibilty and on the observed isotopic distributions; the given m/z values refer in each case to the most intense peak according to the combination of elements each with the highest abundance.

UV/Vis spectra were recorded on a Shimadzu UV-1650 PC spectrometer (λ = 190$-$1100 nm) from *n*-pentane or CH_2Cl_2 solutions in quartz glass cells from the company Hellma with an optical path length of 1 cm at ambient temperature. Molar

---

[1]In some exceptional cases (complexes **41b,g** and **69b**) additionally the values of other characteristic fragments detected at lower intensities are given.

absorbance coefficients (ϵ) at the maximum wavelengths (λ_{max}) were determined in some cases; otherwise, spectral absorbances are given.

Infrared spectra were recorded on a Thermo Nicolet 380 FT-IR or (in the case of complex **41t**) a Bruker FT-IR IFS113V spectrometer as KBr pellets, as nujol mull preparation, or in CH_2Cl_2 solution at ambient temperature (selected data given).

Raman spectra were recorded with a Bruker FT RFS 100 Raman spectrometer with a Nd:YAG laser (excitation wavelength: $\lambda = 1064$ nm) in backscattering (180°) geometry (5 mm aperture); in each measurement 1000 scans were collected.

Elemental analyses were performed using an Elementar VarioEL instrument or (in the cases of complexes **123b,m**) an instrument run by the company Pascher (Remagen-Bandorf); the mean values of two or three independant measurements are given in each case.

Single-crystal X-ray diffraction data were recorded on a Nonius KappaCCD diffractometer[394] equipped with a low-temperature device (Cryostream, Oxford Cryosystems) using graphite monochromated Mo-K_α radiation ($\lambda = 0.71073$ Å). The structures were solved by Patterson methods or Direct Methods (SHELXS-97)[395, 396] and refined by full-matrix least squares on F^2 (SHELXL-97).[396, 397] All non-hydrogens were refined anisotropically. Hydrogen atoms were included isotropically using the riding model on the bound atoms; in some (denoted) cases hydrogen atoms were located in the Fourier difference electron density. Absorption corrections were carried out analytically or semi-empirically from equivalents.

Cyclic voltammetric measurements were performed with an EG&G Potentiostat/Galvanostat M273 in CH_2Cl_2 at a glassy carbon electrode (GCE) with $[^nBu_4N][PF_6]$ (0.1 M) as supporting electrolyte against an AgCl/Ag reference electrode (2 M LiCl in EtOH) and Pt-wire as counter electrode at 25 °C; scan rates were varied between 0.01 and 10 V $\cdot$ s^{-1}. Half cell potentials ($E_{1/2}$) are given in V vs. $E_{1/2}([FeCp_2]^+/[FeCp_2])$ and were determined at a scan rates of 0.1 V $\cdot$ s^{-1}.

10.1.2 Purchased Reagents and Solvents

The following reagents and solvents were purchased and in some cases purified before usage:

Acetic acid (Merck); acetone (Biesterfeld); acetonitrile (Merck); $[D_3]$acetonitrile (Euriso-Top); 1-adamantanecarbonitrile (Acros); aluminum oxide neutral (Merck); ammonia (PraxAir); ammonium hexafluorophosphate (Aldrich); $[D_6]$benzene (Euriso-

Top); benzonitrile (Merck); 1,2-bis(diphenylphosphino)ethane (Aldrich); boron trifluoride diethyl etherate (Acros); bromobenzene (Aldrich); *n*-butyllithium, 1.6 M in *n*-hexane, (Aldrich); *tert*-butyllithium, 1.6 M in *n*-pentane (Aldrich); calcium chloride (KMF); calcium hydride (Acros); [D]chloroform (Merck); 2-chloro-2-methylpropane (Aldrich); chlorotrimethylsilane (Acros); chromium hexacarbonyl (Acros); copper(I) chloride (Aldrich); copper(II) trifluoromethanesulfonate (Aldrich); 12-crown-4 (Acros); cyclohexyl isocyanide (Merck); dichloromethane (Biesterfeld); [D_2]dichloromethane (Euriso-Top); diethyl ether (Prolabo); dimethyl cyanamide (Acros); 1,5-dimethyl-2-pyrrolecarbonitrile (Aldrich); epichlorohydrine (Aldrich); ethanol, technical grade (Hofmann); ethyl cyanoformate (Acros); ethylene glycol dimethyl ether (Merck); ferrocene (Acros); 2-furonitrile (Aldrich); gallium(III) chloride (Aldrich); hydrochloric acid 37 % (Riedel-de Haën); iodomethane (Acros); iron(III) chloride (Alfa Aesar); lithium hexafluorophosphate (Acros); lithium trifluoromethanesulfonate (Acros); methyl trifluoromethanesulfonate (Acros); mineral oil (Fluka); molecular sieves 3 and 4 Å (Merck); molybdenum hexacarbonyl (Acros); pentafluorobenzonitrile (Aldrich); *n*-pentane (Grüssing); petroleum ether 40/60 (Biesterfeld); phosphorus pentoxide (Riedel-de Haën); phosphorus trichloride (Aldrich); pivalonitrile (Acros); potassium bromide (Aldrich); potassium cyanide (Alfa Aesar); potassium tetraphenylborate (Aldrich); pyridine (Merck); silica gel 60, 60-200 mesh (Merck); silica gel silanized 60, 60-200 mesh (Merck); silver(I) trifluoromethanesulfonate (Acros); sodium (Riedel-de Haën); sulfuric acid, 98 % (Merck); sulfuric acid, fuming (Acros); tetrabutylammonium fluoride (Acros); tetrabutylammonium hexafluorophosphate (Fluka); tetrabutylammonium tetraphenylborate (Aldrich); tetrabutylammonium trifluoromethanesulfonate (Alfa Aesar); tetrafluoroboric acid diethyl ether complex (Aldrich); tetrahydrofuran (Aldrich); tetrakisacetonitrile copper(I) trifluoromethanesulfonate (Aldrich); N,N,N',N'-tetramethylethylenediamine (Aldrich); 2-thiophenecarbonitrile (Acros); 3-thiophenecarbonitrile (Acros); thiophene (Aldrich); toluene (Acros); trichloroacetic acid (Merck); triethylamine (Grüssing); trifluoroacetic acid (Acros); trifluoromethanesulfonic acid (Acros); trimethyloxonium tetrafluoroborate (Aldrich); trimethylsilyl cyanide (Merck); tris(pentafluorophenyl)borane (Acros); tungsten hexacarbonyl (Acros).

10.1.3 Reactants Synthesized According to Published Procedures

The following reactants were synthesized according to published procedures:

- Triethyloxonium tetrafluoroborate[398]

- [Bis(trimethylsilyl)methylene]chlorophosphane[318]

- Lithioferrocene[399]

- 1,1'-Dilithioferrocene N,N,N',N'-tetramethyl-1,2-ethanediamine adduct (3:2)[400]

- [Amino(phenyl)carbene]pentacarbonyltungsten(0)[401]

- [Amino(phenyl)carbene]pentacarbonylmolybdenum(0)[402]

- [Amino(phenyl)carbene]pentacarbonylchromium(0)[403]

- [Amino(2-thienyl)carbene]pentacarbonyltungsten(0)[124, 403, 404]

- [Amino(ferrocenyl)carbene]pentacarbonyltungsten(0)[128]

- [2-Bis(trimethylsilyl)methyl-3-phenyl-2H-azaphosphirene-κP]pentacarbonyl-tungsten(0)[122]

- [2-Bis(trimethylsilyl)methyl-3-phenyl-2H-azaphosphirene-κP]pentacarbonyl-molybdenum(0)[123]

- [2-Bis(trimethylsilyl)methyl-3-phenyl-2H-azaphosphirene-κP]pentacarbonyl-chromium(0)[123]

- [2-Bis(trimethylsilyl)methyl-3-(2-thienyl)-2H-azaphosphirene-κP]pentacarbonyl-tungsten(0)[124]

- [2-Bis(trimethylsilyl)methyl-3-ferrocenyl-2H-azaphosphirene-κP]pentacarbonyl-tungsten(0)[128]

- Bis(η^5-cyclopentadienyl)iron(1+) hexafluorophosphate[179]

- Bis(η^5-cyclopentadienyl)iron(1+) tetraphenylborate[405]

- Hydrogen cyanide[406]

Pentacarbonyl[2-(1,2,3,4,5-pentamethyl-2,4-cyclopentadien-1-yl)-3-phenyl-2H-azaphos-phirene-κP]tungsten(0)[125] was kindly provided and synthesized according to the published procedure by Maren Bode and Stefan Fankel, ferrocenecarbonitrile,[407] [2-bis(trimethylsilyl)methyl-3-ferrocenyl-2H-azaphosphirene-κP]pentacarbonylmolybden-um(0),[194] as well as [2-bis(trimethylsilyl)methyl-3-ferrocenyl-2H-azaphosphirene-κP]-pentacarbonylchromium(0)[194] was kindly provided and synthesized according to the published procedure by Stefan Fankel, and lithium tetrakis(pentafluorophenyl)borate[408] was kindly provided and synthesized according to the published procedure by Susanne Sauerbrey.

10.2   SET-Induced Ring Expansion of $2H$-Azaphos-phirene Complexes

10.2.1   Synthesis of [2-Bis(trimethylsilyl)methyl-5-dimethylami-no-3-phenyl-$2H$-1,4,2-diazaphosphole-κP]pentacarbon-yltungsten(0) (41b)

To a stirred solution of 309 mg (0.50 mmol) of $2H$-azaphosphirene complex **35** in 1.5 mL of CH_2Cl_2 were added consecutively 63 μL (0.77 mmol) of dimethyl cyanamide (**36b**) and 30 mg (0.09 mmol) of ferrocinium hexafluorophosphate at ambient temperature. The reaction mixture was stirred for 5 d. After removement of all volatiles in vacuo ($\sim 10^{-2}$ mbar) the product was purified by column chromatography on silica ($-10\,^{\circ}C$, 2×8 cm, petroleum ether/Et_2O: 100/1). The first fraction (yellow) contained ferrocene, and evaporation of the solvents of the second fraction ($\sim 10^{-2}$ mbar) yielded **41b**.

41b: Yellow solid, crystallized from n-pentane at $4\,^{\circ}C$; yield: 203 mg (0.30 mmol, 59 %); mp $122\,^{\circ}C$; ^1H NMR (300.13 MHz, C_6D_6): $\delta = -0.22$ (s_{sat}, $|^2J_{SiH}| = 6.4$ Hz, $|^1J_{CH}| = 119.5$ Hz, 9 H; $Si(CH_3)_3$), 0.50 (s_{sat}, $|^2J_{SiH}| = 6.5$ Hz, $|^1J_{CH}| = 119.7$ Hz, 9 H; $Si(CH_3)_3$), 1.01 (d, $|^2J_{PH}| = 5.8$ Hz, 1 H; $CH(SiMe_3)_2$), 2.78 (s, 3 H; NCH_3), 2.92 (s, 3 H; NCH_3), 7.11 (m_c, 3 H; $meta+para$-H_{phenyl}), 8.17 (m_c, 2 H; $ortho$-H_{phenyl}); $^{13}C\{^1H\}$ NMR (75.5 MHz, C_6D_6): $\delta = 3.1$ (d_{sat}, $|^3J_{PC}| = 1.6$ Hz, $|^1J_{SiC}| = 52.1$ Hz; $Si(CH_3)_3$), 4.1 (d_{sat}, $|^3J_{PC}| = 2.6$ Hz, $|^1J_{SiC}| = 53.1$ Hz; $Si(CH_3)_3$), 22.0 (d, $|^1J_{PC}| = 5.8$ Hz; $CH(SiMe_3)_2$), 37.6 (s; NCH_3), 37.6 (s; NCH_3), 128.8 (s, $meta$-C_{phenyl}), 131.6 (d, $|^3J_{PC}| = 1.9$ Hz; $ortho$-C_{phenyl}), 132.8 (d, $|^2J_{PC}| = 20.7$ Hz; $ipso$-C_{phenyl}), 133.3 (s; $para$-C_{phenyl}), 165.0 (s; PNC), 198.6 (d_{sat}, $|^2J_{PC}| = 6.5$ Hz, $|^1J_{WC}| = 126.7$ Hz; CO_{cis}), 199.6 (d_{sat}, $|^2J_{PC}| = 22.3$ Hz, $|^1J_{WC}| = 143.2$ Hz; CO_{trans}), 200.3 (d_{sat}, $|^{1+4}J_{PC}| = 25.5$ Hz, $|^2J_{WC}| = 3.5$ Hz; PCN); ^{15}N NMR (30.418 MHz, C_6D_6): $\delta = -299$ (NMe_2), -200 ($|^{1+4}J_{PN}| = 55$ Hz, $|^3J_{NH}| = 5$ Hz; N^1); $^{29}Si\{^1H\}$ NMR (59.6 MHz, C_6D_6): $\delta = 2.1$ (d_{sat}, $|^2J_{PSi}| = 11.8$ Hz, $|^1J_{SiC}| = 52.4$ Hz), 2.4 (d_{sat}, $|^2J_{PSi}| = 2.5$ Hz, $|^1J_{SiC}| = 52.5$ Hz); ^{31}P NMR (121.5 MHz, C_6D_6): $\delta = 101.8$ (d_{sat}, $|^1J_{WP}| = 241.6$ Hz, $|^2J_{PH}| = 2.4$ Hz); IR (KBr): $\tilde{\nu} = 2955$ (w, CH_3/CH), 2900 (w, CH_3/CH), 2068 (m, sh, CO), 1980 (m, sh, CO), 1946 (s, br, CO), 1923 (s, CO), 1913 (s, CO), 1606 (m, CN), 1539 cm^{-1} (w, CN); Raman (180 mW): $\tilde{\nu} = 3076$ (m, CH_{phenyl}), 3051 (w, CH_{phenyl}), 2957 (m, CH_3/CH), 2902 (s, CH_3/CH), 2855 (m, CH_3/CH), 2797 (m, CH_3/CH), 2067 (m, CO), 1978 (vs, CO), 1949 (vw, CO), 1918 (m, CO), 1915 (m, CO), 1597 (m, CN), 1538 (m, CN), 446 cm^{-1} (w); UV/Vis (n-pentane): λ_{max} (ϵ [cm^2 $mmol^{-1}$]) = 202 (47406), 227 (79475), 250 (sh, 47464), 288 (17196), 350 (3834), 407 (2614), 421 nm

(2208); CV: $E_{1/2} = -2.001$ V; MS (FAB$^+$, ^{184}W): m/z (%): 688.1 ([M + H]$^+$, 12), 659.1 ([M − CO]$^+$, 49), 631.1 ([M − 2 CO]$^+$, 38), 603.1 ([M − 3 CO]$^+$, 10), 533.1 ([M − 3 CO − Me$_2$NCN]$^+$, 22), 364.2 ([M + H − W(CO)$_5$]$^+$, 100), 191.1 ([Me$_3$SiP(H)C(H)SiMe$_3$]$^+$, 4); MS (EI, ^{184}W): m/z (%): 687.1 ([M]$^+$, 15), 672.1 ([M − CH$_3$]$^+$, 20), 659.1 ([M − CO]$^+$, 65), 631.1 ([M − 2 CO]$^+$, 64), 601.1 ([M − 2 CO − 2 CH$_3$]$^+$, 24), 533.0 ([M − 3 CO − Me$_2$NCN]$^+$, 100), 505.1 ([M − 4 CO − Me$_2$NCN]$^+$, 10), 477.1 ([M − 5 CO − Me$_2$NCN]$^+$, 20), 444.0 ([M − 5 CO − PhCN, 13), 363.2 ([M − W(CO)$_5$]$^+$, 12), 293.1 ([M − W(CO)$_5$ − Me$_2$NCN]$^+$, 15), 190.1 ([Me$_3$SiPC(H)SiMe$_3$]$^+$, 3); 73.1 ([SiMe$_3$]$^+$, 47); elemental analysis (%) calcd. for C$_{22}$H$_{30}$N$_3$O$_5$PSi$_2$W: C 38.44, H 4.40, N 6.11; found: C 38.49, H 4.54, N 5.86.

10.2.2 Synthesis of [2-Bis(trimethylsilyl)methyl-3-phenyl-5-(2-thienyl)-2H-1,4,2-diazaphosphole-κP]pentacarbonyltungsten(0) (41g)

Synthesis of 41g using 0.05 equiv. of [FeCp$_2$][PF$_6$]: To a solution of 617 mg (1.00 mmol) of 2H-azaphosphirene complex **35** in 3 mL of CH$_2$Cl$_2$ were added consecutively 94 μL (1.01 mmol) of 2-thiophenecarbonitrile (**36g**) and 17 mg (0.05 mmol) of ferrocinium hexafluorophosphate. The reaction mixture was stirred for 15 h at ambient temperature. After removement of all volatiles in vacuo ($\sim 10^{-2}$ mbar) the products were separated and purified by column chromatography on silica ($-10\,^\circ$C, 2 × 7 cm). Evaporation of the solvents of the first fraction ($\sim 10^{-2}$ mbar), which was eluated with petroleum ether, gave 6.8 mg (0.037 mmol, 71 % with respect to [FeCp$_2$][PF$_6$]) of ferrocene. Evaporation of the solvents of the second fraction ($\sim 10^{-2}$ mbar), eluated with petroleum ether/Et$_2$O (10:1), gave **41g**; yield: 661 mg (0.91 mmol, 91 %).

Synthesis of 41g using 0.18 equiv. of [FeCp$_2$][PF$_6$]: To a solution of 617 mg (1.00 mmol) of 2H-azaphosphirene complex **35** in 3 mL of CH$_2$Cl$_2$ were added consecutively 94 μL (1.01 mmol) of 2-thiophenecarbonitrile (**36g**) and 60 mg (0.18 mmol) of ferrocinium hexafluorophosphate. The reaction mixture was stirred for 3 h at ambient temperature. After removement of all volatiles in vacuo ($\sim 10^{-2}$ mbar) the products were separated and purified by column chromatography on silica ($-10\,^\circ$C, 2 × 8 cm). Evaporation of the solvents of the first fraction ($\sim 10^{-2}$ mbar), which was eluated with petroleum ether, gave 2.7 mg (0.015 mmol, 8 % with respect to [FeCp$_2$][PF$_6$]) of ferrocene. Evaporation of the solvents of the second fraction ($\sim 10^{-2}$ mbar), eluated with petroleum ether/Et$_2$O (10:1), gave **41g**; yield: 658 mg (0.91 mmol, 91 %).

41g: Orange solid, crystallized from n-pentane at 4 $^\circ$C; mp 117 $^\circ$C; ^{1}H NMR (300.13

MHz, C_6D_6): $\delta = -0.26$ (s_{sat}, $|^2J_{SiH}| = 6.4$ Hz, $|^1J_{CH}| = 119.7$ Hz, 9 H; $Si(CH_3)_3$), 0.50 (s_{sat}, $|^2J_{SiH}| = 6.4$ Hz, $|^1J_{CH}| = 119.9$ Hz, 9 H; $Si(CH_3)_3$), 1.06 (d, $|^2J_{PH}| = 3.8$ Hz, 1 H; $CH(SiMe_3)_2$), 6.65 (dd, $|^3J_{HH}| = 5.0$ and 3.8 Hz, 1H; thienyl-C^4H), 6.88 (dd, $|^3J_{HH}| = 5.0$ Hz, $|^4J_{HH}| = 1.1$ Hz, 1H; thienyl-C^5H), 7.12 (m$_c$, 3 H; $meta+para$-H_{phenyl}), 8.07 (dd, $|^3J_{HH}| = 3.8$ Hz, $|^4J_{HH}| = 1.1$ Hz, 1H; thienyl-C^3H), 8.23 (m$_c$, 2 H; $ortho$-H_{phenyl}); $^{13}C\{^1H\}$ NMR (75.5 MHz, C_6D_6): $\delta = 2.9$ (d$_{sat}$, $|^3J_{PC}| = 2.3$ Hz, $|^1J_{SiC}| = 52.5$ Hz; $Si(CH_3)_3$), 3.8 (d$_{sat}$, $|^3J_{PC}| = 2.9$ Hz, $|^1J_{SiC}| = 53.0$ Hz; $Si(CH_3)_3$), 19.1 (d, $|^1J_{PC}| = 4.8$ Hz; $CH(SiMe_3)_2$), 128.7 (d, $|^{5+6}J_{PC}| = 0.8$ Hz; thienyl-C^4), 129.0 (s; $meta$-C_{phenyl}), 131.9 (d, $|^3J_{PC}| = 2.3$ Hz; $ortho$-C_{phenyl}), 132.5 (d, $|^2J_{PC}| = 22.6$ Hz; $ipso$-C_{phenyl}), 133.5 (s; thienyl-C^5), 133.8 (d, $|^5J_{PC}| = 0.6$ Hz; $para$-C_{phenyl}), 134.0 (d, $|^4J_{PC}| = 0.8$ Hz; thienyl-C^3), 138.8 (d, $|^3J_{PC}| = 14.2$ Hz; thienyl-C^2), 165.2 (d, $|^{2+3}J_{PC}| = 4.2$ Hz; PNC), 197.6 (d$_{sat}$, $|^2J_{PC}| = 6.1$ Hz, $|^1J_{WC}| = 126.7$ Hz; CO_{cis}), 198.3 (d$_{sat}$, $|^2J_{PC}| = 22.3$ Hz, $|^1J_{WC}| = 144.2$ Hz; CO_{trans}), 202.3 (d$_{sat}$, $|^{1+4}J_{PC}| = 23.3$ Hz, $|^2J_{WC}| = 3.6$ Hz; PCN); ^{15}N NMR (30.418 MHz, C_6D_6): $\delta = -116$ ($|^{1+4}J_{PN}| = 50$ Hz, $|^3J_{NH}| = 5$ Hz; N^1); $^{29}Si\{^1H\}$ NMR (59.6 MHz, C_6D_6): $\delta = 3.3$ (d$_{sat}$, $|^2J_{PSi}| = 2.7$ Hz, $|^1J_{SiC}| = 53.1$ Hz), 3.6 (d$_{sat}$, $|^2J_{PSi}| = 11.8$ Hz, $|^1J_{SiC}| = 52.6$ Hz); ^{31}P NMR (121.5 MHz, C_6D_6): $\delta = 110.1$ (d$_{sat}$, $|^1J_{WP}| = 231.4$ Hz, $|^2J_{PH}| = 3.0$ Hz); IR (KBr): $\tilde{\nu} = 2955$ (w, CH_3/CH), 2898 (w, CH_3/CH), 2073 (m, sh, CO), 2001 (m, sh, CO), 1924 (s, CO), 1908 (s, CO), 1566 (m, CN), 1560 (m, CN), 1253 cm^{-1} (m, thienyl); UV/Vis (n-pentane): λ_{max} (ϵ [cm^2 mmol^{-1}]) = 212 (50945), 232 (77993), 251 (sh, 46218), 291 (23949), 309 (sh, 24947), 317 (25367), 330 (sh, 20798), 435 nm (3571); CV: $E_{1/2} = -1.672$ V; MS (FAB$^+$, ^{184}W): m/z (%): 727.0 ($[M+H]^+$, 19), 698.1 ($[M-CO]^+$, 23), 670.1 ($[M-2CO]^+$, 70), 533.0 ($[M-3CO-C_5H_3NS]^+$, 9) 477.0 ($[M-5CO-C_5H_3NS]^+$, 28), 403.1 ($[M+H-W(CO)_5]^+$, 100), 191.1 ($[Me_3SiP(H)C(H)SiMe_3]^+$, 8); MS (EI, ^{184}W): m/z (%): 726.1 ($[M]^+$, 15), 698.1 ($[M-CO]^+$, 43), 670.1 ($[M-2CO]^+$, 100), 533.1 ($[M-3CO-C_5H_3NS]^+$, 45), 505.1 ($[M-4CO-C_5H_3NS]^+$, 9), 477.1 ($[M-5CO-C_5H_3NS]^+$, 28), 402.1 ($[M-W(CO)_5]^+$, 44), 299.1 ($[M-W(CO)_5-PhCN]^+$, 20), 190.1 ($[Me_3SiPC(H)SiMe_3]^+$, 21), 73.1 ($[SiMe_3]^+$, 49); elemental analysis (%) calcd. for $C_{24}H_{27}N_2O_5PSSi_2W$: C 39.68, H 3.75, N 3.86, S 4.41; found: C 39.68, H 3.82, N 3.87, S 4.57.

10.2.3 Reactions of [2-Bis(trimethylsilyl)methyl-3-phenyl-2H-azaphosphirene-κP]pentacarbonyltungsten(0) (35) with Hetaryl Carbonitriles 36d–g in the Presence of 0.05 Equivalents of Ferrocinium Hexafluorophosphate

To a solution of 123 mg (0.20 mmol) of 2H-azaphosphirene complex **35** in 0.6 mL of CH_2Cl_2 were added consecutively the appropriate nitrile (**36d**: 24 mg, 0.20 mmol;

36e: 18 μL, 0.21 mmol; **36f**: 19 μL, 0.21 mmol; **36g**: 19 μL, 0.20 mmol) and 3 mg
(0.01 mmol) of ferrocinium hexafluorophosphate. The reaction mixtures were stirred
for 6 h at ambient temperature, and the formation of **41d**–**g** was evidenced by ^{31}P$\{^1$H$\}$
NMR spectroscopy (121.5 MHz, CH$_2$Cl$_2$): δ = 108.5 (s$_{sat}$, $|^1J_{PW}|$ = 232.7 Hz; **41d**),
110.8 (s$_{sat}$, $|^1J_{PW}|$ = 230.2 Hz; **41e**), 109.1 (s$_{sat}$, $|^1J_{PW}|$ = 228.9 Hz; **41f**), 110.4 (s$_{sat}$,
$|^1J_{PW}|$ = 230.2 Hz; **41g**).

10.2.4 Investigations on the Dependance of the Reaction Progression of 35 with 2-Thiophenecarbonitrile on the Amount of Ferrocinium Hexafluorophosphate

To solutions of 123 mg (0.20 mmol) of 2H-azaphosphirene complex **35** in 0.6 mL of
CH$_2$Cl$_2$ were added consecutively 19 μL (0.20 mmol) of 2-thiophenecarbonitrile (**36g**)
and different amounts of ferrocinium hexafluorophosphate (0.7 mg, 0.002 mmol; 1.3
mg, 0.004 mmol; 2.0 mg, 0.006 mmol; 2.6 mg, 0.008 mmol; 3.3 mg, 0.010 mmol; 6.6
mg, 0.020 mmol; 9.9 mg, 0.030 mmol; 13.2 mg, 0.040 mmol). Product ratios were
estimated by ^{31}P$\{^1$H$\}$ NMR spectroscopic signal integration (30 °C, 100 scans each,
measurement duration 159 s, recorded reaction time corresponds to the end of the
respective measurement; Fig. 3.1, Section 3.1).

For investigations corresponding to Fig. 3.2 (Section 3.1), a solution of 1.6 mg (0.005
mmol) of ferrocinium hexafluorophosphate and 19 μL (0.20 mmol) of 2-thiophene-
carbonitrile (**36g**) in 0.6 mL of CH$_2$Cl$_2$ was added to 123 mg (0.20 mmol) of 2H-aza-
phosphirene complex **35** in an NMR tube. Product ratios were estimated by ^{31}P$\{^1$H$\}$
NMR spectroscopic signal integration (30 °C, 32 scans each, measurement duration 56
s).

10.2.5 Reaction of 2-Thiophenecarbonitrile with Ferrocinium Hexafluorophosphate

To a solution of 0.1 mL (1 mmol) of 2-thiophenecarbonitrile (**36g**) in 3 mL of CH$_2$Cl$_2$
was added 60 mg (0.18 mmol) of ferrocinium hexafluorophosphate. The reaction mix-
ture was stirred for 2 h at ambient temperature. After removement of all volatiles in
vacuo ($\sim 10^{-2}$ mbar) the residue was subjected to column chromatography on silica
(-10 °C, 3×5 cm). Upon eluation with pure petroleum ether no solid material was
obtained.

10.2.6   Reaction of [2-Bis(trimethylsilyl)methyl-3-phenyl-2H-azaphosphirene-κP]pentacarbonyltungsten(0) (35) with 2-Thiophenecarbonitrile in the Presence of Tetra-n-Butylammonium Hexafluorophosphate

To a solution of 123 mg (0.20 mmol) of 2H-azaphosphirene complex **35** in 0.6 mL of CH$_2$Cl$_2$ were added consecutively 15.5 mg (0.20 mmol) of [^{n}Bu$_4$N][PF$_6$] and 19 μL (0.04 mmol) of 2-thiophenecarbonitrile (**36g**). The reaction mixture was stirred for 4 d at ambient temperature and was then analyzed by ^{31}P NMR spectroscopy. It contained about 96 % of unreacted **35** and minor amounts of unidentified product **A** and complex **44** (the resonance of hexafluorophosphate was not taken into account for ratio estimation). ^{31}P NMR (121.5 MHz, CH$_2$Cl$_2$, 25 °C): $\delta = -109.9$ (s$_{sat}$, $|^1J_{PW}| = 293.7$ Hz; **35** (96 %)), 77.5 (d$_{sat}$, $|^1J_{WP}| = 276.7$ Hz, $|^1J_{PH}| = 328.1$ Hz; **44** (3 %)), 156.8 (d, $|^1J_{PF}| = 803.6$ Hz; **A** (<1 %)).

10.2.7

pentacarbonyltungsten(0) (**35**) with 2-Thiophenecarbonitrile in the Presence of Silver(I) Trifluoromethanesulfon-
ate]Reaction of [2-Bis(trimethylsilyl)methyl-3-phenyl-2H-azaphosphirene-κP]pentacarbonyltungsten(0) (**35**) with 2-Thiophenecarbonitrile in the Presence of Silver(I) Trifluoromethanesulfonate To a solution of 62 mg (0.10 mmol) of 2H-azaphosphirene complex **35** in 0.7 mL of CH$_2$Cl$_2$ in an NMR tube were added consecutively 10 μL (0.11 mmol) of 2-thiophenecarbonitrile (**36g**) and 5 mg (0.02 mmol) of silver(I) trifluoromethanesulfonate at ambient temperature. Immediately upon addition of Ag[OTf] the formation of a grey-brownish precipitate was observed, and after 14.5 h the formation of **41g** was evidenced by ^{31}P NMR spectroscopy (121.5 MHz, CH$_2$Cl$_2$, 25 °C): $\delta = 110.4$ (s$_{sat}$, $|^1J_{PW}| = 230.2$ Hz).

10.2.8   Reaction of [2-Bis(trimethylsilyl)methyl-3-phenyl-2H-azaphosphirene-κP]pentacarbonyltungsten(0) (35) with 2-Thiophenecarbonitrile in the Presence of Copper(II) Trifluoromethanesulfonate

To a solution of 62 mg (0.10 mmol) of 2H-azaphosphirene complex **35** in 0.7 mL of CH$_2$Cl$_2$ in an NMR tube were added consecutively 10 μL (0.11 mmol) of 2-thiophene-

carbonitrile (**36g**) and 6 mg (0.02 mmol) of copper(II) trifluoromethanesulfonate at ambient temperature. Ater 4 h the formation of **41g** was evidenced by ^{31}P NMR spectroscopy (121.5 MHz, CH$_2$Cl$_2$, 25 °C): $\delta = 110.4$ (s$_{sat}$, $|^1J_{PW}| = 230.2$ Hz).

10.2.9 Attempted Synthesis of [2-Bis(trimethylsilyl)methyl-3-phenyl-2H-1,4,2-diazaphosphole-κP]pentacarbonyl-tungsten(0) (41h) Using Ferrocinium Hexafluorophosphate

To a solution of 123 mg (0.20 mmol) of 2H-azaphosphirene complex **35** in 0.6 mL of CH$_2$Cl$_2$ were added consecutively 20 μL (0.51 mmol) of hydrogen cyanide (**36h**) and 12 mg (0.04 mmol) of ferrocinium hexafluorophosphate. The mixture was stirred at ambient temperature. After 4 d the reaction mixture containing unreacted **35**, complexes **41c,h**, and unidentified products **A**–**E** was analyzed by ^{31}P{^{1}H} and ^{19}F{^{1}H} NMR spectroscopy. ^{31}P{^{1}H} NMR (121.5 MHz, CH$_2$Cl$_2$): $\delta = -143.5$ (sept, $|^1J_{PF}| = 714.0$ Hz, PF$_6^-$ (3 %)), -109.9 (s$_{sat}$, $|^1J_{PW}| = 293.7$ Hz; **35** (16 %)), 105.5 (s$_{sat}$, $|^1J_{PW}| = 225.1$ Hz; **41h** (20 %)), 110.7 (s$_{sat}$, $|^1J_{PW}| = 227.6$ Hz; **41c** (5 %)), 161.2 (s$_{sat}$, $|^1J_{PW}| = 289.9$ Hz; **A** (6 %)), 191.2 (d, $|^1J_{PF}| = 989.3$ Hz; **B** (4 %)), 197.3 (d, $|^1J_{PF}| = 824.0$ Hz; **C** (9 %)), 206.2 (d, $|^1J_{PF}| = 841.8$ Hz; **D** (3 %)), 206.9 (d, $|^1J_{PF}| = 855.8$ Hz; **E** (1 %)); ^{19}F{^{1}H} NMR (282.4 MHz, CH$_2$Cl$_2$): $\delta = -117.2$ (d, $|^1J_{PF}| = 823.5$ Hz; **C** (9 %)), -111.4 (d, $|^1J_{PF}| = 854.9$ Hz; **E** (1 %)), -109.1 (d, $|^1J_{PF}| = 841.5$ Hz; **D** (3 %)), -72.5 (d, $|^1J_{PF}| = 713.6$ Hz; PF$_6^-$ (3 %)), -31.0 (d, $|^1J_{PF}| = 991.8$ Hz; **B** (4 %)). After removement of all volatiles in vacuo ($\sim 10^{-2}$ mbar) the crude product mixture was subjected to column chromatography on silica (-30 °C, 2 $\times$ 12 cm), but the products could not completely be separated.

10.2.10 Attempted Synthesis of [2-Bis(trimethylsilyl)methyl-5-ethoxycarbonyl-3-phenyl-2H-1,4,2-diazaphosphole-κP]pentacarbonyltungsten(0) (41i) Using Ferrocinium Hexafluorophosphate

To a solution of 123 mg (0.20 mmol) of 2H-azaphosphirene complex **35** in 0.6 mL of CH$_2$Cl$_2$ were added consecutively 30 μL (0.30 mmol) of ethyl cyanoformate **36i** and 12 mg (0.04 mmol) of ferrocinium hexafluorophosphate. The mixture was stirred at ambient temperature. After 6 d the reaction mixture containing unreacted **35**, complex **41c**, and unidentified products **A**–**D** was analyzed by ^{31}P{^{1}H} and ^{19}F{^{1}H}

NMR spectroscopy. $^{31}P\{^1H\}$ NMR (121.5 MHz, CH_2Cl_2): $\delta = -143.8$ (sept, $|^1J_{PF}| = 714.0$ Hz; PF_6^- (6 %)), -110.1 (s_{sat}, $|^1J_{PW}| = 293.7$ Hz; **35** (41 %)), 18.5 (d, $|^1J_{PF}| = 1044.0$ Hz; **A** (3 %)), 110.7 (s_{sat}, $|^1J_{PW}| = 227.6$ Hz; **41c** (21 %)), 160.8 (s_{sat}, $|^1J_{PW}| = 284.8$ Hz; **B** (6 %)), 177.2 (d, $|^1J_{PF}| = 967.7$ Hz; **C** (2 %)), 197.3 (d, $|^1J_{PF}| = 822.7$ Hz; **D** (12 %)); $^{19}F\{^1H\}$ NMR (282.4 MHz, CH_2Cl_2): $\delta = -117.2$ (d, $|^1J_{PF}| = 823.5$ Hz; **D** (12 %)), -74.4 (d, $|^1J_{PF}| = 968.3$ Hz; **C** (2 %)), -73.8 (d, $|^1J_{PF}| = 712.5$ Hz; PF_6^- (6 %)), -66.7 (d, $|^1J_{PF}| = 1046.8$ Hz; **A** (3 %)).

10.2.11 Attempted Synthesis of [2-Bis(trimethylsilyl)methyl-5-pentafluorophenyl-3-phenyl-2H-1,4,2-diazaphosphole-κP]pentacarbonyltungsten(0) (41j) Using Ferrocinium Hexafluorophosphate

To a solution of 123 mg (0.20 mmol) of 2H-azaphosphirene complex **35** in 0.6 mL of CH_2Cl_2 were added consecutively 160 μL (1.27 mmol) of pentafluorobenzonitrile (**36j**) and 12 mg (0.04 mmol) of ferrocinium hexafluorophosphate. The mixture was stirred at ambient temperature. After 6 d the reaction mixture containing unreacted **35** and **36j**, complex **41c**, and unidentified products **A**–**E** was analyzed by $^{31}P\{^1H\}$ and $^{19}F\{^1H\}$ NMR spectroscopy. $^{31}P\{^1H\}$ NMR (121.5 MHz, CH_2Cl_2): $\delta = -110.4$ (s_{sat}, $|^1J_{PW}| = 293.7$ Hz; **35** (48 %)), 18.4 (d, $|^1J_{PF}| = 1041.4$ Hz; **A** (3 %)), 110.7 (s_{sat}, $|^1J_{PW}| = 228.9$ Hz; **41c** (12 %)), 160.9 (s_{sat}, $|^1J_{PW}| = 282.3$ Hz; **B** (5 %)), 176.3 (s; **C** (5 %)), 183.1 (s; **D** (5 %)), 197.4 (d_{sat}, $|^1J_{PF}| = 824.0$ Hz, $|^1J_{PW}| = 286.1$ Hz; **E** (11 %)); $^{19}F\{^1H\}$ NMR (282.4 MHz, CH_2Cl_2): $\delta = -160.6$ (m_c; **36j**), -144.7 (m_c; **36j**), -134.0 (m_c; **36j**), -117.6 (d, $|^1J_{PF}| = 823.5$ Hz; **E** (11 %)), -75.5 (d, $|^1J_{PF}| = 713.6$ Hz; PF_6^-), -67.6 (d, $|^1J_{PF}| = 1041.2$ Hz; **A** (3 %)).

10.2.12 Reaction of [2-Bis(trimethylsilyl)methyl-3-phenyl-2H-azaphosphirene-κP]pentacarbonyltungsten(0) (35) with 2-Thiophenecarbonitrile in the Presence of Ferrocinium Tetraphenylborate

To a solution of 62 mg (0.10 mmol) of 2H-azaphosphirene complex **35** in 0.3 mL of CH_2Cl_2 were added consecutively 10 μL (0.11 mmol) of 2-thiophenecarbonitrile (**36g**) and 9 mg (0.02 mmol) of ferrocinium tetraphenylborate. The mixture was stirred for 8 h at ambient temperature; complete formation of **41g** was evidenced by $^{31}P\{^1H\}$ NMR spectroscopy (121.5 MHz, CH_2Cl_2): $\delta = 110.4$ (s_{sat}, $|^1J_{PW}| = 230.2$ Hz).

10.2.13 Attempted Synthesis of [2-Bis(trimethylsilyl)methyl-3-phenyl-2*H*-1,4,2-diazaphosphole-κP]pentacarbonyltungsten(0) (41h) Using Ferrocinium Tetraphenylborate

To a solution of 123 mg (0.20 mmol) of 2*H*-azaphosphirene complex **35** in 0.6 mL of CH$_2$Cl$_2$ were added consecutively 20 μL (0.51 mmol) of hydrogen cyanide (**36h**) and 18 mg (0.04 mmol) of ferrocinium tetraphenylborate. The mixture was stirred at ambient temperature. After 4 d the reaction mixture containing unreacted **35**, complexes **41c,h**, and unidentified products **A**–**C** was analyzed by ^{31}P{^{1}H} NMR spectroscopy. ^{31}P{^{1}H} NMR (121.5 MHz, CH$_2$Cl$_2$): $\delta = -109.9$ (s$_{sat}$, $|^1J_{PW}| = 293.7$ Hz; **35** (37 %)), -68.9 (s$_{sat}$, $|^1J_{PW}| = 242.9$ Hz; **A** (17 %)), 13.2 (s$_{sat}$, $|^1J_{PW}| = 236.5$ Hz; **B** (8 %)), 20.7 (s$_{sat}$, $|^1J_{PW}| = 236.5$ Hz; **C** (3 %)), 105.5 (s$_{sat}$, $|^1J_{PW}| = 223.8$ Hz, **41h** (3 %)), 110.6 (s$_{sat}$, $|^1J_{PW}| = 227.6$ Hz; **41c** (13 %)).

10.2.14 Attempted Synthesis of [2-Bis(trimethylsilyl)methyl-5-ethoxycarbonyl-3-phenyl-2*H*-1,4,2-diazaphosphole-κP]pentacarbonyltungsten(0) (41i) Using Ferrocinium Tetraphenylborate

To a solution of 123 mg (0.20 mmol) of 2*H*-azaphosphirene complex **35** in 0.6 mL of CH$_2$Cl$_2$ were added consecutively 30 μL (0.30 mmol) of ethyl cyanoformate (**36i**) and 18 mg (0.04 mmol) of ferrocinium tetraphenylborate. The mixture was stirred at ambient temperature. After 6 d the reaction mixture containing unreacted **35**, complex **41c**, and unidentified products **A**–**F** was analyzed by ^{31}P{^{1}H} NMR spectroscopy. ^{31}P{^{1}H} NMR (121.5 MHz, CH$_2$Cl$_2$): $\delta = -110.1$ (s$_{sat}$, $|^1J_{PW}| = 293.7$ Hz; **35** (81 %)), 34.1 (s; **A** (10 %)), 54.5 (s; **B** (1 %)), 97.4 (s; **C** (1 %)), 110.7 (s; **41c** (1 %)), 163.3 (s; **D** (1 %)), 184.5 (s; **E** (1 %)), 204.9 (s; **F** (1 %)).

10.2.15 Attempted Synthesis of [2-Bis(trimethylsilyl)methyl-5-pentafluorophenyl-3-phenyl-2*H*-1,4,2-diazaphosphole-κP]pentacarbonyltungsten(0) (41j) Using Ferrocinium Tetraphenylborate

To a solution of 123 mg (0.20 mmol) of 2*H*-azaphosphirene complex **35** in 0.6 mL of CH$_2$Cl$_2$ were added consecutively 160 μL (1.27 mmol) of pentafluorobenzonitrile

(**36j**) and 18 mg (0.04 mmol) of ferrocinium hexafluorophosphate. The mixture was stirred at ambient temperature. After 6 d the reaction mixture containing unreacted **35** and **36j**, complex **41c**, and unidentified products **A**–**G** was analyzed by $^{31}P\{^1H\}$ and $^{19}F\{^1H\}$ NMR spectroscopy. $^{31}P\{^1H\}$ NMR (121.5 MHz, CH_2Cl_2): $\delta = -110.4$ (s_{sat}, $|^1J_{PW}| = 295.0$ Hz; **35** (69 %)), 40.0 (s; **A** (1 %)), 54.4 (s_{sat}, $|^1J_{PW}| = 270.8$ Hz; **B** (1 %)), 95.5 (s_{sat}, $|^1J_{PW}| = 277.2$ Hz; **C** (3 %)), 110.7 (s; **41c** (1 %)), 126.1 (s; **D** (1 %)), 172.5 (s_{sat}, $^1J_{PW} = 309.0$ Hz; **E** (6 %)), 176.2 (s_{sat}, $|^1J_{PW}| = 277.2$ Hz; **F** (3 %)), 183.0 (s_{sat}, $|^1J_{PW}| = 254.3$ Hz; **G** (9 %)); $^{19}F\{^1H\}$ NMR: $\delta = -134.0$ (m_c; **36j**), -144.7 (m_c; **36j**), -160.6 (m_c; **36j**).

10.2.16 Attempted Synthesis of [2-Bis(trimethylsilyl)methyl-5-pentafluorophenyl-3-phenyl-2*H*-1,4,2-diazaphosphole-κP]pentacarbonyltungsten(0) (41j) Using Silver(I) Trifluoromethanesulfonate

To a solution of 62 mg (0.10 mmol) of 2*H*-azaphosphirene complex **35** in 0.7 mL of CH_2Cl_2 in an NMR tube were added consecutively 13 μL (0.10 mmol) of pentafluorobenzonitrile (**36j**) and 5 mg (0.02 mmol) of silver(I) trifluoromethanesulfonate at ambient temperature. Immediately upon addition of Ag[OTf] the mixture turned green-brownish, and the formation of a grey-brownish precipitate was observed. After 85 min the reaction mixture containing unreacted **35** and complex **41c** was analyzed by $^{31}P\{^1H\}$ NMR spectroscopy (121.5 MHz, CH_2Cl_2, 30 °C): $\delta = -109.6$ (s_{sat}, $|^1J_{PW}| = 296.3$ Hz; **35** (76 %)), 110.6 (s_{sat}, $|^1J_{PW}| = 227.6$ Hz; **41c** (16 %)).

10.2.17 Reaction of [2-Bis(trimethylsilyl)methyl-3-ferrocenyl-2*H*-azaphosphirene-κP]pentacarbonyltungsten(0) (67) with Ferrocinium Hexafluorophosphate in the Absence of Nitriles

To a solution of 243 mg (0.34 mmol) of 2*H*-azaphosphirene complex **67** in 2.1 mL of CH_2Cl_2 was added 35 mg (0.11 mmol) of ferrocinium hexafluorophosphate, and the mixture was stirred for 24 h at ambient temperature. The formation of **69l** was evidenced by $^{31}P\{^1H\}$ NMR spectroscopic reaction monitoring. After removement of all volatiles in vacuo ($\sim 10^{-2}$ mbar) the deep purple residue was subjected to column chromatography on silica (-25 °C, 2×10 cm), but a complete purification of **69l** was not achieved.

10.2.18 Synthesis of [2-Bis(trimethylsilyl)methyl-3,5-diferro-cenyl-2H-1,4,2-diazaphosphole-κP]pentacarbonyltungsten(0) (69l)

To a solution of 579 mg (0.80 mmol) of 2H-azaphosphirene complex **67** in 4.8 mL of CH$_2$Cl$_2$ were added consecutively 189 mg (0.90 mmol) of ferrocenecarbonitrile (**36l**) and 48 mg (0.15 mmol) of ferrocinium hexafluorophosphate at ambient temperature. The reaction mixture was stirred for 2 h at ambient temperature. After removement of all volatiles in vacuo ($\sim 10^{-2}$ mbar) the products were separated and purified by column chromatography on silica ($-15\,^{\circ}$C, 2×10 cm). Evaporation of the solvents of the first fraction ($\sim 10^{-2}$ mbar), which was eluated with petroleum ether, gave 18 mg (0.10 mmol, 67 %, with respect to [FeCp$_2$][PF$_6$]) of ferrocene. Evaporation of the solvents of the second fraction ($\sim 10^{-2}$ mbar), eluated with petroleum ether/Et$_2$O (10:1) gave **69l**.

69l: Purple solid; yield: 493 mg (0.53 mmol, 66 %); mp 174 $^{\circ}$C; ^{1}H NMR (300.13 MHz, C$_6$D$_6$): $\delta = -0.13$ (s$_{sat}$, $|^2J_{SiH}| = 6.3$ Hz, $|^1J_{CH}| = 119.7$ Hz, 9 H; Si(CH$_3$)$_3$), 0.35 (s$_{sat}$, $^2J_{SiH} = 6.3$ Hz, $|^1J_{CH}| = 119.3$ Hz, 9 H; Si(CH$_3$)$_3$), 1.29 (d, $|^2J_{PH}| = 6.5$ Hz, 1 H; CH(SiMe$_3$)$_2$), 4.14 (s, 5 H; Cp-CH unsubst.), 4.22 (s, 5 H; Cp-CH unsubst.), 4.23 (m$_c$, 2 H; Cp-C^{3+4}H at diazaphosphole-C^3), 4.28 (m$_c$, 2 H; Cp-C^{3+4}H at diazaphosphole-C^5), 4.94 (m$_c$, 1 H; Cp-C$^{2/5}$H at diazaphosphole-C^3), 5.11 (m$_c$, 1 H; Cp-C$^{2/5}$H at diazaphosphole-C^3), 5.15 (m$_c$, 1 H; Cp-C$^{2/5}$H at diazaphosphole-C^5), 5.25 (m$_c$, 1 H; Cp-C$^{2/5}$H at diazaphosphole-C^5); ^{13}C$\{^1$H$\}$ NMR (75.5 MHz, C$_6$D$_6$): $\delta = 2.9$ (d, $|^3J_{PC}| = 2.3$ Hz; Si(CH$_3$)$_3$), 3.5 (d, $|^3J_{PC}| = 2.3$ Hz; Si(CH$_3$)$_3$), 23.7 (d, $|^1J_{PC}| = 5.2$ Hz; CH(SiMe$_3$)$_2$), 69.9 (s; Cp-C$^{2/5}$ at diazaphosphole-C^5), 70.3 (s; Cp-C unsubst.), 70.5 (s; Cp-C$^{2/5}$ at diazaphosphole-C^3), 70.9 (s; Cp-C$^{3/4}$ at diazaphosphole-C^3), 71.3 (s; Cp-C unsubst.), 71.4 (s; Cp-C$^{3/4}$ at diazaphosphole-C^5), 72.2 (d, $|^4J_{PC}| = 1.0$ Hz; Cp-C$^{3/4}$ at diazaphosphole-C^3), 72.3 (d, $|^4J_{PC}| = 2.6$ Hz; Cp-C$^{2/5}$ at diazaphosphole-C^5), 73.0 (s; Cp-C$^{3/4}$ at diazaphosphole-C^5), 76.4 (d, $|^3J_{PC}| = 1.9$ Hz; Cp-C$^{2/5}$ at diazaphosphole-C^3), 77.7 (d, $|^3J_{PC}| = 12.9$ Hz; Cp-C^1 at diazaphosphole-C^5), 81.4 (d, $|^2J_{PC}| = 29.7$ Hz; Cp-C^1 at diazaphosphole-C^3), 175.1 (d, $|^{2+3}J_{PC}| = 5.8$ Hz; PNC), 197.9 (d$_{sat}$, $|^2J_{PC}| = 6.1$ Hz, $|^1J_{WC}| = 126.4$ Hz; CO$_{cis}$), 198.6 (d, $|^2J_{PC}| = 22.0$ Hz; CO$_{trans}$), 206.6 (d$_{sat}$, $|^{1+4}J_{PC}| = 27.5$ Hz, $|^2J_{WC}| = 3.9$ Hz; PCN); ^{29}Si$\{^1$H$\}$ NMR (59.6 MHz, C$_6$D$_6$): $\delta = 1.1$ (d, $|^2J_{PSi}| = 8.0$ Hz), 2.4 (d, $|^2J_{PSi}| = 4.9$ Hz); ^{31}P NMR (121.5 MHz, C$_6$D$_6$): $\delta = 114.4$ (d$_{sat}$, $|^1J_{WP}| = 234.0$ Hz, $|^2J_{PH}| = 6.5$ Hz); IR (KBr): $\tilde{\nu} = 2961$ (w, CH$_3$/CH), 2925 (w, CH$_3$/CH), 2900 (w, CH$_3$/CH), 2067 (m, sh, CO), 1979 (m, sh, CO), 1947 (s, CO), 1927 (s, CO), 1921 (s, CO), 1556 (m, CN), 1506 cm^{-1} (w, CN); UV/Vis (n-pentane): λ_{max} (abs.) = 203 (sh, 1.110), 205 (1.143), 227 (0.955), 249 (sh, 0.614), 296 (0.209), 345 (sh, 0.102), 404 (0.054), 539 nm (0.055); CV: $E_{1/2} = 0.206$

and 0.288 V; MS (FAB$^+$, ^{184}W): m/z (%): 935.9 ([M + H]$^+$, 11), 880.0 ([M − 2 CO]$^+$, 30), 796.0 ([M − 5 CO]$^+$, 10), 613.0 ([M + H − W(CO)$_5$]$^+$, 85), 612.1 ([M − W(CO)$_5$]$^+$, 100); elemental analysis (%) calcd. for C$_{34}$H$_{37}$Fe$_2$N$_2$O$_5$PSi$_2$W: C 43.61, H 3.98, N 2.99; found: C 43.87, H 4.12, N 2.88.

10.2.19   Reactions of 2H-Azaphosphirene Complexes 35, 67, and 70–73 with Ferrocinium Hexafluorophosphate in the Absence of Nitriles

In an NMR tube 0.10 mmol 2H-azaphosphirene complex of **35** (61.7 mg), **70** (52.9 mg), **71** (48.6 mg), **67** (93.6 mg), **72** (84.8 mg), or **73** (80.4 mg) and 33.1 mg (0.10 mmol) of ferrocinium hexafluorophosphate were dissolved in 0.6 mL of CH$_2$Cl$_2$. The reactions were monitored by ^{31}P{^{1}H} NMR spectroscopy (results given in Tab. 3.4 and Fig. 3.10, Section 3.3).

10.2.20   Attempted Synthesis of [2-Bis(trimethylsilyl)methyl-3,5-diphenyl-2H-1,4,2-diazaphosphole-κP]pentacarbonylmolybdenum(0) (74c) and [2-Bis(trimethylsilyl)methyl-3,5-diphenyl-2H-1,4,2-diazaphosphole-κP]pentacarbonylchromium(0) (75c) Using Ferrocinium Hexafluorophosphate

Attempted synthesis of complex 74c using 0.05 equiv. of [FeCp$_2$][PF$_6$]: To a solution of 265 mg (0.50 mmol) of 2H-azaphosphirene complex **70** in 1.5 mL of CH$_2$Cl$_2$ were added consecutively 52 μL (0.51 mmol) of benzonitrile (**36c**) and 9 mg (0.05 mmol) of ferrocinium hexafluorophosphate. The reaction mixture was stirred at ambient temperature (monitoring by ^{31}P{^{1}H} NMR spectroscopy). After 24 h it contained complex **74c**, ligand **50c**, unreacted **70**, and unidentified by-products **A** and **B**. ^{31}P{^{1}H} NMR (121.5 MHz, CH$_2$Cl$_2$): δ = −83.3 (s; **70** (48 %)), −76.6 (s; **A** (2 %)), 103.2 (s; **50c** (17 %)), 130.0 (s; **74c** (24 %)), 133.4 (s; **B** (2 %)). After removement of all volatiles in vacuo ($\sim 10^{-2}$ mbar) the crude product mixture was subjected to column chromatography on silica (−30 °C, 2 × 12 cm), but the products could not completely be separated.

Attempted synthesis of complex 74c using 0.18 equiv. of [FeCp$_2$][PF$_6$]: To a solution of 185 mg (0.35 mmol) of 2H-azaphosphirene complex **70** in 2 mL of CH$_2$Cl$_2$

were added consecutively 36 μL (0.35 mmol) of benzonitrile (**36c**) and 22.5 mg (0.07 mmol) of ferrocinium hexafluorophosphate. The reaction mixture was stirred for 6 h at ambient temperature, and after removement of all volatiles in vacuo ($\sim 10^{-2}$ mbar) the crude product mixture was subjected to column chromatography on silica ($-30\,°C$, 2×12 cm), but the products could not completely be separated.

Attempted synthesis of complex 75c using 0.05 equiv. of [FeCp$_2$][PF$_6$]: To a solution of 243 mg (0.50 mmol) of 2*H*-azaphosphirene complex **71** in 1.5 mL of CH$_2$Cl$_2$ were added consecutively 52 μL (0.51 mmol) of benzonitrile (**36c**) and 9 mg (0.05 mmol) of ferrocinium hexafluorophosphate. The reaction mixture was stirred at ambient temperature (monitoring by ^{31}P{^{1}H} NMR spectroscopy). After 24 h it contained complex **75c**, ligand **50c**, and unreacted **71**. ^{31}P{^{1}H} NMR (121.5 MHz, CH$_2$Cl$_2$): $\delta = -53.4$ (s; **71** (51 %)), 103.1 (s; **50c** (11 %)), 153.1 (s; **75c** (34 %)). after removement of all volatiles in vacuo ($\sim 10^{-2}$ mbar) the crude product mixture was subjected to column chromatography on silica ($-30\,°C$, 2×12 cm), but the products could not completely be separated.

10.2.21 Investigations on the Progression of Reactions of [2-Bis(trimethylsilyl)methyl-3-phenyl-2*H*-azaphosphirene-κP]pentacarbonyltungsten(0) (35) and [2-Bis(trimethyl-silyl)methyl-3-phenyl-2*H*-azaphosphirene-κP]pentacar-bonylchromium(0) (71) with Benzonitrile in the Presence of Ferrocinium Hexafluorophosphate

A solution of 16 μL (0.16 mmol) of benzonitrile (**36c**) in 0.6 mL of CH$_2$Cl$_2$ was added to 0.10 mmol of 2*H*-azaphosphirene complex **35** (64 mg) or **71** (50 mg) and 7.2 mg (0.02 mmol) of ferrocinium hexafluorophosphate in an NMR tube. Product ratios were estimated by ^{31}P{^{1}H} NMR spectroscopic signal integration (30 °C, 100 scans each, measurement duration 159 s, recorded reaction time corresponds to the end of the respective measurement; results given in Fig. 3.12, Section 3.4).

10.3 Acid-Induced Ring Expansion of 2*H*-Azaphosphirene Complexes

10.3.1 Synthesis of [2-Bis(trimethylsilyl)methyl-5-dimethylamino-3-phenyl-2*H*-1,4,2-diazaphosphole-*κP*]pentacarbonyltungsten(0) (41b)

To a stirred solution of 216 mg (0.35 mmol) of 2*H*-azaphosphirene complex **35** in 3.8 mL of CH_2Cl_2 were added consecutively 30 μL (0.37 mmol) of dimethyl cyanamide (**36b**) and 33 μL (0.38 mmol) of TfOH at ambient temperature. The initially yellow colored solution turned deep red. Subsequently, 53 μL (0.38 mmol) of NEt_3 was added at ambient temperature while the reaction mixture turned yellow again. After removement of all volatiles in vacuo ($\sim 10^{-2}$ mbar) the product was purified by column chromatography on silica ($-30\,^\circ$C, 2×9 cm, petroleum ether/Et_2O: 100/1). Evaporation of the solvents of the first fraction ($\sim 10^{-2}$ mbar) yielded 181 mg (0.26 mmol, 75 %) of **41b**; for analytical data see Section 10.2.1.

10.3.2 Synthesis of [2-Bis(trimethylsilyl)methyl-3-phenyl-5-(2-thienyl)-2*H*-1,4,2-diazaphosphole-*κP*]pentacarbonyltungsten(0) (41g)

Synthesis of 41g using stoichiometric amounts of TfOH: To a stirred solution of 508 mg (0.82 mmol) of 2*H*-azaphosphirene complex **35** in 11 mL of CH_2Cl_2 were added consecutively 120 μL (1.29 mmol) of 2-thiophenecarbonitrile (**36g**) and 73 μL (0.83 mmol) of TfOH at ambient temperature. The initially yellow colored solution turned deep green. Subsequently, 200 μL (1.42 mmol) of NEt_3 was added at $-5\,^\circ$C while the reaction mixture turned orange. After removement of all volatiles in vacuo ($\sim 10^{-2}$ mbar) the crude product was dissolved in petroleum ether, filtered through celite, and purified by column chromatography on silica ($-30\,^\circ$C, 2×9 cm, petroleum ether/Et_2O: 100/1). Evaporation of the solvents of the first fraction ($\sim 10^{-2}$ mbar) yielded 391 mg (0.54 mmol, 65 %) of **41g**.

Synthesis of 41g using catalytic amounts of TfOH: To a stirred solution of 211 mg (0.34 mmol) of 2*H*-azaphosphirene complex **35** in 4.2 mL of CH_2Cl_2 were added consecutively 32 μL (0.34 mmol) of 2-thiophenecarbonitrile (**36g**) and 3 μL (0.03 mmol, 0.1 equiv.) of TfOH at ambient temperature. The completeness of the reaction was checked by ^{31}P$\{^1$H$\}$ NMR reaction monitoring. After 24 h 5 μL (0.04

mmol) of NEt$_3$ was added at ambient temperature. Then, all volatiles were removed in vacuo ($\sim 10^{-2}$ mbar), and **41g** was purified by column chromatography on silica ($-30\,^\circ$C, 2×7 cm, petroleum ether/Et$_2$O: 100/1). Evaporation of the solvents of the first fraction ($\sim 10^{-2}$ mbar) yielded 160 mg (0.22 mmol, 64 %) of **41g**; for analytical data see Section 10.2.2.

10.3.3 Synthesis of [2-Bis(trimethylsilyl)methyl-5-methyl-3-phenyl-2H-1,4,2-diazaphosphole-κP]pentacarbonyl-tungsten(0) (41m)

To a stirred solution of 400 mg (0.65 mmol) of 2H-azaphosphirene complex **35** in 8 mL of CH$_2$Cl$_2$ were added consecutively 35 μL (0.67 mmol) of acetonitrile (**36m**) and 57 μL (0.65 mmol) of TfOH at ambient temperature. The initially yellow colored solution turned deep purple. Subsequently, 92 μL (0.66 mmol) of NEt$_3$ was added at ambient temperature while the reaction mixture turned yellow again. After removement of all volatiles in vacuo ($\sim 10^{-2}$ mbar) the product was purified by column chromatography on silica ($-30\,^\circ$C, 2×8 cm, petroleum ether/Et$_2$O: 100/1). Evaporation of the solvents of the first fraction ($\sim 10^{-2}$ mbar) yielded **41m**.

41m: Yellow solid; yield: 282 mg (0.43 mmol, 66 %); mp 71$\,^\circ$C (decomp.); ^{1}H NMR (300.13 MHz, C$_6$D$_6$): $\delta = -0.24$ (s$_{sat}$, $|^2J_{SiH}| = 6.3$ Hz, $|^1J_{CH}| = 119.8$ Hz, 9 H; Si(CH$_3$)$_3$), 0.47 (s$_{sat}$, $|^2J_{SiH}| = 6.3$ Hz, $|^1J_{CH}| = 119.2$ Hz, 9 H; Si(CH$_3$)$_3$), 0.94 (d, $|^2J_{PH}| = 4.1$ Hz, 1 H; CH(SiMe$_3$)$_2$), 2.43 (s, 3 H; CH$_3$), 7.10 (m$_c$, 3 H; $meta$+$para$-H$_{phenyl}$), 8.16 (m$_c$, 2 H; $ortho$-H$_{phenyl}$); ^{13}C$\{^1$H$\}$ NMR (75.5 MHz, C$_6$D$_6$): $\delta = 2.9$ (d$_{sat}$, $|^3J_{PC}| = 1.9$ Hz, $|^1J_{SiC}| = 52.4$ Hz; Si(CH$_3$)$_3$), 3.8 (d$_{sat}$, $|^3J_{PC}| = 2.6$ Hz, $|^1J_{SiC}| = 53.3$ Hz; Si(CH$_3$)$_3$), 17.6 (d, $|^1J_{PC}| = 4.2$ Hz; CH(SiMe$_3$)$_2$), 22.2 (d, $|^3J_{PC}| = 11.3$ Hz; CH$_3$), 129.9 (s; $meta$-C$_{phenyl}$), 131.8 (d, $|^3J_{PC}| = 2.3$ Hz; $ortho$-C$_{phenyl}$), 132.3 (d, $|^2J_{PC}| = 23.3$ Hz; $ipso$-C$_{phenyl}$), 133.7 (s; $para$-C$_{phenyl}$), 174.0 (d, $|^{2+3}J_{PC}| = 7.1$ Hz; PNC), 197.7 (d$_{sat}$, $|^2J_{PC}| = 6.1$ Hz, $|^1J_{WC}| = 126.9$ Hz; CO$_{cis}$), 198.2 (d$_{sat}$, $|^2J_{PC}| = 22.3$ Hz, $|^1J_{WC}| = 144.0$ Hz; CO$_{trans}$), 202.1 (d$_{sat}$, $|^{1+4}J_{PC}| = 22.6$ Hz, $|^2J_{WC}| = 3.2$ Hz; PCN); ^{15}N NMR (30.418 MHz, C$_6$D$_6$): $\delta = -116$ ($|^{1+4}J_{PN}| = 55$ Hz, $|^3J_{NH}| = 6$ Hz; N^1), -52 (N^4); ^{29}Si$\{^1$H$\}$ NMR (59.6 MHz, C$_6$D$_6$): $\delta = 3.3$ (d, $|^2J_{PSi}| = 2.5$ Hz), 3.7 (d, $|^2J_{PSi}| = 12.2$ Hz); ^{31}P NMR (121.5 MHz, C$_6$D$_6$): $\delta = 108.7$ (d$_{sat}$, $|^1J_{WP}| = 228.9$ Hz, $|^2J_{PH}| = 3.8$ Hz); IR (KBr): $\tilde{\nu} = 2958$ (w, CH$_3$/CH), 2900 (w, CH$_3$/CH), 2071 (m, sh, CO), 1982 (m, sh, CO), 1952 (s, br, CO), 1930 (s, CO), 1568 cm^{-1} (w, CN); Raman (202 mW): $\tilde{\nu} = 3073$ (m, CH$_{phenyl}$), 2996 (w, CH$_3$/CH), 2962 (m, CH$_3$/CH), 2901 (s, CH$_3$/CH), 2853 (w, CH$_3$/CH), 2068 (s, CO), 1977 (vs, CO), 1955 (m, CO), 1926 (s, CO), 1915 (m, CO), 1596 (m, CN), 1566 (m, CN), 440 cm^{-1} (w); UV/Vis (n-pentane):

λ_{max} (ϵ [cm^2 mmol^{-1}]) = 208 (sh, 65644), 228 (92836), 250 (sh, 50961), 289 (17777), 312 (sh, 14946), 425 nm (2963); CV: $E_{1/2}$ = -1.792 V; MS (FAB$^+$, ^{184}W): m/z (%): 659.0 ([M + H]$^+$, 16), 602.0 ([M $-$ 2 CO]$^+$, 38), 335.2 ([M + H $-$ W(CO)$_5$]$^+$, 100), 191.1 ([Me$_3$SiP(H)C(H)SiMe$_3$]$^+$, 40); elemental analysis (%) calcd. for C$_{22}$H$_{30}$N$_3$O$_5$PSi$_2$W: C 38.31, H 4.13, N 4.25; found: C 38.23, H 4.19, N 4.13.

10.3.4 Synthesis of [2-Bis(trimethylsilyl)methyl-5-(2-methyl-prop-2-yl)-3-phenyl-2*H*-1,4,2-diazaphosphole-κP]penta-carbonyltungsten(0) (41r)

To a stirred solution of 300 mg (0.49 mmol) of 2*H*-azaphosphirene complex **35** in 6 mL of CH$_2$Cl$_2$ were added consecutively 54 μL (0.49 mmol) of pivalonitrile (**36r**) and 43 μL (0.49 mmol) of TfOH at $-30\,^\circ$C. The initially yellow colored solution turned deep purple. After 3 min the cooling bath was removed and 69 μL (0.49 mmol) of NEt$_3$ was added while the reaction mixture turned brownish yellow. Then, all volatiles were removed in vacuo ($\sim 10^{-2}$ mbar), and the product was purified by column chromatography on silica ($-30\,^\circ$C, 2 $\times$ 8 cm, petroleum ether/Et$_2$O: 10/1). Evaporation of the solvents of the first fraction ($\sim 10^{-2}$ mbar) yielded **41r**.

41r: Yellow solid; yield: 311 mg (0.44 mmol, 91 %); mp 72 $^\circ$C; ^{1}H NMR (300.13 MHz, C$_6$D$_6$): δ = -0.27 (s$_{sat}$, $|^2J_{SiH}|$ = 6.2 Hz, $|^1J_{CH}|$ = 119.7 Hz, 9 H; Si(CH$_3$)$_3$), 0.46 (s$_{sat}$, $|^1J_{CH}|$ = 120.6 Hz, 9 H; Si(CH$_3$)$_3$), 0.98 (d, $|^2J_{PH}|$ = 3.9 Hz, 1 H; C*H*(SiMe$_3$)$_2$), 1.41 (d$_{sat}$, $|^5J_{PH}|$ = 0.5 Hz, $|^1J_{CH}|$ = 126.0 Hz, 9 H; C(CH$_3$)$_3$), 7.16 (m$_c$, 3 H; *meta+para*-H$_{phenyl}$), 8.11 (m$_c$, 2 H; *ortho*-H$_{phenyl}$); ^{13}C\{^{1}H\} NMR (75.5 MHz, C$_6$D$_6$): δ = 3.0 (d$_{sat}$, $|^3J_{PC}|$ = 1.9 Hz, $|^1J_{SiC}|$ = 52.4 Hz; Si(CH$_3$)$_3$), 3.9 (d$_{sat}$, $|^3J_{PC}|$ = 2.6 Hz, $|^1J_{SiC}|$ = 53.0 Hz; Si(CH$_3$)$_3$), 17.8 (d, $|^1J_{PC}|$ = 4.2 Hz; *C*H(SiMe$_3$)$_2$), 27.8 (s; C(*C*H$_3$)$_3$), 38.6 (d, $|^3J_{PC}|$ = 9.7 Hz; *C*(CH$_3$)$_3$), 128.8 (s; *meta*-C$_{phenyl}$), 131.9 (d, $|^3J_{PC}|$ = 1.9 Hz; *ortho*-C$_{phenyl}$), 132.3 (d, $|^2J_{PC}|$ = 24.2 Hz; *ipso*-C$_{phenyl}$), 133.5 (s; *para*-C$_{phenyl}$), 182.9 (d, $|^{2+3}J_{PC}|$ = 8.4 Hz; PNC), 197.7 (d$_{sat}$, $|^2J_{PC}|$ = 6.1 Hz, $|^1J_{WC}|$ = 126.4 Hz; CO$_{cis}$), 198.3 (d$_{sat}$, $|^2J_{PC}|$ = 22.3 Hz, $|^1J_{WC}|$ = 144.5 Hz; CO$_{trans}$), 201.2 (d$_{sat}$, $|^{1+4}J_{PC}|$ = 22.3 Hz, $|^2J_{WC}|$ = 3.2 Hz; PCN); ^{29}Si\{^{1}H\} NMR (59.6 MHz, C$_6$D$_6$): δ = 3.3 (d$_{sat}$, $|^2J_{PSi}|$ = 3.5 Hz, $|^1J_{SiC}|$ = 53.2 Hz), 3.8 (d$_{sat}$, $|^2J_{PSi}|$ = 12.0 Hz, $|^1J_{SiC}|$ = 52.5 Hz); ^{31}P NMR (121.5 MHz, C$_6$D$_6$): δ = 108.3 (s$_{sat}$, $|^1J_{WP}|$ = 228.9 Hz); IR (KBr): $\tilde{\nu}$ = 2961 (m, CH$_3$/CH), 2928 (w, CH$_3$/CH), 2905 (w, CH$_3$/CH), 2070 (m, sh, CO), 1981 (m, sh, CO), 1935 (s, CO), 1920 (s, CO), 1568 (m, CN), 1262.2 (m, δ_s(^{t}Bu)), 1253.1 cm^{-1} (m, δ_s(^{t}Bu)); UV/Vis (*n*-pentane): λ_{max} (abs.) = 204 (0.481), 209 (0.487), 212 (0.504), 217 (0.590), 221 (sh, 0.689), 226 (sh, 0.775), 230 (0.811), 250 (sh, 0.766), 292 (0.173), 309 (sh, 0.162), 349 (0.073), 419 nm (0.039); MS

(FAB$^+$, ^{184}W): m/z (%): 700.2 ([M + H]$^+$, 19), 644.1 ([M − 2 CO]$^+$, 22), 561.0 ([M −
3 CO − C(CH$_3$)$_3$]$^+$, 31), 514.0 ([(OC)$_5$W(Me$_3$Si)PC(H)SiMe$_3$]$^+$, 22), 377.2 ([M + H −
W(CO)$_5$]$^+$, 100); elemental analysis (%) calcd. for C$_{24}$H$_{33}$N$_2$O$_5$PSi$_2$W: C 41.15, H
4.75, N 4.00; found: C 41.74, H 5.21, N 3.65.

10.3.5 Synthesis of [5-(1-Adamantyl)-2-bis(trimethylsilyl)methyl-3-phenyl-2H-1,4,2-diazaphosphole-κP]pentacarbonyltungsten(0) (41s)

To a stirred solution of 400 mg (0.65 mmol) of 2H-azaphosphirene complex **35** in 8 mL
of CH$_2$Cl$_2$ were added consecutively 115 mg (0.71 mmol) of 1-adamantanecarbonitrile
(**36s**) and 62 μL (0.71 mmol) of TfOH at −30 °C. The initially yellow colored solution
turned deep purple. The cooling bath was removed after the addition, and after 5
min 100 μL (0.71 mmol) of NEt$_3$ was added while the reaction mixture turned orange.
Then, all volatiles were removed in vacuo ($\sim 10^{-2}$ mbar), and the product was purified
by column chromatography on silica (−30 °C, 2 × 8 cm, petroleum ether/Et$_2$O: 10/1).
Evaporation of the solvents of the first fraction ($\sim 10^{-2}$ mbar) yielded **41s**.

41s: Yellow solid, crystallized from n-pentane at 4 °C; yield: 370 mg (0.60 mmol,
93 %); mp 135 °C; ^{1}H NMR (300.13 MHz, C$_6$D$_6$): δ = −0.23 (s$_{sat}$, $|^2J_{SiH}|$ = 6.5 Hz,
$|^1J_{CH}|$ = 119.7 Hz, 9 H; Si(CH$_3$)$_3$), 0.50 (s$_{sat}$, $|^2J_{SiH}|$ = 6.5 Hz, $|^1J_{CH}|$ = 119.9 Hz,
9 H; Si(CH$_3$)$_3$), 1.01 (d, $|^2J_{PH}|$ = 4.0 Hz, 1 H; CH(SiMe$_3$)$_2$), 1.70 (m$_c$, 6 H; adamantyl-
C^{2,8,9}H$_2$), 2.00 (m$_c$, 3 H; adamantyl-C^{3,5,7}H), 2.20 (m$_c$, 6 H; adamantyl-C^{4,6,10}H$_2$), 7.16
(m$_c$, 3 H; $meta+para$-H$_{phenyl}$), 8.17 (m$_c$, 2 H; $ortho$-H$_{phenyl}$); ^{13}C{^{1}H} NMR (75.5 MHz,
C$_6$D$_6$): δ = 3.1 (d$_{sat}$, $|^3J_{PC}|$ = 1.9 Hz, $|^1J_{SiC}|$ = 52.4 Hz; Si(CH$_3$)$_3$), 3.9 (d$_{sat}$, $|^3J_{PC}|$ =
2.6 Hz, $|^1J_{SiC}|$ = 53.3 Hz; Si(CH$_3$)$_3$), 17.7 (d, $|^1J_{PC}|$ = 4.2 Hz; CH(SiMe$_3$)$_2$), 28.5 (s;
adamantyl-C^{3,5,7}H), 37.0 (s; adamantyl-C^{4,6,10}H$_2$), 39.8 (s; adamantyl-C^{2,8,9}H$_2$), 40.8
(d, $|^3J_{PC}|$ = 10.0 Hz; adamantyl-C^1), 128.8 (s; $meta$-C$_{phenyl}$), 131.9 (d, $|^3J_{PC}|$ = 1.9
Hz; $ortho$-C$_{phenyl}$), 132.5 (d, $|^2J_{PC}|$ = 24.2 Hz; $ipso$-C$_{phenyl}$), 133.5 (d, $|^5J_{PC}|$ = 0.4
Hz; $para$-C$_{phenyl}$), 182.2 (d, $|^{2+3}J_{PC}|$ = 8.4 Hz; PNC), 197.8 (d$_{sat}$, $|^2J_{PC}|$ = 5.8 Hz,
$|^1J_{WC}|$ = 126.7 Hz; CO$_{cis}$), 198.4 (d$_{sat}$, $|^2J_{PC}|$ = 22.3 Hz, $|^1J_{WC}|$ = 144.8 Hz; CO$_{trans}$),
201.0 (d$_{sat}$, $|^{1+4}J_{PC}|$ = 22.3 Hz, $|^2J_{WC}|$ = 3.2 Hz; PCN); ^{29}Si{^{1}H} NMR (59.6 MHz,
C$_6$D$_6$): δ = 3.3 (d$_{sat}$, $|^2J_{PSi}|$ = 3.5 Hz, $|^1J_{SiC}|$ = 53.2 Hz), 3.8 (d$_{sat}$, $|^2J_{PSi}|$ = 12.2 Hz,
$|^1J_{SiC}|$ = 52.3 Hz); ^{31}P NMR (121.5 MHz, C$_6$D$_6$): δ = 107.0 (d$_{sat}$, $|^1J_{WP}|$ = 228.9 Hz,
$|^2J_{PH}|$ = 3.8 Hz); IR (KBr): $\tilde{\nu}$ = 2906 (m, CH$_3$/CH), 2854 (w, CH$_3$/CH), 2072 (m,
sh, CO), 1996 (m, sh, CO), 1948 (s, CO), 1927 (s, CO), 1562 cm^{-1} (m, CN); UV/Vis
(n-pentane): λ_{max} (abs.) = 204 (0.935), 210 (sh, 0.999), 230 (1.625), 250 (sh, 0.950),
292 (0.297), 304 (sh, 0.285), 418 nm (0.051); MS (FAB$^+$, ^{184}W): m/z (%): 779.2

$([M + H]^+, 12)$, 722.2 $([M - 3\,CO]^+, 30)$, 514.0 $([(OC)_5W(Me_3Si)PC(H)SiMe_3]^+, 24)$, 486.0 $([M + H - CH(SiMe_3)_2 - C_{10}H_{15}]^+, 33)$, 455.2 $([M + H - W(CO)_5]^+, 100)$, 191.1 $([Me_3SiP(H)C(H)SiMe_3]^+, 12)$; elemental analysis (%) calcd. for $C_{30}H_{39}N_2O_5PSi_2W$: C 46.28, H 5.05, N 3.60; found: C 46.81, H 5.09, N 3.56.

10.3.6 Synthesis of [2-Bis(trimethylsilyl)methyl-3-phenyl-5-tri-methylsilyl-2*H*-1,4,2-diazaphosphole-κP]pentacarbon-yltungsten(0) (41t)

To a stirred solution of 270 mg (0.44 mmol) of 2*H*-azaphosphirene complex **35** in 5 mL of CH_2Cl_2 were added consecutively 60 μL (0.47 mmol) of trimethylsilyl cyanide (**36t**) and 40 μL (0.46 mmol) of TfOH at ambient temperature. The initially yellow colored solution turned deep purple. Subsequently, 66 μL (0.47 mmol) of NEt_3 was added at ambient temperature while the reaction mixture turned orange. After removement of all volatiles in vacuo ($\sim 10^{-2}$ mbar) the crude product was dissolved in petroleum ether, filtered through celite, and purified by column chromatography on silica ($-30\,°C$, 2×7 cm, petroleum ether/Et_2O: 100/1). Evaporation of the solvents of the first fraction ($\sim 10^{-2}$ mbar) yielded **41t**.

41t: Yellow oil; yield: 24 mg (0.03 mmol, 8 %); ^1H NMR (300.13 MHz, C_6D_6): $\delta = -0.26$ (s_{sat}, $|^2J_{SiH}| = 6.5$ Hz, $|^1J_{CH}| = 119.8$ Hz, 9 H; CHSi(CH_3)$_3$), 0.40 (s_{sat}, $|^2J_{SiH}| = 6.9$ Hz, $|^1J_{CH}| = 119.5$ Hz, 9 H; Si(CH_3)$_3$), 0.48 (s_{sat}, $|^2J_{SiH}| = 6.6$ Hz, $|^1J_{CH}| = 119.0$ Hz, 9 H; CHSi(CH_3)$_3$), 0.99 (d, $|^2J_{PH}| = 4.5$ Hz, 1 H; CH(SiMe$_3$)$_2$), 7.10 (m_c, 3 H; *meta*+*para*-H$_{phenyl}$), 8.17 (m_c, 2 H; *ortho*-H$_{phenyl}$); $^{13}C\{^1H\}$ NMR (75.5 MHz, C_6D_6): $\delta = -2.6$ (s; Si(CH$_3$)$_3$), 2.9 (d, $|^3J_{PC}| = 1.9$ Hz; CHSi(CH_3)$_3$), 3.8 (d, $|^3J_{PC}| = 2.6$ Hz; CHSi(CH_3)$_3$), 17.0 (d, $|^1J_{PC}| = 5.8$ Hz; CH(SiMe$_3$)$_2$), 128.9 (s; *meta*-C$_{phenyl}$), 132.1 (d, $|^3J_{PC}| = 1.9$ Hz; *ortho*-C$_{phenyl}$), 132.5 (d, $|^2J_{PC}| = 26.2$ Hz; *ipso*-C$_{phenyl}$), 133.3 (d, $|^5J_{PC}| = 0.7$ Hz; *para*-C$_{phenyl}$), 188.5 (d, $|^{2+3}J_{PC}| = 15.2$ Hz; PNC), 197.8 (d_{sat}, $|^2J_{PC}| = 5.8$ Hz, $|^1J_{WC}| = 126.7$ Hz; CO$_{cis}$), 198.2 (d, $|^2J_{PC}| = 22.0$ Hz; CO$_{trans}$), 199.4 (d_{sat}, $|^{1+4}J_{PC}| = 19.1$ Hz, $|^2J_{WC}| = 3.6$ Hz; PCN); $^{29}Si\{^1H\}$ NMR (59.6 MHz, C_6D_6): $\delta = 3.4$ (d, $|^2J_{PSi}| = 2.9$ Hz; CHSi(CH$_3$)$_3$), 4.3 (d, $|^3J_{PSi}| = 11.8$ Hz; Si(CH$_3$)$_3$), 4.4 (d, $|^2J_{PSi}| = 14.9$ Hz; CHSi(CH$_3$)$_3$); ^{31}P NMR (121.5 MHz, C_6D_6): $\delta = 109.4$ (d_{sat}, $|^1J_{WP}| = 223.8$ Hz, $|^2J_{PH}| = 4.5$ Hz); IR (KBr): $\tilde{\nu} = 2962$ (m, CH$_3$/CH), 2072 (m, CO), 1949 cm^{-1} (s, CO); UV/Vis (*n*-pentane): λ_{max} (abs.) = 231 (1.292) 251 (sh, 0.693), 284 (0.207), 313 (sh, 0.182), 346 (sh, 0.084), 432 nm (0.030); MS (FAB$^+$, ^{184}W): m/z (%): 717.0 ($[M + H]^+$, 16), 576.0 ($[M - 5\,CO]^+$, 6), 514.0 ($[(OC)_5W(Me_3Si)PC(H)SiMe_3]^+$, 32), 393.1 ($[M + H - W(CO)_5]^+$, 56), 307.0 ($[mNBA + H]^+$, 100).

10.3.7 Synthesis of [5-Dimethylamino-2-(1,2,3,4,5-pentamethyl-2,4-cyclopentadien-1-yl)-3-phenyl-2H-1,4,2-diazaphos-phole-κP]pentacarbonyltungsten(0) (122b)

To a stirred solution of 150 mg (0.25 mmol) of 2H-azaphosphirene complex **121** in 7.5 mL of CH$_2$Cl$_2$ were added consecutively 24 μL (0.29 mmol) of dimethyl cyanamide (**36b**) and a solution of 24 μL (0.27 mmol) of TfOH in 2.5 mL of CH$_2$Cl$_2$ at $-78\,^{\circ}$C. The initially yellow colored solution turned deep red. After 5 min the cooling bath was removed, and after 4 min 24 μL (0.30 mmol) of pyridine was added while the reaction mixture turned light orange. Then, all volatiles were removed in vacuo ($\sim 10^{-2}$ mbar), and the product was purified by column chromatography on neutral Al$_2$O$_3$ ($-35\,^{\circ}$C, 2 $\times$ 8 cm, petroleum ether/Et$_2$O: 10/1). Evaporation of the solvents of the first fraction ($\sim 10^{-2}$ mbar) yielded **122b**.

122b: Yellow solid; yield: 43 mg (0.06 mmol, 25 %); mp 102 $^{\circ}$C; ^{1}H NMR (300.13 MHz, C$_6$D$_6$): δ = 1.23 (d, $|^3J_{PH}|$ = 15.5 Hz, 3 H; Cp*-C^1–CH$_3$), 1.36 (m$_c$, 3 H; Cp*–CH$_3$), 1.41 (m$_c$, 6 H; Cp*–CH$_3$), 2.19 (br, 3 H; Cp*–CH$_3$), 2.90 (s, 3 H; NCH$_3$), 2.96 (s, 3 H; NCH$_3$), 7.06 (m$_c$, 3 H; $meta$+$para$-H$_{phenyl}$), 8.00 (m$_c$, 2 H; $ortho$-H$_{phenyl}$); ^{13}C$\{^1$H$\}$ NMR (75.5 MHz, C$_6$D$_6$): δ = 10.8 (d, $|J_{PC}|$ = 1.3 Hz; Cp*–CH$_3$), 11.4 (d, $|J_{PC}|$ = 1.6 Hz; Cp*–CH$_3$), 12.4 (s; Cp*–CH$_3$), 13.1 (d, $|J_{PC}|$ = 2.3 Hz; Cp*–CH$_3$), 15.0 (s; Cp*-C^1–CH$_3$), 37.6 (s; NCH$_3$), 37.9 (s; NCH$_3$), 63.9 (s; Cp*-C^1), 128.2 (s; $meta$-C$_{phenyl}$), 130.6 (d, $|^3J_{PC}|$ = 1.9 Hz; $ortho$-C$_{phenyl}$), 132.6 (s; $para$-C$_{phenyl}$), 134.4 (d, $|^2J_{PC}|$ = 19.4 Hz; $ipso$-C$_{phenyl}$), 135.3 (d, $|J_{PC}|$ = 2.9 Hz; Cp*-C), 138.8 (d, $|J_{PC}|$ = 1.6 Hz; Cp*-C), 139.2 (d, $|J_{PC}|$ = 4.5 Hz; Cp*-C), 141.0 (d, $|J_{PC}|$ = 7.1 Hz; Cp*-C), 166.3 (d, $|^{2+3}J_{PC}|$ = 3.6 Hz; PNC), 197.4 (d$_{sat}$, $|^2J_{PC}|$ = 6.5 Hz, $|^1J_{WC}|$ = 126.2 Hz; CO$_{cis}$), 198.3 (d, $|^2J_{PC}|$ = 25.2 Hz; CO$_{trans}$), 199.3 (d$_{sat}$, $|^{1+4}J_{PC}|$ = 24.6 Hz, $|^2J_{WC}|$ = 3.2 Hz; PCN); ^{31}P NMR (121.5 MHz, C$_6$D$_6$): δ = 118.5 (m$_c$, $|^1J_{WP}|$ = 244.1 Hz); IR (KBr): $\tilde{\nu}$ = 2960 (w, CH$_3$), 2923 (w, CH$_3$), 2859 (w, CH$_3$), 2067 (m, sh, CO), 1949 (s, CO), 1917 (s, CO), 1914 (s, CO), 1605 cm^{-1} (w, CN); UV/Vis (n-pentane): λ_{max} (abs.) = 205 (sh, 0.461), 226 (0.657), 251 (sh, 0.396), 284 (0.154), 348 (0.049) 400 nm (0.028); MS (EI, ^{184}W): m/z (%): 663.0 ([M]$^+$, 16), 607.1 ([M$-$2 CO]$^+$, 13), 579.1 ([M$-$3 CO]$^+$, 14), 527.9 ([M$-$C5Me5]$^+$, 75), 499.9 ([M$-$C5Me5$-$CO]$^+$, 39), 471.9 ([M$-$C5Me5$-$2 CO]$^+$, 100), 443.9 ([M$-$C5Me5$-$3 CO]$^+$, 10), 388.0 ([M$-$C5Me5$-$5 CO]$^+$, 10), 135.1 (C5Me5$^+$, 69).

10.3.8   Synthesis of [2-Bis(trimethylsilyl)methyl-5-dimethylamino-3-phenyl-2H-1,4,2-diazaphosphol-1-ium-κP]pentacarbonyltungsten(0) Trifluoromethanesulfonate (123b)

To a stirred solution of 400 mg (0.65 mmol) of 2H-azaphosphirene complex **35** in 8 mL of CH$_2$Cl$_2$ were added consecutively 56 μL (0.69 mmol) of dimethyl cyanamide (**36b**) and 57 μL (0.65 mmol) of TfOH at $-60\,°$C while the initially yellow colored solution turned deep red. After all volatiles were removed in vacuo ($\sim 10^{-2}$ mbar) the red solid residue was washed with n-pentane. Then, the product (**123b**) was dried in vacuo ($\sim 10^{-2}$ mbar).

123b: Red solid, crystallized from CH$_2$Cl$_2$/n-pentane at $-20\,°$C; yield: 475 mg (0.57 mmol, 88 %); mp 86 °C (decomp.); ^{1}H NMR (300.13 MHz, CD$_2$Cl$_2$): $\delta = 0.14$ (s$_{sat}$, $|^2J_{SiH}| = 6.0$ Hz, $|^1J_{CH}| = 120.1$ Hz, 9 H; Si(CH$_3$)$_3$), 0.47 (s$_{sat}$, $|^2J_{SiH}| = 6.1$ Hz, $|^1J_{CH}|$ = 121.0 Hz, 9 H; Si(CH$_3$)$_3$), 1.45 (d, $|^2J_{PH}| = 6.7$ Hz, 1 H; CH(SiMe$_3$)$_2$), 3.59 (s, 3 H; NCH$_3$), 3.77 (s, 3 H; NCH$_3$), 7.69 (m$_c$, 2 H; $meta$-H$_{phenyl}$), 7.81 (m$_c$, 1 H; $para$-H$_{phenyl}$), 8.24 (m$_c$, 2 H; $ortho$-H$_{phenyl}$), 10.09 (d, $|^{2+5}J_{PH}| = 22.9$ Hz, $h_{1/2} = 7.8$ Hz, 1 H; NH); ^{13}C{^{1}H} NMR (75.5 MHz, CD$_2$Cl$_2$): $\delta = 3.1$ (d$_{sat}$, $|^3J_{PC}| = 2.6$ Hz, $|^1J_{SiC}| = 53.0$ Hz; Si(CH$_3$)$_3$), 3.3 (d$_{sat}$, $|^3J_{PC}| = 3.6$ Hz, $|^1J_{SiC}| = 53.0$ Hz; Si(CH$_3$)$_3$), 21.9 (d, $|^1J_{PC}|$ = 16.5 Hz; CH(SiMe$_3$)$_2$), 40.2 (s; NCH$_3$), 41.3 (s; NCH$_3$), 120.6 (q, $|^1J_{FC}| = 320.0$ Hz; CF$_3$), 130.0 (s; $meta$-C$_{phenyl}$), 130.5 (d, $|^2J_{PC}| = 21.3$ Hz; $ipso$-C$_{phenyl}$), 131.8 (d, $|^3J_{PC}| = 4.5$ Hz; $ortho$-C$_{phenyl}$), 137.0 (s; $para$-C$_{phenyl}$), 162.4 (d, $|^{2+3}J_{PC}| = 10.3$ Hz; PNC), 195.9 (d$_{sat}$, $|^2J_{PC}| = 5.8$ Hz, $|^1J_{WC}| = 127.4$ Hz; CO$_{cis}$), 196.8 (d$_{sat}$, $|^2J_{PC}| =$ 27.5 Hz, $|^1J_{WC}| = 142.0$ Hz; CO$_{trans}$), 196.9 (d, $|^{1+4}J_{PC}| = 3.2$ Hz; PCN); ^{15}N NMR (30.418 MHz, CD$_2$Cl$_2$): $\delta = -269$ (NMe$_2$), -264 ($|^{1+4}J_{PN}| = 22$ Hz, $|^1J_{NH}| = 92$ Hz; N^{1}H); ^{15}N NMR (30.418 MHz, CDCl$_3$): $\delta = -269$ (NMe$_2$), -264 ($|^{1+4}J_{PN}| =$ 15 Hz, $|^1J_{NH}| = 92$ Hz, $|^3J_{NH}| = 4$ Hz; N^{1}H); ^{29}Si{^{1}H} NMR (59.6 MHz, CD$_2$Cl$_2$): $\delta = 4.4$ (d$_{sat}$, $|^2J_{PSi}| = 6.9$ Hz, $|^1J_{SiC}| = 53.1$ Hz), 4.7 (d, $|^2J_{PSi}| = 1.1$ Hz); ^{31}P NMR (121.5 MHz, CD$_2$Cl$_2$): $\delta = 105.7$ (dd$_{sat}$, $|^1J_{WP}| = 251.8$ Hz, $|^{2+5}J_{PH}| = 23.0$ Hz, $|^2J_{PH}| = 6.7$ Hz); IR (KBr): $\tilde{\nu} = 3067$ (w, CH$_{phenyl}$), 2988 (w, CH$_3$/CH), 2960 (w, CH$_3$/CH), 2903 (w, CH$_3$/CH), 2837 (w, CH$_3$/CH), 2079 (m, sh, CO), 2001 (m, sh, CO), 1956 (s, sh, CO), 1940 (s, sh, CO), 1922 (s, sh, CO), 1658 (m, CN), 1523 cm^{-1} (w, CN); IR (CH$_2$Cl$_2$): $\tilde{\nu} = 2079$ (m, sh, CO), 1997 (w, CO), 1950 (s, CO), 1660 (m, CN), 1598 cm^{-1} (w, CN); Raman (40 mW): $\tilde{\nu} = 3071$ (s, CH$_{phenyl}$), 2957 (s, CH$_3$/CH), 2902 (s, CH$_3$/CH), 2078 (s, CO), 1996 (s, CO), 1958 (w, CO), 1944 (w, CO), 1923 (w, CO), 1660 (w, CN), 1596 (s, CN), 439 cm^{-1} (w); UV/Vis (CH$_2$Cl$_2$): λ_{max} (ϵ [cm^2 mmol^{-1}]) = 234 (91193), 301 (28253), 306 (28253), 335 (sh, 20715), 463 nm (3187); MS (FAB$^+$, ^{184}W): m/z (%): 688.1 ([M]$^+$, 19), 659.1 ([M$-$CO$-$H]$^+$, 16), 631.0 ([M$-$2 CO$-$H]$^+$, 14), 364.2 ([M$-$W(CO)$_5$]$^+$, 100); elemental analysis (%) calcd.

for C$_{23}$H$_{31}$F$_3$N$_3$O$_8$PSSi$_2$W: C 32.98, H 3.73, N 5.02; found: C 32.42, H 3.76, N 5.38.

10.3.9 Reaction of [2-Bis(trimethylsilyl)methyl-5-dimethylamino-3-phenyl-2H-1,4,2-diazaphosphole-κP]pentacarbonyltungsten(0) (41b) with Trifluoromethanesulfonic Acid

To a stirred solution of 70 mg (0.10 mmol) of 2H-1,4,2-diazaphosphole complex **41b** in 1.1 mL of CH$_2$Cl$_2$ was added 9 μL (0.10 mmol) of TfOH at $-30\,^\circ$C. The initially yellow colored solution turned deep red. After warming to room temperature and removement of all volatiles in vacuo ($\sim 10^{-2}$ mbar) the crude product was dissolved in CDCl$_3$, and the solution was subjected to multinuclear (^{1}H, ^{13}C, ^{29}Si, ^{31}P) NMR experiments, which evidenced the formation of **123b** (Section 10.3.8).

10.3.10 Synthesis of [2-Bis(trimethylsilyl)methyl-5-methyl-3-phenyl-2H-1,4,2-diazaphospholium-κP]pentacarbonyltungsten(0) Trifluoromethanesulfonate (123m)

To a stirred solution of 140 mg (0.23 mmol) of 2H-azaphosphirene complex **35** in 1.4 mL of CH$_2$Cl$_2$ were added consecutively 12 μL (0.23 mmol) of acetonitrile (**36m**) and 20 μL (0.23 mmol) of TfOH at $-68\,^\circ$C while the initially yellow colored solution turned deep purple. After the addition the cooling bath was removed and 29 mL of n-pentane was added under rigorous stirring. The light brownish overlaying solution was removed with a syringe, and the purple residue was washed with n-pentane until the overlaying solution was colorless. Then, the product (**123m**) was dried in vacuo ($\sim 10^{-2}$ mbar).

123m: Purple solid; yield: 139 mg (0.17 mmol, 76 %); mp 115 $^\circ$C (decomp.); ^{1}H NMR (300.13 MHz, CD$_2$Cl$_2$, $-10\,^\circ$C): $\delta = -0.05$ (s, 9 H; Si(CH$_3$)$_3$), 0.59 (s, 9 H; Si(CH$_3$)$_3$), 1.42 (d, $|^2J_{PH}| = 4.7$ Hz, 1 H; CH(SiMe$_3$)$_2$), 2.91 (s, 3 H; CH$_3$), 7.76 (m$_c$, 2 H; $meta$-H$_{phenyl}$), 7.88 (m$_c$, 1 H; $para$-H$_{phenyl}$), 8.31 (m$_c$, 2 H; $ortho$-H$_{phenyl}$), 14.7 (br, $h_{1/2} = 45$ Hz, 1 H; NH); ^{31}P NMR (121.5 MHz, CD$_2$Cl$_2$): $\delta = 118.0$ (d$_{sat}$, $|^1J_{WP}| = 239.1$ Hz, $|J_{PH}| = 16.5$ Hz; 67 %), 114.7 (d$_{sat}$, $|^1J_{WP}| = 245.4$ Hz, $|J_{PH}| = 22.9$ Hz; 33 %); IR (KBr): $\tilde{\nu} = 2958$ (w, CH$_3$/CH), 2904 (w, CH$_3$/CH), 2852 (w, CH$_3$/CH), 2078 (m, sh, CO), 2004 (m, CO), 1961 (s, br, CO), 1949 (s, sh, CO), 1935 (s, sh, CO), 1659 cm^{-1} (w, CN); Raman (15 mW): $\tilde{\nu} = 2905$ (m, CH$_3$/CH), 2077 (s, CO), 1990 (s, CO), 1968 (w, CO), 1947 (m, CO), 1932 (vw, CO), 1663 cm^{-1} (w, CN); UV/Vis (CH$_2$Cl$_2$): λ_{max} (ϵ [cm^2 mmol^{-1}]) = 233 (86263), 251 (50900), 288 (16803), 320 (12022), 357

(8155), 550 nm (2250); HR-MS (ESI$^+$) calcd. for $C_{22}H_{28}F_3N_2O_8PSSi_2W$: 659.0778; found: 659.0872; dev. 0.0094; elemental analysis (%) calcd. for $C_{22}H_{28}F_3N_2O_8PSSi_2W$: C 32.68, H 3.49, N 3.46; found: C 31.75, H 3.51, N 3.65.

10.3.11 Reaction of [2-Bis(trimethylsilyl)methyl-3-phenyl-2H-azaphosphirene-κP]pentacarbonyltungsten(0) (35) with Trifluoromethanesulfonic Acid in the Presence of 2-Thiophenecarbonitrile, Pivalonitrile, 1-Adamantanecarbonitrile, or Trimethylsilyl Cyanide

To a stirred stirred solution of 200 mg (0.32 mmol) of 2H-azaphosphirene complex **35** and the appropriate nitrile (**36g**: 31 μL, 0.33 mmol; **36r**: 36 μL, 0.32 mmol; **36s**: 52 mg, 0.32 mmol; **36t**: 43 μL, 0.32 mmol) in 4 mL of CD_2Cl_2 (**36g** and **36s**) or CH_2Cl_2 (**36r** and **36t**) was added 29 μL (0.33 mmol) of TfOH at $-68\,^\circ$C while the initially yellow colored solution turned deep green in the case of **36g** and deep purple in the cases of **36r**–**t**. Subsequently, the reaction mixtures were analyzed by ^{1}H, ^{31}P, and 2D ^{1}H,^{31}P HMQC NMR spectroscopy.

123g: ^{1}H NMR (300.13 MHz, CD_2Cl_2): δ = 0.22 (s$_{sat}$, $|^2J_{SiH}|$ = 6.1 Hz, 9 H; Si(CH$_3$)$_3$), 0.43 (s$_{sat}$, $|^2J_{SiH}|$ = 6.2 Hz, 9 H; Si(CH$_3$)$_3$), 1.70 (d, $|^2J_{PH}|$ = 9.4 Hz, 1 H; CH(SiMe$_3$)$_2$), 7.73 (m$_c$, 3 H; $meta$+$para$-H$_{phenyl}$), 8.32 (m$_c$, 2 H; $ortho$-H$_{phenyl}$), 13.26 (d, $|J_{PH}|$ = 23.0 Hz, $h_{1/2}$ = 14 Hz, 1 H; NH); ^{31}P NMR (121.5 MHz, CD_2Cl_2): δ = 115.6 (dd$_{sat}$, $|^1J_{WP}|$ = 245.4 Hz, $|J_{PH}|$ = 24.2 Hz, $|^2J_{PH}|$ = 8.9 Hz).

123r: ^{31}P NMR (121.5 MHz, CH_2Cl_2): δ = 116.2 (d$_{sat}$, $|^1J_{WP}|$ = 244.1 Hz, $|J_{PH}|$ = 19.1 Hz).

123s: ^{1}H NMR (300.13 MHz, CD_2Cl_2): δ = 0.01 (s, 9 H; Si(CH$_3$)$_3$), 0.63 (s, 9 H; Si(CH$_3$)$_3$), 1.50 (d, $|^2J_{PH}|$ = 9.4 Hz, 1 H; CH(SiMe$_3$)$_2$), 8.52 (m$_c$, 2 H; $ortho$-H$_{phenyl}$), 14.01 (d, $|J_{PH}|$ = 17.7 Hz, $h_{1/2}$ = 27 Hz, 1 H; NH); ^{31}P NMR (121.5 MHz, CD_2Cl_2): δ = 115.8 (dd$_{sat}$, $|^1J_{WP}|$ = 241.6 Hz, $|J_{PH}|$ = 19.1 Hz, $|^2J_{PH}|$ = 2.5 Hz).

123t: ^{31}P NMR (121.5 MHz, CH_2Cl_2): δ = 122.7 (d$_{sat}$, $|^1J_{WP}|$ = 232.7 Hz, $|J_{PH}|$ = 16.5 Hz).

10.3.12 Synthesis of [5-Dimethylamino-2-(1,2,3,4,5-pentamethyl-2,4-cyclopentadien-1-yl)-3-phenyl-2H-1,4,2-diazaphos-phol-1-ium-κP]pentacarbonyltungsten(0) Trifluoro-methanesulfonate (124b)

To a stirred solution of 100 mg (0.17 mmol) of 2H-azaphosphirene complex **121** in 5 mL of CH$_2$Cl$_2$ were added consecutively 14 μL (0.17 mmol) of dimethyl cyanamide (**36b**) and a solution of 15 μL (0.17 mmol) of TfOH in 2 mL of CH$_2$Cl$_2$ at $-78\,^\circ$C while the initially yellow colored solution turned deep red. After all volatiles were removed in vacuo ($\sim 10^{-2}$ mbar) the red solid residue was washed with n-pentane. Then, the product (**124b**) was dried in vacuo ($\sim 10^{-2}$ mbar).

124b: Red solid; yield: 129 mg (0.16 mmol, 94 %); mp 102 $^\circ$C (decomp.); ^{1}H NMR (300.13 MHz, CD$_2$Cl$_2$): δ = 1.31 (m$_c$, 3 H; Cp*–CH$_3$), 1.44 (m$_c$, 3 H; Cp*–CH$_3$), 1.54 (m$_c$, 3 H; Cp*–CH$_3$), 1.67 (d, $|^3J_{PH}|$ = 20.4 Hz, 3 H; Cp*-C^1–CH$_3$), 2.20 (br, 3 H; Cp*–CH$_3$), 3.59 (s, 3 H; NCH$_3$), 3.79 (s, 3 H; NCH$_3$), 7.55 (m$_c$, 2 H; $meta$-H$_{phenyl}$), 7.80 (m$_c$, 1 H; $para$-H$_{phenyl}$), 7.95 (m$_c$, 2 H; $ortho$-H$_{phenyl}$), 10.35 (d, $|^{2+5}J_{PH}|$ = 23.2 Hz, $h_{1/2}$ = 6.4 Hz, 1 H; NH); ^{13}C{^{1}H} NMR (75.5 MHz, CD$_2$Cl$_2$): δ = 9.8 (br; Cp*–CH$_3$), 10.7 (br; Cp*–CH$_3$), 11.2 (br; Cp*–CH$_3$), 12.7 (br; Cp*–CH$_3$), 15.0 (br; Cp*-C^1–CH$_3$), 39.4 (s; NCH$_3$), 40.8 (s; NCH$_3$), 66.3 (br; Cp*-C^1), 120.1 (q, $|^1J_{FC}|$ = 319.4 Hz; CF$_3$), 128.3 (s; $meta$-C$_{phenyl}$), 130.7 (d, $|^3J_{PC}|$ = 3.9 Hz; $ortho$-C$_{phenyl}$), 131.0 (d, $|^2J_{PC}|$ = 19.7 Hz; $ipso$-C$_{phenyl}$), 132.1 (br; Cp*-C), 136.1 (s; $para$-C$_{phenyl}$), 139.0 (br; Cp*-C), 141.2 (br; Cp*-C), 144.4 (br; Cp*-C), 161.0 (d, $|^{2+3}J_{PC}|$ = 8.1 Hz; PNC), 193.6 (d, $|^{1+4}J_{PC}|$ = 1.3 Hz; PCN), 194.7 (d$_{sat}$, $|^2J_{PC}|$ = 6.1 Hz, $|^1J_{WC}|$ = 126.7 Hz; CO$_{cis}$), 195.9 (d, $|^2J_{PC}|$ = 29.7 Hz; CO$_{trans}$); ^{15}N NMR (30.418 MHz, CD$_2$Cl$_2$): δ = -273 (NMe$_2$), -268 ($|^{1+4}J_{PN}|$ = 35 Hz, $|^1J_{NH}|$ = 93 Hz; N^{1}H); ^{31}P NMR (121.5 MHz, CD$_2$Cl$_2$): δ = 114.9 (br$_{sat}$, $|^1J_{WP}|$ = 251.8 Hz); IR (KBr): $\tilde{\nu}$ = 2980 (w, CH$_3$/CH), 2933 (w, CH$_3$/CH), 2861 (w, CH$_3$/CH), 2080 (m, sh, CO), 1997 (s, CO), 1943 (s, br, CO), 1659 (m, CN), 1517 cm^{-1} (w, CN); UV/Vis (n-pentane): λ_{max} (abs.) = 233 (1.909), 238 (2.451), 301 (0.696), 320 (sh, 0.632), 445 nm (0.069); MS (FAB$^+$, ^{184}W): m/z (%): 664.1 ([M]$^+$, 58), 528.0 ([M – CO – C$_5$Me$_5$ – H]$^+$, 27), 472.0 ([M – 2 CO – C$_5$Me$_5$ – H]$^+$, 17), 340.2 ([M – W(CO)$_5$]$^+$, 31), 206.1 ([M + H – W(CO)$_5$ – C$_5$Me$_5$]$^+$, 100).

10.3.13 Synthesis of [2-Bis(trimethylsilyl)methyl-5-dimethyl-amino-3-ferrocenyl-2H-1,4,2-diazaphosphole-κP]pentacarbonyltungsten(0) (69b)

To a stirred solution of 1.400 g (1.93 mmol) of 2H-azaphosphirene complex **67** in 35 mL of CH$_2$Cl$_2$ were added consecutively 170 μL (2.09 mmol) of dimethyl cyanamide (**36b**) and 170 μL (1.93 mmol) of TfOH at ambient temperature. The initially red colored solution turned deep blue, and the formation of protonated intermediate **127b** was evidenced by ^{31}P NMR spectroscopy (121.5 MHz, CH$_2$Cl$_2$): $\delta = 102.6$ (dd$_{sat}$, $|^1J_{WP}| = 253.0$ Hz, $|^{2+5}J_{PH}| = 22.9$ Hz, $|^2J_{PH}| = 11.4$ Hz). Subsequently, 270 μL (1.92 mmol) of NEt$_3$ was added at ambient temperature while the reaction mixture turned red again. After removement of all volatiles in vacuo ($\sim 10^{-2}$ mbar) the crude product was dissolved in petroleum ether, filtered through celite, and purified by column chromatography on silica ($-35\,^{\circ}$C, 3 $\times$ 10 cm, petroleum ether/Et$_2$O: 10/1). Evaporation of the solvents of the first fraction ($\sim 10^{-2}$ mbar) yielded **69b**.

69b: Red solid; yield: 824 mg (1.04 mmol, 54 %); mp 147 $^{\circ}$C; ^{1}H NMR (300.13 MHz, C$_6$D$_6$): $\delta = -0.02$ (s$_{sat}$, $|^2J_{SiH}| = 6.5$ Hz, $|^1J_{CH}| = 119.8$ Hz, 9 H; Si(CH$_3$)$_3$), 0.36 (s$_{sat}$, $|^2J_{SiH}| = 6.5$ Hz, $|^1J_{CH}| = 119.1$ Hz, 9 H; Si(CH$_3$)$_3$), 1.30 (d, $|^2J_{PH}| = 7.9$ Hz, 1 H; CH(SiMe$_3$)$_2$), 2.83 (s, 3 H; NCH$_3$), 2.95 (s, 3 H; NCH$_3$), 4.13 (s, 5 H; Cp-CH unsubst.), 4.21 (m$_c$, 1 H; Cp-C$^{3/4}$H), 4.24 (m$_c$, 1 H; Cp-C$^{3/4}$H), 4.91 (m$_c$, 1 H; Cp-C$^{2/5}$H), 5.10 (m$_c$, 1 H; Cp-C$^{2/5}$H); ^{13}C$\{^1$H$\}$ NMR (75.5 MHz, C$_6$D$_6$): $\delta = 3.2$ (d$_{sat}$, $|^3J_{PC}| = 2.3$ Hz, $|^1J_{SiC}| = 52.5$ Hz; Si(CH$_3$)$_3$), 3.6 (d$_{sat}$, $|^3J_{PC}| = 2.6$ Hz, $|^1J_{SiC}| = 53.1$ Hz; Si(CH$_3$)$_3$), 25.2 (d, $|^1J_{PC}| = 10.0$ Hz; CH(SiMe$_3$)$_2$), 37.6 (s; NCH$_3$), 37.6 (s; NCH$_3$), 70.5 (s; Cp-C$^{3/4}$), 71.0 (s; Cp-C unsubst.), 71.1 (s; Cp-C$^{3/4}$), 71.5 (s; Cp-C$^{2/5}$), 75.6 (d, $|^3J_{PC}| = 1.9$ Hz; Cp-C$^{2/5}$), 79.9 (d, $|^2J_{PC}| = 26.5$ Hz; Cp-C^1), 165.0 (s; PNC), 198.5 (d$_{sat}$, $|^2J_{PC}| = 6.5$ Hz, $|^1J_{WC}| = 126.6$ Hz; CO$_{cis}$), 199.8 (d$_{sat}$, $|^2J_{PC}| = 22.0$ Hz, $|^1J_{WC}| = 143.5$ Hz; CO$_{trans}$), 206.5 (d, $|^{1+4}J_{PC}| = 26.8$ Hz; PCN); ^{29}Si$\{^1$H$\}$ NMR (59.6 MHz, C$_6$D$_6$): $\delta = -0.1$ (d$_{sat}$, $|^2J_{PSi}| = 7.3$ Hz, $|^1J_{SiC}| = 52.5$ Hz), 1.6 (d$_{sat}$, $|^2J_{PSi}| = 3.5$ Hz, $|^1J_{SiC}| = 53.0$ Hz); ^{31}P NMR (121.5 MHz, C$_6$D$_6$): $\delta = 106.5$ (d$_{sat}$, $|^1J_{WP}| = 241.6$ Hz, $|^2J_{PH}| = 7.8$ Hz); IR (KBr): $\tilde{\nu} = 2962$ (w, CH$_3$/CH), 2930 (w, CH$_3$/CH), 2905 (w, CH$_3$/CH), 2876 (w, CH$_3$/CH), 2071 (m, sh, CO), 1991 (m, CO), 1950 (s, CO), 1928 (s, CO), 1906 (s, CO), 1602 (m, CN), 1550 cm^{-1} (w, CN); UV/Vis (n-pentane): λ_{max} (abs.) $= 200$ (sh, 0.855), 205 (0.973), 231 (0.983), 252 (sh, 0.562), 299 (0.173), 352 (0.087), 385 (sh, 0.068), 520 (0.021); MS (FAB$^+$, ^{184}W): m/z (%): 796.0 ([M + H]$^+$, 15), 767.0 ([M $-$ CO]$^+$, 3), 739.0 ([M $-$ 2 CO]$^+$, 1), 711.0 ([M $-$ 3 CO]$^+$, 1), 683.0 ([M $-$ 4 CO]$^+$, 3), 655.0 ([M $-$ 5 CO]$^+$, 1), 472.1 ([M + H $-$ W(CO)$_5$]$^+$, 100); elemental analysis (%) calcd. for C$_{26}$H$_{34}$FeN$_3$O$_5$PSi$_2$W: C 39.26, H 4.31, N 5.28; found: C 39.37, H 4.30, N 5.29.

10.3.14 Synthesis of [2-Bis(trimethylsilyl)methyl-3,5-diferro-cenyl-2H-1,4,2-diazaphosphole-κP]pentacarbonyltungsten(0) (69l)

A solution of 24 μL (0.27 mmol) of TfOH in 3.5 mL of CH_2Cl_2 was added to a stirred solution of 198 mg (0.27 mmol) of 2H-azaphosphirene complex **67** and 58 mg (0.28 mmol) of ferrocenecarbonitrile (**36l**) in 5.5 mL of CH_2Cl_2 at $-40\,^\circ$C while the initially red colored solution turned deep turquois. After the addition the cooling bath was removed, and after 10 min 23 μL (0.28 mmol) of pyridine was added while the reaction mixture turned deep purple. After removement of all volatiles in vacuo ($\sim 10^{-2}$ mbar) the crude product was purified by column chromatography on silica ($-15\,^\circ$C, 2 × 7 cm, petroleum ether/Et$_2$O: 10/1). Evaporation of the solvents of the first fraction ($\sim 10^{-2}$ mbar) yielded 154 mg (0.16 mmol, 60 %) **69l**; for analytical data see Section 10.2.18.

10.3.15 Synthesis of [2-Bis(trimethylsilyl)methyl-5-dimethyl-amino-3-(2-thienyl)-2H-1,4,2-diazaphosphole-κP]pen-tacarbonyltungsten(0) (126b)

To a stirred solution of 310 mg (0.50 mmol) of 2H-azaphosphirene complex **125** in 6.2 mL of CH_2Cl_2 were added consecutively 42 μL (0.52 mmol) of dimethyl cyanamide (**36b**) and 42 μL (0.48 mmol) of TfOH at ambient temperature. The initially yellow colored solution turned deep red, and the formation of protonated intermediate **128b** was evidenced by ^{31}P NMR spectroscopy (121.5 MHz, CH_2Cl_2): δ = 103.0 (dd$_{sat}$, $|^1J_{WP}|$ = 256.9 Hz, $|^{2+5}J_{PH}|$ = 22.9 Hz, $|^2J_{PH}|$ = 5.1 Hz). Subsequently, 68 μL (0.48 mmol) of NEt$_3$ was added at ambient temperature while the reaction mixture turned yellow again. After removement of all volatiles in vacuo ($\sim 10^{-2}$ mbar) the crude product was dissolved in petroleum ether, filtered through celite, and purified by column chromatography on silica ($-35\,^\circ$C, 2 × 10 cm, petroleum ether/Et$_2$O: 100/1). Evaporation of the solvents of the first fraction ($\sim 10^{-2}$ mbar) yielded **126b**.

126b: Orange solid; yield: 246 mg (0.35 mmol, 71 %); mp 133$\,^\circ$C; ^{1}H NMR (300.13 MHz, C$_6$D$_6$): δ = -0.14 (s$_{sat}$, $|^1J_{CH}|$ = 119.4 Hz, 9 H; Si(CH$_3$)$_3$), 0.51 (s$_{sat}$, $|^1J_{CH}|$ = 119.5 Hz, 9 H; Si(CH$_3$)$_3$), 1.04 (d, $|^2J_{PH}|$ = 3.3 Hz, 1 H; CH(SiMe$_3$)$_2$), 2.80 (s, 3 H; NCH$_3$), 2.92 (s, 3 H; NCH$_3$), 6.78 (dd, $|^3J_{HH}|$ = 5.0 and 3.9 Hz, 1 H; thienyl-C^{4}H), 6.95 (d, $|^3J_{HH}|$ = 5.0 Hz, 1 H; thienyl-C^{5}H), 7.87 (d, $|^3J_{HH}|$ = 3.8 Hz, 1 H; thienyl-C^{3}H); ^{13}C{^{1}H} NMR (75.5 MHz, C$_6$D$_6$): δ = 3.0 (d$_{sat}$, $|^3J_{PC}|$ = 1.6 Hz, $|^1J_{SiC}|$ = 52.1 Hz; Si(CH$_3$)$_3$), 4.0 (d$_{sat}$, $|^3J_{PC}|$ = 2.6 Hz, $|^1J_{SiC}|$ = 53.2 Hz; Si(CH$_3$)$_3$), 23.2 (d, $|^1J_{PC}|$ =

5.8 Hz; CH(SiMe$_3$)$_2$), 37.6 (s; NCH$_3$), 37.7 (s; NCH$_3$), 128.4 (s; thienyl-C^4), 133.7 (s; thienyl-C^5), 137.2 (s; thienyl-C^3), 137.9 (d, $|^2J_{PC}|$ = 25.2 Hz; thienyl-C^2), 165.1 (d, $|^{2+3}J_{PC}|$ = 0.6 Hz; PNC), 193.3 (d$_{sat}$, $|^{1+4}J_{PC}|$ = 25.2 Hz, $|^2J_{WC}|$ = 3.6 Hz; PCN), 198.5 (d$_{sat}$, $|^2J_{PC}|$ = 6.8 Hz, $|^1J_{WC}|$ = 126.7 Hz; CO$_{cis}$), 199.7 (d$_{sat}$, $|^2J_{PC}|$ = 22.3 Hz, $|^1J_{WC}|$ = 142.9 Hz; CO$_{trans}$); ^{29}Si{^{1}H} NMR (59.6 MHz, C$_6$D$_6$): δ = 1.7 (d$_{sat}$, $|^2J_{PSi}|$ = 12.0 Hz, $|^1J_{SiC}|$ = 52.7 Hz), 2.1 (d$_{sat}$, $|^2J_{PSi}|$ = 2.5 Hz, $|^1J_{SiC}|$ = 52.7 Hz); ^{31}P NMR (121.5 MHz, C$_6$D$_6$): δ = 104.0 (d$_{sat}$, $|^1J_{WP}|$ = 245.4 Hz, $|^2J_{PH}|$ = 2.2 Hz); IR (KBr): $\tilde{\nu}$ = 2962 (w, CH$_3$/CH), 2930 (w, CH$_3$/CH), 2901 (w, CH$_3$/CH), 2878 (w, CH$_3$/CH), 2066 (m, sh, CO), 1976 (m, sh, CO), 1942 (s, CO), 1929 (s, CO), 1906 (s, CO), 1604 (m, CN), 1540 (w, CN), 1262 (m, thienyl), 1251 cm^{-1} (m, thienyl); UV/Vis (n-pentane): λ_{max} (abs.) = 204 (0.538), 209 (sh, 0.564), 212 (0.583), 217 (0.666), 221 (sh, 0.759), 225 (sh, 0.873), 232 (1.034), 250 (sh, 0.601), 292 (0.159), 325 (0.222), 341 (0.176), 413 nm (0.054); MS (FAB$^+$, ^{184}W): m/z (%): 694.0 ([M + H]$^+$, 7), 664.9 ([M − CO]$^+$, 29), 636.9 ([M − 2 CO]$^+$, 27), 581.0 ([M − 4 CO]$^+$, 29), 370.1 ([M + H − W(CO)$_5$]$^+$, 100); elemental analysis (%) calcd. for C$_{20}$H$_{28}$N$_3$O$_5$PSSi$_2$W: C 34.64, H 4.07, N 6.06, S 4.62; found: C 34.69, H 4.08, N 6.16, S 4.80.

10.3.16 Synthesis of [2-Bis(trimethylsilyl)methyl-3,5-di(2-thienyl)-2H-1,4,2-diazaphosphole-κP]pentacarbonyltungsten(0) (126g)

To a stirred solution of 250 mg (0.40 mmol) of 2H-azaphosphirene complex **125** in 5.5 mL of CH$_2$Cl$_2$ were added consecutively 40 μL (0.43 mmol) of 2-thiophenecarbonitrile (**36g**) and 37 μL (0.42 mmol) of TfOH at ambient temperature. The initially yellow colored solution turned deep green. Subsequently, 58 μL (0.41 mmol) of NEt$_3$ was added at ambient temperature while the reaction mixture turned brownish yellow. Then, all volatiles were removed in vacuo ($\sim$ 10^{-2} mbar), and the product was purified by column chromatography on silica ($-$20 °C, 2 × 8 cm, petroleum ether/Et$_2$O: 100/1). Evaporation of the solvents of the first fraction ($\sim$ 10^{-2} mbar) yielded **126g**.

126g: Orange solid; yield: 193 mg (0.26 mmol, 66 %); mp 128 °C; ^{1}H NMR (300.13 MHz, C$_6$D$_6$): δ = −0.18 (s$_{sat}$, $|^2J_{SiH}|$ = 6.3 Hz, $|^1J_{CH}|$ = 119.7 Hz, 9 H; Si(CH$_3$)$_3$), 0.53 (s$_{sat}$, $|^2J_{SiH}|$ = 6.2 Hz, $|^1J_{CH}|$ = 120.1 Hz, 9 H; Si(CH$_3$)$_3$), 1.09 (d, $|^2J_{PH}|$ = 3.7 Hz, 1 H; CH(SiMe$_3$)$_2$), 6.63 (dd, $|^3J_{HH}|$ = 4.8 and 3.9 Hz, 1 H; thienyl-C^{4}H at diazaphosphole-C^5), 6.74 (dd, $|^3J_{HH}|$ = 5.0 and 3.9 Hz, 1 H; thienyl-C^{4}H at diazaphosphole-C^3), 6.88 (dd, $|^3J_{HH}|$ = 4.8, $|^4J_{HH}|$ = 1.1 Hz, 1 H; thienyl-C^{5}H at diazaphosphole-C^5), 6.89 (ddd, $|^{5+6}J_{PH}|$ = 1.2, $|^3J_{HH}|$ = 5.0, $|^4J_{HH}|$ = 1.1 Hz, 1 H; thienyl-C^{5}H at diazaphosphole-C^3), 7.86 (dd, $|^3J_{HH}|$ = 3.9, $|^4J_{HH}|$ = 1.0 Hz, 1 H; thienyl-C^{3}H at diazaphosphole-C^3),

8.05 (dd, $|^3J_{HH}| = 3.8$, $|^4J_{HH}| = 1.2$ Hz, 1 H; thienyl-C^{3}H at diazaphosphole-C^5);
^{13}C$\{^1$H$\}$ NMR (75.5 MHz, C$_6$D$_6$): $\delta = 2.7$ (d$_{sat}$, $|^3J_{PC}| = 2.3$ Hz, $|^1J_{SiC}| = 52.4$ Hz;
Si(CH$_3$)$_3$), 3.7 (d$_{sat}$, $|^3J_{PC}| = 2.9$ Hz, $|^1J_{SiC}| = 53.3$ Hz; Si(CH$_3$)$_3$), 20.0 (d, $|^1J_{PC}| = $
4.8 Hz; CH(SiMe$_3$)$_2$), 128.6 (s; thienyl-C^4 at diazaphosphole-C^3), 128.6 (d, $|^{5+6}J_{PC}| = $
0.9 Hz; thienyl-C^4 at diazaphosphole-C^5), 133.4 (s; thienyl-C^5 at diazaphosphole-C^5),
134.2 (d, $|^4J_{PC}| = 0.9$ Hz; thienyl-C^3 at diazaphosphole-C^5), 134.7 (s; thienyl-C^5 at
diazaphosphole-C^3), 137.8 (s; thienyl-C^3 at diazaphosphole-C^3), 137.8 (d, $|^2J_{PC}| = $
27.8 Hz; thienyl-C^2 at diazaphosphole-C^3), 138.5 (d, $|^3J_{PC}| = 14.5$ Hz; thienyl-C^2 at
diazaphosphole-C^5), 165.5 (d, $|^{2+3}J_{PC}| = 5.5$ Hz; PNC), 195.2 (d$_{sat}$, $|^{1+4}J_{PC}| = 22.3$
Hz, $|^2J_{WC}| = 3.6$ Hz; PCN), 197.6 (d$_{sat}$, $|^2J_{PC}| = 6.1$ Hz, $|^1J_{WC}| = 126.7$ Hz; CO$_{cis}$),
198.4 (d$_{sat}$, $|^2J_{PC}| = 22.6$ Hz, $|^1J_{WC}| = 143.5$ Hz; CO$_{trans}$); ^{29}Si$\{^1$H$\}$ NMR (59.6 MHz,
C$_6$D$_6$): $\delta = 3.5$ (d$_{sat}$, $|^2J_{PSi}| = 11.8$ Hz, $|^1J_{SiC}| = 52.5$ Hz), 3.5 (d$_{sat}$, $|^2J_{PSi}| = 2.5$ Hz,
$|^1J_{SiC}| = 53.4$ Hz); ^{31}P NMR (121.5 MHz, C$_6$D$_6$): $\delta = 110.4$ (d$_{sat}$, $|^1J_{WP}| = 235.2$ Hz,
$|^2J_{PH}| = 3.3$ Hz); IR (KBr): $\tilde{\nu} = 2963$ (w, CH$_3$/CH), 2904 (w, CH$_3$/CH), 2069 (m,
sh, CO), 1977 (m, sh, CO), 1935 (s, CO), 1925 (s, CO), 1557 (m, CN), 1545 (m, CN),
1261 cm^{-1} (m, thienyl); UV/Vis (n-pentane): λ_{max} (ϵ [cm^2 mmol^{-1}]) = 232 (59618),
249 (sh, 38120), 287 (sh, 13985), 329 (sh, 16862), 341 (19260), 353 (sh, 17262), 444
nm (2557); CV: $E_{1/2} = -1.635$ V; MS (FAB$^+$, ^{184}W): m/z (%): 733.0 ([M + H]$^+$,
11), 704.0 ([M − CO]$^+$, 17), 676.1 ([M − 2 CO]$^+$, 34), 648.0 ([M − 3 CO]$^+$, 49), 592.0
([M − 5 CO]$^+$, 13), 509.1 ([M + H − W(CO)$_5$]$^+$, 100); elemental analysis (%) calcd. for
C$_{22}$H$_{25}$N$_2$O$_5$PS$_2$Si$_2$W: C 36.07, H 3.44, N 3.82, S 8.75; found: C 35.82, H 3.38, N 4.18,
S 8.62.

10.3.17 Synthesis of [2-Bis(trimethylsilyl)methyl-3-phenyl-$2H$-1,4,2-diazaphosphole-κP]pentacarbonyltungsten(0) (41h) and [2-Bis(trimethylsilyl)methyl-3-phenyl-$2H$-1,4,2-diazaphosphole-κN^1]pentacarbonyltungsten(0) (129h)

Consecutively, 100 μL (2.54 mmol) of hydrogen cyanide (**36h**) and a solution of 129
μL (1.47 mmol) of TfOH in 12 mL of CH$_2$Cl$_2$ were slowly added to a stirred solution of
892 mg (1.44 mmol) of $2H$-azaphosphirene complex **35** in 40 mL of CH$_2$Cl$_2$ at $-78\,$°C.
During the addition the initially yellow colored solution turned deep brown. It was
stirred further 5 min, then the reaction solution was warmed to ambient temperature
within 20 min while a slow color change to an intense deep purple was observed.
Upon subsequent addition of 130 μL (1.61 mmol) of pyridine the reaction mixture
turned brownish yellow. After removement of all volatiles in vacuo ($\sim 10^{-2}$ mbar)
the products were purified by column chromatography on silica ($-30\,$°C, 2 × 21 cm,
petroleum ether/Et$_2$O: 10/1). Evaporation of the solvents of the first fraction ($\sim 10^{-2}$

mbar) gave a mixture of **41h** and **129h** (ratio $5 : 1$).

41h and **129h**: Orange solid; yield: 519 mg (0.81 mmol, 65 %); mp 101 °C (decomp.); IR (KBr): $\tilde{\nu}$ = 2955 (w, CH_3/CH), 2901 (w, CH_3/CH), 2072 (m, sh, CO), 1985 (w, sh, CO), 1940 (s, CO), 1924 (s, CO), 1912 (s, CO), 1705 (w, CN), 1557 cm^{-1} (w, CN); UV/Vis (n-pentane): λ_{max} (abs.) = 229 (2.232), 248 (sh, 1.348), 296 (0.394), 312 (0.395), 398 (0.090), 433 nm (0.089); MS (FAB$^+$, ^{184}W): m/z (%): 645.1 ([M + H]$^+$, 20), 588.0 ([M − 2 CO]$^+$, 12), 561.1 ([M + H − 3 CO]$^+$, 10), 321.1 ([M + H − W(CO)$_5$]$^+$, 100); elemental analysis (%) calcd. for $C_{20}H_{25}N_2O_5PSi_2W$: C 37.28, H 3.91, N 4.35; found: C 37.43, H 4.07, N 4.16.

41h: Crystallized from n-pentane at 4 °C; ^{1}H NMR (300.13 MHz, C_6D_6): δ = −0.28 (s_{sat}, $|^2J_{SiH}|$ = 6.5 Hz, $|^1J_{CH}|$ = 120.9 Hz, 9 H; Si(CH$_3$)$_3$), 0.45 (s_{sat}, $|^2J_{SiH}|$ = 6.4 Hz, $|^1J_{CH}|$ = 119.2 Hz, 9 H; Si(CH$_3$)$_3$), 0.98 (d, $|^2J_{PH}|$ = 4.0 Hz, 1 H; CH(SiMe$_3$)$_2$), 7.09 (m$_c$, 3 H; $meta+para$-H$_{phenyl}$), 8.03 (d, $|^{3+4}J_{PH}|$ = 33.6 Hz, 1 H; CH), 8.16 (m$_c$, 2 H; $ortho$-H$_{phenyl}$); ^{13}C{^{1}H} NMR (75.5 MHz, C_6D_6): δ = 2.9 (d$_{sat}$, $|^3J_{PC}|$ = 2.3 Hz, $|^1J_{SiC}|$ = 52.5 Hz; Si(CH$_3$)$_3$), 3.7 (d$_{sat}$, $|^3J_{PC}|$ = 2.9 Hz, $|^1J_{SiC}|$ = 53.2 Hz; Si(CH$_3$)$_3$), 17.3 (d, $|^1J_{PC}|$ = 3.9 Hz; CH(SiMe$_3$)$_2$), 129.0 (s; $meta$-C$_{phenyl}$), 131.9 (d, $|^3J_{PC}|$ = 2.3 Hz; $ortho$-C$_{phenyl}$), 132.4 (d, $|^2J_{PC}|$ = 23.6 Hz; $ipso$-C$_{phenyl}$), 133.9 (d, $|^5J_{PC}|$ = 0.7 Hz; $para$-C$_{phenyl}$), 162.7 (d, $|^{2+3}J_{PC}|$ = 7.8 Hz; PNC), 197.5 (d$_{sat}$, $|^2J_{PC}|$ = 5.8 Hz, $|^1J_{WC}|$ = 126.6 Hz; CO$_{cis}$), 197.7 (d$_{sat}$, $|^2J_{PC}|$ = 22.6 Hz, $|^1J_{WC}|$ = 144.7 Hz; CO$_{trans}$), 203.0 (d$_{sat}$, $|^{1+4}J_{PC}|$ = 22.0 Hz, $|^2J_{WC}|$ = 3.2 Hz; PCN); ^{15}N NMR (30.418 MHz, CDCl$_3$): δ = −86 ($|^{1+4}J_{PN}|$ = 54 Hz, $|^2J_{NH}|$ = 14 Hz; N^1), −64 ($|^{2+3}J_{PN}|$ = 9 Hz, $|^2J_{NH}|$ = 15 Hz; N^4); ^{29}Si{^{1}H} NMR (59.6 MHz, C_6D_6): δ = 3.6 (d$_{sat}$, $|^2J_{PSi}|$ = 2.7 Hz, $|^1J_{SiC}|$ = 53.2 Hz), 4.5 (d$_{sat}$, $|^2J_{PSi}|$ = 12.2 Hz, $|^1J_{SiC}|$ = 52.5 Hz); ^{31}P NMR (121.5 MHz, C_6D_6): δ = 105.6 (dd$_{sat}$, $|^1J_{WP}|$ = 227.6 Hz, $|^{3+4}J_{PH}|$ = 33.5 Hz, $|^2J_{PH}|$ = 4.0 Hz).

129h: ^{1}H NMR (300.13 MHz, C_6D_6): δ = −0.06 (s$_{sat}$, $|^2J_{SiH}|$ = 6.4 Hz, 18 H; Si(CH$_3$)$_3$), 1.77 (d, $|^2J_{PH}|$ = 13.9 Hz, 1 H; CH(SiMe$_3$)$_2$), 7.00–7.19 (m$_c$, 3 H; $meta+para$-H$_{phenyl}$), 7.69 (m$_c$, 2 H; $ortho$-H$_{phenyl}$), 8.41 (d, $|^{3+4}J_{PH}|$ = 6.6 Hz, 1 H; CH); ^{13}C{^{1}H} NMR (75.5 MHz, C_6D_6): δ = 1.9 (d$_{sat}$, $|^3J_{PC}|$ = 5.1 Hz, $|^1J_{SiC}|$ = 52.5 Hz; Si(CH$_3$)$_3$), 17.9 (d, $|^1J_{PC}|$ = 55.0 Hz; CH(SiMe$_3$)$_2$), 128.6 (d, $|^3J_{PC}|$ = 10.1 Hz; $ortho$-C$_{phenyl}$), 129.4 (d, $|^4J_{PC}|$ = 0.9 Hz; $meta$-C$_{phenyl}$), 133.2 (d, $|^5J_{PC}|$ = 3.2 Hz; $para$-C$_{phenyl}$), 135.2 (d, $|^2J_{PC}|$ = 15.2 Hz; $ipso$-C$_{phenyl}$), 170.3 (d, $|^{2+3}J_{PC}|$ = 14.2 Hz; PNC), 198.4 (d$_{sat}$, $|^3J_{PC}|$ = 2.7 Hz, $|^1J_{WC}|$ = 129.8 Hz; CO$_{cis}$), 201.0 (d, $|^3J_{PC}|$ = 1.7 Hz; CO$_{trans}$), 208.5 (d, $|^{1+4}J_{PC}|$ = 35.5 Hz; PCN); ^{15}N NMR (30.418 MHz, CDCl$_3$): δ = −165 ($|^{1+4}J_{PN}|$ = 68 Hz, $|^2J_{NH}|$ = 10 Hz; N^1), −53 ($|^{2+3}J_{PN}|$ = 24 Hz, $|^2J_{NH}|$ = 14 Hz; N^4); ^{29}Si{^{1}H} NMR (59.6 MHz, C_6D_6): δ = 7.4 (d, $|^2J_{PSi}|$ = 8.9 Hz); ^{31}P NMR (121.5 MHz, C_6D_6): δ = 121.2 (br).

10.3.18 Attempted Synthesis of [2-Bis(trimethylsilyl)methyl-3-ferrocenyl-2H-1,4,2-diazaphosphole-κP]pentacarbonyltungsten(0) (69h) and [2-Bis(trimethylsilyl)methyl-3-ferrocenyl-2H-1,4,2-diazaphosphole-κN^1]pentacarbonyltungsten(0) (130h)

Consecutively, 100 μL (2.54 mmol) of hydrogen cyanide (**36h**) and a solution of 40 μL (0.46 mmol) of TfOH in 4 mL of CH$_2$Cl$_2$ were slowly added to a stirred solution of 320 mg (0.44 mmol) of 2H-azaphosphirene complex **67** in 12.5 mL of CH$_2$Cl$_2$ at $-78\,^\circ$C. During the addition the initially red colored solution turned deep turquoise. While warming to room temperature within 20 min a slow color change to an intense deep purple was observed. After the addition of 38 μL (0.47 mmol) of pyridine all volatiles were removed in vacuo ($\sim 10^{-2}$ mbar), and the deep purple crude product was dissolved in 35 mL of diethyl ether and filtered through celite. Then, all volatiles were removed in vacuo ($\sim 10^{-2}$ mbar), which afforded a mixture of complexes **69h** and **130h** (ratio $1:2$) as a deep purple oil.

69h: ^{1}H NMR (300.13 MHz, C$_6$D$_6$): $\delta = 0.12$ (s, 9 H; Si(CH$_3$)$_3$), 0.37 (s, 9 H; Si(CH$_3$)$_3$), 1.25 (d, $|^2J_{PH}| = 9.8$ Hz, 1 H; CH(SiMe$_3$)$_2$), 4.30 (s, 5 H; Cp-CH unsubst.), 8.28 (d, $|^{3+4}J_{PH}| = 33.5$ Hz, 1 H; CH); ^{13}C\{^{1}H\} NMR (75.5 MHz, C$_6$D$_6$): $\delta = 2.8$ (d, $|^3J_{PC}| = 2.3$ Hz; Si(CH$_3$)$_3$), 3.2 (d, $|^3J_{PC}| = 2.9$ Hz; Si(CH$_3$)$_3$), 17.9 (d, $|^1J_{PC}| = 9.4$ Hz; CH(SiMe$_3$)$_2$), 161.7 (d, $|^{2+3}J_{PC}| = 8.1$ Hz; PNC), 197.2 (d$_{sat}$, $|^2J_{PC}| = 6.1$ Hz, $|^1J_{WC}| = 126.7$ Hz; CO$_{cis}$), 198.1 (d, $|^2J_{PC}| = 22.3$ Hz; CO$_{trans}$), 210.1 (d, $|^{1+4}J_{PC}| = 22.3$ Hz; PCN); ^{29}Si\{^{1}H\} NMR (59.6 MHz, C$_6$D$_6$): $\delta = 2.7$ (d, $|^2J_{PSi}| = 4.5$ Hz), 3.1 (d, $|^2J_{PSi}| = 7.4$ Hz); ^{31}P NMR (121.5 MHz, C$_6$D$_6$): $\delta = 107.6$ (dd$_{sat}$, $|^1J_{WP}| = 226.3$ Hz, $|^{3+4}J_{PH}| = 33.4$ Hz, $|^2J_{PH}| = 9.7$ Hz).

130h: ^{1}H NMR (300.13 MHz, C$_6$D$_6$): $\delta = 0.16$ (s, 18 H; Si(CH$_3$)$_3$), 1.58 (d, $|^2J_{PH}| = 12.7$ Hz, 1 H; CH(SiMe$_3$)$_2$), 4.17 (s, 5 H; Cp-CH unsubst.), 4.81 (m$_c$, 2 H; Cp-C^{2+5}H), 4.95 (m$_c$, 2 H; Cp-C^{3+4}H), 8.57 (d, $|^{3+4}J_{PH}| = 7.2$ Hz, 1 H; CH); ^{13}C\{^{1}H\} NMR (75.5 MHz, C$_6$D$_6$): $\delta = 2.0$ (d$_{sat}$, $|^3J_{PC}| = 5.5$ Hz, $|^1J_{SiC}| = 52.4$ Hz; Si(CH$_3$)$_3$), 16.9 (d, $|^1J_{PC}| = 56.3$ Hz; CH(SiMe$_3$)$_2$), 69.9 (s; Cp-C$^{3/4}$), 69.9 (s; Cp-C$^{3/4}$), 71.9 (d, $|^4J_{PC}| = 0.8$ Hz; Cp-C unsubst.), 73.9 (br; Cp-C^{2+5}), 78.7 (d, $|^2J_{PC}| = 16.5$ Hz; Cp-C^1), 171.4 (d, $|^{2+3}J_{PC}| = 12.0$ Hz; PNC), 198.2 (d$_{sat}$, $|^3J_{PC}| = 3.2$ Hz, $|^1J_{WC}| = 130.0$ Hz; CO$_{cis}$), 201.4 (d$_{sat}$, $|^3J_{PC}| = 1.9$ Hz, $|^1J_{WC}| = 149.5$ Hz; CO$_{trans}$), 215.4 (d, $|^{1+4}J_{PC}| = 38.5$ Hz; PCN); ^{15}N NMR (30.418 MHz, CD$_2$Cl$_2$): $\delta = -170$ ($|^{1+4}J_{PN}| = 65$ Hz, $|^2J_{NH}| = 10$ Hz; N^1), -60 ($|^{2+3}J_{PN}| = 6$ Hz, $|^2J_{NH}| = 14$ Hz; N^4); ^{29}Si\{^{1}H\} NMR (59.6 MHz, C$_6$D$_6$): $\delta = 6.7$ (d$_{sat}$, $|^2J_{PSi}| = 9.8$ Hz, $|^1J_{SiC}| = 52.7$ Hz); ^{31}P NMR (121.5 MHz, C$_6$D$_6$): $\delta = 116.3$ (br).

10.3.19   Synthesis of [2-Bis(trimethylsilyl)methyl-3-(2-thienyl)-2*H*-1,4,2-diazaphosphole-κP]pentacarbonyltungsten(0) (126h) and [2-Bis(trimethylsilyl)methyl-3-(2-thienyl)-2*H*-1,4,2-diazaphosphole-κN^1]pentacarbonyltungsten(0) (131h)

Consecutively, 200 μL (4.47 mmol) of hydrogen cyanide (**36h**) and a solution of 179 μL (2.04 mmol) of TfOH in 24 mL of CH_2Cl_2 were slowly added to a stirred solution of 1.247 g (2.00 mmol) of 2*H*-azaphosphirene complex **125** in 40 mL of CH_2Cl_2 at $-78\,^\circ$C. During the addition the initially yellow colored solution turned deep brown. It was stirred further 2 min, then the reaction solution was warmed to ambient temperature within 20 min while a slow color change to an intense deep purple was observed. Upon subsequent addition of 165 μL (2.04 mmol) of pyridine the reaction mixture turned brownish red. After removal of all volatiles in vacuo ($\sim 10^{-2}$ mbar) the products were purified by column chromatography on neutral Al_2O_3 ($-50\,^\circ$C, 3 $\times$ 7 cm, petroleum ether/Et_2O: 1/1). Evaporation of the solvents of the first fraction ($\sim 10^{-2}$ mbar) gave a mixture of **126h** and **131h** (ratio 24 : 1).

126h and **131h**: Orange solid; yield: 852 mg (1.31 mmol, 66 %); mp 117 $^\circ$C (decomp.); IR (KBr): $\tilde{\nu}$ = 2979 (w, CH_3/CH), 2958 (w, CH_3/CH), 2905 (w, CH_3/CH), 2070 (m, sh, CO), 1983 (vw, CO), 1944 (m, CO), 1924 (s, CO), 1917 (s, CO), 1553 (w, CN), 1518 (w, CN), 1254 cm^{-1} (m, thienyl); UV/Vis (*n*-pentane): λ_{max} (abs.) = 233 (1.803), 251 (sh, 0.965), 293 (0.216), 347 (0.319), 370 (sh, 0.252), 438 (0.066); MS (EI, ^{184}W): m/z (%): 650.0 ($[M]^+$, 28), 622.0 ($[M-CO]^+$, 12), 594.0 ($[M-2\,CO]^+$, 91), 538.0 ($[M-4\,CO]^+$, 31), 510.0 ($[M-5\,CO]^+$, 32), 465.0 ($[M-4\,CO-SiMe_3]^+$, 24), 326.1 ($[M-W(CO)_5]^+$, 21), 190.0 ($[PCH(SiMe_3)_2]^+$, 25); 73.0 ($[SiMe_3]^+$, 100); elemental analysis (%) calcd. for $C_{18}H_{23}N_2O_5PSi_2W$: C 33.24, H 3.56, N 4.31; found: C 33.22, H 3.52, N 4.24.

126h: Crystallized from *n*-pentane at 4 $^\circ$C; ^{1}H NMR (300.13 MHz, C_6D_6): δ = -0.24 (s$_{sat}$, $|^2J_{SiH}|$ = 6.4 Hz, $|^1J_{CH}|$ = 119.8 Hz, 9 H; Si(CH_3)$_3$), 0.45 (s$_{sat}$, $|^2J_{SiH}|$ = 6.4 Hz, $|^1J_{CH}|$ = 120.2 Hz, 9 H; Si(CH_3)$_3$), 0.97 (dd, $|^2J_{PH}|$ = 4.1 Hz, $|^5J_{HH}|$ = 0.6 Hz, 1 H; C*H*(SiMe$_3$)$_2$), 6.69 (dd, $|^3J_{HH}|$ = 5.0 and 3.8 Hz, 1 H; thienyl-C^{4}H), 6.81 (ddd, $|^{5+6}J_{PH}|$ = 1.2 Hz, $|^3J_{HH}|$ = 5.0 Hz, $|^4J_{HH}|$ = 0.9 Hz, 1 H; thienyl-C^{5}H), 7.75 (dd, $|^3J_{HH}|$ = 3.8 Hz, $|^4J_{HH}|$ = 0.9 Hz, 1 H; thienyl-C^{3}H), 7.87 (dd, $|^{3+4}J_{PH}|$ = 34.2 Hz, $|^5J_{HH}|$ = 0.6 Hz, 1 H; CH); ^{13}C{^{1}H} NMR (75.5 MHz, C_6D_6): δ = 2.8 (d$_{sat}$, $|^3J_{PC}|$ = 2.0 Hz, $|^1J_{SiC}|$ = 52.4 Hz; Si(CH_3)$_3$), 3.6 (d$_{sat}$, $|^3J_{PC}|$ = 2.8 Hz, $|^1J_{SiC}|$ = 53.5 Hz; Si(CH_3)$_3$), 18.1 (d, $|^1J_{PC}|$ = 3.4 Hz; C*H*(SiMe$_3$)$_2$), 128.6 (s; thienyl-C^4), 134.9 (s; thienyl-C^5), 138.0 (d, $|^2J_{PC}|$ = 28.8 Hz; thienyl-C^2), 138.1 (s; thienyl-C^3), 162.9 (d,

$|^{2+3}J_{PC}| = 9.2$ Hz; PNC), 195.7 (d$_{sat}$, $|^{1+4}J_{PC}| = 21.1$ Hz, $|^2J_{WC}| = 3.6$ Hz; PCN), 197.4 (d$_{sat}$, $|^2J_{PC}| = 6.1$ Hz, $|^1J_{WC}| = 126.9$ Hz; CO$_{cis}$), 197.8 (d$_{sat}$, $|^2J_{PC}| = 23.0$ Hz, $|^1J_{WC}| = 144.2$ Hz; CO$_{trans}$); ^{15}N NMR (30.418 MHz, C$_6$D$_6$): $\delta = -89$ ($|^{1+4}J_{PN}| = 38$ Hz, $|^2J_{NH}| = 14$ Hz; N^1), -66 ($|^{2+3}J_{PN}| = 24$ Hz, $|^2J_{NH}| = 15$ Hz; N^4); ^{15}N NMR (30.418 MHz, CD$_2$Cl$_2$): $\delta = -88$ ($|^{1+4}J_{PN}| = 60$ Hz, $|^2J_{NH}| = 13$ Hz; N^1), -66 ($|^{2+3}J_{PN}| = 8$ Hz, $|^2J_{NH}| = 15$ Hz; N^4); ^{29}Si\{^{1}H\} NMR (59.6 MHz, C$_6$D$_6$): $\delta = 3.4$ (d$_{sat}$, $|^2J_{PSi}| = 2.9$ Hz, $|^1J_{SiC}| = 53.4$ Hz), 4.1 (d$_{sat}$, $|^2J_{PSi}| = 12.2$ Hz, $|^1J_{SiC}| = 52.5$ Hz); ^{31}P NMR (121.5 MHz, C$_6$D$_6$): $\delta = 105.4$ (dd$_{sat}$, $|^1J_{WP}| = 232.3$ Hz, $|^{3+4}J_{PH}| = 34.2$ Hz, $|^2J_{PH}| = 2.5$ Hz).

131h: ^{1}H NMR (300.13 MHz, C$_6$D$_6$): $\delta = 0.00$ (s$_{sat}$, $|^1J_{SiH}| = 6.5$ Hz, 18 H; Si(CH$_3$)$_3$), 1.70 (d, $|^2J_{PH}| = 13.2$ Hz, 1 H; CH(SiMe$_3$)$_2$), 6.57 (m$_c$; thienyl-C^{4}H), 6.90 (m$_c$; thienyl-C^{5}H), 7.36 (m$_c$; thienyl-C^{3}H), 8.26 (d, $|^{3+4}J_{PH}| = 7.1$ Hz, 1 H; CH); ^{13}C\{^{1}H\} NMR (75.5 MHz, C$_6$D$_6$): $\delta = 2.0$ (d, $|^3J_{PC}| = 5.4$ Hz; Si(CH$_3$)$_3$), 17.9 (d, $|^1J_{PC}| = 56.6$ Hz; CH(SiMe$_3$)$_2$), 128.4 (s; thienyl-C^5), 128.8 (d, $|^{4+5}J_{PC}| = 2.9$ Hz; thienyl-C^4), 132.8 (d, $|^3J_{PC}| = 8.4$ Hz; thienyl-C^3), 139.8 (d, $|^2J_{PC}| = 18.8$ Hz; thienyl-C^2), 171.0 (d, $|^{2+3}J_{PC}| = 12.0$ Hz; PNC), 198.3 (d, $|^3J_{PC}| = 2.9$ Hz; CO$_{cis}$), 199.5 (d, $|^{1+4}J_{PC}| = 35.9$ Hz; PCN), 201.0 (d, $|^3J_{PC}| = 1.9$ Hz; CO$_{trans}$); ^{15}N NMR (30.418 MHz, CD$_2$Cl$_2$): $\delta = -56$ (N^4); ^{29}Si\{^{1}H\} NMR (59.6 MHz, C$_6$D$_6$): $\delta = 7.1$ (d, $|^2J_{PSi}| = 10.0$ Hz); ^{31}P NMR (121.5 MHz, C$_6$D$_6$): $\delta = 118.6$ (br).

10.3.20 Investigations on the Temperature Dependance of the Chemical Equilibrium of Complexes 41h/129h, 69h/130h, and 126h/131h

In an NMR tube 49 mg (0.076 mmol) of **41h** and **129h** were dissolved in 0.52 mL of toluene. Subjecting the mixture to ^{31}P\{^{1}H\} NMR (121.5 MHz) at different temperatures revealed the following ratios of **41h/129h** as estimated by signal integration:
$-10\,°$C: 92 : 8
$+30\,°$C: 84 : 16
$+60\,°$C: 79 : 21
In an NMR tube 43 mg (0.057 mmol) of **69h** and **130h** were dissolved in 0.4 mL of toluene. Subjecting the mixture to ^{31}P\{^{1}H\} NMR (121.5 MHz) at different temperatures revealed the following ratios of **69h/130h** as estimated by signal integration:
$-80\,°$C: 38 : 62
$+45\,°$C: 35 : 65
In an NMR tube 28 mg (0.043 mmol) of **126h** and **131h** were dissolved in 0.4 mL of toluene. Subjecting the mixture to ^{31}P\{^{1}H\} NMR (121.5 MHz) at different tempera-

tures revealed the following ratios of **126h/131h** as estimated by signal integration:

−80 °C: 96 : 4

+45 °C: 94 : 6.

10.3.21 Synthesis of [2-Bis(trimethylsilyl)methyl-5-dimethyl-amino-3-phenyl-2H-1,4,2-diazaphosphole-κP]pentacarbonylmolybdenum(0) (74b)

To a stirred solution of 273 mg (0.52 mmol) of 2H-azaphosphirene complex **70** in 7 mL of CH_2Cl_2 were added consecutively 45 μL (0.55 mmol) of dimethyl cyanamide (**36b**) and 46 μL (0.52 mmol) of TfOH at −30 °C while the initially yellow colored solution turned deep red. After the addition the cooling bath was removed, and after 2 min 74 μL (0.53 mmol) of NEt$_3$ was added while the reaction mixture turned light orange. Then, all volatiles were removed in vacuo ($\sim 10^{-2}$ mbar), and the product was purified by column chromatography on silica (−30 °C, 2 × 6 cm, petroleum ether/Et$_2$O: 100/1). Evaporation of the solvents of the first fraction ($\sim 10^{-2}$ mbar) yielded **74b**.

74b: Yellow solid, crystallized from n-pentane at 4 °C; yield: 274 mg (0.46 mmol, 89 %); mp 104 °C (decomp.); ^{1}H NMR (300.13 MHz, C_6D_6): $\delta = -0.18$ (s$_{sat}$, $|^2J_{SiH}| =$ 6.2 Hz, $|^1J_{CH}| = 119.5$ Hz, 9 H; Si(CH$_3$)$_3$), 0.51 (s$_{sat}$, $|^2J_{SiH}| = 6.4$ Hz, $|^1J_{CH}| = 119.8$ Hz, 9 H; Si(CH$_3$)$_3$), 0.91 (d, $|^2J_{PH}| = 2.4$ Hz, 1 H; CH(SiMe$_3$)$_2$), 2.82 (s, 3 H; NCH$_3$), 2.98 (s, 3 H; NCH$_3$), 7.16 (m$_c$, 3 H; $meta$+$para$-H$_{phenyl}$), 8.17 (m$_c$, 2 H; $ortho$-H$_{phenyl}$); ^{13}C$\{^1$H$\}$ NMR (75.5 MHz, C_6D_6): $\delta = 3.1$ (d$_{sat}$, $|^3J_{PC}| = 1.6$ Hz, $|^1J_{SiC}| = 52.0$ Hz; Si(CH$_3$)$_3$), 3.9 (d$_{sat}$, $|^3J_{PC}| = 2.6$ Hz, $|^1J_{SiC}| = 52.9$ Hz; Si(CH$_3$)$_3$), 21.4 (d, $|^1J_{PC}| =$ 11.6 Hz; CH(SiMe$_3$)$_2$), 37.7 (s; NCH$_3$), 37.7 (s; NCH$_3$), 128.9 (s; $meta$-C$_{phenyl}$), 131.3 (d, $|^3J_{PC}| = 2.6$ Hz; $ortho$-C$_{phenyl}$), 133.1 (d, $|^2J_{PC}| = 20.4$ Hz; $ipso$-C$_{phenyl}$), 133.2 (s; $para$-C$_{phenyl}$), 164.7 (d, $|^{2+3}J_{PC}| = 0.7$ Hz; PNC), 201.3 (d, $|^{1+4}J_{PC}| = 29.7$ Hz; PCN), 206.5 (d, $|^2J_{PC}| = 8.4$ Hz; CO$_{cis}$), 211.1 (d, $|^2J_{PC}| = 23.0$ Hz; CO$_{trans}$); ^{29}Si$\{^1$H$\}$ NMR (59.6 MHz, C_6D_6): $\delta = 2.2$ (d$_{sat}$, $|^2J_{PSi}| = 11.8$ Hz, $|^1J_{SiC}| = 52.0$ Hz), 2.3 (d$_{sat}$, $|^2J_{PSi}| = 1.3$ Hz, $|^1J_{SiC}| = 53.0$ Hz); ^{31}P NMR (121.5 MHz, C_6D_6): $\delta = 122.7$ (s); IR (KBr): $\tilde{\nu} = 2957$ (w, CH$_3$/CH), 2930 (w, CH$_3$/CH), 2901 (w, CH$_3$/CH), 2855 (w, CH$_3$/CH), 2070 (m, sh, CO), 1988 (m, sh, CO), 1952 (s, CO), 1929 (s, CO), 1919 (s, CO), 1604 (m, CN), 1538 cm^{-1} (w, CN); UV/Vis (n-pentane): λ_{max} (abs.) = 208 (sh, 0.758), 228 (1.013), 234 (1.016), 250 (sh, 0.828), 286 (0.306), 348 (0.080), 396 nm (0.058); MS (FAB$^+$, ^{98}Mo): m/z (%): 602.0 ([M + H]$^+$, 3), 545.1 ([M − 2 CO]$^+$, 21), 447.0 ([M + H − 5 CO − CH$_3$]$^+$, 16), 364.2 ([M + H − W(CO)$_5$]$^+$, 100); MS (EI, ^{98}Mo): m/z (%): 601.1 ([M]$^+$, 4), 573.1 ([M − CO]$^+$, 11), 545.1 ([M − 2 CO]$^+$, 21), 447.0 ([M − 3 CO − Me$_2$NCN]$^+$, 37), 363.2 ([M − Mo(CO)$_5$]$^+$, 94), 290.1 ([M − Mo(CO)$_5$ − SiMe$_3$]$^+$,

84), 190.0 ([Me$_3$SiPC(H)SiMe$_3$]$^+$, 22), 73.0 ([SiMe$_3$]$^+$, 100); elemental analysis (%) calcd. for C$_{22}$H$_{30}$MoN$_3$O$_5$PSi$_2$: C 44.07, H 5.04, N 7.01; found: C 44.20, H 5.06, N 6.85.

10.3.22 Synthesis of [2-Bis(trimethylsilyl)methyl-5-dimethyl-amino-3-phenyl-2H-1,4,2-diazaphosphole-κP]pentacar-bonylchromium(0) (75b)

To a stirred solution of 250 mg (0.51 mmol) of 2H-azaphosphirene complex **71** in 7 mL of CH$_2$Cl$_2$ were added consecutively 45 μL (0.55 mmol) of dimethyl cyanamide (**36b**) and 46 μL (0.52 mmol) of TfOH at $-30\,^{\circ}$C while the initially yellow colored solution turned deep red. After the addition the cooling bath was removed, and after 1 min 74 μL (0.53 mmol) of NEt$_3$ was added while the reaction mixture turned light red. Then, all volatiles were removed in vacuo ($\sim 10^{-2}$ mbar), and the product was purified by column chromatography on silica ($-30\,^{\circ}$C, 2 $\times$ 6 cm, petroleum ether/Et$_2$O: 100/1). Evaporation of the solvents of the first fraction ($\sim 10^{-2}$ mbar) yielded **75b**.

75b: Orange solid, crystallized from n-pentane at 4$\,^{\circ}$C; yield: 242 mg (0.44 mmol, 85 %); mp 110$\,^{\circ}$C; ^{1}H NMR (300.13 MHz, C$_6$D$_6$): $\delta = -0.19$ (s$_{sat}$, $|^2J_{SiH}| = 6.5$ Hz, $|^1J_{CH}| = 119.6$ Hz, 9 H; Si(CH$_3$)$_3$), 0.50 (s$_{sat}$, $|^2J_{SiH}| = 6.5$ Hz, $|^1J_{CH}| = 119.7$ Hz, 9 H; Si(CH$_3$)$_3$), 1.02 (d, $|^2J_{PH}| = 2.7$ Hz, 1 H; CH(SiMe$_3$)$_2$), 2.80 (s, 3 H; NCH$_3$), 2.95 (s, 3 H; NCH$_3$), 7.16 (m$_c$, 3 H; $meta$+$para$-H$_{phenyl}$), 8.15 (m$_c$, 2 H; $ortho$-H$_{phenyl}$); ^{13}C$\{^1$H$\}$ NMR (75.5 MHz, C$_6$D$_6$): $\delta = 3.2$ (d$_{sat}$, $|^3J_{PC}| = 1.9$ Hz, $|^1J_{SiC}| = 52.0$ Hz; Si(CH$_3$)$_3$), 4.1 (d$_{sat}$, $|^3J_{PC}| = 2.3$ Hz, $|^1J_{SiC}| = 53.0$ Hz; Si(CH$_3$)$_3$), 22.5 (d, $|^1J_{PC}| = 9.7$ Hz; CH(SiMe$_3$)$_2$), 37.6 (s; NCH$_3$), 37.7 (s; NCH$_3$), 128.7 (s; $meta$-C$_{phenyl}$), 131.6 (d, $|^3J_{PC}| = 1.6$ Hz; $ortho$-C$_{phenyl}$), 133.1 (s; $para$-C$_{phenyl}$), 133.2 (d, $|^2J_{PC}| = 20.7$ Hz; $ipso$-C$_{phenyl}$), 163.7 (s; PNC), 200.5 (d, $|^{1+4}J_{PC}| = 31.7$ Hz; PCN), 217.4 (d, $|^2J_{PC}| = 12.6$ Hz; CO$_{cis}$), 222.0 (d, $|^2J_{PC}| = 6.8$ Hz; CO$_{trans}$); ^{29}Si$\{^1$H$\}$ NMR (59.6 MHz, C$_6$D$_6$): $\delta = 1.4$ (d$_{sat}$, $|^2J_{PSi}| = 11.0$ Hz, $|^1J_{SiC}| = 52.2$ Hz), 2.3 (d$_{sat}$, $|^2J_{PSi}| = 3.3$ Hz, $|^1J_{SiC}| = 53.0$ Hz); ^{31}P NMR (121.5 MHz, C$_6$D$_6$): $\delta = 146.3$ (s); IR (KBr): $\tilde{\nu} = 2959$ (w, CH$_3$/CH), 2931 (w, CH$_3$/CH), 2901 (w, CH$_3$/CH), 2855 (w, CH$_3$/CH), 2059 (m, sh, CO), 1981 (m, sh, CO), 1927 (s, CO), 1917 (s, CO), 1606 (m, CN), 1538 cm^{-1} (w, CN); UV/Vis (n-pentane): λ_{max} (abs.) = 202 (sh, 0.901), 209 (sh, 1.012), 225 (1.217), 234 (sh, 1.156), 253 (sh, 0.951), 286 (0.458), 351 (0.102), 390 (0.082), 439 nm (sh, 0.049); MS (FAB$^+$, ^{52}Cr): m/z (%): 443.1 ([M$-$4 CO]$^+$, 76), 415.1 ([M$-$5 CO]$^+$, 100), 400.1 ([M$-$5 CO$-$CH$_3$]$^+$, 46), 364.2 ([M$+$H$-$W(CO)$_5$]$^+$, 63); MS (EI, ^{52}Cr): m/z (%): 555.1 ([M]$^+$, 48), 540.1 ([M$-$CH$_3$]$^+$, 29), 527.1 ([M$-$CO]$^+$, 11), 443.1 ([M$-$4 CO]$^+$, 52), 415.1 ([M$-$5 CO]$^+$, 100), 400.1 ([M$-$5 CO$-$CH$_3$]$^+$, 67), 363.1 ([M$-$

Cr(CO)$_5$]$^+$, 36), 290.1 ([M $-$ Cr(CO)$_5$ $-$ SiMe$_3$]$^+$, 31), 73.0 ([SiMe$_3$]$^+$, 48); elemental analysis (%) calcd. for C$_{22}$H$_{30}$CrN$_3$O$_5$PSi$_2$: C 47.56, H 5.44, N 7.56; found: C 47.09, H 5.66, N 7.36.

10.3.23 Attempted Synthesis of 2-Bis(trimethylsilyl)methyl-5-dimethylamino-3-phenyl-2H-1,4,2-diazaphosphole (50b) and Characterization of 2-Bis(trimethylsilyl)-methyl-5-dimethylamino-3-phenyl-2H-1,4,2-diazaphos-phol-1-ium Trifluoromethanesulfonate (147b)

To a stirred solution of 100 mg (0.19 mmol) of 2H-azaphosphirene complex **70** in 4 mL of CH$_2$Cl$_2$ were added consecutively 16 μL (0.20 mmol) of dimethyl cyanamide (**36b**) and 17 μL (0.19 mmol) of TfOH at $-60\,^{\circ}$C while the initially yellow colored solution turned deep red. After 6 min the cooling bath was removed, and the reaction mixture turned brownish while warming to room temperature. The protonated intermediate **145b** was identified by ^{31}P NMR spectroscopy (121.5 MHz, CH$_2$Cl$_2$): $\delta = 130.6$ (d, $|^{2+5}J_{PH}| = 22.9$ Hz, $|^2J_{PH}| = 6.4$ Hz). After 7 h n-pentane was added under rigorous stirring and the formation of a brownish green precipitate was observed, which was separated, washed with n-pentane, and subjected to multinuclear NMR and diverse shift-correlated 2D NMR experiments in CD$_2$Cl$_2$.

147b: ^{1}H NMR (300.13 MHz, CD$_2$Cl$_2$): $\delta = 0.01$ (s$_{sat}$, $|^2J_{SiH}| = 6.5$ Hz, $|^1J_{CH}| = 120.7$ Hz, 9 H; Si(CH$_3$)$_3$), 0.27 (d$_{sat}$, $|^4J_{PH}| = 0.7$ Hz, $|^1J_{CH}| = 118.3$ Hz, 9 H; Si(CH$_3$)$_3$), 0.93 (d, $|^2J_{PH}| = 4.0$ Hz, 1 H; CH(SiMe$_3$)$_2$), 3.49 (d, $|^{5+6}J_{PH}| = 2.6$ Hz, 3 H; NCH$_3$), 3.67 (d, $|^{5+6}J_{PH}| = 1.7$ Hz, 3 H; NCH$_3$), 7.62 (m$_c$, 2 H; $meta$-H$_{phenyl}$), 7.75 (m$_c$, 1 H; $para$-H$_{phenyl}$), 7.95 (m$_c$, 2 H; $ortho$-H$_{phenyl}$), 9.78 (d, $|^{2+5}J_{PH}| = 28.3$ Hz, $h_{1/2} = 9.1$ Hz, 1 H; NH); ^{13}C{^{1}H} NMR (75.5 MHz, CD$_2$Cl$_2$): $\delta = 1.3$ (d$_{sat}$, $|^3J_{PC}| = 7.8$ Hz, $|^1J_{SiC}| = 52.4$ Hz; Si(CH$_3$)$_3$), 1.9 (d$_{sat}$, $|^3J_{PC}| = 3.2$ Hz, $|^1J_{SiC}| = 52.5$ Hz; Si(CH$_3$)$_3$), 21.1 (d, $|^1J_{PC}| = 63.7$ Hz; CH(SiMe$_3$)$_2$), 39.6 (d, $|^{4+5}J_{PC}| = 1.3$ Hz; NCH$_3$), 41.1 (d, $|^{4+5}J_{PC}| = 1.9$ Hz; NCH$_3$), 120.7 (q, $|^1J_{FC}| = 319.7$ Hz; CF$_3$), 129.8 (d, $|^3J_{PC}| = 10.3$ Hz; $ortho$-C$_{phenyl}$), 129.9 (s; $meta$-C$_{phenyl}$), 132.6 (d, $|^2J_{PC}| = 17.8$ Hz; $ipso$-C$_{phenyl}$), 135.7 (d, $|^5J_{PC}| = 1.6$ Hz; $para$-C$_{phenyl}$), 165.9 (d, $|^{2+3}J_{PC}| = 0.4$ Hz; PNC), 211.8 (d, $|^{1+4}J_{PC}| = 40.4$ Hz; PCN); ^{15}N NMR (30.418 MHz, CD$_2$Cl$_2$): $\delta = -277$ (NMe$_2$), -276 ($|^{1+4}J_{PN}| = 28$ Hz, $|^1J_{NH}| = 91$ Hz; N^{1}H); ^{29}Si{^{1}H} NMR (59.6 MHz, CD$_2$Cl$_2$): $\delta = 5.3$ (d, $|^2J_{PSi}| = 3.5$ Hz), 5.8 (d, $|^2J_{PSi}| = 17.4$ Hz); ^{31}P NMR (121.5 MHz, CD$_2$Cl$_2$): $\delta = 100.7$ (d, $|^2J_{PH}| = 28.0$ Hz).

Subsequently, **147b** was dissolved in 4 mL of CH$_2$Cl$_2$, 32 μL (0.40 mmol, 2 equiv.) of

pyridine was added at $-30\,^\circ$C, and n-pentane was added under rigorous stirring while
the formation of a brownish precipitate was observed. The overlaying solution was
transferred into another flask and all volatiles were removed in vacuo ($\sim 10^{-2}$ mbar).
The crude product was dissolved in 17 mL of n-pentane and filtered over silanized
silica gel at $-50\,^\circ$C. Evaporation of the solvent ($\sim 10^{-2}$ mbar) gave **50b**.

50b: Yellow oil; yield: 14.7 mg (0.04 mmol, 21 %); ^{1}H NMR (300.13 MHz, C_6D_6):
$\delta = 0.26$ (br, 18 H; $Si(CH_3)_3$), 0.75 (d_{sat}, $|^2J_{PH}| = 0.8$ Hz, $|^2J_{SiH}| = 8.8$ Hz, 1 H;
$CH(SiMe_3)_2$), 3.11 (s, 6 H; $N(CH_3)_2$), 7.16 (m_c, 3 H; $meta+para$-H_{phenyl}), 8.01 (m_c,
2 H; $ortho$-H_{phenyl}); $^{13}C\{^1H\}$ NMR (75.5 MHz, C_6D_6): $\delta = 2.0$ (br_{sat}, $|^1J_{SiC}| = 51$
Hz; $Si(CH_3)_3$), 18.6 (d_{sat}, $|^1J_{PC}| = 56.9$ Hz, $|^1J_{SiC}| = 39.0$ Hz; $CH(SiMe_3)_2$), 38.2
(s; $N(CH_3)_2$), 128.5 (d, $|^3J_{PC}| = 8.1$ Hz; $ortho$-C_{phenyl}), 129.1 (s; $meta$-C_{phenyl}), 131.4
(d, $|^5J_{PC}| = 2.3$ Hz; $para$-C_{phenyl}), 135.8 (d, $|^2J_{PC}| = 15.8$ Hz; $ipso$-C_{phenyl}), 167.4 (d,
$|^{2+3}J_{PC}| = 1.1$ Hz; PNC), 210.6 (d, $|^{1+4}J_{PC}| = 52.4$ Hz; PCN); ^{31}P NMR (121.5 MHz,
C_6D_6): $\delta = 95.4$ (s).

10.3.24 Reaction of [2-Bis(trimethylsilyl)methyl-3-phenyl-2H-azaphosphirene-κP]pentacarbonylchromium(0) (71) with Dimethyl Cyanamide and Trifluoromethanesulfonic Acid

To a stirred solution of 97 mg (0.20 mmol) of 2H-azaphosphirene complex **71** in 4
mL of CH_2Cl_2 were added consecutively 16 μL (0.20 mmol) of dimethyl cyanamide
(**36b**) and 17 μL (0.19 mmol) of TfOH at $-60\,^\circ$C while the initially yellow colored
solution turned deep red. The protonated intermediate **146b** was identified by ^{31}P
NMR spectroscopy (121.5 MHz, CH_2Cl_2): $\delta = 157.7$ (d, $|^{2+5}J_{PH}| = 22.9$ Hz, $|^2J_{PH}|$
$= 8.9$ Hz).

10.3.25 Synthesis of [2-Bis(trimethylsilyl)methyl-4-(N-cyclo-hexylimino)-2-phenyl-2,3-dihydro-1,3-azaphosphete-κP]-pentacarbonyltungsten(0) (149)

To a stirred solution of 300 mg (0.49 mmol) of 2H-azaphosphirene complex **35** in 5.4
mL of CH_2Cl_2 were added consecutively 60 μL (0.50 mmol) of cyclohexyl isocyanide
(**148**) and 43 μL (0.49 mmol) of TfOH at $-30\,^\circ$C. The initially yellow colored solution
turned deep red. The cooling bath was removed after 1 min, and after 5 min 69 μL
(0.49 mmol) of NEt_3 was added while the reaction mixture turned brownish yellow.

Then, all volatiles were removed in vacuo ($\sim 10^{-2}$ mbar), and the product was purified by column chromatography on silica ($-30\,°C$, 2×8 cm, petroleum ether/Et$_2$O: 10/1). Evaporation of the solvents of the first fraction ($\sim 10^{-2}$ mbar) yielded **149**.

149: Yellow solid, crystallized from n-pentane at $4\,°C$; yield: 286 mg (0.39 mmol, 81); mp $122\,°C$ (decomp.); ^{1}H NMR (300.13 MHz, C$_6$D$_6$): $\delta = -0.03$ (s$_{sat}$, $|^2J_{SiH}|$ = 6.5 Hz, $|^1J_{CH}|$ = 119.6 Hz, 9 H; Si(CH$_3$)$_3$), 0.46 (s$_{sat}$, $|^2J_{SiH}|$ = 6.1 Hz, $|^1J_{CH}|$ = 119.0 Hz, 9 H; Si(CH$_3$)$_3$), 1.25 (m$_c$, 2 H; Cy-C^{4}H$_2$), 1.27 (m$_c$, 2 H; Cy-C^{3+5}H$_{ax/eq}$), 1.48 (d, $|^2J_{PH}|$ = 9.3 Hz, 1 H; CH(SiMe$_3$)$_2$), 1.67 (m$_c$, 2 H; Cy-C^{2+6}H$_{ax/eq}$), 1.71 (m$_c$, 2 H; Cy-C^{3+5}H$_{ax/eq}$), 1.84 (m$_c$, 2 H; Cy-C^{2+6}H$_{ax/eq}$), 4.59 (m$_c$, 1 H; Cy-C^{1}H), 7.08 (m$_c$, 3 H; $meta+para$-H$_{phenyl}$), 8.09 (m$_c$, 2 H; $ortho$-H$_{phenyl}$); ^{13}C$\{^1$H$\}$ NMR (75.5 MHz, C$_6$D$_6$): $\delta = 2.5$ (d$_{sat}$, $|^3J_{PC}|$ = 3.2 Hz, $|^1J_{SiC}|$ = 53.2 Hz; Si(CH$_3$)$_3$), 3.0 (d$_{sat}$, $|^3J_{PC}|$ = 2.3 Hz, $|^1J_{SiC}|$ = 52.7 Hz; Si(CH$_3$)$_3$), 24.5 (s; Cy-C^{5}H$_2$), 24.6 (s; Cy-C^{3}H$_2$), 25.7 (d, $|^1J_{PC}|$ = 24.6 Hz; CH(SiMe$_3$)$_2$), 26.0 (s; Cy-C^{4}H$_2$), 34.2 (d, $|^4J_{PC}|$ = 0.6 Hz; Cy-C^{6}H$_2$), 34.6 (d, $|^4J_{PC}|$ = 1.3 Hz; Cy-C^{2}H$_2$), 58.9 (d, $|^3J_{PC}|$ = 11.5 Hz; Cy-C^{1}H), 129.0 (s; $meta$-C$_{phenyl}$), 129.9 (d, $|^3J_{PC}|$ = 1.9 Hz; $ortho$-C$_{phenyl}$), 132.9 (d, $|^2J_{PC}|$ = 20.7 Hz; $ipso$-C$_{phenyl}$), 133.9 (s; $para$-C$_{phenyl}$), 156.6 (d, $|^{1+3}J_{PC}|$ = 67.2 Hz; PC(NCy)N), 197.3 (d$_{sat}$, $|^2J_{PC}|$ = 5.8 Hz, $|^1J_{WC}|$ = 125.9 Hz; CO$_{cis}$), 198.5 (d$_{sat}$, $|^{1+3}J_{PC}|$ = 8.4 Hz, $|^2J_{WC}|$ = 3.3 Hz; PC(Ph)N), 199.2 (d$_{sat}$, $|^2J_{PC}|$ = 23.6 Hz, $|^1J_{WC}|$ = 143.5 Hz; CO$_{trans}$); ^{29}Si$\{^1$H$\}$ NMR (59.6 MHz, C$_6$D$_6$): $\delta = 1.4$ (d$_{sat}$, $|^2J_{PSi}|$ = 9.4 Hz, $|^1J_{SiC}|$ = 52.5 Hz), 2.5 (d$_{sat}$, $|^2J_{PSi}|$ = 2.9 Hz, $|^1J_{SiC}|$ = 53.0 Hz); ^{31}P NMR (121.5 MHz, C$_6$D$_6$): $\delta = 104.0$ (d$_{sat}$, $|^1J_{WP}|$ = 220.0 Hz, $|^2J_{PH}|$ = 9.4 Hz); IR (KBr): $\tilde{\nu}$ = 2929 (w, CH$_3$/CH$_2$/CH), 2903 (w, CH$_3$/CH$_2$/CH), 2854 (w, CH$_3$/CH$_2$/CH), 2071 (m, sh, CO), 1987 (m, sh, CO), 1947 (s, CO), 1930 (s, CO), 1906 (s, CO), 1679 (w, CN), 1597 (w, CN), 1505 (w, CN), 1479 (w, CN), 1445 cm^{-1} (w, CN); UV/Vis (n-pentane): λ_{max} (abs.) = 203 (0.527), 208 (sh, 0.517), 212 (sh, 0.530), 217 (0.631), 221 (sh, 0.747), 224 (sh, 0.823), 229 (sh, 0.923), 234 (0.975), 290 (0.277), 350 (0.044), 397 nm (sh, 0.032); MS (EI, ^{184}W): m/z (%): 726.1 ([M]$^+$, 85), 670.1 ([M-2 CO]$^+$, 64), 642.1 ([M-3 CO]$^+$, 40), 614.1 ([M-4 CO]$^+$, 85), 586.1 ([M-5 CO]$^+$, 100), 73.0 ([SiMe$_3$]$^+$, 77); MS (ESI$^+$, ^{184}W): m/z (%): 727.1 ([M$+$H]$^+$, 100), 403.2 ([M$+$H$-$W(CO)$_5$]$^+$, 25); elemental analysis (%) calcd. for C$_{26}$H$_{35}$N$_2$O$_5$PSi$_2$W: C 42.98, H 4.86, N 3.86; found: C 42.96, H 4.80, N 3.82.

10.3.26 Characterization of [2-Bis(trimethylsilyl)methyl-4-(N-cyclohexylimino)-hydrogeno-2-phenyl-2,3-dihydro-1,3-azaphosphete-κP(1+)]pentacarbonyltungsten(0) Trifluoromethanesulfonate (154)

To a stirred solution of 200 mg (0.32 mmol) of 2H-azaphosphirene complex **35** in 2 mL of CH$_2$Cl$_2$ were added consecutively 39 μL (0.32 mmol) of cyclohexyl isocyanide (**148**) and 28 μL (0.32 mmol) of TfOH at $-30\,^\circ$C while the initially yellow colored solution turned deep red. After the addition the cooling bath was removed and 60 mL of n-pentane was added under rigorous stirring. The overlaying solution was removed with a syringe and the red residue was washed with n-pentane until the overlaying solution was colorless. Then, complex **154** was dried in vacuo ($\sim 10^{-2}$ mbar), subsequently dissolved in CD$_2$Cl$_2$, and subjected to multinuclear and diverse shift-correlated 2D NMR experiments.

154: ^{1}H NMR (300.13 MHz, CD$_2$Cl$_2$): $\delta = 0.17$ (s, 9 H; Si(CH$_3$)$_3$), 0.48 (s, 9 H; Si(CH$_3$)$_3$), 1.29 (m$_c$, 2 H; Cy-C^{4}H$_2$), 1.38 (m$_c$, 1 H; Cy-C$^{3/5}$H$_{ax/eq}$), 1.45 (m$_c$, 1 H; Cy-C$^{3/5}$H$_{ax/eq}$), 1.73 (m$_c$, 1 H; Cy-C$^{3/5}$H$_{ax/eq}$), 1.78 (m$_c$, 1 H; Cy-C^{2}H$_{ax/eq}$), 1.84 (m$_c$, 1 H; Cy-C^{6}H$_{ax/eq}$), 1.93 (m$_c$, 1 H; Cy-C$^{3/5}$H$_{ax/eq}$), 2.06 (m$_c$, 1 H; Cy-C^{2}H$_{ax/eq}$), 2.13 (m$_c$, 1 H; Cy-C^{6}H$_{ax/eq}$), 2.23 (d, $|^2J_{PH}| = 15.2$ Hz, 1 H; CH(SiMe$_3$)$_2$), 4.51 (m$_c$, 1 H; Cy-C^{1}H), 7.76 (m$_c$, 2 H; $meta$-H$_{phenyl}$), 7.99 (m$_c$, 1 H; $para$-H$_{phenyl}$), 8.15 (m$_c$, 2 H; $ortho$-H$_{phenyl}$), 12.07 (br, $h_{1/2} = 40$ Hz, 1 H; NH); ^{13}C$\{^1$H$\}$ NMR (75.5 MHz, CD$_2$Cl$_2$): $\delta = 3.7$ (d, $|^3J_{PC}| = 4.2$ Hz; Si(CH$_3$)$_3$), 2.1 (d, $|^3J_{PC}| = 2.6$ Hz; Si(CH$_3$)$_3$), 17.9 (d, $|^1J_{PC}| = 27.8$ Hz; CH(SiMe$_3$)$_2$), 24.4 (s; Cy-C$^{5/3}$H$_2$), 24.6 (s; Cy-C$^{3/5}$H$_2$), 24.6 (s; Cy-C^{4}H$_2$), 30.4 (s; Cy-C^{6}H$_2$), 32.5 (s; Cy-C^{2}H$_2$), 58.3 (d, $|^3J_{PC}| = 1.3$ Hz; Cy-C^{1}H), 120.4 (q, $|^1J_{FC}| = 319.7$ Hz; CF$_3$), 130.2 (d, $|^2J_{PC}| = 14.5$ Hz; $ipso$-C$_{phenyl}$), 130.5 (s; $meta$-C$_{phenyl}$), 132.2 (d, $|^3J_{PC}| = 3.9$ Hz; $ortho$-C$_{phenyl}$), 140.0 (s; $para$-C$_{phenyl}$), 179.8 (d, $|^{1+3}J_{PC}| = 24.2$ Hz; PC(NCy)N), 195.7 (d$_{sat}$, $|^2J_{PC}| = 5.5$ Hz, $|^1J_{WC}| = 126.7$ Hz; CO$_{cis}$), 196.6 (d, $|^2J_{PC}| = 27.5$ Hz; CO$_{trans}$), 211.9 (d, $|^{1+3}J_{PC}| = 14.9$ Hz; PC(Ph)N); ^{29}Si$\{^1$H$\}$ NMR (59.6 MHz, CD$_2$Cl$_2$): $\delta = 3.2$ (d, $|^2J_{PSi}| = 3.5$ Hz), 6.1 (d, $|^2J_{PSi}| = 12.2$ Hz); ^{31}P NMR (121.5 MHz, CD$_2$Cl$_2$): $\delta = 106.9$ (dd$_{sat}$, $|^1J_{WP}| = 240.3$ Hz, $|^2J_{PH}| = 15.3$ Hz, $|^3J_{PH}| = 6.4$ Hz).

10.3.27 Reaction of [2-Bis(trimethylsilyl)methyl-3-phenyl-2*H*-azaphosphirene-κP]pentacarbonyltungsten(0) (35) with Dimethyl Cyanamide in the Presence of Tetrafluoroboric Acid Diethyl Ether Complex

To a stirred solution of 40 mg (0.07 mmol) of 2*H*-azaphosphirene complex **35** in 0.8 mL of CH_2Cl_2 were added consecutively and 6 μL (0.07 mmol) of dimethyl cyanamide (**36b**) and 10 μL (0.07 mmol) of $HBF_4 \cdot Et_2O$ at $-7\,°C$. The initially yellow colored solution turned deep red. After 5 min the cooling bath was removed and 11 μL (0.08 mmol) of NEt_3 was added while the reaction solution turned yellow again. Subsequently, the reaction mixture containing complexes **41b** and **79a** was analyzed by ^{31}P NMR spectroscopy (121.5 MHz, CH_2Cl_2, 25 °C): $\delta = 101.6$ (s_{sat}, $|^1J_{PW}| = 239.1$ Hz; **41b** (84 %)), 197.4 (ddd, $|^1J_{PF}| = 824.0$ Hz, $|^2J_{PH}| = 11.4$ Hz, $|^3J_{PH}| = 52.8$ Hz; **79a** (9 %)).

10.3.28 Reaction of [2-Bis(trimethylsilyl)methyl-3-phenyl-2*H*-azaphosphirene-κP]pentacarbonyltungsten(0) (35) with Dimethyl Cyanamide in the Presence of Fuming Sulfuric Acid

To a stirred solution of 58 mg (0.09 mmol) of 2*H*-azaphosphirene complex **35** in 3 mL of CH_2Cl_2 were added consecutively 8 μL (0.10 mmol) of dimethyl cyanamide (**36b**) and 6 μL (0.09 mmol) of $H_2SO_4 \cdot (SO_3)_x$ ($w(SO_3) \approx 0.2$) at $-27\,°C$. The initially yellow colored solution turned deep red. After 5 min the cooling bath was removed, and after 5 min 27 μL (0.19 mmol) of NEt_3 was added while the reaction solution turned yellow again. Subsequently, the reaction mixture containing complex **41b** and unidentified products **A**–**D** was analyzed by $^{31}P\{^1H\}$ NMR spectroscopy (121.5 MHz, CH_2Cl_2, 25 °C): $\delta = 33.0$ (s; **A** (1 %)), 101.7 (s_{sat}, $|^1J_{PW}| = 240.3$ Hz; **41b** (45 %)), 130.0 (s; **B** (1 %)), 145.0 (s; **C** (16 %)), 150.7 (s_{sat}, $|^1J_{PW}| = 288.6$ Hz; **D** (37 %)).

10.3.29 Reaction of [2-Bis(trimethylsilyl)methyl-3-phenyl-2H-azaphosphirene-κP]pentacarbonyltungsten(0) (35) with Dimethyl Cyanamide in the Presence of Sulfuric Acid

To a stirred solution of 40 mg (0.07 mmol) of 2H-azaphosphirene complex **35** in 0.8 mL of CH$_2$Cl$_2$ were added consecutively 6 μL (0.07 mmol) of dimethyl cyanamide (**36b**) and 4 μL (0.08 mmol) of H$_2$SO$_4$ at -31 °C. The initially yellow colored solution turned deep red. After 1 min the cooling bath was removed, and after 5 min 12 μL (0.15 mmol) of pyridine was added while the reaction solution turned yellow again and the formation of a colorless precipitate was observed. Subsequently, the reaction mixture containing complex **41b** and unidentified products **A**–**R** was analyzed by ^{31}P$\{^1$H$\}$ NMR spectroscopy (121.5 MHz, CH$_2$Cl$_2$, 25 °C): δ = 11.0 (s; **A** (3 %)), 18.1 (s; **B** (5 %)), 25.1 (s; **C** (3 %)), 27.3 (s; **D** (1 %)), 44.2 (s; **E** (1 %)), 44.6 (s; **F** (3 %)), 47.3 (s$_{sat}$, $|^1J_{PW}|$ = 274.7 Hz; **G** (10 %)), 54.0 (s; **H** (2 %)), 57.1 (s; **I** (1 %)), 69.2 (s; **J** (2 %)), 75.3 (s; **K** (6 %)), 79.4 (s$_{sat}$, $|^1J_{PW}|$ = 279.7 Hz; **L** (10 %)), 101.4 (s$_{sat}$, $|^1J_{PW}|$ = 240.3 Hz; **41b** (34 %)), 115.3 (s; **M** (3 %)), 124.1 (s; **N** (1 %)), 144.3 (s; **O** (1 %)), 149.8 (s$_{sat}$, $|^1J_{PW}|$ = 287.4 Hz; **P** (8 %)), 152.7 (s; **Q** (2 %)), 165.9 (s; **R** (1 %)).

10.3.30 Reaction of [2-Bis(trimethylsilyl)methyl-3-phenyl-2H-azaphosphirene-κP]pentacarbonyltungsten(0) (35) with Dimethyl Cyanamide in the Presence of Trifluoroacetic Acid

To a stirred solution of 35 mg (0.06 mmol) of 2H-azaphosphirene complex **35** in 0.6 mL of CH$_2$Cl$_2$ were added consecutively 5 μL (0.06 mmol) of dimethyl cyanamide (**36b**) and 5 μL (0.07 mmol) of trifluoroacetic acid at ambient temperature. The initially yellow colored solution turned deep red. Subsequently, 9 μL (0.06 mmol) of NEt$_3$ was added while the reaction solution turned yellow again. The formation of **41b** was evidenced by ^{31}P NMR spectroscopy (121.5 MHz, CH$_2$Cl$_2$): δ = 101.5 (s$_{sat}$, $|^1J_{PW}|$ = 240.3 Hz).

10.3.31   Reaction of [2-Bis(trimethylsilyl)methyl-3-phenyl-$2H$-azaphosphirene-κP]pentacarbonyltungsten(0) (35) with Dimethyl Cyanamide in the Presence of Trichloroacetic Acid

To a stirred solution of 40 mg (0.07 mmol) of $2H$-azaphosphirene complex **35** in 0.4 mL of CH_2Cl_2 were added consecutively 6 μL (0.07 mmol) of dimethyl cyanamide (**36b**) and a solution of 11 mg (0.07 mmol) of trichloroacetic acid in 0.4 mL of CH_2Cl_2 at ambient temperature. The initially yellow colored solution turned deep red. After 10 min 6 μL (0.07 mmol) of pyridine was added while the reaction solution turned yellow again. Subsequently, the reaction mixture containing complex **41b** and unidentified products **A**–**D** was analyzed by $^{31}P\{^1H\}$ NMR spectroscopy (121.5 MHz, CH_2Cl_2, 25 °C): $\delta = 58.3$ (s; **A** (1 %)), 59.9 (s; **B** (32 %)), 72.5 (s; **C** (1 %)), 98.1 (s; **D** (4 %)), 101.3 (s_{sat}, $|^1J_{PW}| = 240.3$ Hz; **41b** (62 %)).

10.3.32   Reaction of [2-Bis(trimethylsilyl)methyl-3-phenyl-$2H$-azaphosphirene-κP]pentacarbonyltungsten(0) (35) with Dimethyl Cyanamide in the Presence of Triethylammonium Trifluoromethanesulfonate

To a stirred solution of 1.6 mL (11.4 mmol) of NEt_3 in 50 mL of CH_2Cl_2 was added 1.0 mL (11.4 mmol) of TfOH at ambient temperature. After the addition all volatiles were removed in vacuo ($\sim 10^{-2}$ mbar), and the product was washed with n-pentane, giving triethylammonium trifluoromethanesulfonate as colorless solid. [Et_3NH][OTf]: ^1H NMR (300.13 MHz, CD_2Cl_2, 30 °C): $\delta = 1.29$ (t, $|^3J_{HH}| = 7.4$ Hz, 9 H; CH_3), 3.14 (q, br, $|^3J_{HH}| = 6.8$ Hz, 6 H; CH_2), 8.08 (s, br, 1 H; NH); $^{13}C\{^1H\}$ NMR (75.5 MHz, CD_2Cl_2, 30 °C): $\delta = 8.5$ (s; CH_3), 47.0 (s; CH_2), 120.4 (q, $|^1J_{CF}| = 319.5$ Hz; CF_3); $^{19}F\{^1H\}$ NMR (282.4 MHz, CD_2Cl_2, 30 °C): $\delta = -79.3$. A solution of 40 mg (0.16 mmol) of [Et_3NH][OTf] in 0.5 mL of CH_2Cl_2 was added to a solution of 43 mg (0.07 mmol) of $2H$-azaphosphirene complex **35** and 6 μL (0.07 mmol) of dimethyl cyanamide (**36b**) in 0.3 mL of CH_2Cl_2 at ambient temperature. No color change was observed, and after 1 d ^{31}P NMR spectroscopy revealed no evidence for conversion of **35**. Analysis after 7 d revealed besides the resonance of complex **35** a resonance that is presumably assigned to free ligand **50b** together with resonances of unidentified products **A**–**C**. $^{31}P\{^1H\}$ NMR (121.5 MHz, CH_2Cl_2): $\delta = -110.3$ (s_{sat}, $|^1J_{PW}| = 293.7$ Hz; **35** (79 %)), 97.0 (s; **50b** (3 %)), 122.0 (br; **A** (2 %)), 126.6 (br; **B** (12 %)), 145.0 (s; **C** (3 %)).

10.3.33 Reaction of [2-Bis(trimethylsilyl)methyl-3-phenyl-2H-azaphosphirene-κP]pentacarbonyltungsten(0) (35) with Dimethyl Cyanamide in the Presence of Acetic Acid

To a stirred solution of 40 mg (0.07 mmol) of 2H-azaphosphirene complex **35** in 0.8 mL of CH$_2$Cl$_2$ were added consecutively 6 μL (0.07 mmol) of dimethyl cyanamide (**36b**) and 4 μL (0.07 mmol) of acetic acid at ambient temperature. No color change was observed, and after 1 d ^{31}P NMR spectroscopy revealed no evidence for conversion of **35**. Analysis after 5 d revealed the resonances of complex **35** and unidentified products **A** and **B**. ^{31}P{^{1}H} NMR (121.5 MHz, CH$_2$Cl$_2$): $\delta = -109.8$ (s$_{sat}$, $|^1J_{PW}| = 293.7$ Hz; **35** (72 %)), 87.9 (s$_{sat}$, $|^1J_{PW}| = 275.9$ Hz; **A** (14 %)), 151.7 (s$_{sat}$, $|^1J_{PW}| = 286.1$ Hz; **B** (24 %)).

10.3.34 Reaction of [2-Bis(trimethylsilyl)methyl-3-phenyl-2H-azaphosphirene-κP]pentacarbonyltungsten(0) (35) with Dimethyl Cyanamide in the Presence of Boron Trifluoride Diethyl Etherate

To a stirred solution of 35 mg (0.06 mmol) of 2H-azaphosphirene complex **35** in 0.6 mL of CH$_2$Cl$_2$ were added consecutively 5 μL (0.06 mmol) of dimethyl cyanamide (**36b**) and 8 μL (0.06 mmol) of boron trifluoride diethyl etherate at ambient temperature. The initially yellow colored solution turned deep red. Subsequently, the reaction mixture containing complexes **41b** and **174** and unidentified product **A** was analyzed by ^{31}P{^{1}H} NMR spectroscopy (121.5 MHz, CH$_2$Cl$_2$): $\delta = 101.6$ (s$_{sat}$, $|^1J_{PW}| = 239.1$ Hz; **41b** (62 %)), 111.8 (d, $|^1J_{PF}| = 773.1$ Hz; **A** (13 %)), 204.0 (d, $|^1J_{PF}| = 845.6$ Hz; **174** (3 %)).

10.3.35 Reaction of [2-Bis(trimethylsilyl)methyl-3-phenyl-2H-azaphosphirene-κP]pentacarbonyltungsten(0) (35) with Dimethyl Cyanamide in the Presence of Tris(pentafluorophenyl)borane

A solution of 60 mg (0.10 mmol) of 2H-azaphosphirene complex **35** in 0.4 mL of CH$_2$Cl$_2$ was added to a stirred solution of 52 mg (0.10 mmol) of tris(pentafluorophenyl)borane and 9 μL (0.11 mmol) of dimethyl cyanamide (**36b**) in 0.4 mL of CH$_2$Cl$_2$ at

ambient temperature. The reaction mixture turned deep red. After 6 d the mixture containing complex **41b** and unidentified products **A** and **B** was analyzed by ^{31}P{^{1}H} NMR spectroscopy (121.5 MHz, CH$_2$Cl$_2$, 25 °C): $\delta = 101.6$ (s$_{sat}$, $|^1J_{PW}| = 240.3$ Hz; **41b** (97 %)), 133.2 (s; **A** (2 %)), 148.7 (s; **B** (1 %)).

10.3.36 Reaction of [2-Bis(trimethylsilyl)methyl-3-phenyl-2H-azaphosphirene-κP]pentacarbonyltungsten(0) (35) with Dimethyl Cyanamide in the Presence of Lithium Hexafluorophosphate

To a stirred solution of 50 mg (0.08 mmol) of 2H-azaphosphirene complex **35** in 1.0 mL of CH$_2$Cl$_2$ were added consecutively 7 μL (0.09 mmol) of dimethyl cyanamide (**36b**) and 13 mg (0.09 mmol) of lithium hexafluorophosphate at ambient temperature. The initially yellow colored solution turned red. The reaction mixture containing [**Li–41b**], complexes **79a,b**, and unidentified products **A**–**F** was analyzed by ^{31}P{^{1}H} NMR NMR spectroscopy. ^{31}P{^{1}H} NMR (121.5 MHz, CH$_2$Cl$_2$): $\delta = -144.5$ (sept, $|^1J_{PF}| = 710.8$ Hz, PF$_6^-$. -110.7 (s$_{sat}$, $|^1J_{PW}| = 295.0$ Hz; **35** (10 %)), -20.6 (t, $|^1J_{PF}| = 958.8$ Hz; **A** (11 %)), 17.0 (d, $|^1J_{PF}| = 1068.1$ Hz; **B** (2 %)), 17.7 (d, $|^1J_{PF}| = 1045.2$ Hz; **C** (4 %)), 99.4 (s; **D** (4 %)), 102 (br, $h_{1/2} = 70$ Hz; [**Li–41b**]$^+$ (53 %)), 123.0 (s$_{sat}$, $|^1J_{PW}| = 255.6$ Hz; **E** (2 %)), 160.1 (s$_{sat}$, $|^1J_{PW}| = 289.9$ Hz; **F** (4 %)), 192.5 (d$_{sat}$, $|^1J_{PF}| = 858.3$ Hz, $|^1J_{PW}| = 281.0$ Hz; **79b** (2 %)), 196.2 (d, $|^1J_{PF}| = 820.2$ Hz, $h_{1/2} = 20$ Hz; **79a** (8 %)). After 3 d the reaction mixture containing complexes **41b**, **79a,b**, and unidentified products **A**–**D** was analyzed by ^{31}P{^{1}H} and ^{19}F{^{1}H} NMR spectroscopy. ^{31}P{^{1}H} NMR (121.5 MHz, CH$_2$Cl$_2$): $\delta = -144.5$ (sept, $|^1J_{PF}| = 710.8$ Hz, PF$_6^-$; -20.6 (t, $|^1J_{PF}| = 958.8$ Hz; **A** (13 %)), 91.5 (br; **B** (15 %)), 99.4 (s; **C** (9 %)), 100.9 (s$_{sat}$, $|^1J_{PW}| = 241.6$ Hz; **41b** (44 %)), 123.0 (s$_{sat}$, $|^1J_{PW}| = 255.6$ Hz; **D** (4 %)), 192.5 (d$_{sat}$, $|^1J_{PF}| = 858.3$ Hz, $|^1J_{PW}| = 281.0$ Hz; **79b** (12 %)), 196.2 (d, $|^1J_{PF}| = 820.2$ Hz, $h_{1/2} = 20$ Hz; **79a** (3 %)), ^{19}F{^{1}H} NMR (282.4 MHz, CH$_2$Cl$_2$): $\delta = -117.3$ (d, $|^1J_{PF}| = 825.8$ Hz; **79a**). -114.5 (d, $|^1J_{PF}| = 858.3$ Hz; **79b**), -83.9 (d, $|^1J_{PF}| = 953.7$ Hz; **A**), -73.7 (d, $|^1J_{PF}| = 711.3$ Hz; PF$_6^-$).

10.3.37 Reaction of [2-Bis(trimethylsilyl)methyl-3-phenyl-2*H*-azaphosphirene-κP]pentacarbonyltungsten(0) (35) with Dimethyl Cyanamide in the Presence of Lithium Trifluoromethanesulfonate

A solution of 40 mg (0.07 mmol) of 2*H*-azaphosphirene complex **35** and 6 μL (0.07 mmol) of dimethyl cyanamide (**36b**) in 1.0 mL of CH$_2$Cl$_2$ was added to 10 mg (0.06 mmol) of lithium trifluoromethanesulfonate at ambient temperature. No color change was observed, and after 1 d the reaction mixture containing unreacted **35**, complex **41b**, and unidentified product **A** was analyzed by ^{31}P{^{1}H} NMR spectroscopy (121.5 MHz, CH$_2$Cl$_2$): $\delta = -110.7$ (s$_{sat}$, $|^1J_{PW}| = 295.0$ Hz; **35** (72 %)), 100.9 (s$_{sat}$, $|^1J_{PW}| = 239.1$ Hz; **41b** (19 %)), 154.8 (s; **A** (6 %)).

10.3.38 Reaction of [2-Bis(trimethylsilyl)methyl-3-phenyl-2*H*-azaphosphirene-κP]pentacarbonyltungsten(0) (35) with Dimethyl Cyanamide in the Presence of Lithium Trifluoromethanesulfonate in THF

To a stirred solution of 31 mg (0.05 mmol) of 2*H*-azaphosphirene complex **35** in 0.7 mL of THF were added consecutively 5 μL (0.06 mmol) of dimethyl cyanamide (**36b**) and 8 mg (0.05 mmol) of lithium trifluoromethanesulfonate at ambient temperature. No color change was observed, and ^{31}P NMR spectroscopy revealed no evidence for conversion of **35**.

10.3.39 Reaction of [2-Bis(trimethylsilyl)methyl-3-phenyl-2*H*-azaphosphirene-κP]pentacarbonyltungsten(0) (35) with Dimethyl Cyanamide in the Presence of Lithium Trifluoromethanesulfonate and 12-Crown-4

To a stirred solution of 40 mg (0.07 mmol) of 2*H*-azaphosphirene complex **35** in 0.7 mL of CH$_2$Cl$_2$ were added consecutively 6 μL (0.07 mmol) of dimethyl cyanamide (**36b**), 12 μL (0.07 mmol) of 12-crown-4, and 11 mg (0.07 mmol) of lithium trifluoromethanesulfonate at ambient temperature. No color change was observed, and ^{31}P NMR spectroscopy revealed no evidence for conversion of **35**.

10.3.40   Reaction of [2-Bis(trimethylsilyl)methyl-3-phenyl-2*H*-azaphosphirene-κ*P*]pentacarbonyltungsten(0) (35) with Dimethyl Cyanamide in the Presence of Lithium Tetrakis(pentafluorophenyl)borate

A solution of 60 mg (0.10 mmol) of 2*H*-azaphosphirene complex **35** in 0.4 mL of CH_2Cl_2 was added to a stirred solution of 85 mg (0.12 mmol) of lithium tetrakis(penta-fluorophenyl)borate and 9 μL (0.11 mmol) of dimethyl cyanamide (**36b**) in 0.4 mL of CH_2Cl_2 at ambient temperature. The reaction mixture turned red. After 2 d the mixture containing complex **41b** and unidentified product **A** was analyzed by $^{31}P\{^1H\}$ NMR spectroscopy (121.5 MHz, CH_2Cl_2, 25 °C): $\delta = 101.5$ (s_{sat}, $|^1J_{PW}| = 239.1$ Hz; **41b** (85 %)), 110.5 (s_{sat}, $|^1J_{PW}| = 263.2$ Hz; **A** (15 %)).

10.3.41   Reaction of [2-Bis(trimethylsilyl)methyl-3-phenyl-2*H*-azaphosphirene-κ*P*]pentacarbonyltungsten(0) (35) with Dimethyl Cyanamide in the Presence of Copper(I) Chloride

In an NMR tube 44 mg (0.07 mmol) of 2*H*-azaphosphirene complex **35**, 9 mg (0.09 mmol) of copper(I) chloride, and 6 μL (0.07 mmol) of dimethyl cyanamide (**36b**) were dissolved in 0.8 mL of CH_2Cl_2 at ambient temperature, and the reaction mixture containing complexes **46** and **155** was analyzed by $^{31}P\{^1H\}$ NMR spectroscopy (121.5 MHz, CH_2Cl_2, 25 °C): $\delta = 133.0$ (s_{sat}, $|^1J_{PW}| = 263.2$ Hz; **155** (30 %)), 149.6 (s_{sat}, $|^1J_{PW}| = 256.9$ Hz; **46** (73 %)).

10.3.42   Reaction of [2-Bis(trimethylsilyl)methyl-3-phenyl-2*H*-azaphosphirene-κ*P*]pentacarbonyltungsten(0) (35) with Dimethyl Cyanamide in the Presence of Tetrakisacetonitrile Copper(I) Trifluoromethanesulfonate

In an NMR tube 40 mg (0.07 mmol) of 2*H*-azaphosphirene complex **35**, 29 mg (0.08 mmol) of tetrakisacetonitrile copper(I) trifluoromethanesulfonate, and 6 μL (0.07 mmol) of dimethyl cyanamide (**36b**) were dissolved in 0.8 mL of CH_2Cl_2 at ambient temperature. The initially yellow colored solution turned red. After 24 h the mixture containing complexes **46**, **155**, **41b,m**, and **156**, which is in equilibrium with **35**, was

analyzed by ^{31}P{^{1}H} NMR spectroscopy (121.5 MHz, CH$_2$Cl$_2$, 25 °C): $\delta = -92.3$ (s$_{sat}$, $|^1J_{PW}| = 294.5$ Hz; **156/35** (30 %)), 101.7 (s$_{sat}$, $|^1J_{PW}| = 240.3$ Hz; **41b** (14 %)), 110.0 (s$_{sat}$, $|^1J_{PW}| = 226.3$ Hz; **41m** (3 %)), 132.9 (s$_{sat}$, $|^1J_{PW}| = 263.2$ Hz; **155** (27 %)), 149.7 (s$_{sat}$, $|^1J_{PW}| = 259.4$ Hz; **46** (11 %)).

10.3.43 Reaction of [2-Bis(trimethylsilyl)methyl-3-phenyl-2H-azaphosphirene-κP]pentacarbonyltungsten(0) (35) with Tetrakisacetonitrile Copper(I) Trifluoromethanesulfonate

Stoichiometric reaction of complex 35 with [Cu(MeCN)$_4$][OTf]: In an NMR tube 41 mg (0.07 mmol) of 2H-azaphosphirene complex **35** and 27 mg (0.07 mmol) of tetrakisacetonitrile copper(I) trifluoromethanesulfonate were dissolved in 0.4 mL of CD$_2$Cl$_2$ at ambient temperature while the initially yellow colored solution turned red. Subsequently, the mixture containing complex **41m** (27 %) and complex **156**, which is in equilibrium with **35** (70 %), was analyzed by ^{1}H and ^{31}P NMR spectroscopy.

156/35: ^{1}H NMR (300.13 MHz, CD$_2$Cl$_2$, 25 °C): $\delta = 0.15$ (s$_{sat}$, $|^2J_{SiH}| = 6.4$ Hz, 9 H; Si(CH$_3$)$_3$), 0.33 (s$_{sat}$, $|^2J_{SiH}| = 6.0$ Hz, 9 H; Si(CH$_3$)$_3$), 0.93 (d, $|^2J_{PH}| = 2.6$ Hz, 1 H; CH(SiMe$_3$)$_2$), 2.14 (s, 12 H; CH$_3$CN), 7.72 (m$_c$, 3 H; *meta*+*para*-H$_{phenyl}$), 8.11 (m$_c$, 2 H; *ortho*-H$_{phenyl}$); ^{31}P NMR (121.5 MHz, CD$_2$Cl$_2$, 25 °C): $\delta = -84.2$ (s$_{sat}$, $|^1J_{PW}| = 297.5$ Hz).

After 56 h the mixture containing complex **41m** and unidentified product **A** was analyzed by ^{31}P{^{1}H} NMR spectroscopy (121.5 MHz, CD$_2$Cl$_2$, 25 °C): $\delta = 110.3$ (s$_{sat}$, $|^1J_{PW}| = 228.9$ Hz; **41m** (18 %)), 96.4 (br, $h_{1/2} = 55$ Hz; **A** (73 %)).

Reaction of [Cu(MeCN)$_4$][OTf] with two equiv. of 35: A solution of 10 mg (0.03 mmol) of tetrakisacetonitrile copper(I) trifluoromethanesulfonate in 0.4 mL of CH$_2$Cl$_2$ was added to a solution of 40 mg (0.07 mmol) of 2H-azaphosphirene complex **35** in 0.4 mL of CH$_2$Cl$_2$ in an NMR tube at ambient temperature. The initially yellow colored mixture turned slowly red, and ^{31}P{^{1}H} NMR spectroscopic monitoring (121.5 MHz, CH$_2$Cl$_2$, 25 °C) revealed a resonance at $\delta = -99.0$ (s$_{sat}$, $|^1J_{PW}| \approx 290$ Hz, $h_{1/2} = 57$ Hz) assigned to complex **156** being in equilibrium with complex **35**.

10.3.44 Reaction of [2-Bis(trimethylsilyl)methyl-3-phenyl-2H-azaphosphirene-κP]pentacarbonyltungsten(0) (35) with Acetonitrile in the Presence of Tetrakisacetonitrile Copper(I) Trifluoromethanesulfonate

To a stirred solution of 40 mg (0.07 mmol) of 2H-azaphosphirene complex **35** in 0.4 mL of CH$_2$Cl$_2$ were added consecutively 4 μL (0.08 mmol) of acetonitrile (**36m**) and a solution of 27 mg (0.07 mmol) of tetrakisacetonitrile copper(I) trifluoromethanesulfonate in 0.4 mL of CH$_2$Cl$_2$ at $-33\,^{\circ}$C. Upon warming to room temperature the initially yellow colored solution turned red. After 14 h the mixture containing complex **41m** and unidentified products **A**–**C** was analyzed by ^{31}P$\{^1$H$\}$ NMR spectroscopy (121.5 MHz, CH$_2$Cl$_2$, 25 $^{\circ}$C): $\delta = 110.3$ (s$_{sat}$, $|^1J_{PW}| = 228.9$ Hz; **41m** (86 %)), 162.3 (s; **A** (6 %)), 163.0 (s; **B** (3 %)), 175.8 (s; **C** (5 %)).

10.3.45 Consecutive Reaction of Acetonitrile (36m) with Trifluoromethanesulfonic Acid, [2-Bis(trimethylsilyl)methyl-3-phenyl-2H-azaphosphirene-κP]pentacarbonyltungsten(0) (35), and Triethylamine

To a stirred solution of 9 μL (0.17 mmol) of acetonitrile (**36m**) in 2 mL of CD$_2$Cl$_2$ was added 15 μL (0.17 mmol) of TfOH at ambient temperature. The mixture was subjected to ^{1}H and ^{19}F$\{^1$H$\}$ NMR spectroscopy: ^{1}H NMR (300.13 MHz, CD$_2$Cl$_2$, 30 $^{\circ}$C): $\delta = 2.09$ (s; CH$_3$), 12.27 (br; OH); ^{19}F$\{^1$H$\}$ NMR (282.4 MHz, CD$_2$Cl$_2$, 30 $^{\circ}$C): $\delta = -78.2$. Subsequently, 100 mg (0.16 mmol) of 2H-azaphosphirene complex **35** in 1 mL of CH$_2$Cl$_2$ was added at ambient temperature while the reaction mixture turned deep red. Upon addition of NEt$_3$ the solution turned yellow again, and the formation of **41m** was evidenced by ^{31}P$\{^1$H$\}$ NMR spectroscopy. ^{31}P$\{^1$H$\}$ NMR (121.5 MHz, CD$_2$Cl$_2$/CH$_2$Cl$_2$): $\delta = 109.1$ (s$_{sat}$, $|^1J_{WP}| = 228.9$ Hz).

10.3.46 Consecutive Reaction of [2-Bis(trimethylsilyl)methyl-3-phenyl-2*H*-azaphosphirene-κP]pentacarbonyltungsten(0) (35) with Trifluoromethanesulfonic Acid, Dimethyl Cyanamide, and Triethylamine

To a stirred solution of 200 mg (0.32 mmol) of 2*H*-azaphosphirene complex **35** in 1.0 mL of CD_2Cl_2 was added 43 μL (0.49 mmol) of TfOH at $-61\,°C$. While the initially yellow colored solution was allowed to reach room temperature it turned deep red. Then, the reaction mixture was subjected to multinuclear (^{1}H, ^{13}C, ^{15}N, ^{29}Si, ^{31}P) NMR and diverse shift-correlated 2D NMR experiments. After 24 h was added 40 μL (0.49 mmol) of dimethyl cyanamide (**36b**), and the formation of **171b** was evidenced by multinuclear NMR experiments. After 4 h was added 110 μL (0.78 mmol) of NEt$_3$, and the formation of **172b** was evidenced by multinuclear NMR experiments.

169: ^{1}H NMR (300.13 MHz, CD_2Cl_2, $-17\,°C$): $\delta = 0.04$ (s$_{sat}$, $|^2J_{SiH}| = 6.9$ Hz, 9 H; Si(CH$_3$)$_3$), 7.73 (m$_c$, 2 H; *meta*-H$_{phenyl}$), 7.91 (m$_c$, 1 H; *para*-H$_{phenyl}$), 8.17 (m$_c$, 2 H; *ortho*-H$_{phenyl}$), 8.52 (d$_{sat}$, $|^2J_{PH}| = 1.5$ Hz, $|^2J_{SiH}| = 1.3$ Hz, 1 H; CH), 12.09 (d, $|^3J_{PH}| = 16$ Hz, 1 H; NH$_2$), 12.13 (br, 1 H; NH$_2$); ^{13}C{^{1}H} NMR (75.5 MHz, CD_2Cl_2, $-17\,°C$): $\delta = -0.3$ (d, $|^3J_{PC}| = 5.3$ Hz; Si(CH$_3$)$_3$), 119.1 (q, $|^1J_{FC}| = 317.8$ Hz; CF$_3$), 127.9 (*ipso*-C$_{phenyl}$), 130.6 (s; *meta*-C$_{phenyl}$), 131.9 (d, $|^3J_{PC}| = 2.3$ Hz; *ortho*-C$_{phenyl}$), 138.6 (s; *para*-C$_{phenyl}$), 174.6 (d, $|^1J_{PC}| = 26.5$ Hz; CH), 189.6 (PCN), 192.8 (d, $|^2J_{PC}| = 9.1$ Hz; CO$_{cis}$), 206.6 (d, $|^2J_{PC}| = 103.1$ Hz; CO$_{trans}$); ^{15}N NMR (30.418 MHz, CD_2Cl_2, $-17\,°C$): $\delta = -198$ (NH$_2$); ^{29}Si{^{1}H} NMR (59.6 MHz, CD_2Cl_2, $-17\,°C$): $\delta = -0.3$ (d, $|^2J_{PSi}| = 18.7$ Hz); ^{31}P NMR (121.5 MHz, CD_2Cl_2, $-17\,°C$): $\delta = 223.3$ (s$_{sat}$, $|^1J_{WP}| = 293.0$ Hz).

170: ^{1}H NMR (300.13 MHz, CD_2Cl_2, $-17\,°C$): $\delta = 0.29$ (s$_{sat}$, $|^2J_{SiH}| = 6.6$ Hz, 9 H; Si(CH$_3$)$_3$), 3.81 (d, $|^2J_{PH}| = 14.3$ Hz, 1 H; CH), 7.63 (m$_c$, 2 H; *meta*-H$_{phenyl}$), 7.82–7.85 (m$_c$, 1 H; *para*-H$_{phenyl}$), 8.10 (m$_c$, 2 H; *ortho*-H$_{phenyl}$), 10.50 (br, 1 H; NH$_2$), 11.08 (br, 1 H; NH$_2$); ^{13}C{^{1}H} NMR (75.5 MHz, CD_2Cl_2, $-17\,°C$): $\delta = 1.1$ (d, $|^3J_{PC}| = 7.1$ Hz; Si(CH$_3$)$_3$), 37.0 (d, $|^1J_{PC}| = 108$ Hz; CH), 128.2 (*ortho*-C$_{phenyl}$), 129.8 (*meta*-C$_{phenyl}$), 133.1 (*ipso*-C$_{phenyl}$), 136.5 (*para*-C$_{phenyl}$), 192.5 (d, $|^2J_{PC}| = 10.0$ Hz; CO$_{cis}$), 206.4 (d, $|^1J_{PC}| = 100.0$ Hz; PCN); ^{15}N NMR (30.418 MHz, CD_2Cl_2, $-50\,°C$): $\delta = -211$ (NH$_2$); ^{29}Si{^{1}H} NMR (59.6 MHz, CD_2Cl_2, $-10\,°C$): $\delta = 10.0$ (d, $|^2J_{PSi}| = 31$ Hz); ^{31}P NMR (121.5 MHz, CD_2Cl_2, $-17\,°C$): $\delta = -50.6$ (d$_{sat}$, $|^{1+2}J_{WP}| = 21.4$ Hz, $|^2J_{PH}| = 14.0$ Hz).

171b: ^{1}H NMR (300.13 MHz, CD_2Cl_2): $\delta = -0.02$ (s$_{sat}$, $|^2J_{SiH}| = 6.9$ Hz, 9 H; Si(CH$_3$)$_3$), 1.89 (d, $|^2J_{HH}| = 15.3$ Hz, 1 H; C*H$_2$*SiMe$_3$), 2.52 (dd, $|^2J_{PH}| = 10.9$ Hz, $|^2J_{HH}| = 15.3$ Hz, 1 H; C*H$_2$*SiMe$_3$), 3.53 (s, 3 H; NCH$_3$), 3.77 (s, 3 H; NCH$_3$), 7.68 (m$_c$,

2 H; *meta*-H$_{phenyl}$), 7.82 (m$_c$, 1 H; *para*-H$_{phenyl}$), 8.23 (m$_c$, 2 H; *ortho*-H$_{phenyl}$), 10.67 (d, $|^{2+5}J_{PH}|$ = 22.4 Hz, $h_{1/2}$ = 7.6 Hz, 1 H; NH); ^{13}C{^{1}H} NMR (75.5 MHz, CD$_2$Cl$_2$):[2] δ = 0.7 (d, $^3J_{PC}$ = 2 Hz; Si(CH$_3$)$_3$), 26.6 (*C*H$_2$(SiMe$_3$)), 39.8 (s; NCH$_3$), 41.0 (s; NCH$_3$), 129.8 (s; *meta*-C$_{phenyl}$), 131.0 (d, $|^3J_{PC}|$ = 2 Hz; *ortho*-C$_{phenyl}$), 131.3 (d, $|^2J_{PC}|$ = 21 Hz; *ipso*-C$_{phenyl}$), 137.1 (s; *para*-C$_{phenyl}$), 162.6 (s; PNC), 197.0 (d, $|^{1+4}J_{PC}|$ = 16 Hz; PCN), ^{15}N NMR (30.418 MHz, CD$_2$Cl$_2$): δ = -270 (NMe$_2$), -269 ($|^{1+4}J_{PN}|$ = 19 Hz, $|^1J_{NH}|$ = 93 Hz, $|^3J_{NH}|$ = 3 Hz, NH); ^{29}Si{^{1}H} NMR (59.6 MHz, CD$_2$Cl$_2$): δ = 3.9 (d, $|^2J_{PSi}|$ = 12.1 Hz); ^{31}P NMR (121.5 MHz, CD$_2$Cl$_2$): δ = 102.8 (dd$_{sat}$, $|^1J_{WP}|$ = 267.0 Hz, $|^{2+5}J_{PH}|$ = 23 Hz, $|^2J_{PH}|$ = 11.4 Hz).

10.3.47 Synthesis of [5-Dimethylamino-3-phenyl-2-trimethyl-silylmethyl-2*H*-1,4,2-diazaphosphole-κP]pentacarbon-yltungsten(0) (172b)

To a stirred solution of 200 mg (0.32 mmol) of 2*H*-azaphosphirene complex **35** in 1 mL of CH$_2$Cl$_2$ was added 43 μL (0.49 mmol) of TfOH at $-61\,°$C while the initially yellow colored solution turned deep red. Then, the cooling bath was removed, and after 10 min 40 μL (0.49 mmol) of dimethyl cyanamide (**36b**) was added. The reaction mixture was stirred for 4 h at ambient temperature, and, subsequently, 69 μL (0.49 mmol) of NEt$_3$ was added at ambient temperature while the reaction mixture turned brownish yellow. After removal of all volatiles in vacuo ($\sim 10^{-2}$ mbar) the product was purified by column chromatography on silica ($-30\,°$C, 3 $\times$ 7 cm, petroleum ether/Et$_2$O: 10/1). Evaporation of the solvents of the second fraction ($\sim 10^{-2}$ mbar) yielded **172b**.

172b: Yellow solid, crystallized from *n*-pentane at 4 °C; yield: 89 mg (0.14 mmol, 59 %, with respect to TfOH); mp 152 °C (decomp.); ^{1}H NMR (300.13 MHz, C$_6$D$_6$): δ = -0.05 (s$_{sat}$, $|^2J_{SiH}|$ = 6.6 Hz, $|^1J_{CH}|$ = 120.2 Hz, 9 H; Si(CH$_3$)$_3$), 1.57 (dd, $|^2J_{PH}|$ = 9.7 Hz, $|^2J_{HH}|$ = 14.3 Hz, 1 H; C*H*$_2$SiMe$_3$), 1.76 (dd, $|^2J_{PH}|$ = 3.9 Hz, $|^2J_{HH}|$ = 14.3 Hz, 1 H; C*H*$_2$SiMe$_3$), 2.82 (s, 3 H; NCH$_3$), 2.93 (s, 3 H; NCH$_3$), 7.12 (m$_c$, 3 H; *meta+para*-H$_{phenyl}$), 8.13 (m$_c$, 2 H; *ortho*-H$_{phenyl}$); ^{13}C{^{1}H} NMR (75.5 MHz, C$_6$D$_6$): δ = 0.3 (d$_{sat}$, $|^3J_{PC}|$ = 1.9 Hz, $|^1J_{SiC}|$ = 52.7 Hz; Si(CH$_3$)$_3$), 23.9 (d, $|^1J_{PC}|$ = 12.3 Hz; *C*H$_2$(SiMe$_3$)), 37.7 (s; NCH$_3$), 37.8 (s; NCH$_3$), 129.3 (s; *meta*-C$_{phenyl}$), 130.3 (d, $|^3J_{PC}|$ = 2.3 Hz; *ortho*-C$_{phenyl}$), 132.0 (d, $|^2J_{PC}|$ = 21.0 Hz; *ipso*-C$_{phenyl}$), 133.5 (s; *para*-C$_{phenyl}$), 166.1 (d, $|^{2+3}J_{PC}|$ = 0.3 Hz; PNC), 197.4 (d$_{sat}$, $|^2J_{PC}|$ = 7.1 Hz, $|^1J_{WC}|$ = 125.8 Hz; CO$_{cis}$), 200.2 (d$_{sat}$, $|^2J_{PC}|$ = 21.7 Hz, $|^1J_{WC}|$ = 144.7 Hz; CO$_{trans}$), 200.6 (d$_{sat}$, $|^{1+4}J_{PC}|$ = 15.5 Hz, $|^2J_{WC}|$ = 3.2 Hz; PCN); ^{15}N NMR (30.418 MHz, C$_6$D$_6$):

---

[2]Estimated from 2D ^{1}H,^{13}C gsHSQC and gsHMQC NMR experiments.

$\delta = -298$ (NMe$_2$), -203 ($|^{1+4}J_{PN}| = 59$ Hz, N^1); ^{29}Si$\{^1$H$\}$ NMR (59.6 MHz, C$_6$D$_6$): $\delta = 2.5$ (d$_{sat}$, $|^2J_{PSi}| = 8.9$ Hz, $|^1J_{SiC}| = 52.6$ Hz); ^{31}P NMR (121.5 MHz, C$_6$D$_6$): $\delta = 95.8$ (dd$_{sat}$, $|^1J_{WP}| = 242.9$ Hz, $|^2J_{PH}| = 9.4$ and 3.5 Hz); IR (KBr): $\tilde{\nu} = 2962$ (m, CH$_3$/CH$_2$), 2928 (w, CH$_3$/CH$_2$), 2903 (w, CH$_3$/CH$_2$), 2070 (m, sh, CO), 1982 (m, sh, CO), 1954 (s, CO), 1946 (s, CO), 1934 (s, CO), 1915 (s, CO), 1900 (s, CO), 1609 (m, CN), 1598 (m, CN), 1543 cm^{-1} (w, CN); UV/Vis (n-pentane): λ_{max} (abs.) = 205 (1.078), 209 (sh, 1.195), 212 (sh, 1.279), 217 (sh, 1.529), 222 (sh, 1.785), 227 (sh, 1.995), 232 (2.097), 252 (sh, 1.083), 287 (0.454), 295 (sh, 0.412), 306 (sh, 0.286), 345 (0.127), 411 nm (sh, 0.061); MS (FAB$^+$, ^{184}W): m/z (%): 616.1 ([M + H]$^+$, 31), 587.1 ([M − CO]$^+$, 46), 559.1 ([M − 2 CO]$^+$, 37), 531.1 ([M − 3 CO]$^+$, 37), 292.1 ([M + H − W(CO)$_5$]$^+$, 100); MS (EI, ^{184}W): m/z (%): 615.0 ([M]$^+$, 35), 587.0 ([M − CO]$^+$, 55), 559.0 ([M − 2 CO]$^+$, 44), 529.0 ([M − 2 CO − 2 CH$_3$]$^+$, 100), 501.0 ([M − 3 CO − 2 CH$_3$]$^+$, 31), 473.0 ([M − 4 CO − 2 CH$_3$]$^+$, 70), 73.0 ([SiMe$_3$]$^+$, 26); elemental analysis (%) calcd. for C$_{19}$H$_{22}$N$_3$O$_5$PSiW: C 37.09, H 3.60, N 6.83; found: C 36.89, H 3.78, N 6.56.

10.3.48 Reaction of Pentacarbonyl[2-(1,2,3,4,5-pentamethyl-2,4-cyclopentadien-1-yl)-3-phenyl-2H-azaphosphirene-κP]tungsten(0) (121) with Trifluoromethanesulfonic Acid

To a stirred solution of 54 mg (0.09 mmol) of 2H-azaphosphirene complex **121** in 2.5 mL of CH$_2$Cl$_2$ was added 8 μL (0.09 mmol) of TfOH at $-80\,^{\circ}$C while the initially yellow colored solution turned deep wine-red. The reaction solution was subjected to multinuclear (^{1}H, ^{13}C, ^{31}P) NMR and diverse shift-correlated 2D NMR experiments.

[**H−121**][OTf]: ^{1}H NMR (300.13 MHz, CD$_2$Cl$_2$, $-70\,^{\circ}$C): $\delta = 1.34$ (d, $|^3J_{PH}| = 14.7$ Hz, 3 H; Cp*-C^1-CH$_3$), 1.84 (m$_c$, 3 H; Cp*−CH$_3$), 1.95 (m$_c$, 9 H; Cp*−CH$_3$), 7.57 (m$_c$, 2 H; H$_{phenyl}$), 7.70 (m$_c$, 1 H; H$_{phenyl}$), 8.11 (m$_c$, 2 H; H$_{phenyl}$), 12.84 (d, $|^{2+3}J_{PH}| = 15.0$ Hz, $h_{1/2} = 8$ Hz, 1 H; NH); ^{13}C$\{^1$H$\}$ NMR (75.5 MHz, CD$_2$Cl$_2$, $-70\,^{\circ}$C): $\delta = 64.3$ (d, $|^1J_{PC}| = 10.0$ Hz; Cp*-C^1), 119.9 (q, $|^1J_{FC}| = 318.1$ Hz; CF$_3$), 184.1 (d, $|^{1+2}J_{PC}| = 13.4$ Hz; PCN); ^{31}P NMR (121.5 MHz, CD$_2$Cl$_2$, $-70\,^{\circ}$C): $\delta = -61.4$ (m$_c$, $|^1J_{WP}| = 263.2$ Hz).

10.3.49 Consecutive Reaction of Pentacarbonyl[2-(1,2,3,4,5-pentamethyl-2,4-cyclopentadien-1-yl)-3-phenyl-2*H*-aza-phosphirene-κP]tungsten(0) (121) with Trifluoromethane-sulfonic Acid and Dimethyl Cyanamide

To a stirred solution of 54 mg (0.09 mmol) of 2*H*-azaphosphirene complex **121** in 2.5 mL of CH_2Cl_2 was added 8 μL (0.09 mmol) of TfOH at $-80\,^{\circ}$C while the initially yellow colored solution turned deep wine-red. Subsequently, a solution of 8 μL (0.10 mmol) of dimethyl cyanamide (**36b**) in 1 mL of CH_2Cl_2 was added slowly at $-80\,^{\circ}$C. During the addition the reaction solution brightened up noticeably, and the formation of **124b** was evidenced by $^{31}P\{^1H\}$ NMR spectroscopy (121.5 MHz, CH_2Cl_2): $\delta = 115.0$ (s_{sat}, $|^1J_{WP}| = 251.8$ Hz).

10.3.50 Consecutive Reaction of Pentacarbonyl[2-(1,2,3,4,5-pentamethyl-2,4-cyclopentadien-1-yl)-3-phenyl-2*H*-aza-phosphirene-κP]tungsten(0) (121) with Trifluoromethane-sulfonic Acid and Triethylamine

To a stirred solution of 54 mg (0.09 mmol) of 2*H*-azaphosphirene complex **121** in 2.5 mL of CH_2Cl_2 8 μL (0.09 mmol) of TfOH was added at $-80\,^{\circ}$C while the initially yellow colored solution turned deep wine-red. Upon subsequent addition of a solution of 13 μL (0.09 mmol) of NEt_3 in 1 mL of CH_2Cl_2 at $-80\,^{\circ}$C the reaction solution turned light yellow. The regeneration of **121** was evidenced by $^{31}P\{^1H\}$ NMR spectroscopy (121.5 MHz, CH_2Cl_2): $\delta = -108.6$ (s_{sat}, $|^1J_{WP}| = 284.8$ Hz).

10.3.51 Reaction of [2-Bis(trimethylsilyl)methyl-3-phenyl-2*H*-azaphosphirene-κP]pentacarbonyltungsten(0) (35) with Tetrafluoroboric Acid Diethyl Ether Complex

To a stirred solution of 300 mg (0.49 mmol) of 2*H*-azaphosphirene complex **35** in 12 mL of CH_2Cl_2 was added 68 μL (0.50 mmol) of $HBF_4 \cdot Et_2O$ at $-65\,^{\circ}$C while the initially yellow colored solution turned deep red. After the reaction mixture was allowed to reach room temperature all volatiles were removed in vacuo ($\sim 10^{-2}$ mbar), and the crude product was washed with *n*-pentane. This afforded a 2.2:1 mixture of complexes **173** and **79b**, which were dried in vacuo ($\sim 10^{-2}$ mbar).

173 and **79b**: Red solid; yield: 185 mg; mp 54 °C (decomp.); IR (KBr): $\tilde{\nu}$ = 3325 (w, NH), 3108 (w, NH), 2961 (w, CH$_3$/CH), 2903 (w, CH$_3$/CH), 2085 (m, sh, CO (**173**)), 2077 (m, sh, CO (**79b**)), 2004 (m, CO), 1943 (s, CO), 1083 cm^{-1} (m, δ_{NH}); UV/Vis (CH$_2$Cl$_2$): λ_{max} (abs.) = 236 (1.830), 289 (0.248), 336 (0.109), 410 nm (0.020); HR-MS (ESI$^+$) calcd. for C$_{19}$H$_{26}$FNO$_5$PSi$_2$W ([**79b** + H]$^+$): 638.0574; found: 638.0665; dev. 0.0091.

173: ^{1}H NMR (300.13 MHz, CD$_2$Cl$_2$): δ = 0.26 (s, 9 H; Si(CH$_3$)$_3$), 0.50 (s, 9 H; Si(CH$_3$)$_3$), 1.85 (d, $|^3J_{FH}|$ = 32.5 Hz, 1 H; CH(SiMe$_3$)$_2$), 7.73 (m$_c$, 2 H; $meta$-H$_{phenyl}$), 7.89 (m$_c$, 1 H; $para$-H$_{phenyl}$), 8.13 (m$_c$, 2 H; $ortho$-H$_{phenyl}$), 10.6 (br, 1 H; NH); ^{11}B{^{1}H} NMR (96.3 MHz, CD$_2$Cl$_2$): δ = 0.5 (s); ^{13}C{^{1}H} NMR (75.5 MHz, CD$_2$Cl$_2$): δ = 3.0 (d, $|^3J_{PC}|/|^4J_{FC}|$ = 2.6 Hz; Si(CH$_3$)$_3$), 3.2 (d, $|^3J_{PC}|/|^4J_{FC}|$ = 1.3 Hz; Si(CH$_3$)$_3$), 25.7 (br; CH(SiMe$_3$)$_2$), 128.1 (br; $ipso$-C$_{phenyl}$), 130.6 (br; $meta$-C$_{phenyl}$), 131.0 (br; $ortho$-C$_{phenyl}$), 137.8 (br; $para$-C$_{phenyl}$), 189.6 (br; PCN), 194.7 (dd, $|^2J_{PC}|$ = 6.8 Hz, $|^3J_{FC}|$ = 2.6 Hz; CO$_{cis}$), 195.6 (d, $|^2J_{PC}|$ = 30.4 Hz; CO$_{trans}$); ^{19}F NMR (282.4 MHz, CD$_2$Cl$_2$): δ = −147.2 (s; BF$_3$), −120.3 (dd, $|^1J_{PF}|$ = 888.6 Hz, $|^4J_{FH}|$ = 23.6 Hz; PF); ^{29}Si{^{1}H} NMR (59.6 MHz, CD$_2$Cl$_2$): δ = 3.4 (d, $|^2J_{PSi}|/|^3J_{SiF}|$ = 6.4 Hz), 7.3 (br); ^{31}P NMR (121.5 MHz, CD$_2$Cl$_2$): δ = 189.6 (d$_{sat}$, $|^1J_{WP}|$ = 314.1 Hz, $|^1J_{PF}|$ = 887.6 Hz).

79b: ^{1}H NMR (300.13 MHz, CD$_2$Cl$_2$): δ = 0.22 (d, $|^5J_{FH}|$ = 1.7 Hz, 9 H; Si(CH$_3$)$_3$), 0.39 (s, 9 H; Si(CH$_3$)$_3$), 2.07 (dd, $|^2J_{PH}|$ = 10.7 Hz, $|^3J_{FH}|$ = 0.7 Hz, 1 H; CH(SiMe$_3$)$_2$), 7.56 (m$_c$, 2 H; $meta$-H$_{phenyl}$), 7.68 (m$_c$, 1 H; $para$-H$_{phenyl}$), 8.11 (m$_c$, 2 H; $ortho$-H$_{phenyl}$), 10.6 (br, 1 H; NH); ^{13}C{^{1}H} NMR (75.5 MHz, CD$_2$Cl$_2$): δ = 2.4 (dd, $|^3J_{PC}|$ = 2.6 Hz, $|^4J_{FC}|$ = 2.6 Hz; Si(CH$_3$)$_3$), 3.3 (d, $|^3J_{PC}|/|^4J_{FC}|$ = 2.9 Hz; Si(CH$_3$)$_3$), 31.6 (dd, $|^1J_{PC}|/|^2J_{FC}|$ = 11.5, 5.0 Hz; CH(SiMe$_3$)$_2$), 129.1 (d, $|^4J_{PC}|/|^5J_{FC}|$ = 0.6 Hz; $meta$-C$_{phenyl}$), 129.5 (d, $|^3J_{PC}|$ = 6.1 Hz; $ortho$-C$_{phenyl}$), 134.5 (s; $para$-C$_{phenyl}$), 135.9 (dd, $|^2J_{PC}|/|^3J_{FC}|$ = 40.1, 1.9 Hz; $ipso$-C$_{phenyl}$), 195.9 (dd, $|^2J_{PC}|/|^3J_{FC}|$ = 7.1, 2.9 Hz; CO$_{cis}$), 198.4 (d, $|^2J_{PC}|$ = 28.8 Hz; CO$_{trans}$), 207.8 (dd, $|^1J_{PC}|$ = 14.4 Hz, $|^2J_{FC}|$ = 14.4 Hz; PCN); ^{19}F{^{1}H} NMR (282.4 MHz, CD$_2$Cl$_2$): δ = −113.3 (d$_{sat}$, $|^1J_{PF}|$ = 858.3 Hz, $|^2J_{WF}|$ = 10.1 Hz); ^{29}Si{^{1}H} NMR (59.6 MHz, CD$_2$Cl$_2$): δ = −1.1 (dd, $|^2J_{PSi}|/|^3J_{SiF}|/|^2J_{PSi}|/|^3J_{SiF}|$ = 4.4, 0.7 Hz), 2.7 (dd, $|^2J_{PSi}|/|^3J_{SiF}|/|^2J_{PSi}|/|^3J_{SiF}|$ = 12.4, 6.4 Hz); ^{31}P NMR (121.5 MHz, CD$_2$Cl$_2$): δ = 193.3 (dd$_{sat}$, $|^1J_{WP}|$ = 281.0 Hz, $|^1J_{PF}|$ = 857.0 Hz, $|^2J_{PH}|$ = 11.4 Hz).

Subjecting a mixture of **173** and **79b** to column chromatography (−30 °C, 2 × 8 cm, petroleum ether/Et$_2$O: 10/1) yielded a color change from red to yellow, and a 2.4:1 mixture of **79a,b** was obtained that showed no resonance in an ^{11}B{^{1}H} NMR experiment; for analytical data for complex **79a** see Section 10.3.52. A mixture with the same composition was obtained when a mixture of complexes **173** and **79b** was dissolved in diethyl ether.

10.3.52 Reaction of [2-Bis(trimethylsilyl)methyl-3-phenyl-2H-azaphosphirene-κP]pentacarbonyltungsten(0) (35) with Boron Trifluoride Diethyl Etherate

To a stirred solution of 427 mg (0.69 mmol) of 2H-azaphosphirene complex **35** in 9 mL of CH_2Cl_2 was added 0.1 mL (0.79 mmol) of $BF_3 \cdot Et_2O$ at $-65\,°C$ while the initially yellow colored solution turned orange. Immediately after the addition all volatiles were removed in vacuo ($\sim 10^{-2}$ mbar) at $-65\,°C$, and a yellow solid containing mainly complex **174** was obtained, which was analyzed by multinuclear NMR experiments.

174: ^1H NMR (300.13 MHz, C_6D_6): $\delta = -0.03$ (s, 9 H; $Si(CH_3)_3$), 0.31 (s, 9 H; $Si(CH_3)_3$), 0.79 (t, $|^3J_{HH}| = 7.1$ Hz, 6 H; CH_3 (Et_2O)), 0.93 (d, $|^2J_{PH}|/|^3J_{FH}| = 2.9$ Hz, 1 H; $CH(SiMe_3)_2$), 3.42 (q, $|^3J_{HH}| = 7.1$ Hz, 4 H; CH_2 (Et_2O)), 7.01 (m_c, 2 H; $meta$-H_{phenyl}), 7.54 (m_c, 1 H; $para$-H_{phenyl}), 8.14 (m_c, 2 H; $ortho$-H_{phenyl}); $^{11}B\{^1H\}$ NMR (96.3 MHz, C_6D_6): $\delta = 2.5$ (s); $^{19}F\{^1H\}$ NMR (282.4 MHz, C_6D_6): $\delta = -141.8$ (s; BF_2), -105.1 (d, $|^1J_{PF}| = 846.0$ Hz; PF); $^{31}P\{^1H\}$ NMR (121.5 MHz, CD_2Cl_2): $\delta = 202.5$ (d_{sat}, $h_{1/2} = 13.1$ Hz, $|^1J_{WP}| = 315.3$ Hz, $|^1J_{PF}| = 845.6$ Hz).

Subjecting the product to column chromatography ($-35\,°C$, 2×10 cm) afforded complex **79a** after evaporation of the solvents of the 4th fraction ($\sim 10^{-2}$ mbar), which was eluated with petroleum ether/Et_2O: 1/4.

79a: Yellow solid; yield: 100 mg (0.16 mmol, 23 %); ^1H NMR (300.13 MHz, C_6D_6): $\delta = 0.19$ (d, $|^5J_{FH}| = 1.6$ Hz, 9 H; $Si(CH_3)_3$), 0.35 (s_{sat}, $|^2J_{SiH}| = 6.2$ Hz, 9 H; $Si(CH_3)_3$), 2.08 (d, $|^2J_{PH}| = 10.6$ Hz, 1 H; $CH(SiMe_3)_2$), 7.05 (m_c, 3 H; $meta+para$-H_{phenyl}), 7.17 (m_c, 2 H; $ortho$-H_{phenyl}), 10.15 (dd, $|^3J_{PH}| = 51.5$ Hz, $|^4J_{FH}| = 5.3$ Hz, 1 H; NH); $^{13}C\{^1H\}$ NMR (75.5 MHz, C_6D_6): $\delta = 2.7$ (dd_{sat}, $|^3J_{PC}|/|^4J_{FC}| = 2.7$, 2.3 Hz, $|^1J_{SiC}| = 53.0$ Hz; $Si(CH_3)_3$), 4.2 (d_{sat}, $|^3J_{PC}|/|^4J_{FC}| = 2.9$ Hz, $|^1J_{SiC}| = 54.5$ Hz; $Si(CH_3)_3$), 33.2 (dd, $|^1J_{PC}|/|^2J_{FC}| = 11.3$, 4.1 Hz; $CH(SiMe_3)_2$), 127.2 (dd, $|^3J_{PC}|/|^4J_{FC}| = 3.9$, 1.4 Hz; $ortho$-C_{phenyl}), 129.0 (d, $|^4J_{PC}|/|^5J_{FC}| = 0.6$ Hz; $meta$-C_{phenyl}), 130.7 (d, $|^5J_{PC}|/|^6J_{FC}| = 0.3$ Hz; $para$-C_{phenyl}), 138.7 (dd, $|^2J_{PC}|/|^3J_{FC}| = 26.9$, 2.1 Hz; $ipso$-C_{phenyl}), 184.7 (dd, $|^1J_{PC}|/|^2J_{FC}| = 42.0$, 17.6 Hz; PCN), 196.3 (dd, $|^2J_{PC}|/|^3J_{FC}| = 7.7$, 3.0 Hz; CO_{cis}), 198.8 (d, $|^2J_{PC}| = 28.2$ Hz; CO_{trans}); $^{19}F\{^1H\}$ NMR (282.4 MHz, C_6D_6): $\delta = -116.0$ (d_{sat}, $|^1J_{PF}| = 824.9$ Hz, $|^2J_{WF}| = 13.4$ Hz, $|^3J_{SiF}| = 5.0$ Hz); ^{31}P NMR (121.5 MHz, C_6D_6): $\delta = 196.7$ (ddd_{sat}, $|^1J_{WP}| = 288.6$ Hz, $|^1J_{PF}| = 824.0$ Hz, $|^2J_{PH}| = 10.8$ Hz, $|^3J_{PH}| = 51.5$ Hz); MS (FAB$^+$, ^{184}W): m/z (%): 638.0 ([M + H]$^+$, 30), 609.1 ([M − CO]$^+$, 85), 581.0 ([M − 2 CO]$^+$, 100), 497.0 ([M − 3 CO]$^+$, 40), 314.1 ([M + H − W(CO)$_5$]$^+$, 66).

10.4 Attempted Synthesis of *N*-Heterocyclic Carbenes with Phosphorus in the Backbone

10.4.1 Reaction of [2-Bis(trimethylsilyl)methyl-3-phenyl-2*H*-1,4,2-diazaphosphole-κ*P*]pentacarbonyltungsten(0) (41h) and [2-Bis(trimethylsilyl)methyl-3-phenyl-2*H*-1,4,2-diazaphosphole-κ*N*¹]pentacarbonyltungsten(0) (129h) with Methyl Trifluoromethanesulfonate and Trifluoromethanesulfonic Acid

To a stirred solution of 50 mg (0.08 mmol) of a mixture of 2*H*-1,4,2-diazaphosphole complexes **41h** and **129h** in 0.6 mL of CD_2Cl_2 were added consecutively 0.2 mL (1.77 mmol) of MeOTf and a solution of 2 µL (0.02 mmol) of TfOH in 0.1 mL (0.88 mmol) of MeOTf at −40 °C while the initially orange colored solution turned deep purple. After the addition the solution was allowed to reach room temperature, and the formation of **189** was evidenced by (^{1}H, ^{13}C, ^{31}P) NMR and diverse shift-correlated 2D NMR experiments.

189: ^{1}H NMR (300.13 MHz, CD_2Cl_2): δ = 0.40 (s, 9 H; Si(CH$_3$)$_3$), 1.97 (dd, $|^2J_{HH}|$ = 12.6 Hz, $|^5J_{HH}|$ = 2.6 Hz, 1 H; CH_2SiMe$_3$), 3.22 (dd, $|^2J_{PH}|$ = 21.3 Hz, $|^2J_{HH}|$ = 12.6 Hz, 1 H; CH_2SiMe$_3$), 4.26 (s, 3 H; NCH$_3$), 7.79 (m$_c$, 2 H; *meta+para*-H$_{phenyl}$), 7.87 (m$_c$, 3 H; *ortho*-H$_{phenyl}$), 8.29 (dd, $|^{3+4}J_{PH}|$ = 32.7 Hz, $|^5J_{HH}|$ = 2.3 Hz, 1 H; CH); ^{13}C{^{1}H} NMR (75.5 MHz, CD_2Cl_2): δ = 0.3 (d$_{sat}$, $|^3J_{PC}|$ = 3.3 Hz, $|^1J_{SiC}|$ = 53.2 Hz; Si(CH$_3$)$_3$), 17.2 (d, $|^1J_{PC}|$ = 11.9 Hz; CH_2SiMe$_3$), 40.5 (d, $|^{3+4}J_{PC}|$ = 2.2 Hz; NCH$_3$), 120.4 (q, $|^1J_{FC}|$ = 318.0 Hz; CF$_3$), 125.3 (d, $|^2J_{PC}|$ = 10.8 Hz; *ipso*-C$_{phenyl}$), 130.5 (s; *meta*-C$_{phenyl}$), 130.5 (d, $|^3J_{PC}|$ = 2.4 Hz; *ortho*-C$_{phenyl}$), 137.4 (d, $|^3J_{PC}|$ = 0.6 Hz; *para*-C$_{phenyl}$), 151.5 (d, $|^{2+3}J_{PC}|$ = 13.7 Hz; PNC), 192.9 (d$_{sat}$, $|^2J_{PC}|$ = 6.1 Hz, $|^1J_{WC}|$ = 126.4 Hz; CO$_{cis}$), 195.2 (d, $|^2J_{PC}|$ = 23.4 Hz; CO$_{trans}$), 203.1 (d, $|^{1+4}J_{PC}|$ = 9.7 Hz; PCN); ^{31}P NMR (121.5 MHz, CD_2Cl_2): δ = 130.6 (dd$_{sat}$, $|^1J_{WP}|$ = 253.1 Hz, $|^{3+4}J_{PH}|$ = 32.3 Hz, $|^2J_{PH}|$ = 21.0 Hz).

10.4.2 Synthesis of [2-Methyl-3-(2-thienyl)-2*H*-1,4,2-diazaphosphole-κ*P*]pentacarbonyltungsten(0) (190)

Consecutively, a solution of 505 mg (2.01 mmol) of triethylammonium trifluoromethanesulfonate (synthesis: Section 10.3.32) in 1.5 mL of THF and a solution of 369 mg (1.41

mmol) of tetra-n-butylammonium fluoride in 1.4 mL of THF were slowly added to a stirred solution of 251 mg (0.39 mmol) of a mixture of complexes **126h** and **131h** in 30 mL of THF at $-78\,$°C. During the addition the orange colored solution brightened up noticeably. It was stirred further 20 min at $-78\,$°C. Then, all volatiles were removed in vacuo ($\sim 10^{-2}$ mbar), the crude product was dissolved in n-pentane, filtered through celite, and dried in vacuo ($\sim 10^{-2}$ mbar).

190: Yellow solid, crystallized from n-pentane at $4\,$°C; yield: 132 mg (0.26 mmol, 68 %); mp 104 °C (decomp.); ^{1}H NMR (300.13 MHz, C$_6$D$_6$): $\delta = 1.27$ (d, $|^2J_{PH}| = 7.5$ Hz, 3 H; CH$_3$), 6.61 (dd, $|^3J_{HH}| = 5.0$ and 3.9 Hz, 1 H; thienyl-C^{4}H), 6.86 (ddd, $|^{5+6}J_{PH}| = 1.2$ Hz, $|^3J_{HH}| = 5.0$ Hz, $|^4J_{HH}| = 1.2$ Hz, 1 H; thienyl-C^{5}H), 7.53 (dd, $|^3J_{HH}| = 3.8$ Hz, $|^4J_{HH}| = 1.0$ Hz, 1 H; thienyl-C^{3}H), 7.96 (d, $|^{3+4}J_{PH}| = 34.7$ Hz, 1 H; CH); ^{13}C$\{^1$H$\}$ NMR (75.5 MHz, C$_6$D$_6$): $\delta = 17.7$ (d, $|^1J_{PC}| = 24.9$ Hz; CH$_3$), 129.3 (s; thienyl-C^4), 135.3 (s; thienyl-C^5), 136.2 (s; thienyl-C^3), 136.6 (d, $|^2J_{PC}| = 29.4$ Hz; thienyl-C^2), 165.5 (d, $|^{2+3}J_{PC}| = 10.3$ Hz; PNC), 195.0 (d$_{sat}$, $|^{1+4}J_{PC}| = 8.7$ Hz, $|^2J_{WC}| = 3.6$ Hz; PCN), 195.3 (d$_{sat}$, $|^2J_{PC}| = 6.5$ Hz, $|^1J_{WC}| = 125.1$ Hz; CO$_{cis}$), 198.1 (d$_{sat}$, $|^2J_{PC}| = 23.3$ Hz, $|^1J_{WC}| = 145.5$ Hz; CO$_{trans}$); ^{31}P NMR (121.5 MHz, C$_6$D$_6$): $\delta = 95.7$ (dq$_{sat}$, $|^1J_{WP}| = 240.3$ Hz, $|^3J_{PH}| = 34.4$ Hz, $|^2J_{PH}| = 7.4$ Hz); IR (KBr): $\tilde{\nu} = 2962$ (w, CH$_3$), 2924 (w, CH$_3$), 2924 (w, CH$_3$), 2077 (m, sh, CO), 1989 (m, CO), 1923 (s, CO), 1554 (m, CN), 1513 (w, CN), 1262 cm^{-1} (w, thienyl); UV/Vis (n-pentane): λ_{max} (abs.) = 233 (1.397), 252 (sh, 0.503), 295 (0.154), 345 (0.245), 422 nm (0.044); MS (EI, ^{184}W): m/z (%): 505.9 ([M]$^+$, 78), 477.9 ([M$-$CO]$^+$, 64), 449.9 ([M$-$2 CO]$^+$, 80), 422.0 ([M$-$3 CO]$^+$, 15), 393.9 ([M$-$4 CO]$^+$, 78), 365.9 ([M$-$5 CO]$^+$, 100), 311.9 ([M$-$4 CO$-$C$_4$H$_3$S]$^+$, 43), 181.9 ([M$-$W(CO)$_5$]$^+$, 18).

10.4.3 Attempted Synthesis of 2-Bis(trimethylsilyl)methyl-3-phenyl-5-(2-thienyl)-2H-1,4,2-diazaphosphole (50g) via Decomplexation of Complex 41g with 1,2-Bis(diphenylphosphino)ethane (DPPE)

A solution of 335 mg (0.46 mmol) of 2H-1,4,2-diazaphosphole complex **41g** and 184 mg (0.46 mmol) of DPPE in 2.5 mL of toluene was heated 3 h at 105 °C while the reaction solution turned brownish. The mixture containing **50g** and complexes **191** and **192** was analyzed by ^{31}P$\{^1$H$\}$ NMR spectroscopy (121.5 MHz, toluene): $\delta = 101.8$ (s; **50g**), 41.9 (s$_{sat}$, $|^1J_{WP}| = 232.7$ Hz; **192**), 13.8 (d$_{sat}$, $|^1J_{WP}| = 239.7$ Hz, $|^3J_{PP}| = 36.9$ Hz; **191**), -11.9 (d, $|^3J_{PP}| = 36.9$ Hz; **191**). After removement of all volatiles in vacuo ($\sim 10^{-2}$ mbar) the yellow crude product was dissolved in n-pentane and filtered through silica at $-50\,$°C. Then, all volatiles were removed in vacuo ($\sim 10^{-2}$ mbar),

and the crude product was subjected to column chromatography on silica ($-50\,^{\circ}$C, 2
$\times$ 8 cm), but a complete purification of **50g** was not achieved.

10.4.4   Attempted Synthesis of 2-Bis(trimethylsilyl)methyl-3-phenyl-2*H*-1,4,2-diazaphosphole (50h) via Decomplexation of Complexes 41h and 129h in Acetonitrile

A solution of 300 mg (0.47 mmol) of a mixture of 2*H*-1,4,2-diazaphosphole complexes
41h and **129h** in 8 mL of CH$_3$CN was heated for 80 min at 75 $^{\circ}$C while the reaction
solution turned brownish. After removement of all volatiles in vacuo ($\sim 10^{-2}$ mbar)
the crude product mixture was subjected to column chromatography on silica ($-30\,^{\circ}$C,
2 $\times$ 12 cm), but the products could not completely be separated.

Therefore, a solution of 30 mg (0.05 mmol) of a mixture of 2*H*-1,4,2-diazaphosphole
complexes **41h** and **129h** in 0.8 mL of CD$_3$CN in an NMR tube was heated for 80 min
at 75 $^{\circ}$C while the reaction solution turned brownish. The reaction solution containing
50h was subjected to ^{1}H and ^{31}P NMR experiments.

50h: ^{1}H NMR (300.13 MHz, CD$_3$CN): $\delta = 0.06$ (s, 18 H; Si(CH$_3$)$_3$), 1.48 (d, $|^5J_{HH}|$
$= 0.7$ Hz, 1 H; CH(SiMe$_3$)$_2$), 7.51 (m$_c$, 3 H; *meta+para*-H$_{phenyl}$), 7.91 (m$_c$, 2 H; *ortho*-
H$_{phenyl}$), 8.55 (dd, $|^{3+4}J_{PH}| = 18.3$ Hz, $|^5J_{HH}| = 0.7$ Hz, 1 H; CH); ^{31}P NMR (121.5
MHz, CD$_3$CN): $\delta = 97.6$ (d, $|^{3+4}J_{PH}| = 17.2$ Hz).

10.4.5   Attempted Synthesis of 2-Bis(trimethylsilyl)methyl-3-(2-thienyl)-2*H*-1,4,2-diazaphosphole (193h) via Decomplexation of Complexes 126h and 131h in Acetonitrile

A solution of 200 mg (0.31 mmol) of a mixture of 2*H*-1,4,2-diazaphosphole complexes
126h and **131h** in 5 mL of acetonitrile was heated 145 min at 75 $^{\circ}$C while the re-
action solution turned brownish. After the decomplexation was complete 100 mL of
n-pentane was added under rigorous stirring. The light orange colored crude prod-
uct was filtered, dried in vacuo ($\sim 10^{-2}$ mbar), and subjected to multinuclear NMR
experiments in C$_6$D$_6$. After removement of all volatiles in vacuo ($\sim 10^{-2}$ mbar) the
crude product mixture was subjected to column chromatography on silica ($-30\,^{\circ}$C, 2
$\times$ 12 cm), but the products could not completely be separated.

193h: ^{1}H NMR (300.13 MHz, C$_6$D$_6$): $\delta = 0.09$ (d$_{sat}$, $|^4J_{PH}| = 0.3$ Hz, $|^2J_{SiH}| = 6.3$
Hz, $|^1J_{CH}| = 119.6$ Hz, 18 H; Si(CH$_3$)$_3$), 0.99 (d, $|^5J_{HH}| = 0.8$ Hz, 1 H; CH(SiMe$_3$)$_2$),

6.69 (ddd, $|^{5+6}J_{PH}| = 0.9$ Hz, $|^3J_{HH}| = 5.0$ and 3.7 Hz, 1 H; thienyl-C^4H), 6.91 (ddd, $|^{5+6}J_{PH}| = 1.0$ Hz, $|^3J_{HH}| = 5.2$ Hz, $|^4J_{HH}| = 1.0$ Hz, 1 H; thienyl-C^5H), 7.41 (ddd, $|^4J_{PH}| = 2.6$ Hz, $|^3J_{HH}| = 3.7$ Hz, $|^4J_{HH}| = 1.0$ Hz, 1 H; thienyl-C^3H), 8.50 (dd, $|^{3+4}J_{PH}| = 18.8$ Hz, $|^5J_{HH}| = 0.9$ Hz, 1 H; CH); ^{13}C{^{1}H} NMR (75.5 MHz, C_6D_6): $\delta = 1.5$ (d$_{sat}$, $|^3J_{PC}| = 3.9$ Hz, $|^1J_{SiC}| = 52.4$ Hz; Si(CH$_3$)$_3$), 18.8 (d, $|^1J_{PC}| = 45.9$ Hz; CH(SiMe$_3$)$_2$), 128.5 (d, $|^{4+5}J_{PC}| = 2.6$ Hz; thienyl-C^4), 130.5 (d, $|^{4+5}J_{PC}| = 3.9$ Hz; thienyl-C^5), 130.8 (d, $|^3J_{PC}| = 7.1$ Hz; thienyl-C^3), 140.1 (d, $|^2J_{PC}| = 21.0$ Hz; thienyl-C^2), 162.2 (d, $|^{2+3}J_{PC}| = 3.6$ Hz; PNC), 199.3 (d, $|^{1+4}J_{PC}| = 44.6$ Hz; PCN); ^{29}Si{^{1}H} NMR (59.6 MHz, C_6D_6): $\delta = 5.5$ (d$_{sat}$, $|^2J_{PSi}| = 2.5$ Hz, $|^1J_{SiC}| = 52.3$ Hz); ^{31}P NMR (121.5 MHz, C_6D_6): $\delta = 96.1$ (d, $|^{3+4}J_{PH}| = 19.1$ Hz).

10.5 Synthesis of a Bis-2H-azaphosphirene Complex

10.5.1 Synthesis of μ-{(1,1'-Ferrocenediyl)bis[(ethoxy)carbene]}-bis(pentacarbonyltungsten(0)) (198)

To a stirred solution of 11.8 g (14.3 mmol) of 1,1'-dilithioferrocene N,N,N',N'-tetra-methyl-1,2-ethanediamine adduct (3:2) (**197**) in 360 mL of DME was added 30.3 g (86.1 mmol) of tungsten hexacarbonyl at $-50\,^{\circ}$C while the reaction mixture turned deep red. After removement of all volatiles in vacuo ($\sim 10^{-2}$ mbar) the red-brownish residue was dissolved in 360 mL of deoxygenated water, covered with 100 mL of diethyl ether, and 18 g (94.8 mmol) of triethyloxonium tetrafluoroborate was slowly added at ambient temperature. During the reaction the mixture turned purple and the deep purple crude product precipitated from the water phase, which was filtered off, washed with diethyl ether, dried in vacuo ($\sim 10^{-2}$ mbar), and was then purified by soxhlet extraction for 7 d with diethyl ether, which gave **198**.

198: Deep purple solid; yield: 12.7 g (13.4 mmol, 31 %); mp 243$\,^{\circ}$C; ^{1}H NMR (300.13 MHz, CDCl$_3$): $\delta = 1.63$ (t, $|^3J_{HH}| = 7.1$ Hz, 6 H; CH$_3$), 4.90 (q, $|^3J_{HH}| = 7.1$ Hz, 6 H; CH$_2$), 4.82 (dd, $|^3J_{HH}| = 2.3$ Hz, $|^4J_{HH}| = 1.9$ Hz, 4 H; Cp-$C^{3+4/2+5}$H), 5.02 (dd, $|^3J_{HH}| = 2.3$ Hz, $|^4J_{HH}| = 1.9$ Hz, 4 H; Cp-$C^{2+5/3+4}$H); ^{13}C{^{1}H} NMR (75.5 MHz, CDCl$_3$): $\delta = 15.3$ (s; CH$_3$), 74.5 (s; CH$_2$), 76.9 (s; Cp-$C^{3+4/2+5}$), 77.2 (s; Cp-$C^{2+5/3+4}$), 96.1 (s; Cp-C^1), 197.6 (s; CO$_{cis}$), 202.2 (s; CO$_{trans}$), 308.4 (s; C$_{carbene}$); IR (nujol): $\tilde{\nu} =$ 2064 (m, sh, CO), 1971 (m, CO), 1927 (s, CO), 1909 cm^{-1} (s, CO); UV/Vis (CH$_2$Cl$_2$): λ_{max} (abs.) = 242 (1.152), 289 (sh, 0.152), 352 (0.094), 375 (0.171) 435 (0.180), 557 nm (sh, 0.049); MS (EI, ^{184}W): m/z (%): 945.9 ([M]$^+$, 62), 750.0 ([M $-$ 7 CO]$^+$, 23), 722.0

([M $-$ 8 CO]$^+$, 42), 694.0 ([M $-$ 9 CO]$^+$, 19), 666.0 ([M $-$ 10 CO]$^+$, 33), 636.0 ([M $-$ 9 CO $-$ 2 CH$_3$CH$_2$]$^+$, 41), 453.0 ([M $-$ C(OEt)(W(CO)$_5$) $-$ 4 CO]$^+$, 100). elemental analysis (%) calcd. for C$_{26}$H$_{28}$FeO$_{12}$W$_2$: C 33.01, H 1.92; found: C 32.68, H 2.08.

10.5.2 Synthesis of μ-{(1,1'-Ferrocenediyl)bis[(amino)carbene-κC]}bis(pentacarbonyltungsten(0)) (199)

Gaseous ammonia was introduced for 4.5 h into a solution of 2.50 g (2.64 mmol) of bis(ethoxy)carbene complex **198** in 1 L of CH$_2$Cl$_2$ at 0 °C. Then, all volatiles were removed in vacuo ($\sim 10^{-2}$ mbar), and the product was purified by column chromatography on silica (-15 °C, 2 × 5 cm, petroleum ether/CH$_2$Cl$_2$: 1/8). Evaporation of the solvents of the 3rd fraction ($\sim 10^{-2}$ mbar) yielded **199**.

199: Red solid; yield: 1.45 g (1.63 mmol, 62 %); mp 181 °C; ^{1}H NMR (300.13 MHz, CD$_2$Cl$_2$): δ = 4.81 (dd, $|^3J_{HH}|$ = 2.5 Hz, $|^4J_{HH}|$ = 1.9 Hz, 4 H; Cp-C$^{3+4/2+5}$H), 4.88 (dd, $|^3J_{HH}|$ = 2.5 Hz, $|^4J_{HH}|$ = 1.9 Hz, 4 H; Cp-C$^{2+5/3+4}$H), 8.24 (br, $h_{1/2}$ = 17 Hz, 2 H; NH), 8.60 (br, $h_{1/2}$ = 17 Hz, 2 H; NH); ^{13}C{^{1}H} NMR (75.5 MHz, CD$_2$Cl$_2$): δ = 72.8 (s; Cp-C$^{2+5/2+5}$), 76.2 (s; Cp-C$^{3+4/3+4}$), 90.3 (s; Cp-C^1), 197.6 (s$_{sat}$, $|^1J_{WC}|$ = 127.4 Hz; CO$_{cis}$), 202.6 (s$_{sat}$, $|^1J_{WC}|$ = 127.4 Hz; CO$_{trans}$), 253.5 (s$_{sat}$, $|^1J_{WC}|$ = 89.2 Hz; C$_{carbene}$); IR (nujol): $\tilde\nu$ = 3457 (w, NH), 3354 (w, NH), 2059 (m, sh, CO), 1988 (m, CO), 1970 (m, CO), 1910 (s, CO), 1890 (s, CO), 1870 (s, CO), 1856 (s, CO), 1637 cm^{-1} (m, CN); UV/Vis (CH$_2$Cl$_2$): λ_{max} (abs.) = 243 (1.690), 288 (0.218), 363 (0.201), 407 (0.237), 506 nm (sh, 0.043); MS (EI, ^{184}W): m/z (%): 887.9 ([M]$^+$, 42), 720.0 ([M $-$ 6 CO]$^+$, 14), 664.0 ([M $-$ 8 CO]$^+$, 16), 606.0 ([M $-$ 9 CO $-$ 2 NH$_2$]$^+$, 68), 268.0 ([W(CO)$_3$]$^+$, 100); HR-MS (ESI$^+$) calcd. for C$_{22}$H$_{12}$FeN$_2$O$_{10}$W$_2$ + Na: 910.8764; found: 910.8778; dev. 0.0014.

10.5.3 Attempted Synthesis of μ-{1,1'-Bis-($2R^*,2'R^*/2R^*,2'S^*$)-[2-bis(trimethylsilyl)methyl-2H-azaphosphiren-3-yl-κP]-ferrocene}bis(pentacarbonyltungsten(0)) (202a,b)

Reaction of μ-{(1,1'-ferrocenediyl)bis[(amino)carbene-κC]}bis(pentacarbonyltungsten(0)) (199) with [bis(trimethylsilyl)methylene]chlorophosphane in the presence of triethylamine: In a 250 mL three-necked flask equipped with a dropping funnel 370 mg (1.64 mmol) of [bis(trimethylsilyl)methylene]chlorophosphane (**194**) was dissolved in 30 mL of Et$_2$O and 7 mL of NEt$_3$. A solution of 694 mg (0.78 mmol) of bis(aminocarbene) complex **199** in 200 mL of Et$_2$O, 30 mL of CH$_2$Cl$_2$, and 10

mL of THF was added dropwise under continuous heating at 30 °C within 3.5 h. After the addition the reaction mixture was stirred for 65 h at ambient temperature. Then, all volatiles were removed in vacuo ($\sim 10^{-2}$ mbar), and the crude product mixture was subjected to column chromatography on silica (-20 °C, 2×10 cm). It was eluated with a mixture of petroleum ether and Et$_2$O while the polarity was continuously increased; 9 fractions were collected.

Evaporation of the solvents of the 7th fraction ($\sim 10^{-2}$ mbar) yielded **201**: red solid, crystallized from Et$_2$O at 4 °C; estimated yield: 40 mg (0.37 mmol, 2 %). Due to the low yield only ^{1}H and ^{31}P NMR data could be obtained.

201: ^{1}H NMR (300.13 MHz, C$_6$D$_6$): $\delta = -0.03$ (s$_{sat}$, $|^2J_{SiH}| = 6.4$ Hz, $|^1J_{CH}| = 121.1$ Hz, 9 H; Si(CH$_3$)$_3$), 0.16 (s$_{sat}$, $|^2J_{SiH}| = 6.3$ Hz, $|^1J_{CH}| = 118.4$ Hz, 9 H; Si(CH$_3$)$_3$), 0.58 (d, $|^2J_{PH}| = 3.4$ Hz, 1 H; CH(SiMe$_3$)$_2$), 4.06 (m$_c$, 1 H; Cp-H), 4.09 (m$_c$, 2 H; Cp-H), 4.30 (m$_c$, 1 H; Cp-H), 4.41 (m$_c$, 1 H; Cp-H), 4.54 (m$_c$, 1 H; Cp-H), 4.67 (m$_c$, 1 H; Cp-H), 4.71 (m$_c$, 1 H; Cp-H), 7.58 (br, $h_{1/2} = 12.7$ Hz, 1 H; NH), 8.26 (br, $h_{1/2} = 12.0$ Hz, 1 H; NH); ^{31}P NMR (121.5 MHz, C$_6$D$_6$): $\delta = -112.8$ (s$_{sat}$, $|^1J_{WP}| = 296.3$ Hz).

Reaction of μ-{(1,1'-ferrocenediyl)bis[(amino)carbene-κC]}bis(pentacarbonyltungsten(0)) (199) with [bis(trimethylsilyl)methylene]bromophosphane in the presence of triethylamine: In a 500 mL three-necked flask equipped with a dropping funnel 555 mg (2.06 mmol) of [bis(trimethylsilyl)methylene]bromophosphane (**194**) was dissolved in 15 mL of CH$_2$Cl$_2$ and 3.5 mL of NEt$_3$. A solution of 555 mg (0.63 mmol) of bis(aminocarbene) complex **199** in 250 mL of CH$_2$Cl$_2$ was added dropwise within 3.5 h. After the addition the reaction mixture was analyzed by ^{31}P{^{1}H} NMR spectroscopy, which revealed the formation of several unidentified products.

Consecutive reaction of μ-{(1,1'-ferrocenediyl)bis[(amino)carbene-κC]}-bis(pentacarbonyltungsten(0)) (199) with n-butyllithium and [bis(trimethylsilyl)methylene]chlorophosphane in the presence of triethylamine: To a solution of 1.142 g (1.29 mmol) of bis(aminocarbene) complex **199** in 125 mL of Et$_2$O was slowly added 1.7 mL (2.72 mmol; 1.6 M) of n-butyllithium at -10 °C. After the addition the reaction mixture was stirred for 20 min at -10 °C and for 10 min at ambient temperature. Then, all volatiles were removed in vacuo ($\sim 10^{-2}$ mbar), and the red-brownish residue was washed with n-pentane. Subsequently, it was dissolved in 40 mL of Et$_2$O, and 578 mg (2.57 mmol) of [bis(trimethylsilyl)methylene]bromophosphane (**194**) was slowly added at ambient temperature. Subjecting the reaction solution to ^{31}P{^{1}H} NMR spectroscopy revealed the formation of several unidentified products.

10.5.4 Synthesis of μ-{(1,1'-Ferrocenediyl)bis[N-(amino)carbene-κC][bis(trimethylsilyl)methyl]phosphane}bis(pentacarbonyltungsten(0)) (205)

To a stirred solution of 440 mg (0.50 mmol) of bis(aminocarbene) complex **199** in 30 mL of CH$_2$Cl$_2$ were added consecutively 140 μL (0.62 mmol) of [bis(trimethylsilyl)-methylene]chlorophosphane (**194**) and 13 mL of NEt$_3$ at ambient temperature. The initially red colored solution turned deep brown. After the mixture was stirred for 1.5 h at ambient temperture all volatiles were removed in vacuo ($\sim 10^{-2}$ mbar), and the product was purified by column chromatography on silica ($-10\,°$C, 2×8 cm, petroleum ether/CH$_2$Cl$_2$: 1/1). Evaporation of the solvents of the first fraction ($\sim 10^{-2}$ mbar) yielded **205**.

205: Red-brown solid, crystallized from Et$_2$O at 4 °C; yield: 328 mg (0.31 mmol, 62 %); mp 183 °C; ^{1}H NMR (300.13 MHz, CDCl$_3$): $\delta = 0.39$ (d$_{sat}$, $|^4J_{PH}| = 0.9$ Hz, $|^2J_{SiH}| = 6.0$ Hz, $|^1J_{CH}| = 119.3$ Hz, 18 H; Si(CH$_3$)$_3$), 0.96 (d, $|^2J_{PH}| = 13.6$ Hz, 1 H; CH(SiMe$_3$)$_2$), 4.28 (m$_c$, 1 H; Cp-H), 4.54 (m$_c$, 1 H; Cp-H), 4.70 (m$_c$, 1 H; Cp-H), 4.80 (m$_c$, 1 H; Cp-H), 9.39 (d, $|^2J_{PH}| = 4.5$ Hz, 2 H; NH); ^{13}C{^{1}H} NMR (75.5 MHz, CDCl$_3$): $\delta = 2.3$ (d$_{sat}$, $|^3J_{PC}| = 5.1$ Hz, $|^1J_{SiC}| = 53.3$ Hz; Si(CH$_3$)$_3$), 20.5 (d, $|^1J_{PC}| = 51.4$ Hz; CH(SiMe$_3$)$_2$), 71.3 (d, $|^4J_{PC}| = 2.2$ Hz; Cp-C$^{2/5}$), 72.2 (s; Cp-C$^{3/4}$), 75.1 (d, $|^4J_{PC}| = 1.5$ Hz; Cp-C$^{2/5}$), 77.7 (s; Cp-C$^{3/4}$), 92.0 (d, $|^3J_{PC}| = 6.0$ Hz; Cp-C^1), 198.4 (s$_{sat}$, $|^1J_{WC}| = 127.9$ Hz; CO$_{cis}$), 203.0 (d, $|^4J_{PC}| = 0.9$ Hz; CO$_{trans}$), 279.5 (d$_{sat}$, $|^2J_{PC}| = 1.6$ Hz, $|^1J_{WC}| = 93.8$ Hz; C$_{carbene}$); ^{29}Si{^{1}H} NMR (59.6 MHz, CDCl$_3$): $\delta = 0.0$ (d, $|^2J_{PSi}| = 15.8$ Hz); ^{31}P NMR (121.5 MHz, CDCl$_3$): $\delta = 66.0$ (s); IR (KBr): $\tilde{\nu} = 3305$ (w, NH), 2959 (w, CH$_3$/CH), 2065 (m, sh, CO), 2060 (m, sh, CO), 1996 (m, CO), 1988 (m, sh, CO), 1977 (m, CO), 1937 (m, CO), 1924 (m, CO), 1914 (s, CO), 1898 (m, CO), 1970 cm^{-1} (s, CO); UV/Vis (CH$_2$Cl$_2$): λ_{max} (abs.) = 235 (1.194), 242 (1.189), 375 (0.171) 403 (0.190), 429 nm (0.225); MS (EI, ^{184}W): m/z (%): 1076.5 ([M]$^+$, 2), 73.1 ([SiMe$_3$]$^+$, 100). elemental analysis (%) calcd. for C$_{29}$H$_{29}$FeN$_2$O$_{10}$PSi$_2$W$_2$: C 32.36, H 2.72, N 2.60; found: 32.23, H 2.82, N 2.49.

10.5.5   Synthesis of μ-{1,1'-Bis-($2R^*$,2'R^*/$2R^*$,2'S^*)-[2-bis(tri-methylsilyl)methyl-$2H$-azaphosphiren-3-yl-κP]ferrocene}-bis(pentacarbonyltungsten(0)) (202a,b) and μ-(1-{2,3-Bis[bis(trimethylsilyl)methyl]-2,3-dihydro-1,2,3-azadiphos-phete-4-yl-κP^2}-1'-(cyano-κN)ferrocene)bis(pentacarbon-yltungsten(0)) (207)

To a stirred solution of 204 mg (0.19 mmol) of ferrocenophane complex **205** in 7.6 mL of CH_2Cl_2 were added consecutively 0.2 mL (0.89 mmol) of [bis(trimethylsilyl)methylene]-chlorophosphane (**194**) and 2.8 mL of NEt_3 at ambient temperature. After the mixture was stirred for 1.5 h at ambient temperture all volatiles were removed in vacuo ($\sim 10^{-2}$ mbar), and the crude product was extracted with n-pentane at $-30\,^{\circ}$C. Evaporation of the solvent of the second fraction ($\sim 10^{-2}$ mbar) yielded **207**.

207: Red solid; estimated yield: 70 mg (0.06 mmol, 29 %); ^{1}H NMR (300.13 MHz, C_6D_6): $\delta = -0.02$ (br, 9 H; σ^4-P–CH(Si(CH_3)$_3$)$_2$), 0.22 (br, 9 H; σ^4-P–CH(Si(CH_3)$_3$)$_2$), 0.33 (br, 18 H; σ^3-P–CH(Si(CH_3)$_3$)$_2$), 1.06 (dd, $|^2J_{PH}| = 22.0$ Hz, $|^{3+5}J_{PH}| = 6.7$ Hz, 1 H; CH(SiMe$_3$)$_2$), 1.81 (dd, $|^2J_{PH}| = 24.0$ Hz, $|^{3+5}J_{PH}| = 4.0$ Hz, 1 H; CH(SiMe$_3$)$_2$), 3.85 (m$_c$, 1 H; Cp-H), 3.93 (m$_c$, 2 H; Cp-H), 4.01 (m$_c$, 1 H; Cp-H), 4.14 (m$_c$, 1 H; Cp-H), 4.31 (m$_c$, 2 H; Cp-H), 4.61 (m$_c$, 1 H; Cp-H); ^{13}C{^{1}H} NMR (75.5 MHz, C_6D_6): $\delta = 1.7$ (br; σ^4-P–CH(Si(CH_3)$_3$)$_2$), 2.8 (br; σ^4-P–CH(Si(CH_3)$_3$)$_2$), 3.6 (br; σ^3-P–CH(Si(CH_3)$_3$)$_2$), 16.5 (dd, $|J_{PC}| = 79.5$ Hz, $|J_{PC}| = 7.1$ Hz; CH(SiMe$_3$)$_2$), 34.7 (dd, $|J_{PC}| = 20.7$ Hz, $|J_{PC}| = 10.3$ Hz; CH(SiMe$_3$)$_2$), 70.4 (m$_c$; Cp-C), 71.9 (m$_c$; Cp-C), 72.2 (m$_c$; Cp-C), 73.4 (m$_c$; Cp-C), 73.7 (m$_c$; Cp-C), 74.8 (m$_c$; Cp-C), 75.5 (m$_c$; Cp-C), 87.4 (dd, $|J_{PC}| = 30.4$ Hz, $|J_{PC}| = 26.5$ Hz; Cp-C^1 at dihydroazadiphosphete-C^4), 197.0 (s$_{sat}$, $|^1J_{WC}| = 130.0$ Hz; CO$_{cis}$ of CN–W(CO)$_5$), 197.1 (dd, $|J_{PC}| = 41.4$ Hz, $|J_{PC}| = 7.8$ Hz; PCN), 198.1 (d, $|^2J_{PC}| = 7.1$ Hz; CO$_{cis}$ of P–W(CO)$_5$), 198.6 (d, $|^2J_{PC}| = 29.1$ Hz; CO$_{trans}$ of P–W(CO)$_5$), 199.9 (s; CO$_{trans}$ of CN–W(CO)$_5$); ^{31}P NMR (121.5 MHz, C_6D_6): $\delta = 77.5$ (ddd$_{sat}$, $|^1J_{WP}| = 254.3$ Hz, $|^{1+3}J_{PP}| = 115.7$ Hz, $|^2J_{PH}| = 22.3$ Hz, $|^{3+5}J_{PH}| = 2.5$ Hz; σ^4-P), 90.5 (ddd, $|^{1+3}J_{PP}| = 117.0$ Hz, $|^2J_{PH}| = 22.9$ Hz, $|^{3+5}J_{PH}| = 5.7$ Hz; σ^3-P); MS (ESI$^+$, ^{184}W): m/z (%): 1265.0 ([M + H]$^+$, 56), 1237.0 ([M + H − CO]$^+$, 16), 941.1 ([M + H − W(CO)$_5$]$^+$, 100), 617.1 ([M + H − 2 W(CO)$_5$]$^+$, 38); HR-MS (ESI$^+$) calcd. for $C_{36}H_{47}FeN_2O_{10}P_2Si_4W_2$: 1265.0150; found: 1265.0118; dev. 0.0032.

Subsequently, the residue was subjected to soxhlet extraction with n-pentane for 3 d. Then, the product was purified by column chromatography on silica ($-15\,^{\circ}$C, 1 × 10 cm, petroleum ether/Et$_2$O: 10/1). Evaporation of the solvents of the first fraction ($\sim 10^{-2}$ mbar) yielded a mixture of diastereomers **202a,b**.

202a,b:[3] Red solid; yield: 33 mg (0.31 mmol, 14 %); mp 119 °C (decomp.); ^{1}H NMR (300.13 MHz, CD$_2$Cl$_2$): δ = 0.09 (s, 18 H; Si(CH$_3$)$_3$), 0.20 (s, 18 H; Si(CH$_3$)$_3$), 0.66 (d, $|^2J_{PH}|$ = 2.9 Hz, 2 H; CH(SiMe$_3$)$_2$), 4.70 (m$_c$, 2 H; Cp-H), 4.77 (m$_c$, 2 H; Cp-H), 4.94 (m$_c$, 2 H; Cp-H), 5.21 (m$_c$, 2 H; Cp-H); ^{13}C$\{^1$H$\}$ NMR (75.5 MHz, CD$_2$Cl$_2$): δ = 1.1 (d, $|^3J_{PC}|$ = 3.9 Hz; Si(CH$_3$)$_3$), 1.9 (d, $|^3J_{PC}|$ = 2.6 Hz; Si(CH$_3$)$_3$), 28.9 (d, $|^1J_{PC}|$ = 22.0 Hz; CH(SiMe$_3$)$_2$), 71.5 (s; Cp-C), 71.9 (s; Cp-C), 72.0 (s; Cp-C), 72.4 (s; Cp-C), 75.0 (s; Cp-C), 75.1 (s; Cp-C), 75.4 (s; Cp-C), 75.5 (s; Cp-C), 189.5 (s; PCN), 189.6 (s; PCN), 196.5 (d, $|^2J_{PC}|$ = 9.1 Hz; CO$_{cis}$), 209.6 (d, $|^2J_{PC}|$ = 32.3 Hz; CO$_{trans}$); ^{29}Si$\{^1$H$\}$ NMR (59.6 MHz, CD$_2$Cl$_2$): δ = 0.1 (d, $|^2J_{PSi}|$ = 9.1 Hz), 2.4 (d, $|^2J_{PSi}|$ = 6.4 Hz); ^{31}P NMR (121.5 MHz, CD$_2$Cl$_2$): δ = −113.6 (s$_{sat}$, $|^1J_{WP}|$ = 292.5 Hz), −113.2 (s$_{sat}$, $|^1J_{WP}|$ = 302.6 Hz); UV/Vis (CH$_2$Cl$_2$): λ_{max} (abs.) = 451 (0.016), 382 (sh, 0.066), 346 (0.104), 288 (0.252), 252 (sh, 0.846), 234 nm (1.369); MS (ESI$^+$, ^{184}W): m/z (%): 1265.0 ([M + H]$^+$, 100), 941.1 ([M + H − W(CO)$_5$]$^+$, 18), 855.1 ([M − W(CO)$_5$ − 3 CO]$^+$, 36); MS (MALDI$^+$/TOF, ^{184}W): m/z (%): 1264.4 ([M]$^+$); HR-MS (ESI$^+$) calcd. for C$_{36}$H$_{47}$FeN$_2$O$_{10}$P$_2$Si$_4$W$_2$: 1265.0150; found: 1265.0165; dev. 0.0015.

---

[3]Not all NMR data could be unambiguously assigned to either **202a** or **202b**.

Bibliography

[1] a) *The Chemistry of Heterocyclic Compounds: Small Ring Heterocycles, Part 1, Vol. 42* (Ed.: A. Hassner), Wiley, New York, **1983**; b) *The Chemistry of Heterocyclic Compounds: Small Ring Heterocycles, Part 2, Vol. 42* (Ed.: A. Hassner), Wiley, New York, **1983**; c) *The Chemistry of Heterocyclic Compounds: Small Ring Heterocycles, Part 3, Vol. 42* (Ed.: A. Hassner), Wiley, New York, **1985**; d) T. L. Gilchrist, *Heterocyclic Chemistry*, 2nd ed., Longman, Harlow, **1992**.

[2] Discovery of aziridine: a) S. Gabriel, *Ber. Dtsch. Chem. Ges.* **1888**, *21*, 1049−1057; b) C. C. Howard, W. Marckwald, *Ber. Dtsch. Chem. Ges.* **1899**, *32*, 2036−2038; c) W. Marckwald, *Ber. Dtsch. Chem. Ges.* **1900**, *33*, 764−766.

[3] *Aziridines and Epoxides in Organic Synthesis* (Ed.: A. K. Yudin), Wiley-VCH, Weinheim, **2006**.

[4] a) D. Tanner, *Angew. Chem.* **1994**, *106*, 625−646; *Angew. Chem., Int. Ed. Engl.* **1994**, *33*, 599−690; b) J. B. Sweeney, *Chem. Soc. Rev.* **2002**, *31*, 247−258.

[5] Discovery of oxirane: A. Wurtz, *C. R. Hebd. Seances Acad. Sci.* **1859**, *48*, 101−105.

[6] a) W. A. Nugent, T. V. RajanBabu, *J. Am. Chem. Soc.* **1988**, *110*, 8561−8562; b) E. N. Jacobsen, M. H. Wu in *Comprehensive Asymmetric Catalysis I-III, Vol. 9* (Eds.: E. N. Jacobsen, A. Pfaltz, H. Yamamoto), Springer, Berlin, **1999**, p. 1309; c) A. Gansäuer, H. Bluhm, *Chem. Rev.* **2000**, *100*, 2771−2788; d) K. Dassbjerg, H. Svith, S. Grimme, M. Gerenkamp, C. Mück-Lichtenfeld, A. Gansäuer, A. Barchuk, *Top. Curr. Chem.* **2006**, *263*, 39−69.

[7] G. W. Coates, D. R. Moore, *Angew. Chem.* **2004**, *116*, 6784−6806; *Angew. Chem., Int. Ed.* **2004**, *43*, 6618−6639.

[8] F. Mathey, *Chem. Rev.* **1990**, *90*, 997−1025.

[9] *Phosphorus-Carbon Heterocyclic Chemistry: The Rise of a New Domain* (Ed.: F. Mathey), Pergamon Press, Amsterdam, **2001**.

[10] a) M. Sander, *Chem. Rev.* **1966**, *66*, 297−339; b) W. Adam, R. M. Bargon, *Chem. Rev.* **2004**, *104*, 251−261; c) S. K. Richardson, A. R. Howell, *Synthesis* **2007**, *18*, 2755−2778.

[11] a) H.-H. Otto, T. Schirmeister, *Chem. Rev.* **1997**, *97*, 133−171; b) J. C. Powers, J. L. Asgian, Ö. D. Ekici, K. E. James, *Chem. Rev.* **2002**, *102*, 4639−4750; c) R. Leung-Toung, W. Li, T. F. Tam, K. Karimian, *Curr. Med. Chem.* **2002**, *9*, 979−1002; d) F. Lecaille, J. Kaleta, D. Brömme, *Chem. Rev.* **2002**, *102*, 4459−4488; e) T. Schirmeister, U. Käppler, *Mini-Rev. Med. Chem.* **2003**, *3*, 361−373.

[12] For recent advances in cationic ring opening polymerization of cyclic ethers see e.g.: P. Kubisa, *J. Polym. Sci., Part A: Polym. Chem.* **2003**, *41*, 457−468.

[13] For an example of living ring opening polymerization of aziridines see: I. C. Stewart, C. C. Lee, R. G. Bergman, F. D. Toste, *J. Am. Chem. Soc.* **2005**, *127*, 17616−17617.

[14] For an example of polymerization of a phosphirane see: S. Kobayashi, J. Kadokawa, *Macromol. Rapid Commun.* **1994**, *15*, 567−571; for examples of polymerizations of thiiranes see, e.g.: a) T. Imai, K. Hayakawa, T. Satoh, H. Kaga, T. Kakuchi, *J. Polym. Sci., Part A: Polym. Chem.* **2002**, *40*, 3443−3448; b) M. L. Tebaldi de Sordi, M. A. Ceschi, C. L. Petzhold, A. H. E. Muller, *Macromol. Rapid Commun.* **2007**, *28*, 63−71.

[15] a) T. M. Trnka, R. H. Grubbs, *Acc. Chem. Res.* **2001**, *34*, 18−29; b) W. A. Herrmann, *Angew. Chem.* **2002**, *114*, 1342−1363; *Angew. Chem., Int. Ed.* **2002**, *41*, 1290−1309.

[16] B. H. Lipshutz, *Chem. Rev.* **1986**, *86*, 795−819.

[17] a) *Topics in Heterocyclic Chemistry: Heterocyclic Antitumor Antibiotics*, 1st ed. (Ed.: M. Lee), Springer, Berlin, **2006**; b) *Topics in Heterocyclic Chemistry: Bioactive Heterocycles I*, 1st ed. (Ed.: S. Eguchi), Springer, Berlin, **2006**; c) *Topics in Heterocyclic Chemistry: Bioactive Heterocycles II*, 1st ed. (Ed.: S. Eguchi), Springer, Berlin, **2007**; d) *Topics in Heterocyclic Chemistry: Bioactive Heterocycles III*, 1st ed. (Ed.: M. T. H. Khan), Springer, Berlin, **2007**; e) *Topics in Heterocyclic Chemistry: Bioactive Heterocycles IV*, 1st ed. (Ed.: M. T. H. Khan), Springer, Berlin, **2007**; f) *Topics in Heterocyclic Chemistry: Bioactive Heterocycles V*, 1st ed. (Ed.: M. T. H. Khan), Springer, Berlin, **2007**; g) *Topics in*

Heterocyclic Chemistry: QSAR and Molecular Modeling Studies in Heterocyclic Drugs I, 1st ed. (Ed.: S. P. Gupta), Springer, Berlin, **2006**; h) *Topics in Heterocyclic Chemistry: QSAR and Molecular Modeling Studies in Heterocyclic Drugs II*, 1st ed. (Ed.: S. P. Gupta), Springer, Berlin, **2006**.

[18] a) G. E. Ham, *J. Org. Chem.* **1964**, *29*, 3052−3055; b) 0. Mitsunobu in *Comprehensive Organic Synthesis, Vol. 7* (Eds.: B. M. Trost, I. Fleming), Pergamon, Oxford, **1991**, p. 65.

[19] M. Chandrasekhar, G. Sekar, V. K. Singh, *Tetrahedron Lett.* **2000**, *41*, 10079−10083.

[20] R. V. Anand, G. Pandey, V. K. Singh, *Tetrahedron Lett.* **2002**, *43*, 3975−3976.

[21] J. M. Concellón, E. Riego, *J. Org. Chem.* **2003**, *68*, 6407−6410.

[22] I. D. G. Watson, A. K. Yudin, *J. Org. Chem.* **2003**, *68*, 5160−5167.

[23] C. Gaebert, J. Mattay, *Tetrahedron* **1997**, *53*, 14297−14316.

[24] a) M. Nakagawa, M. Kawahara, *Org. Lett.* **2000**, *2*, 953−955; b) I. Prathap, P. Srihari, S. K. Pandey, B. V. S. Reddy, J. S. Yadav, *Tetrahedron Lett.* **2001**, *42*, 9089−9092; c) R. J. Madhushaw, C.-C. Hu, R.-S. Liu, *Org. Lett.* **2002**, *4*, 4151−4153; d) C.-H. Ding, L.-X. Dai, X.-L. Hou, *Synlett* **2004**, 1691−1694.

[25] A. Sudo, Y. Morioko, E. Koizumi, F. Sanda, T. Endo, *Tetrahedron Lett.* **2003**, *44*, 7889−7891.

[26] a) J. O. Baeg, H. Alper, *J. Org. Chem.* **1992**, *57*, 157−162; b) J. O. Baeg, C. Bensimon, H. Alper, *J. Am. Chem. Soc.* **1995**, *117*, 4700−4701; c) H. Maas, C. Bensimon, H. Alper, *J. Org. Chem.* **1998**, *63*, 17−20; d) T. Munegumi, I. Azumaya, T. Kato, H. Masu, S. Saito, *Org. Lett.* **2006**, *8*, 379−382.

[27] a) T. Hiyama, H. Koide, S. Fujita, H. Nozaki, *Tetrahedron* **1973**, *29*, 3137−3139; b) J. Legters, J. G. H. Willems, L. Thijs, B. Zwanenburg, *Recl. Trav. Chim. Pays-Bas* **1992**, *111*, 59−68.

[28] S. Gandhi, A. Bisai, B. A. B. Prasad, V. K. Singh, *J. Org. Chem.* **2007**, *72*, 2133−2142.

[29] a) B. A. B. Prasad, G. Pandey, V. K. Singh, *Tetrahedron Lett.* **2004**, *45*, 1137−1141; b) V. K. Yadav, V. Sriramurthy, *J. Am. Chem. Soc.* **2005**, *127*, 16366−16367.

[30] E. Brunn, R. Huisgen, *Tetrahedron Lett.* **1971**, *12*, 473−476.

[31] a) T. Brigaud, E. Laurent, R. Tardevil, Z. Cebulska, R. Bartnik, *J. Chem. Res. Synop.* **1994**, *8*, 330−331; b) C. Gaebert, C. Siegner, J. Mattay, M. Toubartz, S. Steenken, *J. Chem. Soc., Perkin Trans. 2* **1998**, 2735−2739.

[32] P. D. Pohlhaus, R. K. Bowman, J. S. Johnson, *J. Am. Chem. Soc.* **2004**, *126*, 2294−2295.

[33] C. Gaebert, J. Mattay, M. Toubartz, S. Steenken, B. Müller, T. Bally, *Chem. Eur. J.* **2005**, *11*, 1294−1304.

[34] R. K. Bowman, J. S. Johnson, *J. Org. Chem.* **2004**, *69*, 8537−8540.

[35] a) R. I. Wagner, *US Pat.* 3086053, **1963**, (*Chem. Abstr.* **1963**, *59*, 10124); b) R. I. Wagner, *US Pat.* 3086056, **1963**, (*Chem. Abstr.* **1964**, *60*, 559); c) R. I. Wagner, L. V. D. Freeman, H. Goldwhite, D. G. Rowsell, *J. Am. Chem. Soc.* **1967**, *89*, 1102−1104.

[36] E. Niecke, M. Leuer, M. Nieger, *Chem. Ber.* **1989**, *122*, 453−461.

[37] E. Niecke, J. Böske, D. Gudat, W. Güth, M. Lysek, E. Symalla, *Nova Acta Leopold.* **1985**, *59*, 83.

[38] H. Quast, M. Heuschmann, *Chem. Ber.* **1982**, *115*, 901−909.

[39] F. Mercier, B. Deschamps, F. Mathey, *J. Am. Chem. Soc.* **1989**, *111*, 9098−9100.

[40] A. Marinetti, C. Charrier, F. Mathey, J. Fischer, *Organometallics* **1985**, *4*, 2134−2138.

[41] G. Märkl, W. Hölzl, I. Trötsch-Schaller, *Tetrahedron Lett.* **1987**, *28*, 2693−2696.

[42] A. Marinetti, F. Mathey, *Tetrahedron* **1989**, *45*, 3061−3070.

[43] a) R. Benn, R. Mynott, W. J. Richter, G. Schroth, *Tetrahedron* **1984**, *40*, 3273−3276; b) B. A. Arbuzov, E. N. Dianova, R. T. Galiaskarova, A. Schmidpeter, *Chem. Ber.* **1987**, *120*, 597−599.

[44] A. Marinetti, F. Mathey, *Organometallics* **1984**, *3*, 456−461.

[45] A. Marinetti, F. Mathey, *Organometallics* **1984**, *3*, 1492−1495.

[46] A. Maercker, W. Brieden, *Chem. Ber.* **1991**, *124*, 933−938.

[47] a) D. C. R. Hockless, M. A. McDonald, M. Pabel, S. B. Wild, *J. Chem. Soc., Chem. Commun.* **1995**, 257−258; b) D. C. R. Hockless, M. A. McDonald, M. Pabel, S. B. Wild, *J. Organomet. Chem.* **1997**, *529*, 189−196.

[48] a) T. J. Katz, C. R. Nicholson, C. A. Reilly, *J. Am. Chem. Soc.* **1966**, *88*, 3832−3842; b) T. J. Katz, J. C. Carnahan, Jr., G. M. Clarke, N. Action, *J. Am. Chem. Soc.* **1970**, *92*, 734−735; c) W. J. Richter, *Angew. Chem.* **1982**, *94*, 932−933; *Angew. Chem., Int. Ed. Engl.* **1982**, *21*, 292−293; d) W. J. Richter, *Chem. Ber.* **1983**, *116*, 3293−3300; e) N. S. Rao, L. D. Quin, *J. Am. Chem. Soc.* **1983**, *105*, 5960−5961; f) G. Märkl, B. Alig, *Tetrahedron Lett.* **1983**, *24*, 3981−3984; g) W. J. Richter, *Chem. Ber.* **1985**, *118*, 1575−1579; h) W. J. Richter, *Chem. Ber.* **1985**, *118*, 97−106; i) L. D. Quin, N. S. Rao, R. J. Topping, A. T. McPhail, *J. Am. Chem. Soc.* **1986**, *108*, 4519−4526; j) L. D. Quin, N. S. Rao, J. Szewczyk, *Phosphorus, Sulfur Silicon Relat. Elem.* **1986**, *27*, 109−117; k) L. D. Quin, E.-Y. Yao, J. Szewczyk, *Tetrahedron Lett.* **1987**, *28*, 1077−1080; l) G. Märkl, H. J. Beckh, M. L. Ziegler, B. Nuber, *Angew. Chem.* **1987**, *99*, 1214−1216; *Angew. Chem., Int. Ed. Engl.* **1987**, *26*, 1134−1141.

[49] N. H. Tran Huy, L. Ricard, F. Mathey, *Organometallics* **2007**, *26*, 3614−3616.

[50] M. Regitz, B. Arnold, D. Danion, H. Schubert, G. Fusser, *Bull. Soc. Chim. Belg.* **1981**, *90*, 615−631.

[51] a) T. L. Gilchrist, E. Gymer, C. W. Rees, *Chem. Commun.* **1971**, 1519−1520; b) G. Mitchell, C. W. Rees, *J. Chem. Soc., Perkin Trans. 1* **1987**, 413−422.

[52] A. Padwa, A. D. Woolhouse in *Comprehensive Heterocyclic Chemistry, Vol. 7* (Eds.: A. R. Katritzky, C. W. Rees), Pergamon, Oxford, **1984**, p. 47 ff.

[53] F. Palacios, A. M. Ochoa de Retana, E. Martínez de Marigorta, J. M. de los Santos, *Eur. J. Org. Chem.* **2001**, 2401−2414.

[54] A. Marinetti, F. Mathey, *J. Am. Chem. Soc.* **1985**, *107*, 4700−4706.

[55] 0. Wagner, G. Maas, M. Regitz, *Angew. Chem.* **99**, *1987*, 1328−1330; *Angew. Chem., Int. Ed.* **26**, *1987*, 1257−1259.

[56] F. Mathey, M. Regitz in *Comprehensive Heterocyclic Chemistry, Vol. 1A* (Eds.: A. R. Katritzky, C. W. Rees, E. F. V. Scriven), Pergamon, Oxford, **1996**, p. 277.

[57] F. Mathey, *Acc. Chem. Res.* **1992**, *25*, 90−96.

[58] M. Regitz, H. Heydt, 0. Wagner, W. Schnurr, M. Ehle, J. Hoffmann, *Phosphorus, Sulfur Silicon Relat. Elem.* **1990**, *49*, 341−344.

[59] M. Sanchez, R. Réau, C. J. Marsden, M. Regitz, G. Bertrand, *Chem. Eur. J.* **1999**, *5*, 274−279.

[60] O. Wagner, M. Ehle, M. Regitz, *Angew. Chem.* **1989**, *101*, 227−229; *Angew. Chem., Int. Ed. Engl.* **1989**, *28*, 225−226.

[61] a) A. Igau, H. Grützmacher, A. Baceiredo, G. Bertrand, *J. Am. Chem. Soc.* **1988**, *110*, 6463−6466; b) A. Igau, A. Baceiredo, G. Trinquier, G. Bertrand, *Angew. Chem.* **1989**, *101*, 617−618; *Angew. Chem., Int. Ed. Engl.* **1989**, *28*, 621−622; c) G. R. Gillette, A. Baceiredo, G. Bertrand, *Angew. Chem.* **1990**, *102*, 1486−1488; *Angew. Chem., Int. Ed. Engl.* **1990**, *29*, 1429−1431; d) G. Alcaraz, R. Reed, A. Baceiredo, G. Bertrand, *J. Chem. Soc., Chem. Commun.* **1993**, 1354−1355.

[62] D. Bourissou, O. Guerret, F. P. Gabbaš, G. Bertrand, *Chem. Rev.* **2000**, *100*, 39−91.

[63] a) R. Armbrust, M. Sanchez, R. Réau U. Bergsträßer, M. Regitz, G. Bertrand, *J. Am. Chem. Soc.* **1995**, *117*, 10785−10786; b) M. Sanchez, R. Réau, F. Dahan, M. Regitz, G. Bertrand, *Angew. Chem.* **1996**, *108*, 2386−2388; *Angew. Chem., Int. Ed. Engl.* **1996**, *35*, 2228−2230; c) M. Sanchez, R. Réau, H. Gornitzka, F. Dahan, M. Regitz, G. Bertrand, *J. Am. Chem. Soc.* **1997**, *119*, 9720−9728.

[64] A. Marinetti, F. Mathey, J. Fischer, A. Mitschler, *J. Am. Chem. Soc.* **1982**, *104*, 4484−4485.

[65] F. Mathey, *Angew. Chem.* **1987**, *99*, 285−296; *Angew. Chem., Int. Ed. Engl.* **1987**, *26*, 275−286.

[66] The first phosphirenium salts were obtained via reaction of in situ generated phosphenium salts with alkynes: K. S. Fongers, H. Hogeveen, R. F Kingma, *Tetrahedron Lett.* **1983**, *24*, 643−646.

[67] E. W. Koos, J. P. Vander Kooi, E. E. Green, J. K. Stille, *J. Chem. Soc., Chem. Commun.* **1972**, 1085−1086; b) H. Quast, M. Heuschmann, *J. Chem. Soc., Chem. Commun.* **1979**, 390−392.

[68] a) J. Svara, A. Marinetti, F. Mathey, *Organometallics* **1986**, *5*, 1161−1167; b) S. Haber, R. Boese, M. Regitz, *Angew. Chem.* **1990**, *102*, 1523−1525; *Angew. Chem., Int. Ed. Engl.* **1990**, *29*, 1436−1438; c) H. Memmesheimer, M. Regitz, *Rev. Heteroatom. Chem.* **1994**, *10*, 61; d) S. Haber, M. Schmitz, U. Bergsträßer, J. Hoffmann, M. Regitz, *Chem. Eur. J.* **1999**, *5*, 1581−1589.

[69] R. Streubel, H. Wilkens, U. Rohde, A. Ostrowski, J. Jeske, F. Ruthe, P. G. Jones, *Eur. J. Inorg. Chem.* **1999**, 1567−1579.

[70] A. Marinetti, J. Fischer, F. Mathey, *J. Am. Chem. Soc.* **1985**, *107*, 5001−5002.

[71] a) D. Carmichael, P. B. Hitchcock, J. F. Nixon, F. Mathey, A. Pidcock, *J. Chem. Soc., Chem. Commun.* **1986**, 762−763; b) S. S. Al-Juaid, D. Carmichael, P. B. Hitchcock, S. Lochschmidt, A. Marinetti, F. Mathey, J. F. Nixon, *J. Chem. Soc., Chem. Commun.,* **1988**, 1156−1158; c) F. A. Ajulu, D. Carmichael, P. B. Hitchcock, F. Mathey, M. F. Meidine, J. F. Nixon, L. Ricard, M. L. Riley, *J. Chem. Soc., Chem. Commun.* **1992**, 750−752.

[72] A. Marinetti, F. Mathey, *Tetrahedron Lett.* **1987**, *28*, 5021−5024.

[73] A. Espinosa Ferao, B. Deschamps, F. Mathey, *Bull. Soc. Chim. Fr.* **1993**, *130*, 695−699.

[74] a) N. H. Tran Huy, L. Ricard, F. Mathey, *Organometallics* **1997**, *16*, 4501−4504; b) B. Wang, K. A. Nguyen, G. N. Srinivas, C. L. Watkins, S. Menzer, A. L. Spek, K. Lammertsma, *Organometallics* **1999**, *18*, 796−799; c) N. H. Tran Huy, L. Ricard, F. Mathey, *J. Organomet. Chem.* **1999**, *582*, 53−57.

[75] a) A. D. Averin, N. V. Lukashev, M. A. Kazankova, I. P. Beletskaya, *Mendeleev Commun.* **1993**, 68−70; b) M. Link, E. Niecke, M. Nieger, *Chem. Ber.* **1994**, *127*, 313−319.

[76] a) L. Ricard, N. Maigrot, C. Charrier, F. Mathey, *Angew. Chem.* **1987**, *99*, 590−591; *Angew. Chem., Int. Ed. Engl.* **1987**, *26*, 548−549; b) M. L. Sierra, C. Charrier, L. Ricard, F. Mathey, *Bull. Soc. Chim. Fr.* **1993**, *130*, 521.

[77] K. Dietliker, H. Heimgartner, *Helv. Chim. Acta* **1983**, *66*, 262−295.

[78] M. K. G. Mekhael, R. J. Smith, S. Bienz, A. Linden, H. Heimgartner, *Z. Naturforsch.* **2002**, *57b*, 444−452.

[79] N. J. Leonard, B. Zwanenburg, *J. Am. Chem. Soc.* **1967**, *89*, 4456−4465.

[80] S. Sato, H. Kato, M. Ohta, *Bull. Chem. Soc. Jpn.* **1967**, *40*, 1014.

[81] F. W. Fowler, A. Hassner, *J. Am. Chem. Soc.* **1968**, *90*, 2875−2881.

[82] C. Bernard-Henriet, R. Hoet, L. Ghosez, *Tetrahedron Lett.* **1981**, *22*, 4717−4720.

[83] N. J. Leonard, E. F. Muth, V. Nair, *J. Org. Chem.* **1968**, *2*, 827−828.

[84] a) A. Hassner, F. W. Fowler, *J. Am. Chem. Soc.* **1968**, *90*, 2869−2875; b) R. M. Carlson, S. Y. Lee, *Tetrahedron Lett.* **1969**, *10*, 4001−4004; c) S.-M. Lee, T.-F. Lai, M. P. Sammes, *J. Chem. Res. (S)* **1992**, 266−267; d) M. Haddach, R. Pastor, J. G. Riess, *Tetrahedron* **1993**, *49*, 4627−4638; e) M. M. H. Verstappen, G. J. A. Ariaans, B. Zwanenburg, *J. Am. Chem. Soc.* **1996**, *118*, 8491−8492; f)

M. J. Alves, T. L. Gilchrist, J. H. Sousa, *J. Chem. Soc., Perkin Trans. 1* **1999**, 1305−1310; g) M. J. Alves, P. M. T. Ferreira, H. L. S. Maia, L. S. Monteiro, T. L. Gilchrist, *Tetrahedron Lett.* **2000**, *41*, 4991−4995.

[85] a) K. Dietliker, U. Schmid, G. Mukherjee-Müller, H. Heimgartner, *Chimia* **1978**, *32*, 164−166; b) P. F. Dos Santos Filho, U. Schuchardt, *J. Organomet. Chem.* **1984**, *264*, 385−394.

[86] H. Alper, S. Wollowitz, *J. Am. Chem. Soc.* **1975**, *97*, 3541−3543.

[87] H. Heimgartner, *Angew. Chem.* **1991**, *103*, 271−279; *Angew. Chem., Int. Ed. Engl.* **1991**, *30*, 238−264.

[88] F. Arnhold, S. Chaloupka, A. Linden, H. Heimgartner, *Helv. Chim. Acta* **1995**, *78*, 899−909.

[89] a) B. Hostettler, J. P. Obrecht, R. Prewo, J. H. Bieri, H. Heimgartner, *Helv. Chim. Acta* **1986**, *69*, 298−304; b) A. Rahm, A. Linden, B. R. Vincent, H. Heimgartner, M. Mühlstädt, B. Schulze, *Helv. Chim. Acta* **1991**, *74*, 1002−1010; c) A. S. Orahovats, A. Linden, H. Heimgartner, *Helv. Chim. Acta* **1992**, *75*, 2515−2519; d) M. Schläpfer-Dähler, H. Heimgartner, *Helv. Chim. Acta* **1993**, *76*, 2398−2406; e) A. S. Orahovats, S. S. Bratovanov, A. Linden, H. Heimgartner, *Helv. Chim. Acta* **1996**, *79*, 1121−1128; f) T. R. Mihova, A. Linden, H. Heimgartner, *Helv. Chim. Acta* **1996**, *79*, 2067−2074; g) T. R. Mihova, A. Linden, H. Heimgartner, *Heterocycles* **1998**, *49*, 215−232.

[90] M. Hugener, H. Heimgartner, *Helv. Chim. Acta* **1995**, *78*, 1490−1498.

[91] In the Neber rearrangement 2*H*-azirenium derivatives were first proposed: a) P. W. Neber, A. Burgard, *Justus Liebigs Ann. Chem.* **1932**, *493*, 281−294; b) M. J. Hatch, D. J. Cram, *J. Am. Chem. Soc.* **1953**, *75*, 38−44.

[92] B. P. Chandrasekhar, U. Schmid, R. Schmid, H. Heimgartner, H. Schmid, *Helv. Chim. Acta* **1975**, *58*, 1191−1200.

[93] M. Rens, L. Ghosez, *Tetrahedron Lett.* **1970**, *11*, 3765−3768.

[94] R. Flammang, S. Lacombe, A. Laurent, A. Maquestiau, B. Marquet, S. Novkova, *Tetrahedron* **1986**, *42*, 315−328.

[95] a) T. Nishiwaki, *J. Chem. Soc., Chem. Commun.* **1972**, 565−566; b) N. Kanomata, T. Nakata, *Heterocycles* **1998**, *48*, 2551−2558.

[96] D. Knittel, *Synthesis* **1985**, *2*, 186−188.

[97] The first nitrilium ylides and their 1,3-dipolar cycloadditions: R. Huisgen, H. Stangl, H. J. Sturm, H. Wagenhofer, *Angew. Chem.* **1962**, *74*, 31; *Angew. Chem., Int. Ed. Engl.* **1962**, *1*, 50.

[98] 1,3-Dipolar cycloadditions of nitrilium ylides: a) R. Huisgen, *Angew. Chem.* **1963**, *75*, 604−637; *Angew. Chem., Int. Ed. Engl.* **1963**, *2*, 565−632; b) R. Huisgen, H. Stangl, H. J. Sturm, H. Wagenhofer, *Angew. Chem.* **1963**, *75*, 742−754; *Angew. Chem., Int. Ed. Engl.* **1963**, *2*, 633−645.

[99] Isolation of the first stable nitrilium ylide: E. P. Janulis, Jr., S. R. Wilson, A. J. Arduengo, III, *Tetrahedron Lett.* **1984**, *25*, 405−408.

[100] a) A. F. Hegarty, S. J. Eustace, N. M. Tynan, N.-N. Pham-Tran, M. T. Nguyen, *J. Chem. Soc., Perkin Trans. 2* **2001**, 1239−1246; b) S. Fergus, S. J. Eustace, A. F. Hegarty, *J. Org. Chem.* **2004**, *69*, 4663−4669.

[101] A. Demoulin, H. Gorissen, A.-M. Hesbain-Frisque, L. Ghosez, *J. Am. Chem. Soc.* **1975**, *97*, 4409−4410.

[102] J. Barluenga, M. Tomas, *Adv. Heterocycl. Chem.* **1993**, *57*, 1−80.

[103] a) A. Padwa, J. Smolanoff, *J. Am. Chem. Soc.* **1971**, *93*, 548−550; b) A. Padwa, S. Clough, M. Dharan, J. Smolanoff, S. I. Wetmore, Jr., *J. Am. Chem. Soc.* **1972**, *94*, 1395−1397; c) A. Padwa, S. I. Wetmore, Jr., *J. Chem. Soc., Chem. Commun.* **1972**, 1116−1117; d) N. Gakis, M. Märky, H.-J. Hansen, H. Schmid, *Helv. Chim. Acta* **1972**, *55*, 748−752; e) A. Padwa, J. Smolanoff, *J. Am. Chem. Soc.* **1973**, *95*, 1945−1954; f) A. Padwa, M. Dharan, J. Smolanoff, S. I. Wetmore, Jr., *J. Am. Chem. Soc.* **1973**, *95*, 1954−1961; g) A. Padwa, J. Smolanoff, S. I. Wetmore, Jr., *J. Org. Chem.* **1973**, *38*, 1333−1340; h) A. Padwa, S. I. Wetmore, Jr., *J. Org. Chem.* **1974**, *39*, 1396−1400; i) A. Orahovats, H. Heimgartner, H. Schmid, W. Heinzelmann, *Helv. Chim. Acta* **1975**, *58*, 2662−2677; j) A. Padwa, *Acc. Chem. Res.* **1976**, *9*, 371−378; k) A. Padwa, *Chem. Rev.* **1977**, *77*, 37−68. l) T. Kitamura S. Kobayashi, H. Taniguchi, *Tetrahedron Lett.* **1979**, *20*, 1619−1622; m) T. Kitamura, S. Kobayashi, H. Taniguchi, *J. Org. Chem.* **1984**, *49*, 4755−4760.

[104] a) F. Müller, J. Mattay, *Angew. Chem.* **1991**, *103*, 1352−1353; *Angew. Chem., Int. Ed. Engl.* **1991**, *30*, 1336−1337; b) F. Müller, J. Mattay, *Chem. Rev.* **1993**, *93*, 99−117.

[105] M. K. G. Mekhael, S. Bienz, A. Linden, H. Heimgartner, *Helv. Chim. Acta* **2004**, *87*, 2385−2404.

[106] G. A. Olah, R. H. Schlosberg, *J. Am. Chem. Soc.* **1968**, *90*, 2726−2727.

[107] For a recent review on weakly coordinating anions see: I. Krossing, I. Raabe, *Angew. Chem.* **2004**, *116*, 2116−2142; *Angew. Chem., Int. Ed.* **2004**, *43*, 2066−2090.

[108] a) J. F. Coetzee, I. M. Kolthoff, *J. Am. Chem. Soc.* **1957**, *79*, 6110−6115; b) I. M. Kolthoff, S. Bruckenstein, M. K. Chantooni, Jr., *J. Am. Chem. Soc.* **1961**, *83*, 3927−3935; c) J. F. Coetzee, G. R. Padmanabhan, *J. Am. Chem. Soc.* **1965**, *87*, 5005−5010.

[109] H. Bader, H.-J. Hansen, *Helv. Chim. Acta* **1978**, *61*, 286−304.

[110] a) J. J. Ritter, P. P. Minieri, *J. Am. Chem. Soc.* **1948**, *70*, 4045−4048; b) J. J. Ritter, J. Kalish, *J. Am. Chem. Soc.* **1948**, *70*, 4048−4050; c) L. I. Krimen, D. J. Cota, *Org. React.* **1969**, *17*, 213−325.

[111] G. Alcaraz, U. Wecker, A. Baceiredo, F. Dahan, G. Bertrand, *Angew. Chem.* **1995**, *107*, 1358−1359; *Angew. Chem., Int. Ed. Engl.* **1995**, *34*, 1246−1248.

[112] V. Piquet, A. Baceiredo, H. Gornitzka, F. Dahan, G. Bertrand, *Chem. Eur. J.* **1997**, *3*, 1757−1764.

[113] K. B. Dillon, F. Mathey, J. F. Nixon, *Phosphorus: The Carbon Copy*, Wiley, New York, **1998**.

[114] R. Streubel, *Top. Curr. Chem.* **2003**, *223*, 91−109.

[115] W. Rösch, T. Facklam, M. Regitz, *Tetrahedron* **1987**, *43*, 3247−3256.

[116] M. Rahmoune, Y. Y. C. Yeung Lamko, R. Carrie, F. Tonnard, *New. J. Chem.* **1989**, *13*, 891−898.

[117] a) R. S. Winburn, B. R. Reems, M. R. Hoffmann, C. McMichael Rohlfing, *Main Group Chem.* **1996**, *1*, 189−196; b) O. Kwon, M. L. McKee, *J. Phys. Chem. A* **2001**, *105*, 478−483; c) N.-N. Pham-Tran, B. Hajgató, T. Veszprémi, M. T. Nguyen, *Phys. Chem. Chem. Phys.* **2001**, *3*, 1588−1597; d) R. R. Pandey, Y. G. Khait, M. R. Hoffmann, *J. Mol. Struct. (Theochem.)* **2001**, *542*, 177−188; e) Y. Ding, Z. Li, X. Huang, C. Sun, *Theor. Chem. Acc.* **2001**, *107*, 1−7; f) T. P. M. Goumans, A. W. Ehlers, K. Lammertsma, E.-U. Würthwein, *Eur. J. Org. Chem.* **2003**, 2941−2946.

[118] R. Streubel, J. Jeske, P. G. Jones, R. Herbst-Irmer, *Angew. Chem.* **1994**, *106*, 115−117; *Angew. Chem., Int. Ed. Engl.* **1994**, *33*, 80−82.

[119] R. Streubel, *Coord. Chem. Rev.* **2002**, *227*, 175−192.

[120] H. Heydt, *Science of Synthesis* **2002**, *9*, 125−133.

[121] R. Streubel, A. Kusenberg, *Phosphorus, Sulfur Silicon Relat. Elem.* **1994**, *93−94*, 281−284.

[122] R. Streubel, A. Ostrowski, S. Priemer, U. Rohde, J. Jeske, P. G. Jones, *Eur. J. Inorg. Chem.* **1998**, 257−261.

[123] R. Streubel, F. Ruthe, P. G. Jones, *Eur. J. Inorg. Chem.* **1998**, 571−574.

[124] R. Streubel, S. Priemer, F. Ruthe, P. G. Jones, D. Gudat, *Eur. J. Inorg. Chem.* **1998**, 575−578.

[125] R. Streubel, U. Rohde, J. Jeske, F. Ruthe, P. G. Jones, *Eur. J. Inorg. Chem.* **1998**, 2005−2012.

[126] R. Streubel, N. Hoffmann, H.-M. Schiebel, F. Ruthe, P. G. Jones, *Eur. J. Inorg. Chem.* **2002**, 957−967.

[127] C. Neumann, E. Ionescu, U. Schiemann, M. Schlenker, M. Bode, F. Ruthe, P. G. Jones, R. Streubel, *J. Organomet. Chem.* **2002**, *643−644*, 253−264.

[128] R. Streubel, M. Beckmann, C. Neumann, S. Fankel, H. Helten, O. Feier-Iova, P. G. Jones, M. Nieger, **2009**, 2090−2095.

[129] M. J. S. Dewar, G. P. Ford, *J. Am. Chem. Soc.* **1979**, *101*, 783−791.

[130] D. Gonbeau, G. Pfister-Guillouzo, *Inorg. Chem.* **1987**, *26*, 1799−1805.

[131] A. Marinetti, F. Mathey, *Organometallics* **1984**, *3*, 456−461.

[132] D. Gonbeau, G. Pfister-Guillouzo, A. Marinetti, F. Mathey, *Organometallics* **1985**, *24*, 4133−4140.

[133] a) A. W. Ehlers, K. Lammertsma, E. J. Baerends, *Organometallics* **1998**, *17*, 2738−2742; b) S. Creve, K. Pierloot, M. T. Nguyen, *Chem. Phys. Lett.* **1998**, *285*, 429−437; c) G. Frison, F. Mathey, A. Sevin, *J. Organomet. Chem.* **1998**, *570*, 225−234; d) S. Creve, K. Pierloot, M. T. Nguyen, L. G. Vanquickenborne, *Eur. J. Inorg. Chem.* **1999**, 107−115; e) S. Grigoleit, A. Alijah, A. B. Rozhenko, R. Streubel, W. W. Schoeller, *J. Organomet. Chem.* **2002**, *643−644*, 223−230.

[134] R. Streubel, H. Wilkens, F. Ruthe, P. G. Jones, *Chem. Commun.* **2000**, 2543−2454.

[135] E. Ionescu, P. G. Jones, R. Streubel, *Chem. Commun.* **2002**, 2204−2205.

[136] E. Ionescu, H. Wilkens, R. Streubel in *Organosilicon Chemistry VI, From Molecules to Materials*, 1st ed. (Eds.: N. Auner, J. Weis), Wiley-VCH, Weinheim, **2005**, p. 202−208.

[137] R. Streubel, E. Ionescu, N. Hoffmann, *Phosphorus, Sulfur Silicon Relat. Elem.* **2004**, *179*, 809−811.

[138] A. Ostrowski, J. Jeske, P. G. Jones, R. Streubel, *J. Chem. Soc., Chem. Commun.* **1995**, 2507−2508.

[139] R. Streubel, H. Wilkens, A. Ostrowski, C. Neumann, F. Ruthe, P. G. Jones, *Angew. Chem.* **1997**, *109*, 1549−1550; *Angew. Chem., Int. Ed. Engl.* **1997**, *36*, 1492−1494.

[140] A. Ostrowski, J. Jeske, F. Ruthe, P. G. Jones, R. Streubel, *Z. Anorg. Allg. Chem.* **1997**, *623*, 1897−1902.

[141] R. Streubel, H. Wilkens, F. Ruthe, P. G. Jones, *Z. Anorg. Allg. Chem.* **1999**, *625*, 102−106.

[142] R. Streubel, M. Bode, U. Schiemann, C. Wismach, P. G. Jones, A. Monsees, *Z. Anorg. Allg. Chem.* **2004**, *630*, 1215−1219.

[143] R. Streubel, U. Schiemann, P. G. Jones, J. Grunenberg, H.-M. Schiebel, D. Gudat, *Angew. Chem.* **2001**, *113*, 2531−2534; *Angew. Chem., Int. Ed.* **2001**, *40*, 2471−2474.

[144] A. Ostrowski, J. Jeske, P. G. Jones, R. Streubel, *Z. Anorg. Allg. Chem.* **2001**, *627*, 1135−1140.

[145] R. Streubel, A. Ostrowski, H. Wilkens, F. Ruthe, J. Jeske, P. G. Jones, *Angew. Chem.* **1997**, *109*, 409−413; *Angew. Chem., Int. Ed. Engl.* **1997**, *36*, 378−381.

[146] H. Wilkens, F. Ruthe, P. G. Jones, R. Streubel, *Chem. Eur. J.* **1998**, *4*, 1542−1553.

[147] H. Wilkens, F. Ruthe, P. G. Jones, R. Streubel, *Chem. Commun.* **1998**, 1529−1530.

[148] H. Wilkens, A. Ostrowski, J. Jeske, F. Ruthe, P. G. Jones, R. Streubel, *Organometallics* **1999**, *18*, 5627−5642.

[149] R. Streubel, N. Hoffmann, F. Ruthe, P. G. Jones, *Polyhedron* **2002**, *21*, 119−124.

[150] N. Hoffmann, C. Wismach, L. Ernst, H.-M. Schiebel, P. G. Jones, R. Streubel, *Eur. J. Inorg. Chem.* **2003**, 1815−1821.

[151] F. G. N. Cloke, P. B. Hitchcock, J. F. Nixon, U. Schiemann, R. Streubel, D. J. Wilson, *Chem. Commun.* **2000**, 1659−1660.

[152] R. Streubel, H. Wilkens, F. Ruthe, P. G. Jones, *Organometallics* **2006**, *25*, 4830−4834.

[153] H. Wilkens, Ph.D. Thesis, University of Braunschweig, **2000**.

[154] R. Streubel, H. Wilkens, *Phosphorus, Sulfur Silicon Relat. Elem.* **1999**, *144−146*, 473−476.

[155] R. Streubel, H. Wilkens, F. Ruthe, P. G. Jones, *Tetrahedron* **2000**, *56*, 21−26.

[156] H. Wilkens, J. Jeske, P. G. Jones, R. Streubel, *Chem. Commun.* **1997**, 2317−2318.

[157] R. Streubel, U. Schiemann, N. Hoffmann, Y. Schiemann, P. G. Jones, D. Gudat, *Organometallics* **2000**, *19*, 475−481.

[158] H. Wilkens, R. Streubel, *Phosphorus, Sulfur Silicon Relat. Elem.* **1997**, *124−125*, 83−92.

[159] A. A. Khan, C. Neumann, C. Wismach, P. G. Jones, R. Streubel, *J. Organomet. Chem.* **2003**, *682*, 212−217.

[160] R. Streubel, C. Neumann, *Heteroat. Chem.* **2002**, *13*, 72−76.

[161] R. Streubel, H. Wilkens, P. G. Jones, *Chem. Commun.* **1999**, 2127−2128.

[162] M. Bode, M. Nieger, R. Streubel, *Organometallics* **2007**, *26*, 245−246.

[163] R. Streubel, H. Wilkens, P. G. Jones, *Chem. Eur. J.* **2000**, *6*, 3997−4000.

[164] O. W. Webster, W. Mahler, R. E. Benson, *J. Am. Chem. Soc.* **1962**, *84*, 3678−3684;

[165] a) L. Eberson, *Electron Transfer Reactions in Organic Chemistry*, Springer, Berlin, **1987**; b) D. Astruc, *Electron Transfer and Radical Processes in Transition-Metal Chemistry*, VCH Publishers, New York, **1995**.

[166] N. G. Connelly, T. Damhus, R. M. Hartshorn, A. T. Hutton, *Nomenclature of Inorganic Chemistry – IUPAC Recommendations 2005*, RSC Publishing, Cambridge, **2005**, p. 227.

[167] C. Neumann, Ph.D. Thesis, University of Braunschweig, **2007**.

[168] R. Streubel, C. Neumann, P. G. Jones, *J. Chem. Soc., Dalton Trans.* **2000**, 2495−2496.

[169] R. Streubel, H. Wilkens, C. Neumann, *Phosphorus, Sulfur Silicon Relat. Elem.* **2002**, *177*, 1563−1565.

[170] C. Neumann, A. Prehn Junquera, C. Wismach, P. G. Jones, R. Streubel, *Tetrahedron* **2003**, *59*, 6213−6220.

[171] A. A. Khan, C. Wismach, P. G. Jones, R. Streubel, *J. Chem. Soc., Dalton Trans.* **2003**, 2483−2487.

[172] R. Streubel, A. Ostrowski, H. Wilkens, S. Priemer, U. Rohde, *Phosphorus, Sulfur Silicon Relat. Elem.* **1997**, *124−125*, 93−102.

[173] H. Helten, C. Neumann, A. Espinosa, P. G. Jones, M. Nieger, R. Streubel, *Eur. J. Inorg. Chem.* **2007**, 4669−4678.

[174] A. H. Cowley, S. W. Hall, R. A. Jones, C. M. Nunn, *J. Chem. Soc., Chem. Commun.* **1988**, 867−868.

[175] S. Berger, S. Braun, H.-O. Kalinowski, *NMR-Spektroskopie von Nichtmetallen,* ^{31}*P-NMR-Spektroskopie, Vol. 3*, Georg Thieme, Stuttgart, **1993**, p. 103.

[176] D. T. Davies, *Aromatic Heterocyclic Chemsistry*, Oxford University Press, Oxford, **1992**.

[177] P. W. Atkins, *Physical Chemistry*, 5th ed., Oxford University Press, Oxford, **1994**.

[178] M. Schmittel, A. Burghart, *Angew. Chem.* **1997**, *109*, 2658−2699; *Angew. Chem., Int. Ed. Engl.* **1997**, *36*, 2550−2589.

[179] N. G. Connelly, W. E. Geiger, *Chem. Rev.* **1996**, *96*, 877−910.

[180] S. P. Schmidt, F. Basolo, W. C. Trogler, *Inorg. Chim. Acta* **1987**, *131*, 181−189.

[181] a) J. H. Weinmaier, H. Tautz, A. Schmidpeter, S. Pohl, *J. Organomet. Chem.* **1980**, *185*, 53−68; b) K. Karaghiosoff, W. S. Sheldrick, A. Schmidpeter, *Chem. Ber.* **1986**, *119*, 3213−3226.

[182] H. Dehne in Houben-Weyl, *Meth. Org. Chem., Vol. E 8d*, **1994**, p. 305.

[183] C. Hay, M. Hissler, C. Fischmeister, J. Rault-Berthelot, L. Toupet, L. Nyulászi, R. Réau, *Chem. Eur. J.* **2001**, *7*, 4222−4236.

[184] F. H. Allen, O. Kennard, D. G. Watson, L. Brammer, A. G. Orpen, R. Taylor, *J. Chem. Soc., Perkin Trans. 2* **1987**, S1−S19.

[185] G. Barbarella, M. Zambianchi, L. Antolini, P. Ostoja, P. Maccagnani, A. Bongini, E. A. Marseglia, E. Tedesco, G. Gigli, R. Cingolani, *J. Am. Chem. Soc.* **1999**, *121*, 8920−8926.

[186] S. W. Kirtley in *Comprehensive Organometallic Chemistry, Vol. 3* (Ed.: G. Wilkinson), Pergamon Press, Oxford, **1982**.

[187] R. E. Martin, F. Diederich, *Angew. Chem.* **1999**, *111*, 1440−1469; *Angew. Chem., Int. Ed.* **1999**, *38*, 1350−1377.

[188] M. A. Alvarez, G. García, M. E. García, V. Riera, M. A. Ruiz, *Organometallics* **1999**, *18*, 4509−4517.

[189] a) Y. S. Sohn, D. N. Hendrickson, H. B. Gray, *J. Am. Chem. Soc.* **1971**, *93*, 3603−3612; b) K. Naka, T. Uemura, Y. Chujo, *Macromolecules* **2000**, *33*, 6965−6969.

[190] S. Barlow, H. E. Bunting, C. Ringham, J. C. Green, G. U. Bublitz, S. G. Boxer, J. W. Perry, S. R. Marder, *J. Am. Chem. Soc.* **1999**, *121*, 3715−3723.

[191] a) S. J. Higgins, C. L. Jones, S. M. Francis, *Synth. Met.* **1998**, *98*, 211−214; b) G. E. Southard, M. D. Curtis, *Organometallics* **2001**, *20*, 508−522.

[192] M. Schlenker, Diploma Thesis, University of Braunschweig, **2002**.

[193] O. Feier, Thesis, University of Bonn, **2004**.

[194] H. Helten, S. Fankel, O. Feier-Iova, M. Nieger, A. Espinosa Ferao, R. Streubel, *Eur. J. Inorg. Chem.* **2009**, 3226−3237.

[195] O. Stelzer, R. Schmutzler, *J. Chem. Soc. A* **1971**, 2867−2873.

[196] A. Özbolat, G. von Frantzius, W. Hoffbauer, R. Streubel, *Dalton Trans.* **2008**, 2674−2676.

[197] a) A. Özbolat-Schön, R. Streubel, manuscript in preparation; b) A. Özbolat-Schön, planned dissertation, University of Bonn.

[198] J. E. Huheey, E. A. Keiter, R. L. Keiter, *Inorganic Chemistry, Principles of Structure and Reactivity*, 4th ed., HarperCollins College Publishers, New York, **1993**, p. 46f.

[199] R. E. Winters, R. W. Kiser, *Inorg. Chem.* **1965**, *4*, 157−161.

[200] D. R. Lloyd, E. W. Schlag, *Inorg. Chem.* **1969**, *8*, 2544−2655.

[201] B. R. Higginson, D. R. Lloyd, P. Burroughs, D. M. Gibson, A. F. Orchard, *J. Chem. Soc., Faraday Trans. 2* **1973**, *69*, 1659−1668.

[202] C. J. Pickett, D. Pletcher, *J. Chem. Soc., Dalton Trans.* **1975**, 879−886.

[203] S. B. Clendenning, J. C. Green, C. F. Nixon, *J. Chem. Soc., Dalton Trans.* **2000**, 1707−1712.

[204] J. Heinze, *Angew. Chem.* **1984**, *96*, 823−916; *Angew. Chem., Int. Ed. Engl.* **1984**, *23*, 831−847.

[205] R. J. Gale, R. Job, *Inorg. Chem.* **1981**, *20*, 42−45.

[206] TURBOMOLE V5.9.1: a) R. Ahlrichs, M. Bär, M. Häser, H. Horn, C. Kölmel, *Chem. Phys. Lett.* **1989**, *162*, 165−169; b) module RELAX: M. v. Arnim, R. Ahlrichs, *J. Chem. Phys.* **1999**, *111*, 9183−9190.

[207] a) P. A. M. Dirac, *Proc. Royal Soc. (London) A* **1929**, *123*, 714−733; b) J. C. Slater, *Phys. Rev.* **1951**, *81*, 385−390.

[208] S. H. Vosko, L. Wilk, M. Nusair, *Can. J. Phys.* **1980**, *58*, 1200−1211.

[209] A. D. Becke, *Phys. Rev. A* **1988**, *38*, 3098−3100.

[210] J. P. Perdew, *Phys. Rev. B* **1986**, *33*, 8822−8824.

[211] a) K. Eichkorn, O. Treutler, H. Öhm, M. Häser, R. Ahlrichs, *Chem. Phys. Lett.* **1995**, *240*, 283−290; b) K. Eichkorn, O. Treutler, H. Öhm, M. Häser, R. Ahlrichs, *Chem. Phys. Lett.* **1995**, *242*, 652−660; c) K. Eichkorn, F. Weigend, O. Treutler, R. Ahlrichs, *Theor. Chem. Acc.* **1997**, *97*, 119−124.

[212] A. Schäfer, H. Horn, R. Ahlrichs, *J. Chem. Phys.* **1992**, *97*, 2571−2577.

[213] D. Andrae, U. Häußermann, M. Dolg, H. Stoll, H. Preuß, *Theor. Chim. Acta* **1990**, *77*, 123−141.

[214] A. Klamt and G. Schüürmann, *J. Chem. Soc. Perkin Trans. 2* **1993**, 799−805.

[215] A. Bondi, *J. Phys. Chem.* **1964**, *68*, 441−451.

[216] T. Helgaker, *Chem. Phys. Lett.* **1991**, *182*, 503−510.

[217] a) P. Deglmann, F. Furche, R. Ahlrichs, *Chem. Phys. Lett.* **2002**, *362*, 511−518;
       b) P. Deglmann, F. Furche, *J. Chem. Phys.* **2002**, *117*, 9535−9538; c) P.
       Deglmann, K. May, F. Furche, R. Ahlrichs, *Chem. Phys. Lett.* **2004**, *384*,
       103−107.

[218] A. Schäfer, C. Huber, R. Ahlrichs, *J. Chem. Phys.* **1994**, *100*, 5829−5835.

[219] Gaussian 03, Revision D.02, M. J. Frisch, G. W. Trucks, H. B. Schlegel, G. E.
       Scuseria, M. A. Robb, J. R. Cheeseman, J. A. Montgomery, Jr., T. Vreven, K.
       N. Kudin, J. C. Burant, J. M. Millam, S. S. Iyengar, J. Tomasi, V. Barone, B.
       Mennucci, M. Cossi, G. Scalmani, N. Rega, G. A. Petersson, H. Nakatsuji, M.
       Hada, M. Ehara, K. Toyota, R. Fukuda, J. Hasegawa, M. Ishida, T. Nakajima,
       Y. Honda, O. Kitao, H. Nakai, M. Klene, X. Li, J. E. Knox, H. P. Hratchian, J.
       B. Cross, V. Bakken, C. Adamo, J. Jaramillo, R. Gomperts, R. E. Stratmann,
       O. Yazyev, A. J. Austin, R. Cammi, C. Pomelli, J. W. Ochterski, P. Y. Ayala,
       K. Morokuma, G. A. Voth, P. Salvador, J. J. Dannenberg, V. G. Zakrzewski, S.
       Dapprich, A. D. Daniels, M. C. Strain, O. Farkas, D. K. Malick, A. D. Rabuck,
       K. Raghavachari, J. B. Foresman, J. V. Ortiz, Q. Cui, A. G. Baboul, S. Clifford,
       J. Cioslowski, B. B. Stefanov, G. Liu, A. Liashenko, P. Piskorz, I. Komaromi, R.
       L. Martin, D. J. Fox, T. Keith, M. A. Al Laham, C. Y. Peng, A. Nanayakkara, M.
       Challacombe, P. M. W. Gill, B. Johnson, W. Chen, M. W. Wong, C. Gonzalez,
       J. A. Pople, Gaussian, Inc., Wallingford CT, **2004**.

[220] a) V. Barone, M. Cossi, *J. Phys. Chem. A* **1998**, *102*, 1995−2001; b) M. Cossi,
       N. Rega, G. Scalmani, V. Barone, *J. Comp. Chem.* **2003**, *24*, 669−681.

[221] a) J. P. Foster, F. Weinhold, *J. Am. Chem. Soc.* **1980**, *102*, 7211−7218; b) A. E.
       Reed, F. Weinhold, *J. Chem. Phys.* **1983**, *78*, 4066−4073; c) A. E. Reed, R. B.
       Weinstock, F. Weinhold, *J. Chem. Phys.* **1985**, *83*, 735−746; d) J. E. Carpenter,
       Ph.D. Thesis, University of Wisconsin, Madison, WI, **1987**; e) J. E. Carpenter,
       F. Weinhold, *J. Mol. Struct. (Theochem)* **1988**, *169*, 41−62; f) A. E. Reed, L.
       A. Curtiss, F. Weinhold, *Chem. Rev.* **1988**, *88*, 899−926.

[222] a) E. van Lenthe, E. J. Baerends, J. G. Snijders, *J. Chem. Phys.* **1993**, *99*,
       4597−4610; b) E. van Lenthe, E. J. Baerends, J. G. Snijders, *J. Chem. Phys.*
       1994, *101*, 9783−9792; c) E. van Lenthe, A. E. Ehlers, E. J. Baerends, *J. Chem.
       Phys.* **1999**, *110*, 8943−8953.

[223] a) E. van Lenthe, J. G. Snijders, E. J. Baerends, *J. Chem. Phys.* **1996**, *105*, 6505−6516; b) E. van Lenthe, R. van Leeuwen, E. J. Baerends, J. G. Snijders, *Int. J. Quantum Chem.* **1996**, *57*, 281−293.

[224] ADF2008.01, SCM, Theoretical Chemistry, Vrije Universiteit, Amsterdam, The Netherlands, http://www.scm.com; contributors: E. J. Baerends, J. Autschbach, A. Bérces, F. M. Bickelhaupt, C. Bo, P. M. Boerrigter, L. Cavallo, D. P. Chong, L. Deng, R. M. Dickson, D. E. Ellis, M. van Faassen, L. Fan, T. H. Fischer, C. Fonseca Guerra, S. J. A. van Gisbergen, A. W. Götz, J. A. Groeneveld, O. V. Gritsenko, M. Grüning, F. E. Harris, P. van den Hoek, C. R. Jacob, H. Jacobsen, L. Jensen, G. van Kessel, F. Kootstra, M. V. Krykunov, E. van Lenthe, D. A. McCormack, A. Michalak, J. Neugebauer, V. P. Nicu, V. P. Osinga, S. Patchkovskii, P. H. T. Philipsen, D. Post, C. C. Pye, W. Ravenek, J. I. Rodríguez, P. Ros, P. R. T. Schipper, G. Schreckenbach, J. G. Snijders, M. Solà, M. Swart, D. Swerhone, G. te Velde, P. Vernooijs, L. Versluis, L. Visscher, O. Visser, F. Wang, T. A. Wesolowski, E. M. van Wezenbeek, G. Wiesenekker, S. K. Wolff, T. K. Woo, A. L. Yakovlev, T. Ziegler; a) C. Fonseca Guerra, J. G. Snijders, G. te Velde, E. J. Baerends, *Theor. Chem. Acc.* **1998**, *99*, 391−403; b) G. te Velde, F. M. Bickelhaupt, S. J. A. van Gisbergen, C. Fonseca Guerra, E. J. Baerends, J. G. Snijders, T. Ziegler, *J. Comput. Chem.* **2001**, *22*, 931−967.

[225] a) E. van Lenthe, E. J. Baerends, *J. Comput. Chem.* **2003**, *24*, 1142−1156; b) D. P. Chong, E. van Lenthe, S. J. A. van Gisbergen, E. J. Baerends, *J. Comput. Chem.* **2004**, *25*, 1030−1036.

[226] J. W. Rabalais, L. O. Werme, T. Bergmark, L. Karlsson, M. Hussain, K. Siegbahn, *J. Chem. Phys.* **1972**, *57*, 1185−1192.

[227] MOLDEN 4.7: G. Schaftenaar, J. H. Noordik, *J. Comput.-Aided Mol. Des.* **2000**, *14*, 123−134.

[228] E. Ruiz, J. Cirera, S. Alvarez, *Coord. Chem. Rev.* **2005**, *249*, 2649−2660.

[229] K. E. Torraca, L. McElwee-White, *Coord. Chem. Rev.* **2000**, *206−207*, 469−491.

[230] A. D. Becke, *J. Chem. Phys.* **1993**, *98*, 5648−5652.

[231] C. Lee, W. Yang, R. G. Parr, *Phys. Rev. B.* **1988**, *37*, 785−789.

[232] B. Miehlich, A. Savin, H. Stoll, H. Preuss, *Chem. Phys. Lett.* **1989**, *157*, 200−206.

[233] a) R. Ditchfield, W. J. Hehre, J. A. Pople, *J. Chem. Phys.* **1971**, *54*, 724−728; b) W. J. Hehre, R. Ditchfield, J. A. Pople, *J. Chem. Phys.* **1972**, *56*, 2257−2261;

c) P. C. Hariharan, J. A. Pople, *Theo. Chim. Acta* **1973**, *28*, 213−222; d) P. C. Hariharan, J. A. Pople, *Mol. Phys.* **1974**, *27*, 209−214; e) M. S. Gordon, *Chem. Phys. Lett.* **1980**, *76*, 163−168; f) M. M. Francl, W. J. Pietro, W. J. Hehre, J. S. Binkley, D. J. DeFrees, J. A. Pople, M. S. Gordon, *J. Chem. Phys.* **1982**, *77*, 3654−3665; g) R. C. Binning Jr., L. A. Curtiss, *J. Comp. Chem.* **1990**, *11*, 1206−1216; h) J.-P. Blaudeau, M. P. McGrath, L. A. Curtiss, L. Radom, *J. Chem. Phys.* **1997**, *107*, 5016−5021; i) V. A. Rassolov, J. A. Pople, M. A. Ratner, T. L. Windus, *J. Chem. Phys.* **1998**, *109*, 1223−1229; j) V. A. Rassolov, M. A. Ratner, J. A. Pople, P. C. Redfern, L. A. Curtiss, *J. Comp. Chem.* **2001**, *22*, 976−984.

[234] T. Clark, J. Chandrasekhar, G. W. Spitznagel, P. v. R. Schleyer, *J. Comp. Chem.* **1983**, *4*, 294−301.

[235] a) P. J. Hay, W. R. Wadt, *J. Chem. Phys.* **1985**, *82*, 270−283; b) W. R. Wadt, P. J. Hay, *J. Chem. Phys.* **1985**, *82*, 284−298; c) P. J. Hay, W. R. Wadt, *J. Chem. Phys.* **1985**, *82*, 299−310.

[236] a) R. Krishnan, J. S. Binkley, R. Seeger, J. A. Pople, *J. Chem. Phys.* **1980**, *72*, 650−654; b) A. D. McLean, G. S. Chandler, *J. Chem. Phys.* **1980**, *72*, 5639−5648.

[237] a) V. Lloveras, A. Caballero, A. Tárraga, M. D. Velasco, A. Espinosa, K. Wurst, D. J. Evans, J. Vidal-Gancedo, C. Rovira, P. Molina, J. Veciana, *Eur. J. Inorg. Chem.* **2005**, 2436−2450; b) A. Caballero, A. Espinosa, A. Tárraga, P. Molina, *J. Org. Chem.* **2008**, *73*, 5489−5497.

[238] S. Lupan, M. Kapon, M. Cais, F. H. Herbstein, *Angew. Chem.* **1972**, *84*, 1104−1106; *Angew. Chem., Int. Ed. Engl.* **1972**, *11*, 1025−1027.

[239] a) D. R. Christ, N. J. Leonard, *Angew. Chem.* **1969**, *23*, 953−1008; *Angew. Chem. Int. Ed. Engl.* **1969**, *8*, 962−974; b) T.-H. Chuang, K. B. Sharpless, *Org. Lett.* **2000**, *2*, 3555−3557; c) V. H. Dahanukar, A. I. Zavialov, *Curr. Op. Drug Discov. Develop.* **2002**, *5*, 918−927.

[240] E. Niecke, D. Gudat, E. Symalla, *Angew. Chem.* **1986**, *98*, 817−818; *Angew. Chem., Int. Ed. Engl.* **1986**, *25*, 834−835.

[241] G. Etemad-Moghadam, M. Rifqui, P. Layrolle, J. Berlan, M. Koenig, *Tetrahedron Lett.* **1991**, *32*, 5965−5968; b) M. Rifqui, G. Etemad-Moghadam, J. Berlan, M. Koenig, *Main Group Chem.* **1997**, *2*, 37−41.

[242] a) D. Bourissou, Y. Canac, M. I. Collado, A. Baceiredo, G. Bertrand, *J. Am. Chem. Soc.* **1997**, *119*, 9923−9924; b) D. Bourissou, Y. Canac, H. Gornitzka, C. J. Marsden, A. Baceiredo, G. Bertrand, *Eur. J. Inorg. Chem.* **1999**, 1479−1488.

[243] For an expample of a kinetically controlled protonation see: S. Ekici, D. Gudat, M. Nieger, L. Nyulaszi, E. Niecke, *Angew. Chem.* **2002**, *114*, 3515−3519; *Angew. Chem., Int. Ed.* **2002**, *41*, 3367−3371.

[244] S. Berger, S. Braun, H.-O. Kalinowski, *NMR-Spektroskopie von Nichtmetallen,* ^{15}N-*NMR-Spektroskopie, Vol. 2*, Georg Thieme, Stuttgart, New York **1992**, p. 25ff.

[245] B. Clement, T. Kämpchen, *Chem. Ber.* **1986**, *119*, 1101−1104.

[246] M. Alei, Jr., L. O. Morgan, W. E. Wageman, T. W. Whaley, *J. Am. Chem. Soc.* **1980**, *102*, 2881−2887.

[247] F. A. Cotton, C. S. Kraihanzel, *J. Am. Chem. Soc.* **1962**, *84*, 4432−4438.

[248] a) M. Bigorgne, R. Poilblanc, M. Pankowski, *Spectrochim. Acta* **1970**, *26*, 1217−1224; b) F. T. Delbeke, G. P. van der Kelen, *J. Organomet. Chem.* **1974**, *64*, 239−244.

[249] M. Nee, J. D. Roberts, *Biochemistry* **1982**, *21*, 4920−4926.

[250] M. Alei, Jr., P. J. Vergamini, W. E. Wageman, *J. Am. Chem. Soc.* **1979**, *101*, 5415−5417.

[251] T. G. Appleton, J. R. Hall, S. F. Ralph, C. S. M. Thompson, *Aust. J. Chem.* **1988**, *41*, 1425−1432.

[252] T. G. Appleton, J. R. Hall, S. F. Ralph, *Inorg. Chem.* **1988**, *27*, 4435−4437.

[253] L. Pazderski, E. Szłyk, J. Sitkowski, B. Kamieński, L. Kozerski, J. Toušek, R. Marek, *Magn. Reson. Chem.* **2006**, *44*, 163−170.

[254] R. W. Schurko, R. E. Wasylishen, *J. Phys. Chem. A* **2000**, *104*, 3410−3420.

[255] G. C. van Stein, G. van Koten, K. Vrieze, C. Brevard, A. L. Spek, *J. Am. Chem. Soc.* **1984**, *106*, 4486−4492.

[256] B. Wrackmeyer, K. Schamel, M. Herberhold, *Z. Naturforsch.* **1989**, *44b*, 55−62.

[257] a) R. Hagen, J. P. Warren, D. H. Hunter, J. D. Roberts, *J. Am. Chem. Soc.* **1973**, *95*, 5712−5716; b) H. Motschi, P. S. Pregosin, L. M. Venanzi, *Helv. Chim. Acta* **1979**, *62*, 667−677; c) H. van der Poel, G. van Koten, D. M. Grove, P. S. Pregosin, K. A. Ostoja Starzewski, *Helv. Chim. Acta* **1981**, *64*, 1174−1182; d) C. J. Boreham, J. A. Broomhead, D. P. Fairlie, *Aust. J. Chem.* **1981**, *34*, 659−664; e) M. Watabe, M. Takahashi, A. Yamasaki, *Inorg. Chem.* **1983**, *22*, 2650−2651; f) G. C. van Stein, G. van Koten, K. Vrieze, A. L. Spek, E. A. Klop, C. Brevard, *Inorg. Chem.* **1985**, *24*, 1367−1375; g) H. Bissinger, W. Beck, *Z. Naturforsch.* **1985**, *40b*, 507−511; h) P. S. Pregosin, R. Rüedi, C. Anklin, *Magn. Reson. Chem.* **1986**, *24*, 255−258; i) K. Isobe, K. Nanjo, Y. Nakamura, S. Kawaguchi, *Bull. Soc. Chem. Jpn.* **1986**, *59*, 2141−2149; j) Y. Nakashima, M. Muto, K. Kawano, Y. Kyogoku, Y. Yoshikawa, *Bull. Soc. Chem. Jpn.* **1989**, *62*, 2455−2460.

[258] J. C. Jeffrey, T. B. Rauchfuss, *Inorg. Chem.* **1979**, *18*, 2658−2666.

[259] a) J. A. Davies, F. R. Hartley, *Chem. Rev.* **1981**, *81*, 79−90; b) P. Braunstein, F. Naud, *Angew. Chem.* **2001**, *113*, 702−722; *Angew. Chem., Int. Ed.* **2001**, *40*, 680−699; c) P. Braunstein, N. M. Boag, *Angew. Chem.* **2001**, *113*, 2493−2500; *Angew. Chem., Int. Ed.* **2001**, *40*, 2427−2433; d) L. H. Gade, *J. Organomet. Chem.* **2002**, *661*, 85−94; e) W. E. Piers, D. J. H. Emslie, *Coord. Chem. Rev.* **2002**, *233−234*, 131−155; f) C. J. Elsevier, J. Reedijk, P. H. Walton, M. D. Ward, *Dalton Trans.* **2003**, 1869−1880.

[260] a) M. Pfeiffer, T. Stey, H. Jehle, B. Klüpfel, W. Malisch, V. Chandrasekhar, Dietmar Stalke, *Chem. Commun.* **2001**, 337−338; b) A. Murso, D. Stalke, *Eur. J. Inorg. Chem.* **2004**, 4272−4277; c) A. Murso, D. Stalke, *Dalton Trans.* **2004**, 2563−2569; d) T. Stey, D. Stalke, *Z. Anorg. Allg. Chem.* **2005**, *631*, 2931−2936; e) T. Stey, M. Pfeiffer, J. Henn, S. K. Pandey, D. Stalke, *Chem. Eur. J.* **2007**, *13*, 3636−3642.

[261] F. Baier, Z. Fei, H. Gornitzka, A. Murso, S. Neufeld, M. Pfeiffer, I. Rüdenauer, A. Steiner, T. Stey, D. Stalke, *J. Organomet. Chem.* **2002**, *661*, 111−127.

[262] T. Stey, J. Henn, D. Stalke, *Chem. Commun.* **2007**, 413−415.

[263] a) C. G. Arena, G. Bruno, G. De Munno, E. Rotondo, D. Drommi, F. Faraone, *Inorg. Chem.* **1993**, *32*, 1601−1606; b) C. Amatore, A. Fuxa, A. Jutand, *Chem. Eur. J.* **2000**, *6*, 1474−1482.

[264] a) J. C. Decius, *J. Chem. Phys.* **1963**, *38*, 241−248; b) L. H. Jones, *J. Mol. Spectr.* **1970**, *36*, 398−403; c) J. Grunenberg, R. Streubel, G. von Frantzius, W.

Marten, *J. Chem. Phys.* **2003**, *119*, 165−169; d) K. Brandhorst, J. Grunenberg, *Chem. Soc. Rev.* **2008**, *119*, 1558−1567.

[265] C. Roques, M. R. Mazieres, J.-P. Majoral, M. Sanchez, *J. Org. Chem.* **1989**, *54*, 5535−5539.

[266] R. Streubel, Habilitationsschrift, University of Braunschweig, **1997**.

[267] E. Ionescu, G. von Frantzius, P. G. Jones, R. Streubel, *Organometallics* **2005**, *24*, 2237−2240.

[268] E. Ionescu, Ph.D. Thesis, University of Bonn, **2005**.

[269] a) L. P. Hammett, A. J. Dreyrup, *J. Am. Chem. Soc.* **1932**, *54*, 2721−2739; b) L. P. Hammett, *Chem. Rev.* **1935**, *16*, 67−79.

[270] S. Saito, S. Saito, T. Ohwada, K. Shudo, *Chem. Pharm. Bull.* **1991**, *39*, 2718−2720.

[271] a) M. H. A. Benvenutti, P. B. Hitchcock, J. L. Kiplinger, J. F. Nixon, T. G. Richmond, *J. Chem. Soc., Chem. Commun.* **1997**, 1539−1540; b) M. Yoshifuji, Y. Ichikawa, N. Yamada, K. Toyota, *J. Chem. Soc., Chem. Commun.* **1998**, 27−28; c) P. Kramkowski, M. Scheer, *Eur. J. Inorg. Chem.* **2000**, 1869−1876; d) C. Peters, H. Disteldorf, E. Fuchs, S. Werner, S. Stutzmann, J. Bruckmann, C. Krüger, P. Binger, H. Heydt, M. Regitz, *Eur. J. Org.Chem.* **2001**, 3425−3435; e) C. Jones, C. Schulten, A. Stasch, *J. Chem. Soc., Dalton Trans.* **2007**, 1929−1933.

[272] M. Hesse, H. Meier, B. Zeeh, *Spektroskopische Methoden in der organischen Chemie*, 7th ed., Georg Thieme, Stuttgart, New York, **2005**, p. 49ff.

[273] see e.g.: a) A. H. Cowley, R. A. Kemp, *Chem. Rev.* **1985**, *85*, 367−382; M. Sanchez, M. R. Mazières, L. Lamandé, R. Wolf in *Multiple Bonds in Low Coordination Phosphorus Chemistry* (Eds.: M. Regitz, O. J. Scherer), Georg Thieme, Stuttgart, **1990**, p. 129−148; c) D. Gudat, *Coord. Chem. Rev.* **1997**, *163*, 71−106; d) W. W. Schoeller, *Top. Curr. Chem.* **2003**, *229*, 75−94.

[274] E. Cancès, B. Mennucci, *J. Math. Chem.* **1998**, *23*, 309−326.

[275] B. Mennucci, E. Cancès, J. Tomasi, *J. Phys. Chem. B* **1997**, *101*, 10506−10517.

[276] E. Cancès, B. Mennucci, J. Tomasi, *J. Chem. Phys.* **1997**, *107*, 3032−3041.

[277] H. Helten, G. von Frantzius, G. Schnakenburg, J. Daniels, R. Streubel, *Eur. J. Inorg. Chem.* **2009**, 2062−2065.

[278] a) F. L. Hirshfeld, *Theor. Chim. Acta* **1977**, *44*, 129−138; b) K. B. Wiberg, P. R. Rablen, *J. Comp. Chem.* **1993**, *14*, 1504−1518.

[279] a) A. Kraft, A. C. Grimsdale, A. B. Holmes, *Angew. Chem.* **1998**, *110*, 416−443; *Angew. Chem., Int. Ed.* **1998**, *37*, 403−428; b) K. Müllen, G. Wegner, *Electronic Materials: The Oligomer Approach*, Wiley-VCH, Weinheim, **1998**; c) *Handbook of Conducting Polymers* (Eds. T. A. Skotheim, R. L. Elsenbaumer, J. R. Reynolds), Marcel Dekker, New York, **1998**.

[280] a) J. Roncali, *Chem. Rev.* **1997**, *97*, 173−205; b) F. Garnier, *Acc. Chem. Res.* **1998**, *32*, 209−215; c) R. E. Martin, F. Diederich, *Angew. Chem.* **1999**, *111*, 1440−1469; *Angew. Chem., Int. Ed.* **1999**, *38*, 1350−1377; d) J. M. Tour, *Acc. Chem. Res.* **2000**, *33*, 791−804; e) U. Mitschke, P. Bäuerle, *J. Mater. Chem.* **2000**, *10*, 1471−1507; f) J. L. Segura, N. Martin, *J. Mater. Chem.* **2000**, *10*, 2403−2435; g) F. Fichou, *J. Mater. Chem.* **2000**, *10*, 571−588; h) T-Q. Nguyen, J. Wu, V. Doan, B. J. Schwartz, S. H. Tolbert, *Science* **2000**, *288*, 652−656; i) M. A. Baldo, M. E. Thompson, S. R. Forrest, *Nature* **2000**, *403*, 750−752; j) Y. Shi, C. Zhang, H. Zhang, J. H. Bechtel, L. R. Dalton, B. H. Robinson, W. H. Steier, *Science* **2000**, *288*, 119−122.

[281] a) Z. Zhou, T. Maruyama, T. Kanbara, T. Ikeda, K. Ichimura, T. Yamamoto, K. Tokuda, *J. Chem. Soc., Chem. Commun.* **1991**, 1210−1212; b) T. Yamamoto, Z.-H. Zhou, T. Kanbara, M. Shimura, K. Kizu, T. Maruyama, Y. Nakamura, T. Fukuda, B. L. Lee, N. Ooba, S. Tomura, T. Kurihara, T. Kaino, K. Kubota, S. Sasaki, *J. Am. Chem. Soc.* **1996**, *118*, 10389−10399; c) Q. T. Zhang, J. T. Tour, *J. Am. Chem. Soc.* **1998**, *120*, 5355−5362; d) D. J. Irvin, C. J. Dubois, J. R. Reynolds, *Chem. Commun.* **1999**, 2121−2122.

[282] S. Yamagushi, Y. Itami, K. Tamao, *Organometallics* **1998**, *17*, 4910−4916.

[283] S. Yamagushi, T. Goto, K. Tamao, *Angew. Chem.* **2000**, *112*, 1761−1763; *Angew. Chem., Int. Ed.* **2000**, *39*, 1695−1697;

[284] a) J. P. Ferraris, R. G. Andrus, D. C. Hrncir, *J. Chem. Soc., Chem. Commun.* **1989**, 1318−1320; b) K. Tamao, S. Yamagushi, M. Shiozaki, Y. Nakagawa, Y. Ito, *J. Am. Chem. Soc.* **1992**, *114*, 5867−5869; c) R. J. P. Corriu, W. E. Douglas, Z.-X Yang, *J. Organomet. Chem.* **1993**, *456*, 35−39; d) I. Albert, T. Marks, M. Ratner, *J. Am. Chem. Soc.* **1997**, *119*, 6575−6582; e) S. Yamagushi, Y. Itami, K. Tamao, *Organometallics* **1998**, *17*, 4910−4916; f) A. Hucke, M. P. Cava, *J. Org. Chem.* **1998**, *63*, 7413−7417; g) B. Jiang, T. D. Tilley, *J. Am. Chem. Soc.* **1999**, *121*, 9744−9745; h) C.-F. Lee, L.-M.Yang, T.-Y. Hwu, A.-S. Feng, J.-C. Tseng, T.-Y. Luh, *J. Am. Chem. Soc.* **2000**, *122*, 4992−4993; i) S. Yamagushi,

T. Goto, K. Tamao, *Angew. Chem.* **2000**, *112*, 1761−1763; *Angew. Chem., Int. Ed.* **2000**, *39*, 1695−1697; j) M. C. Suh, B. Jiang, T. D. Tilley, *Angew. Chem.* **2000**, *112*, 2992−2995; *Angew. Chem., Int. Ed.* **2000**, *39*, 2870−2873; k) B. L. Lucht, M. A. Buretea, T. D. Tilley, *Organometallics* **2000**, *19*, 3469−3475.

[285] a) S. Yamagushi, K. Tamao, *J. Chem. Soc., Dalton Trans.* **1998**, 3693−3702; b) S. Yamagushi, T. Endo, M. Uchida, T. Izumizawa, K. Furukawa, K. Tamao, *Chem. Eur. J.* **2000**, *6*, 1683−1692.

[286] K. Tamao, M. Uchida, T. Izumizawa, K. Furukawa, S. Yamaguchi, *J. Am. Chem. Soc.* **1996**, *118*, 11974−11975.

[287] T. Baumgartner, W. Bergmans, T. Kárpáti, T. Neumann, M. Nieger, L. Nyulászi, *Chem. Eur. J.* **2005**, *11*, 4687−4699.

[288] Y. Dienes, M. Eggenstein, T. Neumann, U. Englert, T. Baumgartner, *Dalton Trans.* **2006**, 1424−1433.

[289] S. S. H. Mao, T. D. Tilley, *Macromolecules* **1997**, *30*, 5566−5569.

[290] For reviews on phosphole containing π-conjugated materials see a) T. Baumgartner, R. Réau, *Chem. Rev.* **2006**, *106*, 4681−4727; b) M. G. Hobbs, T. Baumgartner, *Eur. J. Inorg. Chem.* **2007**, 3611−3628.

[291] T. Baumgartner, T. Neumann, B. Wirges, *Angew. Chem.* **2004**, *116*, 6323−6328; *Angew. Chem., Int. Ed.* **2004**, *43*, 6197−6201.

[292] S. Durben, Y. Dienes, T. Baumgartner, *Org. Lett.* **2006**, *8*, 5893−5896.

[293] Y. Dienes, S. Durben, T. Kárpáti, T. Neumann, U. Englert, L. Nyulászi, T. Baumgartner, *Chem. Eur. J.* **2007**, *13*, 7487−7500.

[294] a) H. Weiss, R. Ahlrichs, M. Häser *J. Chem. Phys.* **1993**, *99*, 1262−1270; b) *Density functional theory for excited states: equilibrium structure and electronic spectra*, F. Furche, D. Rappoport, Chapter III in *Computational Photochemistry, Vol. 16* (Ed. M. Olivucci), Elsevier, Amsterdam, **2005**; c) R. Bauernschmitt, R. Ahlrichs, *J. Chem. Phys.* **1996**, *104*, 9047−9052.

[295] R. Bauernschmitt, R. Ahlrichs, *Chem. Phys. Lett.* **1996**, *256*, 454−464.

[296] a) S.-A. Chen, G.-W. Hwang, *Macromolecules* **1996**, *29*, 3950−3955; b) Y. Liu, M. Liu, *Thin Solid Films* **2002**, *415*, 248−252.

[297] A. J. Arduengo, III, R. L. Harlow, M. Kline, *J. Am. Chem. Soc.* **1991**, *113*, 361−363.

[298] a) T. Weskamp, W. C. Schattenmann, M. Spiegler, W. A. Herrmann, *Angew. Chem.* **1998**, *110*, 2631−2633; *Angew. Chem., Int. Ed.* **1998**, *37*, 2490−2493; b) M. Scholl, S. Ding, C. W. Lee, R. H. Grubbs, *Org. Lett.* **1999**, *1*, 953−956; c) J. Huang, E. D. Stevens, S. P. Nolan, J. L. Peterson, *J. Am. Chem. Soc.* **1999**, *121*, 2674−2678; d) A. Fürstner, *Angew. Chem.* **2000**, *112*, 3140−3172; *Angew. Chem., Int. Ed.* **2000**, *39*, 3012−3043; e) L. Jafarpour, S. P. Nolan, *Adv. Organomet. Chem.* **2000**, *46*, 181−222; f) T. M. Trnka, R. H. Grubbs, *Acc. Chem. Res.* **2001**, *34*, 18−29; g) L. Jafarpour, S. P. Nolan, *J. Organomet. Chem.* **2001**, *617−618*, 17−27; h) W. A. Herrmann, *Angew. Chem.* **2002**, *114*, 1342−1363; *Angew. Chem., Int. Ed.* **2002**, *41*, 1290−1309.

[299] a) H. M. Lee, T. Jiang, E. D. Stevens, S. P. Nolan, *Organometallics* **2001**, *20*, 1255−1258; b) A. C. Hillier, H. M. Lee, E. D. Stevens, S. P. Nolan, *Organometallics* **2001**, *20*, 4246−4252; c) L. D. Vasquez-Serrano, B. T. Owens, J. M. Buriak, *Chem. Commun.* **2002**, 2518−2519.

[300] I. E. Markò, S. Stérin, O. Buisine, G. Mignani, P. Branlard, B. Tinant, J.-P. Declerq, *Science* **2002**, *298*, 204−206.

[301] a) G. A. Grasa, M. S. Viciu, J. Huang, S. P. Nolan, *J. Org. Chem.* **2001**, *66*, 7729−7737; b) G. A. Grasa, M. S. Viciu, J. Huang, C. Zhang, M. L. Trudell, S. P. Nolan, *Organometallics* **2002**, *21*, 2866−2873; c) M. S. Viciu, R. F. Germaneau, S. P. Nolan, *Org. Lett.* **2002**, *4*, 4053−4056; d) O. Navarro, R. A. Kelly III, S. P. Nolan, *J. Am. Chem. Soc.* **2003**, *125*, 16194−16195.

[302] D. Enders, K. Breuer, G. Raabe, J. Runsink, J. H. Teles, J.-P. Melder, K. Ebel, S. Brode, *Angew. Chem.* **1995**, *107*, 1119−1122;

[303] a) V. Lavallo, Y. Canac, C. Präsang, B. Donnadieu, G. Bertrand, *Angew. Chem.* **2005**, *117*, 5851−5855; *Angew. Chem., Int. Ed.* **2005**, *44*, 5705−5709; b) V. Lavallo, Y. Canac, A. Dehope, B. Donnadieu, G. Bertrand, *Angew. Chem.* **2005**, *117*, 7402−7405; *Angew. Chem., Int. Ed.* **2005**, *44*, 7236−7239; c) R. Jazzar, R. D. Dewhurst, J. B. Bourg, B. Donnadieu, Y. Canac, G. Bertrand, *Angew. Chem.* **2007**, *119*, 2957−2960; *Angew. Chem., Int. Ed.* **2007**, *46*, 2899−2902; d) G. D. Frey, V. Lavallo, B. Donnadieu, W.W. Schoeller, G. Bertrand, *Science* **2007**, *316*, 439−441.

[304] J.-B. Bourg, M. Song, M. Soleilhavoup, B. Donnadieu, G. Bertrand, International Conference on Heteroatom Chemistry, **2007**, poster 4.

[305] E. Niecke, A. Fuchs, M. Nieger, O. Schmidt, W. W. Schoeller, *Angew. Chem.* **1999**, *111*, 3216−3219; *Angew. Chem., Int. Ed.* **1999**, *38*, 3031−3034. *Angew. Chem., Int. Ed. Engl.* **1995**, *34*, 1021−1023.

[306] D. Martin, A. Baceiredo, H. Gornitzka, W. W. Schoeller, G. Bertrand, *Angew. Chem.* **2005**, *117*, 1728−1731; *Angew. Chem., Int. Ed.* **2005**, *44*, 1700−1703.

[307] W. W. Schoeller, D. Schroeder, A. B. Rozhenko, *J. Organomet. Chem.* **2005**, *690*, 6079−6088.

[308] E. Despagnet-Ayoub, R. H. Grubbs, *J. Am. Chem. Soc.* **2004**, *126*, 10198−10199.

[309] a) C. A. Dyker, S. D. Riegel, N. Burford, M. D. Lumsden, A. Decken, *J. Am. Chem. Soc.* **2007**, *129*, 7464−7474; b) J. J. Weigand, S. D. Riegel, N. Burford, A. Decken, *J. Am. Chem. Soc.* **2007**, *129*, 7969−7976.

[310] a) W. Jiang, C. B. Knobler, M. D. Mortimer, M. F. Hawthorne, *Angew. Chem.* **1995**, *107*, 1470−1473; *Angew. Chem., Int. Ed. Engl.* **1995**, *34*, 1332−1334; b) B. T. King, Z. Janoušek, B. Grüner, M. Trammell, B. C. Noll, J. Michl, *J. Am. Chem. Soc.* **1996**, *118*, 3313−3314.

[311] D. Stasko, C. A. Reed, *J. Am. Chem. Soc.* **2002**, *124*, 1148−1149.

[312] see e.g., E. V. Banide, B. C. Molloy, Y. Ortin, H. Müller-Bunz, M. J. McGlinchey, *Eur. J. Org. Chem.* **2007**, 2611−2622.

[313] F. Mathey, A. Marinetti, F. Mercier, *Synlett* **1992**, 363−370.

[314] N. H. Tran Huy, L. Ricard, F. Mathey, *Organometallics* **1988**, *7*, 1791−1795.

[315] For a modified approach using *N*-methylimidazole instead of 2,2'-bipyridyl see: E. Deschamps, F. Mathey, *J. Org. Chem.* **1990**, *55*, 2494−2498.

[316] For a modified approach using iodine as oxidant and *N*-methylimidazole as ligand see: A. Marinetti, F. Mathey, J. Fischer, A. Mitschler, *J. Chem. Soc., Chem. Commun.* **1984**, 45−46.

[317] K. H. Dötz, H. Fischer, P. Hofmann, F. R. Kreissl, U. Schubert, K. Weiss, *Transition Metal Carbene Complexes*, (Ed.: D. Seyferth), Verlag Chemie, Weinheim, **1983**.

[318] a) R. Appel, A. Westerhaus, *Tetrahedron Lett.* **1981**, *22*, 2159−2160; b) K. Issleib, M. Schmidt, C. Wirkner, *Z. Chem.* **1981**, *21*, 357−358.

[319] R. Streubel, S. Priemer, J. Jeske, P. G. Jones, *J. Organomet. Chem.* **2001**, *617−618*, 423−434.

[320] S. Priemer, Ph.D. Thesis, University of Braunschweig, **1999**.

[321] R. Streubel, S. Priemer, F. Ruthe, P. G. Jones, *Eur. J. Inorg. Chem.* **2000**, 1253−1259.

[322] R. Streubel, M. Hobbold, S. Priemer, *J. Organomet. Chem.* **2000**, *613*, 56−59.

[323] R. Streubel, M. Hobbold, J. Jeske, F. Ruthe, P. G. Jones, *J. Organomet. Chem.* **1997**, *529*, 351−356.

[324] E. Niecke, D. Barion, *Tetrahedron Lett.* **1989**, *30*, 459−460.

[325] R. Streubel, L. Ernst, J. Jeske, P. G. Jones, *J. Chem. Soc., Chem. Commun.* **1995**, 2113−2114.

[326] B. Denise, A. Parlier, H. Rudler, *J. Organomet. Chem.* **1988**, *354*, C23−C25.

[327] P. Hohenberg, W. Kohn, *Phys. Rev.* **1964**, *136*, B864−B871.

[328] W. Kohn, L. J. Sham, *Phys. Rev.* **1965**, *140*, A1133−A1138.

[329] F. Block, *Z. Physik* **1929**, *57*, 545.

[330] P. A. M. Dirac, *Proc. Cambridge Phil. Soc.* **1930**, *26*, 376−385.

[331] R. M. Dreizler, E. K. U. Gross, *Density Functional Theory*, Springer, Berlin, **1990**.

[332] D. M. Ceperley, *Phys. Rev. B* **1978**, *18*, 3126−3138.

[333] D. M. Ceperley, B. J. Alder, *Phys. Rev. Lett.* **1980**, *45*, 566−569.

[334] F. Jensen, *Introduction to Computational Chemistry*, Wiley, Chichester, New York, Weinheim, Brisbane, Singapore, Toronto, **1999**.

[335] J. D. Perdew, Y. Wang, *Phys. Rev. B* **1986**, *33*, 8800−8802.

[336] G. Ortiz, P. Ballone, *Phys. Rev. B* **1991**, *43*, 6376−6387.

[337] J. P. Perdew, *Phys. Rev. B* **1986**, *34*, 7406.

[338] J. P. Perdew, J. A. Chevary, S. H. Vosko, K. A. Jackson, M. R. Pederson, D. J. Singh, C. Fiolhais, *Phys. Rev. B* **1992**, *46*, 6671−6687.

[339] R. Colle, O. Salvetti, *Theo. Chem. Acc.* **1975**, *37*, 329−334.

[340] a) T. Schwabe, S. Grimme, *Phys. Chem. Chem. Phys.* **2007**, *9*, 3397−3406. b) T. Schwabe, S. Grimme, *Acc. Chem. Res.* **2008**, *41*, 569−579.

[341] a) S. Grimme, *J. Comput. Chem.* **2004**, *25*, 1463−1473; b) S. Grimme, *J. Comput. Chem.* **2006**, *27*, 1787−1799.

[342] S. Grimme, F. Neese, *J. Chem. Phys.* **2007**, *127*, 154116.

[343] S. Hirata, M. Head-Gordon, *Chem. Phys. Lett.* **1999**, *314*, 291−299.

[344] Y. Zhao, D. G. Truhlar, *Acc. Chem. Res.* **2008**, *41*, 157−167.

[345] S. Ivanov, M. Levy, *Theor. Chem. Acc.* **1999**, *103*, 117−123.

[346] E. Lieb, *Physics as Natural Philosophy: Essays in Honor of Lazlo Tisza on His 75th Birthday*, A. Shimony, H. Fesbach, MIT, Camebridge, MA, **1982**.

[347] R. Ahlrichs, S. Elliot, U. Huniar, *Modern Methods and Algorithms of Quantum Chemistry, Proceedings, Second Edition, Vol. 3* (Ed. J. Grotendorst), John von Neumann Institute for Computing, Jülich, NIC Series, **2000**.

[348] O. Vahtras, J. Almlöf, M. W. Feyereisen, *Chem. Phys. Lett.* **1993**, *213*, 514−518.

[349] H. A. Früchtl, R. A. Kendall, R. J. Harrison, K. G. Dyall, *Int. J. Quant. Chem.* **1997**, *64*, 63−69.

[350] M. Feyereisen, G. Fitzgerald, A. Komornicki, *Chem. Phys. Lett.* **1993**, *208*, 359−363.

[351] D. E. Bernholdt, R. J. Harrison, *Chem. Phys. Lett.* **1996**, *250*, 477−484.

[352] a) S. Ten-no, S. Iwata, *J. Chem. Phys.* **1996**, *105*, 3604−3611; b) S. Ten-no, S. Iwata, *Int. J. Quant. Chem. Symp.* **1996**, *30*, 107−112.

[353] A. P. Rendell, T. J. Lee, *J. Chem. Phys.* **1994**, *101*, 400−408.

[354] R. A. Kendall, H. A. Früchtl, *Theor. Chem. Acc.* **1997**, *97*, 158−163.

[355] J.-L. Rivail, D. Rinaldi, *Chem. Phys.* **1976**, *18*, 233−242.

[356] a) H. Helten, T. Schirmeister, B. Engels, *J. Phys. Chem. A* **2004**, *108*, 7691−7701; b) H. Helten, T. Schirmeister, B. Engels, *J. Org. Chem.* **2005**, *70*, 233−237; c) R. Vicik, H. Helten, T. Schirmeister, B. Engels, *ChemMedChem* **2006,**, *1*, 1021−1028.

[357] C. J. Cramer, D. G. Truhlar, *Chem. Rev.* **1999**, *99*, 2161−2200.

[358] N. Metropolis, A. W. Rosenbluth, M. N. Rosenbluth, A. H. Teller, E. Teller, *J. Chem. Phys.* **1953**, *21*, 1087−1092.

[359] B. J. Alder, T. E. Wainwright, *J. Chem. Phys.* **1957**, *57*, 1208−1209.

[360] A. Rahman, F. M. Stillinger, *J. Chem. Phys.* **1971**, *57*, 3336−3359.

[361] a) A. Ben-Naim, *Water and Aqueous Solutions*, Plenum Press, New York, **1974**; b) A. Ben-Naim, *J. Phys. Chem.* **1978**, *82*, 792−803; c) A. Ben-Naim, *Solvation Thermodynamics*, Plenum Press, New York, **1987**.

[362] J. Tomasi, M. Persico, *Chem. Rev.* **1994**, *94*, 2027−2094.

[363] S. Miertuš, E. Scrocco, J. Tomasi, *Chem. Phys.* **1981**, *55*, 117−129.

[364] S. Miertuš, J. Tomasi, *Chem. Phys.* **1982**, *65*, 239−245.

[365] J. L. Pascual-Ahuir, E. Silla, J. Tomasi, R. Bonaccorsi, *J. Comput. Chem.* **1987**, *8*, 778−787.

[366] M. A. Aguilar, F. J. Olivares del Valle, J. Tomasi, *J. Chem. Phys.* **1993**, *98*, 7375−7384.

[367] E. L. Coitiño, J. Tomasi, R. Cammi, *J. Comput. Chem.* **1995**, *16*, 20−30.

[368] H. Hoshi, M. Sakurai, Y. Inoue, R. Chûjô, *J. Chem. Phys.* **1987**, *87*, 1107−1115.

[369] H. Hoshi, M. Sakurai, Y. Inoue, R. Chûjô, *J. Mol. Struct. (Theochem)* **1988**, *180*, 267−281.

[370] B. Wang, G. P. Ford, *J. Chem. Phys.* **1992**, *97*, 4162−4169.

[371] a) M. L. Drummond, *J. Chem. Phys.* **1988**, *88*, 5014−5020; M. L. Drummond, *J. Chem. Phys.* **1988**, *88*, 5021−5026.

[372] a) R. J. Zauhar, R. S. Morgan, *J. Mol. Biol.* **1985**, *186*, 815−820; b) R. J. Zauhar, R. S. Morgan, *J. Comput. Chem.* **1990**, *11*, 603−622; c) R. J. Zauhar, *J. Comput. Chem.* **1991**, *12*, 575−583; d) T. Fox, N. Rösch, R. J. Zauhar, *J. Comput. Chem.* **1993**, *14*, 253−262.

[373] J. A. Grant, R. L. Williams, H. A. Scheraga, *Biopolymers* **1990**, *30*, 929−949.

[374] a) A. Klamt, *J. Phys. Chem.* **1995**, *99*, 2224−2235; b) A. Klamt, V. J. Jonas, *J. Chem. Phys.* **1996**, *105*, 9972−9981.

[375] S. Yomosa, *J. Phys. Soc. Jpn.* **1974**, *36*, 1655−1660.

[376] a) C. J. F. Böttcher, *Theory of Electric Polarization, Vol. I*, Elsevier, Amsterdam, **1973**; b) C. J. F. Böttcher, *Theory of Electric Polarization, Vol. II*, Elsevier, Amsterdam, **1978**.

[377] J. Langlet, P. Claverie, J. Caillet, A. Pullman, *J. Phys. Chem.* **1988**, *92*, 1617−1631.

[378] J. G. Kirkwood, *Theory of Liquids* (Ed.: B. J. Alder), Gordon and Breach, New York, **1968**.

[379] A. A. Rashin, M. A. Bukatin, J. Andzelm, A. T. Hagler, *Biophys. Chem.* **1994**, *51*, 375−392.

[380] a) F. J. Olivares del Valle, J. Tomasi, *Chem. Phys.* **1991**, *150*, 139−150; b) F. J. Olivares del Valle, R. Bonaccorsi, R. Cammi, J. Tomasi, *J. Mol. Struct. (Theochem.)* **1991**, *230*, 295−312; c) F. J. Olivares del Valle, M. A. Aguilar, *J. Comput. Chem.* **1992**, *13*, 115−134; d) F. J. Olivares del Valle, M. A. Aguilar, S. Tolosa, *J. Mol. Struct. (Theochem.)* **1993**, *279*, 223−231; e) F. J. Olivares del Valle, M. A. Aguilar, *J. Mol. Struct. (Theochem.)* **1993**, *280*, 25−47.

[381] a) J. G. Ángyán, *Int. J. Quantum Chem.* **1993**, *47*, 469−483; b) J. G. Ángyán, *Chem. Phys. Lett.* **1995**, *241*, 51−56.

[382] M. W. Wong, M. J. Frisch, K. B. Wiberg, *J. Am. Chem. Soc.* **1991**, *113*, 4776−4482.

[383] J.-L. Rivail, *Compt. Rend. Acad. Sci. Paris* **1990**, *311*, 307.

[384] A. Fortunelli, *J. Mol. Struct. (Theochem.)* **1995**, *357*, 117−124.

[385] O. Tapia, E. Poulain, F. Sussman, *Theor. Chim. Acta* **1978**, *47*, 171−174.

[386] M. A. Aguilar, F. J. Olivares del Valle, J. Tomasi, *J. Chem. Phys.* **1993**, *98*, 7375−7384.

[387] M. Persico, J. Tomasi, *Croat. Chem. Acta* **1984**, *57*, 1395.

[388] E. L. Coitiño, J. Tomasi, O. N. Ventura, *J. Chem. Soc., Faraday Trans.* **1994**, *90*, 1745−1755.

[389] A. Bernhardsson, R. Lindh, G. Karlström, B. O. Roos, *Chem. Phys. Lett.* **1996**, *251*, 141−149.

[390] a) K. V. Mikkelsen, H. Ågren end H. J. A. Jensen, T. Helgaker, *J. Chem. Phys.* **1988**, *89*, 3086−3095; b) K. V. Mikkelsen, P. Jørgensen, H. J. A. Fensen, *J. Chem. Phys.* **1994**, *100*, 6597−6607; c) O. Christiansen, K. V. Mikkelsen, *J. Chem. Phys.* **1999**, *110*, 1365−1375.

[391] M. Reguero, R. R. Pappalardo, M. A. Robb, H. S. Rzepa, *J. Chem. Soc., Perkin Trans. 2* **1993**, 1499−1502.

[392] a) C. J. Cramer, D. G. Truhlar, *J. Am. Chem. Soc.* **1991**, *113*, 8305−8311; b) C. J. Cramer, D. G. Truhlar, *Science* **1992**, *256*, 213−217; c) C. J. Cramer, D. G. Truhlar, *J. Comput. Chem.* **1992**, *13*, 1089−1097; d) C. J. Cramer, D. G. Truhlar, *J. Comput.-Aid. Mol. Des.* **1992**, *6*, 629−666.

[393] a) D. D. Perrin, W. L. F. Armarego, D. R. Perrin, *Purification of Laboratory Chemicals*, Pergamon Press, Oxford, **1988**; b) Autorenkollektiv, *Organikum*, 20th ed., VEB Deutscher Verlag der Wissenschaften, Berlin, **1996**.

[394] a) Collect data collection software, Nonius B.V., **1999**; b) Z. Otwinoski, W. Minor in *Processing of X-ray Diffraction Data Collected in Oscillation Mode, Methods in Enzymology, Vol. 276: Macromolecular Crystallography, Part A* (Eds.: C. W. Carter, Jr., R. M. Sweet), Academic Press, **1997**, p. 307−326.

[395] SHELXS-97, G. M. Sheldrick, *Acta Crystallogr., Sect. A* **1990**, *46*, 467−473.

[396] G. M. Sheldrick, *Acta Crystallogr., Sect. A* **2008**, *64*, 112−122.

[397] SHELXL-97, G. M. Sheldrick, University of Göttingen, **1997**.

[398] H. Meerwein, G. Hinz, P. Hofmann, E. Kroning, E. Pfeil, *J. prakt. Chem.* **1937**, *147*, 257−285.

[399] R. Sanders, U. T. Mueller-Westerhoff, *J. Organomet. Chem.* **1996**, *512*, 219−224.

[400] I. R. Butler, W. R. Cullen, J. Ni, S. J. Rettig, *Organometallics* **1985**, *4*, 2196−2201.

[401] G. M. Bodner, S. B. Kahl, K. Bork, B. N. Storhoff, J. E. Wuller, L. J. Todd, *Inorg. Chem.* **1973**, *12*, 1071−1074.

[402] K. H. Dötz, *Chem. Ber.* **1980**, *113*, 3597−3604.

[403] E. O. Fischer, H. J. Kollmeier, *Chem. Ber.* **1971**, *104*, 1339−1346.

[404] J. A. Connor, E. M. Jones, *J. Chem. Soc. A* **1971**, 1974−1979.

[405] S. B. Harkins, J. C. Peters, *J. Am. Chem. Soc.* **2004**, *126*, 2885−2893.

[406] Patricia Panne, Ph.D. Thesis, University of Cologne, **2004**.

[407] A. N. Nesmeyanov, E. G. Perevalova, L. P. Yuryeva, K. I. Grandberg, *Izv. Akad. Nauk SSSR, Ser. Khim.* **1962**, 1772−1777.

[408] a) A. G. Massey, A. J. Park, F. G. A. Stone, *Proc. Chem. Soc. London* **1963**, 212; b) A. G. Massey, A. J. Park, *J. Organomet. Chem.* **1964**, *2*, 245−250.

[409] H. D. Flack, *Acta Crystallorg. Sect. A* **1983**, *39*, 876−881.

Appendix A

List of Abbreviations and Symbols

Å	Ångstrøm
abs.	absorbance
Ad	1-adamantyl
Ar	aryl
ASC	apparent surface charge
au	atomic units
aug	augmented
ax	axial
B2PLYP	double-hybrid density functional by Grimme
B3	three parameter hybrid functional by Becke
B3LYP	combination of Becke's three parameter hybrid functional and the correlation functional by Lee, Yang, and Parr
B88	gradient corrected exchange functional by Becke
BEM	boundary element method
BLYP	combination of the local Slater-Dirac exchange functional, Becke's gradient corrected exchange functional B88, and the correlation functional by Lee, Yang, and Parr
bp	boiling point
BP86	combination of the local Slater-Dirac exchange functional, the correlation functional by Vosko, Wilk, and Nusair (VWN (V)), Becke's gradient corrected exchange functional B88, and the gradient corrected correlation functional by Perdew (P86)
br	broad
°C	grad Celsius
calcd.	calculated

cat.	catalyst or catalytic amount
CCSD	coupled cluster with singles and doubles
cf.	compare
CID	collision-induced dissociation
COSMO	conductor-like screening model
COSY	correlation spectroscopy
Cp	2,4-cyclopentadien-1-yl or η^5-cyclopentadienyl/cyclopentadienide
Cp*	1,2,3,4,5-pentamethyl-2,4-cyclopentadien-1-yl
CPE	conjugated polyelectrolyte
CV	cyclic voltammetry or cyclic voltammogram
Cy	cyclohexyl
d	day(s) or doublet (NMR) or distance
d_{sat}	doublet with satellites (NMR)
δ	chemical shift
decomp.	decomposition
DEPT	distorsionless enhancement by polarisation transfer
dev.	deviation
DFT	density functional theory
DFT-D	density functional theory including dispersion correction by Grimme
DHDF	double-hybrid density functional
Dipp	2,6-diisopropylphenyl
DMAD	dimethyl acetylenedicarboxylate
DPPE	1,2-bis(diphenylphosphino)ethane
Δx	difference $x_2 - x_1$
E	electrode potential
$E_{1/2}$	half cell potential
E_{pa}	anodic peak potential
E_{pc}	cathodic peak potential
ϵ	molar absorbance coefficient
ε	relative permittivity or orbital energy
ECP	effective core potential
ed.	edition
Ed.	editor
Eds.	editors
EI	electron ionization / electron impact
eq	equatorial
Eq(s).	equation(s)
equiv.	equivalent(s)
ESI$^+$	electrospray ionization (positive mode)

Et	ethyl
ET	electron transfer
F	Faraday constant
FAB$^+$	fast atom bombardement (positive mode)
Fc	ferrocenyl
Fig.	figure
FT	fourier transformation
g	gram
G	Gibbs free energy
GCE	glassy carbon electrode
GGA	general gradient approximation
gs	gradient selected
h	hour(s)
$h_{1/2}$	full width at half maximum
H	enthalpy
$\{^1\text{H}\}$	^{1}H broad band decoupled
η	hapto; specifies coordinating carbon atom(s)
HE	high-energy
HMBC	heteronuclear multiple bond correlation
HMQC	heteronuclear multiple quantum coherence
HOMO	highest occupied molecular obital
HR	high resolution
HSQC	heteronuclear single quantum coherence
Hz	Hertz
i_{pa}	anodic peak current
i_{pc}	cathodic peak current
ICT	intramolecular charge transfer
IEF	integral equation formalism
INEPT	insensitive nuclei enhanced by polarisation transfer
i-Pr / ^{i}Pr	isopropyl
IR	infrared (spectroscopy)
J	Joule
$\lvert^x J_{AB}\rvert$	magnitude of coupling constant of nuclei A and B over x bonds
k	kilo or rate constant
K	Kelvin
κ	specifies coordinating atom(s)
L	liter
λ	wavelength or specifier of bonding number
LanL2DZ	Los Alamos effective core potential plus double-ζ basis set DZ

LDA	local density approximation
LE	low-energy
LMCT	ligand−metal charge transfer
LSDA	local spin density approximation
LUMO	lowest unoccupied molecular obital
LYP	gradient corrected correlation functional by Lee, Yang, and Parr
m	meter or medium (IR)
m_c	multiplet (centered) (NMR)
M	metal or mega or $mol \cdot L^{-1}$
$[M]^+$	molecule radical cation
μ	micro
M05	density functional by Truhlar
M06	density functional by Truhlar
$MALDI^+$	matrix-assisted laser desorption/ionization (positive mode)
MCSCF	multi-configurational self-consistent field
MD	molecular dynamics
Me	methyl
Mes	mesityl
Mes*	2,4,6-tris(*tert*-butyl)phenyl
min	minute(s)
MLCT	metal−ligand charge transfer
*m*NBA	*meta*-nitrobenzyl alcohol
mol	mole
mp	melting point
MP2	Møller-Plesset perturbation theory second order
MS	mass spectrometry
m/z	mass charge ratio
n	nano
$\tilde{\nu}$	wavenumber
NBO	natural bond orbital population analysis
n-Bu / ^{n}Bu	*n*-butyl
NHC	*N*-heterocyclic carbene
NImag	number of imaginary frequencies
NMR	nuclear magnetic resonance (spectroscopy)
No.	number
NOESY	Nuclear Overhauser enhancement correlation spectroscopy
OLED	organic light-emitting diode
p	pico
p.	page

P86	gradient corrected correlation functional by Perdew
PCM	polarizable continuum model
PET	photoinduced electron transfer
Ph	phenyl
pip	1-piperidino
ppm	parts per million
PW86	gradient corrected exchange functional by Perdew and Wang (1986)
PW91	gradient corrected correlation functional by Perdew and Wang (1991)
Py	pyridine
R	common organic substituent
RI	resolution of the identity
r.t.	room temperature
s	second(s) or singlet (NMR) or strong (IR)
s_{sat}	singlet with satellites (NMR)
σ	specifies coordination number
SCE	standard calomel electrode
SCF	self-consistent field
SCRF	self-consistent Reaction field
SET	single-electron transfer
sh	sharp (IR) or shoulder (UV/Vis)
SOMO	singly occupied molecular orbital
SVP	split valence shell basis set by Ahlrichs and coworkers including polarization functions for hydrogen atoms
SV(P)	split valence shell basis set by Ahlrichs and coworkers
t	triplet (NMR)
t_{sat}	triplet with satellites (NMR)
T	temperature
Tab.	table
TBAF	tetra-n-butylammonium fluoride
t-Bu / ^{t}Bu	$tert$-butyl
TCA	trichloroacetic acid
TCNE	tetracyanoethylene
TDA	Tamm-Dancoff approximation
TD-DFT	time-dependent density functional theory
Tf	trifluoromethanesulfonyl
TFA	trifluoroacetic acid
TFD	Thomas-Fermi-Dirac theory
Th	2-thienyl
THF / thf	tetrahydrofuran

TMEDA	N,N,N',N'-tetramethyl-1,2-ethanediamine
TMS	tetramethylsilane
TOF	time of flight
TRIM	trust radius image minimization algorithm
TZ2P	valence-triple-ζ basis set by Baerends and coworkers
TZVP	valence-triple-ζ basis set by Ahlrichs and coworkers
UV/Vis	ultraviolet/visual (spectroscopy)
Vol.	volume
vs	very strong (IR)
vs.	versus
vw	very weak (IR)
VWN	correlation functional by Vosko, Wilk, and Nusair
w	weak (IR)
ZORA	zeroth order regular approximation to the Dirac equation
6-311G(d,p)	valence-triple-ζ basis set by Pople and coworkers
6-31G(d)	valence-double-ζ basis set by Pople and coworkers
$\circ$	grad

Appendix B

Details on TD-DFT Calculations

Time-Dependent DFT (TD-DFT)[294, 295] calculations were carried out with the TUR-BOMOLE V5.8 program package.[206] If not otherwise denoted, "approach I" was employed, which means, calculations of vertical singlet excitations were done using the B3LYP[230, 231] density functional in combination with the SV(P)[212] basis set and effective core potential ECP-60-MWB[213] for the core electrons of tungsten on geometries obtained at the RI-BLYP[209, 211, 231]/SV(P)[212]/ECP-60-MWB(W)[213] level of theory. Stationary points were characterized as minima by analytical vibrational frequencies calculations.[217]

In order to check the reliability of the results obtained using approach I, additionally, two further methods, II and III, were applied for complex **41h** (Tab. B.1), the latter as a good case in point. Approach II was chosen to get an estimate for the error that is made by applying different density functionals for geometry optimization and TD-DFT single point calculation, respectively (BLYP and B3LYP, which is done by approach I). Here, geometry optimization was carried out also on the B3LYP/SV(P)/ECP-60-MWB(W) level. Comparison of the results obtained with both methods reveals that the differences both in ocsillator strengths and wavenumbers ($\Delta \tilde{\nu} < 650$ cm^{-1}) are rather small, whereas all wavenumbers predicted by method I are somewhat larger. The respective contributions of the different molecular orbitals to each excitation agree for both methods qualitatively and, to a large extend, also quantitatively. Approach III may be considered as a higher benchmark. Here, the B3LYP functional in combination with a larger basis set, the valence-triple-ζ basis TZVP[218] (and ECP-60-MWB for W), was employed for treatment of electronic excitations of **41h** on the geometry optimized using B3LYP/SV(P)/ECP-60-MWB(W). Compared to method I, all excitation energies are slightly larger, but the differences are below 500 cm^{-1}, and the oscillator strengths predicted with the two approaches are in good agreement as well.

Moreover, the qualitative pictures derived from an analysis of the contributing molecular orbitals are almost identical. The only difference is a switch of HOMO−4 and HOMO−5 as an effect of the basis: for example, using methods I and II the major contribution to transition No. 4 is provided by HOMO−4, while in the case of method III it is the HOMO−5. The reason for that is just a shift in the ordering of orbital energies. In other words, HOMO−5 generated by method III has a similar shape, and thus, may be regarded as equivalent to HOMO−4 obtained with methods I and II, and vice versa.

Table B.1: Vertical singlet excitations for complex **41h** calculated with three different methods I–III (only the major orbital contributions given).

No.	$\tilde{\nu}$ [cm^{-1}]	λ [nm]	Oscillator strength	Orbital contributions			$|c|^2$ [%]
(I) TD-B3LYP/SV(P)/ECP-60-MWB(W) // RI-BLYP/SV(P)/ECP-60-MWB(W)							
2	20295	493	0.0244	**HOMO−1**	→	**LUMO**	98
4	26636	375	0.0190	**HOMO−4**	→	**LUMO**	41
				HOMO−3	→	**LUMO**	32
				HOMO−5	→	**LUMO**	22
10	30064	333	0.2194	**HOMO−3**	→	**LUMO**	58
				HOMO−4	→	**LUMO**	16
(II) TD-B3LYP/SV(P)/ECP-60-MWB(W) // B3LYP/SV(P)/ECP-60-MWB(W)							
2	20461	489	0.0252	**HOMO−1**	→	**LUMO**	98
4	27057	370	0.0155	**HOMO−4**	→	**LUMO**	54
				HOMO−3	→	**LUMO**	33
				HOMO−5	→	**LUMO**	8
10	30692	326	0.2119	**HOMO−3**	→	**LUMO**	57
				HOMO−4	→	**LUMO**	20
(III) TD-B3LYP/TZVP/ECP-60-MWB(W) // B3LYP/SV(P)/ECP-60-MWB(W)							
2	20591	486	0.0250	**HOMO−1**	→	**LUMO**	97
4	27110	369	0.0209	**HOMO−5**	→	**LUMO**	48
				HOMO−3	→	**LUMO**	34
				HOMO−4	→	**LUMO**	13
10	30283	330	0.2074	**HOMO−3**	→	**LUMO**	55
				HOMO−5	→	**LUMO**	18

Selected molecular orbitals (method I) of κP-complexes **41h** and **126h** are displayed in Figures B.1 and B.2, and for complex **126h** the most intense electronic transitions calculated with method I are given in Table B.2; data are plotted in Figure B.3 in

comparison to the UV/Vis spectrum of the mixture of **126h** and **131h**.
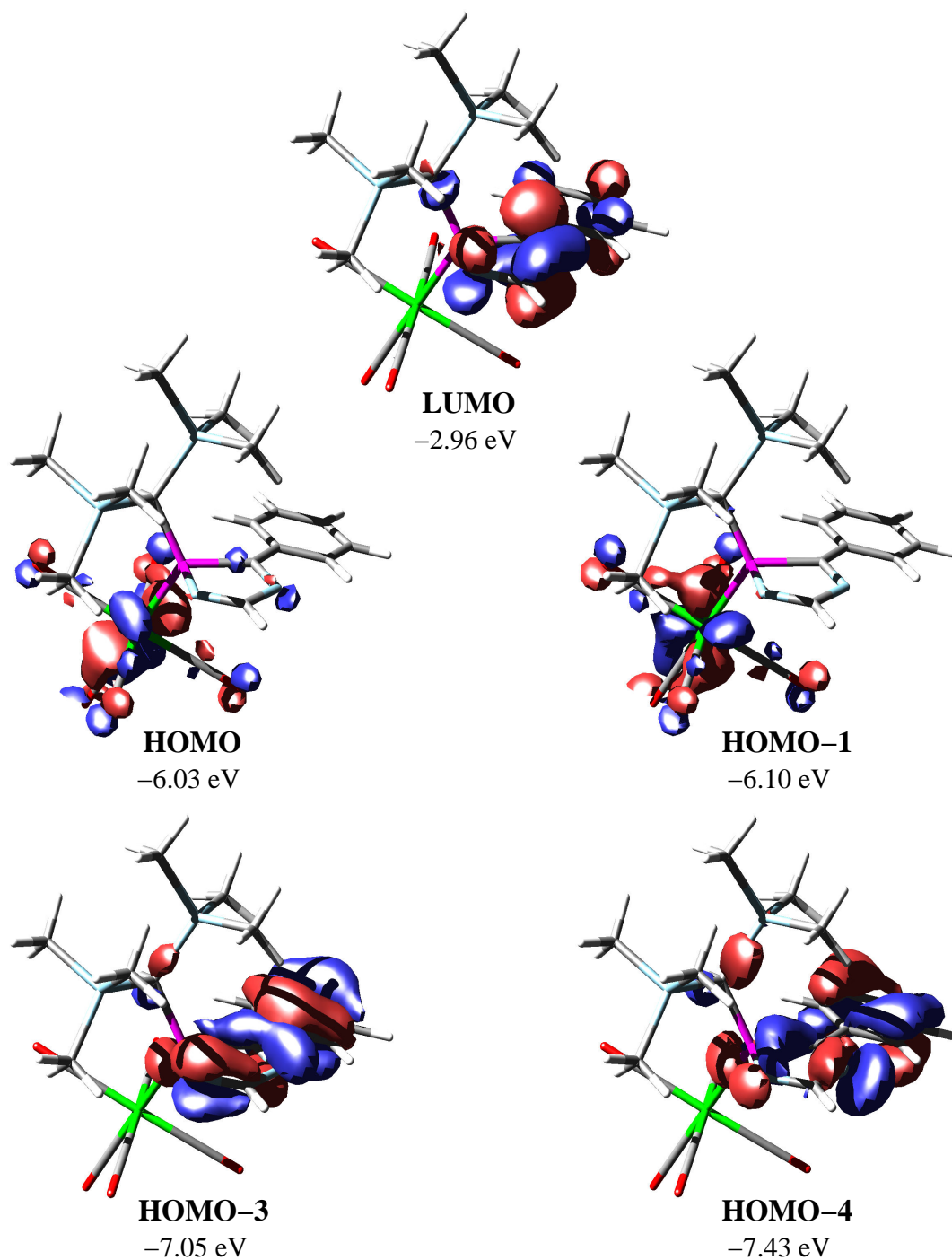
Figure B.1: Visualization of selected molecular orbitals calculated for complex **41h** (B3LYP/SV(P)/ECP-60-MWB(W)//RI-BLYP/SV(P)/ECP-60-MWB(W); isovalue 0.04 au).
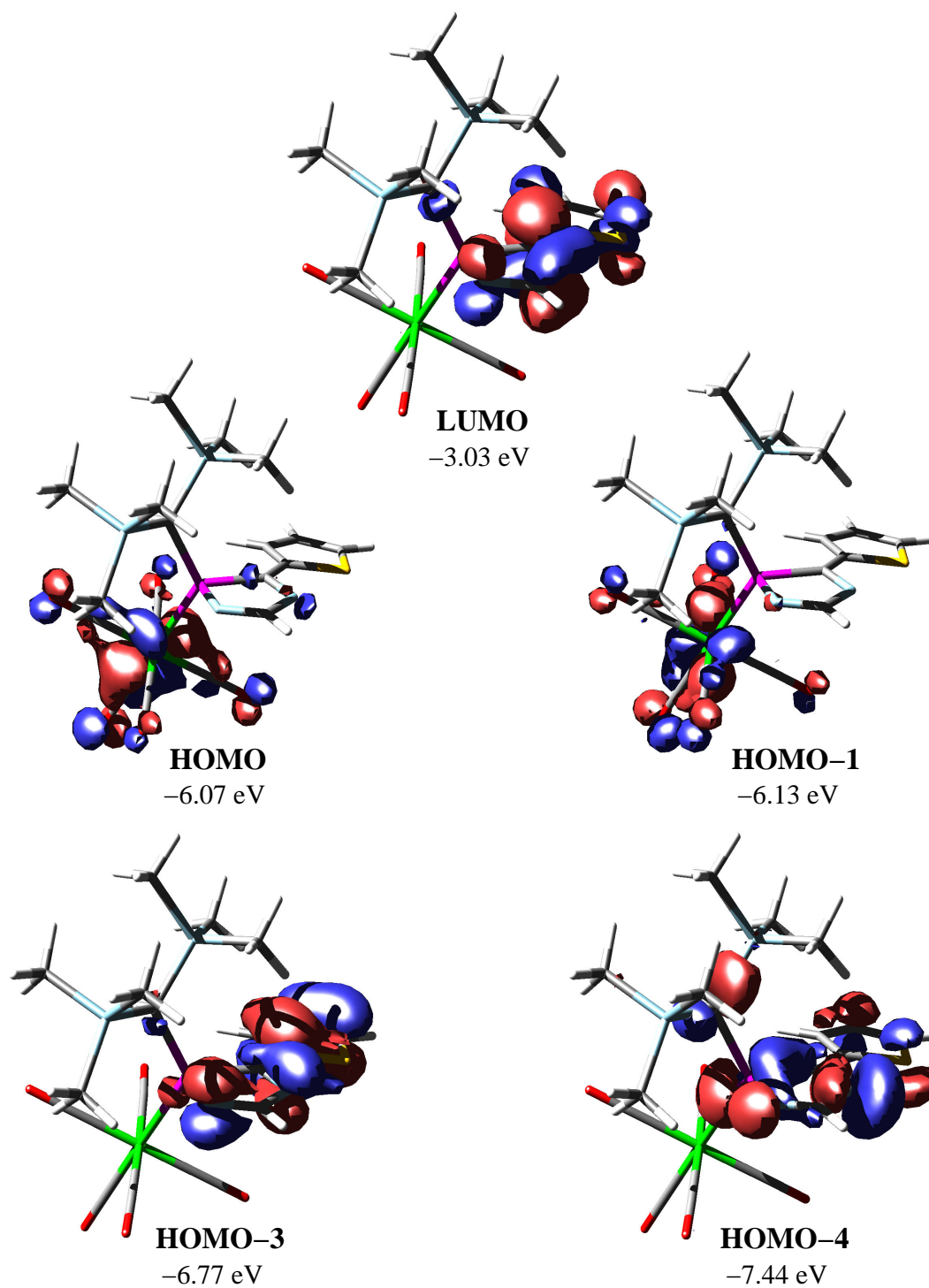
Figure B.2:   Visualization of selected molecular orbitals calculated for complex
126h (B3LYP/SV(P)/ECP-60-MWB(W)//RI-BLYP/SV(P)/ECP-60-MWB(W); iso-
value 0.04 au).

For both complexes **41h** and **126h** the lowest-lying transitions having considerable oscillator strengths occur from HOMO−1 to the LUMO and constitute MLCT processes, since HOMO−1 corresponds to a metal d orbital and the LUMO is of π type.

Table B.2: Calculated vertical singlet excitations for complex **126h** (TD-B3LYP/SV(P)/ ECP-60-MWB(W)//RI-BLYP/SV(P)/ECP-60-MWB(W)). Only the major orbital contributions are given.

No.	$\tilde{\nu}$ [cm^{-1}]	λ [nm]	Oscillator strength	Orbital contributions			$|c|^2$ [%]
2	20015	500	0.0215	**HOMO−1**	$\rightarrow$	**LUMO**	96
4	26335	380	0.0851	**HOMO−4**	$\rightarrow$	**LUMO**	45
				HOMO−3	$\rightarrow$	**LUMO**	44
7	28005	357	0.1678	**HOMO−3**	$\rightarrow$	**LUMO**	39
				HOMO−4	$\rightarrow$	**LUMO**	32

Two further excitations are worth mentioning: i) The absorption No. 4 in both cases and ii) the absorptions No. 10 (**41h**) and No. 7 (**126h**), respectively. Both are characterized by contributions of HOMO−3 and HOMO−4 to the initial state, and the excitation occurs to the LUMO. The HOMO−3 is clearly identified as a π orbital delocalized over the two conjugated rings in both cases. Also HOMO−4 exhibits π characteristics, but, additionally, a considerable contribution of the nitrogen lone pairs (especially of N^4), which is significantly more pronounced for complex **126h**. As these orbitals contribute to both excitations at almost equal ratios, none of the latter can be classified exclusively either as $\pi-\pi^*$ or as $n-\pi^*$ transition. Comparison of the experimental spectrum of **126h** and **131h** with the data calculated for complex **126h** reveals that the absorption maximum at $\tilde{\nu}_{max} = 28800$ cm^{-1} may result from a superposition of the two excitations.
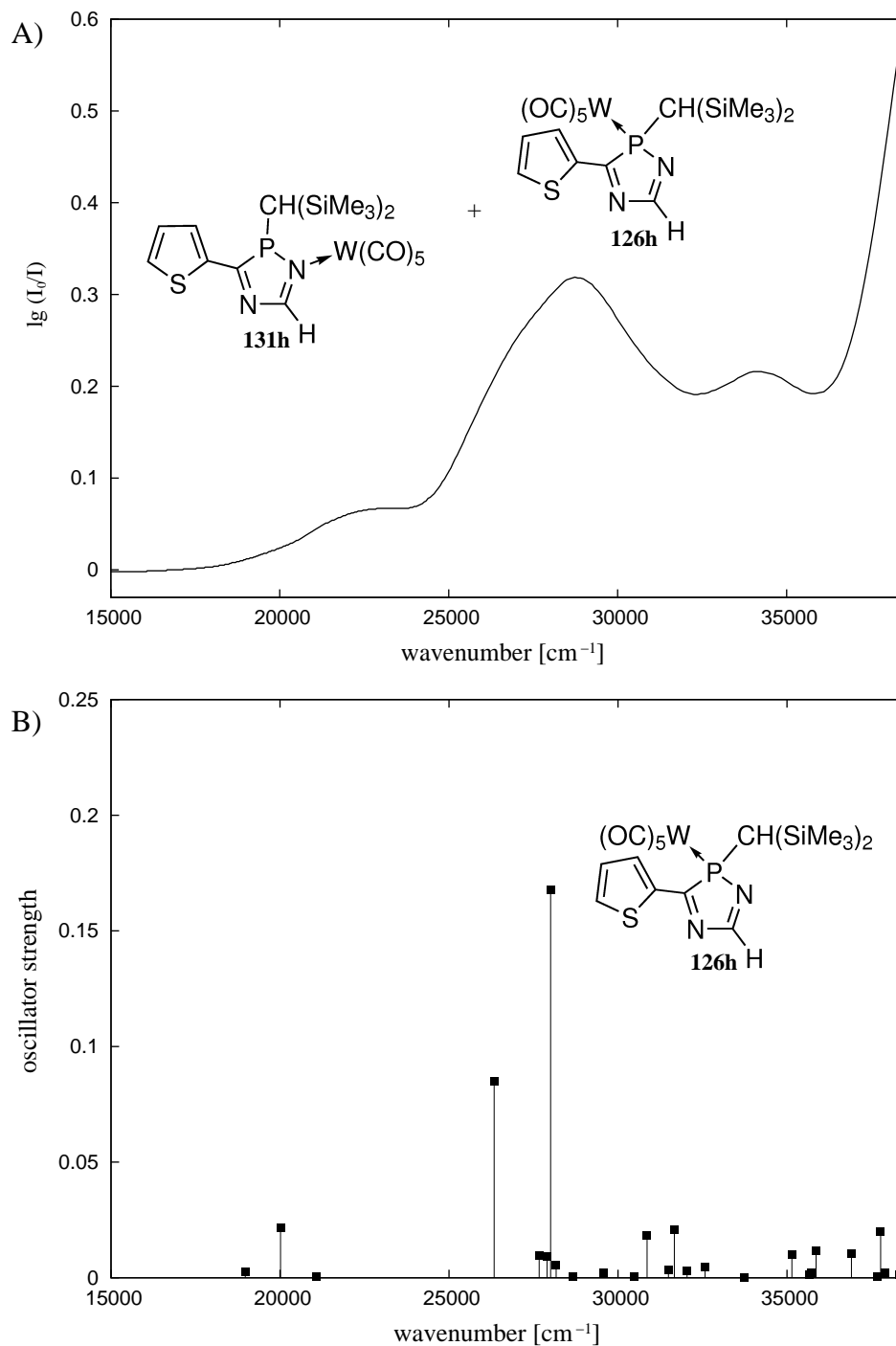
Figure B.3: A) UV/Vis spectrum of a mixture of complexes **126h** and **131h** (*n*-pentane). B) Calculated vertical singlet excitations for complex **126h** (TD-B3LYP/SV(P)/ECP-60-MWB(W)//RI-BLYP/SV(P)/ECP-60-MWB(W)).

Appendix C

Spectroscopic Data for $2H$-1,4,2-Diazaphosphole Derivatives

In Tables C.1 and C.2 selected $^{13}C\{^1H\}$ NMR and IR spectroscopic data of $2H$-1,4,2-diazaphosphole derivatives displayed in Figure C.1 are compiled for comparison.

41b,g,h,m,r–t, 69b,h,l, 74b
75b, 122b, 126b,g,h, 172b, 190

123b, 124b, 171b

189

129h, 130h, 131h

147b

50b,h, 193h

M = W; **74**: M = Mo; **75**: M = Cr   R = NMe₂ (**b**), Ph (**c**), 2-thienyl (**g**), H (**h**), Fc (**l**),
                                         CH₃ (**m**), ^{t}Bu (**r**),1-adamantyl (**s**), SiMe₃ (**t**)

41, 69, 74, 75, 126: R' = CH(SiMe₃)₂	**41, 50, 74, 75, 122, 129, 172**: R'' = Ph
122: R' = Cp*	**69, 130**: R'' = Fc
172: R' = CH₂SiMe₃	**126, 131, 190, 193**: R'' = thienyl
190: R' = CH₃	
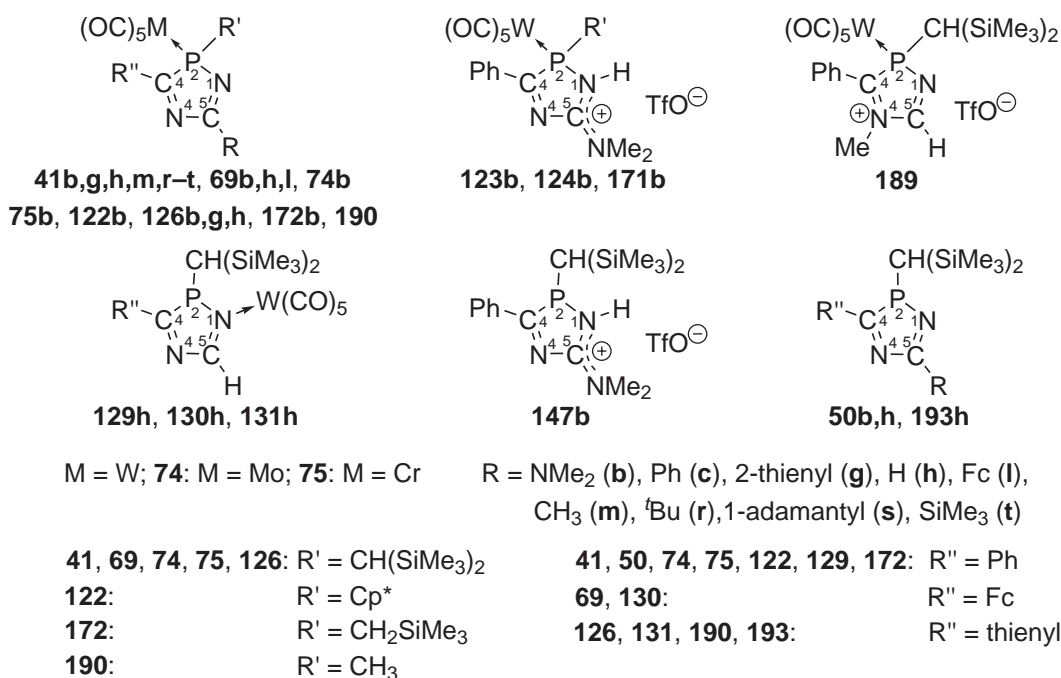
Figure C.1: $2H$-1,4,2-Diazaphosphole and $2H$-1,4,2-diazaphosphole complex derivatives.

Table C.1: Comparison of $^{13}\text{C}\{^1\text{H}\}$ NMR spectroscopic data for 2*H*-1,4,2-diazaphosphole derivatives presented in this work (see Fig. C.1 for atom numbering).

No.	δ_{C^3}	$\lvert^{1+4}J_{PC^3}\rvert$ [Hz]	δ_{C^5}	$\lvert^{2+3}J_{PC^5}\rvert$ [Hz]	$\delta^{\ddagger}_{C\text{exo}}$	$\lvert^1 J_{PC^e}\rvert$ [Hz]	$\delta_C(\text{CO}_{cis})$	$\lvert^2 J_{PC^c}\rvert$ [Hz]	$\lvert^1 J_{WC^c}\rvert$ [Hz]	$\delta_C(\text{CO}_{trans})$	$\lvert^2 J_{PC^t}\rvert$ [Hz]	$\lvert^1 J_{WC^t}\rvert$ [Hz]
41b	200.3	25.5	165.0	–	22.0	5.8	198.6	6.5	126.7	199.6	22.3	143.2
41g	202.3	23.3	165.2	4.2	19.1	4.8	197.6	6.1	126.7	198.3	22.3	144.2
41h	203.0	22.0	162.7	7.8	17.3	3.9	197.5	5.8	126.6	197.7	22.6	144.7
41m	202.1	22.6	174.0	7.1	17.6	4.2	197.7	6.1	126.9	198.2	22.3	144.0
41r	201.2	23.3	182.9	8.4	17.8	4.2	197.7	6.1	126.4	198.3	22.3	144.5
41s	201.0	23.3	182.2	8.4	17.7	4.2	197.8	5.8	126.7	198.4	22.3	144.8
41t	199.4	19.1	188.5	15.2	17.0	5.8	197.8	5.8	126.7	198.2	22.0	*
50b	210.6	52.4	167.4	1.1	18.6	56.9	–	–	–	–	–	–
50h	199.3	44.6	162.2	3.6	18.8	45.9	–	–	–	–	–	–
69b	206.5	26.8	165.0	–	25.2	10.0	198.5	6.5	126.6	199.8	22.0	143.5
69h	210.1	22.3	161.7	8.1	17.9	9.4	197.2	6.1	126.7	198.1	22.3	*
69l	206.6	27.5	175.1	5.8	23.7	5.2	197.9	6.1	126.4	198.6	22.0	*
74b	201.3	29.7	164.7	0.7	21.4	11.6	206.5	8.4	–	211.1	23.0	–
75b	200.5	31.7	163.7	0.8	22.5	9.7	217.4	12.6	–	222.0	6.8	–
122b	199.3	24.6	166.3	3.6	63.9	1.3	197.4	6.5	126.2	198.3	25.2	*
123b†	196.9	3.2	162.4	10.3	21.9	16.5	195.9	5.8	127.4	196.8	27.5	142.0
124b†	193.6	1.3	161.0	8.1	66.3	*	194.7	6.1	126.7	195.9	29.7	*

349

No.	δ_{C^3}	$\|^{1+4}J_{PC^3}\|$ [Hz]	δ_{C^5}	$\|^{2+3}J_{PC^5}\|$ [Hz]	$\delta_{C^{exo}}^{\ddagger}$	$\|^1J_{PC^e}\|$ [Hz]	$\delta_C(CO_{cis})$	$\|J_{PC^c}\|$ [Hz]	$\|^1J_{WC^c}\|$ [Hz]	$\delta_C(CO_{trans})$	$\|J_{PC^t}\|$ [Hz]	$\|^1J_{WC^t}\|$ [Hz]
126b	193.3	25.2	165.1	0.6	23.2	5.8	198.5	6.8	126.7	199.7	22.3	142.9
126g	195.2	22.3	165.5	5.5	20.0	4.8	197.6	6.1	126.7	198.4	22.6	143.5
126h	195.7	21.1	162.9	9.2	18.1	3.4	197.4	6.1	126.9	197.8	23.0	144.2
129h	208.5	35.5	170.3	14.2	17.9	55.0	198.4	2.7	129.8	201.0	1.7	*
130h	215.4	38.5	171.4	12.0	16.9	56.3	198.2	3.2	130.0	201.4	1.9	149.5
131h	199.5	35.9	171.0	12.0	17.9	56.6	198.3	2.9	*	201.0	1.9	*
147b	211.8	40.4	165.9	0.4	21.1	63.7	–	–	–	–	–	–
171b[†]	197.0	~16	162.6	*	26.6	*	*	*	*	*	*	*
172b	200.6	15.5	166.1	0.3	23.9	12.3	197.4	7.1	125.8	200.2	21.7	144.7
189	203.1	9.7	151.5	13.7	17.2	11.9	193.9	6.1	126.4	195.2	23.4	*
190	195.0	8.7	165.5	10.3	17.7	24.9	195.3	6.5	125.1	198.1	23.3	145.5
193h	199.3	44.6	162.2	3.6	18.8	45.9	–	–	–	–	–	–

All data recorded in C_6D_6 solution, except for [†] recorded in CD_2Cl_2 solution.

[‡]Exocyclic P-bonded carbon. *Not resolved.

Table C.2: Comparison of IR spectroscopic data for $2H$-1,4,2-diazaphosphole complexes presented in this work (Fig. C.1).

No.	A_1(CO) [cm^{-1}]	B_1(CO) [cm^{-1}]	E /A_1(CO) [cm^{-1}]	ν(CN) [cm^{-1}]	ν(thienyl) [cm^{-1}]
41b	2068	1980	1946, 1923, 1913	1606, 1539	–
41g	2073	2001	1924, 1908	1566, 1560	1253
41h[†]	2072	1985	1940, 1924, 1912	1705, 1557	–
41m	2071	1982	1952, 1930	1597, 1568	–
41r	2070	1981	1935, 1920	1568	–
41s	2072	1996	1948, 1927	1562	–
41t	2072	2000	1949		–
69b	2071	1991	1950, 1928, 1906	1602, 1550	–
69l	2067	1979	1947, 1927, 1921	1556, 1506	–
74b	2070	1988	1952, 1929, 1919	1604, 1538	–
75b	2059	1981	1927, 1917	1606, 1538	–
122b	2067	1988	1945, 1917, 1914	1605	–
123b	2079	2001	1956, 1940, 1922	1658, 1598	–
123b[†]	2079	1997	1950	1660, 1598	–
123m	2078	2004	1961, 1949, 1935	1659	–
124b	2080	1997	1943	1659, 1517	–
126b	2066	1976	1942, 1929, 1906	1604, 1540	1262, 1251
126g	2069	1977	1935, 1925	1557, 1545	1261
126h	2070	1983	1944, 1924, 1917	1553, 1518	1254
172b	2070	1982	1954, 1946, 1934, 1915, 1900	1609, 1598, 1543	– –
190	2077	1989	1923	1554, 1513	1262

All data recorded as KBr pellets, except for [†]recorded in CH$_2$Cl$_2$ solution.

Appendix D

Structural Data for $2H$-1,4,2-Diazaphosphole Complexes

In the following tables, selected structural data of $2H$-1,4,2-diazaphosphole complexes displayed in Figure D.1, which were determined by single-crystal X-ray diffractometry are compiled for comparison.
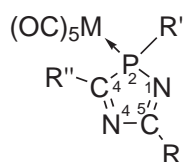
41b,g,h,s
69b,l, 74b, 75b
126b,g,h
172b, 190

M = W
74: M = Mo
75: M = Cr
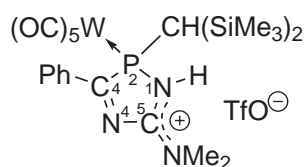
R = NMe$_2$ (**b**), 2-thienyl (**g**), H (**h**), Fc (**l**), 1-adamantyl (**s**)

41, **69**, **74**, **75**, **126**: R' = CH(SiMe$_3$)$_2$
172:   R' = CH$_2$SiMe$_3$
190:   R' = CH$_3$

41, **74**, **75**, **172**: R'' = Ph
69:   R'' = Fc
126, **190**:   R'' = thienyl

Figure D.1: Structurally characterized $2H$-1,4,2-diazaphosphole complexes.

Table D.1: Comparison of bond distances [Å] for 2*H*-1,4,2-diazaphosphole complexes presented in this work (see Fig. D.1 for atom numbering).

No.	P–M	P–C^{e†}	P–C^3	C^3–N^4	N^4–C^5	C^5–N^1	N^1–P	C^5–E^{e‡}	C^3–C^{ar}	M–CO^{tr}	M–CO$^{cis\sharp}$
41b	2.5340(14)	1.838(5)	1.884(5)	1.294(6)	1.429(7)	1.312(8)	1.682(4)	1.333(8)	1.467(8)	1.989(5)	2.042
41g	2.5306(10)	1.835(3)	1.877(4)	1.304(5)	1.424(5)	1.293(5)	1.707(3)	1.441(5)	1.457(6)	2.008(4)	2.046
41h	2.5362(10)	1.819(3)	1.861(4)	1.296(4)	1.408(5)	1.280(5)	1.715(3)	–	1.472(5)	1.996(5)	2.045
41s	2.5296(15)	1.827(4)	1.875(4)	1.295(5)	1.445(5)	1.281(4)	1.704(4)	1.500(5)	1.462(5)	1.997(4)	2.053
69b	2.5359(8)	1.849(3)	1.859(3)	1.292(4)	1.443(4)	1.307(4)	1.683(3)	1.337(4)	1.452(4)	2.000(4)	2.046
69l	2.5283(10)	1.824(4)	1.882(3)	1.299(4)	1.423(5)	1.301(4)	1.697(3)	1.451(5)	1.464(5)	2.012(4)	2.044
74b	2.5487(10)	1.830(4)	1.877(4)	1.293(5)	1.417(6)	1.315(5)	1.673(3)	1.341(6)	1.462(6)	2.003(4)	2.043
75b	2.4208(6)	1.828(2)	1.887(2)	1.292(3)	1.416(3)	1.311(2)	1.682(2)	1.337(3)	1.465(3)	1.870(2)	1.906
123b	2.5077(15)	1.821(5)	1.844(6)	1.299(7)	1.397(7)	1.345(7)	1.740(5)	1.319(7)	1.466(7)	2.011(7)	2.064
126b	2.5266(8)	1.818(3)	1.879(3)	1.295(4)	1.428(4)	1.305(4)	1.683(2)	1.343(4)	1.448(4)	2.005(4)	2.046
126g	2.5377(9)	1.824(4)	1.858(4)	1.296(5)	1.426(4)	1.294(5)	1.705(3)	1.445(5)	1.441(5)	2.009(4)	2.045
126h	2.5252(8)	1.823(3)	1.869(3)	1.309(4)	1.413(4)	1.281(4)	1.708(3)	–	1.445(4)	2.000(3)	2.053
172b	2.505(3)	1.826(11)	1.853(10)	1.300(12)	1.466(13)	1.305(13)	1.663(8)	1.334(12)	1.454(13)	2.027(12)	2.036
190	2.4763(9)	1.813(4)	1.848(4)	1.308(4)	1.433(5)	1.278(5)	1.713(3)	–	1.434(5)	2.007(4)	2.051

†Exocyclic P,C bond. ‡Exocyclic C,C or C,N bond. ♯Mean value. M = W, Mo, Cr.

Table D.2: Comparison of bond angles [°] for 2H-1,4,2-diazaphosphole complexes presented in this work (see Fig. D.1 for atom numbering).

No.	M-P-C^{et}†	N^1-P-C^3	M-P-N^1	M-P-C^3	C^{et}-P-N^1	C^{et}-P-C^3	P-C^3-N^4	C^3-N^4-C^5	N^4-C^5-N^1	C^5-N^1-P
41b	120.86(17)	90.7(2)	113.01(17)	110.69(16)	103.9(2)	113.3(2)	109.0(3)	110.5(4)	120.1(5)	109.2(4)
41g	119.31(12)	90.11(17)	112.44(11)	110.98(12)	102.15(16)	117.35(17)	109.2(3)	110.1(3)	121.0(3)	109.1(3)
41h	126.06(13)	90.53(16)	110.79(11)	104.41(12)	102.02(16)	117.13(17)	109.1(3)	109.7(3)	122.7(3)	107.4(3)
41s	124.00(13)	90.51(17)	112.10(12)	107.57(13)	103.10(18)	114.36(17)	108.8(3)	110.9(3)	119.8(4)	109.7(3)
69b	130.89(10)	90.74(13)	107.78(9)	109.14(10)	105.96(14)	104.99(14)	110.7(2)	108.7(3)	120.5(3)	109.0(2)
69l	121.33(11)	90.40(15)	114.13(11)	105.07(12)	101.61(16)	120.11(16)	108.6(3)	110.5(3)	120.4(3)	109.2(3)
74b	121.47(11)	90.91(17)	112.78(11)	110.16(11)	103.80(17)	113.32(16)	109.2(3)	110.0(3)	120.8(4)	108.7(3)
75b	119.98(7)	90.35(10)	113.16(7)	111.68(7)	103.63(10)	113.79(9)	109.18(18)	110.16(18)	120.8(2)	108.93(18)
123b	127.44(19)	86.5(2)	112.84(18)	107.66(18)	106.2(2)	108.6(3)	113.6(4)	110.8(5)	116.4(5)	112.0(4)
126b	118.77(10)	90.14(13)	116.40(9)	109.53(10)	103.88(13)	114.62(13)	110.0(2)	109.4(3)	120.7(3)	109.5(2)
126g	127.74(12)	90.55(16)	107.55(11)	105.67(11)	106.68(15)	112.25(16)	109.7(2)	109.5(3)	121.4(3)	108.0(2)
126h	121.64(10)	90.17(14)	112.60(10)	107.77(10)	102.39(14)	117.55(14)	109.2(2)	109.5(3)	122.1(3)	108.6(2)
172b	119.2(4)	92.0(4)	114.3(3)	116.0(3)	106.2(5)	105.3(5)	109.8(7)	108.9(8)	119.7(9)	109.3(7)
190	119.86(14)	91.04(16)	115.50(12)	115.39(11)	103.99(18)	106.8(2)	109.8(3)	108.5(3)	122.6(3)	107.4(3)

†Exocyclic P-bonded carbon. M = W, Mo, Cr.

Torsion angles [°] between 2H-1,4,2-diazaphosphole and 3-aryl rings with respect to least-squares planes.

41b	41g	41h	41s	69b	69l	74b	75b	123b	126b	126g	126h	172b	190†
8.9	4.3	15.3	12.6	18.1	31.8	8.6	7.6	9.2	11.9	6.1	16.6	2.8	24.0

†Molecule is disordered in the crystal; only the value for the prevailing conformation is given.

Appendix E

List of Structures Determined by X-Ray Crystallography
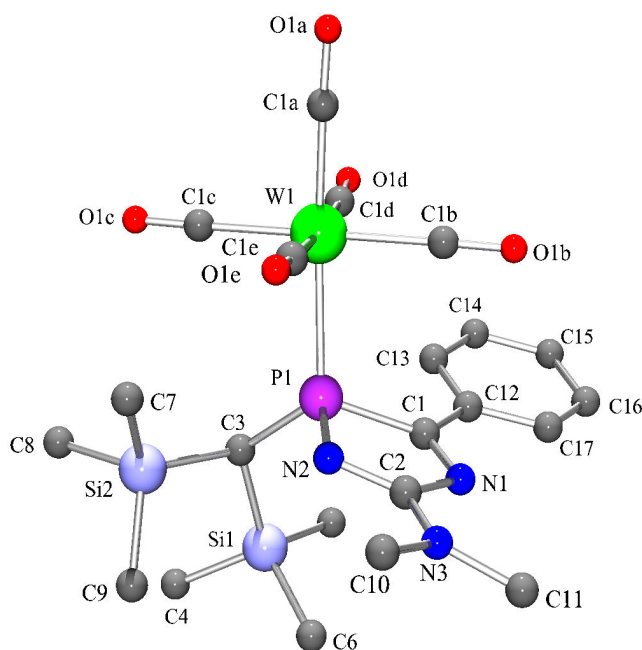
Figure E.1: Fully numbered picture of the molecular structure of complex **41b** in the crystal (hydrogen atoms are omitted for clarity). Selected bond lengths [Å] and angles [º]: W(1)–C(1a) 1.989(5), W(1)–P(1) 2.5340(14), P(1)–C(3) 1.838(5), P(1)–N(2) 1.682(4), P(1)–C(1) 1.884(5), C(1)–N(1) 1.294(6), N(1)–C(2) 1.429(7), C(2)–N(2) 1.312(8), C(2)–N(3) 1.333(8), C(1)–C(12) 1.467(8), N(2)–P(1)–C(1) 90.7(2), W(1)–P(1)–C(3) 120.86(17), W(1)–P(1)–C(1) 110.69(16), W(1)–P(1)–N(2) 113.01(17), C(3)–P(1)–C(1) 113.3(2), C(3)–P(1)–N(2) 103.9(2), P(1)–C(1)–N(1) 109.0(3), C(1)–N(1)–C(2) 110.5(4), N(1)–C(2)–N(2) 120.1(5), C(2)–N(2)–P(1) 109.2(4), P(1)–C(1)–C(12) 129.0(4), N(2)–C(2)–N(3) 123.8(6).
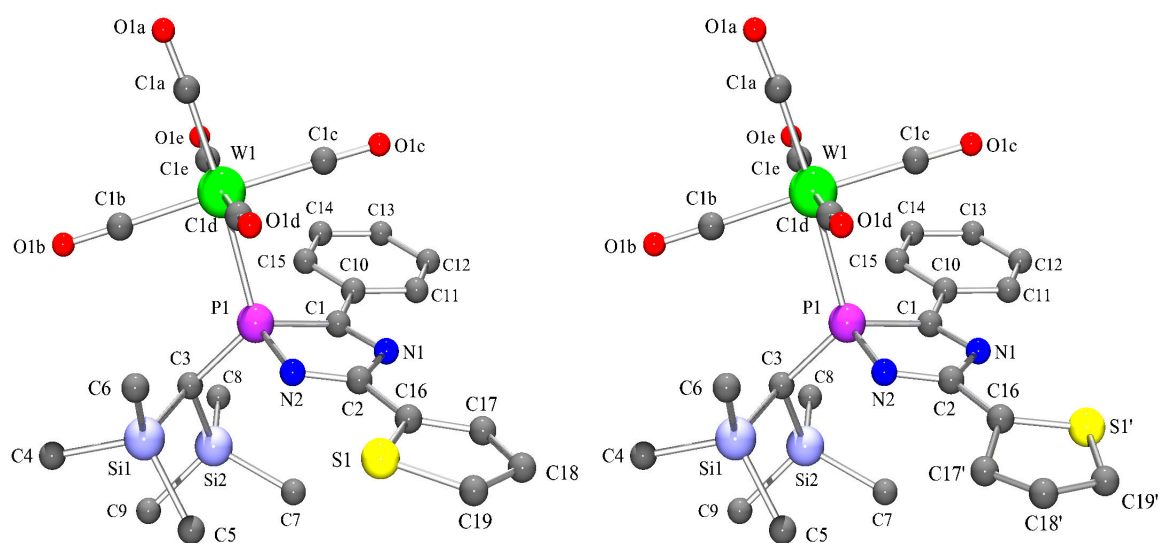
Figure E.2: Fully numbered picture of the molecular structure of complex **41g** in the crystal (left: major conformation, 81 %; right: minor conformation, 19 %; hydrogen atoms are omitted for clarity). Selected bond lengths [Å] and angles [°]: W(1)–C(1a) 2.008(4), W(1)–P(1) 2.531(10), P(1)–C(3) 1.835(3), P(1)–N(2) 1.707(3), P(1)–C(1) 1.877(4), C(1)–N(1) 1.304(5), N(1)–C(2) 1.424(5), C(2)–N(2) 1.293(5), C(2)–C(16) 1.441(5), C(1)–C(10) 1.457(6), N(2)–P(1)–C(1) 90.1(2), W(1)–P(1)–C(3) 119.31(12), W(1)–P(1)–C(1) 110.98(12), W(1)–P(1)–N(2) 112.44(11), C(3)–P(1)–C(1) 117.35(17), C(3)–P(1)–N(2) 102.15(16), P(1)–C(1)–N(1) 109.2(3), C(1)–N(1)–C(2) 110.1(3), N(1)–C(2)–N(2) 121.0(3), C(2)–N(2)–P(1) 109.1(3), P(1)–C(1)–C(10) 129.3(3), N(2)–C(2)–C(16) 121.5(4).
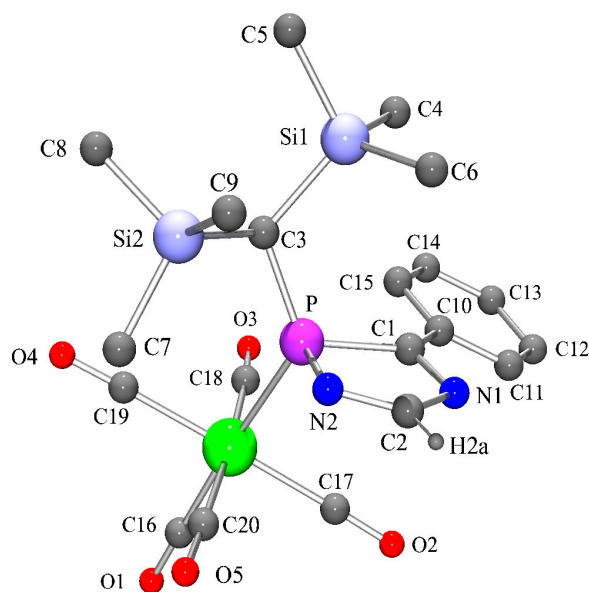
Figure E.3: Fully numbered picture of the molecular structure of complex **41h** in the crystal (except for H2a all hydrogen atoms are omitted for clarity). Selected bond lengths [Å] and angles [°]: W–C(16) 1.996(5), W–P 2.5362(10), P–C(3) 1.819(3), P–N(2) 1.715(3), P–C(1) 1.861(4), C(1)–N(1) 1.296(4), N(1)–C(2) 1.408(5), C(2)–N(2) 1.280(5), C(1)–C(10) 1.472(5), N(2)–P–C(1) 90.53(16), W–P–C(3) 126.06(13), W–P–C(1) 104.41(12), W–P–N(2) 110.79(11), C(3)–P–C(1) 117.13(17), C(3)–P–N(2) 102.02(16), P–C(1)–N(1) 109.1(3), C(1)–N(1)–C(2) 109.7(3), N(1)–C(2)–N(2) 122.7(3), C(2)–N(2)–P 107.4(3), P–C(1)–C(10) 120.8(3).
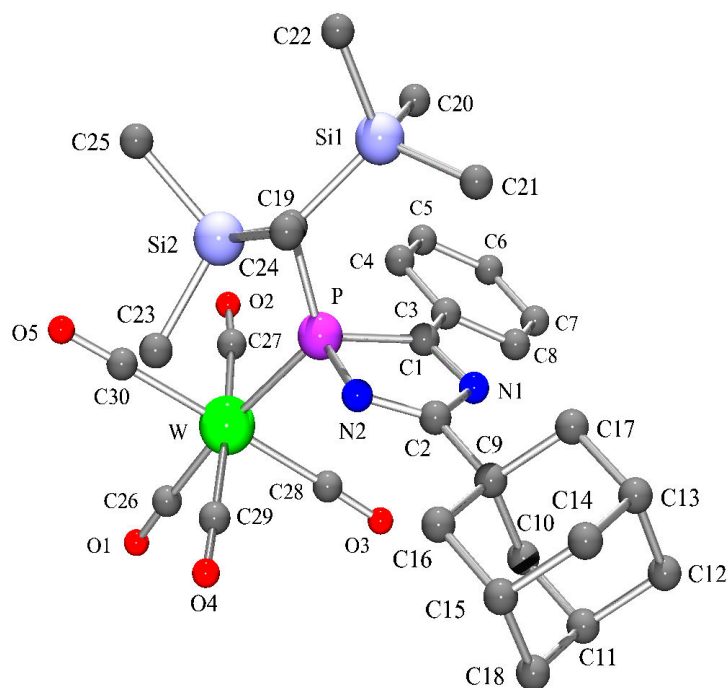
Figure E.4: Fully numbered picture of the molecular structure of complex **41s** in the crystal (hydrogen atoms are omitted for clarity). Selected bond lengths [Å] and angles [°]: W–C(26) 1.997(4), W–P 2.5296(15), P–C(19) 1.827(4), P–N(2) 1.704(4), P–C(1) 1.875(4), C(1)–N(1) 1.295(5), N(1)–C(2) 1.445(5), C(2)–N(2) 1.281(4), C(2)–C(9) 1.500(5), C(1)–C(3) 1.462(5), N(2)–P–C(1) 90.51(17), W–P–C(19) 124.00(13), W–P–C(1) 107.57(13), W–P–N(2) 112.10(12), C(19)–P–C(1) 114.36(17), C(19)–P–N(2) 103.10(18), P–C(1)–N(1) 108.8(3), C(1)–N(1)–C(2) 110.9(3), N(1)–C(2)–N(2) 119.8(4), C(2)–N(2)–P 109.7(3), P–C(1)–C(3) 129.7(3), N(2)–C(2)–C(9) 125.3(4).
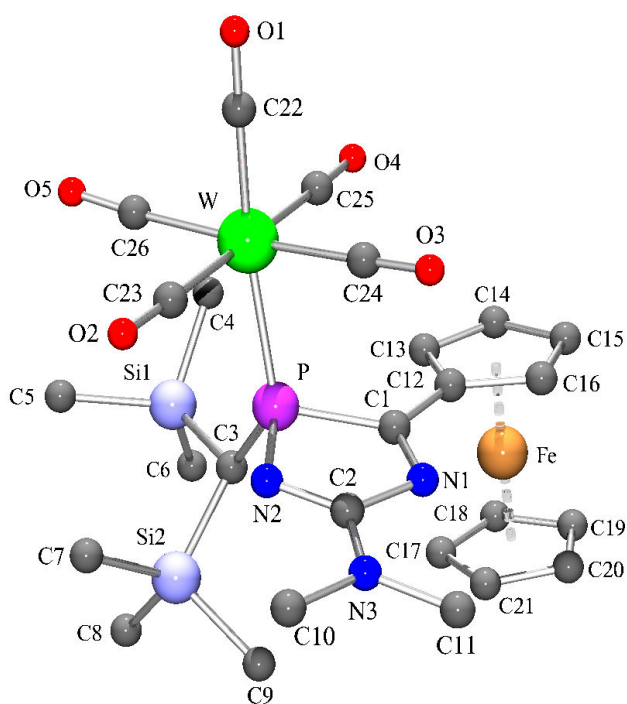
Figure E.5: Fully numbered picture of the molecular structure of complex **69b** in the crystal (hydrogen atoms are omitted for clarity). Selected bond lengths [Å] and angles [°]: W–C(22) 2.000(4), W–P 2.5359(8), P–C(3) 1.849(3), P–N(2) 1.683(3), P–C(1) 1.859(3), C(1)–N(1) 1.292(4), N(1)–C(2) 1.443(4), C(2)–N(2) 1.307(4), C(2)–N(3) 1.337(4), C(1)–C(12) 1.452(4), N(2)–P–C(1) 90.74(13), W–P–C(3) 130.89(10), W–P–C(1) 109.14(10), W–P–N(2) 107.78(9), C(3)–P–C(1) 104.99(14), C(3)–P–N(2) 105.96(14), P–C(1)–N(1) 110.7(2), C(1)–N(1)–C(2) 108.7(3), N(1)–C(2)–N(2) 120.5(3), C(2)–N(2)–P 109.0(2), P–C(1)–C(12) 126.0(2), N(2)–C(2)–N(3) 123.4(3).
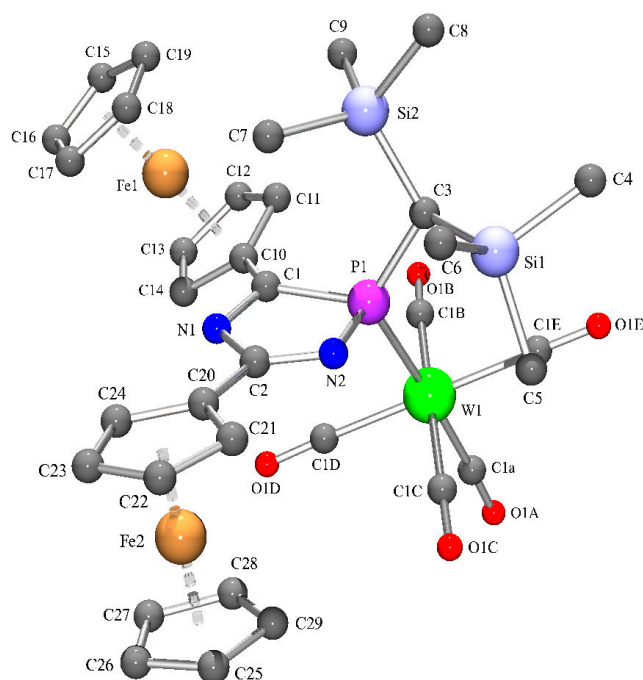
Figure E.6: Fully numbered picture of the molecular structure of complex **69l** in the crystal (hydrogen atoms are omitted for clarity). Selected bond lengths [Å] and angles [°]: W(1)–C(1a) 2.012(4), W(1)–P(1) 2.5283(10), P(1)–C(3) 1.824(4), P(1)–N(2) 1.697(3), P(1)–C(1) 1.882(3), C(1)–N(1) 1.299(4), N(1)–C(2) 1.423(5), C(2)–N(2) 1.301(4), C(2)–C(20) 1.451(5), C(1)–C(10) 1.464(5), N(2)–P(1)–C(1) 90.40(15), W(1)–P(1)–C(3) 121.33(11), W(1)–P(1)–C(1) 105.07(12), W(1)–P(1)–N(2) 114.13(11), C(3)–P(1)–C(1) 120.11(16), C(3)–P(1)–N(2) 101.61(16), P(1)–C(1)–N(1) 108.6(3), C(1)–N(1)–C(2) 110.5(3), N(1)–C(2)–N(2) 120.4(3), C(2)–N(2)–P(1) 109.2(3), P(1)–C(1)–C(10) 128.2(3), N(2)–C(2)–C(20) 121.9(3).
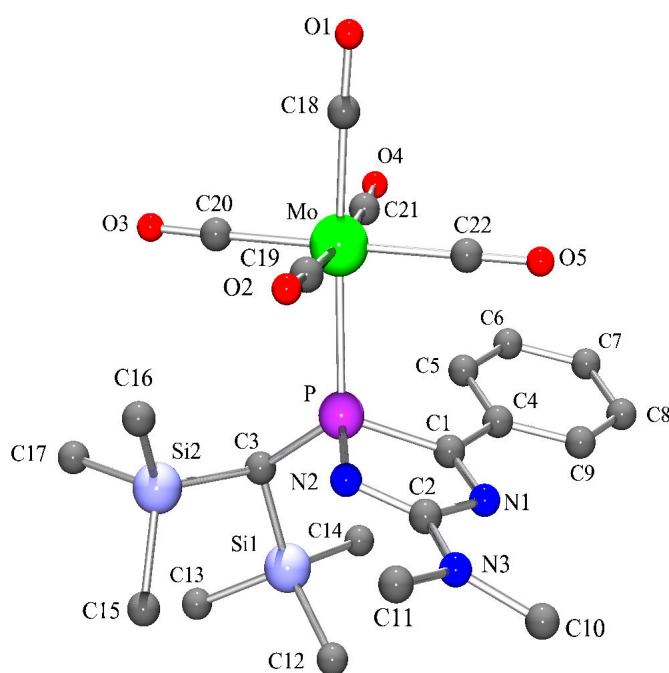
Figure E.7: Fully numbered picture of the molecular structure of complex **74b** in the crystal (hydrogen atoms are omitted for clarity). Selected bond lengths [Å] and angles [°]: Mo–C(18) 2.003(4), Mo–P 2.5487(10), P–C(3) 1.830(4), P–N(2) 1.673(3), P–C(1) 1.877(4), C(1)–N(1) 1.293(5), N(1)–C(2) 1.417(6), C(2)–N(2) 1.315(5), C(2)–N(3) 1.341(6), C(1)–C(4) 1.462(6), N(2)–P–C(1) 90.91(17), Mo–P–C(3) 121.47(11), Mo–P–C(1) 110.16(11), Mo–P–N(2) 112.78(11), C(3)–P–C(1) 113.32(16), C(3)–P–N(2) 103.80(17), P–C(1)–N(1) 109.2(3), C(1)–N(1)–C(2) 110.0(3), N(1)–C(2)–N(2) 120.8(4), C(2)–N(2)–P 108.7(3), P–C(1)–C(4) 130.0(3), N(2)–C(2)–N(3) 123.0(4).
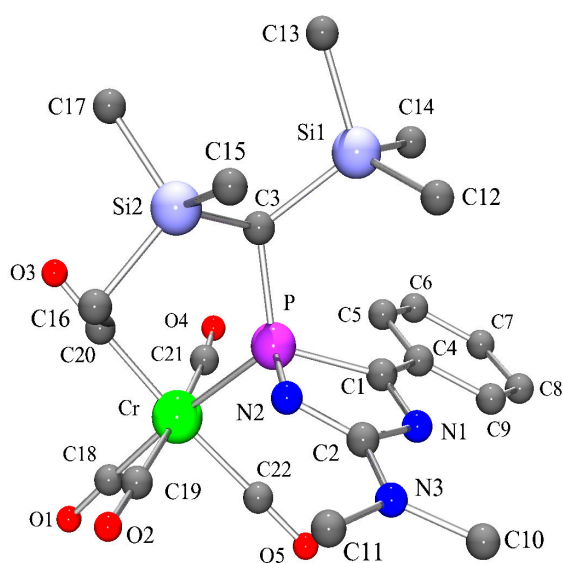
Figure E.8: Fully numbered picture of the molecular structure of complex **75b** in the crystal (hydrogen atoms are omitted for clarity). Selected bond lengths [Å] and angles [°]: Cr–C(18) 1.870(2), Cr–P 2.4208(6), P–C(3) 1.828(2), P–N(2) 1.682(2), P–C(1) 1.887(2), C(1)–N(1) 1.292(3), N(1)–C(2) 1.416(3), C(2)–N(2) 1.311(2), C(2)–N(3) 1.337(3), C(1)–C(4) 1.465(3), N(2)–P–C(1) 90.35(10), Cr–P–C(3) 119.98(7), Cr–P–C(1) 111.68(7), Cr–P–N(2) 113.16(7), C(3)–P–C(1) 113.79(9), C(3)–P–N(2) 103.63(10), P–C(1)–N(1) 109.18(18), C(1)–N(1)–C(2) 110.16(18), N(1)–C(2)–N(2) 120.8(2), C(2)–N(2)–P 108.93(18), P–C(1)–C(4) 129.38(17), N(2)–C(2)–N(3) 122.1(2).
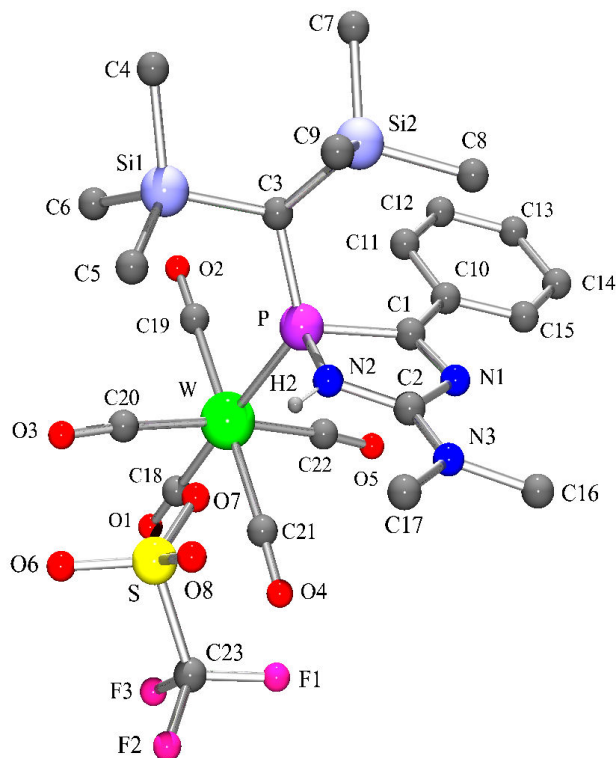
Figure E.9: Fully numbered picture of the molecular structure of complex **123b** in the crystal (except for H2 all hydrogen atoms are omitted for clarity). Selected bond lengths [Å] and angles [°]: W–C(18) 2.011(7), W–P 2.5077(15), P–C(3) 1.821(5), P–N(2) 1.740(5), P–C(1) 1.844(6), C(1)–N(1) 1.299(7), N(1)–C(2) 1.397(7), C(2)–N(2) 1.345(7), C(2)–N(3) 1.319(7), C(1)–C(10) 1.466(7), N(2)···O(7) 2.821(6), N(2)–P–C(1) 86.5(2), W–P–C(3) 127.44(19), W–P–C(1) 107.66(18), W–P–N(2) 112.84(18), C(3)–P–C(1) 108.6(3), C(3)–P–N(2) 106.2(2), P–C(1)–N(1) 113.6(4), C(1)–N(1)–C(2) 110.8(5), N(1)–C(2)–N(2) 116.4(5), C(2)–N(2)–P 112.0(4), P–C(1)–C(10) 126.6(4), N(2)–C(2)–N(3) 125.5(5).
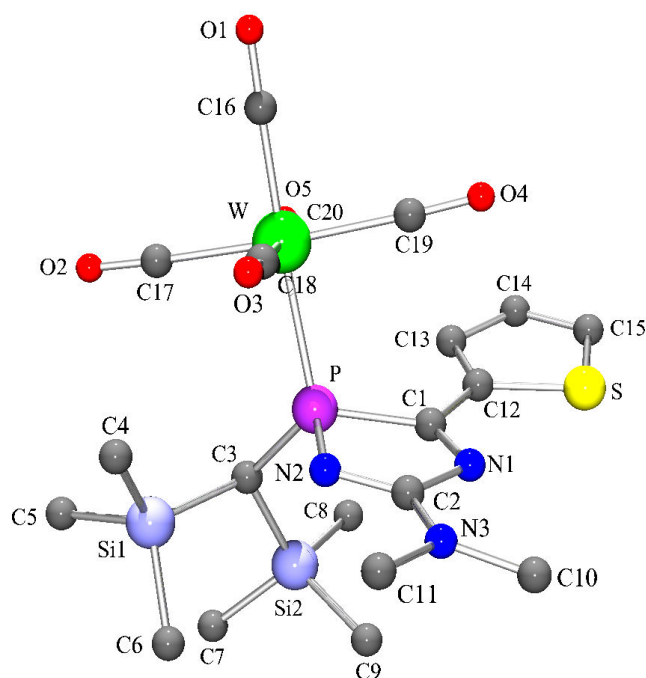
Figure E.10: Fully numbered picture of the molecular structure of complex **126b** in the crystal (hydrogen atoms and most atom labels are omitted for clarity). Selected bond lengths [Å] and angles [º]: W–C(16) 2.005(4), W–P 2.5266(8), P–C(3) 1.818(3), P–N(2) 1.683(2), P–C(1) 1.879(3), C(1)–N(1) 1.295(4), N(1)–C(2) 1.428(4), C(2)–N(2) 1.305(4), C(2)–N(3) 1.343(4), C(1)–C(12) 1.448(4), N(2)–P–C(1) 90.14(13), W–P–C(3) 118.77(10), W–P–C(1) 109.53(10), W–P–N(2) 116.40(9), C(3)–P–C(1) 114.62(13), C(3)–P–N(2) 103.88(13), P–C(1)–N(1) 110.0(2), C(1)–N(1)–C(2) 109.4(3), N(1)–C(2)–N(2) 120.7(3), C(2)–N(2)–P 109.5(2), P–C(1)–C(12) 129.2(2), N(2)–C(2)–N(3) 123.6(3).
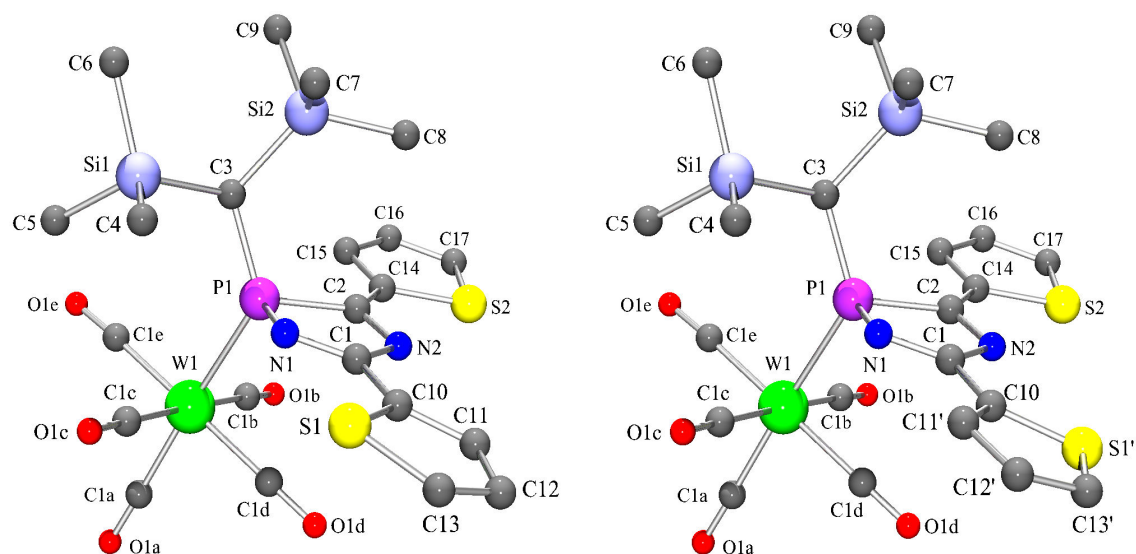
Figure E.11: Fully numbered picture of the molecular structure of complex **126g** in the crystal (left: major conformation, 59 %; right: minor conformation, 41 %; hydrogen atoms are omitted for clarity). Selected bond lengths [Å] and angles [°]: W(1)–C(1a) 2.009(4), W(1)–P(1) 2.5377(9), P(1)–C(3) 1.824(4), P(1)–N(1) 1.705(3), P(1)–C(2) 1.858(4), C(2)–N(2) 1.296(5), N(2)–C(1) 1.426(4), C(1)–N(1) 1.294(5), C(1)–C(10) 1.445(5), C(2)–C(14) 1.441(5), N(1)–P(1)–C(2) 90.55(16), W(1)–P(1)–C(3) 127.74(12), W(1)–P(1)–C(2) 105.67(11), W(1)–P(1)–N(1) 107.55(11), C(3)–P(1)–C(2) 112.25(16), C(3)–P(1)–N(1) 106.68(15), P(1)–C(2)–N(2) 109.7(2), C(2)–N(2)–C(1) 109.5(3), N(2)–C(1)–N(1) 121.4(3), C(1)–N(1)–P(1) 108.0(2), P(1)–C(2)–C(14) 127.3(3), N(1)–C(1)–C(10) 122.0(3).
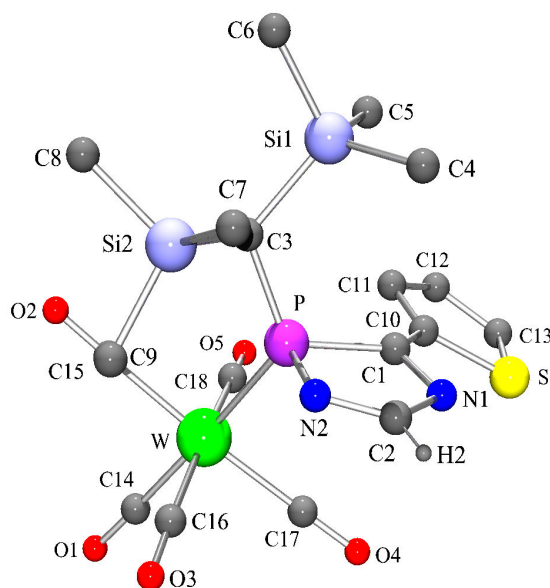
Figure E.12: Fully numbered picture of the molecular structure of complex **126h** in the crystal (except for H2 all hydrogen atoms are omitted for clarity). Selected bond lengths [Å] and angles [°]: W–C(14) 2.000(3), W–P 2.5252(8), P–C(3) 1.823(3), P–N(2) 1.708(3), P–C(1) 1.869(3), C(1)–N(1) 1.309(4), N(1)–C(2) 1.413(4), C(2)–N(2) 1.281(4), C(1)–C(10) 1.445(4), N(2)–P–C(1) 90.17(14), W–P–C(3) 121.64(10), W–P–C(1) 107.77(10), W–P–N(2) 112.60(10), C(3)–P–C(1) 117.55(14), C(3)–P–N(2) 102.39(14), P–C(1)–N(1) 109.2(2), C(1)–N(1)–C(2) 109.5(3), N(1)–C(2)–N(2) 122.1(3), C(2)–N(2)–P 108.6(2), P–C(1)–C(10) 129.7(2).
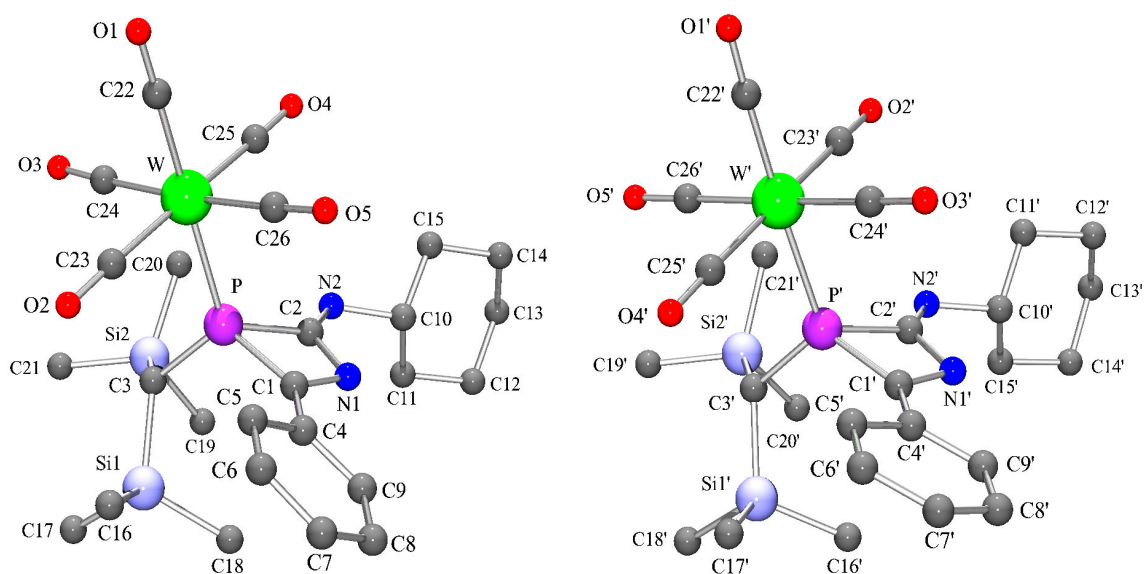
Figure E.13: Fully numbered picture of the molecular structure of complex **149** in the crystal (two independent molecules in the asymmetric unit; hydrogen atoms are omitted for clarity). Selected bond lengths [Å] and angles [°]: W–C(22) 2.005(6), W–P 2.4987(13), P–C(3) 1.834(5), P–C(1) 1.878(6), P–C(2) 1.874(6), C(1)–N(1) 1.312(7), N(1)–C(2) 1.436(7), C(2)–N(2) 1.239(7), C(1)–C(4) 1.443(8), C(1)–P–C(2) 68.0(3), W–P–C(3) 118.22(18), W–P–C(1) 114.68(16), W–P–C(2) 120.74(16), C(3)–P–C(1) 114.4(2), C(3)–P–C(2) 110.9(2), P–C(1)–N(1) 98.4(4), C(1)–N(1)–C(2) 99.4(5), N(1)–C(2)–P 94.2(4), P–C(1)–C(4) 138.3(5), P–C(2)–N(2) 135.3(4); W'–C(22') 1.988(6), W'–P' 2.4982(13), P'–C(3') 1.832(6), P'–C(1') 1.868(6), P'–C(2') 1.868(6), C(1')–N(1') 1.315(7), N(1')–C(2') 1.450(7), C(2')–N(2') 1.238(7), C(1')–C(4') 1.457(8), C(1')–P'–C(2') 68.1(3), W'–P'–C(3') 117.97(18), W'–P'–C(1') 114.50(18), W'–P'–C(2') 120.30(17), C(3')–P'–C(1') 116.2(3), C(3')–P'–C(2') 110.2(2), P'–C(1')–N(1') 99.1(4), C(1')–N(1')–C(2') 98.3(5), N(1')–C(2')–P' 94.2(4), P'–C(1')–C(4') 137.0(4), P'–C(2')–N(2') 134.6(5).
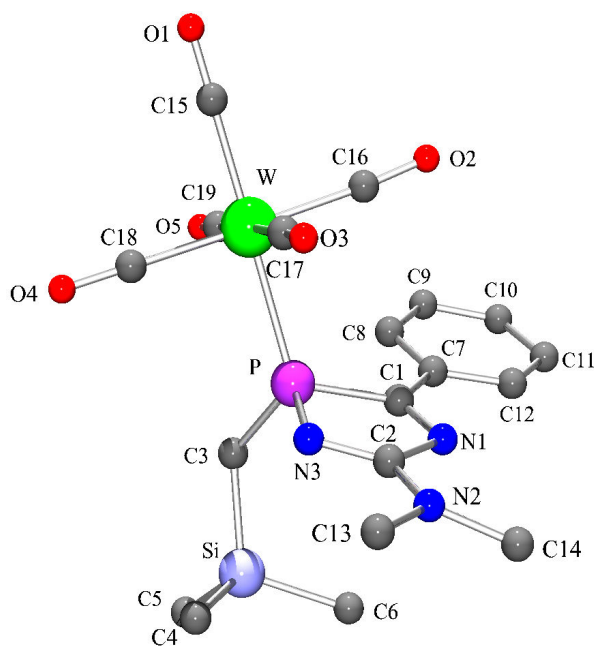
Figure E.14: Fully numbered picture of the molecular structure of complex **172b** in the crystal (hydrogen atoms are omitted for clarity). Selected bond lengths [Å] and angles [°]: W–C(15) 2.027(12), W–P 2.505(3), P–C(3) 1.826(11), P–N(3) 1.663(8), P–C(1) 1.853(10), C(1)–N(1) 1.300(12), N(1)–C(2) 1.466(13), C(2)–N(3) 1.305(13), C(2)–N(2) 1.334(12), C(1)–C(7) 1.454(13), N(3)–P–C(1) 92.0(4), W–P–C(3) 119.2(4), W–P–C(1) 116.0(3), W–P–N(3) 114.3(3), C(3)–P–C(1) 105.3(5), C(3)–P–N(3) 106.2(5), P–C(1)–N(1) 109.8(7), C(1)–N(1)–C(2) 108.9(8), N(1)–C(2)–N(3) 119.7(9), C(2)–N(3)–P 109.3(7), P–C(1)–C(7) 127.7(8), N(3)–C(2)–N(2) 125.9(10).
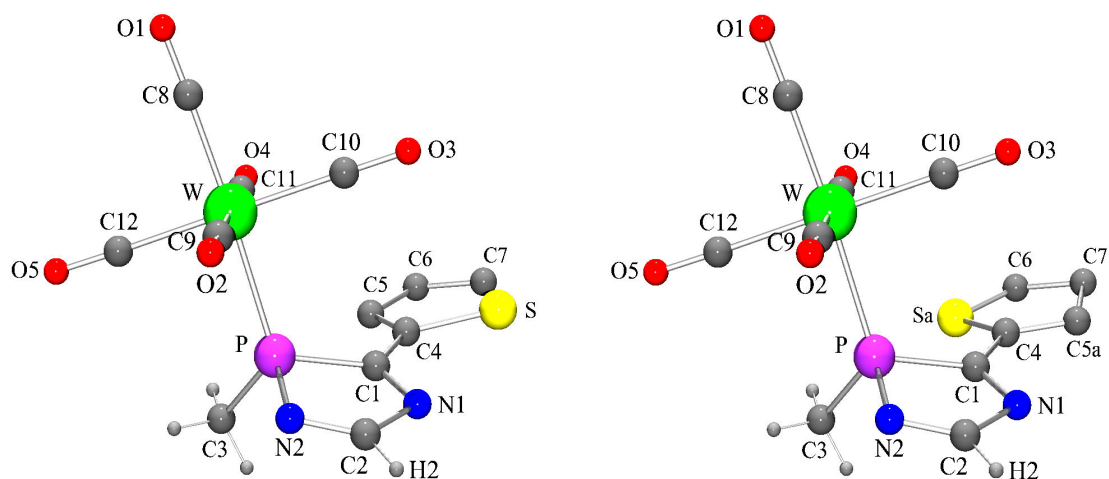
Figure E.15: Fully numbered picture of the molecular structure of complex **190** in the crystal (left: major conformation, 81 %; right: minor conformation, 19 %; hydrogen atoms of the 2-thienyl moiety are omitted for clarity). Selected bond lengths [Å] and angles [º]: W–C(8) 2.007(4), W–P 2.4763(9), P–C(3) 1.813(4), P–N(2) 1.713(3), P–C(1) 1.848(4), C(1)–N(1) 1.308(4), N(1)–C(2) 1.433(5), C(2)–N(2) 1.278(5), C(1)–C(4) 1.434(5), N(2)–P–C(1) 91.04(16), W–P–C(3) 119.86(14), W–P–C(1) 115.39(11), W–P–N(2) 115.50(12), C(3)–P–C(1) 106.8(2), C(3)–P–N(2) 103.99(18), P–C(1)–N(1) 109.8(3), C(1)–N(1)–C(2) 108.5(3), N(1)–C(2)–N(2) 122.6(3), C(2)–N(2)–P 107.4(3), P–C(1)–C(4) 126.0(3).
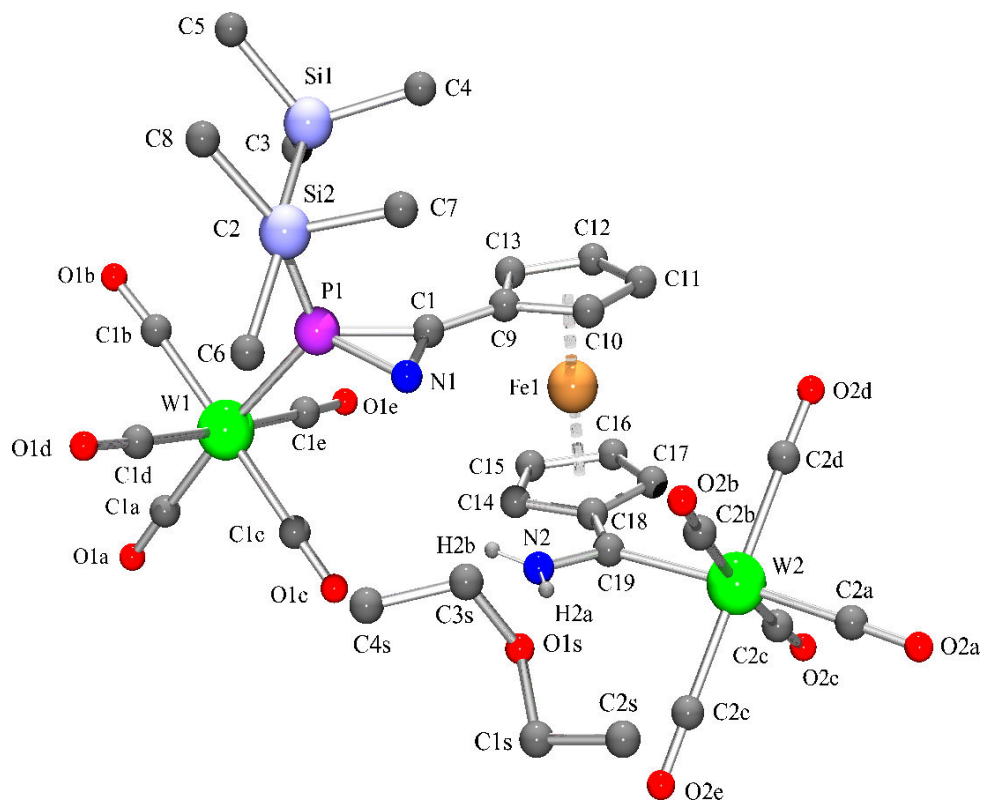
Figure E.16: Fully numbered picture of the molecular structure of complex **201** in the crystal (except for H2a and H2b all hydrogen atoms are omitted for clarity). Selected bond lengths [Å] and angles [°]: W(1)–C(1a) 1.986(5), W(1)–P(1) 2.4827(11), P(1)–N(1) 1.798(4), P(1)–C(1) 1.769(4), N(1)–C(1) 1.280(5), C(1)–C(9) 1.440(6), C(18)–C(19) 1.472(6), C(19)–N(2) 1.313(5), C(19)–W(2) 2.223(4), W(2)–C(2a) 2.005(5), N(1)–P(1)–C(1) 42.05(17), W(1)–P(1)–C(2) 122.34(14), W(1)–P(1)–N(1) 120.29(12), W(1)–P(1)–C(1) 124.34(13), C(2)–P(1)–N(1) 109.58(18), C(2)–P(1)–C(1) 111.63(18), P(1)–C(1)–C(9) 153.1(3), N(1)–C(1)–C(9) 136.7(4), C(18)–C(19)–N(2) 113.0(4), C(18)–C(19)–W(2) 126.4(3), N(2)–C(19)–W(2) 120.5(3).
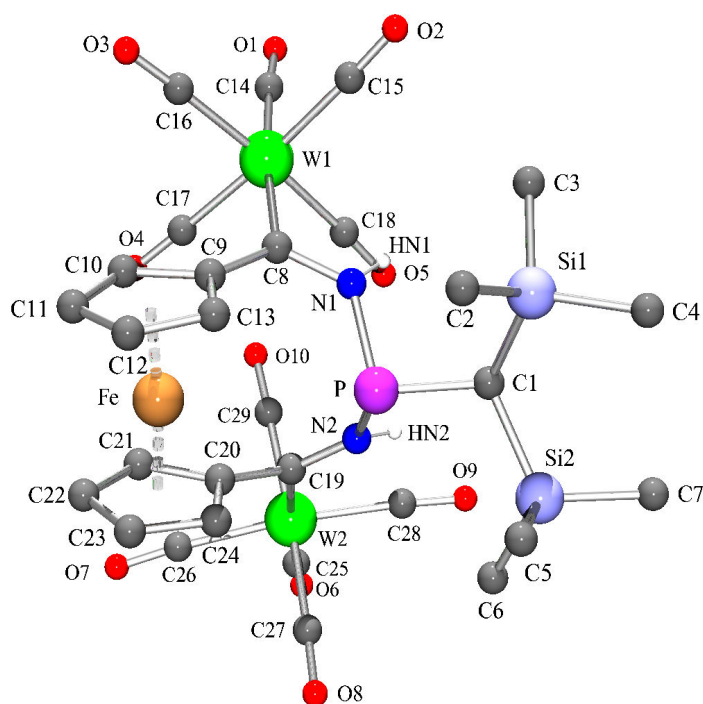
Figure E.17: Fully numbered picture of the molecular structure of complex **205** in the crystal (except for HN1 and HN2 all hydrogen atoms are omitted for clarity). Selected bond lengths [Å] and angles [°]: P–C(1) 1.816(3), P–N(1) 1.769(3), P–N(2) 1.787(3), N(1)–C(8) 1.362(4), N(2)–C(19) 1.325(4), C(8)–W(1) 2.207(3), C(19)–W(2) 2.206(3), C(8)–C(9) 1.462(4), C(19)–C(20) 1.484(4), W(1)–C(14) 2.024(3), W(2)–C(25) 2.023(4), C(1)–P–N(1) 99.04(13), C(1)–P–N(2) 99.64(14), N(1)–P–N(2) 94.25(13), P–N(1)–C(8) 129.2(2), P–N(2)–C(19) 131.3(2), N(1)–C(8)–C(9) 115.0(3), N(2)–C(19)–C(20) 116.3(3), N(1)–C(8)–W(1) 118.4(2), N(2)–C(19)–W(2) 122.5(2), C(9)–C(8)–W(1) 126.5(2), C(20)–C(19)–W(2) 120.3(2).
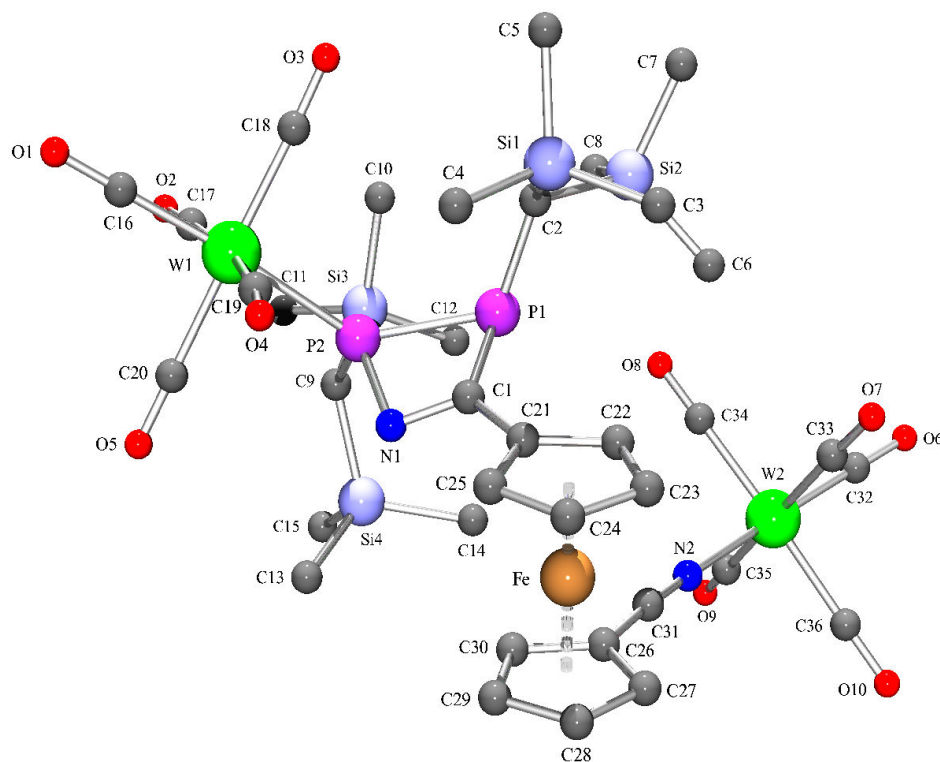
Figure E.18: Fully numbered picture of the molecular structure of complex **207** in the crystal
(hydrogen atoms are omitted for clarity). Selected bond lengths [Å] and angles [º]: W(1)–
C(16) 2.006(4), W(1)–P(2) 2.5188(8), P(2)–C(9) 1.833(3), P(2)–P(1) 2.2543(11), P(2)–N(1)
1.751(3), P(1)–C(2) 1.861(3), P(1)–C(1) 1.841(3), C(1)–N(1) 1.305(4), C(1)–C(21) 1.458(4),
C(26)–C(31) 1.416(5), C(31)–N(2) 1.153(5), N(2)–W(2) 2.177(3), W(2)–C(32) 1.970(4),
P(1)–P(2)–N(1) 78.43(10), W(1)–P(2)–C(9) 112.51(10), W(1)–P(2)–P(1) 131.35(4), W(1)–
P(2)–N(1) 110.65(10), C(9)–P(2)–P(1) 108.39(11), C(9)–P(2)–N(1) 109.07(15), P(2)–P(1)–
C(2) 117.99(11), C(2)–P(1)–C(1) 116.51(15), P(2)–P(1)–C(1) 69.74(10), P(1)–C(1)–N(1)
107.8(2), C(1)–N(1)–P(2) 100.4(2), P(1)–C(1)–C(21) 128.9(2), N(1)–C(1)–C(21) 122.8(3),
C(26)–C(31)–N(2) 175.5(4), C(31)–N(2)–W(2) 170.6(3).

Appendix F

Crystallographic Data and Refinement Parameters for Unpublished Structures

F.1 Data for Complex 41h
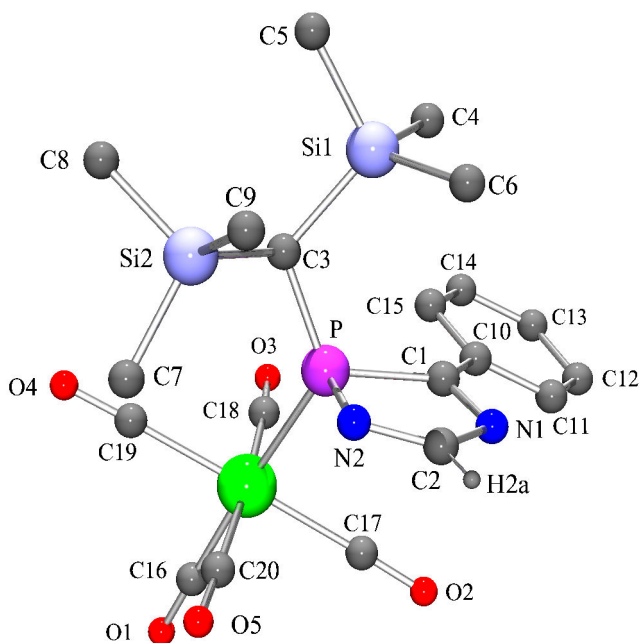
Figure F.1: Molecular structure of complex **41h** (GSTR005) in the crystal (except for H2a all hydrogen atoms are omitted for clarity).

Table F.1: Crystal data and structure refinement for GSTR005.

Identification code	GSTR005
Empirical formula	$C_{20}H_{25}N_2O_5PSi_2W$
Formula weight	644.42
Temperature	123(2) K
Wavelength	0.71073 Å
Crystal system, space group	Monoclinic, P $2_1/c$
Unit cell dimensions	a = 10.2655(5) Å, $\alpha = 90°$
	b = 18.7396(10) Å, $\beta = 98.340(3)°$
	c = 13.4211(5) Å, $\gamma = 90°$
Volume	2554.5(2) Å^3
Z, Calculated density	4, 1.676 Mg/m^3
Absorption coefficient	4.710 mm^{-1}
F(000)	1264
Crystal size	0.40 x 0.08 x 0.08 mm
θ range for data collection	2.91 to 27.50°
Limiting indices	$-13 \leq h \leq 13$, $-23 \leq k \leq 24$, $-9 \leq l \leq 17$
Reflections collected / unique	14073 / 5516 [$R_{int} = 0.0448$]
Completeness to $\theta = 27.50$	93.9 %
Absorption correction	Semi-empirical from equivalents
Max. and min. transmission	0.68770 and 0.59827
Refinement method	Full-matrix least-squares on F^2
Data / restraints / parameters	5516 / 0 / 281
Goodness-of-fit on F^2	0.959
Final R indices [I>2σ(I)]	$R_1 = 0.0304$, $wR_2 = 0.0611$
R indices (all data)	$R_1 = 0.0460$, $wR_2 = 0.0647$
Largest diff. peak and hole	1.462 and -1.670 e $\cdot$ A^{-3}

Table F.2: Atomic coordinates (x 10^4) and equivalent isotropic displacement parameters ($\text{Å}^2 \cdot 10^3$) for GSTR005. U(eq) is defined as one third of the trace of the orthogonalized U_{ij} tensor.

	x	y	z	U(eq)
C(1)	5951(4)	4238(2)	8614(3)	20(1)
C(2)	4791(4)	4032(2)	9850(3)	25(1)
C(3)	3627(4)	3421(2)	7318(2)	19(1)
C(4)	4106(4)	4854(2)	6186(3)	33(1)
C(5)	1450(4)	4225(2)	5923(3)	29(1)
C(6)	2597(4)	4902(2)	7952(3)	29(1)
C(7)	2741(4)	2032(2)	8469(3)	34(1)
C(8)	1517(5)	2398(2)	6368(3)	38(1)
C(9)	992(4)	3279(2)	8231(3)	34(1)
C(10)	6987(4)	4557(2)	8104(3)	22(1)
C(11)	7866(4)	5046(2)	8614(3)	32(1)
C(12)	8851(4)	5345(2)	8146(4)	43(1)
C(13)	8947(4)	5168(2)	7157(4)	41(1)
C(14)	8096(4)	4682(3)	6651(3)	34(1)
C(15)	7120(4)	4372(2)	7121(3)	27(1)
C(16)	8154(4)	1675(3)	8881(3)	32(1)
C(17)	7941(4)	3111(2)	9511(3)	28(1)
C(18)	7689(4)	2710(3)	7347(3)	30(1)
C(19)	5668(4)	1742(2)	7626(3)	32(1)
C(20)	5934(4)	2063(2)	9739(3)	28(1)
N(1)	5756(3)	4459(2)	9495(2)	24(1)
N(2)	4290(3)	3482(2)	9374(2)	21(1)
O(1)	8934(3)	1237(2)	9080(2)	45(1)
O(2)	8593(3)	3476(2)	10051(2)	38(1)
O(3)	8209(3)	2813(2)	6673(2)	37(1)
O(4)	5055(3)	1342(2)	7111(2)	54(1)
O(5)	5469(3)	1839(2)	10399(2)	39(1)
P	5030(1)	3391(1)	8315(1)	18(1)
Si(1)	2956(1)	4343(1)	6876(1)	22(1)
Si(2)	2235(1)	2789(1)	7606(1)	26(1)
W	6785(1)	2429(1)	8560(1)	20(1)

Table F.3: Bond lengths [Å] and angles [º] for GSTR005.

C(1)-N(1)	1.296(4)	C(8)-H(8C)	0.9800
C(1)-C(10)	1.472(5)	C(9)-Si(2)	1.867(4)
C(1)-P	1.861(4)	C(9)-H(9A)	0.9800
C(2)-N(2)	1.280(5)	C(9)-H(9B)	0.9800
C(2)-N(1)	1.408(5)	C(9)-H(9C)	0.9800
C(2)-H(2A)	0.9500	C(10)-C(15)	1.390(5)
C(3)-P	1.819(3)	C(10)-C(11)	1.394(5)
C(3)-Si(1)	1.922(4)	C(11)-C(12)	1.384(6)
C(3)-Si(2)	1.937(4)	C(11)-H(11A)	0.9500
C(3)-H(3A)	1.0000	C(12)-C(13)	1.385(6)
C(4)-Si(1)	1.867(4)	C(12)-H(12A)	0.9500
C(4)-H(4A)	0.9800	C(13)-C(14)	1.371(6)
C(4)-H(4B)	0.9800	C(13)-H(13A)	0.9500
C(4)-H(4C)	0.9800	C(14)-C(15)	1.387(5)
C(5)-Si(1)	1.871(4)	C(14)-H(14A)	0.9500
C(5)-H(5A)	0.9800	C(15)-H(15A)	0.9500
C(5)-H(5B)	0.9800	C(16)-O(1)	1.150(5)
C(5)-H(5C)	0.9800	C(16)-W	1.996(5)
C(6)-Si(1)	1.863(4)	C(17)-O(2)	1.140(5)
C(6)-H(6A)	0.9800	C(17)-W	2.056(4)
C(6)-H(6B)	0.9800	C(18)-O(3)	1.133(5)
C(6)-H(6C)	0.9800	C(18)-W	2.056(5)
C(7)-Si(2)	1.858(4)	C(19)-O(4)	1.143(5)
C(7)-H(7A)	0.9800	C(19)-W	2.032(4)
C(7)-H(7B)	0.9800	C(20)-O(5)	1.146(4)
C(7)-H(7C)	0.9800	C(20)-W	2.035(4)
C(8)-Si(2)	1.867(4)	N(2)-P	1.715(3)
C(8)-H(8A)	0.9800	P-W	2.5362(10)
C(8)-H(8B)	0.9800		
N(1)-C(1)-C(10)	120.8(3)	C(10)-C(11)-H(11A)	119.8
N(1)-C(1)-P	109.1(3)	C(11)-C(12)-C(13)	119.7(4)
C(10)-C(1)-P	128.7(3)	C(11)-C(12)-H(12A)	120.1
N(2)-C(2)-N(1)	122.7(3)	C(13)-C(12)-H(12A)	120.1
N(2)-C(2)-H(2A)	118.7	C(14)-C(13)-C(12)	120.3(4)
N(1)-C(2)-H(2A)	118.7	C(14)-C(13)-H(13A)	119.8
P-C(3)-Si(1)	117.6(2)	C(12)-C(13)-H(13A)	119.8
P-C(3)-Si(2)	111.26(18)	C(13)-C(14)-C(15)	120.2(4)

Si(1)-C(3)-Si(2)	111.68(18)	C(13)-C(14)-H(14A)	119.9
P-C(3)-H(3A)	105.0	C(15)-C(14)-H(14A)	119.9
Si(1)-C(3)-H(3A)	105.0	C(14)-C(15)-C(10)	120.3(4)
Si(2)-C(3)-H(3A)	105.0	C(14)-C(15)-H(15A)	119.9
Si(1)-C(4)-H(4A)	109.5	C(10)-C(15)-H(15A)	119.9
Si(1)-C(4)-H(4B)	109.5	O(1)-C(16)-W	178.8(4)
H(4A)-C(4)-H(4B)	109.5	O(2)-C(17)-W	178.5(4)
Si(1)-C(4)-H(4C)	109.5	O(3)-C(18)-W	174.9(4)
H(4A)-C(4)-H(4C)	109.5	O(4)-C(19)-W	178.5(4)
H(4B)-C(4)-H(4C)	109.5	O(5)-C(20)-W	178.1(4)
Si(1)-C(5)-H(5A)	109.5	C(1)-N(1)-C(2)	109.7(3)
Si(1)-C(5)-H(5B)	109.5	C(2)-N(2)-P	107.4(3)
H(5A)-C(5)-H(5B)	109.5	N(2)-P-C(3)	102.02(16)
Si(1)-C(5)-H(5C)	109.5	N(2)-P-C(1)	90.53(16)
H(5A)-C(5)-H(5C)	109.5	C(3)-P-C(1)	117.13(17)
H(5B)-C(5)-H(5C)	109.5	N(2)-P-W	110.79(11)
Si(1)-C(6)-H(6A)	109.5	C(3)-P-W	126.06(13)
Si(1)-C(6)-H(6B)	109.5	C(1)-P-W	104.41(12)
H(6A)-C(6)-H(6B)	109.5	C(6)-Si(1)-C(4)	107.9(2)
Si(1)-C(6)-H(6C)	109.5	C(6)-Si(1)-C(5)	111.10(19)
H(6A)-C(6)-H(6C)	109.5	C(4)-Si(1)-C(5)	103.87(18)
H(6B)-C(6)-H(6C)	109.5	C(6)-Si(1)-C(3)	111.65(16)
Si(2)-C(7)-H(7A)	109.5	C(4)-Si(1)-C(3)	112.95(18)
Si(2)-C(7)-H(7B)	109.5	C(5)-Si(1)-C(3)	109.14(18)
H(7A)-C(7)-H(7B)	109.5	C(7)-Si(2)-C(8)	107.1(2)
Si(2)-C(7)-H(7C)	109.5	C(7)-Si(2)-C(9)	104.1(2)
H(7A)-C(7)-H(7C)	109.5	C(8)-Si(2)-C(9)	112.7(2)
H(7B)-C(7)-H(7C)	109.5	C(7)-Si(2)-C(3)	116.33(18)
Si(2)-C(8)-H(8A)	109.5	C(8)-Si(2)-C(3)	105.65(19)
Si(2)-C(8)-H(8B)	109.5	C(9)-Si(2)-C(3)	111.15(18)
H(8A)-C(8)-H(8B)	109.5	C(16)-W-C(19)	90.03(18)
Si(2)-C(8)-H(8C)	109.5	C(16)-W-C(20)	87.79(17)
H(8A)-C(8)-H(8C)	109.5	C(19)-W-C(20)	89.93(17)
H(8B)-C(8)-H(8C)	109.5	C(16)-W-C(18)	88.14(17)
Si(2)-C(9)-H(9A)	109.5	C(19)-W-C(18)	87.31(17)
Si(2)-C(9)-H(9B)	109.5	C(20)-W-C(18)	175.07(17)
H(9A)-C(9)-H(9B)	109.5	C(16)-W-C(17)	88.91(17)
Si(2)-C(9)-H(9C)	109.5	C(19)-W-C(17)	178.94(16)
H(9A)-C(9)-H(9C)	109.5	C(20)-W-C(17)	90.04(16)
H(9B)-C(9)-H(9C)	109.5	C(18)-W-C(17)	92.65(16)

C(15)-C(10)-C(11)	119.0(4)	C(16)-W-P	175.00(11)
C(15)-C(10)-C(1)	121.1(4)	C(19)-W-P	92.54(13)
C(11)-C(10)-C(1)	119.9(4)	C(20)-W-P	87.93(12)
C(12)-C(11)-C(10)	120.5(4)	C(18)-W-P	96.26(12)
C(12)-C(11)-H(11A)	119.8	C(17)-W-P	88.52(12)

Table F.4: Anisotropic displacement parameters ($\mathring{A}^2 \cdot 10^3$) for GSTR005. The anisotropic displacement factor exponent takes the form: $-2\pi^2[h^2a^{*2}U_{11} + ... + 2hka^*b^*U_{12}]$.

	U(11)	U(22)	U(33)	U(23)	U(13)	U(12)
C(1)	17(2)	17(2)	25(2)	2(2)	-1(2)	5(2)
C(2)	29(3)	25(2)	20(2)	-2(2)	5(2)	6(2)
C(3)	17(2)	23(2)	17(2)	-1(2)	1(1)	1(2)
C(4)	29(3)	32(3)	38(2)	13(2)	3(2)	8(2)
C(5)	27(3)	33(3)	26(2)	3(2)	-2(2)	6(2)
C(6)	28(3)	24(2)	34(2)	1(2)	-2(2)	3(2)
C(7)	26(3)	31(3)	44(3)	4(2)	4(2)	-10(2)
C(8)	40(3)	32(3)	38(3)	0(2)	-5(2)	-7(2)
C(9)	25(3)	41(3)	36(2)	4(2)	8(2)	-5(2)
C(10)	17(2)	17(2)	32(2)	3(2)	3(2)	1(2)
C(11)	28(3)	23(2)	44(3)	-5(2)	1(2)	-5(2)
C(12)	25(3)	23(3)	80(4)	-2(2)	5(2)	-8(2)
C(13)	26(3)	31(3)	69(3)	19(2)	19(2)	0(2)
C(14)	26(3)	37(3)	41(3)	13(2)	10(2)	3(2)
C(15)	22(3)	27(2)	31(2)	4(2)	0(2)	0(2)
C(16)	35(3)	30(3)	28(2)	-2(2)	0(2)	4(2)
C(17)	30(3)	25(2)	28(2)	6(2)	1(2)	6(2)
C(18)	24(3)	42(3)	23(2)	-3(2)	-6(2)	8(2)
C(19)	35(3)	31(3)	31(2)	0(2)	5(2)	1(2)
C(20)	23(2)	31(3)	26(2)	1(2)	-7(2)	4(2)
N(1)	26(2)	22(2)	25(2)	-4(1)	3(1)	3(2)
N(2)	25(2)	23(2)	16(2)	1(1)	4(1)	2(2)
O(1)	45(2)	38(2)	49(2)	-3(2)	-7(2)	23(2)
O(2)	39(2)	31(2)	39(2)	-3(1)	-11(1)	-4(2)
O(3)	33(2)	56(2)	24(2)	1(1)	9(1)	4(2)
O(4)	57(2)	60(3)	42(2)	-27(2)	1(2)	-14(2)
O(5)	40(2)	49(2)	30(2)	16(2)	5(1)	-2(2)
P	18(1)	18(1)	17(1)	1(1)	2(1)	0(1)
Si(1)	20(1)	23(1)	22(1)	2(1)	0(1)	2(1)

	x	y	z	U(eq)
Si(2)	20(1)	26(1)	30(1)	1(1)	1(1)	-6(1)
W	19(1)	21(1)	18(1)	0(1)	0(1)	3(1)

Table F.5: Hydrogen coordinates (x 10^4) and isotropic displacement parameters ($\mathring{A}^2 \cdot$ 10^3) for GSTR005.

	x	y	z	U(eq)
H(2A)	4499	4158	10466	29
H(3A)	3953	3207	6717	23
H(4A)	4255	4587	5584	40
H(4B)	4946	4923	6625	40
H(4C)	3720	5320	5985	40
H(5A)	785	3958	6224	35
H(5B)	1680	3962	5342	35
H(5C)	1097	4694	5702	35
H(6A)	3406	4970	8427	35
H(6B)	1937	4663	8293	35
H(6C)	2259	5367	7701	35
H(7A)	3165	2216	9119	41
H(7B)	3362	1727	8175	41
H(7C)	1964	1752	8568	41
H(8A)	2201	2137	6081	45
H(8B)	1170	2781	5908	45
H(8C)	803	2070	6466	45
H(9A)	593	3658	7784	40
H(9B)	1425	3491	8862	40
H(9C)	307	2947	8377	40
H(11A)	7789	5174	9288	39
H(12A)	9458	5671	8501	52
H(13A)	9605	5384	6828	49
H(14A)	8176	4557	5977	41
H(15A)	6541	4031	6770	33

Table F.6: Torsion angles [º] for GSTR005.

N(1)-C(1)-C(10)-C(15)	−173.8(4)	Si(1)-C(3)-Si(2)-C(9)	-38.9(2)
P-C(1)-C(10)-C(15)	21.1(5)	O(1)-C(16)-W-C(19)	-95(21)
N(1)-C(1)-C(10)-C(11)	7.2(6)	O(1)-C(16)-W-C(20)	-5(21)
P-C(1)-C(10)-C(11)	−157.9(3)	O(1)-C(16)-W-C(18)	178(100)
C(15)-C(10)-C(11)-C(12)	0.5(6)	O(1)-C(16)-W-C(17)	85(21)

C(1)-C(10)-C(11)-C(12)	179.5(4)	O(1)-C(16)-W-P	26(22)
C(10)-C(11)-C(12)-C(13)	1.2(7)	O(4)-C(19)-W-C(16)	21(15)
C(11)-C(12)-C(13)-C(14)	−1.9(7)	O(4)-C(19)-W-C(20)	-66(15)
C(12)-C(13)-C(14)-C(15)	0.9(7)	O(4)-C(19)-W-C(18)	110(15)
C(13)-C(14)-C(15)-C(10)	0.8(7)	O(4)-C(19)-W-C(17)	22(21)
C(11)-C(10)-C(15)-C(14)	−1.5(6)	O(4)-C(19)-W-P	-154(15)
C(1)-C(10)-C(15)-C(14)	179.5(4)	O(5)-C(20)-W-C(16)	-28(11)
C(10)-C(1)-N(1)-C(2)	−175.3(3)	O(5)-C(20)-W-C(19)	62(11)
P-C(1)-N(1)-C(2)	−7.5(4)	O(5)-C(20)-W-C(18)	6(12)
N(2)-C(2)-N(1)-C(1)	4.9(5)	O(5)-C(20)-W-C(17)	-117(11)
N(1)-C(2)-N(2)-P	0.9(5)	O(5)-C(20)-W-P	154(11)
C(2)-N(2)-P-C(3)	−122.2(3)	O(3)-C(18)-W-C(16)	34(4)
C(2)-N(2)-P-C(1)	−4.3(3)	O(3)-C(18)-W-C(19)	-56(4)
C(2)-N(2)-P-W	101.3(3)	O(3)-C(18)-W-C(20)	0(5)
Si(1)-C(3)-P-N(2)	82.5(2)	O(3)-C(18)-W-C(17)	123(4)
Si(2)-C(3)-P-N(2)	−48.1(2)	O(3)-C(18)-W-P	-148(4)
Si(1)-C(3)-P-C(1)	−14.3(3)	O(2)-C(17)-W-C(16)	-28(15)
Si(2)-C(3)-P-C(1)	−144.98(18)	O(2)-C(17)-W-C(19)	-29(20)
Si(1)-C(3)-P-W	−150.31(12)	O(2)-C(17)-W-C(20)	60(15)
Si(2)-C(3)-P-W	79.1(2)	O(2)-C(17)-W-C(18)	-116(15)
N(1)-C(1)-P-N(2)	7.2(3)	O(2)-C(17)-W-P	148(15)
C(10)-C(1)-P-N(2)	173.7(3)	N(2)-P-W-C(16)	-13.4(15)
N(1)-C(1)-P-C(3)	111.0(3)	C(3)-P-W-C(16)	-136.9(15)
C(10)-C(1)-P-C(3)	−82.4(4)	C(1)-P-W-C(16)	82.8(15)
N(1)-C(1)-P-W	−104.4(3)	N(2)-P-W-C(19)	107.50(17)
C(10)-C(1)-P-W	62.1(3)	C(3)-P-W-C(19)	-16.01(18)
P-C(3)-Si(1)-C(6)	−52.6(3)	C(1)-P-W-C(19)	-156.32(17)
Si(2)-C(3)-Si(1)-C(6)	77.8(2)	N(2)-P-W-C(20)	17.67(17)
P-C(3)-Si(1)-C(4)	69.2(2)	C(3)-P-W-C(20)	-105.85(19)
Si(2)-C(3)-Si(1)-C(4)	−160.39(18)	C(1)-P-W-C(20)	113.85(16)
P-C(3)-Si(1)-C(5)	−175.84(19)	N(2)-P-W-C(18)	-164.93(17)
Si(2)-C(3)-Si(1)-C(5)	−45.4(2)	C(3)-P-W-C(18)	71.55(19)
P-C(3)-Si(2)-C(7)	−24.0(3)	C(1)-P-W-C(18)	-68.75(17)
Si(1)-C(3)-Si(2)-C(7)	−157.72(19)	N(2)-P-W-C(17)	-72.43(17)
P-C(3)-Si(2)-C(8)	−142.6(2)	C(3)-P-W-C(17)	164.06(18)
Si(1)-C(3)-Si(2)-C(8)	83.7(2)	C(1)-P-W-C(17)	23.76(16)
P-C(3)-Si(2)-C(9)	94.8(2)		

F.2 Data for Complex 69b
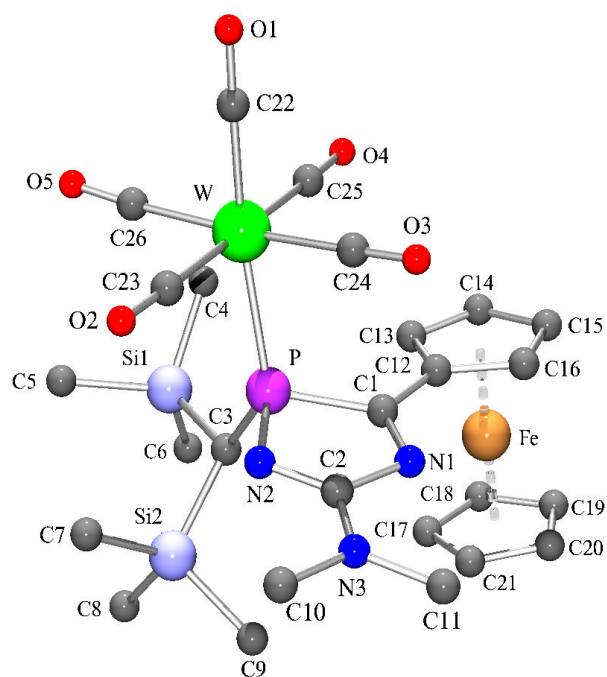
Figure F.2: Molecular structure of complex **69b** (GSTR048) in the crystal (hydrogen atoms are omitted for clarity).

Table F.7: Crystal data and structure refinement for GSTR048.

Identification code	GSTR048
Empirical formula	$C_{26}H_{34}FeN_3O_5PSi_2W$
Formula weight	795.41
Temperature	293(2) K
Wavelength	0.71073 Å
Crystal system, space group	Monoclinic, P $2_1/n$
Unit cell dimensions	a = 16.0145(5) Å, $\alpha = 90^o$
	b = 12.3033(4) Å, $\beta = 103.387(2)^o$
	c = 16.1955(3) Å, $\gamma = 90^o$
Volume	3104.31(15) Å^3
Z, Calculated density	4, 1.702 Mg/m^3
Absorption coefficient	4.337 mm^{-1}
F(000)	1576
Crystal size	0.50 x 0.18 x 0.18 mm
θ range for data collection	2.61 to 27.47^o
Limiting indices	-20 $\leq$ h $\leq$ 19, -14 $\leq$ k $\leq$ 15, -18 $\leq$ l $\leq$ 20
Reflections collected / unique	21506 / 6845 [R$_{int}$ = 0.0336]
Completeness to θ = 27.47	96.3 %
Absorption correction	Analytical
Max. and min. transmission	0.5090 and 0.2203
Refinement method	Full-matrix least-squares on F^2
Data / restraints / parameters	6845 / 0 / 387
Goodness-of-fit on F^2	1.051
Final R indices [I>2σ(I)]	R$_1$ = 0.0257, wR$_2$ = 0.0594
R indices (all data)	R$_1$ = 0.0317, wR$_2$ = 0.0613
Largest diff. peak and hole	3.694 and -1.404 e $\cdot$ A^{-3}

Table F.8: Atomic coordinates (x 10^4) and equivalent isotropic displacement parameters ($\mathring{A}^2 \cdot 10^3$) for GSTR048. U(eq) is defined as one third of the trace of the orthogonalized U$_{ij}$ tensor.

	x	y	z	U(eq)
W	9302(1)	2659(1)	5007(1)	13(1)
Fe	6684(1)	2787(1)	7233(1)	14(1)
P	7694(1)	2841(1)	4844(1)	11(1)
Si(1)	7095(1)	317(1)	4567(1)	16(1)
Si(2)	5994(1)	2288(1)	3569(1)	15(1)
N(1)	7258(2)	4568(2)	5583(2)	14(1)
N(2)	7361(2)	3923(2)	4219(2)	13(1)
N(3)	6929(2)	5703(2)	4377(2)	17(1)
O(1)	11305(2)	2862(2)	5273(2)	32(1)
O(2)	8991(2)	3823(3)	3203(2)	45(1)
O(3)	9370(2)	4943(2)	5941(2)	41(1)
O(4)	9589(2)	1397(2)	6761(2)	24(1)
O(5)	9478(2)	453(2)	4029(2)	36(1)
C(1)	7485(2)	3576(3)	5778(2)	12(1)
C(2)	7188(2)	4720(3)	4686(2)	12(1)
C(3)	6825(2)	1823(3)	4568(2)	13(1)
C(4)	8043(2)	-176(3)	5400(2)	18(1)
C(5)	7287(3)	-111(3)	3522(2)	34(1)
C(6)	6154(2)	-395(3)	4830(3)	35(1)
C(7)	6522(2)	2529(3)	2666(2)	23(1)
C(8)	5150(2)	1222(3)	3208(2)	25(1)
C(9)	5373(2)	3476(3)	3844(2)	23(1)
C(10)	6875(2)	5937(3)	3481(2)	22(1)
C(11)	6722(2)	6587(3)	4884(2)	21(1)
C(12)	7641(2)	3160(3)	6640(2)	13(1)
C(13)	7686(2)	2037(3)	6878(2)	16(1)
C(14)	7803(2)	1970(3)	7769(2)	19(1)
C(15)	7831(2)	3047(3)	8090(2)	17(1)
C(16)	7724(2)	3784(3)	7404(2)	14(1)
C(17)	5546(3)	2219(5)	6529(3)	43(1)
C(18)	5663(3)	1873(4)	7385(3)	44(1)
C(19)	5728(3)	2821(4)	7882(3)	39(1)
C(20)	5658(3)	3725(4)	7345(3)	36(1)
C(21)	5550(2)	3352(4)	6517(3)	37(1)
C(22)	10575(2)	2783(3)	5171(2)	22(1)

C(23)	9099(2)	3425(3)	3852(2)	25(1)
C(24)	9336(2)	4122(3)	5613(2)	23(1)
C(25)	9474(2)	1855(3)	6135(2)	17(1)
C(26)	9378(2)	1231(3)	4381(2)	23(1)

Table F.9: Bond lengths [Å] and angles [°] for GSTR048.

W-C(22)	2.000(4)	C(4)-H(4C)	0.9600
W-C(25)	2.040(3)	C(5)-H(5A)	0.9600
W-C(24)	2.044(4)	C(5)-H(5B)	0.9600
W-C(26)	2.046(4)	C(5)-H(5C)	0.9600
W-C(23)	2.052(4)	C(6)-H(6A)	0.9600
W-P	2.5359(8)	C(6)-H(6B)	0.9600
Fe-C(16)	2.034(3)	C(6)-H(6C)	0.9600
Fe-C(17)	2.037(4)	C(7)-H(7A)	0.9600
Fe-C(21)	2.038(4)	C(7)-H(7B)	0.9600
Fe-C(12)	2.040(3)	C(7)-H(7C)	0.9600
Fe-C(13)	2.045(3)	C(8)-H(8A)	0.9600
Fe-C(18)	2.046(4)	C(8)-H(8B)	0.9600
Fe-C(19)	2.048(4)	C(8)-H(8C)	0.9600
Fe-C(20)	2.050(4)	C(9)-H(9A)	0.9600
Fe-C(15)	2.054(3)	C(9)-H(9B)	0.9600
Fe-C(14)	2.062(4)	C(9)-H(9C)	0.9600
P-N(2)	1.683(3)	C(10)-H(10A)	0.9600
P-C(3)	1.849(3)	C(10)-H(10B)	0.9600
P-C(1)	1.859(3)	C(10)-H(10C)	0.9600
Si(1)-C(5)	1.864(4)	C(11)-H(11A)	0.9600
Si(1)-C(6)	1.875(4)	C(11)-H(11B)	0.9600
Si(1)-C(4)	1.882(3)	C(11)-H(11C)	0.9600
Si(1)-C(3)	1.903(3)	C(12)-C(13)	1.432(5)
Si(2)-C(7)	1.875(4)	C(12)-C(16)	1.436(4)
Si(2)-C(8)	1.877(4)	C(13)-C(14)	1.414(4)
Si(2)-C(9)	1.878(4)	C(13)-H(13)	0.86(4)
Si(2)-C(3)	1.929(3)	C(14)-C(15)	1.421(5)
N(1)-C(1)	1.292(4)	C(14)-H(14)	0.92(4)
N(1)-C(2)	1.443(4)	C(15)-C(16)	1.413(5)
N(2)-C(2)	1.307(4)	C(15)-H(15)	0.96(4)
N(3)-C(2)	1.337(4)	C(16)-H(16)	0.94(4)
N(3)-C(11)	1.447(4)	C(17)-C(21)	1.395(7)
N(3)-C(10)	1.462(4)	C(17)-C(18)	1.421(7)

O(1)-C(22)	1.145(4)	C(17)-H(17)	0.72(5)
O(2)-C(23)	1.137(4)	C(18)-C(19)	1.407(7)
O(3)-C(24)	1.137(4)	C(18)-H(18)	0.84(5)
O(4)-C(25)	1.137(4)	C(19)-C(20)	1.400(7)
O(5)-C(26)	1.145(4)	C(19)-H(19)	0.91(5)
C(1)-C(12)	1.452(4)	C(20)-C(21)	1.390(6)
C(3)-H(3)	0.9800	C(20)-H(20)	0.83(5)
C(4)-H(4A)	0.9600	C(21)-H(21)	0.97(5)
C(4)-H(4B)	0.9600		
C(22)-W-C(25)	89.74(13)	Si(1)-C(5)-H(5C)	109.5
C(22)-W-C(24)	87.50(14)	H(5A)-C(5)-H(5C)	109.5
C(25)-W-C(24)	90.80(13)	H(5B)-C(5)-H(5C)	109.5
C(22)-W-C(26)	87.45(14)	Si(1)-C(6)-H(6A)	109.5
C(25)-W-C(26)	90.92(13)	Si(1)-C(6)-H(6B)	109.5
C(24)-W-C(26)	174.65(13)	H(6A)-C(6)-H(6B)	109.5
C(22)-W-C(23)	91.58(14)	Si(1)-C(6)-H(6C)	109.5
C(25)-W-C(23)	177.97(14)	H(6A)-C(6)-H(6C)	109.5
C(24)-W-C(23)	90.80(15)	H(6B)-C(6)-H(6C)	109.5
C(26)-W-C(23)	87.60(15)	Si(2)-C(7)-H(7A)	109.5
C(22)-W-P	170.44(11)	Si(2)-C(7)-H(7B)	109.5
C(25)-W-P	93.42(9)	H(7A)-C(7)-H(7B)	109.5
C(24)-W-P	83.44(10)	Si(2)-C(7)-H(7C)	109.5
C(26)-W-P	101.51(10)	H(7A)-C(7)-H(7C)	109.5
C(23)-W-P	85.52(10)	H(7B)-C(7)-H(7C)	109.5
C(16)-Fe-C(17)	151.75(18)	Si(2)-C(8)-H(8A)	109.5
C(16)-Fe-C(21)	117.69(17)	Si(2)-C(8)-H(8B)	109.5
C(17)-Fe-C(21)	40.0(2)	H(8A)-C(8)-H(8B)	109.5
C(16)-Fe-C(12)	41.26(12)	Si(2)-C(8)-H(8C)	109.5
C(17)-Fe-C(12)	119.05(15)	H(8A)-C(8)-H(8C)	109.5
C(21)-Fe-C(12)	108.78(15)	H(8B)-C(8)-H(8C)	109.5
C(16)-Fe-C(13)	68.89(13)	Si(2)-C(9)-H(9A)	109.5
C(17)-Fe-C(13)	110.27(16)	Si(2)-C(9)-H(9B)	109.5
C(21)-Fe-C(13)	130.34(15)	H(9A)-C(9)-H(9B)	109.5
C(12)-Fe-C(13)	41.04(13)	Si(2)-C(9)-H(9C)	109.5
C(16)-Fe-C(18)	165.19(17)	H(9A)-C(9)-H(9C)	109.5
C(17)-Fe-C(18)	40.7(2)	H(9B)-C(9)-H(9C)	109.5
C(21)-Fe-C(18)	67.9(2)	N(3)-C(10)-H(10A)	109.5
C(12)-Fe-C(18)	152.69(17)	N(3)-C(10)-H(10B)	109.5
C(13)-Fe-C(18)	119.12(18)	H(10A)-C(10)-H(10B)	109.5

C(16)-Fe-C(19)	127.13(16)	N(3)-C(10)-H(10C)	109.5
C(17)-Fe-C(19)	67.38(17)	H(10A)-C(10)-H(10C)	109.5
C(21)-Fe-C(19)	67.14(17)	H(10B)-C(10)-H(10C)	109.5
C(12)-Fe-C(19)	165.71(17)	N(3)-C(11)-H(11A)	109.5
C(13)-Fe-C(19)	151.85(17)	N(3)-C(11)-H(11B)	109.5
C(18)-Fe-C(19)	40.2(2)	H(11A)-C(11)-H(11B)	109.5
C(16)-Fe-C(20)	107.22(16)	N(3)-C(11)-H(11C)	109.5
C(17)-Fe-C(20)	67.08(19)	H(11A)-C(11)-H(11C)	109.5
C(21)-Fe-C(20)	39.76(17)	H(11B)-C(11)-H(11C)	109.5
C(12)-Fe-C(20)	128.27(16)	C(13)-C(12)-C(16)	107.1(3)
C(13)-Fe-C(20)	167.35(16)	C(13)-C(12)-C(1)	125.8(3)
C(18)-Fe-C(20)	67.6(2)	C(16)-C(12)-C(1)	126.9(3)
C(19)-Fe-C(20)	39.96(19)	C(13)-C(12)-Fe	69.66(18)
C(16)-Fe-C(15)	40.43(13)	C(16)-C(12)-Fe	69.14(17)
C(17)-Fe-C(15)	167.38(19)	C(1)-C(12)-Fe	123.5(2)
C(21)-Fe-C(15)	150.57(18)	C(14)-C(13)-C(12)	108.6(3)
C(12)-Fe-C(15)	68.38(12)	C(14)-C(13)-Fe	70.5(2)
C(13)-Fe-C(15)	67.87(13)	C(12)-C(13)-Fe	69.30(18)
C(18)-Fe-C(15)	128.26(18)	C(14)-C(13)-H(13)	125(2)
C(19)-Fe-C(15)	107.97(15)	C(12)-C(13)-H(13)	127(2)
C(20)-Fe-C(15)	117.54(16)	Fe-C(13)-H(13)	130(2)
C(16)-Fe-C(14)	68.49(14)	C(13)-C(14)-C(15)	107.7(3)
C(17)-Fe-C(14)	130.23(19)	C(13)-C(14)-Fe	69.21(19)
C(21)-Fe-C(14)	168.16(17)	C(15)-C(14)-Fe	69.50(19)
C(12)-Fe-C(14)	68.55(13)	C(13)-C(14)-H(14)	127(2)
C(13)-Fe-C(14)	40.26(12)	C(15)-C(14)-H(14)	125(2)
C(18)-Fe-C(14)	108.79(19)	Fe-C(14)-H(14)	126(2)
C(19)-Fe-C(14)	118.29(16)	C(16)-C(15)-C(14)	108.9(3)
C(20)-Fe-C(14)	150.85(16)	C(16)-C(15)-Fe	69.03(18)
C(15)-Fe-C(14)	40.38(14)	C(14)-C(15)-Fe	70.11(19)
N(2)-P-C(3)	105.96(14)	C(16)-C(15)-H(15)	127(2)
N(2)-P-C(1)	90.74(13)	C(14)-C(15)-H(15)	124(2)
C(3)-P-C(1)	104.99(14)	Fe-C(15)-H(15)	122(2)
N(2)-P-W	107.78(9)	C(15)-C(16)-C(12)	107.7(3)
C(3)-P-W	130.89(10)	C(15)-C(16)-Fe	70.54(19)
C(1)-P-W	109.14(10)	C(12)-C(16)-Fe	69.59(18)
C(5)-Si(1)-C(6)	112.6(2)	C(15)-C(16)-H(16)	125(2)
C(5)-Si(1)-C(4)	106.53(16)	C(12)-C(16)-H(16)	127(2)
C(6)-Si(1)-C(4)	104.11(16)	Fe-C(16)-H(16)	126(2)
C(5)-Si(1)-C(3)	111.16(17)	C(21)-C(17)-C(18)	108.3(4)

C(6)-Si(1)-C(3)	105.04(16)	C(21)-C(17)-Fe	70.0(2)
C(4)-Si(1)-C(3)	117.31(14)	C(18)-C(17)-Fe	70.0(2)
C(7)-Si(2)-C(8)	106.81(16)	C(21)-C(17)-H(17)	122(4)
C(7)-Si(2)-C(9)	114.89(17)	C(18)-C(17)-H(17)	129(4)
C(8)-Si(2)-C(9)	103.58(17)	Fe-C(17)-H(17)	123(4)
C(7)-Si(2)-C(3)	110.68(15)	C(19)-C(18)-C(17)	106.6(4)
C(8)-Si(2)-C(3)	111.22(15)	C(19)-C(18)-Fe	70.0(2)
C(9)-Si(2)-C(3)	109.43(14)	C(17)-C(18)-Fe	69.3(2)
C(1)-N(1)-C(2)	108.7(3)	C(19)-C(18)-H(18)	127(4)
C(2)-N(2)-P	109.0(2)	C(17)-C(18)-H(18)	127(4)
C(2)-N(3)-C(11)	124.0(3)	Fe-C(18)-H(18)	127(4)
C(2)-N(3)-C(10)	119.5(3)	C(20)-C(19)-C(18)	108.6(4)
C(11)-N(3)-C(10)	116.5(3)	C(20)-C(19)-Fe	70.1(2)
N(1)-C(1)-C(12)	123.0(3)	C(18)-C(19)-Fe	69.8(2)
N(1)-C(1)-P	110.7(2)	C(20)-C(19)-H(19)	123(3)
C(12)-C(1)-P	126.0(2)	C(18)-C(19)-H(19)	128(3)
N(2)-C(2)-N(3)	123.4(3)	Fe-C(19)-H(19)	123(3)
N(2)-C(2)-N(1)	120.5(3)	C(21)-C(20)-C(19)	108.1(4)
N(3)-C(2)-N(1)	116.1(3)	C(21)-C(20)-Fe	69.6(2)
P-C(3)-Si(1)	120.10(16)	C(19)-C(20)-Fe	69.9(2)
P-C(3)-Si(2)	109.65(16)	C(21)-C(20)-H(20)	124(3)
Si(1)-C(3)-Si(2)	113.63(16)	C(19)-C(20)-H(20)	128(3)
P-C(3)-H(3)	103.8	Fe-C(20)-H(20)	127(3)
Si(1)-C(3)-H(3)	103.8	C(20)-C(21)-C(17)	108.4(4)
Si(2)-C(3)-H(3)	103.8	C(20)-C(21)-Fe	70.6(2)
Si(1)-C(4)-H(4A)	109.5	C(17)-C(21)-Fe	70.0(3)
Si(1)-C(4)-H(4B)	109.5	C(20)-C(21)-H(21)	127(3)
H(4A)-C(4)-H(4B)	109.5	C(17)-C(21)-H(21)	124(3)
Si(1)-C(4)-H(4C)	109.5	Fe-C(21)-H(21)	118(3)
H(4A)-C(4)-H(4C)	109.5	O(1)-C(22)-W	179.2(3)
H(4B)-C(4)-H(4C)	109.5	O(2)-C(23)-W	178.1(4)
Si(1)-C(5)-H(5A)	109.5	O(3)-C(24)-W	178.3(3)
Si(1)-C(5)-H(5B)	109.5	O(4)-C(25)-W	178.3(3)
H(5A)-C(5)-H(5B)	109.5	O(5)-C(26)-W	175.2(3)

Table F.10: Anisotropic displacement parameters ($\text{Å}^2 \cdot 10^3$) for GSTR048. The anisotropic displacement factor exponent takes the form: $-2\pi^2[h^2a^{*2}U_{11} + ... + 2hka^*b^*U_{12}]$.

	U(11)	U(22)	U(33)	U(23)	U(13)	U(12)
W	11(1)	16(1)	12(1)	1(1)	3(1)	-1(1)
Fe	17(1)	17(1)	10(1)	-2(1)	6(1)	-4(1)
P	13(1)	11(1)	9(1)	0(1)	3(1)	0(1)
Si(1)	16(1)	12(1)	20(1)	-4(1)	2(1)	-1(1)
Si(2)	12(1)	19(1)	12(1)	0(1)	1(1)	-1(1)
N(1)	18(1)	13(1)	12(1)	1(1)	4(1)	1(1)
N(2)	14(1)	13(1)	11(1)	2(1)	4(1)	1(1)
N(3)	29(2)	11(1)	12(1)	1(1)	6(1)	2(1)
O(1)	13(1)	47(2)	35(2)	-3(1)	4(1)	-3(1)
O(2)	28(2)	76(2)	34(2)	33(2)	11(1)	10(2)
O(3)	41(2)	23(2)	59(2)	-15(1)	12(1)	-11(1)
O(4)	28(1)	26(1)	18(1)	5(1)	3(1)	2(1)
O(5)	37(2)	32(2)	44(2)	-15(1)	19(1)	2(1)
C(1)	11(2)	14(2)	12(1)	-1(1)	5(1)	-2(1)
C(2)	12(2)	16(2)	10(1)	2(1)	3(1)	-2(1)
C(3)	12(2)	13(2)	15(2)	1(1)	4(1)	-2(1)
C(4)	20(2)	14(2)	19(2)	-1(1)	5(1)	1(1)
C(5)	39(2)	36(2)	23(2)	-14(2)	-2(2)	11(2)
C(6)	21(2)	17(2)	62(3)	10(2)	1(2)	-4(2)
C(7)	23(2)	32(2)	14(2)	-3(1)	3(1)	-3(2)
C(8)	21(2)	27(2)	23(2)	3(2)	1(1)	-2(2)
C(9)	16(2)	29(2)	21(2)	1(2)	0(1)	4(2)
C(10)	32(2)	17(2)	17(2)	6(1)	6(1)	4(2)
C(11)	27(2)	11(2)	26(2)	-1(1)	6(1)	7(1)
C(12)	14(2)	14(2)	13(1)	0(1)	4(1)	1(1)
C(13)	24(2)	12(2)	14(2)	-1(1)	6(1)	2(1)
C(14)	30(2)	13(2)	13(2)	3(1)	6(1)	2(1)
C(15)	19(2)	20(2)	12(2)	0(1)	2(1)	-1(1)
C(16)	16(2)	12(2)	16(2)	-1(1)	3(1)	0(1)
C(17)	23(2)	71(4)	36(2)	-33(2)	13(2)	-23(2)
C(18)	34(2)	43(3)	60(3)	2(2)	24(2)	-19(2)
C(19)	25(2)	71(3)	25(2)	-4(2)	16(2)	-7(2)
C(20)	21(2)	42(3)	46(3)	-9(2)	9(2)	3(2)
C(21)	15(2)	64(3)	31(2)	8(2)	2(2)	-3(2)
C(22)	21(2)	26(2)	17(2)	-1(1)	4(1)	-1(1)

C(23)	14(2)	35(2)	27(2)	6(2)	7(1)	2(2)
C(24)	16(2)	25(2)	27(2)	0(2)	3(1)	-6(1)
C(25)	12(2)	20(2)	18(2)	-6(1)	2(1)	0(1)
C(26)	19(2)	29(2)	22(2)	0(2)	7(1)	0(2)

Table F.11: Hydrogen coordinates (x 10^4) and isotropic displacement parameters ($\mathring{A}^2 \cdot$ 10^3) for GSTR048.

	x	y	z	U(eq)
H(3)	6520	1892	5025	16
H(4A)	8122	-941	5326	26
H(4B)	7942	-48	5953	26
H(4C)	8549	208	5345	26
H(5A)	7392	-879	3529	51
H(5B)	7777	269	3419	51
H(5C)	6791	58	3081	51
H(6A)	5639	-196	4424	52
H(6B)	6106	-186	5388	52
H(6C)	6236	-1167	4813	52
H(7A)	6295	2029	2214	35
H(7B)	7130	2420	2857	35
H(7C)	6411	3260	2463	35
H(8A)	4740	1479	2716	37
H(8B)	4863	1074	3655	37
H(8C)	5414	569	3068	37
H(9A)	5633	4140	3718	34
H(9B)	5378	3454	4438	34
H(9C)	4792	3441	3517	34
H(10A)	7133	5354	3235	32
H(10B)	7172	6603	3432	32
H(10C)	6283	6008	3188	32
H(11A)	6639	6308	5413	32
H(11B)	6205	6938	4583	32
H(11C)	7184	7103	4993	32
H(13)	7690(20)	1490(30)	6550(20)	20
H(14)	7850(20)	1340(30)	8090(20)	22
H(15)	7860(20)	3220(30)	8670(20)	20
H(16)	7720(20)	4540(30)	7450(20)	17
H(17)	5510(30)	1900(40)	6150(30)	51
H(18)	5680(30)	1230(40)	7560(30)	52

H(19)	5830(30)	2870(40)	8460(30)	46
H(20)	5670(30)	4380(40)	7480(30)	44
H(21)	5570(30)	3780(40)	6020(30)	45

Table F.12: Torsion angles [º] for GSTR048.

C(22)-W-P-N(2)	46.0(6)	Fe-C(15)-C(16)-C(12)	-59.9(2)
C(25)-W-P-N(2)	155.15(13)	C(14)-C(15)-C(16)-Fe	58.9(2)
C(24)-W-P-N(2)	64.74(14)	C(13)-C(12)-C(16)-C(15)	1.0(4)
C(26)-W-P-N(2)	−113.21(14)	C(1)-C(12)-C(16)-C(15)	177.4(3)
C(23)-W-P-N(2)	−26.59(15)	Fe-C(12)-C(16)-C(15)	60.5(2)
C(22)-W-P-C(3)	177.3(6)	C(13)-C(12)-C(16)-Fe	-59.6(2)
C(25)-W-P-C(3)	−73.57(16)	C(1)-C(12)-C(16)-Fe	116.9(3)
C(24)-W-P-C(3)	−163.98(16)	C(17)-Fe-C(16)-C(15)	-174.0(3)
C(26)-W-P-C(3)	18.07(17)	C(21)-Fe-C(16)-C(15)	154.2(2)
C(23)-W-P-C(3)	104.69(17)	C(12)-Fe-C(16)-C(15)	-118.4(3)
C(22)-W-P-C(1)	−51.2(6)	C(13)-Fe-C(16)-C(15)	-80.2(2)
C(25)-W-P-C(1)	57.94(14)	C(18)-Fe-C(16)-C(15)	45.3(8)
C(24)-W-P-C(1)	−32.48(15)	C(19)-Fe-C(16)-C(15)	73.0(3)
C(26)-W-P-C(1)	149.57(15)	C(20)-Fe-C(16)-C(15)	112.5(2)
C(23)-W-P-C(1)	−123.80(15)	C(14)-Fe-C(16)-C(15)	-36.88(19)
C(3)-P-N(2)-C(2)	109.9(2)	C(17)-Fe-C(16)-C(12)	-55.6(4)
C(1)-P-N(2)-C(2)	4.1(2)	C(21)-Fe-C(16)-C(12)	-87.3(2)
W-P-N(2)-C(2)	−106.3(2)	C(13)-Fe-C(16)-C(12)	38.21(18)
C(2)-N(1)-C(1)-C(12)	178.0(3)	C(18)-Fe-C(16)-C(12)	163.7(7)
C(2)-N(1)-C(1)-P	4.2(3)	C(19)-Fe-C(16)-C(12)	-168.5(2)
N(2)-P-C(1)-N(1)	−5.0(2)	C(20)-Fe-C(16)-C(12)	-129.0(2)
C(3)-P-C(1)-N(1)	−111.8(2)	C(15)-Fe-C(16)-C(12)	118.4(3)
W-P-C(1)-N(1)	104.1(2)	C(14)-Fe-C(16)-C(12)	81.57(19)
N(2)-P-C(1)-C(12)	−178.6(3)	C(16)-Fe-C(17)-C(21)	-46.4(4)
C(3)-P-C(1)-C(12)	74.7(3)	C(12)-Fe-C(17)-C(21)	-84.9(3)
W-P-C(1)-C(12)	−69.5(3)	C(13)-Fe-C(17)-C(21)	-129.3(2)
P-N(2)-C(2)-N(3)	178.2(3)	C(18)-Fe-C(17)-C(21)	119.2(4)
P-N(2)-C(2)-N(1)	−2.7(4)	C(19)-Fe-C(17)-C(21)	80.9(3)
C(11)-N(3)-C(2)-N(2)	179.0(3)	C(20)-Fe-C(17)-C(21)	37.4(3)
C(10)-N(3)-C(2)-N(2)	−3.3(5)	C(15)-Fe-C(17)-C(21)	151.6(6)
C(11)-N(3)-C(2)-N(1)	−0.1(5)	C(14)-Fe-C(17)-C(21)	-170.4(2)
C(10)-N(3)-C(2)-N(1)	177.6(3)	C(16)-Fe-C(17)-C(18)	-165.6(3)
C(1)-N(1)-C(2)-N(2)	−1.2(4)	C(21)-Fe-C(17)-C(18)	-119.2(4)
C(1)-N(1)-C(2)-N(3)	177.9(3)	C(12)-Fe-C(17)-C(18)	155.9(3)

N(2)-P-C(3)-Si(1)	143.96(17)	C(13)-Fe-C(17)-C(18)	111.5(3)
C(1)-P-C(3)-Si(1)	−120.85(18)	C(19)-Fe-C(17)-C(18)	-38.3(3)
W-P-C(3)-Si(1)	12.1(2)	C(20)-Fe-C(17)-C(18)	-81.8(3)
N(2)-P-C(3)-Si(2)	9.60(19)	C(15)-Fe-C(17)-C(18)	32.4(8)
C(1)-P-C(3)-Si(2)	104.79(16)	C(14)-Fe-C(17)-C(18)	70.3(3)
W-P-C(3)-Si(2)	−122.29(12)	C(21)-C(17)-C(18)-C(19)	0.6(5)
C(5)-Si(1)-C(3)-P	−86.9(2)	Fe-C(17)-C(18)-C(19)	60.4(3)
C(6)-Si(1)-C(3)-P	151.0(2)	C(21)-C(17)-C(18)-Fe	-59.8(3)
C(4)-Si(1)-C(3)-P	36.0(2)	C(16)-Fe-C(18)-C(19)	35.1(9)
C(5)-Si(1)-C(3)-Si(2)	45.8(2)	C(17)-Fe-C(18)-C(19)	-117.5(4)
C(6)-Si(1)-C(3)-Si(2)	−76.3(2)	C(21)-Fe-C(18)-C(19)	-80.2(3)
C(4)-Si(1)-C(3)-Si(2)	168.71(15)	C(12)-Fe-C(18)-C(19)	-168.6(3)
C(7)-Si(2)-C(3)-P	56.4(2)	C(13)-Fe-C(18)-C(19)	154.8(3)
C(8)-Si(2)-C(3)-P	174.97(16)	C(20)-Fe-C(18)-C(19)	-37.1(3)
C(9)-Si(2)-C(3)-P	−71.2(2)	C(15)-Fe-C(18)-C(19)	71.1(3)
C(7)-Si(2)-C(3)-Si(1)	−81.1(2)	C(14)-Fe-C(18)-C(19)	111.9(3)
C(8)-Si(2)-C(3)-Si(1)	37.4(2)	C(16)-Fe-C(18)-C(17)	152.6(6)
C(9)-Si(2)-C(3)-Si(1)	151.28(17)	C(21)-Fe-C(18)-C(17)	37.3(3)
N(1)-C(1)-C(12)-C(13)	163.7(3)	C(12)-Fe-C(18)-C(17)	-51.1(5)
P-C(1)-C(12)-C(13)	−23.5(5)	C(13)-Fe-C(18)-C(17)	-87.7(3)
N(1)-C(1)-C(12)-C(16)	−12.1(5)	C(19)-Fe-C(18)-C(17)	117.5(4)
P-C(1)-C(12)-C(16)	160.7(3)	C(20)-Fe-C(18)-C(17)	80.4(3)
N(1)-C(1)-C(12)-Fe	75.8(4)	C(15)-Fe-C(18)-C(17)	-171.4(3)
P-C(1)-C(12)-Fe	−111.4(3)	C(14)-Fe-C(18)-C(17)	-130.6(3)
C(16)-Fe-C(12)-C(13)	118.5(3)	C(17)-C(18)-C(19)-C(20)	-0.3(5)
C(17)-Fe-C(12)-C(13)	−88.0(3)	Fe-C(18)-C(19)-C(20)	59.6(3)
C(21)-Fe-C(12)-C(13)	−130.6(2)	C(17)-C(18)-C(19)-Fe	-59.9(3)
C(18)-Fe-C(12)-C(13)	−52.5(4)	C(16)-Fe-C(19)-C(20)	71.0(3)
C(19)-Fe-C(12)-C(13)	158.5(6)	C(17)-Fe-C(19)-C(20)	-80.8(3)
C(20)-Fe-C(12)-C(13)	−170.6(2)	C(21)-Fe-C(19)-C(20)	-37.3(3)
C(15)-Fe-C(12)-C(13)	80.7(2)	C(12)-Fe-C(19)-C(20)	38.9(7)
C(14)-Fe-C(12)-C(13)	37.12(19)	C(13)-Fe-C(19)-C(20)	-171.8(3)
C(17)-Fe-C(12)-C(16)	153.5(2)	C(18)-Fe-C(19)-C(20)	-119.6(4)
C(21)-Fe-C(12)-C(16)	110.9(2)	C(15)-Fe-C(19)-C(20)	111.7(3)
C(13)-Fe-C(12)-C(16)	−118.5(3)	C(14)-Fe-C(19)-C(20)	154.4(2)
C(18)-Fe-C(12)-C(16)	−171.0(4)	C(16)-Fe-C(19)-C(18)	-169.4(3)
C(19)-Fe-C(12)-C(16)	40.0(7)	C(17)-Fe-C(19)-C(18)	38.8(3)
C(20)-Fe-C(12)-C(16)	70.9(3)	C(21)-Fe-C(19)-C(18)	82.4(3)
C(15)-Fe-C(12)-C(16)	−37.83(19)	C(12)-Fe-C(19)-C(18)	158.5(6)
C(14)-Fe-C(12)-C(16)	−81.4(2)	C(13)-Fe-C(19)-C(18)	-52.1(5)

C(16)-Fe-C(12)-C(1)	−121.3(3)	C(20)-Fe-C(19)-C(18)	119.6(4)
C(17)-Fe-C(12)-C(1)	32.2(3)	C(15)-Fe-C(19)-C(18)	-128.7(3)
C(21)-Fe-C(12)-C(1)	−10.4(3)	C(14)-Fe-C(19)-C(18)	-86.0(3)
C(13)-Fe-C(12)-C(1)	120.2(3)	C(18)-C(19)-C(20)-C(21)	-0.1(5)
C(18)-Fe-C(12)-C(1)	67.7(5)	Fe-C(19)-C(20)-C(21)	59.4(3)
C(19)-Fe-C(12)-C(1)	−81.3(7)	C(18)-C(19)-C(20)-Fe	-59.4(3)
C(20)-Fe-C(12)-C(1)	−50.4(3)	C(16)-Fe-C(20)-C(21)	112.8(3)
C(15)-Fe-C(12)-C(1)	−159.1(3)	C(17)-Fe-C(20)-C(21)	-37.6(3)
C(14)-Fe-C(12)-C(1)	157.3(3)	C(12)-Fe-C(20)-C(21)	72.1(3)
C(16)-C(12)-C(13)-C(14)	−0.6(4)	C(13)-Fe-C(20)-C(21)	42.8(9)
C(1)-C(12)-C(13)-C(14)	−177.0(3)	C(18)-Fe-C(20)-C(21)	-81.9(3)
Fe-C(12)-C(13)-C(14)	−59.8(2)	C(19)-Fe-C(20)-C(21)	-119.3(4)
C(16)-C(12)-C(13)-Fe	59.2(2)	C(15)-Fe-C(20)-C(21)	155.4(3)
C(1)-C(12)-C(13)-Fe	−117.2(3)	C(14)-Fe-C(20)-C(21)	-170.6(3)
C(16)-Fe-C(13)-C(14)	81.2(2)	C(16)-Fe-C(20)-C(19)	-127.9(3)
C(17)-Fe-C(13)-C(14)	−129.0(2)	C(17)-Fe-C(20)-C(19)	81.6(3)
C(21)-Fe-C(13)-C(14)	−169.8(2)	C(21)-Fe-C(20)-C(19)	119.3(4)
C(12)-Fe-C(13)-C(14)	119.6(3)	C(12)-Fe-C(20)-C(19)	-168.6(2)
C(18)-Fe-C(13)-C(14)	−85.0(3)	C(13)-Fe-C(20)-C(19)	162.1(7)
C(19)-Fe-C(13)-C(14)	−49.3(4)	C(18)-Fe-C(20)-C(19)	37.3(3)
C(20)-Fe-C(13)-C(14)	155.5(7)	C(15)-Fe-C(20)-C(19)	-85.4(3)
C(15)-Fe-C(13)-C(14)	37.6(2)	C(14)-Fe-C(20)-C(19)	-51.3(5)
C(16)-Fe-C(13)-C(12)	−38.40(18)	C(19)-C(20)-C(21)-C(17)	0.4(5)
C(17)-Fe-C(13)-C(12)	111.4(2)	Fe-C(20)-C(21)-C(17)	60.0(3)
C(21)-Fe-C(13)-C(12)	70.6(3)	C(19)-C(20)-C(21)-Fe	-59.6(3)
C(18)-Fe-C(13)-C(12)	155.4(2)	C(18)-C(17)-C(21)-C(20)	-0.7(5)
C(19)-Fe-C(13)-C(12)	−168.9(3)	Fe-C(17)-C(21)-C(20)	-60.4(3)
C(20)-Fe-C(13)-C(12)	35.8(8)	C(18)-C(17)-C(21)-Fe	59.7(3)
C(15)-Fe-C(13)-C(12)	−82.0(2)	C(16)-Fe-C(21)-C(20)	-83.8(3)
C(14)-Fe-C(13)-C(12)	−119.6(3)	C(17)-Fe-C(21)-C(20)	119.0(4)
C(12)-C(13)-C(14)-C(15)	0.0(4)	C(12)-Fe-C(21)-C(20)	-127.9(3)
Fe-C(13)-C(14)-C(15)	−59.1(2)	C(13)-Fe-C(21)-C(20)	-168.7(3)
C(12)-C(13)-C(14)-Fe	59.1(2)	C(18)-Fe-C(21)-C(20)	81.1(3)
C(16)-Fe-C(14)-C(13)	−82.3(2)	C(19)-Fe-C(21)-C(20)	37.4(3)
C(17)-Fe-C(14)-C(13)	72.7(3)	C(15)-Fe-C(21)-C(20)	-48.8(4)
C(21)-Fe-C(14)-C(13)	41.3(8)	C(14)-Fe-C(21)-C(20)	157.2(7)
C(12)-Fe-C(14)-C(13)	−37.8(2)	C(16)-Fe-C(21)-C(17)	157.2(2)
C(18)-Fe-C(14)-C(13)	113.2(2)	C(12)-Fe-C(21)-C(17)	113.1(2)
C(19)-Fe-C(14)-C(13)	156.0(2)	C(13)-Fe-C(21)-C(17)	72.3(3)
C(20)-Fe-C(14)-C(13)	−169.3(3)	C(18)-Fe-C(21)-C(17)	-37.9(3)

C(15)-Fe-C(14)-C(13)	−119.2(3)	C(19)-Fe-C(21)-C(17)	-81.5(3)
C(16)-Fe-C(14)-C(15)	36.93(19)	C(20)-Fe-C(21)-C(17)	-119.0(4)
C(17)-Fe-C(14)-C(15)	−168.0(2)	C(15)-Fe-C(21)-C(17)	-167.8(3)
C(21)-Fe-C(14)-C(15)	160.6(7)	C(14)-Fe-C(21)-C(17)	38.2(9)
C(12)-Fe-C(14)-C(15)	81.4(2)	C(25)-W-C(22)-O(1)	-70(27)
C(13)-Fe-C(14)-C(15)	119.2(3)	C(24)-W-C(22)-O(1)	21(27)
C(18)-Fe-C(14)-C(15)	−127.6(2)	C(26)-W-C(22)-O(1)	-161(27)
C(19)-Fe-C(14)-C(15)	−84.7(2)	C(23)-W-C(22)-O(1)	112(27)
C(20)-Fe-C(14)-C(15)	−50.0(4)	P-W-C(22)-O(1)	40(28)
C(13)-C(14)-C(15)-C(16)	0.6(4)	C(22)-W-C(23)-O(2)	82(10)
Fe-C(14)-C(15)-C(16)	−58.3(2)	C(25)-W-C(23)-O(2)	-49(12)
C(13)-C(14)-C(15)-Fe	58.9(2)	C(24)-W-C(23)-O(2)	169(10)
C(17)-Fe-C(15)-C(16)	167.0(7)	C(26)-W-C(23)-O(2)	-6(10)
C(21)-Fe-C(15)-C(16)	−51.5(4)	P-W-C(23)-O(2)	-107(10)
C(12)-Fe-C(15)-C(16)	38.59(19)	C(22)-W-C(24)-O(3)	35(12)
C(13)-Fe-C(15)-C(16)	83.0(2)	C(25)-W-C(24)-O(3)	125(12)
C(18)-Fe-C(15)-C(16)	−166.6(2)	C(26)-W-C(24)-O(3)	16(13)
C(19)-Fe-C(15)-C(16)	−126.7(2)	C(23)-W-C(24)-O(3)	-56(12)
C(20)-Fe-C(15)-C(16)	−84.4(2)	P-W-C(24)-O(3)	-142(12)
C(14)-Fe-C(15)-C(16)	120.5(3)	C(22)-W-C(25)-O(4)	-29(10)
C(16)-Fe-C(15)-C(14)	−120.5(3)	C(24)-W-C(25)-O(4)	-116(10)
C(17)-Fe-C(15)-C(14)	46.5(8)	C(26)-W-C(25)-O(4)	59(10)
C(21)-Fe-C(15)-C(14)	−172.0(3)	C(23)-W-C(25)-O(4)	102(11)
C(12)-Fe-C(15)-C(14)	−81.9(2)	P-W-C(25)-O(4)	160(10)
C(13)-Fe-C(15)-C(14)	−37.50(19)	C(22)-W-C(26)-O(5)	-13(4)
C(18)-Fe-C(15)-C(14)	72.9(3)	C(25)-W-C(26)-O(5)	-103(4)
C(19)-Fe-C(15)-C(14)	112.8(2)	C(24)-W-C(26)-O(5)	6(5)
C(20)-Fe-C(15)-C(14)	155.1(2)	C(23)-W-C(26)-O(5)	78(4)
C(14)-C(15)-C(16)-C(12)	−1.0(4)	P-W-C(26)-O(5)	163(4)

F.3   Data for Complex 74b
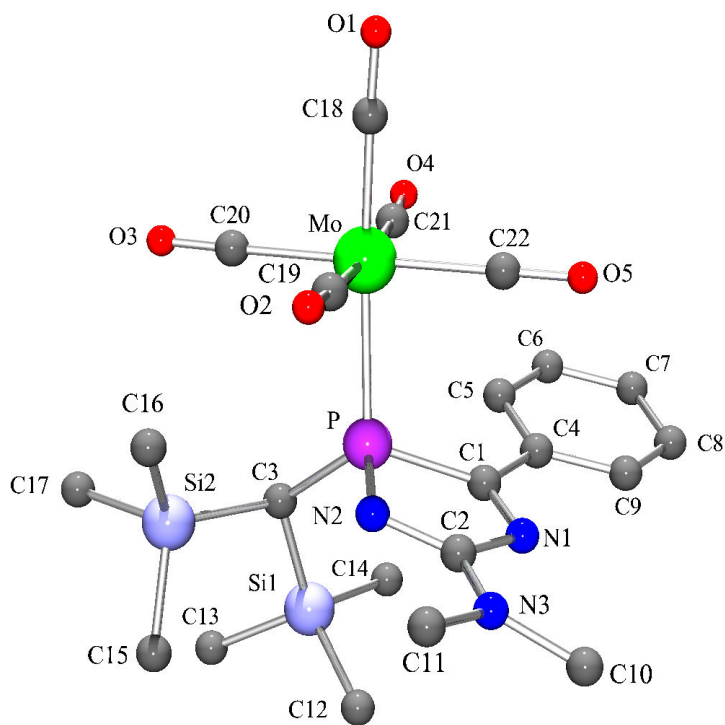
Figure F.3: Molecular structure of complex **74b** (GSTR022) in the crystal (hydrogen atoms are omitted for clarity).

Table F.13: Crystal data and structure refinement for GSTR022.

Identification code	GSTR022
Empirical formula	$C_{22}H_{30}MoN_3O_5PSi_2$
Formula weight	599.58
Temperature	123(2) K
Wavelength	0.71073 Å
Crystal system, space group	Monoclinic, $P2_1$ (No.4)
Unit cell dimensions	a = 9.3471(5) Å, $\alpha = 90°$
	b = 12.7344(11) Å, $\beta = 93.523(4)°$
	c = 11.8746(9) Å, $\gamma = 90°$
Volume	1410.76(18) Å^3
Z, Calculated density	2, 1.411 Mg/m^3
Absorption coefficient	0.641 mm^{-1}
F(000)	616
Crystal size	0.60 x 0.08 x 0.08 mm
θ range for data collection	3.13 to 29.00°
Limiting indices	-12 ≤ h ≤ 12, -17 ≤ k ≤ 15, -16 ≤ l ≤ 11
Reflections collected / unique	10766 / 6251 [R$_{int}$ = 0.0465]
Completeness to θ = 29.00	96.8 %
Absorption correction	Semi-empirical from equivalents
Max. and min. transmission	0.89913 and 0.87878
Refinement method	Full-matrix least-squares on F^2
Data / restraints / parameters	6251 / 1 / 317
Goodness-of-fit on F^2	0.713
Final R indices [I>2σ(I)]	R$_1$ = 0.0380, wR$_2$ = 0.0579
R indices (all data)	R$_1$ = 0.0736, wR$_2$ = 0.0676
Absolute structure parameter[409]	0.54(3)
Largest diff. peak and hole	0.434 and -0.438 e · A^{-3}

Table F.14: Atomic coordinates (x 10^4) and equivalent isotropic displacement parameters ($\text{Å}^2 \cdot 10^3$) for GSTR022. U(eq) is defined as one third of the trace of the orthogonalized U_{ij} tensor.

	x	y	z	U(eq)
C(1)	3835(3)	4492(3)	2783(3)	17(1)
C(2)	4059(5)	2756(4)	2868(4)	19(1)
C(3)	1701(4)	4052(3)	739(3)	19(1)
C(4)	4213(4)	5582(4)	3045(4)	20(1)
C(5)	3263(4)	6404(3)	2745(3)	21(1)
C(6)	3610(5)	7422(4)	3034(4)	24(1)
C(7)	4900(5)	7654(4)	3634(4)	35(1)
C(8)	5849(5)	6850(4)	3907(4)	35(1)
C(9)	5505(4)	5832(4)	3642(4)	30(1)
C(10)	6349(4)	1954(4)	3581(4)	36(1)
C(11)	4185(5)	877(4)	3055(4)	32(1)
C(12)	4752(4)	3439(4)	10(4)	36(1)
C(13)	2540(4)	4410(5)	-1690(3)	29(1)
C(14)	3972(5)	5731(3)	116(4)	32(1)
C(15)	1762(5)	1865(4)	-547(4)	38(1)
C(16)	-337(4)	2051(4)	1145(4)	35(1)
C(17)	-761(4)	3410(4)	-908(4)	42(1)
C(18)	-1210(4)	4393(5)	4873(3)	29(1)
C(19)	105(5)	2684(5)	3877(4)	27(1)
C(20)	-1464(3)	4283(6)	2418(3)	28(1)
C(21)	69(5)	5877(5)	3479(4)	26(1)
C(22)	1806(4)	4412(5)	4846(3)	23(1)
Mo	167(1)	4287(1)	3651(1)	19(1)
N(1)	4706(3)	3745(3)	3103(3)	21(1)
N(2)	2751(3)	2693(3)	2400(3)	19(1)
N(3)	4842(3)	1911(3)	3180(3)	27(1)
O(1)	-1954(3)	4423(4)	5605(2)	43(1)
O(2)	33(3)	1802(3)	4025(3)	41(1)
O(3)	-2370(2)	4333(4)	1729(2)	43(1)
O(4)	-84(3)	6770(3)	3406(3)	39(1)
O(5)	2741(3)	4504(3)	5512(2)	35(1)
P	2074(1)	3906(1)	2261(1)	19(1)
Si(1)	3242(1)	4384(1)	-187(1)	22(1)
Si(2)	625(1)	2862(1)	128(1)	27(1)

Table F.15: Bond lengths [Å] and angles [º] for GSTR022.

C(1)-N(1)	1.293(5)	C(13)-Si(1)	1.864(4)
C(1)-C(4)	1.462(6)	C(13)-H(13A)	0.9800
C(1)-P	1.877(4)	C(13)-H(13B)	0.9800
C(2)-N(2)	1.315(5)	C(13)-H(13C)	0.9800
C(2)-N(3)	1.341(6)	C(14)-Si(1)	1.872(5)
C(2)-N(1)	1.417(6)	C(14)-H(14A)	0.9800
C(3)-P	1.830(4)	C(14)-H(14B)	0.9800
C(3)-Si(1)	1.911(3)	C(14)-H(14C)	0.9800
C(3)-Si(2)	1.935(4)	C(15)-Si(2)	1.868(4)
C(3)-H(3A)	1.0000	C(15)-H(15A)	0.9800
C(4)-C(9)	1.399(6)	C(15)-H(15B)	0.9800
C(4)-C(5)	1.405(6)	C(15)-H(15C)	0.9800
C(5)-C(6)	1.375(6)	C(16)-Si(2)	1.862(4)
C(5)-H(5A)	0.9500	C(16)-H(16A)	0.9800
C(6)-C(7)	1.394(6)	C(16)-H(16B)	0.9800
C(6)-H(6A)	0.9500	C(16)-H(16C)	0.9800
C(7)-C(8)	1.380(6)	C(17)-Si(2)	1.866(5)
C(7)-H(7A)	0.9500	C(17)-H(17C)	0.9800
C(8)-C(9)	1.367(6)	C(17)-H(17B)	0.9800
C(8)-H(8A)	0.9500	C(17)-H(17A)	0.9800
C(9)-H(9A)	0.9500	C(18)-O(1)	1.147(4)
C(10)-N(3)	1.460(5)	C(18)-Mo	2.003(4)
C(10)-H(10A)	0.9800	C(19)-O(2)	1.140(6)
C(10)-H(10B)	0.9800	C(19)-Mo	2.060(6)
C(10)-H(10C)	0.9800	C(20)-O(3)	1.143(4)
C(11)-N(3)	1.457(5)	C(20)-Mo	2.048(4)
C(11)-H(11A)	0.9800	C(21)-O(4)	1.148(6)
C(11)-H(11B)	0.9800	C(21)-Mo	2.036(6)
C(11)-H(11C)	0.9800	C(22)-O(5)	1.149(4)
C(12)-Si(1)	1.858(4)	C(22)-Mo	2.029(4)
C(12)-H(12A)	0.9800	Mo-P	2.5487(10)
C(12)-H(12B)	0.9800	N(2)-P	1.673(3)
C(12)-H(12C)	0.9800		
N(1)-C(1)-C(4)	119.8(4)	Si(2)-C(15)-H(15B)	109.5
N(1)-C(1)-P	109.2(3)	H(15A)-C(15)-H(15B)	109.5
C(4)-C(1)-P	130.0(3)	Si(2)-C(15)-H(15C)	109.5
N(2)-C(2)-N(3)	123.0(4)	H(15A)-C(15)-H(15C)	109.5

N(2)-C(2)-N(1)	120.8(4)	H(15B)-C(15)-H(15C)	109.5
N(3)-C(2)-N(1)	116.1(4)	Si(2)-C(16)-H(16A)	109.5
P-C(3)-Si(1)	119.07(18)	Si(2)-C(16)-H(16B)	109.5
P-C(3)-Si(2)	110.74(19)	H(16A)-C(16)-H(16B)	109.5
Si(1)-C(3)-Si(2)	110.53(18)	Si(2)-C(16)-H(16C)	109.5
P-C(3)-H(3A)	105.1	H(16A)-C(16)-H(16C)	109.5
Si(1)-C(3)-H(3A)	105.1	H(16B)-C(16)-H(16C)	109.5
Si(2)-C(3)-H(3A)	105.1	Si(2)-C(17)-H(17C)	109.5
C(9)-C(4)-C(5)	118.2(4)	Si(2)-C(17)-H(17B)	109.5
C(9)-C(4)-C(1)	120.9(4)	H(17C)-C(17)-H(17B)	109.5
C(5)-C(4)-C(1)	120.9(4)	Si(2)-C(17)-H(17A)	109.5
C(6)-C(5)-C(4)	120.2(4)	H(17C)-C(17)-H(17A)	109.5
C(6)-C(5)-H(5A)	119.9	H(17B)-C(17)-H(17A)	109.5
C(4)-C(5)-H(5A)	119.9	O(1)-C(18)-Mo	176.7(4)
C(5)-C(6)-C(7)	120.7(4)	O(2)-C(19)-Mo	177.7(4)
C(5)-C(6)-H(6A)	119.6	O(3)-C(20)-Mo	176.6(6)
C(7)-C(6)-H(6A)	119.6	O(4)-C(21)-Mo	175.2(4)
C(8)-C(7)-C(6)	119.1(4)	O(5)-C(22)-Mo	178.5(5)
C(8)-C(7)-H(7A)	120.5	C(18)-Mo-C(22)	88.79(14)
C(6)-C(7)-H(7A)	120.5	C(18)-Mo-C(21)	88.8(2)
C(9)-C(8)-C(7)	120.7(4)	C(22)-Mo-C(21)	91.1(2)
C(9)-C(8)-H(8A)	119.6	C(18)-Mo-C(20)	91.99(14)
C(7)-C(8)-H(8A)	119.6	C(22)-Mo-C(20)	175.5(3)
C(8)-C(9)-C(4)	121.0(4)	C(21)-Mo-C(20)	84.5(2)
C(8)-C(9)-H(9A)	119.5	C(18)-Mo-C(19)	87.0(2)
C(4)-C(9)-H(9A)	119.5	C(22)-Mo-C(19)	90.7(2)
N(3)-C(10)-H(10A)	109.5	C(21)-Mo-C(19)	175.35(16)
N(3)-C(10)-H(10B)	109.5	C(20)-Mo-C(19)	93.7(2)
H(10A)-C(10)-H(10B)	109.5	C(18)-Mo-P	171.14(16)
N(3)-C(10)-H(10C)	109.5	C(22)-Mo-P	86.54(10)
H(10A)-C(10)-H(10C)	109.5	C(21)-Mo-P	98.84(12)
H(10B)-C(10)-H(10C)	109.5	C(20)-Mo-P	93.24(10)
N(3)-C(11)-H(11A)	109.5	C(19)-Mo-P	85.53(13)
N(3)-C(11)-H(11B)	109.5	C(1)-N(1)-C(2)	110.0(3)
H(11A)-C(11)-H(11B)	109.5	C(2)-N(2)-P	108.7(3)
N(3)-C(11)-H(11C)	109.5	C(2)-N(3)-C(11)	118.6(3)
H(11A)-C(11)-H(11C)	109.5	C(2)-N(3)-C(10)	124.0(4)
H(11B)-C(11)-H(11C)	109.5	C(11)-N(3)-C(10)	117.3(3)
Si(1)-C(12)-H(12A)	109.5	N(2)-P-C(3)	103.80(17)
Si(1)-C(12)-H(12B)	109.5	N(2)-P-C(1)	90.91(17)

H(12A)-C(12)-H(12B)	109.5	C(3)-P-C(1)	113.32(16)
Si(1)-C(12)-H(12C)	109.5	N(2)-P-Mo	112.78(11)
H(12A)-C(12)-H(12C)	109.5	C(3)-P-Mo	121.47(11)
H(12B)-C(12)-H(12C)	109.5	C(1)-P-Mo	110.16(11)
Si(1)-C(13)-H(13A)	109.5	C(12)-Si(1)-C(13)	110.6(2)
Si(1)-C(13)-H(13B)	109.5	C(12)-Si(1)-C(14)	107.7(2)
H(13A)-C(13)-H(13B)	109.5	C(13)-Si(1)-C(14)	105.7(2)
Si(1)-C(13)-H(13C)	109.5	C(12)-Si(1)-C(3)	112.2(2)
H(13A)-C(13)-H(13C)	109.5	C(13)-Si(1)-C(3)	108.74(16)
H(13B)-C(13)-H(13C)	109.5	C(14)-Si(1)-C(3)	111.79(18)
Si(1)-C(14)-H(14A)	109.5	C(16)-Si(2)-C(17)	107.0(2)
Si(1)-C(14)-H(14B)	109.5	C(16)-Si(2)-C(15)	102.2(2)
H(14A)-C(14)-H(14B)	109.5	C(17)-Si(2)-C(15)	111.2(2)
Si(1)-C(14)-H(14C)	109.5	C(16)-Si(2)-C(3)	116.87(18)
H(14A)-C(14)-H(14C)	109.5	C(17)-Si(2)-C(3)	106.1(2)
H(14B)-C(14)-H(14C)	109.5	C(15)-Si(2)-C(3)	113.35(18)
Si(2)-C(15)-H(15A)	109.5		

Table F.16: Anisotropic displacement parameters ($\text{Å}^2 \cdot 10^3$) for GSTR022. The anisotropic displacement factor exponent takes the form: $-2\pi^2[h^2 a^{*2} U_{11} + ... + 2hka^* b^* U_{12}]$.

	U(11)	U(22)	U(33)	U(23)	U(13)	U(12)
C(1)	18(2)	18(3)	16(2)	0(2)	5(1)	-1(2)
C(2)	20(2)	17(3)	20(3)	1(2)	8(2)	1(2)
C(3)	21(2)	18(3)	18(2)	0(2)	-1(1)	-1(2)
C(4)	17(2)	25(3)	18(3)	-3(2)	-1(2)	-2(2)
C(5)	20(2)	25(3)	18(2)	1(2)	2(2)	-1(2)
C(6)	30(3)	18(3)	25(3)	-2(2)	-3(2)	-1(2)
C(7)	41(3)	22(3)	41(3)	-5(2)	0(2)	-6(2)
C(8)	29(3)	24(3)	49(3)	-3(2)	-13(2)	-7(2)
C(9)	27(2)	24(3)	38(3)	-4(2)	0(2)	5(2)
C(10)	21(2)	31(3)	55(4)	7(3)	-3(2)	4(2)
C(11)	32(3)	16(3)	49(4)	8(2)	6(2)	1(2)
C(12)	28(2)	42(3)	39(3)	-6(2)	8(2)	4(2)
C(13)	37(2)	29(3)	22(2)	-2(3)	6(2)	-1(3)
C(14)	38(2)	31(3)	29(3)	2(2)	9(2)	-10(2)
C(15)	50(3)	29(3)	36(3)	-9(2)	5(2)	-12(2)
C(16)	39(3)	36(3)	30(3)	-10(2)	1(2)	-17(2)
C(17)	33(2)	54(4)	37(3)	-8(3)	-12(2)	-8(2)

C(18)	31(2)	28(3)	26(2)	-1(3)	1(2)	10(3)
C(19)	28(3)	39(4)	15(3)	1(2)	3(2)	-2(2)
C(20)	24(2)	32(2)	30(2)	2(4)	9(2)	-8(3)
C(21)	21(2)	39(4)	17(3)	3(2)	6(2)	7(2)
C(22)	28(2)	22(3)	19(2)	1(2)	3(2)	0(2)
Mo	18(1)	23(1)	17(1)	0(1)	2(1)	1(1)
N(1)	18(2)	19(2)	26(2)	0(2)	2(1)	2(2)
N(2)	20(2)	16(2)	21(2)	0(2)	1(1)	-1(2)
N(3)	23(2)	27(2)	32(2)	7(2)	-1(2)	2(2)
O(1)	42(2)	48(2)	40(2)	5(2)	25(1)	11(2)
O(2)	55(2)	31(2)	38(2)	9(2)	7(2)	-5(2)
O(3)	29(1)	61(2)	36(2)	8(3)	-12(1)	-9(2)
O(4)	51(2)	28(2)	39(2)	2(2)	7(2)	7(2)
O(5)	34(1)	43(3)	28(2)	-1(2)	-10(1)	2(2)
P	18(1)	19(1)	19(1)	-1(1)	0(1)	-2(1)
Si(1)	23(1)	22(1)	21(1)	-2(1)	5(1)	-1(1)
Si(2)	29(1)	30(1)	22(1)	-5(1)	-1(1)	-9(1)

Table F.17: Hydrogen coordinates (x 10^4) and isotropic displacement parameters ($\mathring{A}^2 \cdot 10^3$) for GSTR022.

	x	y	z	U(eq)
H(3A)	1029	4661	652	23
H(5A)	2377	6257	2340	25
H(6A)	2964	7974	2823	29
H(7A)	5122	8355	3853	42
H(8A)	6750	7005	4283	42
H(9A)	6154	5286	3866	36
H(10A)	6654	2688	3651	53
H(10B)	6932	1592	3043	53
H(10C)	6472	1610	4319	53
H(11A)	4291	617	2288	48
H(11B)	3164	926	3194	48
H(11C)	4658	391	3600	48
H(12A)	4398	2725	-135	54
H(12B)	5170	3488	785	54
H(12C)	5484	3608	-518	54
H(13A)	1794	4948	-1789	44
H(13B)	2134	3722	-1897	44
H(13C)	3323	4572	-2173	44

H(14A)	4596	5715	810	48
H(14B)	3178	6219	209	48
H(14C)	4525	5963	-514	48
H(15A)	2412	1538	30	58
H(15B)	2322	2208	-1113	58
H(15C)	1147	1325	-912	58
H(16A)	-1049	2485	1500	53
H(16B)	352	1774	1727	53
H(16C)	-822	1466	744	53
H(17C)	-1376	2840	-1212	63
H(17B)	-290	3751	-1525	63
H(17A)	-1346	3925	-531	63

Table F.18: Torsion angles [º] for GSTR022.

N(1)-C(1)-C(4)-C(9)	-0.2(6)	N(2)-C(2)-N(3)-C(10)	172.7(4)
P-C(1)-C(4)-C(9)	166.7(3)	N(1)-C(2)-N(3)-C(10)	−9.1(6)
N(1)-C(1)-C(4)-C(5)	-177.6(4)	C(2)-N(2)-P-C(3)	119.4(3)
P-C(1)-C(4)-C(5)	-10.7(6)	C(2)-N(2)-P-C(1)	5.1(3)
C(9)-C(4)-C(5)-C(6)	0.1(6)	C(2)-N(2)-P-Mo	−107.3(3)
C(1)-C(4)-C(5)-C(6)	177.5(4)	Si(1)-C(3)-P-N(2)	−79.9(2)
C(4)-C(5)-C(6)-C(7)	-0.5(6)	Si(2)-C(3)-P-N(2)	49.8(2)
C(5)-C(6)-C(7)-C(8)	2.0(7)	Si(1)-C(3)-P-C(1)	17.2(3)
C(6)-C(7)-C(8)-C(9)	-3.1(7)	Si(2)-C(3)-P-C(1)	146.94(18)
C(7)-C(8)-C(9)-C(4)	2.8(7)	Si(1)-C(3)-P-Mo	151.93(15)
C(5)-C(4)-C(9)-C(8)	-1.3(7)	Si(2)-C(3)-P-Mo	−78.3(2)
C(1)-C(4)-C(9)-C(8)	-178.7(4)	N(1)-C(1)-P-N(2)	−5.7(3)
O(1)-C(18)-Mo-C(22)	-40(9)	C(4)-C(1)-P-N(2)	−173.7(4)
O(1)-C(18)-Mo-C(21)	-131(9)	N(1)-C(1)-P-C(3)	−111.1(3)
O(1)-C(18)-Mo-C(20)	145(9)	C(4)-C(1)-P-C(3)	80.8(4)
O(1)-C(18)-Mo-C(19)	51(9)	N(1)-C(1)-P-Mo	109.1(2)
O(1)-C(18)-Mo-P	19(10)	C(4)-C(1)-P-Mo	−59.0(4)
O(5)-C(22)-Mo-C(18)	-112(14)	C(18)-Mo-P-N(2)	16.7(9)
O(5)-C(22)-Mo-C(21)	-23(14)	C(22)-Mo-P-N(2)	75.0(2)
O(5)-C(22)-Mo-C(20)	-12(15)	C(21)-Mo-P-N(2)	165.65(19)
O(5)-C(22)-Mo-C(19)	161(14)	C(20)-Mo-P-N(2)	−109.4(2)
O(5)-C(22)-Mo-P	75(14)	C(19)-Mo-P-N(2)	−15.94(18)
O(4)-C(21)-Mo-C(18)	-30(5)	C(18)-Mo-P-C(3)	140.8(9)
O(4)-C(21)-Mo-C(22)	-119(5)	C(22)-Mo-P-C(3)	−160.9(2)
O(4)-C(21)-Mo-C(20)	62(5)	C(21)-Mo-P-C(3)	−70.3(2)

O(4)-C(21)-Mo-C(19)	-6(7)	C(20)-Mo-P-C(3)	14.7(2)
O(4)-C(21)-Mo-P	154(5)	C(19)-Mo-P-C(3)	108.13(19)
O(3)-C(20)-Mo-C(18)	89(5)	C(18)-Mo-P-C(1)	−83.2(9)
O(3)-C(20)-Mo-C(22)	-11(6)	C(22)-Mo-P-C(1)	−24.9(2)
O(3)-C(20)-Mo-C(21)	1(5)	C(21)-Mo-P-C(1)	65.71(19)
O(3)-C(20)-Mo-C(19)	176(5)	C(20)-Mo-P-C(1)	150.6(2)
O(3)-C(20)-Mo-P	-98(5)	C(19)-Mo-P-C(1)	−115.88(19)
O(2)-C(19)-Mo-C(18)	10(11)	P-C(3)-Si(1)-C(12)	54.5(3)
O(2)-C(19)-Mo-C(22)	99(11)	Si(2)-C(3)-Si(1)-C(12)	−75.4(3)
O(2)-C(19)-Mo-C(21)	-14(13)	P-C(3)-Si(1)-C(13)	177.1(3)
O(2)-C(19)-Mo-C(20)	-82(11)	Si(2)-C(3)-Si(1)-C(13)	47.2(3)
O(2)-C(19)-Mo-P	-175(11)	P-C(3)-Si(1)-C(14)	−66.6(3)
C(4)-C(1)-N(1)-C(2)	173.7(3)	Si(2)-C(3)-Si(1)-C(14)	163.5(2)
P-C(1)-N(1)-C(2)	4.3(4)	P-C(3)-Si(2)-C(16)	19.4(3)
N(2)-C(2)-N(1)-C(1)	-0.5(5)	Si(1)-C(3)-Si(2)-C(16)	153.5(2)
N(3)-C(2)-N(1)-C(1)	-178.7(3)	P-C(3)-Si(2)-C(17)	138.6(2)
N(3)-C(2)-N(2)-P	174.1(3)	Si(1)-C(3)-Si(2)-C(17)	−87.3(2)
N(1)-C(2)-N(2)-P	-4.0(5)	P-C(3)-Si(2)-C(15)	−99.1(2)
N(2)-C(2)-N(3)-C(11)	-3.7(6)	Si(1)-C(3)-Si(2)-C(15)	35.0(3)
N(1)-C(2)-N(3)-C(11)	174.4(4)		

F.4 Data for Complex 75b
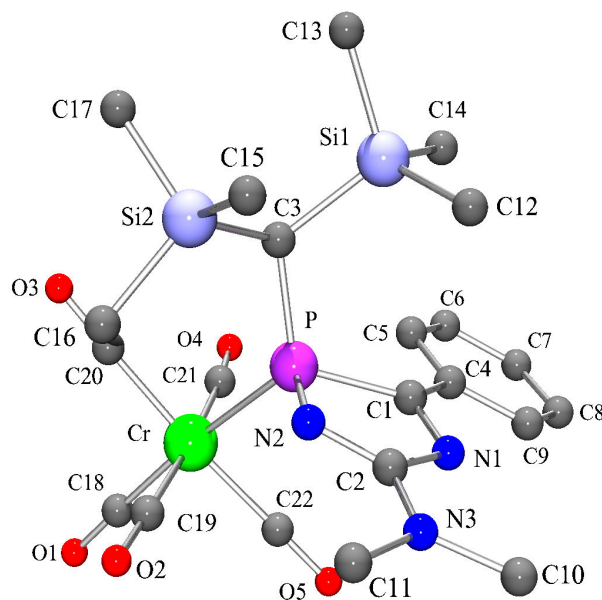
Figure F.4: Molecular structure of complex **75b** (GSTR023) in the crystal (hydrogen atoms are omitted for clarity).

Table F.19: Crystal data and structure refinement for GSTR023.

Identification code	GSTR023
Empirical formula	$C_{22}H_{30}CrN_3O_5PSi_2$
Formula weight	555.64
Temperature	123(2) K
Wavelength	0.71073 Å
Crystal system, space group	Monoclinic, $P2_1$ (No.4)
Unit cell dimensions	a = 9.2995(3) Å, α = 90º
	b = 12.7072(8) Å, β = 92.008(3)º
	c = 11.6982(6) Å, γ = 90º
Volume	1381.53(12) $Å^3$
Z, Calculated density	2, 1.336 Mg/m^3
Absorption coefficient	0.594 mm^{-1}
F(000)	580
Crystal size	0.52 x 0.18 x 0.18 mm
θ range for data collection	2.72 to 28.99º
Limiting indices	-12 $\leq$ h $\leq$ 12, -17 $\leq$ k $\leq$ 15, -10 $\leq$ l $\leq$ 15
Reflections collected / unique	11154 / 6490 [R_{int} = 0.0402]
Completeness to θ = 28.99	98.1 %
Absorption correction	Semi-empirical from equivalents
Max. and min. transmission	0.89804 and 0.86208
Refinement method	Full-matrix least-squares on F^2
Data / restraints / parameters	6490 / 1 / 316
Goodness-of-fit on F^2	0.958
Final R indices [I>2σ(I)]	R_1 = 0.0342, wR_2 = 0.0587
R indices (all data)	R_1 = 0.0481, wR_2 = 0.0619
Absolute structure parameter[409]	0.407(13)
Largest diff. peak and hole	0.416 and -0.378 e · A^{-3}

Table F.20: Atomic coordinates (x 10^4) and equivalent isotropic displacement parameters ($\AA^2 \cdot 10^3$) for GSTR023. U(eq) is defined as one third of the trace of the orthogonalized U_{ij} tensor.

	x	y	z	U(eq)
C(1)	6103(2)	5469(2)	7197(2)	20(1)
C(2)	5853(2)	7205(2)	7080(2)	21(1)
C(3)	8258(2)	5957(2)	9223(2)	20(1)
C(4)	5750(2)	4362(2)	6976(2)	20(1)
C(5)	6707(2)	3552(2)	7255(2)	22(1)
C(6)	6388(2)	2523(2)	6993(2)	27(1)
C(7)	5087(2)	2272(2)	6438(2)	31(1)
C(8)	4108(2)	3067(2)	6171(2)	32(1)
C(9)	4426(2)	4099(2)	6424(2)	26(1)
C(10)	3572(2)	7989(2)	6349(2)	32(1)
C(11)	5747(2)	9081(2)	6829(2)	30(1)
C(12)	5104(2)	6354(2)	9992(2)	33(1)
C(13)	7434(2)	5590(3)	11724(2)	29(1)
C(14)	6221(2)	4123(2)	9972(2)	29(1)
C(15)	7895(3)	8149(2)	10487(2)	36(1)
C(16)	10127(2)	8077(2)	8787(2)	35(1)
C(17)	10601(2)	6749(3)	10893(2)	36(1)
C(18)	11093(2)	5621(3)	5207(2)	30(1)
C(19)	9770(2)	7226(3)	6085(2)	28(1)
C(20)	11194(2)	5823(3)	7530(2)	30(1)
C(22)	8230(2)	5564(2)	5224(2)	25(1)
Cr	9742(1)	5738(1)	6347(1)	15(1)
N(1)	5221(2)	6205(2)	6875(2)	21(1)
N(2)	7150(2)	7287(2)	7547(2)	21(1)
N(3)	5080(2)	8048(2)	6757(2)	24(1)
O(1)	11907(2)	5578(2)	4491(1)	44(1)
O(2)	9842(2)	8102(2)	5888(2)	40(1)
O(3)	12081(2)	5816(2)	8241(1)	42(1)
O(4)	10109(2)	3374(2)	6676(2)	39(1)
O(5)	7332(2)	5456(2)	4535(1)	36(1)
P	7870(1)	6078(1)	7686(1)	19(1)
Si(1)	6757(1)	5527(1)	10203(1)	22(1)
Si(2)	9185(1)	7213(1)	9825(1)	26(1)
C(21)	9894(2)	4259(3)	6558(2)	28(1)

Table F.21: Bond lengths [Å] and angles [°] for GSTR023.

C(1)-N(1)	1.292(3)	C(13)-Si(1)	1.868(2)
C(1)-C(4)	1.465(3)	C(13)-H(13A)	0.9800
C(1)-P	1.887(2)	C(13)-H(13B)	0.9800
C(2)-N(2)	1.311(2)	C(13)-H(13C)	0.9800
C(2)-N(3)	1.337(3)	C(14)-Si(1)	1.869(3)
C(2)-N(1)	1.416(3)	C(14)-H(14A)	0.9800
C(3)-P	1.828(2)	C(14)-H(14B)	0.9800
C(3)-Si(1)	1.917(2)	C(14)-H(14C)	0.9800
C(3)-Si(2)	1.935(2)	C(15)-Si(2)	1.875(3)
C(3)-H(3A)	1.0000	C(15)-H(15A)	0.9800
C(4)-C(5)	1.391(3)	C(15)-H(15B)	0.9800
C(4)-C(9)	1.410(3)	C(15)-H(15C)	0.9800
C(5)-C(6)	1.373(4)	C(16)-Si(2)	1.877(3)
C(5)-H(5A)	0.9500	C(16)-H(16A)	0.9800
C(6)-C(7)	1.390(3)	C(16)-H(16B)	0.9800
C(6)-H(6A)	0.9500	C(16)-H(16C)	0.9800
C(7)-C(8)	1.388(4)	C(17)-Si(2)	1.877(2)
C(7)-H(7A)	0.9500	C(17)-H(17C)	0.9800
C(8)-C(9)	1.373(4)	C(17)-H(17B)	0.9800
C(8)-H(8A)	0.9500	C(17)-H(17A)	0.9800
C(9)-H(9A)	0.9500	C(18)-O(1)	1.150(2)
C(10)-N(3)	1.467(3)	C(18)-Cr	1.870(2)
C(10)-H(10A)	0.9800	C(19)-O(2)	1.139(3)
C(10)-H(10B)	0.9800	C(19)-Cr	1.916(3)
C(10)-H(10C)	0.9800	C(20)-O(3)	1.150(2)
C(11)-N(3)	1.453(3)	C(20)-Cr	1.903(2)
C(11)-H(11A)	0.9800	C(22)-O(5)	1.147(2)
C(11)-H(11B)	0.9800	C(22)-Cr	1.904(2)
C(11)-H(11C)	0.9800	Cr-C(21)	1.901(3)
C(12)-Si(1)	1.872(3)	Cr-P	2.4208(6)
C(12)-H(12A)	0.9800	N(2)-P	1.682(2)
C(12)-H(12B)	0.9800	O(4)-C(21)	1.149(3)
C(12)-H(12C)	0.9800		
N(1)-C(1)-C(4)	120.51(19)	Si(2)-C(15)-H(15B)	109.5
N(1)-C(1)-P	109.18(18)	H(15A)-C(15)-H(15B)	109.5
C(4)-C(1)-P	129.38(17)	Si(2)-C(15)-H(15C)	109.5
N(2)-C(2)-N(3)	122.1(2)	H(15A)-C(15)-H(15C)	109.5

N(2)-C(2)-N(1)	120.8(2)	H(15B)-C(15)-H(15C)	109.5
N(3)-C(2)-N(1)	117.06(19)	Si(2)-C(16)-H(16A)	109.5
P-C(3)-Si(1)	119.31(10)	Si(2)-C(16)-H(16B)	109.5
P-C(3)-Si(2)	111.06(12)	H(16A)-C(16)-H(16B)	109.5
Si(1)-C(3)-Si(2)	110.00(11)	Si(2)-C(16)-H(16C)	109.5
P-C(3)-H(3A)	105.1	H(16A)-C(16)-H(16C)	109.5
Si(1)-C(3)-H(3A)	105.1	H(16B)-C(16)-H(16C)	109.5
Si(2)-C(3)-H(3A)	105.1	Si(2)-C(17)-H(17C)	109.5
C(5)-C(4)-C(9)	118.2(2)	Si(2)-C(17)-H(17B)	109.5
C(5)-C(4)-C(1)	122.06(19)	H(17C)-C(17)-H(17B)	109.5
C(9)-C(4)-C(1)	119.7(2)	Si(2)-C(17)-H(17A)	109.5
C(6)-C(5)-C(4)	121.3(2)	H(17C)-C(17)-H(17A)	109.5
C(6)-C(5)-H(5A)	119.3	H(17B)-C(17)-H(17A)	109.5
C(4)-C(5)-H(5A)	119.3	O(1)-C(18)-Cr	177.8(3)
C(5)-C(6)-C(7)	120.1(2)	O(2)-C(19)-Cr	176.4(2)
C(5)-C(6)-H(6A)	120.0	O(3)-C(20)-Cr	176.3(3)
C(7)-C(6)-H(6A)	120.0	O(5)-C(22)-Cr	179.1(2)
C(8)-C(7)-C(6)	119.3(3)	C(18)-Cr-C(21)	88.00(12)
C(8)-C(7)-H(7A)	120.3	C(18)-Cr-C(20)	92.60(9)
C(6)-C(7)-H(7A)	120.3	C(21)-Cr-C(20)	85.08(12)
C(9)-C(8)-C(7)	120.8(2)	C(18)-Cr-C(22)	89.85(9)
C(9)-C(8)-H(8A)	119.6	C(21)-Cr-C(22)	91.38(12)
C(7)-C(8)-H(8A)	119.6	C(20)-Cr-C(22)	175.62(12)
C(8)-C(9)-C(4)	120.2(2)	C(18)-Cr-C(19)	87.19(13)
C(8)-C(9)-H(9A)	119.9	C(21)-Cr-C(19)	174.60(9)
C(4)-C(9)-H(9A)	119.9	C(20)-Cr-C(19)	92.69(13)
N(3)-C(10)-H(10A)	109.5	C(22)-Cr-C(19)	91.05(11)
N(3)-C(10)-H(10B)	109.5	C(18)-Cr-P	172.73(9)
H(10A)-C(10)-H(10B)	109.5	C(21)-Cr-P	98.29(7)
N(3)-C(10)-H(10C)	109.5	C(20)-Cr-P	91.57(7)
H(10A)-C(10)-H(10C)	109.5	C(22)-Cr-P	86.38(6)
H(10B)-C(10)-H(10C)	109.5	C(19)-Cr-P	86.67(7)
N(3)-C(11)-H(11A)	109.5	C(1)-N(1)-C(2)	110.16(18)
N(3)-C(11)-H(11B)	109.5	C(2)-N(2)-P	108.93(18)
H(11A)-C(11)-H(11B)	109.5	C(2)-N(3)-C(11)	118.92(19)
N(3)-C(11)-H(11C)	109.5	C(2)-N(3)-C(10)	123.3(2)
H(11A)-C(11)-H(11C)	109.5	C(11)-N(3)-C(10)	117.8(2)
H(11B)-C(11)-H(11C)	109.5	N(2)-P-C(3)	103.63(10)
Si(1)-C(12)-H(12A)	109.5	N(2)-P-C(1)	90.35(10)
Si(1)-C(12)-H(12B)	109.5	C(3)-P-C(1)	113.79(9)

H(12A)-C(12)-H(12B)	109.5	N(2)-P-Cr	113.16(7)
Si(1)-C(12)-H(12C)	109.5	C(3)-P-Cr	119.98(7)
H(12A)-C(12)-H(12C)	109.5	C(1)-P-Cr	111.68(7)
H(12B)-C(12)-H(12C)	109.5	C(13)-Si(1)-C(14)	104.97(13)
Si(1)-C(13)-H(13A)	109.5	C(13)-Si(1)-C(12)	110.48(12)
Si(1)-C(13)-H(13B)	109.5	C(14)-Si(1)-C(12)	107.68(12)
H(13A)-C(13)-H(13B)	109.5	C(13)-Si(1)-C(3)	109.20(9)
Si(1)-C(13)-H(13C)	109.5	C(14)-Si(1)-C(3)	112.43(11)
H(13A)-C(13)-H(13C)	109.5	C(12)-Si(1)-C(3)	111.85(11)
H(13B)-C(13)-H(13C)	109.5	C(15)-Si(2)-C(17)	111.63(12)
Si(1)-C(14)-H(14A)	109.5	C(15)-Si(2)-C(16)	102.46(14)
Si(1)-C(14)-H(14B)	109.5	C(17)-Si(2)-C(16)	106.39(11)
H(14A)-C(14)-H(14B)	109.5	C(15)-Si(2)-C(3)	112.93(11)
Si(1)-C(14)-H(14C)	109.5	C(17)-Si(2)-C(3)	106.05(12)
H(14A)-C(14)-H(14C)	109.5	C(16)-Si(2)-C(3)	117.31(11)
H(14B)-C(14)-H(14C)	109.5	O(4)-C(21)-Cr	174.2(2)
Si(2)-C(15)-H(15A)	109.5		

Table F.22: Anisotropic displacement parameters ($\mathring{A}^2 \cdot 10^3$) for GSTR023. The anisotropic displacement factor exponent takes the form: $-2\pi^2[h^2 a^{*2} U_{11} + ... + 2hka^*b^* U_{12}]$.

	U(11)	U(22)	U(33)	U(23)	U(13)	U(12)
C(1)	22(1)	21(2)	16(1)	1(1)	3(1)	0(1)
C(2)	20(1)	20(2)	22(1)	1(1)	3(1)	0(1)
C(3)	19(1)	20(2)	20(1)	0(1)	-1(1)	1(1)
C(4)	21(1)	21(2)	17(1)	-1(1)	1(1)	-3(1)
C(5)	24(1)	18(2)	23(1)	1(1)	-1(1)	-1(1)
C(6)	29(1)	21(2)	31(1)	-1(1)	-3(1)	1(1)
C(7)	38(1)	20(2)	36(2)	-4(1)	-1(1)	-7(1)
C(8)	26(1)	28(2)	41(2)	-1(1)	-7(1)	-7(1)
C(9)	20(1)	25(2)	35(2)	-1(1)	-4(1)	-1(1)
C(10)	23(1)	29(2)	43(2)	4(1)	-1(1)	4(1)
C(11)	33(1)	18(2)	39(2)	4(1)	0(1)	2(1)
C(12)	25(1)	36(2)	38(2)	-5(1)	2(1)	2(1)
C(13)	32(1)	31(2)	24(1)	0(1)	4(1)	-1(1)
C(14)	34(1)	27(2)	27(1)	0(1)	6(1)	-7(1)
C(15)	46(2)	29(2)	33(2)	-9(1)	1(1)	-3(1)
C(16)	38(1)	33(2)	33(2)	-4(1)	0(1)	-16(1)
C(17)	31(1)	48(2)	29(2)	-6(1)	-4(1)	-10(1)

C(18)	29(1)	28(2)	32(1)	2(1)	-1(1)	2(1)
C(19)	26(1)	36(2)	21(1)	2(1)	4(1)	0(1)
C(20)	29(1)	32(2)	29(1)	2(1)	7(1)	-3(1)
C(22)	28(1)	24(2)	22(1)	0(1)	3(1)	2(1)
Cr	14(1)	18(1)	13(1)	1(1)	0(1)	0(1)
N(1)	20(1)	19(1)	23(1)	1(1)	0(1)	0(1)
N(2)	21(1)	19(1)	23(1)	0(1)	-1(1)	-3(1)
N(3)	22(1)	20(1)	31(1)	4(1)	-1(1)	1(1)
O(1)	43(1)	49(2)	41(1)	3(1)	18(1)	8(1)
O(2)	54(1)	31(1)	37(1)	7(1)	5(1)	-4(1)
O(3)	31(1)	56(2)	39(1)	1(1)	-10(1)	-3(1)
O(4)	45(1)	32(2)	40(1)	3(1)	6(1)	7(1)
O(5)	38(1)	44(2)	26(1)	0(1)	-8(1)	-2(1)
P	18(1)	18(1)	20(1)	-1(1)	-1(1)	-2(1)
Si(1)	22(1)	23(1)	21(1)	-1(1)	2(1)	-1(1)
Si(2)	28(1)	26(1)	24(1)	-4(1)	-2(1)	-6(1)
C(21)	26(1)	37(2)	20(1)	3(1)	3(1)	1(1)

Table F.23: Hydrogen coordinates (x 10^4) and isotropic displacement parameters ($\mathring{A}^2 \cdot 10^3$) for GSTR023.

	x	y	z	U(eq)
H(3A)	9004	5393	9299	24
H(5A)	7599	3715	7635	26
H(6A)	7056	1983	7191	33
H(7A)	4870	1562	6242	38
H(8A)	3208	2896	5810	38
H(9A)	3752	4636	6226	32
H(10A)	3264	7252	6326	47
H(10B)	3477	8293	5580	47
H(10C)	2969	8384	6870	47
H(11A)	5602	9382	7587	45
H(11B)	5309	9542	6242	45
H(11C)	6780	9015	6705	45
H(12A)	4780	6331	9186	49
H(12B)	5324	7083	10210	49
H(12C)	4342	6083	10468	49
H(13A)	7740	6310	11906	43
H(13B)	8253	5111	11834	43
H(13C)	6665	5382	12229	43

H(14A)	5536	4076	9318	44
H(14B)	5770	3854	10658	44
H(14C)	7076	3702	9818	44
H(15A)	7186	8387	9904	54
H(15B)	8424	8757	10799	54
H(15C)	7400	7791	11103	54
H(16A)	10909	7682	8445	52
H(16B)	10525	8694	9189	52
H(16C)	9440	8307	8183	52
H(17C)	11037	7357	11286	54
H(17B)	11344	6359	10496	54
H(17A)	10160	6288	11454	54

Table F.24: Torsion angles [º] for GSTR023.

N(1)-C(1)-C(4)-C(5)	176.4(2)	Si(1)-C(3)-P-N(2)	83.73(15)
P-C(1)-C(4)-C(5)	8.7(3)	Si(2)-C(3)-P-N(2)	-45.80(12)
N(1)-C(1)-C(4)-C(9)	-1.1(3)	Si(1)-C(3)-P-C(1)	-12.80(19)
P-C(1)-C(4)-C(9)	-168.86(16)	Si(2)-C(3)-P-C(1)	-142.33(11)
C(9)-C(4)-C(5)-C(6)	0.7(3)	Si(1)-C(3)-P-Cr	-148.90(10)
C(1)-C(4)-C(5)-C(6)	-176.9(2)	Si(2)-C(3)-P-Cr	81.58(12)
C(4)-C(5)-C(6)-C(7)	0.0(4)	N(1)-C(1)-P-N(2)	6.45(16)
C(5)-C(6)-C(7)-C(8)	-1.2(4)	C(4)-C(1)-P-N(2)	175.3(2)
C(6)-C(7)-C(8)-C(9)	1.7(4)	N(1)-C(1)-P-C(3)	111.53(17)
C(7)-C(8)-C(9)-C(4)	-1.0(4)	C(4)-C(1)-P-C(3)	-79.7(2)
C(5)-C(4)-C(9)-C(8)	-0.2(3)	N(1)-C(1)-P-Cr	-108.74(14)
C(1)-C(4)-C(9)-C(8)	177.5(2)	C(4)-C(1)-P-Cr	60.1(2)
O(1)-C(18)-Cr-C(21)	156(6)	C(18)-Cr-P-N(2)	-17.4(7)
O(1)-C(18)-Cr-C(20)	-119(6)	C(21)-Cr-P-N(2)	-167.18(10)
O(1)-C(18)-Cr-C(22)	64(6)	C(20)-Cr-P-N(2)	107.56(12)
O(1)-C(18)-Cr-C(19)	-27(6)	C(22)-Cr-P-N(2)	-76.31(11)
O(1)-C(18)-Cr-P	5(7)	C(19)-Cr-P-N(2)	14.96(10)
O(3)-C(20)-Cr-C(18)	-78(3)	C(18)-Cr-P-C(3)	-140.3(7)
O(3)-C(20)-Cr-C(21)	10(3)	C(21)-Cr-P-C(3)	69.96(12)
O(3)-C(20)-Cr-C(22)	46(4)	C(20)-Cr-P-C(3)	-15.30(14)
O(3)-C(20)-Cr-C(19)	-165(3)	C(22)-Cr-P-C(3)	160.83(13)
O(3)-C(20)-Cr-P	108(3)	C(19)-Cr-P-C(3)	-107.91(12)
O(5)-C(22)-Cr-C(18)	7(16)	C(18)-Cr-P-C(1)	82.8(7)
O(5)-C(22)-Cr-C(21)	-81(16)	C(21)-Cr-P-C(1)	-66.98(11)
O(5)-C(22)-Cr-C(20)	-118(16)	C(20)-Cr-P-C(1)	-152.23(13)

O(5)-C(22)-Cr-C(19)	94(16)	C(22)-Cr-P-C(1)	23.90(12)
O(5)-C(22)-Cr-P	-180(100)	C(19)-Cr-P-C(1)	115.16(11)
O(2)-C(19)-Cr-C(18)	-3(4)	P-C(3)-Si(1)-C(13)	-175.14(15)
O(2)-C(19)-Cr-C(21)	24(5)	Si(2)-C(3)-Si(1)-C(13)	-45.13(16)
O(2)-C(19)-Cr-C(20)	89(4)	P-C(3)-Si(1)-C(14)	68.78(17)
O(2)-C(19)-Cr-C(22)	-93(4)	Si(2)-C(3)-Si(1)-C(14)	-161.22(11)
O(2)-C(19)-Cr-P	-179(100)	P-C(3)-Si(1)-C(12)	-52.53(18)
C(4)-C(1)-N(1)-C(2)	-174.28(18)	Si(2)-C(3)-Si(1)-C(12)	77.48(14)
P-C(1)-N(1)-C(2)	-4.3(2)	P-C(3)-Si(2)-C(15)	97.05(13)
N(2)-C(2)-N(1)-C(1)	-0.6(3)	Si(1)-C(3)-Si(2)-C(15)	-37.25(15)
N(3)-C(2)-N(1)-C(1)	178.10(19)	P-C(3)-Si(2)-C(17)	-140.40(12)
N(3)-C(2)-N(2)-P	-172.88(19)	Si(1)-C(3)-Si(2)-C(17)	85.31(13)
N(1)-C(2)-N(2)-P	5.8(3)	P-C(3)-Si(2)-C(16)	-21.78(16)
N(2)-C(2)-N(3)-C(11)	5.8(3)	Si(1)-C(3)-Si(2)-C(16)	-156.07(12)
N(1)-C(2)-N(3)-C(11)	-172.9(2)	C(18)-Cr-C(21)-O(4)	42(2)
N(2)-C(2)-N(3)-C(10)	-173.1(2)	C(20)-Cr-C(21)-O(4)	-51(2)
N(1)-C(2)-N(3)-C(10)	8.2(3)	C(22)-Cr-C(21)-O(4)	131(2)
C(2)-N(2)-P-C(3)	-121.03(16)	C(19)-Cr-C(21)-O(4)	15(3)
C(2)-N(2)-P-C(1)	-6.41(16)	P-Cr-C(21)-O(4)	-142(2)
C(2)-N(2)-P-Cr	107.44(14)		

F.5   Data for Complex 126b
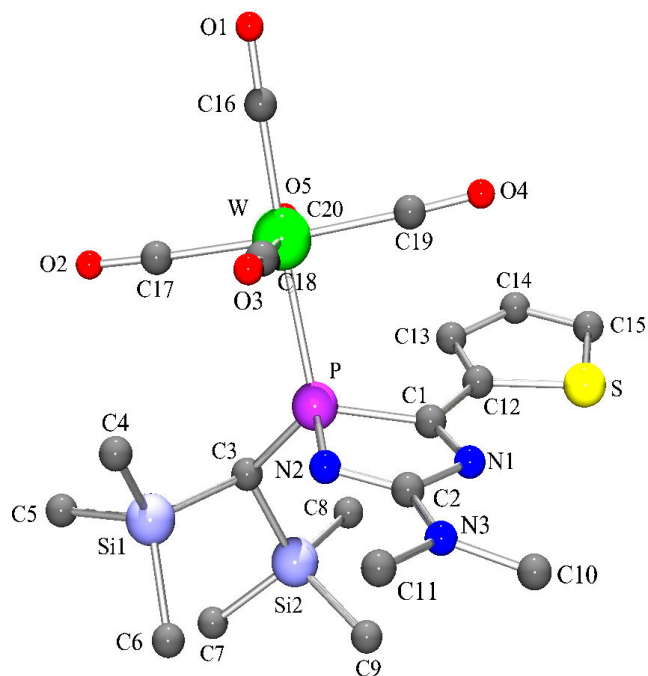
Figure F.5: Molecular structure of complex **126b** (GSTR049) in the crystal (hydrogen atoms are omitted for clarity).

Table F.25: Crystal data and structure refinement for GSTR049.

Identification code	GSTR049
Empirical formula	$C_{20}H_{28}N_3O_5PSSi_2W$
Formula weight	693.51
Temperature	100(2) K
Wavelength	0.71073 Å
Crystal system, space group	Monoclinic, P $2_1/n$
Unit cell dimensions	a = 11.8239(2) Å, α = 90º
	b = 20.2887(5) Å, β = 104.5180(10)º
	c = 11.9270(3) Å, γ = 90º
Volume	2769.83(11) Å^3
Z, Calculated density	4, 1.663 Mg/m^3
Absorption coefficient	4.423 mm^{-1}
F(000)	1368
Crystal size	0.26 x 0.20 x 0.03 mm
θ range for data collection	2.04 to 27.48º
Limiting indices	-15 $\leq$ h $\leq$ 15, -26 $\leq$ k $\leq$ 26, -15 $\leq$ l $\leq$ 15
Reflections collected / unique	44556 / 6333 [R$_{int}$ = 0.0569]
Completeness to θ = 27.48	99.7 %
Absorption correction	Analytical
Max. and min. transmission	0.8787 and 0.3949
Refinement method	Full-matrix least-squares on F^2
Data / restraints / parameters	6333 / 0 / 306
Goodness-of-fit on F^2	0.983
Final R indices [I>2σ(I)]	R$_1$ = 0.0290, wR$_2$ = 0.0511
R indices (all data)	R$_1$ = 0.0435, wR$_2$ = 0.0541
Largest diff. peak and hole	2.001 and -1.875 e $\cdot$ A^{-3}

Table F.26: Atomic coordinates (x 10^4) and equivalent isotropic displacement parameters ($\text{Å}^2 \cdot 10^3$) for GSTR049. U(eq) is defined as one third of the trace of the orthogonalized U_{ij} tensor.

	x	y	z	U(eq)
W	7149(1)	2693(1)	6137(1)	15(1)
P	6970(1)	3600(1)	7535(1)	14(1)
S	9241(1)	5144(1)	6401(1)	21(1)
Si(1)	5873(1)	3075(1)	9448(1)	20(1)
Si(2)	8050(1)	4043(1)	10176(1)	19(1)
N(1)	6952(2)	4821(1)	6816(2)	17(1)
N(2)	5688(2)	4005(1)	7254(2)	16(1)
N(3)	4953(2)	5035(1)	6555(3)	24(1)
O(1)	7105(2)	1656(1)	4158(2)	33(1)
O(2)	6799(2)	1541(1)	7827(2)	39(1)
O(3)	4413(2)	2885(1)	5042(2)	28(1)
O(4)	7937(2)	3741(1)	4495(2)	28(1)
O(5)	9772(2)	2346(1)	7443(2)	27(1)
C(1)	7716(3)	4363(2)	7190(3)	16(1)
C(2)	5830(3)	4601(2)	6900(3)	18(1)
C(3)	7263(2)	3407(1)	9069(3)	15(1)
C(4)	4738(3)	2708(2)	8221(3)	28(1)
C(5)	6362(3)	2386(2)	10510(3)	32(1)
C(6)	5093(3)	3744(2)	10038(3)	29(1)
C(7)	8052(3)	3744(2)	11656(3)	30(1)
C(8)	9627(3)	4097(2)	10191(3)	25(1)
C(9)	7379(3)	4878(2)	9899(3)	27(1)
C(10)	5112(3)	5714(2)	6253(3)	29(1)
C(11)	3765(3)	4833(2)	6557(4)	35(1)
C(12)	8899(3)	4445(2)	7077(3)	16(1)
C(13)	9844(2)	4023(2)	7385(3)	18(1)
C(14)	10835(3)	4272(2)	7059(3)	20(1)
C(15)	10624(3)	4866(2)	6515(3)	22(1)
C(16)	7145(3)	2025(2)	4898(3)	23(1)
C(17)	6867(3)	1962(2)	7218(3)	25(1)
C(18)	5392(3)	2826(2)	5430(3)	21(1)
C(19)	7632(3)	3378(2)	5088(3)	20(1)
C(20)	8846(3)	2495(2)	6948(3)	20(1)

Table F.27: Bond lengths [Å] and angles [º] for GSTR049.

W-C(16)	2.005(4)	C(3)-H(3)	1.0000
W-C(20)	2.038(3)	C(4)-H(4A)	0.9800
W-C(19)	2.044(4)	C(4)-H(4B)	0.9800
W-C(17)	2.046(4)	C(4)-H(4C)	0.9800
W-C(18)	2.054(3)	C(5)-H(5A)	0.9800
W-P	2.5266(8)	C(5)-H(5B)	0.9800
P-N(2)	1.683(2)	C(5)-H(5C)	0.9800
P-C(3)	1.818(3)	C(6)-H(6A)	0.9800
P-C(1)	1.879(3)	C(6)-H(6B)	0.9800
S-C(15)	1.704(3)	C(6)-H(6C)	0.9800
S-C(12)	1.729(3)	C(7)-H(7A)	0.9800
Si(1)-C(4)	1.873(3)	C(7)-H(7B)	0.9800
Si(1)-C(6)	1.874(3)	C(7)-H(7C)	0.9800
Si(1)-C(5)	1.877(4)	C(8)-H(8A)	0.9800
Si(1)-C(3)	1.932(3)	C(8)-H(8B)	0.9800
Si(2)-C(8)	1.864(3)	C(8)-H(8C)	0.9800
Si(2)-C(7)	1.866(3)	C(9)-H(9A)	0.9800
Si(2)-C(9)	1.866(3)	C(9)-H(9B)	0.9800
Si(2)-C(3)	1.913(3)	C(9)-H(9C)	0.9800
N(1)-C(1)	1.295(4)	C(10)-H(10A)	0.9800
N(1)-C(2)	1.428(4)	C(10)-H(10B)	0.9800
N(2)-C(2)	1.305(4)	C(10)-H(10C)	0.9800
N(3)-C(2)	1.343(4)	C(11)-H(11A)	0.9800
N(3)-C(10)	1.449(4)	C(11)-H(11B)	0.9800
N(3)-C(11)	1.463(4)	C(11)-H(11C)	0.9800
O(1)-C(16)	1.148(4)	C(12)-C(13)	1.382(4)
O(2)-C(17)	1.137(4)	C(13)-C(14)	1.416(4)
O(3)-C(18)	1.140(4)	C(13)-H(13)	0.9500
O(4)-C(19)	1.141(4)	C(14)-C(15)	1.361(4)
O(5)-C(20)	1.146(4)	C(14)-H(14)	0.9500
C(1)-C(12)	1.448(4)	C(15)-H(15)	0.9500
C(16)-W-C(20)	92.07(13)	Si(1)-C(5)-H(5B)	109.5
C(16)-W-C(19)	87.58(13)	H(5A)-C(5)-H(5B)	109.5
C(20)-W-C(19)	91.83(12)	Si(1)-C(5)-H(5C)	109.5
C(16)-W-C(17)	90.20(14)	H(5A)-C(5)-H(5C)	109.5
C(20)-W-C(17)	81.60(13)	H(5B)-C(5)-H(5C)	109.5
C(19)-W-C(17)	172.98(12)	Si(1)-C(6)-H(6A)	109.5

C(16)-W-C(18)	88.34(13)	Si(1)-C(6)-H(6B)	109.5
C(20)-W-C(18)	174.21(13)	H(6A)-C(6)-H(6B)	109.5
C(19)-W-C(18)	93.96(12)	Si(1)-C(6)-H(6C)	109.5
C(17)-W-C(18)	92.63(13)	H(6A)-C(6)-H(6C)	109.5
C(16)-W-P	173.56(9)	H(6B)-C(6)-H(6C)	109.5
C(20)-W-P	93.77(9)	Si(2)-C(7)-H(7A)	109.5
C(19)-W-P	89.53(9)	Si(2)-C(7)-H(7B)	109.5
C(17)-W-P	93.33(10)	H(7A)-C(7)-H(7B)	109.5
C(18)-W-P	86.13(9)	Si(2)-C(7)-H(7C)	109.5
N(2)-P-C(3)	103.88(13)	H(7A)-C(7)-H(7C)	109.5
N(2)-P-C(1)	90.14(13)	H(7B)-C(7)-H(7C)	109.5
C(3)-P-C(1)	114.62(13)	Si(2)-C(8)-H(8A)	109.5
N(2)-P-W	116.40(9)	Si(2)-C(8)-H(8B)	109.5
C(3)-P-W	118.77(10)	H(8A)-C(8)-H(8B)	109.5
C(1)-P-W	109.53(10)	Si(2)-C(8)-H(8C)	109.5
C(15)-S-C(12)	91.28(15)	H(8A)-C(8)-H(8C)	109.5
C(4)-Si(1)-C(6)	104.91(16)	H(8B)-C(8)-H(8C)	109.5
C(4)-Si(1)-C(5)	105.72(17)	Si(2)-C(9)-H(9A)	109.5
C(6)-Si(1)-C(5)	112.52(17)	Si(2)-C(9)-H(9B)	109.5
C(4)-Si(1)-C(3)	116.14(15)	H(9A)-C(9)-H(9B)	109.5
C(6)-Si(1)-C(3)	111.26(15)	Si(2)-C(9)-H(9C)	109.5
C(5)-Si(1)-C(3)	106.32(15)	H(9A)-C(9)-H(9C)	109.5
C(8)-Si(2)-C(7)	104.25(16)	H(9B)-C(9)-H(9C)	109.5
C(8)-Si(2)-C(9)	109.18(16)	N(3)-C(10)-H(10A)	109.5
C(7)-Si(2)-C(9)	111.20(17)	N(3)-C(10)-H(10B)	109.5
C(8)-Si(2)-C(3)	111.03(14)	H(10A)-C(10)-H(10B)	109.5
C(7)-Si(2)-C(3)	108.62(15)	N(3)-C(10)-H(10C)	109.5
C(9)-Si(2)-C(3)	112.28(14)	H(10A)-C(10)-H(10C)	109.5
C(1)-N(1)-C(2)	109.4(3)	H(10B)-C(10)-H(10C)	109.5
C(2)-N(2)-P	109.5(2)	N(3)-C(11)-H(11A)	109.5
C(2)-N(3)-C(10)	124.1(3)	N(3)-C(11)-H(11B)	109.5
C(2)-N(3)-C(11)	119.0(3)	H(11A)-C(11)-H(11B)	109.5
C(10)-N(3)-C(11)	116.7(3)	N(3)-C(11)-H(11C)	109.5
N(1)-C(1)-C(12)	119.5(3)	H(11A)-C(11)-H(11C)	109.5
N(1)-C(1)-P	110.0(2)	H(11B)-C(11)-H(11C)	109.5
C(12)-C(1)-P	129.2(2)	C(13)-C(12)-C(1)	129.8(3)
N(2)-C(2)-N(3)	123.6(3)	C(13)-C(12)-S	111.4(2)
N(2)-C(2)-N(1)	120.7(3)	C(1)-C(12)-S	118.8(2)
N(3)-C(2)-N(1)	115.6(3)	C(12)-C(13)-C(14)	112.0(3)
P-C(3)-Si(2)	119.12(16)	C(12)-C(13)-H(13)	124.0

P-C(3)-Si(1)	110.62(15)	C(14)-C(13)-H(13)	124.0
Si(2)-C(3)-Si(1)	111.66(16)	C(15)-C(14)-C(13)	112.4(3)
P-C(3)-H(3)	104.7	C(15)-C(14)-H(14)	123.8
Si(2)-C(3)-H(3)	104.7	C(13)-C(14)-H(14)	123.8
Si(1)-C(3)-H(3)	104.7	C(14)-C(15)-S	112.9(2)
Si(1)-C(4)-H(4A)	109.5	C(14)-C(15)-H(15)	123.6
Si(1)-C(4)-H(4B)	109.5	S-C(15)-H(15)	123.6
H(4A)-C(4)-H(4B)	109.5	O(1)-C(16)-W	177.1(3)
Si(1)-C(4)-H(4C)	109.5	O(2)-C(17)-W	174.6(3)
H(4A)-C(4)-H(4C)	109.5	O(3)-C(18)-W	178.5(3)
H(4B)-C(4)-H(4C)	109.5	O(4)-C(19)-W	177.1(3)
Si(1)-C(5)-H(5A)	109.5	O(5)-C(20)-W	175.1(3)

Table F.28: Anisotropic displacement parameters ($\mathring{A}^2 \cdot 10^3$) for GSTR049. The anisotropic displacement factor exponent takes the form: $-2\pi^2[h^2a^{*2}U_{11} + ... + 2hka^*b^*U_{12}]$.

	U(11)	U(22)	U(33)	U(23)	U(13)	U(12)
W	16(1)	14(1)	16(1)	-1(1)	4(1)	-1(1)
P	13(1)	13(1)	16(1)	1(1)	3(1)	-1(1)
S	21(1)	19(1)	24(1)	3(1)	8(1)	-2(1)
Si(1)	21(1)	22(1)	21(1)	1(1)	10(1)	-3(1)
Si(2)	19(1)	19(1)	16(1)	-2(1)	2(1)	1(1)
N(1)	15(1)	15(1)	21(2)	1(1)	6(1)	-1(1)
N(2)	13(1)	16(1)	20(2)	2(1)	4(1)	0(1)
N(3)	16(1)	21(2)	36(2)	8(1)	6(1)	5(1)
O(1)	30(1)	36(2)	35(2)	-19(1)	9(1)	-5(1)
O(2)	49(2)	26(1)	45(2)	12(1)	17(1)	-3(1)
O(3)	18(1)	31(1)	33(2)	-3(1)	2(1)	-2(1)
O(4)	35(1)	29(1)	22(1)	5(1)	11(1)	-3(1)
O(5)	22(1)	31(1)	27(1)	3(1)	2(1)	7(1)
C(1)	16(2)	17(2)	14(2)	-4(1)	2(1)	-3(1)
C(2)	17(2)	19(2)	18(2)	-1(1)	4(1)	1(1)
C(3)	15(2)	14(2)	16(2)	3(1)	7(1)	2(1)
C(4)	23(2)	32(2)	33(2)	-4(2)	13(2)	-9(2)
C(5)	39(2)	28(2)	34(2)	7(2)	19(2)	0(2)
C(6)	24(2)	32(2)	33(2)	-2(2)	12(2)	1(2)
C(7)	32(2)	35(2)	19(2)	-1(2)	1(2)	-4(2)
C(8)	22(2)	27(2)	24(2)	-1(2)	1(2)	0(1)
C(9)	26(2)	23(2)	30(2)	-7(2)	4(2)	3(2)

C(10)	28(2)	19(2)	38(2)	7(2)	7(2)	6(1)
C(11)	16(2)	34(2)	55(3)	10(2)	8(2)	7(2)
C(12)	19(2)	15(2)	14(2)	-2(1)	3(1)	-2(1)
C(13)	13(2)	22(2)	18(2)	3(1)	2(1)	-3(1)
C(14)	15(2)	26(2)	20(2)	-3(1)	5(1)	-2(1)
C(15)	20(2)	27(2)	20(2)	-2(1)	9(2)	-7(1)
C(16)	15(2)	23(2)	30(2)	-2(2)	4(2)	-4(1)
C(17)	23(2)	21(2)	30(2)	-5(2)	6(2)	-2(1)
C(18)	27(2)	17(2)	20(2)	-1(1)	8(2)	-5(1)
C(19)	18(2)	21(2)	19(2)	-4(1)	1(1)	2(1)
C(20)	28(2)	16(2)	16(2)	0(1)	10(2)	-3(1)

Table F.29: Hydrogen coordinates (x 10^4) and isotropic displacement parameters ($\mathring{A}^2 \cdot 10^3$) for GSTR049.

	x	y	z	U(eq)
H(3)	7806	3021	9178	18
H(4A)	5073	2332	7901	42
H(4B)	4477	3041	7617	42
H(4C)	4072	2560	8505	42
H(5A)	6806	2568	11251	48
H(5B)	6858	2082	10209	48
H(5C)	5678	2150	10625	48
H(6A)	4440	3553	10297	43
H(6B)	4795	4071	9431	43
H(6C)	5637	3957	10694	43
H(7A)	8345	3291	11753	45
H(7B)	7255	3757	11756	45
H(7C)	8558	4028	12236	45
H(8A)	10052	4327	10893	38
H(8B)	9713	4341	9507	38
H(8C)	9946	3652	10179	38
H(9A)	7693	5163	10569	41
H(9B)	6530	4842	9774	41
H(9C)	7561	5069	9210	41
H(10A)	5937	5791	6281	43
H(10B)	4873	6007	6805	43
H(10C)	4635	5803	5470	43
H(11A)	3746	4356	6679	52
H(11B)	3232	4947	5812	52

H(11C)	3522	5062	7182	52
H(13)	9831	3615	7771	22
H(14)	11564	4049	7203	24
H(15)	11189	5100	6229	26

Table F.30: Torsion angles [º] for GSTR049.

C(16)-W-P-N(2)	22.0(9)	C(7)-Si(2)-C(3)-Si(1)	42.2(2)
C(20)-W-P-N(2)	177.07(14)	C(9)-Si(2)-C(3)-Si(1)	-81.24(19)
C(19)-W-P-N(2)	85.27(13)	C(4)-Si(1)-C(3)-P	22.9(2)
C(17)-W-P-N(2)	−101.14(14)	C(6)-Si(1)-C(3)-P	-97.03(19)
C(18)-W-P-N(2)	−8.73(14)	C(5)-Si(1)-C(3)-P	140.14(17)
C(16)-W-P-C(3)	147.4(9)	C(4)-Si(1)-C(3)-Si(2)	158.01(16)
C(20)-W-P-C(3)	−57.60(14)	C(6)-Si(1)-C(3)-Si(2)	38.1(2)
C(19)-W-P-C(3)	−149.40(14)	C(5)-Si(1)-C(3)-Si(2)	-84.72(19)
C(17)-W-P-C(3)	24.19(14)	N(1)-C(1)-C(12)-C(13)	-178.5(3)
C(18)-W-P-C(3)	116.60(14)	P-C(1)-C(12)-C(13)	-12.7(5)
C(16)-W-P-C(1)	−78.3(9)	N(1)-C(1)-C(12)-S	-2.0(4)
C(20)-W-P-C(1)	76.76(13)	P-C(1)-C(12)-S	163.74(18)
C(19)-W-P-C(1)	−15.04(13)	C(15)-S-C(12)-C(13)	0.8(3)
C(17)-W-P-C(1)	158.55(13)	C(15)-S-C(12)-C(1)	-176.2(3)
C(18)-W-P-C(1)	−109.04(13)	C(1)-C(12)-C(13)-C(14)	176.2(3)
C(3)-P-N(2)-C(2)	118.6(2)	S-C(12)-C(13)-C(14)	-0.5(4)
C(1)-P-N(2)-C(2)	3.1(2)	C(12)-C(13)-C(14)-C(15)	-0.2(4)
W-P-N(2)-C(2)	−108.9(2)	C(13)-C(14)-C(15)-S	0.9(4)
C(2)-N(1)-C(1)-C(12)	173.5(3)	C(12)-S-C(15)-C(14)	-1.0(3)
C(2)-N(1)-C(1)-P	5.2(3)	C(20)-W-C(16)-O(1)	-157(6)
N(2)-P-C(1)-N(1)	−5.1(2)	C(19)-W-C(16)-O(1)	-65(6)
C(3)-P-C(1)-N(1)	−110.5(2)	C(17)-W-C(16)-O(1)	122(6)
W-P-C(1)-N(1)	113.1(2)	C(18)-W-C(16)-O(1)	29(6)
N(2)-P-C(1)-C(12)	−172.0(3)	P-W-C(16)-O(1)	-2(7)
C(3)-P-C(1)-C(12)	82.7(3)	C(16)-W-C(17)-O(2)	73(3)
W-P-C(1)-C(12)	−53.7(3)	C(20)-W-C(17)-O(2)	-19(3)
P-N(2)-C(2)-N(3)	176.7(3)	C(19)-W-C(17)-O(2)	1(4)
P-N(2)-C(2)-N(1)	−0.9(4)	C(18)-W-C(17)-O(2)	161(3)
C(10)-N(3)-C(2)-N(2)	174.6(3)	P-W-C(17)-O(2)	-113(3)
C(11)-N(3)-C(2)-N(2)	−0.8(5)	C(16)-W-C(18)-O(3)	59(12)
C(10)-N(3)-C(2)-N(1)	−7.8(5)	C(20)-W-C(18)-O(3)	-35(13)
C(11)-N(3)-C(2)-N(1)	176.8(3)	C(19)-W-C(18)-O(3)	147(12)
C(1)-N(1)-C(2)-N(2)	−3.2(4)	C(17)-W-C(18)-O(3)	-31(12)

C(1)-N(1)-C(2)-N(3)	179.0(3)	P-W-C(18)-O(3)	-124(12)
N(2)-P-C(3)-Si(2)	−86.55(18)	C(16)-W-C(19)-O(4)	-46(5)
C(1)-P-C(3)-Si(2)	10.1(2)	C(20)-W-C(19)-O(4)	46(5)
W-P-C(3)-Si(2)	142.28(12)	C(17)-W-C(19)-O(4)	25(6)
N(2)-P-C(3)-Si(1)	44.83(18)	C(18)-W-C(19)-O(4)	-135(5)
C(1)-P-C(3)-Si(1)	141.49(15)	P-W-C(19)-O(4)	139(5)
W-P-C(3)-Si(1)	−86.34(15)	C(16)-W-C(20)-O(5)	-83(3)
C(8)-Si(2)-C(3)-P	−72.9(2)	C(19)-W-C(20)-O(5)	-171(3)
C(7)-Si(2)-C(3)-P	173.07(17)	C(17)-W-C(20)-O(5)	6(3)
C(9)-Si(2)-C(3)-P	49.7(2)	C(18)-W-C(20)-O(5)	10(4)
C(8)-Si(2)-C(3)-Si(1)	156.22(15)	P-W-C(20)-O(5)	99(3)

F.6 Data for Complex 126g
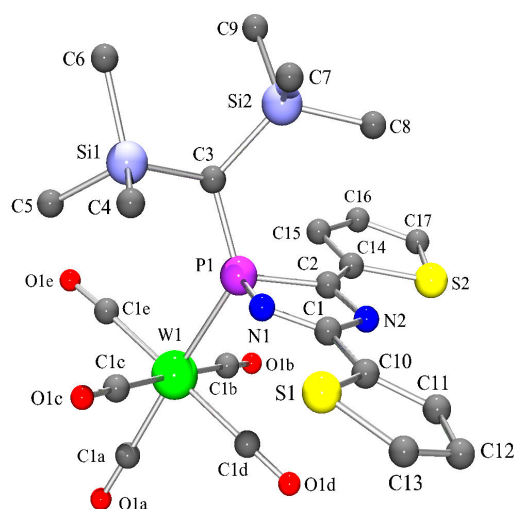
Figure F.6: Molecular structure of complex **126g** (str010) in the crystal (major conformation, 59 %; hydrogen atoms are omitted for clarity).
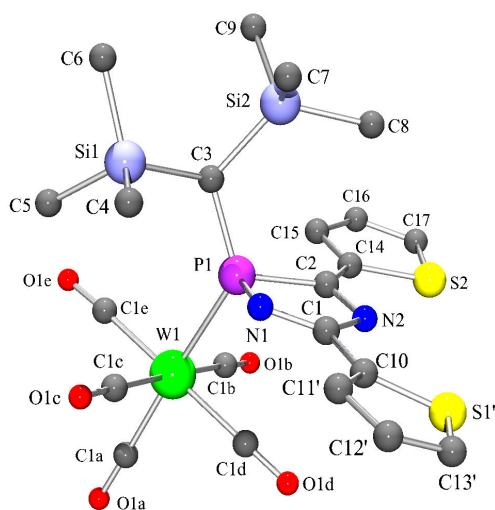
Figure F.7: Molecular structure of complex **126g** (str010) in the crystal (minor conformation, 41 %; hydrogen atoms are omitted for clarity).

Table F.31: Crystal data and structure refinement for str010.

Identification code	str010_m
Empirical formula	$C_{22}H_{25}N_2O_5PSi_2W$
Formula weight	732.56
Temperature	123(2) K
Wavelength	0.71073 Å
Crystal system, space group	Triclinic, P$\bar{1}$ (No.2)
Unit cell dimensions	a = 9.5035(3) Å, α = 75.868(2)º
	b = 10.9580(4) Å, β = 84.937(2)º
	c = 15.4221(7) Å, γ = 65.551(2)º
Volume	1417.64(9) Å^3
Z, Calculated density	2, 1.716 Mg/m^3
Absorption coefficient	4.397 mm^{-1}
F(000)	720
Crystal size	0.35 x 0.20 x 0.15 mm
Diffractometer	Nonius KappaCCD
θ range for data collection	3.00 to 27.47º
Limiting indices	-12 $\leq$ h $\leq$ 12, -13 $\leq$ k $\leq$ 14, -20 $\leq$ l $\leq$ 17
Reflections collected / unique	13970 / 6484 [R_{int} = 0.0401]
Completeness to θ = 27.47	99.6 %
Absorption correction	Semi-empirical from equivalents
Max. and min. transmission	0.53875 and 0.36309
Refinement method	Full-matrix least-squares on F^2
Data / restraints / parameters	6484 / 119 / 309
Goodness-of-fit on F^2	1.040
Final R indices [I>2σ(I)]	R_1 = 0.0291, wR_2 = 0.0668
R indices (all data)	R_1 = 0.0337, wR_2 = 0.0686
Largest diff. peak and hole	1.268 and -2.092 e $\cdot$ A^{-3}

Table F.32: Atomic coordinates (x 10^4) and equivalent isotropic displacement parameters ($\text{Å}^2 \cdot 10^3$) for str010. U(eq) is defined as one third of the trace of the orthogonalized U_{ij} tensor.

	x	y	z	U(eq)
W(1)	1417(1)	7237(1)	3786(1)	18(1)
C(1A)	-36(4)	8331(4)	4613(3)	28(1)
O(1A)	-853(4)	8936(3)	5097(2)	42(1)
C(1B)	2600(5)	8448(4)	3701(3)	29(1)
O(1B)	3214(4)	9152(3)	3696(3)	46(1)
C(1C)	173(4)	6062(4)	3879(2)	23(1)
O(1C)	-537(3)	5431(3)	3918(2)	32(1)
C(1D)	106(4)	8609(4)	2710(3)	23(1)
O(1D)	-619(3)	9388(3)	2108(2)	34(1)
C(1E)	2749(4)	5980(4)	4887(3)	24(1)
O(1E)	3454(4)	5366(3)	5525(2)	36(1)
P(1)	3044(1)	5899(1)	2662(1)	17(1)
N(1)	1810(3)	5869(3)	1937(2)	21(1)
C(1)	1678(4)	6827(4)	1225(2)	19(1)
N(2)	2613(3)	7591(3)	1103(2)	21(1)
C(2)	3533(4)	7160(4)	1788(2)	19(1)
C(3)	4631(4)	4194(4)	2890(2)	19(1)
Si(1)	4002(1)	2744(1)	3508(1)	22(1)
C(4)	2426(5)	2692(5)	2905(3)	34(1)
C(5)	3379(5)	2902(4)	4670(3)	30(1)
C(6)	5692(5)	1031(4)	3686(3)	36(1)
Si(2)	6087(1)	3617(1)	1966(1)	23(1)
C(7)	5503(5)	2625(5)	1351(3)	35(1)
C(8)	6353(5)	4974(4)	1055(3)	38(1)
C(9)	7994(5)	2637(5)	2560(3)	43(1)
C(10)	567(4)	7194(4)	523(2)	24(1)
C(11)	187(9)	8258(8)	-263(5)	26(1)[a]
C(12)	-983(9)	8404(7)	-776(5)	27(1)[a]
C(13)	-1503(9)	7427(8)	-400(5)	32(1)[a]
S(1)	-556(2)	6328(2)	600(1)	30(1)[a]
C(11')	-393(13)	6490(11)	435(7)	26(1)[b]
C(12')	-1356(12)	7070(11)	-287(7)	27(1)[b]
C(13')	-1107(13)	8147(11)	-779(7)	32(1)[b]
S(1')	270(4)	8538(3)	-342(2)	30(1)[b]
C(14)	4653(4)	7705(3)	1854(2)	20(1)

C(15)	5719(4)	7320(4)	2536(3)	24(1)
C(16)	6701(4)	8019(4)	2326(3)	30(1)
C(17)	6397(5)	8890(4)	1504(3)	31(1)
S(2)	4892(1)	8901(1)	967(1)	29(1)

[a] s.o.f. = 0.591(4); [b] s.o.f. = 0.409(4).

Table F.33: Bond lengths [Å] and angles [°] for str010.

W(1)-C(1A)	2.009(4)	Si(1)-C(4)	1.857(4)
W(1)-C(1D)	2.041(4)	Si(1)-C(5)	1.863(4)
W(1)-C(1B)	2.041(4)	Si(1)-C(6)	1.873(4)
W(1)-C(1E)	2.044(4)	Si(2)-C(8)	1.865(4)
W(1)-C(1C)	2.054(4)	Si(2)-C(9)	1.865(5)
W(1)-P(1)	2.5377(9)	Si(2)-C(7)	1.867(4)
C(1A)-O(1A)	1.145(5)	C(10)-C(11)	1.413(8)
C(1B)-O(1B)	1.142(5)	C(10)-C(11')	1.450(9)
C(1C)-O(1C)	1.138(4)	C(10)-S(1')	1.671(5)
C(1D)-O(1D)	1.141(5)	C(10)-S(1)	1.677(4)
C(1E)-O(1E)	1.135(5)	C(11)-C(12)	1.355(9)
P(1)-N(1)	1.705(3)	C(12)-C(13)	1.346(9)
P(1)-C(3)	1.824(4)	C(13)-S(1)	1.756(8)
P(1)-C(2)	1.858(4)	C(11')-C(12')	1.354(12)
N(1)-C(1)	1.294(5)	C(12')-C(13')	1.336(11)
C(1)-N(2)	1.426(4)	C(13')-S(1')	1.764(10)
C(1)-C(10)	1.445(5)	C(14)-C(15)	1.389(5)
N(2)-C(2)	1.296(5)	C(14)-S(2)	1.719(3)
C(2)-C(14)	1.441(5)	C(15)-C(16)	1.407(5)
C(3)-Si(2)	1.927(4)	C(16)-C(17)	1.359(6)
C(3)-Si(1)	1.933(4)	C(17)-S(2)	1.709(4)
C(1A)-W(1)-C(1D)	90.40(16)	P(1)-C(3)-Si(1)	113.56(17)
C(1A)-W(1)-C(1B)	87.37(15)	Si(2)-C(3)-Si(1)	111.02(17)
C(1D)-W(1)-C(1B)	88.76(16)	C(4)-Si(1)-C(5)	109.1(2)
C(1A)-W(1)-C(1E)	87.41(16)	C(4)-Si(1)-C(6)	109.8(2)
C(1D)-W(1)-C(1E)	175.82(14)	C(5)-Si(1)-C(6)	102.9(2)
C(1B)-W(1)-C(1E)	87.58(16)	C(4)-Si(1)-C(3)	112.42(18)
C(1A)-W(1)-C(1C)	91.26(15)	C(5)-Si(1)-C(3)	111.71(17)
C(1D)-W(1)-C(1C)	90.54(14)	C(6)-Si(1)-C(3)	110.50(18)
C(1B)-W(1)-C(1C)	178.46(14)	C(8)-Si(2)-C(9)	105.5(2)
C(1E)-W(1)-C(1C)	93.07(14)	C(8)-Si(2)-C(7)	103.3(2)

C(1A)-W(1)-P(1)	174.96(11)	C(9)-Si(2)-C(7)	114.9(2)
C(1D)-W(1)-P(1)	85.71(10)	C(8)-Si(2)-C(3)	118.14(17)
C(1B)-W(1)-P(1)	95.74(11)	C(9)-Si(2)-C(3)	104.62(19)
C(1E)-W(1)-P(1)	96.66(11)	C(7)-Si(2)-C(3)	110.70(17)
C(1C)-W(1)-P(1)	85.57(10)	C(11)-C(10)-C(1)	130.0(4)
O(1A)-C(1A)-W(1)	178.8(4)	C(1)-C(10)-C(11')	127.5(5)
O(1B)-C(1B)-W(1)	176.0(4)	C(1)-C(10)-S(1')	121.9(3)
O(1C)-C(1C)-W(1)	178.6(3)	C(11')-C(10)-S(1')	110.6(4)
O(1D)-C(1D)-W(1)	179.1(3)	C(11)-C(10)-S(1)	110.1(4)
O(1E)-C(1E)-W(1)	174.9(3)	C(1)-C(10)-S(1)	119.9(3)
N(1)-P(1)-C(3)	106.68(15)	C(12)-C(11)-C(10)	116.6(6)
N(1)-P(1)-C(2)	90.55(16)	C(13)-C(12)-C(11)	108.8(6)
C(3)-P(1)-C(2)	112.25(16)	C(12)-C(13)-S(1)	114.8(6)
N(1)-P(1)-W(1)	107.55(11)	C(10)-S(1)-C(13)	89.7(3)
C(3)-P(1)-W(1)	127.74(12)	C(12')-C(11')-C(10)	115.2(7)
C(2)-P(1)-W(1)	105.67(11)	C(13')-C(12')-C(11')	109.1(8)
C(1)-N(1)-P(1)	108.0(2)	C(12')-C(13')-S(1')	115.8(8)
N(1)-C(1)-N(2)	121.4(3)	C(10)-S(1')-C(13')	89.1(4)
N(1)-C(1)-C(10)	122.0(3)	C(15)-C(14)-C(2)	128.6(3)
N(2)-C(1)-C(10)	116.6(3)	C(15)-C(14)-S(2)	111.5(3)
C(2)-N(2)-C(1)	109.5(3)	C(2)-C(14)-S(2)	119.7(3)
N(2)-C(2)-C(14)	122.8(3)	C(14)-C(15)-C(16)	111.9(3)
N(2)-C(2)-P(1)	109.7(2)	C(17)-C(16)-C(15)	112.7(4)
C(14)-C(2)-P(1)	127.3(3)	C(16)-C(17)-S(2)	112.6(3)
P(1)-C(3)-Si(2)	119.88(19)	C(17)-S(2)-C(14)	91.26(18)

Table F.34: Torsion angles [º] for str010.

C(1D)-W(1)-C(1A)-O(1A)	165(17)	W(1)-P(1)-C(3)-Si(2)	-161.20(11)
C(1B)-W(1)-C(1A)-O(1A)	-106(17)	N(1)-P(1)-C(3)-Si(1)	-64.8(2)
C(1E)-W(1)-C(1A)-O(1A)	-19(17)	C(2)-P(1)-C(3)-Si(1)	-162.49(17)
C(1C)-W(1)-C(1A)-O(1A)	74(17)	W(1)-P(1)-C(3)-Si(1)	64.2(2)
P(1)-W(1)-C(1A)-O(1A)	125(17)	P(1)-C(3)-Si(1)-C(4)	55.6(3)
C(1A)-W(1)-C(1B)-O(1B)	13(6)	Si(2)-C(3)-Si(1)-C(4)	-83.0(2)
C(1D)-W(1)-C(1B)-O(1B)	104(6)	P(1)-C(3)-Si(1)-C(5)	-67.6(2)
C(1E)-W(1)-C(1B)-O(1B)	-74(6)	Si(2)-C(3)-Si(1)-C(5)	153.87(19)
C(1C)-W(1)-C(1B)-O(1B)	41(10)	P(1)-C(3)-Si(1)-C(6)	178.6(2)
P(1)-W(1)-C(1B)-O(1B)	-171(6)	Si(2)-C(3)-Si(1)-C(6)	40.0(2)
C(1A)-W(1)-C(1C)-O(1C)	79(15)	P(1)-C(3)-Si(2)-C(8)	24.5(3)
C(1D)-W(1)-C(1C)-O(1C)	-11(15)	Si(1)-C(3)-Si(2)-C(8)	160.1(2)

C(1B)-W(1)-C(1C)-O(1C)	51(18)	P(1)-C(3)-Si(2)-C(9)	141.3(2)
C(1E)-W(1)-C(1C)-O(1C)	166(15)	Si(1)-C(3)-Si(2)-C(9)	-83.0(2)
P(1)-W(1)-C(1C)-O(1C)	-97(15)	P(1)-C(3)-Si(2)-C(7)	-94.3(2)
C(1A)-W(1)-C(1D)-O(1D)	78(23)	Si(1)-C(3)-Si(2)-C(7)	41.3(3)
C(1B)-W(1)-C(1D)-O(1D)	-9(23)	N(1)-C(1)-C(10)-C(11)	175.2(6)
C(1E)-W(1)-C(1D)-O(1D)	20(24)	N(2)-C(1)-C(10)-C(11)	-3.8(7)
C(1C)-W(1)-C(1D)-O(1D)	169(100)	N(1)-C(1)-C(10)-C(11')	-8.3(8)
P(1)-W(1)-C(1D)-O(1D)	-105(23)	N(2)-C(1)-C(10)-C(11')	172.7(7)
C(1A)-W(1)-C(1E)-O(1E)	-33(4)	N(1)-C(1)-C(10)-S(1')	173.4(3)
C(1D)-W(1)-C(1E)-O(1E)	26(5)	N(2)-C(1)-C(10)-S(1')	-5.6(5)
C(1B)-W(1)-C(1E)-O(1E)	55(4)	N(1)-C(1)-C(10)-S(1)	-2.2(5)
C(1C)-W(1)-C(1E)-O(1E)	-124(4)	N(2)-C(1)-C(10)-S(1)	178.7(3)
P(1)-W(1)-C(1E)-O(1E)	150(4)	C(1)-C(10)-C(11)-C(12)	-176.1(6)
C(1A)-W(1)-P(1)-N(1)	-4.5(13)	C(11')-C(10)-C(11)-C(12)	6.8(10)
C(1D)-W(1)-P(1)-N(1)	-44.11(15)	S(1')-C(10)-C(11)-C(12)	-165(4)
C(1B)-W(1)-P(1)-N(1)	-132.43(17)	S(1)-C(10)-C(11)-C(12)	1.6(9)
C(1E)-W(1)-P(1)-N(1)	139.34(15)	C(10)-C(11)-C(12)-C(13)	-1.4(11)
C(1C)-W(1)-P(1)-N(1)	46.76(16)	C(11)-C(12)-C(13)-S(1)	0.6(10)
C(1A)-W(1)-P(1)-C(3)	-133.2(13)	C(11)-C(10)-S(1)-C(13)	-0.9(5)
C(1D)-W(1)-P(1)-C(3)	-172.82(17)	C(1)-C(10)-S(1)-C(13)	177.0(4)
C(1B)-W(1)-P(1)-C(3)	98.86(19)	C(11')-C(10)-S(1)-C(13)	-35(3)
C(1E)-W(1)-P(1)-C(3)	10.64(17)	S(1')-C(10)-S(1)-C(13)	1.2(4)
C(1C)-W(1)-P(1)-C(3)	-81.95(17)	C(12)-C(13)-S(1)-C(10)	0.2(7)
C(1A)-W(1)-P(1)-C(2)	91.2(13)	C(11)-C(10)-C(11')-C(12')	-3.7(12)
C(1D)-W(1)-P(1)-C(2)	51.58(15)	C(1)-C(10)-C(11')-C(12')	179.1(8)
C(1B)-W(1)-P(1)-C(2)	-36.74(17)	S(1')-C(10)-C(11')-C(12')	-2.5(12)
C(1E)-W(1)-P(1)-C(2)	-124.96(15)	S(1)-C(10)-C(11')-C(12')	144(4)
C(1C)-W(1)-P(1)-C(2)	142.46(15)	C(10)-C(11')-C(12')-C(13')	3.3(15)
C(3)-P(1)-N(1)-C(1)	-121.8(2)	C(11')-C(12')-C(13')-S(1')	-2.8(15)
C(2)-P(1)-N(1)-C(1)	-8.4(3)	C(11)-C(10)-S(1')-C(13')	9(3)
W(1)-P(1)-N(1)-C(1)	98.3(2)	C(1)-C(10)-S(1')-C(13')	179.2(5)
P(1)-N(1)-C(1)-N(2)	6.9(4)	C(11')-C(10)-S(1')-C(13')	0.7(7)
P(1)-N(1)-C(1)-C(10)	-172.1(3)	S(1)-C(10)-S(1')-C(13')	-5.1(5)
N(1)-C(1)-N(2)-C(2)	0.2(4)	C(12')-C(13')-S(1')-C(10)	1.3(10)
C(10)-C(1)-N(2)-C(2)	179.2(3)	N(2)-C(2)-C(14)-C(15)	-178.7(4)
C(1)-N(2)-C(2)-C(14)	178.3(3)	P(1)-C(2)-C(14)-C(15)	7.1(6)
C(1)-N(2)-C(2)-P(1)	-6.6(3)	N(2)-C(2)-C(14)-S(2)	-4.3(5)
N(1)-P(1)-C(2)-N(2)	9.0(3)	P(1)-C(2)-C(14)-S(2)	-178.47(19)
C(3)-P(1)-C(2)-N(2)	117.3(3)	C(2)-C(14)-C(15)-C(16)	175.3(4)
W(1)-P(1)-C(2)-N(2)	-99.4(2)	S(2)-C(14)-C(15)-C(16)	0.5(4)

N(1)-P(1)-C(2)-C(14)	-176.2(3)	C(14)-C(15)-C(16)-C(17)	-0.8(5)
C(3)-P(1)-C(2)-C(14)	-67.9(3)	C(15)-C(16)-C(17)-S(2)	0.7(5)
W(1)-P(1)-C(2)-C(14)	75.4(3)	C(16)-C(17)-S(2)-C(14)	-0.4(3)
N(1)-P(1)-C(3)-Si(2)	69.8(2)	C(15)-C(14)-S(2)-C(17)	-0.1(3)
C(2)-P(1)-C(3)-Si(2)	-27.9(2)	C(2)-C(14)-S(2)-C(17)	-175.4(3)

Table F.35: Hydrogen bonds for str010 [Å and °].

D-H...A	d(D-H)	d(H...A)	d(D...A)	<(DHA)
C(3)-H(3)...O(1E)#1	1.00	2.41	3.407(4)	172.8
C(15)-H(15)...O(1E)#1	0.95	2.59	3.525(5)	167.9

Symmetry transformations used to generate equivalent atoms:

#1 −x+1, −y+1, −z+1

F.7   Data for Complex 126h
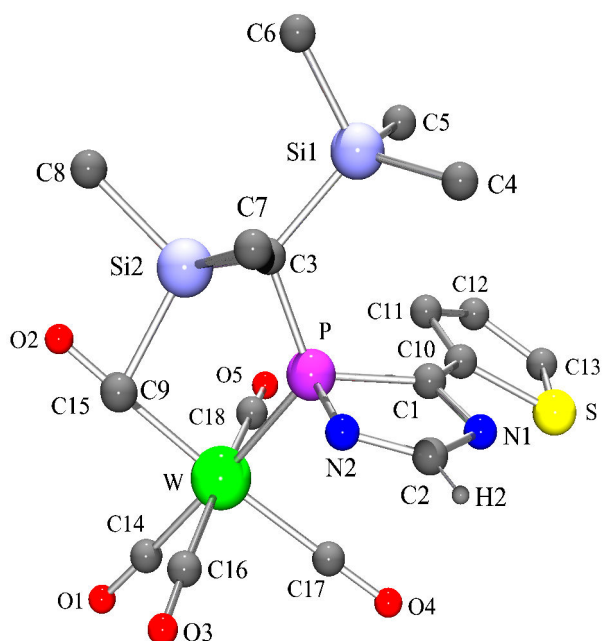
Figure F.8: Molecular structure of complex **126h** (GSTR036) in the crystal (except for H2 all hydrogen atoms are omitted for clarity).

Table F.36: Crystal data and structure refinement for GSTR036.

Identification code	GSTR036
Empirical formula	$C_{18}H_{23}N_2O_5PSSi_2W$
Formula weight	650.44
Temperature	100(2) K
Wavelength	0.71073 Å
Crystal system, space group	Monoclinic, C $2/c$
Unit cell dimensions	a = 27.6553(6) Å, $\alpha = 90º$
	b = 8.3362(2) Å, $\beta = 110.8330(10)º$
	c = 22.5825(5) Å, $\gamma = 90º$
Volume	4865.80(19) Å^3
Z, Calculated density	8, 1.776 Mg/m^3
Absorption coefficient	5.029 mm^{-1}
F(000)	2544
Crystal size	0.33 x 0.17 x 0.09 mm
θ range for data collection	1.58 to 27.49º
Limiting indices	$-35 \leq h \leq 32, -10 \leq k \leq 10, -25 \leq l \leq 29$
Reflections collected / unique	23882 / 5469 [R$_{int}$ = 0.0639]
Completeness to θ = 27.49	98.0 %
Absorption correction	Analytical
Max. and min. transmission	0.6688 and 0.2844
Refinement method	Full-matrix least-squares on F^2
Data / restraints / parameters	5469 / 0 / 330
Goodness-of-fit on F^2	1.034
Final R indices [I>2σ(I)]	R$_1$ = 0.0245, wR$_2$ = 0.0487
R indices (all data)	R$_1$ = 0.0328, wR$_2$ = 0.0556
Largest diff. peak and hole	1.250 and -1.755 e $\cdot$ A^{-3}

Table F.37: Atomic coordinates (x 10^4) and equivalent isotropic displacement parameters ($\mathring{A}^2 \cdot 10^3$) for GSTR036. U(eq) is defined as one third of the trace of the orthogonalized U_{ij} tensor.

	x	y	z	U(eq)
W	8807(1)	2112(1)	5034(1)	12(1)
O(1)	9149(1)	945(3)	6450(1)	28(1)
O(2)	9966(1)	3295(3)	5330(1)	23(1)
O(3)	9017(1)	-1543(3)	4794(1)	23(1)
O(4)	7622(1)	1093(3)	4655(1)	26(1)
O(5)	8530(1)	5432(3)	5539(1)	26(1)
P	8617(1)	2833(1)	3887(1)	12(1)
S	6997(1)	4604(1)	3541(1)	20(1)
N(1)	7655(1)	2372(4)	3161(1)	20(1)
N(2)	8478(1)	1193(3)	3402(1)	16(1)
Si(1)	8823(1)	5379(1)	2938(1)	16(1)
Si(2)	9582(1)	2419(1)	3520(1)	15(1)
C(1)	7926(1)	3488(4)	3543(1)	15(1)
C(2)	7990(1)	1167(4)	3091(2)	20(1)
C(3)	9086(1)	3902(4)	3635(1)	13(1)
C(4)	8345(1)	4421(5)	2225(2)	26(1)
C(5)	8525(2)	7151(4)	3172(2)	23(1)
C(6)	9374(2)	6187(5)	2732(2)	31(1)
C(7)	9376(2)	1702(5)	2682(2)	22(1)
C(8)	10216(1)	3499(5)	3767(2)	22(1)
C(9)	9709(1)	572(5)	4016(2)	19(1)
C(10)	7661(1)	4749(4)	3745(1)	16(1)
C(11)	7852(1)	6078(4)	4104(2)	19(1)
C(12)	7459(2)	6999(4)	4209(2)	24(1)
C(13)	6982(1)	6335(5)	3938(2)	25(1)
C(14)	9011(1)	1399(4)	5935(2)	19(1)
C(15)	9554(1)	2856(4)	5225(2)	17(1)
C(16)	8953(1)	-215(4)	4854(1)	16(1)
C(17)	8045(1)	1461(4)	4798(2)	19(1)
C(18)	8629(1)	4288(4)	5330(2)	17(1)

Table F.38: Bond lengths [$\mathring{A}$] and angles [º] for GSTR036.

W-C(14)	2.000(3)	C(1)-C(10)	1.445(4)
W-C(15)	2.051(4)	C(2)-H(2)	0.94(4)

W-C(16)	2.052(4)	C(3)-H(3)	1.01(4)
W-C(18)	2.053(3)	C(4)-H(4A)	0.9800
W-C(17)	2.055(3)	C(4)-H(4B)	0.9800
W-P	2.5252(8)	C(4)-H(4C)	0.9800
O(1)-C(14)	1.151(4)	C(5)-H(5A)	0.9800
O(2)-C(15)	1.139(4)	C(5)-H(5B)	0.9800
O(3)-C(16)	1.137(4)	C(5)-H(5C)	0.9800
O(4)-C(17)	1.138(4)	C(6)-H(6A)	0.9800
O(5)-C(18)	1.140(4)	C(6)-H(6B)	0.9800
P-N(2)	1.708(3)	C(6)-H(6C)	0.9800
P-C(3)	1.823(3)	C(7)-H(7A)	0.80(4)
P-C(1)	1.869(3)	C(7)-H(7B)	0.98(4)
S-C(13)	1.706(4)	C(7)-H(7C)	1.03(4)
S-C(10)	1.733(3)	C(8)-H(8A)	0.88(4)
N(1)-C(1)	1.309(4)	C(8)-H(8B)	1.02(4)
N(1)-C(2)	1.413(4)	C(8)-H(8C)	0.96(4)
N(2)-C(2)	1.281(4)	C(9)-H(9A)	0.97(4)
Si(1)-C(5)	1.857(3)	C(9)-H(9B)	0.99(4)
Si(1)-C(4)	1.861(3)	C(9)-H(9C)	0.86(4)
Si(1)-C(6)	1.873(4)	C(10)-C(11)	1.363(5)
Si(1)-C(3)	1.926(3)	C(11)-C(12)	1.416(5)
Si(2)-C(9)	1.863(4)	C(11)-H(11)	0.98(3)
Si(2)-C(7)	1.870(4)	C(12)-C(13)	1.359(5)
Si(2)-C(8)	1.870(4)	C(12)-H(12)	0.91(4)
Si(2)-C(3)	1.933(3)	C(13)-H(13)	1.08(4)
C(14)-W-C(15)	88.70(13)	Si(1)-C(4)-H(4C)	109.5
C(14)-W-C(16)	85.19(13)	H(4A)-C(4)-H(4C)	109.5
C(15)-W-C(16)	94.20(13)	H(4B)-C(4)-H(4C)	109.5
C(14)-W-C(18)	86.83(13)	Si(1)-C(5)-H(5A)	109.5
C(15)-W-C(18)	90.30(12)	Si(1)-C(5)-H(5B)	109.5
C(16)-W-C(18)	170.74(12)	H(5A)-C(5)-H(5B)	109.5
C(14)-W-C(17)	94.42(13)	Si(1)-C(5)-H(5C)	109.5
C(15)-W-C(17)	176.61(12)	H(5A)-C(5)-H(5C)	109.5
C(16)-W-C(17)	87.40(13)	H(5B)-C(5)-H(5C)	109.5
C(18)-W-C(17)	88.54(13)	Si(1)-C(6)-H(6A)	109.5
C(14)-W-P	174.41(9)	Si(1)-C(6)-H(6B)	109.5
C(15)-W-P	88.29(9)	H(6A)-C(6)-H(6B)	109.5
C(16)-W-P	90.32(8)	Si(1)-C(6)-H(6C)	109.5
C(18)-W-P	97.90(9)	H(6A)-C(6)-H(6C)	109.5

C(17)-W-P	88.71(9)	H(6B)-C(6)-H(6C)	109.5
N(2)-P-C(3)	102.39(14)	Si(2)-C(7)-H(7A)	111(3)
N(2)-P-C(1)	90.17(14)	Si(2)-C(7)-H(7B)	106(2)
C(3)-P-C(1)	117.55(14)	H(7A)-C(7)-H(7B)	110(4)
N(2)-P-W	112.60(10)	Si(2)-C(7)-H(7C)	108(2)
C(3)-P-W	121.64(10)	H(7A)-C(7)-H(7C)	112(4)
C(1)-P-W	107.77(10)	H(7B)-C(7)-H(7C)	110(3)
C(13)-S-C(10)	91.30(17)	Si(2)-C(8)-H(8A)	106(3)
C(1)-N(1)-C(2)	109.5(3)	Si(2)-C(8)-H(8B)	111(2)
C(2)-N(2)-P	108.6(2)	H(8A)-C(8)-H(8B)	109(3)
C(5)-Si(1)-C(4)	109.74(17)	Si(2)-C(8)-H(8C)	115(2)
C(5)-Si(1)-C(6)	105.53(18)	H(8A)-C(8)-H(8C)	113(3)
C(4)-Si(1)-C(6)	109.18(18)	H(8B)-C(8)-H(8C)	102(3)
C(5)-Si(1)-C(3)	110.69(14)	Si(2)-C(9)-H(9A)	111(3)
C(4)-Si(1)-C(3)	112.28(16)	Si(2)-C(9)-H(9B)	108(2)
C(6)-Si(1)-C(3)	109.19(15)	H(9A)-C(9)-H(9B)	105(3)
C(9)-Si(2)-C(7)	105.62(18)	Si(2)-C(9)-H(9C)	116(3)
C(9)-Si(2)-C(8)	105.20(18)	H(9A)-C(9)-H(9C)	111(3)
C(7)-Si(2)-C(8)	111.83(18)	H(9B)-C(9)-H(9C)	104(3)
C(9)-Si(2)-C(3)	116.03(15)	C(11)-C(10)-C(1)	130.3(3)
C(7)-Si(2)-C(3)	111.42(15)	C(11)-C(10)-S	111.3(2)
C(8)-Si(2)-C(3)	106.66(16)	C(1)-C(10)-S	118.3(2)
N(1)-C(1)-C(10)	119.2(3)	C(10)-C(11)-C(12)	112.5(3)
N(1)-C(1)-P	109.2(2)	C(10)-C(11)-H(11)	123(2)
C(10)-C(1)-P	129.7(2)	C(12)-C(11)-H(11)	124(2)
N(2)-C(2)-N(1)	122.1(3)	C(13)-C(12)-C(11)	112.5(3)
N(2)-C(2)-H(2)	119(2)	C(13)-C(12)-H(12)	125(3)
N(1)-C(2)-H(2)	119(2)	C(11)-C(12)-H(12)	122(3)
P-C(3)-Si(1)	117.59(16)	C(12)-C(13)-S	112.3(3)
P-C(3)-Si(2)	110.33(17)	C(12)-C(13)-H(13)	128(2)
Si(1)-C(3)-Si(2)	112.30(15)	S-C(13)-H(13)	119(2)
P-C(3)-H(3)	107.6(19)	O(1)-C(14)-W	176.5(3)
Si(1)-C(3)-H(3)	103.0(19)	O(2)-C(15)-W	178.8(3)
Si(2)-C(3)-H(3)	104.9(19)	O(3)-C(16)-W	174.0(3)
Si(1)-C(4)-H(4A)	109.5	O(4)-C(17)-W	178.5(3)
Si(1)-C(4)-H(4B)	109.5	O(5)-C(18)-W	174.2(3)
H(4A)-C(4)-H(4B)	109.5		

Table F.39: Anisotropic displacement parameters ($\mathring{A}^2 \cdot 10^3$) for GSTR036. The anisotropic displacement factor exponent takes the form: $-2\pi^2[h^2 a^{*2} U_{11} + ... + 2hka^*b^*U_{12}]$.

	U(11)	U(22)	U(33)	U(23)	U(13)	U(12)
W	11(1)	14(1)	13(1)	0(1)	5(1)	0(1)
O(1)	26(1)	42(2)	17(1)	7(1)	9(1)	5(1)
O(2)	13(1)	26(1)	29(1)	-4(1)	7(1)	-6(1)
O(3)	27(1)	16(1)	26(1)	0(1)	9(1)	2(1)
O(4)	17(1)	25(2)	37(1)	-2(1)	11(1)	-6(1)
O(5)	24(1)	26(1)	30(1)	-10(1)	10(1)	3(1)
P	11(1)	12(1)	13(1)	-2(1)	4(1)	0(1)
S	15(1)	26(1)	21(1)	1(1)	9(1)	6(1)
N(1)	14(2)	23(2)	20(1)	-5(1)	5(1)	1(1)
N(2)	14(1)	16(1)	19(1)	-5(1)	7(1)	-1(1)
Si(1)	19(1)	16(1)	13(1)	2(1)	6(1)	2(1)
Si(2)	12(1)	18(1)	15(1)	0(1)	6(1)	1(1)
C(1)	15(2)	16(2)	13(1)	1(1)	5(1)	2(1)
C(2)	19(2)	19(2)	21(2)	-9(2)	7(1)	-1(2)
C(3)	12(2)	15(2)	12(1)	-1(1)	4(1)	-1(1)
C(4)	31(2)	26(2)	16(2)	-3(2)	2(2)	10(2)
C(5)	31(2)	17(2)	19(2)	2(1)	8(2)	2(2)
C(6)	35(2)	33(2)	32(2)	14(2)	18(2)	2(2)
C(7)	20(2)	29(2)	21(2)	-4(2)	11(2)	2(2)
C(8)	16(2)	27(2)	26(2)	0(2)	10(2)	1(2)
C(9)	16(2)	21(2)	23(2)	1(2)	9(1)	3(2)
C(10)	15(2)	20(2)	15(2)	3(1)	6(1)	4(1)
C(11)	22(2)	19(2)	18(2)	0(1)	8(1)	-1(2)
C(12)	39(2)	15(2)	22(2)	2(2)	16(2)	7(2)
C(13)	31(2)	24(2)	23(2)	8(2)	16(2)	14(2)
C(14)	15(2)	22(2)	23(2)	-2(2)	11(1)	2(2)
C(15)	24(2)	14(2)	14(2)	-1(1)	7(1)	2(2)
C(16)	13(2)	24(2)	12(2)	3(1)	4(1)	0(2)
C(17)	23(2)	14(2)	21(2)	1(1)	11(1)	0(2)
C(18)	12(2)	20(2)	19(2)	-1(1)	6(1)	0(1)

Table F.40: Hydrogen coordinates (x 10^4) and isotropic displacement parameters ($\mathring{A}^2 \cdot$ 10^3) for GSTR036.

	x	y	z	U(eq)
H(4A)	8076	3890	2342	39
H(4B)	8521	3626	2053	39
H(4C)	8187	5243	1904	39
H(5A)	8738	7478	3603	34
H(5B)	8177	6874	3158	34
H(5C)	8503	8036	2878	34
H(6A)	9246	7001	2400	47
H(6B)	9535	5311	2578	47
H(6C)	9631	6670	3109	47
H(2)	7848(15)	300(50)	2819(18)	29(10)
H(3)	9296(13)	4620(40)	3999(16)	18(9)
H(7A)	9093(17)	1330(50)	2571(18)	29(12)
H(7B)	9629(15)	870(50)	2679(17)	27(10)
H(7C)	9400(16)	2650(50)	2400(20)	37(12)
H(8A)	10438(17)	2830(50)	3700(19)	30(11)
H(8B)	10341(14)	3800(50)	4237(19)	31(10)
H(8C)	10207(15)	4520(50)	3568(18)	32(11)
H(9A)	9844(15)	840(50)	4460(20)	39(12)
H(9B)	9992(15)	-30(50)	3943(17)	32(11)
H(9C)	9459(16)	-100(50)	3931(18)	29(11)
H(11)	8220(13)	6330(40)	4280(14)	11(8)
H(12)	7527(16)	7950(50)	4422(19)	29(11)
H(13)	6615(15)	6770(50)	3941(17)	30(10)

Table F.41: Torsion angles [º] for GSTR036.

C(14)-W-P-N(2)	56.0(11)	C(7)-Si(2)-C(3)-P	92.5(2)
C(15)-W-P-N(2)	113.57(13)	C(8)-Si(2)-C(3)-P	-145.19(17)
C(16)-W-P-N(2)	19.37(13)	C(9)-Si(2)-C(3)-Si(1)	-161.68(17)
C(18)-W-P-N(2)	−156.36(13)	C(7)-Si(2)-C(3)-Si(1)	-40.8(2)
C(17)-W-P-N(2)	−68.02(14)	C(8)-Si(2)-C(3)-Si(1)	81.52(19)
C(14)-W-P-C(3)	−65.9(11)	N(1)-C(1)-C(10)-C(11)	-175.7(3)
C(15)-W-P-C(3)	−8.40(15)	P-C(1)-C(10)-C(11)	21.6(5)
C(16)-W-P-C(3)	−102.60(15)	N(1)-C(1)-C(10)-S	7.0(4)
C(18)-W-P-C(3)	81.66(15)	P-C(1)-C(10)-S	-155.7(2)
C(17)-W-P-C(3)	170.01(16)	C(13)-S-C(10)-C(11)	0.3(3)

C(14)-W-P-C(1)	153.9(10)	C(13)-S-C(10)-C(1)	178.1(3)
C(15)-W-P-C(1)	−148.58(15)	C(1)-C(10)-C(11)-C(12)	-178.4(3)
C(16)-W-P-C(1)	117.23(14)	S-C(10)-C(11)-C(12)	-0.9(4)
C(18)-W-P-C(1)	−58.51(14)	C(10)-C(11)-C(12)-C(13)	1.2(4)
C(17)-W-P-C(1)	29.84(15)	C(11)-C(12)-C(13)-S	-1.0(4)
C(3)-P-N(2)-C(2)	−122.5(2)	C(10)-S-C(13)-C(12)	0.4(3)
C(1)-P-N(2)-C(2)	−4.1(2)	C(15)-W-C(14)-O(1)	-52(5)
W-P-N(2)-C(2)	105.2(2)	C(16)-W-C(14)-O(1)	42(5)
C(2)-N(1)-C(1)-C(10)	−172.7(3)	C(18)-W-C(14)-O(1)	-142(5)
C(2)-N(1)-C(1)-P	−6.7(3)	C(17)-W-C(14)-O(1)	129(5)
N(2)-P-C(1)-N(1)	6.6(2)	P-W-C(14)-O(1)	6(6)
C(3)-P-C(1)-N(1)	110.7(2)	C(14)-W-C(15)-O(2)	-108(13)
W-P-C(1)-N(1)	−107.3(2)	C(16)-W-C(15)-O(2)	167(100)
N(2)-P-C(1)-C(10)	170.6(3)	C(18)-W-C(15)-O(2)	-21(13)
C(3)-P-C(1)-C(10)	−85.3(3)	C(17)-W-C(15)-O(2)	49(14)
W-P-C(1)-C(10)	56.8(3)	P-W-C(15)-O(2)	77(13)
P-N(2)-C(2)-N(1)	1.2(4)	C(14)-W-C(16)-O(3)	35(3)
C(1)-N(1)-C(2)-N(2)	4.1(5)	C(15)-W-C(16)-O(3)	123(3)
N(2)-P-C(3)-Si(1)	87.01(19)	C(18)-W-C(16)-O(3)	4(3)
C(1)-P-C(3)-Si(1)	−9.8(2)	C(17)-W-C(16)-O(3)	-60(3)
W-P-C(3)-Si(1)	−146.30(11)	P-W-C(16)-O(3)	-148(3)
N(2)-P-C(3)-Si(2)	−43.54(17)	C(14)-W-C(17)-O(4)	-148(12)
C(1)-P-C(3)-Si(2)	−140.32(15)	C(15)-W-C(17)-O(4)	55(13)
W-P-C(3)-Si(2)	83.15(16)	C(16)-W-C(17)-O(4)	-63(12)
C(5)-Si(1)-C(3)-P	68.8(2)	C(18)-W-C(17)-O(4)	125(12)
C(4)-Si(1)-C(3)-P	−54.2(2)	P-W-C(17)-O(4)	27(12)
C(6)-Si(1)-C(3)-P	−175.45(19)	C(14)-W-C(18)-O(5)	-17(3)
C(5)-Si(1)-C(3)-Si(2)	−161.57(17)	C(15)-W-C(18)-O(5)	-106(3)
C(4)-Si(1)-C(3)-Si(2)	75.4(2)	C(16)-W-C(18)-O(5)	13(3)
C(6)-Si(1)-C(3)-Si(2)	−45.8(2)	C(17)-W-C(18)-O(5)	77(3)
C(9)-Si(2)-C(3)-P	−28.4(2)	P-W-C(18)-O(5)	166(3)

F.8 Data for Complex 190
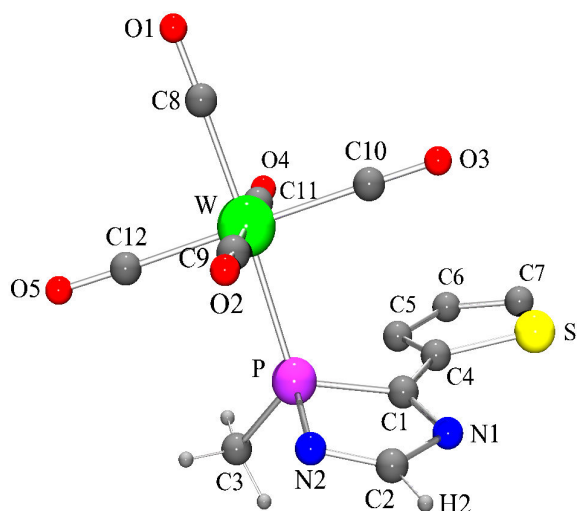
Figure F.9: Molecular structure of complex **190** (GSTR040) in the crystal (major conformation, 81 %; hydrogen atoms of the 2-thienyl moiety are omitted for clarity).
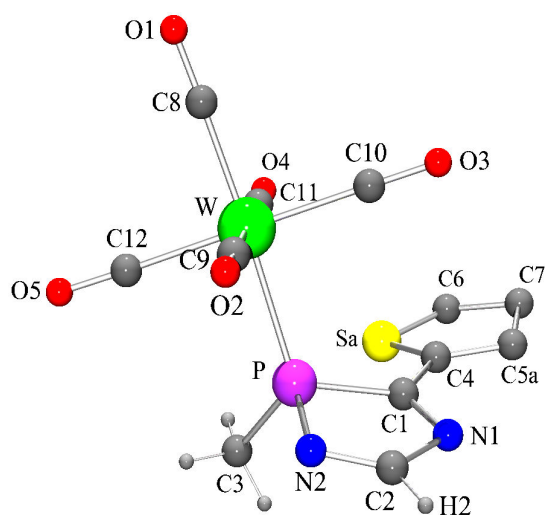
Figure F.10: Molecular structure of complex **190** (GSTR040) in the crystal (minor conformation, 19 %; hydrogen atoms of the 2-thienyl moiety are omitted for clarity).

Table F.42: Crystal data and structure refinement for GSTR040.

Identification code	GSTR040
Empirical formula	$C_{12}H_7N_2O_5PSW$
Formula weight	506.08
Temperature	100(2) K
Wavelength	0.71073 Å
Crystal system, space group	Triclinic, $P\bar{1}$
Unit cell dimensions	a = 6.7855(2) Å, $\quad \alpha = 95.964(2)$º
	b = 10.4987(4) Å, $\quad \beta = 100.540(2)$º
	c = 11.5844(4) Å, $\quad \gamma = 107.410(2)$º
Volume	763.02(5) Å^3
Z, Calculated density	2, 2.203 Mg/m^3
Absorption coefficient	7.834 mm^{-1}
F(000)	476
Crystal size	0.43 x 0.17 x 0.04 mm
θ range for data collection	2.97 to 25.50º
Limiting indices	$-8 \leq h \leq 8$, $-12 \leq k \leq 12$, $-14 \leq l \leq 14$
Reflections collected / unique	14278 / 2824 [$R_{int} = 0.0522$]
Completeness to $\theta = 25.50$	99.6 %
Absorption correction	Analytical
Max. and min. transmission	0.7244 and 0.1336
Refinement method	Full-matrix least-squares on F^2
Data / restraints / parameters	2824 / 0 / 224
Goodness-of-fit on F^2	1.016
Final R indices [I$>2\sigma$(I)]	$R_1 = 0.0209$, $wR_2 = 0.0422$
R indices (all data)	$R_1 = 0.0236$, $wR_2 = 0.0429$
Largest diff. peak and hole	0.753 and -1.858 e · A^{-3}

Table F.43: Atomic coordinates (x 10^4) and equivalent isotropic displacement parameters ($\text{\AA}^2 \cdot 10^3$) for GSTR040. U(eq) is defined as one third of the trace of the orthogonalized U_{ij} tensor.

	x	y	z	U(eq)
W	7029(1)	8407(1)	6869(1)	11(1)
P	6701(2)	7543(1)	8758(1)	14(1)
C(1)	5853(6)	5681(4)	8637(3)	15(1)
C(2)	9124(6)	6511(4)	9773(3)	21(1)
C(3)	5203(7)	8145(5)	9707(4)	23(1)
C(4)	3877(6)	4745(4)	7948(3)	16(1)
C(6)	292(7)	3787(4)	6979(4)	26(1)
C(5)	1960(13)	4961(8)	7628(7)	26(1)
C(7)	1049(7)	2740(5)	6804(4)	27(1)
C(5A)	3430(60)	3410(30)	7580(30)	27(1)
S	3651(3)	3112(2)	7403(1)	20(1)
SA	1656(14)	5164(8)	7687(8)	20(1)
C(8)	7282(6)	9191(4)	5373(3)	15(1)
C(9)	10252(6)	9137(4)	7510(3)	15(1)
C(10)	7237(6)	6606(4)	6113(3)	17(1)
C(11)	3815(6)	7683(4)	6229(3)	16(1)
C(12)	6828(6)	10204(4)	7633(3)	15(1)
N(1)	7417(5)	5316(3)	9173(3)	18(1)
N(2)	9045(5)	7704(3)	9712(3)	21(1)
O(1)	7385(5)	9654(3)	4526(2)	26(1)
O(2)	12034(4)	9545(3)	7880(2)	22(1)
O(3)	7318(4)	5597(3)	5695(2)	25(1)
O(4)	2025(4)	7286(3)	5845(2)	24(1)
O(5)	6755(4)	11217(3)	8041(2)	22(1)

Table F.44: Bond lengths [$\text{\AA}$] and angles [$^{\text{o}}$] for GSTR040.

W-C(8)	2.007(4)	C(3)-H(3C)	0.97(4)
W-C(11)	2.045(4)	C(4)-C(5A)	1.34(3)
W-C(9)	2.051(4)	C(4)-C(5)	1.378(9)
W-C(12)	2.052(4)	C(4)-SA	1.678(8)
W-C(10)	2.055(4)	C(4)-S	1.716(4)
W-P	2.4763(9)	C(6)-C(5)	1.424(9)
P-N(2)	1.713(3)	C(6)-H(6)	0.98(5)
P-C(3)	1.813(4)	C(5)-H(5)	0.9500

P-C(1)	1.848(4)	C(7)-C(5A)	1.60(4)
C(1)-N(1)	1.308(4)	C(7)-H(7)	0.91(6)
C(1)-C(4)	1.434(5)	C(5A)-H(5A)	0.9500
C(2)-N(2)	1.278(5)	C(8)-O(1)	1.144(4)
C(2)-N(1)	1.433(5)	C(9)-O(2)	1.136(4)
C(2)-H(2)	0.96(4)	C(10)-O(3)	1.139(5)
C(3)-H(3A)	0.97(5)	C(11)-O(4)	1.144(5)
C(3)-H(3B)	0.96(5)	C(12)-O(5)	1.137(4)
C(8)-W-C(11)	88.30(14)	H(3A)-C(3)-H(3B)	111(4)
C(8)-W-C(9)	91.59(14)	P-C(3)-H(3C)	113(2)
C(11)-W-C(9)	179.87(14)	H(3A)-C(3)-H(3C)	112(4)
C(8)-W-C(12)	88.25(14)	H(3B)-C(3)-H(3C)	109(4)
C(11)-W-C(12)	90.57(14)	C(5A)-C(4)-C(5)	104.1(16)
C(9)-W-C(12)	89.35(14)	C(5A)-C(4)-C(1)	127.2(16)
C(8)-W-C(10)	92.03(14)	C(5)-C(4)-C(1)	128.3(5)
C(11)-W-C(10)	89.56(14)	C(5A)-C(4)-SA	110.1(17)
C(9)-W-C(10)	90.52(14)	C(5)-C(4)-SA	6.6(6)
C(12)-W-C(10)	179.70(13)	C(1)-C(4)-SA	122.0(4)
C(8)-W-P	177.24(10)	C(5A)-C(4)-S	8.9(16)
C(11)-W-P	91.65(10)	C(5)-C(4)-S	110.4(4)
C(9)-W-P	88.45(10)	C(1)-C(4)-S	121.3(3)
C(12)-W-P	89.00(10)	SA-C(4)-S	116.7(4)
C(10)-W-P	90.73(10)	C(5)-C(6)-H(6)	126(3)
N(2)-P-C(3)	103.99(18)	C(4)-C(5)-C(6)	113.5(6)
N(2)-P-C(1)	91.04(16)	C(4)-C(5)-H(5)	123.2
C(3)-P-C(1)	106.8(2)	C(6)-C(5)-H(5)	123.2
N(2)-P-W	115.50(12)	C(5A)-C(7)-H(7)	133(4)
C(3)-P-W	119.86(14)	C(4)-C(5A)-C(7)	111(2)
C(1)-P-W	115.39(11)	C(4)-C(5A)-H(5A)	124.3
N(1)-C(1)-C(4)	123.9(3)	C(7)-C(5A)-H(5A)	124.3
N(1)-C(1)-P	109.8(3)	O(1)-C(8)-W	178.1(3)
C(4)-C(1)-P	126.0(3)	O(2)-C(9)-W	179.0(3)
N(2)-C(2)-N(1)	122.6(3)	O(3)-C(10)-W	178.9(3)
N(2)-C(2)-H(2)	129(2)	O(4)-C(11)-W	178.4(3)
N(1)-C(2)-H(2)	109(2)	O(5)-C(12)-W	178.2(3)
P-C(3)-H(3A)	102(3)	C(1)-N(1)-C(2)	108.5(3)
P-C(3)-H(3B)	109(3)	C(2)-N(2)-P	107.4(3)

Table F.45: Anisotropic displacement parameters ($\mathring{A}^2 \cdot 10^3$) for GSTR040. The anisotropic displacement factor exponent takes the form: $-2\pi^2[h^2a^{*2}U_{11} + ... + 2hka^*b^*U_{12}]$.

	U(11)	U(22)	U(33)	U(23)	U(13)	U(12)
W	10(1)	12(1)	12(1)	0(1)	-1(1)	4(1)
P	15(1)	14(1)	12(1)	1(1)	-1(1)	6(1)
C(1)	19(2)	19(2)	11(2)	5(2)	4(2)	9(2)
C(2)	15(2)	27(2)	18(2)	6(2)	-2(2)	8(2)
C(3)	32(3)	26(3)	15(2)	1(2)	4(2)	16(2)
C(4)	19(2)	20(2)	12(2)	5(2)	4(2)	8(2)
C(6)	25(2)	26(2)	25(2)	5(2)	2(2)	9(2)
C(5)	25(2)	26(2)	25(2)	5(2)	2(2)	9(2)
C(7)	27(2)	21(2)	26(2)	0(2)	0(2)	2(2)
C(5A)	27(2)	21(2)	26(2)	0(2)	0(2)	2(2)
S	22(1)	13(1)	22(1)	0(1)	-2(1)	6(1)
SA	22(1)	13(1)	22(1)	0(1)	-2(1)	6(1)
C(8)	15(2)	10(2)	18(2)	-3(2)	0(2)	5(2)
C(9)	21(2)	15(2)	12(2)	1(2)	3(2)	10(2)
C(10)	12(2)	22(2)	17(2)	5(2)	-1(2)	5(2)
C(11)	25(2)	13(2)	11(2)	0(2)	1(2)	9(2)
C(12)	8(2)	21(2)	16(2)	5(2)	1(2)	5(2)
N(1)	18(2)	18(2)	20(2)	5(1)	1(1)	9(2)
N(2)	18(2)	23(2)	16(2)	3(1)	-5(1)	5(2)
O(1)	32(2)	24(2)	21(2)	7(1)	6(1)	8(1)
O(2)	10(2)	29(2)	22(1)	-1(1)	-1(1)	3(1)
O(3)	23(2)	17(2)	33(2)	-5(1)	4(1)	8(1)
O(4)	12(2)	27(2)	28(2)	-2(1)	-4(1)	4(1)
O(5)	20(2)	16(2)	28(2)	-4(1)	5(1)	7(1)

Table F.46: Hydrogen coordinates (x 10^4) and isotropic displacement parameters ($\mathring{A}^2 \cdot 10^3$) for GSTR040.

	x	y	z	U(eq)
H(5)	1770	5812	7821	31
H(5A)	4391	2928	7767	32
H(2)	10230(60)	6240(40)	10220(30)	15(10)
H(3A)	6080(70)	9080(50)	9980(40)	30(12)
H(3B)	3840(80)	8080(50)	9240(40)	46(14)
H(3C)	5010(70)	7650(40)	10360(40)	32(12)

H(6)	-1180(80)	3730(50)	6690(40)	46(14)
H(7)	280(90)	1890(60)	6430(50)	56(16)

Table F.47: Torsion angles [º] for GSTR040.

C(8)-W-P-N(2)	-97(2)	SA-C(4)-C(5A)-C(7)	11(3)
C(11)-W-P-N(2)	174.03(16)	S-C(4)-C(5A)-C(7)	-128(12)
C(9)-W-P-N(2)	-6.05(16)	C(11)-W-C(8)-O(1)	52(10)
C(12)-W-P-N(2)	-95.43(16)	C(9)-W-C(8)-O(1)	-128(10)
C(10)-W-P-N(2)	84.44(16)	C(12)-W-C(8)-O(1)	-39(10)
C(8)-W-P-C(3)	29(2)	C(10)-W-C(8)-O(1)	142(10)
C(11)-W-P-C(3)	-60.3(2)	P-W-C(8)-O(1)	-37(12)
C(9)-W-P-C(3)	119.6(2)	C(8)-W-C(9)-O(2)	141(19)
C(12)-W-P-C(3)	30.2(2)	C(11)-W-C(9)-O(2)	106(79)
C(10)-W-P-C(3)	-149.9(2)	C(12)-W-C(9)-O(2)	53(19)
C(8)-W-P-C(1)	159(2)	C(10)-W-C(9)-O(2)	-127(19)
C(11)-W-P-C(1)	69.63(16)	P-W-C(9)-O(2)	-36(19)
C(9)-W-P-C(1)	-110.46(16)	C(8)-W-C(10)-O(3)	-113(16)
C(12)-W-P-C(1)	160.17(16)	C(11)-W-C(10)-O(3)	-25(16)
C(10)-W-P-C(1)	-19.96(16)	C(9)-W-C(10)-O(3)	155(16)
N(2)-P-C(1)-N(1)	-7.5(3)	C(12)-W-C(10)-O(3)	92(31)
C(3)-P-C(1)-N(1)	-112.5(3)	P-W-C(10)-O(3)	67(16)
W-P-C(1)-N(1)	111.5(2)	C(8)-W-C(11)-O(4)	12(11)
N(2)-P-C(1)-C(4)	179.2(3)	C(9)-W-C(11)-O(4)	47(84)
C(3)-P-C(1)-C(4)	74.2(4)	C(12)-W-C(11)-O(4)	100(11)
W-P-C(1)-C(4)	-61.8(3)	C(10)-W-C(11)-O(4)	-80(11)
N(1)-C(1)-C(4)-C(5A)	-11(2)	P-W-C(11)-O(4)	-171(11)
P-C(1)-C(4)-C(5A)	161(2)	C(8)-W-C(12)-O(5)	-39(10)
N(1)-C(1)-C(4)-C(5)	160.4(5)	C(11)-W-C(12)-O(5)	-127(10)
P-C(1)-C(4)-C(5)	-27.2(7)	C(9)-W-C(12)-O(5)	52(10)
N(1)-C(1)-C(4)-SA	157.8(5)	C(10)-W-C(12)-O(5)	115(27)
P-C(1)-C(4)-SA	-29.7(6)	P-W-C(12)-O(5)	141(10)
N(1)-C(1)-C(4)-S	-19.4(5)	C(4)-C(1)-N(1)-C(2)	-179.9(3)
P-C(1)-C(4)-S	153.0(2)	P-C(1)-N(1)-C(2)	6.7(4)
C(5A)-C(4)-C(5)-C(6)	-4.3(17)	N(2)-C(2)-N(1)-C(1)	-2.6(5)
C(1)-C(4)-C(5)-C(6)	-177.5(4)	N(1)-C(2)-N(2)-P	-3.3(5)
SA-C(4)-C(5)-C(6)	-159(5)	C(3)-P-N(2)-C(2)	113.3(3)
S-C(4)-C(5)-C(6)	2.3(7)	C(1)-P-N(2)-C(2)	5.7(3)
C(5)-C(4)-C(5A)-C(7)	8(2)	W-P-N(2)-C(2)	-113.2(3)
C(1)-C(4)-C(5A)-C(7)	-178.5(9)		

F.9   Data for Complex 201
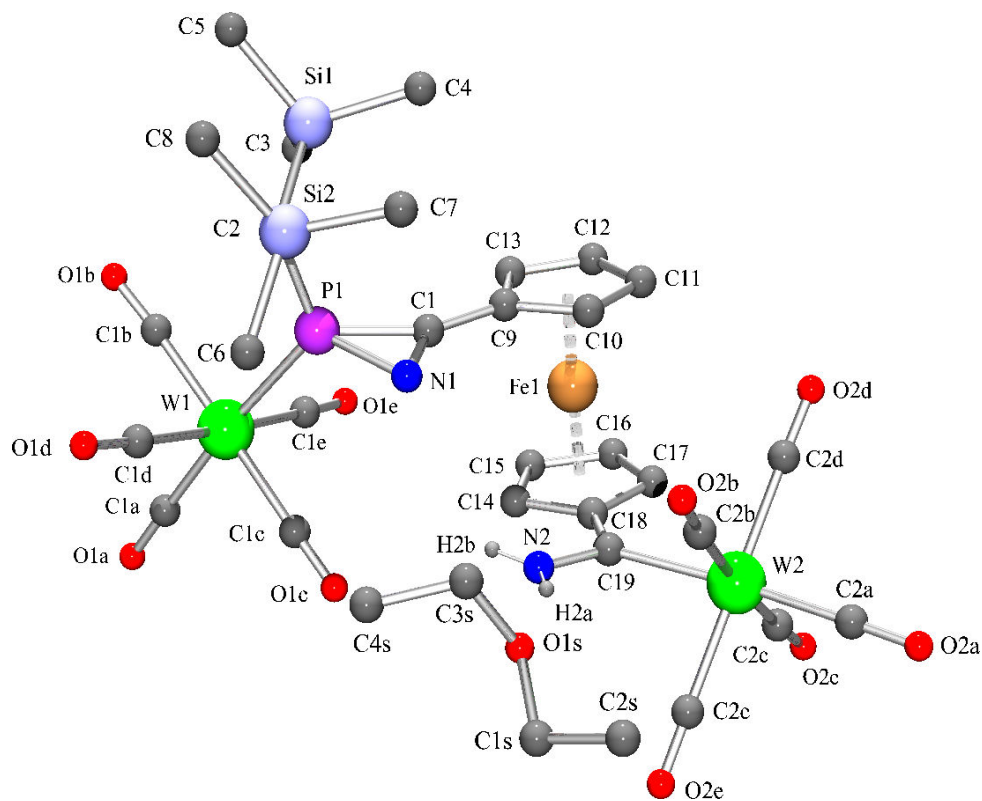
Figure F.11: Molecular structure of complex **201** (str006) in the crystal (except for H2a and H2b all hydrogen atoms are omitted for clarity).

Table F.48: Crystal data and structure refinement for str006.

Identification code	str006_m
Empirical formula	$C_{33}H_{39}FeN_2O_{11}PSi_2W_2$
	$C_{29}H_{29}FeN_2O_{10}PSi_2W_2 - Et_2O$
Formula weight	1150.36
Temperature	123(2) K
Wavelength	0.71073 Å
Crystal system, space group	Monoclinic, P $2_1/c$ (No.14)
Unit cell dimensions	a = 9.5311(1) Å, $\alpha = 90°$
	b = 38.0849(4) Å, $\beta = 112.270(1)°$
	c = 12.3869(1) Å, $\gamma = 90°$
Volume	4160.94(7) Å^3
Z, Calculated density	4, 1.836 Mg/m^3
Absorption coefficient	6.010 mm^{-1}
F(000)	2224
Crystal size	0.25 x 0.20 x 0.10 mm
Diffractometer	Nonius KappaCCD
θ range for data collection	3.15 to 27.48°
Limiting indices	-12 $\leq$ h $\leq$ 12, -49 $\leq$ k $\leq$ 49, -16 $\leq$ l $\leq$ 16
Reflections collected / unique	40069 / 9395 [$R_{int} = 0.0661$]
Completeness to θ = 27.48	98.6 %
Absorption correction	Semi-empirical from equivalents
Max. and min. transmission	0.49299 and 0.35312
Refinement method	Full-matrix least-squares on F^2
Data / restraints / parameters	9395 / 4 / 475
Goodness-of-fit on F^2	1.007
Final R indices [I>2σ(I)]	$R_1 = 0.0338$, $wR_2 = 0.0817$
R indices (all data)	$R_1 = 0.0418$, $wR_2 = 0.0844$
Largest diff. peak and hole	2.537 and -2.304 e $\cdot$ A^{-3}

Table F.49: Atomic coordinates (x 10^4) and equivalent isotropic displacement parameters ($\mathring{A}^2 \cdot 10^3$) for str006. U(eq) is defined as one third of the trace of the orthogonalized U_{ij} tensor.

	x	y	z	U(eq)
W(1)	5369(1)	5291(1)	2813(1)	23(1)
C(1A)	4264(6)	4923(2)	3308(4)	45(1)
O(1A)	3650(6)	4708(1)	3621(4)	83(2)
C(1B)	5855(5)	4937(1)	1772(4)	27(1)
O(1B)	6047(4)	4737(1)	1154(3)	41(1)
C(1C)	4803(5)	5661(1)	3780(4)	33(1)
O(1C)	4509(4)	5868(1)	4309(3)	53(1)
C(1D)	3475(5)	5408(1)	1375(4)	30(1)
O(1D)	2440(4)	5460(1)	556(3)	43(1)
C(1E)	7299(6)	5152(1)	4187(4)	34(1)
O(1E)	8375(4)	5066(1)	4931(3)	53(1)
P(1)	6848(1)	5769(1)	2380(1)	19(1)
N(1)	7000(4)	6191(1)	3065(3)	24(1)
C(1)	8251(4)	6021(1)	3454(3)	20(1)
C(2)	6946(4)	5822(1)	954(3)	20(1)
Si(1)	8846(1)	5680(1)	924(1)	23(1)
C(3)	9457(5)	5267(1)	1793(4)	32(1)
C(4)	10330(5)	6022(1)	1550(4)	32(1)
C(5)	8568(5)	5573(2)	-614(4)	44(1)
Si(2)	6023(1)	6247(1)	193(1)	28(1)
C(6)	4188(5)	6306(1)	387(4)	38(1)
C(7)	7205(6)	6643(1)	758(5)	42(1)
C(8)	5570(7)	6193(2)	-1421(4)	49(1)
C(9)	9770(5)	6082(1)	4280(3)	22(1)
C(10)	10393(5)	6414(1)	4797(3)	26(1)
C(11)	11893(5)	6351(1)	5578(4)	30(1)
C(12)	12218(5)	5989(1)	5561(4)	31(1)
C(13)	10920(5)	5820(1)	4765(3)	26(1)
Fe(1)	10396(1)	6060(1)	6045(1)	19(1)
C(14)	8592(5)	5903(1)	6420(3)	23(1)
C(15)	9835(5)	5676(1)	6976(4)	27(1)
C(16)	11050(5)	5881(1)	7733(3)	27(1)
C(17)	10579(5)	6233(1)	7653(3)	24(1)
C(18)	9024(5)	6256(1)	6833(3)	22(1)
C(19)	8113(4)	6579(1)	6478(3)	23(1)

N(2)	6785(5)	6526(1)	5642(4)	37(1)
W(2)	8736(1)	7106(1)	7283(1)	20(1)
C(2A)	9121(5)	7591(1)	7964(4)	31(1)
O(2A)	9313(4)	7870(1)	8350(3)	49(1)
C(2B)	7843(5)	7330(1)	5651(4)	29(1)
O(2B)	7410(4)	7461(1)	4763(3)	46(1)
C(2C)	9749(5)	6907(1)	8927(4)	30(1)
O(2C)	10353(4)	6813(1)	9851(3)	50(1)
C(2D)	10801(5)	7106(1)	7121(4)	30(1)
O(2D)	11936(4)	7111(1)	7048(3)	47(1)
C(2E)	6684(5)	7098(1)	7475(4)	28(1)
O(2E)	5581(4)	7083(1)	7616(3)	41(1)
C(2S)	3911(6)	7624(1)	5051(5)	47(1)
C(1S)	3403(5)	7251(1)	4837(4)	39(1)
O(1S)	4436(4)	7035(1)	4548(3)	36(1)
C(3S)	4142(6)	7021(2)	3328(4)	47(1)
C(4S)	2879(7)	6772(2)	2697(5)	67(2)

Table F.50: Bond lengths [Å] and angles [º] for str006.

W(1)-C(1A)	1.986(5)	C(13)-Fe(1)	2.051(4)
W(1)-C(1B)	2.035(5)	Fe(1)-C(14)	2.034(4)
W(1)-C(1E)	2.046(5)	Fe(1)-C(17)	2.042(4)
W(1)-C(1D)	2.048(5)	Fe(1)-C(18)	2.046(4)
W(1)-C(1C)	2.050(5)	Fe(1)-C(15)	2.054(4)
W(1)-P(1)	2.4827(11)	Fe(1)-C(16)	2.058(4)
C(1A)-O(1A)	1.154(6)	Fe(1)-Cp(1)	1.655(2)
C(1B)-O(1B)	1.143(5)	Fe(1)-Cp(2)	1.649(2)
C(1C)-O(1C)	1.126(6)	C(14)-C(15)	1.415(6)
C(1D)-O(1D)	1.132(5)	C(14)-C(18)	1.444(6)
C(1E)-O(1E)	1.137(6)	C(15)-C(16)	1.417(6)
P(1)-C(1)	1.769(4)	C(16)-C(17)	1.405(6)
P(1)-N(1)	1.798(4)	C(17)-C(18)	1.448(6)
P(1)-C(2)	1.815(4)	C(18)-C(19)	1.472(6)
N(1)-C(1)	1.280(5)	C(19)-N(2)	1.313(5)
C(1)-C(9)	1.440(6)	C(19)-W(2)	2.223(4)
C(2)-Si(1)	1.905(4)	N(2)-H(2A)	0.883(14)
C(2)-Si(2)	1.910(4)	N(2)-H(2B)	0.884(14)
Si(1)-C(4)	1.863(5)	W(2)-C(2A)	2.005(5)
Si(1)-C(5)	1.866(5)	W(2)-C(2C)	2.041(5)

Si(1)-C(3)	1.870(5)	W(2)-C(2D)	2.052(5)
Si(2)-C(7)	1.853(5)	W(2)-C(2B)	2.057(5)
Si(2)-C(6)	1.868(5)	W(2)-C(2E)	2.057(4)
Si(2)-C(8)	1.889(5)	C(2A)-O(2A)	1.150(5)
C(9)-C(13)	1.436(6)	C(2B)-O(2B)	1.134(5)
C(9)-C(10)	1.440(6)	C(2C)-O(2C)	1.128(5)
C(9)-Fe(1)	2.039(4)	C(2D)-O(2D)	1.120(5)
C(10)-C(11)	1.411(6)	C(2E)-O(2E)	1.131(5)
C(10)-Fe(1)	2.050(4)	C(2S)-C(1S)	1.493(7)
C(11)-C(12)	1.412(7)	C(1S)-O(1S)	1.428(6)
C(11)-Fe(1)	2.055(4)	O(1S)-C(3S)	1.430(6)
C(12)-C(13)	1.413(6)	C(3S)-C(4S)	1.498(8)
C(12)-Fe(1)	2.059(4)		
C(1A)-W(1)-C(1B)	90.2(2)	C(14)-Fe(1)-C(15)	40.50(17)
C(1A)-W(1)-C(1E)	88.6(2)	C(9)-Fe(1)-C(15)	126.77(17)
C(1B)-W(1)-C(1E)	90.42(18)	C(17)-Fe(1)-C(15)	68.07(18)
C(1A)-W(1)-C(1D)	91.5(2)	C(18)-Fe(1)-C(15)	69.05(17)
C(1B)-W(1)-C(1D)	86.02(17)	C(10)-Fe(1)-C(15)	164.78(17)
C(1E)-W(1)-C(1D)	176.44(18)	C(13)-Fe(1)-C(15)	107.94(18)
C(1A)-W(1)-C(1C)	90.9(2)	C(14)-Fe(1)-C(11)	163.88(19)
C(1B)-W(1)-C(1C)	176.88(18)	C(9)-Fe(1)-C(11)	68.17(16)
C(1E)-W(1)-C(1C)	92.52(19)	C(17)-Fe(1)-C(11)	106.79(18)
C(1D)-W(1)-C(1C)	91.04(18)	C(18)-Fe(1)-C(11)	125.14(19)
C(1A)-W(1)-P(1)	174.82(13)	C(10)-Fe(1)-C(11)	40.20(17)
C(1B)-W(1)-P(1)	93.69(13)	C(13)-Fe(1)-C(11)	67.90(19)
C(1E)-W(1)-P(1)	87.97(14)	C(15)-Fe(1)-C(11)	153.83(18)
C(1D)-W(1)-P(1)	92.19(13)	C(14)-Fe(1)-C(16)	68.14(17)
C(1C)-W(1)-P(1)	85.37(13)	C(9)-Fe(1)-C(16)	162.94(18)
O(1A)-C(1A)-W(1)	178.4(5)	C(17)-Fe(1)-C(16)	40.09(17)
O(1B)-C(1B)-W(1)	176.4(4)	C(18)-Fe(1)-C(16)	68.82(17)
O(1C)-C(1C)-W(1)	178.8(4)	C(10)-Fe(1)-C(16)	153.74(18)
O(1D)-C(1D)-W(1)	176.9(4)	C(13)-Fe(1)-C(16)	124.68(18)
O(1E)-C(1E)-W(1)	177.8(4)	C(15)-Fe(1)-C(16)	40.30(17)
C(1)-P(1)-N(1)	42.05(17)	C(11)-Fe(1)-C(16)	119.25(17)
C(1)-P(1)-C(2)	111.63(18)	C(14)-Fe(1)-C(12)	155.14(19)
N(1)-P(1)-C(2)	109.58(18)	C(9)-Fe(1)-C(12)	68.22(17)
C(1)-P(1)-W(1)	124.34(13)	C(17)-Fe(1)-C(12)	123.83(17)
N(1)-P(1)-W(1)	120.29(12)	C(18)-Fe(1)-C(12)	161.61(18)
C(2)-P(1)-W(1)	122.34(14)	C(10)-Fe(1)-C(12)	68.07(19)

C(1)-N(1)-P(1)	67.8(2)	C(13)-Fe(1)-C(12)	40.21(17)
N(1)-C(1)-C(9)	136.7(4)	C(15)-Fe(1)-C(12)	119.88(19)
N(1)-C(1)-P(1)	70.2(2)	C(11)-Fe(1)-C(12)	40.16(19)
C(9)-C(1)-P(1)	153.1(3)	C(16)-Fe(1)-C(12)	106.75(18)
P(1)-C(2)-Si(1)	112.8(2)	Cp(1)-Fe(1)-Cp(2)	178.0(2)
P(1)-C(2)-Si(2)	113.0(2)	C(15)-C(14)-C(18)	108.8(4)
Si(1)-C(2)-Si(2)	119.7(2)	C(15)-C(14)-Fe(1)	70.5(2)
C(4)-Si(1)-C(5)	111.7(2)	C(18)-C(14)-Fe(1)	69.7(2)
C(4)-Si(1)-C(3)	109.1(2)	C(14)-C(15)-C(16)	108.1(4)
C(5)-Si(1)-C(3)	107.3(2)	C(14)-C(15)-Fe(1)	69.0(2)
C(4)-Si(1)-C(2)	111.7(2)	C(16)-C(15)-Fe(1)	70.0(3)
C(5)-Si(1)-C(2)	108.3(2)	C(17)-C(16)-C(15)	108.7(4)
C(3)-Si(1)-C(2)	108.65(19)	C(17)-C(16)-Fe(1)	69.4(2)
C(7)-Si(2)-C(6)	108.5(2)	C(15)-C(16)-Fe(1)	69.7(2)
C(7)-Si(2)-C(8)	110.5(3)	C(16)-C(17)-C(18)	108.7(4)
C(6)-Si(2)-C(8)	107.5(2)	C(16)-C(17)-Fe(1)	70.6(2)
C(7)-Si(2)-C(2)	113.7(2)	C(18)-C(17)-Fe(1)	69.4(2)
C(6)-Si(2)-C(2)	108.5(2)	C(14)-C(18)-C(17)	105.8(4)
C(8)-Si(2)-C(2)	108.0(2)	C(14)-C(18)-C(19)	128.0(4)
C(13)-C(9)-C(1)	126.0(4)	C(17)-C(18)-C(19)	126.2(4)
C(13)-C(9)-C(10)	107.7(4)	C(14)-C(18)-Fe(1)	68.8(2)
C(1)-C(9)-C(10)	126.3(4)	C(17)-C(18)-Fe(1)	69.1(2)
C(13)-C(9)-Fe(1)	69.9(2)	C(19)-C(18)-Fe(1)	125.0(3)
C(1)-C(9)-Fe(1)	124.2(3)	N(2)-C(19)-C(18)	113.0(4)
C(10)-C(9)-Fe(1)	69.8(2)	N(2)-C(19)-W(2)	120.5(3)
C(11)-C(10)-C(9)	107.2(4)	C(18)-C(19)-W(2)	126.4(3)
C(11)-C(10)-Fe(1)	70.1(2)	C(19)-N(2)-H(2A)	114(3)
C(9)-C(10)-Fe(1)	69.0(2)	C(19)-N(2)-H(2B)	114(3)
C(10)-C(11)-C(12)	109.1(4)	H(2A)-N(2)-H(2B)	131(5)
C(10)-C(11)-Fe(1)	69.7(2)	C(2A)-W(2)-C(2C)	88.91(19)
C(12)-C(11)-Fe(1)	70.1(3)	C(2A)-W(2)-C(2D)	90.68(18)
C(11)-C(12)-C(13)	108.5(4)	C(2C)-W(2)-C(2D)	89.35(18)
C(11)-C(12)-Fe(1)	69.7(3)	C(2A)-W(2)-C(2B)	88.53(19)
C(13)-C(12)-Fe(1)	69.6(2)	C(2C)-W(2)-C(2B)	176.03(18)
C(12)-C(13)-C(9)	107.6(4)	C(2D)-W(2)-C(2B)	87.65(18)
C(12)-C(13)-Fe(1)	70.2(2)	C(2A)-W(2)-C(2E)	89.84(18)
C(9)-C(13)-Fe(1)	69.0(2)	C(2C)-W(2)-C(2E)	89.43(18)
C(14)-Fe(1)-C(9)	109.13(16)	C(2D)-W(2)-C(2E)	178.67(19)
C(14)-Fe(1)-C(17)	68.90(17)	C(2B)-W(2)-C(2E)	93.59(17)
C(9)-Fe(1)-C(17)	156.25(17)	C(2A)-W(2)-C(19)	175.44(17)

C(14)-Fe(1)-C(18)	41.45(17)	C(2C)-W(2)-C(19)	93.23(17)
C(9)-Fe(1)-C(18)	121.11(16)	C(2D)-W(2)-C(19)	93.37(16)
C(17)-Fe(1)-C(18)	41.48(16)	C(2B)-W(2)-C(19)	89.54(17)
C(14)-Fe(1)-C(10)	127.34(17)	C(2E)-W(2)-C(19)	86.16(16)
C(9)-Fe(1)-C(10)	41.25(16)	O(2A)-C(2A)-W(2)	178.7(4)
C(17)-Fe(1)-C(10)	119.90(18)	O(2B)-C(2B)-W(2)	176.9(4)
C(18)-Fe(1)-C(10)	107.55(17)	O(2C)-C(2C)-W(2)	176.4(4)
C(14)-Fe(1)-C(13)	121.31(18)	O(2D)-C(2D)-W(2)	178.8(5)
C(9)-Fe(1)-C(13)	41.11(16)	O(2E)-C(2E)-W(2)	177.2(4)
C(17)-Fe(1)-C(13)	160.55(17)	O(1S)-C(1S)-C(2S)	112.7(4)
C(18)-Fe(1)-C(13)	156.78(16)	C(1S)-O(1S)-C(3S)	114.1(4)
C(10)-Fe(1)-C(13)	68.98(18)	O(1S)-C(3S)-C(4S)	111.8(5)

Table F.51: Torsion angles [º] for str006.

C(1B)-W(1)-C(1A)-O(1A)	105(21)	C(11)-C(12)-Fe(1)-C(9)	81.5(3)
C(1E)-W(1)-C(1A)-O(1A)	14(21)	C(13)-C(12)-Fe(1)-C(9)	-38.4(3)
C(1D)-W(1)-C(1A)-O(1A)	-169(100)	C(11)-C(12)-Fe(1)-C(17)	-75.2(3)
C(1C)-W(1)-C(1A)-O(1A)	-78(21)	C(13)-C(12)-Fe(1)-C(17)	164.9(3)
P(1)-W(1)-C(1A)-O(1A)	-34(23)	C(11)-C(12)-Fe(1)-C(18)	-42.7(7)
C(1A)-W(1)-C(1B)-O(1B)	64(6)	C(13)-C(12)-Fe(1)-C(18)	-162.6(5)
C(1E)-W(1)-C(1B)-O(1B)	152(6)	C(11)-C(12)-Fe(1)-C(10)	36.9(2)
C(1D)-W(1)-C(1B)-O(1B)	-28(6)	C(13)-C(12)-Fe(1)-C(10)	-83.0(3)
C(1C)-W(1)-C(1B)-O(1B)	-47(8)	C(11)-C(12)-Fe(1)-C(13)	119.9(4)
P(1)-W(1)-C(1B)-O(1B)	-120(6)	C(11)-C(12)-Fe(1)-C(15)	-157.6(2)
C(1A)-W(1)-C(1C)-O(1C)	168(25)	C(13)-C(12)-Fe(1)-C(15)	82.6(3)
C(1B)-W(1)-C(1C)-O(1C)	-81(25)	C(13)-C(12)-Fe(1)-C(11)	-119.9(4)
C(1E)-W(1)-C(1C)-O(1C)	80(25)	C(11)-C(12)-Fe(1)-C(16)	-115.8(3)
C(1D)-W(1)-C(1C)-O(1C)	-100(25)	C(13)-C(12)-Fe(1)-C(16)	124.4(3)
P(1)-W(1)-C(1C)-O(1C)	-8(25)	C(9)-Fe(1)-C(14)-C(15)	124.7(3)
C(1A)-W(1)-C(1D)-O(1D)	-79(8)	C(17)-Fe(1)-C(14)-C(15)	-80.5(3)
C(1B)-W(1)-C(1D)-O(1D)	11(8)	C(18)-Fe(1)-C(14)-C(15)	-119.6(3)
C(1E)-W(1)-C(1D)-O(1D)	12(10)	C(10)-Fe(1)-C(14)-C(15)	167.3(3)
C(1C)-W(1)-C(1D)-O(1D)	-170(8)	C(13)-Fe(1)-C(14)-C(15)	81.0(3)
P(1)-W(1)-C(1D)-O(1D)	105(8)	C(11)-Fe(1)-C(14)-C(15)	-157.8(5)
C(1A)-W(1)-C(1E)-O(1E)	78(13)	C(16)-Fe(1)-C(14)-C(15)	-37.3(3)
C(1B)-W(1)-C(1E)-O(1E)	-12(13)	C(12)-Fe(1)-C(14)-C(15)	45.4(5)
C(1D)-W(1)-C(1E)-O(1E)	-13(15)	C(9)-Fe(1)-C(14)-C(18)	-115.7(2)
C(1C)-W(1)-C(1E)-O(1E)	169(100)	C(17)-Fe(1)-C(14)-C(18)	39.1(2)
P(1)-W(1)-C(1E)-O(1E)	-106(13)	C(10)-Fe(1)-C(14)-C(18)	-73.1(3)

C(1A)-W(1)-P(1)-C(1)	10(2)	C(13)-Fe(1)-C(14)-C(18)	-159.4(2)
C(1B)-W(1)-P(1)-C(1)	-128.3(2)	C(15)-Fe(1)-C(14)-C(18)	119.6(3)
C(1E)-W(1)-P(1)-C(1)	-38.0(2)	C(11)-Fe(1)-C(14)-C(18)	-38.2(7)
C(1D)-W(1)-P(1)-C(1)	145.6(2)	C(16)-Fe(1)-C(14)-C(18)	82.3(3)
C(1C)-W(1)-P(1)-C(1)	54.7(2)	C(12)-Fe(1)-C(14)-C(18)	165.0(4)
C(1A)-W(1)-P(1)-N(1)	-40(2)	C(18)-C(14)-C(15)-C(16)	-0.2(5)
C(1B)-W(1)-P(1)-N(1)	-178.29(18)	Fe(1)-C(14)-C(15)-C(16)	59.3(3)
C(1E)-W(1)-P(1)-N(1)	-87.99(19)	C(18)-C(14)-C(15)-Fe(1)	-59.5(3)
C(1D)-W(1)-P(1)-N(1)	95.56(19)	C(9)-Fe(1)-C(15)-C(14)	-75.8(3)
C(1C)-W(1)-P(1)-N(1)	4.70(19)	C(17)-Fe(1)-C(15)-C(14)	82.8(3)
C(1A)-W(1)-P(1)-C(2)	174(2)	C(18)-Fe(1)-C(15)-C(14)	38.0(2)
C(1B)-W(1)-P(1)-C(2)	35.70(19)	C(10)-Fe(1)-C(15)-C(14)	-41.8(8)
C(1E)-W(1)-P(1)-C(2)	126.0(2)	C(13)-Fe(1)-C(15)-C(14)	-117.5(3)
C(1D)-W(1)-P(1)-C(2)	-50.5(2)	C(11)-Fe(1)-C(15)-C(14)	166.2(4)
C(1C)-W(1)-P(1)-C(2)	-141.3(2)	C(16)-Fe(1)-C(15)-C(14)	119.6(4)
C(2)-P(1)-N(1)-C(1)	-100.9(3)	C(12)-Fe(1)-C(15)-C(14)	-159.8(2)
W(1)-P(1)-N(1)-C(1)	109.1(2)	C(14)-Fe(1)-C(15)-C(16)	-119.6(4)
P(1)-N(1)-C(1)-C(9)	178.0(5)	C(9)-Fe(1)-C(15)-C(16)	164.6(3)
C(2)-P(1)-C(1)-N(1)	95.7(3)	C(17)-Fe(1)-C(15)-C(16)	-36.8(3)
W(1)-P(1)-C(1)-N(1)	-98.9(2)	C(18)-Fe(1)-C(15)-C(16)	-81.6(3)
N(1)-P(1)-C(1)-C(9)	-176.9(8)	C(10)-Fe(1)-C(15)-C(16)	-161.4(6)
C(2)-P(1)-C(1)-C(9)	-81.3(7)	C(13)-Fe(1)-C(15)-C(16)	122.9(3)
W(1)-P(1)-C(1)-C(9)	84.2(7)	C(11)-Fe(1)-C(15)-C(16)	46.6(5)
C(1)-P(1)-C(2)-Si(1)	60.2(3)	C(12)-Fe(1)-C(15)-C(16)	80.6(3)
N(1)-P(1)-C(2)-Si(1)	105.2(2)	C(14)-C(15)-C(16)-C(17)	-0.1(5)
W(1)-P(1)-C(2)-Si(1)	-105.61(19)	Fe(1)-C(15)-C(16)-C(17)	58.6(3)
C(1)-P(1)-C(2)-Si(2)	-79.5(2)	C(14)-C(15)-C(16)-Fe(1)	-58.6(3)
N(1)-P(1)-C(2)-Si(2)	-34.5(3)	C(14)-Fe(1)-C(16)-C(17)	-82.8(3)
W(1)-P(1)-C(2)-Si(2)	114.72(18)	C(9)-Fe(1)-C(16)-C(17)	-166.8(5)
P(1)-C(2)-Si(1)-C(4)	-79.3(3)	C(18)-Fe(1)-C(16)-C(17)	-38.1(3)
Si(2)-C(2)-Si(1)-C(4)	57.4(3)	C(10)-Fe(1)-C(16)-C(17)	48.8(5)
P(1)-C(2)-Si(1)-C(5)	157.3(3)	C(13)-Fe(1)-C(16)-C(17)	163.4(3)
Si(2)-C(2)-Si(1)-C(5)	-66.0(3)	C(15)-Fe(1)-C(16)-C(17)	-120.3(4)
P(1)-C(2)-Si(1)-C(3)	41.1(3)	C(11)-Fe(1)-C(16)-C(17)	81.3(3)
Si(2)-C(2)-Si(1)-C(3)	177.8(2)	C(12)-Fe(1)-C(16)-C(17)	123.0(3)
P(1)-C(2)-Si(2)-C(7)	77.2(3)	C(14)-Fe(1)-C(16)-C(15)	37.5(3)
Si(1)-C(2)-Si(2)-C(7)	-59.3(3)	C(9)-Fe(1)-C(16)-C(15)	-46.6(7)
P(1)-C(2)-Si(2)-C(6)	-43.6(3)	C(17)-Fe(1)-C(16)-C(15)	120.3(4)
Si(1)-C(2)-Si(2)-C(6)	179.8(2)	C(18)-Fe(1)-C(16)-C(15)	82.2(3)
P(1)-C(2)-Si(2)-C(8)	-159.8(2)	C(10)-Fe(1)-C(16)-C(15)	169.1(4)

Si(1)-C(2)-Si(2)-C(8)	63.6(3)	C(13)-Fe(1)-C(16)-C(15)	-76.3(3)
N(1)-C(1)-C(9)-C(13)	165.3(5)	C(11)-Fe(1)-C(16)-C(15)	-158.4(3)
P(1)-C(1)-C(9)-C(13)	-18.9(9)	C(12)-Fe(1)-C(16)-C(15)	-116.7(3)
N(1)-C(1)-C(9)-C(10)	-12.5(8)	C(15)-C(16)-C(17)-C(18)	0.3(5)
P(1)-C(1)-C(9)-C(10)	163.3(5)	Fe(1)-C(16)-C(17)-C(18)	59.1(3)
N(1)-C(1)-C(9)-Fe(1)	76.5(6)	C(15)-C(16)-C(17)-Fe(1)	-58.8(3)
P(1)-C(1)-C(9)-Fe(1)	-107.8(6)	C(14)-Fe(1)-C(17)-C(16)	80.7(3)
C(13)-C(9)-C(10)-C(11)	0.0(4)	C(9)-Fe(1)-C(17)-C(16)	170.4(4)
C(1)-C(9)-C(10)-C(11)	178.2(4)	C(18)-Fe(1)-C(17)-C(16)	119.8(4)
Fe(1)-C(9)-C(10)-C(11)	59.9(3)	C(10)-Fe(1)-C(17)-C(16)	-157.4(3)
C(13)-C(9)-C(10)-Fe(1)	-59.9(3)	C(13)-Fe(1)-C(17)-C(16)	-44.7(7)
C(1)-C(9)-C(10)-Fe(1)	118.2(4)	C(15)-Fe(1)-C(17)-C(16)	37.0(3)
C(9)-C(10)-C(11)-C(12)	0.0(5)	C(11)-Fe(1)-C(17)-C(16)	-115.7(3)
Fe(1)-C(10)-C(11)-C(12)	59.2(3)	C(12)-Fe(1)-C(17)-C(16)	-75.1(3)
C(9)-C(10)-C(11)-Fe(1)	-59.2(3)	C(14)-Fe(1)-C(17)-C(18)	-39.1(2)
C(10)-C(11)-C(12)-C(13)	0.0(5)	C(9)-Fe(1)-C(17)-C(18)	50.7(5)
Fe(1)-C(11)-C(12)-C(13)	59.0(3)	C(10)-Fe(1)-C(17)-C(18)	82.8(3)
C(10)-C(11)-C(12)-Fe(1)	-59.0(3)	C(13)-Fe(1)-C(17)-C(18)	-164.5(5)
C(11)-C(12)-C(13)-C(9)	0.1(5)	C(15)-Fe(1)-C(17)-C(18)	-82.7(3)
Fe(1)-C(12)-C(13)-C(9)	59.1(3)	C(11)-Fe(1)-C(17)-C(18)	124.5(3)
C(11)-C(12)-C(13)-Fe(1)	-59.1(3)	C(16)-Fe(1)-C(17)-C(18)	-119.8(4)
C(1)-C(9)-C(13)-C(12)	-178.2(4)	C(12)-Fe(1)-C(17)-C(18)	165.1(3)
C(10)-C(9)-C(13)-C(12)	-0.1(5)	C(15)-C(14)-C(18)-C(17)	0.4(4)
Fe(1)-C(9)-C(13)-C(12)	-59.9(3)	Fe(1)-C(14)-C(18)-C(17)	-59.6(3)
C(1)-C(9)-C(13)-Fe(1)	-118.3(4)	C(15)-C(14)-C(18)-C(19)	178.5(4)
C(10)-C(9)-C(13)-Fe(1)	59.8(3)	Fe(1)-C(14)-C(18)-C(19)	118.5(4)
C(13)-C(9)-Fe(1)-C(14)	-116.0(3)	C(15)-C(14)-C(18)-Fe(1)	59.9(3)
C(1)-C(9)-Fe(1)-C(14)	4.5(4)	C(16)-C(17)-C(18)-C(14)	-0.4(5)
C(10)-C(9)-Fe(1)-C(14)	125.3(3)	Fe(1)-C(17)-C(18)-C(14)	59.4(3)
C(13)-C(9)-Fe(1)-C(17)	163.0(4)	C(16)-C(17)-C(18)-C(19)	-178.6(4)
C(1)-C(9)-Fe(1)-C(17)	-76.4(6)	Fe(1)-C(17)-C(18)-C(19)	-118.8(4)
C(10)-C(9)-Fe(1)-C(17)	44.4(5)	C(16)-C(17)-C(18)-Fe(1)	-59.8(3)
C(13)-C(9)-Fe(1)-C(18)	-160.2(3)	C(9)-Fe(1)-C(18)-C(14)	84.0(3)
C(1)-C(9)-Fe(1)-C(18)	-39.7(4)	C(17)-Fe(1)-C(18)-C(14)	-117.4(3)
C(10)-C(9)-Fe(1)-C(18)	81.1(3)	C(10)-Fe(1)-C(18)-C(14)	127.1(2)
C(13)-C(9)-Fe(1)-C(10)	118.6(4)	C(13)-Fe(1)-C(18)-C(14)	49.6(5)
C(1)-C(9)-Fe(1)-C(10)	-120.8(5)	C(15)-Fe(1)-C(18)-C(14)	-37.2(2)
C(1)-C(9)-Fe(1)-C(13)	120.5(5)	C(11)-Fe(1)-C(18)-C(14)	167.9(2)
C(10)-C(9)-Fe(1)-C(13)	-118.6(4)	C(16)-Fe(1)-C(18)-C(14)	-80.5(3)
C(13)-C(9)-Fe(1)-C(15)	-74.2(3)	C(12)-Fe(1)-C(18)-C(14)	-159.8(5)

C(1)-C(9)-Fe(1)-C(15)	46.3(4)	C(14)-Fe(1)-C(18)-C(17)	117.4(3)
C(10)-C(9)-Fe(1)-C(15)	167.1(3)	C(9)-Fe(1)-C(18)-C(17)	-158.7(2)
C(13)-C(9)-Fe(1)-C(11)	80.9(3)	C(10)-Fe(1)-C(18)-C(17)	-115.6(3)
C(1)-C(9)-Fe(1)-C(11)	-158.5(4)	C(13)-Fe(1)-C(18)-C(17)	167.0(4)
C(10)-C(9)-Fe(1)-C(11)	-37.7(3)	C(15)-Fe(1)-C(18)-C(17)	80.2(3)
C(13)-C(9)-Fe(1)-C(16)	-38.3(7)	C(11)-Fe(1)-C(18)-C(17)	-74.8(3)
C(1)-C(9)-Fe(1)-C(16)	82.2(7)	C(16)-Fe(1)-C(18)-C(17)	36.8(3)
C(10)-C(9)-Fe(1)-C(16)	-157.0(5)	C(12)-Fe(1)-C(18)-C(17)	-42.4(7)
C(13)-C(9)-Fe(1)-C(12)	37.5(3)	C(14)-Fe(1)-C(18)-C(19)	-122.3(4)
C(1)-C(9)-Fe(1)-C(12)	158.1(4)	C(9)-Fe(1)-C(18)-C(19)	-38.4(4)
C(10)-C(9)-Fe(1)-C(12)	-81.1(3)	C(17)-Fe(1)-C(18)-C(19)	120.3(4)
C(11)-C(10)-Fe(1)-C(14)	165.8(3)	C(10)-Fe(1)-C(18)-C(19)	4.8(4)
C(9)-C(10)-Fe(1)-C(14)	-75.8(3)	C(13)-Fe(1)-C(18)-C(19)	-72.7(6)
C(11)-C(10)-Fe(1)-C(9)	-118.4(4)	C(15)-Fe(1)-C(18)-C(19)	-159.5(4)
C(11)-C(10)-Fe(1)-C(17)	80.6(3)	C(11)-Fe(1)-C(18)-C(19)	45.6(4)
C(9)-C(10)-Fe(1)-C(17)	-161.0(2)	C(16)-Fe(1)-C(18)-C(19)	157.1(4)
C(11)-C(10)-Fe(1)-C(18)	124.1(3)	C(12)-Fe(1)-C(18)-C(19)	77.9(7)
C(9)-C(10)-Fe(1)-C(18)	-117.5(3)	C(14)-C(18)-C(19)-N(2)	-3.6(6)
C(11)-C(10)-Fe(1)-C(13)	-80.2(3)	C(17)-C(18)-C(19)-N(2)	174.1(4)
C(9)-C(10)-Fe(1)-C(13)	38.2(2)	Fe(1)-C(18)-C(19)-N(2)	85.6(5)
C(11)-C(10)-Fe(1)-C(15)	-161.3(6)	C(14)-C(18)-C(19)-W(2)	172.6(3)
C(9)-C(10)-Fe(1)-C(15)	-42.9(8)	C(17)-C(18)-C(19)-W(2)	-9.7(6)
C(9)-C(10)-Fe(1)-C(11)	118.4(4)	Fe(1)-C(18)-C(19)-W(2)	-98.1(3)
C(11)-C(10)-Fe(1)-C(16)	46.6(5)	N(2)-C(19)-W(2)-C(2A)	21(2)
C(9)-C(10)-Fe(1)-C(16)	165.0(4)	C(18)-C(19)-W(2)-C(2A)	-155(2)
C(11)-C(10)-Fe(1)-C(12)	-36.9(3)	N(2)-C(19)-W(2)-C(2C)	139.3(4)
C(9)-C(10)-Fe(1)-C(12)	81.5(3)	C(18)-C(19)-W(2)-C(2C)	-36.7(4)
C(12)-C(13)-Fe(1)-C(14)	-157.7(3)	N(2)-C(19)-W(2)-C(2D)	-131.2(4)
C(9)-C(13)-Fe(1)-C(14)	83.5(3)	C(18)-C(19)-W(2)-C(2D)	52.9(4)
C(12)-C(13)-Fe(1)-C(9)	118.8(4)	N(2)-C(19)-W(2)-C(2B)	-43.6(4)
C(12)-C(13)-Fe(1)-C(17)	-40.5(7)	C(18)-C(19)-W(2)-C(2B)	140.5(3)
C(9)-C(13)-Fe(1)-C(17)	-159.3(5)	N(2)-C(19)-W(2)-C(2E)	50.1(4)
C(12)-C(13)-Fe(1)-C(18)	166.1(4)	C(18)-C(19)-W(2)-C(2E)	-125.9(4)
C(9)-C(13)-Fe(1)-C(18)	47.3(6)	C(2C)-W(2)-C(2A)-O(2A)	-108(20)
C(12)-C(13)-Fe(1)-C(10)	80.5(3)	C(2D)-W(2)-C(2A)-O(2A)	163(20)
C(9)-C(13)-Fe(1)-C(10)	-38.3(2)	C(2B)-W(2)-C(2A)-O(2A)	75(20)
C(12)-C(13)-Fe(1)-C(15)	-115.3(3)	C(2E)-W(2)-C(2A)-O(2A)	-19(20)
C(9)-C(13)-Fe(1)-C(15)	125.9(3)	C(19)-W(2)-C(2A)-O(2A)	10(21)
C(12)-C(13)-Fe(1)-C(11)	37.1(3)	C(2A)-W(2)-C(2B)-O(2B)	54(8)
C(9)-C(13)-Fe(1)-C(11)	-81.7(3)	C(2C)-W(2)-C(2B)-O(2B)	4(10)

C(12)-C(13)-Fe(1)-C(16)	-74.0(3)	C(2D)-W(2)-C(2B)-O(2B)	-37(8)
C(9)-C(13)-Fe(1)-C(16)	167.2(2)	C(2E)-W(2)-C(2B)-O(2B)	144(8)
C(9)-C(13)-Fe(1)-C(12)	-118.8(4)	C(19)-W(2)-C(2B)-O(2B)	-130(8)
C(10)-C(11)-Fe(1)-C(14)	-44.8(7)	C(2A)-W(2)-C(2C)-O(2C)	-28(7)
C(12)-C(11)-Fe(1)-C(14)	-165.1(5)	C(2D)-W(2)-C(2C)-O(2C)	62(7)
C(10)-C(11)-Fe(1)-C(9)	38.7(3)	C(2B)-W(2)-C(2C)-O(2C)	22(9)
C(12)-C(11)-Fe(1)-C(9)	-81.7(3)	C(2E)-W(2)-C(2C)-O(2C)	-118(7)
C(10)-C(11)-Fe(1)-C(17)	-116.7(3)	C(19)-W(2)-C(2C)-O(2C)	156(7)
C(12)-C(11)-Fe(1)-C(17)	123.0(3)	C(2A)-W(2)-C(2D)-O(2D)	24(26)
C(10)-C(11)-Fe(1)-C(18)	-74.8(3)	C(2C)-W(2)-C(2D)-O(2D)	-65(26)
C(12)-C(11)-Fe(1)-C(18)	164.8(2)	C(2B)-W(2)-C(2D)-O(2D)	112(26)
C(12)-C(11)-Fe(1)-C(10)	-120.3(4)	C(2E)-W(2)-C(2D)-O(2D)	-89(29)
C(10)-C(11)-Fe(1)-C(13)	83.2(3)	C(19)-W(2)-C(2D)-O(2D)	-159(26)
C(12)-C(11)-Fe(1)-C(13)	-37.2(2)	C(2A)-W(2)-C(2E)-O(2E)	-107(9)
C(10)-C(11)-Fe(1)-C(15)	169.0(4)	C(2C)-W(2)-C(2E)-O(2E)	-18(9)
C(12)-C(11)-Fe(1)-C(15)	48.7(5)	C(2D)-W(2)-C(2E)-O(2E)	6(15)
C(10)-C(11)-Fe(1)-C(16)	-158.4(3)	C(2B)-W(2)-C(2E)-O(2E)	164(9)
C(12)-C(11)-Fe(1)-C(16)	81.3(3)	C(19)-W(2)-C(2E)-O(2E)	75(9)
C(10)-C(11)-Fe(1)-C(12)	120.3(4)	C(2S)-C(1S)-O(1S)-C(3S)	-89.1(5)
C(11)-C(12)-Fe(1)-C(14)	170.2(3)	C(1S)-O(1S)-C(3S)-C(4S)	-79.8(6)
C(13)-C(12)-Fe(1)-C(14)	50.4(5)		

Table F.52: Hydrogen bonds for str006 [Å and º].

D-H...A	d(D-H)	d(H...A)	d(D...A)	<(DHA)
N(2)-H(2A)...O(1S)	0.883(14)	2.034(19)	2.882(5)	161(4)
N(2)-H(2B)...O(1C)	0.884(14)	2.58(3)	3.315(6)	141(4)
C(14)-H(14)...O(1A)#1	0.95	2.60	3.147(6)	117.3
C(16)-H(16)...O(1B)#2	0.95	2.65	3.495(6)	148.5
C(4)-H(4C)...O(1D)#3	0.98	2.64	3.468(6)	141.9
C(5)-H(5B)...O(1D)#3	0.98	2.61	3.443(6)	142.8
C(13)-H(13)...O(1E)#2	0.95	2.56	3.431(6)	151.9
C(10)-H(10)...O(2A)#4	0.95	2.40	3.211(6)	143.2
C(4S)-H(4S1)...O(2C)#5	0.98	2.66	3.437(7)	136.8
C(1S)-H(1S1)...O(2D)#6	0.99	2.64	3.557(6)	153.2

Symmetry transformations used to generate equivalent atoms:

#1 −x+1, −y+1, −z+1

#2 −x+2, −y+1, −z+1

#3 x+1, y, z

#4 x, −y+3/2, z−1/2

#5 x−1, y, z−1

#6 x−1, y, z

F.10   Data for Complex 205
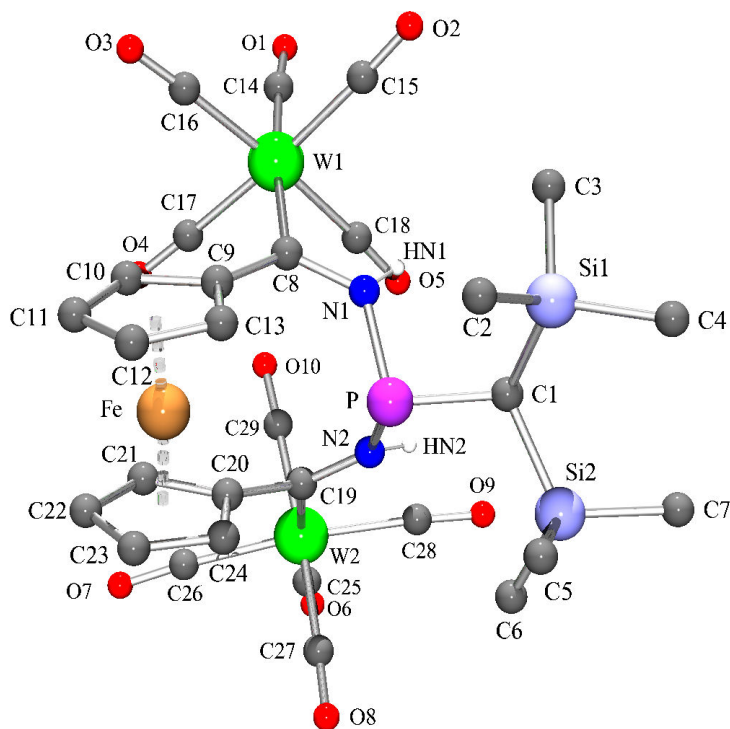
Figure F.12: Molecular structure of complex **205** (GSTR004) in the crystal (except for HN1 and HN2 all hydrogen atoms are omitted for clarity).

Table F.53: Crystal data and structure refinement for GSTR004.

Identification code	GSTR004
Empirical formula	$C_{29}H_{29}FeN_2O_{10}PSi_2W_2$
Formula weight	1076.24
Temperature	123(2) K
Wavelength	0.71073 Å
Crystal system, space group	Monoclinic, P $2_1/n$
Unit cell dimensions	a = 12.6934(2) Å, $\quad \alpha = 90º$
	b = 13.5261(2) Å, $\quad \beta = 98.1493(6)º$
	c = 20.7751(3) Å, $\quad \gamma = 90º$
Volume	3530.90(9) Å^3
Z, Calculated density	4, 2.025 Mg/m^3
Absorption coefficient	7.073 mm^{-1}
F(000)	2056
Crystal size	0.20 x 0.08 x 0.07 mm
θ range for data collection	3.01 to 28.75º
Limiting indices	$-17 \leq h \leq 17, -18 \leq k \leq 18, -28 \leq l \leq 27$
Reflections collected / unique	38919 / 9154 [$R_{int} = 0.0568$]
Completeness to $\theta = 28.75$	99.9 %
Absorption correction	Semi-empirical from equivalents
Max. and min. transmission	0.63328 and 0.46064
Refinement method	Full-matrix least-squares on F^2
Data / restraints / parameters	9154 / 0 / 439
Goodness-of-fit on F^2	0.924
Final R indices [I>2σ(I)]	$R_1 = 0.0241, wR_2 = 0.0446$
R indices (all data)	$R_1 = 0.0372, wR_2 = 0.0465$
Extinction coefficient	0.00016(2)
Largest diff. peak and hole	1.973 and -1.642 e $\cdot$ A^{-3}

Table F.54: Atomic coordinates (x 10^4) and equivalent isotropic displacement parameters ($\mathring{A}^2 \cdot 10^3$) for GSTR004. U(eq) is defined as one third of the trace of the orthogonalized U_{ij} tensor.

	x	y	z	U(eq)
C(1)	10364(2)	7710(2)	4045(1)	15(1)
C(2)	10605(3)	5432(2)	4214(2)	26(1)
C(3)	11421(3)	6810(3)	5343(2)	30(1)
C(4)	12607(3)	6614(3)	4215(2)	30(1)
C(5)	10575(3)	6946(3)	2692(2)	24(1)
C(6)	9786(3)	9047(3)	2809(2)	29(1)
C(7)	12073(3)	8621(3)	3278(2)	27(1)
C(8)	8011(2)	7022(2)	5116(1)	14(1)
C(9)	7272(2)	6321(2)	4757(1)	16(1)
C(10)	6164(2)	6208(2)	4832(1)	19(1)
C(11)	5704(3)	5479(2)	4399(2)	21(1)
C(12)	6508(3)	5107(2)	4053(2)	20(1)
C(13)	7464(3)	5619(2)	4261(2)	18(1)
C(14)	7841(3)	8435(3)	6912(2)	22(1)
C(15)	9276(3)	7103(3)	6467(2)	23(1)
C(16)	7108(3)	6478(3)	6352(2)	29(1)
C(17)	6394(3)	8251(3)	5696(2)	30(1)
C(18)	8498(3)	8956(3)	5724(2)	23(1)
C(19)	7350(2)	8800(2)	3751(1)	17(1)
C(20)	6583(2)	7995(2)	3540(1)	16(1)
C(21)	5524(2)	7908(2)	3701(2)	20(1)
C(22)	4998(3)	7133(2)	3326(2)	22(1)
C(23)	5710(3)	6727(2)	2933(2)	22(1)
C(24)	6689(3)	7246(2)	3067(1)	19(1)
C(25)	6456(3)	11808(3)	3564(2)	34(1)
C(26)	5244(3)	10069(2)	3446(2)	23(1)
C(27)	6929(3)	10160(3)	2696(2)	31(1)
C(28)	8357(3)	10820(3)	3811(2)	47(1)
C(29)	6688(3)	10473(3)	4621(2)	33(1)
Fe	6317(1)	6599(1)	3896(1)	15(1)
N(1)	8871(2)	7262(2)	4823(1)	16(1)
N(2)	8362(2)	8537(2)	3891(1)	16(1)
O(1)	7896(2)	8864(2)	7394(1)	29(1)
O(2)	10044(2)	6755(2)	6714(1)	37(1)
O(3)	6659(2)	5823(2)	6507(1)	47(1)

O(4)	5563(2)	8536(2)	5496(1)	47(1)
O(5)	8816(2)	9663(2)	5519(1)	37(1)
O(6)	6275(2)	12639(2)	3522(2)	56(1)
O(7)	4344(2)	9979(2)	3301(1)	36(1)
O(8)	6959(2)	10013(2)	2157(1)	53(1)
O(9)	9199(2)	11155(2)	3878(2)	90(2)
O(10)	6581(3)	10566(2)	5158(1)	56(1)
P	8976(1)	7347(1)	3985(1)	14(1)
Si(1)	11241(1)	6650(1)	4443(1)	17(1)
Si(2)	10712(1)	8079(1)	3208(1)	17(1)
W(1)	7853(1)	7713(1)	6060(1)	17(1)
W(2)	6842(1)	10360(1)	3662(1)	19(1)

Table F.55: Bond lengths [Å] and angles [º] for GSTR004.

C(1)-P	1.816(3)	C(13)-Fe	2.034(3)
C(1)-Si(2)	1.921(3)	C(13)-H(13A)	0.9500
C(1)-Si(1)	1.929(3)	C(14)-O(1)	1.151(4)
C(1)-H(1)	1.0000	C(14)-W(1)	2.024(3)
C(2)-Si(1)	1.866(3)	C(15)-O(2)	1.137(4)
C(2)-H(2A)	0.9800	C(15)-W(1)	2.055(4)
C(2)-H(2B)	0.9800	C(16)-O(3)	1.125(4)
C(2)-H(2C)	0.9800	C(16)-W(1)	2.053(4)
C(3)-Si(1)	1.864(3)	C(17)-O(4)	1.145(4)
C(3)-H(3A)	0.9800	C(17)-W(1)	2.033(4)
C(3)-H(3B)	0.9800	C(18)-O(5)	1.143(4)
C(3)-H(3C)	0.9800	C(18)-W(1)	2.036(4)
C(4)-Si(1)	1.863(3)	C(19)-N(2)	1.325(4)
C(4)-H(4A)	0.9800	C(19)-C(20)	1.484(4)
C(4)-H(4B)	0.9800	C(19)-W(2)	2.206(3)
C(4)-H(4C)	0.9800	C(20)-C(24)	1.431(4)
C(5)-Si(2)	1.864(3)	C(20)-C(21)	1.435(4)
C(5)-H(5A)	0.9800	C(20)-Fe	2.074(3)
C(5)-H(5B)	0.9800	C(21)-C(22)	1.417(5)
C(5)-H(5C)	0.9800	C(21)-Fe	2.049(3)
C(6)-Si(2)	1.872(3)	C(21)-H(21A)	0.9500
C(6)-H(6A)	0.9800	C(22)-C(23)	1.412(4)
C(6)-H(6B)	0.9800	C(22)-Fe	2.041(3)
C(6)-H(6C)	0.9800	C(22)-H(22A)	0.9500
C(7)-Si(2)	1.863(3)	C(23)-C(24)	1.420(4)

C(7)-H(7A)	0.9800	C(23)-Fe	2.046(3)
C(7)-H(7B)	0.9800	C(23)-H(23A)	0.9500
C(7)-H(7C)	0.9800	C(24)-Fe	2.047(3)
C(8)-N(1)	1.362(4)	C(24)-H(24A)	0.9500
C(8)-C(9)	1.462(4)	C(25)-O(6)	1.149(4)
C(8)-W(1)	2.207(3)	C(25)-W(2)	2.023(4)
C(9)-C(10)	1.445(4)	C(26)-O(7)	1.145(4)
C(9)-C(13)	1.448(4)	C(26)-W(2)	2.052(4)
C(9)-Fe	2.048(3)	C(27)-O(8)	1.143(4)
C(10)-C(11)	1.405(4)	C(27)-W(2)	2.044(4)
C(10)-Fe	2.051(3)	C(28)-O(9)	1.151(4)
C(10)-H(10A)	0.9500	C(28)-W(2)	2.004(4)
C(11)-C(12)	1.421(4)	C(29)-O(10)	1.151(4)
C(11)-Fe	2.054(3)	C(29)-W(2)	2.033(4)
C(11)-H(11A)	0.9500	N(1)-P	1.769(3)
C(12)-C(13)	1.410(4)	N(1)-HN1	0.82(3)
C(12)-Fe	2.053(3)	N(2)-P	1.787(3)
C(12)-H(12A)	0.9500	N(2)-HN2	0.83(3)
P-C(1)-Si(2)	110.65(16)	C(23)-C(24)-C(20)	108.6(3)
P-C(1)-Si(1)	108.89(15)	C(23)-C(24)-Fe	69.65(17)
Si(2)-C(1)-Si(1)	112.85(15)	C(20)-C(24)-Fe	70.68(17)
P-C(1)-H(1)	108.1	C(23)-C(24)-H(24A)	125.7
Si(2)-C(1)-H(1)	108.1	C(20)-C(24)-H(24A)	125.7
Si(1)-C(1)-H(1)	108.1	Fe-C(24)-H(24A)	125.6
Si(1)-C(2)-H(2A)	109.5	O(6)-C(25)-W(2)	177.3(3)
Si(1)-C(2)-H(2B)	109.5	O(7)-C(26)-W(2)	174.5(3)
H(2A)-C(2)-H(2B)	109.5	O(8)-C(27)-W(2)	177.3(3)
Si(1)-C(2)-H(2C)	109.5	O(9)-C(28)-W(2)	174.7(4)
H(2A)-C(2)-H(2C)	109.5	O(10)-C(29)-W(2)	177.7(3)
H(2B)-C(2)-H(2C)	109.5	C(13)-Fe-C(22)	158.71(13)
Si(1)-C(3)-H(3A)	109.5	C(13)-Fe-C(23)	124.71(13)
Si(1)-C(3)-H(3B)	109.5	C(22)-Fe-C(23)	40.42(13)
H(3A)-C(3)-H(3B)	109.5	C(13)-Fe-C(24)	110.72(12)
Si(1)-C(3)-H(3C)	109.5	C(22)-Fe-C(24)	68.18(13)
H(3A)-C(3)-H(3C)	109.5	C(23)-Fe-C(24)	40.61(12)
H(3B)-C(3)-H(3C)	109.5	C(13)-Fe-C(9)	41.53(12)
Si(1)-C(4)-H(4A)	109.5	C(22)-Fe-C(9)	155.10(13)
Si(1)-C(4)-H(4B)	109.5	C(23)-Fe-C(9)	164.40(12)
H(4A)-C(4)-H(4B)	109.5	C(24)-Fe-C(9)	129.38(12)

Si(1)-C(4)-H(4C)	109.5	C(13)-Fe-C(21)	160.45(13)
H(4A)-C(4)-H(4C)	109.5	C(22)-Fe-C(21)	40.52(13)
H(4B)-C(4)-H(4C)	109.5	C(23)-Fe-C(21)	68.14(13)
Si(2)-C(5)-H(5A)	109.5	C(24)-Fe-C(21)	68.24(12)
Si(2)-C(5)-H(5B)	109.5	C(9)-Fe-C(21)	122.98(13)
H(5A)-C(5)-H(5B)	109.5	C(13)-Fe-C(10)	68.74(12)
Si(2)-C(5)-H(5C)	109.5	C(22)-Fe-C(10)	117.51(13)
H(5A)-C(5)-H(5C)	109.5	C(23)-Fe-C(10)	151.13(13)
H(5B)-C(5)-H(5C)	109.5	C(24)-Fe-C(10)	166.56(13)
Si(2)-C(6)-H(6A)	109.5	C(9)-Fe-C(10)	41.28(12)
Si(2)-C(6)-H(6B)	109.5	C(21)-Fe-C(10)	107.50(13)
H(6A)-C(6)-H(6B)	109.5	C(13)-Fe-C(12)	40.36(12)
Si(2)-C(6)-H(6C)	109.5	C(22)-Fe-C(12)	120.60(13)
H(6A)-C(6)-H(6C)	109.5	C(23)-Fe-C(12)	104.94(13)
H(6B)-C(6)-H(6C)	109.5	C(24)-Fe-C(12)	121.19(13)
Si(2)-C(7)-H(7A)	109.5	C(9)-Fe-C(12)	68.85(13)
Si(2)-C(7)-H(7B)	109.5	C(21)-Fe-C(12)	157.65(13)
H(7A)-C(7)-H(7B)	109.5	C(10)-Fe-C(12)	67.72(13)
Si(2)-C(7)-H(7C)	109.5	C(13)-Fe-C(11)	68.45(13)
H(7A)-C(7)-H(7C)	109.5	C(22)-Fe-C(11)	102.57(13)
H(7B)-C(7)-H(7C)	109.5	C(23)-Fe-C(11)	116.24(13)
N(1)-C(8)-C(9)	115.0(3)	C(24)-Fe-C(11)	153.21(13)
N(1)-C(8)-W(1)	118.4(2)	C(9)-Fe-C(11)	68.96(12)
C(9)-C(8)-W(1)	126.5(2)	C(21)-Fe-C(11)	121.82(13)
C(10)-C(9)-C(13)	105.7(3)	C(10)-Fe-C(11)	40.03(12)
C(10)-C(9)-C(8)	125.3(3)	C(12)-Fe-C(11)	40.48(12)
C(13)-C(9)-C(8)	129.0(3)	C(13)-Fe-C(20)	125.60(13)
C(10)-C(9)-Fe	69.45(17)	C(22)-Fe-C(20)	68.42(12)
C(13)-C(9)-Fe	68.72(17)	C(23)-Fe-C(20)	68.42(13)
C(8)-C(9)-Fe	125.7(2)	C(24)-Fe-C(20)	40.64(12)
C(11)-C(10)-C(9)	109.1(3)	C(9)-Fe-C(20)	111.84(12)
C(11)-C(10)-Fe	70.11(17)	C(21)-Fe-C(20)	40.75(12)
C(9)-C(10)-Fe	69.26(16)	C(10)-Fe-C(20)	127.98(13)
C(11)-C(10)-H(10A)	125.4	C(12)-Fe-C(20)	158.48(12)
C(9)-C(10)-H(10A)	125.4	C(11)-Fe-C(20)	161.01(13)
Fe-C(10)-H(10A)	126.8	C(8)-N(1)-P	129.2(2)
C(10)-C(11)-C(12)	108.0(3)	C(8)-N(1)-HN1	109(2)
C(10)-C(11)-Fe	69.86(18)	P-N(1)-HN1	117(2)
C(12)-C(11)-Fe	69.71(18)	C(19)-N(2)-P	131.3(2)
C(10)-C(11)-H(11A)	126.0	C(19)-N(2)-HN2	115(2)

C(12)-C(11)-H(11A)	126.0	P-N(2)-HN2	113(2)
Fe-C(11)-H(11A)	126.0	N(1)-P-N(2)	94.25(13)
C(13)-C(12)-C(11)	108.6(3)	N(1)-P-C(1)	99.04(13)
C(13)-C(12)-Fe	69.12(19)	N(2)-P-C(1)	99.64(14)
C(11)-C(12)-Fe	69.81(18)	C(4)-Si(1)-C(3)	105.79(17)
C(13)-C(12)-H(12A)	125.7	C(4)-Si(1)-C(2)	107.27(16)
C(11)-C(12)-H(12A)	125.7	C(3)-Si(1)-C(2)	110.27(16)
Fe-C(12)-H(12A)	127.0	C(4)-Si(1)-C(1)	114.29(15)
C(12)-C(13)-C(9)	108.4(3)	C(3)-Si(1)-C(1)	108.94(15)
C(12)-C(13)-Fe	70.52(19)	C(2)-Si(1)-C(1)	110.16(15)
C(9)-C(13)-Fe	69.74(17)	C(7)-Si(2)-C(5)	112.26(15)
C(12)-C(13)-H(13A)	125.8	C(7)-Si(2)-C(6)	106.00(17)
C(9)-C(13)-H(13A)	125.8	C(5)-Si(2)-C(6)	108.63(16)
Fe-C(13)-H(13A)	125.5	C(7)-Si(2)-C(1)	111.13(15)
O(1)-C(14)-W(1)	175.9(3)	C(5)-Si(2)-C(1)	107.05(14)
O(2)-C(15)-W(1)	177.2(3)	C(6)-Si(2)-C(1)	111.81(14)
O(3)-C(16)-W(1)	177.0(4)	C(14)-W(1)-C(17)	91.84(13)
O(4)-C(17)-W(1)	178.5(4)	C(14)-W(1)-C(18)	87.39(13)
O(5)-C(18)-W(1)	176.9(3)	C(17)-W(1)-C(18)	88.07(14)
N(2)-C(19)-C(20)	116.3(3)	C(14)-W(1)-C(16)	94.18(13)
N(2)-C(19)-W(2)	122.5(2)	C(17)-W(1)-C(16)	88.15(15)
C(20)-C(19)-W(2)	120.3(2)	C(18)-W(1)-C(16)	175.95(14)
C(24)-C(20)-C(21)	106.5(3)	C(14)-W(1)-C(15)	87.08(13)
C(24)-C(20)-C(19)	126.9(3)	C(17)-W(1)-C(15)	176.01(14)
C(21)-C(20)-C(19)	126.0(3)	C(18)-W(1)-C(15)	95.72(14)
C(24)-C(20)-Fe	68.67(17)	C(16)-W(1)-C(15)	88.09(14)
C(21)-C(20)-Fe	68.70(17)	C(14)-W(1)-C(8)	173.97(12)
C(19)-C(20)-Fe	134.1(2)	C(17)-W(1)-C(8)	90.85(12)
C(22)-C(21)-C(20)	108.5(3)	C(18)-W(1)-C(8)	87.30(12)
C(22)-C(21)-Fe	69.46(19)	C(16)-W(1)-C(8)	91.30(12)
C(20)-C(21)-Fe	70.56(18)	C(15)-W(1)-C(8)	90.60(11)
C(22)-C(21)-H(21A)	125.8	C(28)-W(2)-C(25)	85.87(15)
C(20)-C(21)-H(21A)	125.8	C(28)-W(2)-C(29)	92.81(17)
Fe-C(21)-H(21A)	125.8	C(25)-W(2)-C(29)	88.33(15)
C(23)-C(22)-C(21)	108.4(3)	C(28)-W(2)-C(27)	90.46(17)
C(23)-C(22)-Fe	69.95(19)	C(25)-W(2)-C(27)	94.29(15)
C(21)-C(22)-Fe	70.02(19)	C(29)-W(2)-C(27)	175.95(15)
C(23)-C(22)-H(22A)	125.8	C(28)-W(2)-C(26)	172.16(15)
C(21)-C(22)-H(22A)	125.8	C(25)-W(2)-C(26)	86.90(14)
Fe-C(22)-H(22A)	125.8	C(29)-W(2)-C(26)	89.98(14)

C(22)-C(23)-C(24)	108.0(3)	C(27)-W(2)-C(26)	87.08(14)
C(22)-C(23)-Fe	69.62(19)	C(28)-W(2)-C(19)	91.23(14)
C(24)-C(23)-Fe	69.74(18)	C(25)-W(2)-C(19)	176.72(14)
C(22)-C(23)-H(23A)	126.0	C(29)-W(2)-C(19)	93.34(13)
C(24)-C(23)-H(23A)	126.0	C(27)-W(2)-C(19)	84.20(12)
Fe-C(23)-H(23A)	126.2	C(26)-W(2)-C(19)	95.92(12)

Table F.56: Anisotropic displacement parameters ($\text{Å}^2 \cdot 10^3$) for GSTR004. The anisotropic displacement factor exponent takes the form: $-2\pi^2[h^2a^{*2}U_{11} + ... + 2hka^*b^*U_{12}]$.

	U(11)	U(22)	U(33)	U(23)	U(13)	U(12)
C(1)	16(2)	12(2)	18(2)	1(1)	5(1)	0(1)
C(2)	30(2)	14(2)	31(2)	1(2)	0(2)	4(2)
C(3)	33(2)	30(2)	25(2)	0(2)	-4(2)	8(2)
C(4)	19(2)	35(2)	37(2)	8(2)	6(2)	7(2)
C(5)	26(2)	30(2)	19(2)	-2(2)	8(2)	-1(2)
C(6)	34(2)	28(2)	26(2)	5(2)	13(2)	8(2)
C(7)	26(2)	29(2)	27(2)	-1(2)	10(2)	-6(2)
C(8)	11(2)	14(2)	17(2)	5(1)	2(1)	4(1)
C(9)	18(2)	17(2)	14(1)	5(1)	4(1)	1(1)
C(10)	17(2)	23(2)	16(2)	5(1)	5(1)	-3(1)
C(11)	23(2)	22(2)	19(2)	3(1)	3(1)	-7(1)
C(12)	24(2)	14(2)	21(2)	3(1)	2(1)	-4(1)
C(13)	19(2)	17(2)	19(2)	4(1)	4(1)	1(1)
C(14)	18(2)	25(2)	22(2)	2(2)	4(1)	-1(1)
C(15)	26(2)	25(2)	19(2)	-8(1)	1(2)	-1(2)
C(16)	34(2)	36(2)	18(2)	-4(2)	7(2)	-7(2)
C(17)	25(2)	34(2)	32(2)	-16(2)	8(2)	1(2)
C(18)	22(2)	23(2)	24(2)	-2(2)	4(2)	3(2)
C(19)	18(2)	17(2)	16(2)	0(1)	7(1)	1(1)
C(20)	17(2)	13(2)	18(2)	5(1)	1(1)	3(1)
C(21)	15(2)	16(2)	27(2)	4(1)	1(1)	3(1)
C(22)	17(2)	22(2)	27(2)	5(2)	-1(1)	-3(1)
C(23)	28(2)	19(2)	18(2)	2(1)	-2(1)	-4(2)
C(24)	21(2)	19(2)	16(2)	3(1)	4(1)	-1(1)
C(25)	24(2)	23(2)	50(2)	-3(2)	-14(2)	3(2)
C(26)	24(2)	13(2)	30(2)	5(2)	3(2)	3(1)
C(27)	34(2)	19(2)	42(2)	10(2)	16(2)	3(2)
C(28)	23(2)	18(2)	97(4)	-9(2)	2(2)	7(2)

C(29)	28(2)	29(2)	38(2)	-8(2)	-10(2)	12(2)
Fe	15(1)	14(1)	16(1)	0(1)	3(1)	-2(1)
N(1)	14(1)	17(2)	17(1)	-1(1)	3(1)	-1(1)
N(2)	14(1)	13(2)	22(1)	0(1)	3(1)	-1(1)
O(1)	32(2)	34(2)	22(1)	-10(1)	5(1)	0(1)
O(2)	35(2)	40(2)	33(2)	-9(1)	-6(1)	12(1)
O(3)	64(2)	41(2)	38(2)	1(1)	15(2)	-26(2)
O(4)	25(2)	58(2)	55(2)	-20(2)	-6(1)	16(1)
O(5)	39(2)	27(2)	46(2)	9(1)	7(1)	-1(1)
O(6)	57(2)	14(2)	84(2)	-4(2)	-30(2)	8(1)
O(7)	20(2)	31(2)	53(2)	12(1)	-4(1)	1(1)
O(8)	75(2)	54(2)	34(2)	15(2)	25(2)	7(2)
O(9)	18(2)	33(2)	216(5)	-35(2)	9(2)	-8(1)
O(10)	68(2)	66(2)	30(2)	-10(2)	-9(2)	33(2)
P	13(1)	13(1)	16(1)	0(1)	4(1)	1(1)
Si(1)	14(1)	17(1)	20(1)	0(1)	3(1)	2(1)
Si(2)	17(1)	17(1)	19(1)	2(1)	6(1)	1(1)
W(1)	16(1)	21(1)	16(1)	-2(1)	5(1)	0(1)
W(2)	14(1)	13(1)	30(1)	-1(1)	1(1)	1(1)

Table F.57: Hydrogen coordinates (x 10^4) and isotropic displacement parameters ($\mathring{A}^2 \cdot 10^3$) for GSTR004.

	x	y	z	U(eq)
H(1)	10475	8301	4337	18
H(2A)	10420	5396	3740	38
H(2B)	9958	5362	4417	38
H(2C)	11102	4898	4363	38
H(3A)	10747	6676	5505	45
H(3B)	11646	7490	5453	45
H(3C)	11966	6349	5545	45
H(4A)	12968	7243	4332	45
H(4B)	12563	6508	3745	45
H(4C)	13010	6073	4447	45
H(5A)	9863	6665	2689	37
H(5B)	11112	6460	2868	37
H(5C)	10678	7118	2247	37
H(6A)	9772	9610	3105	43
H(6B)	9069	8770	2707	43
H(6C)	10034	9269	2407	43

H(7A)	12599	8089	3295	40
H(7B)	12210	9017	3676	40
H(7C)	12125	9043	2900	40
H(10A)	5805	6568	5128	22
H(11A)	4982	5272	4346	25
H(12A)	6416	4598	3734	24
H(13A)	8122	5519	4102	22
H(21A)	5227	8304	4008	24
H(22A)	4286	6923	3336	27
H(23A)	5561	6198	2633	26
H(24A)	7311	7118	2874	22
HN1	9270(30)	7620(30)	5069(17)	32(11)
HN2	8780(20)	8990(20)	4017(13)	6(8)

Table F.58: Torsion angles [$^{\text{o}}$] for GSTR004.

N(1)-C(8)-C(9)-C(10)	−157.5(3)	C(11)-C(10)-Fe-C(24)	-171.7(5)
W(1)-C(8)-C(9)-C(10)	22.1(4)	C(9)-C(10)-Fe-C(24)	-51.0(6)
N(1)-C(8)-C(9)-C(13)	21.8(5)	C(11)-C(10)-Fe-C(9)	-120.7(3)
W(1)-C(8)-C(9)-C(13)	−158.6(2)	C(9)-C(10)-Fe-C(21)	119.0(2)
N(1)-C(8)-C(9)-Fe	−68.6(3)	C(9)-C(10)-Fe-C(21)	-120.39(19)
W(1)-C(8)-C(9)-Fe	111.0(2)	C(11)-C(10)-Fe-C(12)	-37.8(2)
C(13)-C(9)-C(10)-C(11)	−0.5(4)	C(9)-C(10)-Fe-C(12)	82.9(2)
C(8)-C(9)-C(10)-C(11)	178.8(3)	C(9)-C(10)-Fe-C(11)	120.7(3)
Fe-C(9)-C(10)-C(11)	58.9(2)	C(11)-C(10)-Fe-C(20)	159.35(19)
C(13)-C(9)-C(10)-Fe	−59.4(2)	C(9)-C(10)-Fe-C(20)	-80.0(2)
C(8)-C(9)-C(10)-Fe	119.9(3)	C(11)-C(12)-Fe-C(13)	120.3(3)
C(9)-C(10)-C(11)-C(12)	1.1(4)	C(13)-C(12)-Fe-C(22)	167.34(17)
Fe-C(10)-C(11)-C(12)	59.5(2)	C(11)-C(12)-Fe-C(22)	-72.3(2)
C(9)-C(10)-C(11)-Fe	−58.4(2)	C(13)-C(12)-Fe-C(23)	126.58(18)
C(10)-C(11)-C(12)-C(13)	−1.2(4)	C(11)-C(12)-Fe-C(23)	-113.1(2)
Fe-C(11)-C(12)-C(13)	58.3(2)	C(13)-C(12)-Fe-C(24)	85.8(2)
C(10)-C(11)-C(12)-Fe	−59.6(2)	C(11)-C(12)-Fe-C(24)	-153.90(19)
C(11)-C(12)-C(13)-C(9)	0.9(4)	C(13)-C(12)-Fe-C(9)	-38.35(17)
Fe-C(12)-C(13)-C(9)	59.7(2)	C(11)-C(12)-Fe-C(9)	82.0(2)
C(11)-C(12)-C(13)-Fe	−58.8(2)	C(13)-C(12)-Fe-C(21)	-164.8(3)
C(10)-C(9)-C(13)-C(12)	−0.2(3)	C(11)-C(12)-Fe-C(21)	-44.5(4)
C(8)-C(9)-C(13)-C(12)	−179.6(3)	C(13)-C(12)-Fe-C(10)	-82.93(19)
Fe-C(9)-C(13)-C(12)	−60.2(2)	C(11)-C(12)-Fe-C(10)	37.39(19)
C(10)-C(9)-C(13)-Fe	59.9(2)	C(13)-C(12)-Fe-C(11)	-120.3(3)

C(8)-C(9)-C(13)-Fe	−119.4(3)	C(13)-C(12)-Fe-C(20)	57.8(4)
N(2)-C(19)-C(20)-C(24)	−47.2(4)	C(11)-C(12)-Fe-C(20)	178.1(3)
W(2)-C(19)-C(20)-C(24)	122.6(3)	C(10)-C(11)-Fe-C(13)	82.2(2)
N(2)-C(19)-C(20)-C(21)	142.7(3)	C(12)-C(11)-Fe-C(13)	-36.94(19)
W(2)-C(19)-C(20)-C(21)	−47.5(4)	C(10)-C(11)-Fe-C(22)	-118.1(2)
N(2)-C(19)-C(20)-Fe	48.2(4)	C(12)-C(11)-Fe-C(22)	122.8(2)
W(2)-C(19)-C(20)-Fe	−142.0(2)	C(10)-C(11)-Fe-C(23)	-158.62(19)
C(24)-C(20)-C(21)-C(22)	−0.9(4)	C(12)-C(11)-Fe-C(23)	82.3(2)
C(19)-C(20)-C(21)-C(22)	170.9(3)	C(10)-C(11)-Fe-C(24)	175.7(3)
Fe-C(20)-C(21)-C(22)	−59.3(2)	C(12)-C(11)-Fe-C(24)	56.6(4)
C(24)-C(20)-C(21)-Fe	58.5(2)	C(10)-C(11)-Fe-C(9)	37.45(19)
C(19)-C(20)-C(21)-Fe	−129.8(3)	C(12)-C(11)-Fe-C(9)	-81.7(2)
C(20)-C(21)-C(22)-C(23)	0.4(4)	C(10)-C(11)-Fe-C(21)	-79.1(2)
Fe-C(21)-C(22)-C(23)	−59.7(2)	C(12)-C(11)-Fe-C(21)	161.73(19)
C(20)-C(21)-C(22)-Fe	60.0(2)	C(12)-C(11)-Fe-C(10)	-119.1(3)
C(21)-C(22)-C(23)-C(24)	0.3(4)	C(10)-C(11)-Fe-C(12)	119.1(3)
Fe-C(22)-C(23)-C(24)	−59.4(2)	C(10)-C(11)-Fe-C(20)	-58.7(5)
C(21)-C(22)-C(23)-Fe	59.7(2)	C(12)-C(11)-Fe-C(20)	-177.8(3)
C(22)-C(23)-C(24)-C(20)	−0.9(4)	C(24)-C(20)-Fe-C(13)	80.4(2)
Fe-C(23)-C(24)-C(20)	−60.2(2)	C(21)-C(20)-Fe-C(13)	-160.85(18)
C(22)-C(23)-C(24)-Fe	59.3(2)	C(19)-C(20)-Fe-C(13)	-40.8(3)
C(21)-C(20)-C(24)-C(23)	1.1(4)	C(24)-C(20)-Fe-C(22)	-81.2(2)
C(19)-C(20)-C(24)-C(23)	−170.6(3)	C(21)-C(20)-Fe-C(22)	37.50(19)
Fe-C(20)-C(24)-C(23)	59.5(2)	C(19)-C(20)-Fe-C(22)	157.5(3)
C(21)-C(20)-C(24)-Fe	−58.5(2)	C(24)-C(20)-Fe-C(23)	-37.58(18)
C(19)-C(20)-C(24)-Fe	129.9(3)	C(21)-C(20)-Fe-C(23)	81.1(2)
C(12)-C(13)-Fe-C(22)	−31.3(4)	C(19)-C(20)-Fe-C(23)	-158.8(3)
C(9)-C(13)-Fe-C(22)	−150.5(3)	C(21)-C(20)-Fe-C(24)	118.7(3)
C(12)-C(13)-Fe-C(23)	−70.7(2)	C(19)-C(20)-Fe-C(24)	-121.2(4)
C(9)-C(13)-Fe-C(23)	170.09(17)	C(24)-C(20)-Fe-C(9)	125.63(18)
C(12)-C(13)-Fe-C(24)	−114.20(19)	C(21)-C(20)-Fe-C(9)	-115.67(19)
C(9)-C(13)-Fe-C(24)	126.58(18)	C(19)-C(20)-Fe-C(9)	4.4(3)
C(12)-C(13)-Fe-C(9)	119.2(2)	C(24)-C(20)-Fe-C(21)	-118.7(3)
C(12)-C(13)-Fe-C(21)	162.6(3)	C(19)-C(20)-Fe-C(21)	120.0(4)
C(9)-C(13)-Fe-C(21)	43.4(4)	C(24)-C(20)-Fe-C(10)	170.05(18)
C(12)-C(13)-Fe-C(10)	80.19(19)	C(21)-C(20)-Fe-C(10)	-71.2(2)
C(9)-C(13)-Fe-C(10)	−39.03(17)	C(19)-C(20)-Fe-C(10)	48.8(3)
C(9)-C(13)-Fe-C(12)	−119.2(2)	C(24)-C(20)-Fe-C(12)	38.1(4)
C(12)-C(13)-Fe-C(11)	37.05(18)	C(21)-C(20)-Fe-C(12)	156.8(3)
C(9)-C(13)-Fe-C(11)	−82.17(18)	C(19)-C(20)-Fe-C(12)	-83.2(5)

C(12)-C(13)-Fe-C(20)	−157.57(18)	C(24)-C(20)-Fe-C(11)	-145.7(4)
C(9)-C(13)-Fe-C(20)	83.2(2)	C(21)-C(20)-Fe-C(11)	-27.0(5)
C(23)-C(22)-Fe-C(13)	−53.6(4)	C(19)-C(20)-Fe-C(11)	93.0(5)
C(21)-C(22)-Fe-C(13)	−172.9(3)	C(9)-C(8)-N(1)-P	32.1(4)
C(21)-C(22)-Fe-C(23)	−119.3(3)	W(1)-C(8)-N(1)-P	-147.57(19)
C(23)-C(22)-Fe-C(24)	37.72(19)	C(20)-C(19)-N(2)-P	-10.1(4)
C(21)-C(22)-Fe-C(24)	−81.6(2)	W(2)-C(19)-N(2)-P	-179.67(15)
C(23)-C(22)-Fe-C(9)	177.3(3)	C(8)-N(1)-P-N(2)	78.9(3)
C(21)-C(22)-Fe-C(9)	57.9(4)	C(8)-N(1)-P-C(1)	179.4(3)
C(23)-C(22)-Fe-C(21)	119.3(3)	C(19)-N(2)-P-N(1)	-88.4(3)
C(23)-C(22)-Fe-C(10)	−155.69(19)	C(19)-N(2)-P-C(1)	171.7(3)
C(21)-C(22)-Fe-C(10)	85.0(2)	Si(2)-C(1)-P-N(1)	-170.91(15)
C(23)-C(22)-Fe-C(12)	−76.6(2)	Si(1)-C(1)-P-N(1)	64.51(17)
C(21)-C(22)-Fe-C(12)	164.11(18)	Si(2)-C(1)-P-N(2)	-74.99(17)
C(23)-C(22)-Fe-C(11)	−115.9(2)	Si(1)-C(1)-P-N(2)	160.44(14)
C(21)-C(22)-Fe-C(11)	124.78(19)	P-C(1)-Si(1)-C(4)	153.46(17)
C(23)-C(22)-Fe-C(20)	81.6(2)	Si(2)-C(1)-Si(1)-C(4)	30.2(2)
C(21)-C(22)-Fe-C(20)	−37.70(18)	P-C(1)-Si(1)-C(3)	-88.47(19)
C(22)-C(23)-Fe-C(13)	159.19(19)	Si(2)-C(1)-Si(1)-C(3)	148.25(17)
C(24)-C(23)-Fe-C(13)	−81.6(2)	P-C(1)-Si(1)-C(2)	32.6(2)
C(24)-C(23)-Fe-C(22)	119.2(3)	Si(2)-C(1)-Si(1)-C(2)	-90.67(19)
C(22)-C(23)-Fe-C(24)	−119.2(3)	P-C(1)-Si(2)-C(7)	171.95(16)
C(22)-C(23)-Fe-C(9)	−175.7(4)	Si(1)-C(1)-Si(2)-C(7)	-65.8(2)
C(24)-C(23)-Fe-C(9)	−56.5(5)	P-C(1)-Si(2)-C(5)	-65.14(19)
C(22)-C(23)-Fe-C(21)	−37.62(19)	Si(1)-C(1)-Si(2)-C(5)	57.2(2)
C(24)-C(23)-Fe-C(21)	81.6(2)	P-C(1)-Si(2)-C(6)	53.7(2)
C(22)-C(23)-Fe-C(10)	49.1(4)	Si(1)-C(1)-Si(2)-C(6)	176.01(17)
C(24)-C(23)-Fe-C(10)	168.4(3)	O(1)-C(14)-W(1)-C(17)	-134(4)
C(22)-C(23)-Fe-C(12)	119.9(2)	O(1)-C(14)-W(1)-C(18)	-46(4)
C(24)-C(23)-Fe-C(12)	−120.8(2)	O(1)-C(14)-W(1)-C(16)	138(4)
C(22)-C(23)-Fe-C(11)	78.2(2)	O(1)-C(14)-W(1)-C(15)	50(4)
C(24)-C(23)-Fe-C(11)	−162.55(19)	O(1)-C(14)-W(1)-C(8)	-17(5)
C(22)-C(23)-Fe-C(20)	−81.6(2)	O(4)-C(17)-W(1)-C(14)	-97(12)
C(24)-C(23)-Fe-C(20)	37.61(18)	O(4)-C(17)-W(1)-C(18)	175(100)
C(23)-C(24)-Fe-C(13)	119.6(2)	O(4)-C(17)-W(1)-C(16)	-3(12)
C(20)-C(24)-Fe-C(13)	−120.99(19)	O(4)-C(17)-W(1)-C(15)	-23(13)
C(23)-C(24)-Fe-C(22)	−37.55(19)	O(4)-C(17)-W(1)-C(8)	88(12)
C(20)-C(24)-Fe-C(22)	81.85(19)	O(5)-C(18)-W(1)-C(14)	-104(5)
C(20)-C(24)-Fe-C(23)	119.4(3)	O(5)-C(18)-W(1)-C(17)	-12(5)
C(23)-C(24)-Fe-C(9)	163.15(19)	O(5)-C(18)-W(1)-C(16)	9(7)

C(20)-C(24)-Fe-C(9)	−77.5(2)	O(5)-C(18)-W(1)-C(15)	169(5)
C(23)-C(24)-Fe-C(21)	−81.3(2)	O(5)-C(18)-W(1)-C(8)	79(5)
C(20)-C(24)-Fe-C(21)	38.05(18)	O(3)-C(16)-W(1)-C(14)	79(6)
C(23)-C(24)-Fe-C(10)	−155.3(5)	O(3)-C(16)-W(1)-C(17)	-13(6)
C(20)-C(24)-Fe-C(10)	−35.9(6)	O(3)-C(16)-W(1)-C(18)	-34(7)
C(23)-C(24)-Fe-C(12)	75.9(2)	O(3)-C(16)-W(1)-C(15)	165(6)
C(20)-C(24)-Fe-C(12)	−164.66(18)	O(3)-C(16)-W(1)-C(8)	-104(6)
C(23)-C(24)-Fe-C(11)	36.6(4)	O(2)-C(15)-W(1)-C(14)	50(6)
C(20)-C(24)-Fe-C(11)	156.0(3)	O(2)-C(15)-W(1)-C(17)	-24(8)
C(23)-C(24)-Fe-C(20)	−119.4(3)	O(2)-C(15)-W(1)-C(18)	137(6)
C(10)-C(9)-Fe-C(13)	−117.2(3)	O(2)-C(15)-W(1)-C(16)	-44(6)
C(8)-C(9)-Fe-C(13)	123.4(3)	O(2)-C(15)-W(1)-C(8)	-135(6)
C(10)-C(9)-Fe-C(22)	37.7(4)	N(1)-C(8)-W(1)-C(14)	7.2(13)
C(13)-C(9)-Fe-C(22)	154.9(3)	C(9)-C(8)-W(1)-C(14)	-172.4(11)
C(8)-C(9)-Fe-C(22)	−81.7(4)	N(1)-C(8)-W(1)-C(17)	123.7(2)
C(10)-C(9)-Fe-C(23)	−148.9(4)	C(9)-C(8)-W(1)-C(17)	-55.9(3)
C(13)-C(9)-Fe-C(23)	−31.7(5)	N(1)-C(8)-W(1)-C(18)	35.7(2)
C(8)-C(9)-Fe-C(23)	91.7(5)	C(9)-C(8)-W(1)-C(18)	-143.9(3)
C(10)-C(9)-Fe-C(24)	166.48(19)	N(1)-C(8)-W(1)-C(16)	-148.1(2)
C(13)-C(9)-Fe-C(24)	−76.3(2)	C(9)-C(8)-W(1)-C(16)	32.3(3)
C(8)-C(9)-Fe-C(24)	47.1(3)	N(1)-C(8)-W(1)-C(15)	-60.0(2)
C(10)-C(9)-Fe-C(21)	78.7(2)	C(9)-C(8)-W(1)-C(15)	120.4(3)
C(13)-C(9)-Fe-C(21)	−164.09(17)	O(9)-C(28)-W(2)-C(25)	-15(5)
C(8)-C(9)-Fe-C(21)	−40.6(3)	O(9)-C(28)-W(2)-C(29)	-103(5)
C(13)-C(9)-Fe-C(10)	117.2(3)	O(9)-C(28)-W(2)-C(27)	79(5)
C(8)-C(9)-Fe-C(10)	−119.4(3)	O(9)-C(28)-W(2)-C(26)	8(6)
C(10)-C(9)-Fe-C(12)	−79.9(2)	O(9)-C(28)-W(2)-C(19)	164(5)
C(13)-C(9)-Fe-C(12)	37.30(17)	O(6)-C(25)-W(2)-C(28)	-23(8)
C(8)-C(9)-Fe-C(12)	160.8(3)	O(6)-C(25)-W(2)-C(29)	70(8)
C(10)-C(9)-Fe-C(11)	−36.36(19)	O(6)-C(25)-W(2)-C(27)	-114(8)
C(13)-C(9)-Fe-C(11)	80.83(19)	O(6)-C(25)-W(2)-C(26)	160(8)
C(8)-C(9)-Fe-C(11)	−155.7(3)	O(6)-C(25)-W(2)-C(19)	-51(10)
C(10)-C(9)-Fe-C(20)	123.25(19)	O(10)-C(29)-W(2)-C(28)	104(9)
C(13)-C(9)-Fe-C(20)	−119.56(18)	O(10)-C(29)-W(2)-C(25)	18(9)
C(8)-C(9)-Fe-C(20)	3.9(3)	O(10)-C(29)-W(2)-C(27)	-112(9)
C(22)-C(21)-Fe-C(13)	172.3(3)	O(10)-C(29)-W(2)-C(26)	-69(9)
C(20)-C(21)-Fe-C(13)	52.9(4)	O(10)-C(29)-W(2)-C(19)	-164(9)
C(20)-C(21)-Fe-C(22)	−119.4(3)	O(8)-C(27)-W(2)-C(28)	134(8)
C(22)-C(21)-Fe-C(23)	37.53(19)	O(8)-C(27)-W(2)-C(25)	-140(8)
C(20)-C(21)-Fe-C(23)	−81.9(2)	O(8)-C(27)-W(2)-C(29)	-10(9)

C(22)-C(21)-Fe-C(24)	81.4(2)	O(8)-C(27)-W(2)-C(26)	-54(8)
C(20)-C(21)-Fe-C(24)	−37.96(18)	O(8)-C(27)-W(2)-C(19)	43(8)
C(22)-C(21)-Fe-C(9)	−154.83(18)	O(7)-C(26)-W(2)-C(28)	1(4)
C(20)-C(21)-Fe-C(9)	85.8(2)	O(7)-C(26)-W(2)-C(25)	24(3)
C(22)-C(21)-Fe-C(10)	−112.1(2)	O(7)-C(26)-W(2)-C(29)	112(3)
C(20)-C(21)-Fe-C(10)	128.50(19)	O(7)-C(26)-W(2)-C(27)	-70(3)
C(22)-C(21)-Fe-C(12)	−38.3(4)	O(7)-C(26)-W(2)-C(19)	-154(3)
C(20)-C(21)-Fe-C(12)	−157.7(3)	N(2)-C(19)-W(2)-C(28)	3.0(3)
C(22)-C(21)-Fe-C(11)	−70.6(2)	C(20)-C(19)-W(2)-C(28)	-166.1(3)
C(20)-C(21)-Fe-C(11)	169.98(18)	N(2)-C(19)-W(2)-C(25)	31(2)
C(22)-C(21)-Fe-C(20)	119.4(3)	C(20)-C(19)-W(2)-C(25)	-138(2)
C(11)-C(10)-Fe-C(13)	−81.4(2)	N(2)-C(19)-W(2)-C(29)	-89.9(3)
C(9)-C(10)-Fe-C(13)	39.26(18)	C(20)-C(19)-W(2)-C(29)	101.0(2)
C(11)-C(10)-Fe-C(22)	76.2(2)	N(2)-C(19)-W(2)-C(27)	93.4(3)
C(9)-C(10)-Fe-C(22)	−163.13(18)	C(20)-C(19)-W(2)-C(27)	-75.8(2)
C(11)-C(10)-Fe-C(23)	42.6(4)	N(2)-C(19)-W(2)-C(26)	179.8(2)
C(9)-C(10)-Fe-C(23)	163.3(3)	C(20)-C(19)-W(2)-C(26)	10.7(2)

F.11   Data for Complex 207
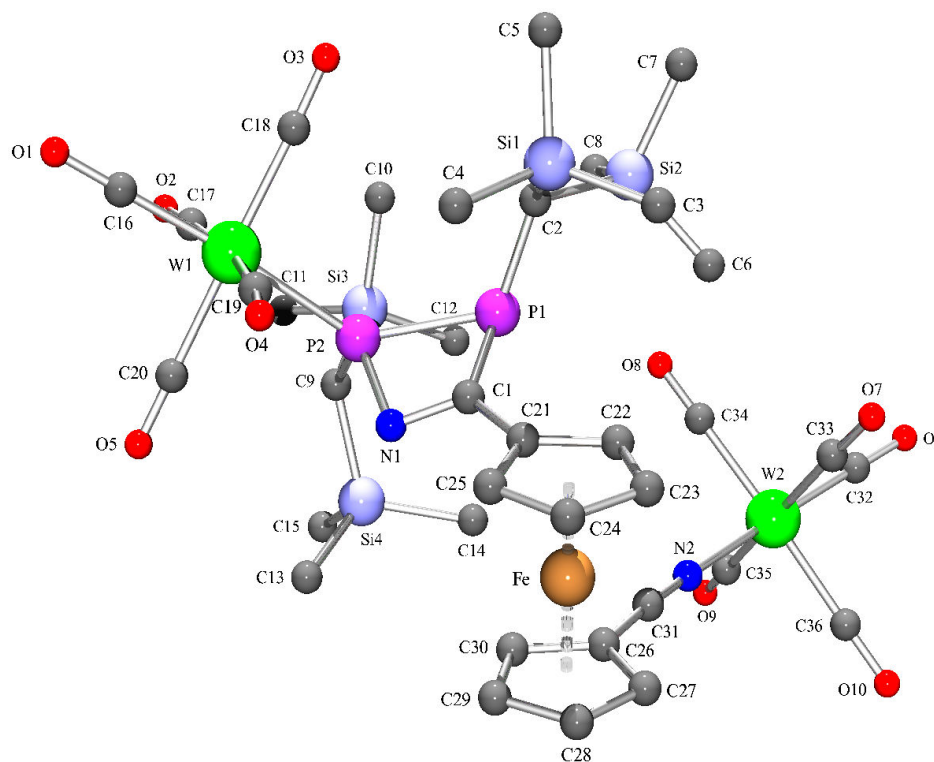
Figure F.13: Molecular structure of complex **207** (GSTR057) in the crystal (hydrogen atoms are omitted for clarity).

Table F.59: Crystal data and structure refinement for GSTR057.

Identification code	GSTR057
Empirical formula	$C_{36}H_{46}FeN_2O_{10}P_2Si_4W_2$
Formula weight	1264.60
Temperature	123(2) K
Wavelength	0.71073 Å
Crystal system, space group	Triclinic, P$\bar{1}$
Unit cell dimensions	a = 11.9658(2) Å, α = 84.768(2)º
	b = 14.4371(3) Å, β = 72.406(2)º
	c = 14.6344(3) Å, γ = 84.245(2)º
Volume	2392.76(8) Å^3
Z, Calculated density	2, 1.755 Mg/m^3
Absorption coefficient	5.312 mm^{-1}
F(000)	1232
Crystal size	0.50 x 0.30 x 0.20 mm
θ range for data collection	1.97 to 29.00º
Limiting indices	-16 $\leq$ h $\leq$ 16, -18 $\leq$ k $\leq$ 19, -19 $\leq$ l $\leq$ 19
Reflections collected / unique	45553 / 12724 [R$_{int}$ = 0.0453]
Completeness to θ = 29.00	100.0 %
Absorption correction	Semi-empirical from equivalents
Max. and min. transmission	0.4163 and 0.1765
Refinement method	Full-matrix least-squares on F^2
Data / restraints / parameters	12724 / 0 / 527
Goodness-of-fit on F^2	1.010
Final R indices [I>2σ(I)]	R$_1$ = 0.0319, wR$_2$ = 0.0802
R indices (all data)	R$_1$ = 0.0388, wR$_2$ = 0.0823
Extinction coefficient	0.00501(18)
Largest diff. peak and hole	1.394 and -1.796 e $\cdot$ A^{-3}

Table F.60: Atomic coordinates (x 10^4) and equivalent isotropic displacement parameters ($\mathring{A}^2 \cdot 10^3$) for GSTR057. U(eq) is defined as one third of the trace of the orthogonalized U$_{ij}$ tensor.

	x	y	z	U(eq)
C(1)	2669(3)	8068(2)	1476(2)	22(1)
C(2)	238(3)	8520(2)	3021(2)	23(1)
C(3)	-795(3)	9160(3)	1297(3)	31(1)
C(4)	1087(4)	10242(3)	1572(3)	33(1)
C(5)	-1279(4)	10332(3)	3031(3)	38(1)
C(6)	-918(4)	6844(3)	2634(3)	34(1)
C(7)	-2472(4)	8277(3)	3942(3)	41(1)
C(8)	-738(4)	7016(3)	4654(3)	36(1)
C(9)	4010(3)	7377(2)	3418(2)	23(1)
C(10)	1782(3)	7889(3)	5100(3)	32(1)
C(11)	3989(4)	6887(3)	5489(3)	35(1)
C(12)	2421(4)	5850(3)	4717(3)	37(1)
C(13)	6058(4)	6870(3)	1614(3)	38(1)
C(14)	3915(4)	5690(3)	2272(3)	35(1)
C(15)	5688(4)	5641(3)	3410(3)	41(1)
C(16)	4140(4)	11149(3)	3370(3)	36(1)
C(17)	3923(4)	9467(3)	4438(3)	31(1)
C(18)	1952(3)	10330(3)	3801(3)	31(1)
C(19)	3677(3)	10454(3)	1795(3)	32(1)
C(20)	5379(4)	9491(3)	2470(3)	41(1)
C(21)	2494(3)	8088(2)	531(2)	23(1)
C(22)	1621(3)	7652(3)	274(2)	27(1)
C(23)	1734(3)	7910(3)	-711(3)	32(1)
C(24)	2675(4)	8494(3)	-1067(3)	32(1)
C(25)	3158(3)	8604(2)	-311(2)	28(1)
C(26)	3599(3)	5835(2)	-346(2)	28(1)
C(27)	3531(4)	6051(3)	-1305(3)	33(1)
C(28)	4412(4)	6657(3)	-1770(3)	38(1)
C(29)	5024(3)	6824(3)	-1120(3)	38(1)
C(30)	4529(3)	6324(3)	-229(3)	30(1)
C(31)	2841(3)	5248(3)	345(3)	29(1)
C(32)	-626(4)	3247(3)	2372(3)	33(1)
C(33)	-407(4)	4839(3)	1262(3)	33(1)
C(34)	563(4)	4629(3)	2907(3)	31(1)
C(35)	1772(4)	2944(3)	2263(3)	36(1)

C(36)	1042(4)	3142(3)	549(3)	34(1)
Fe	3267(1)	7227(1)	-570(1)	23(1)
N(1)	3689(2)	8161(2)	1596(2)	24(1)
N(2)	2194(3)	4758(2)	859(2)	30(1)
O(1)	4402(3)	11857(2)	3510(2)	49(1)
O(2)	4098(3)	9271(2)	5155(2)	43(1)
O(3)	1009(3)	10579(2)	4185(2)	46(1)
O(4)	3792(3)	10784(3)	1045(2)	49(1)
O(5)	6322(3)	9274(3)	2074(3)	64(1)
O(6)	-1479(3)	2880(3)	2724(2)	47(1)
O(7)	-1130(3)	5290(2)	1050(2)	48(1)
O(8)	450(3)	4968(2)	3607(2)	49(1)
O(9)	2257(3)	2376(3)	2613(3)	60(1)
O(10)	1177(3)	2665(2)	-58(2)	54(1)
P(1)	1640(1)	7772(1)	2662(1)	22(1)
P(2)	3266(1)	8311(1)	2831(1)	22(1)
Si(1)	-169(1)	9535(1)	2216(1)	25(1)
Si(2)	-965(1)	7676(1)	3556(1)	27(1)
Si(3)	3042(1)	6996(1)	4671(1)	26(1)
Si(4)	4888(1)	6403(1)	2665(1)	29(1)
W(1)	3680(1)	9911(1)	3142(1)	25(1)
W(2)	771(1)	3927(1)	1706(1)	27(1)

Table F.61: Bond lengths [Å] and angles [º] for GSTR057.

C(1)-N(1)	1.305(4)	C(15)-H(15A)	0.9800
C(1)-C(21)	1.458(4)	C(15)-H(15B)	0.9800
C(1)-P(1)	1.841(3)	C(15)-H(15C)	0.9800
C(1)-P(2)	2.366(3)	C(16)-O(1)	1.153(5)
C(2)-P(1)	1.861(3)	C(16)-W(1)	2.006(4)
C(2)-Si(1)	1.913(3)	C(17)-O(2)	1.137(4)
C(2)-Si(2)	1.915(3)	C(17)-W(1)	2.042(4)
C(2)-H(2A)	1.0000	C(18)-O(3)	1.135(5)
C(3)-Si(1)	1.867(4)	C(18)-W(1)	2.055(4)
C(3)-H(3A)	0.9800	C(19)-O(4)	1.131(5)
C(3)-H(3B)	0.9800	C(19)-W(1)	2.054(4)
C(3)-H(3C)	0.9800	C(20)-O(5)	1.128(6)
C(4)-Si(1)	1.862(4)	C(20)-W(1)	2.030(5)
C(4)-H(4A)	0.9800	C(21)-C(22)	1.429(5)
C(4)-H(4B)	0.9800	C(21)-C(25)	1.436(5)

C(4)-H(4C)	0.9800	C(21)-Fe	2.057(3)
C(5)-Si(1)	1.869(4)	C(22)-C(23)	1.425(5)
C(5)-H(5A)	0.9800	C(22)-Fe	2.052(3)
C(5)-H(5B)	0.9800	C(22)-H(22A)	0.9500
C(5)-H(5C)	0.9800	C(23)-C(24)	1.416(5)
C(6)-Si(2)	1.872(4)	C(23)-Fe	2.052(4)
C(6)-H(6A)	0.9800	C(23)-H(23A)	0.9500
C(6)-H(6B)	0.9800	C(24)-C(25)	1.421(5)
C(6)-H(6C)	0.9800	C(24)-Fe	2.047(4)
C(7)-Si(2)	1.866(4)	C(24)-H(24A)	0.9500
C(7)-H(7A)	0.9800	C(25)-Fe	2.042(3)
C(7)-H(7B)	0.9800	C(25)-H(25A)	0.9500
C(7)-H(7C)	0.9800	C(26)-C(31)	1.416(5)
C(8)-Si(2)	1.871(4)	C(26)-C(30)	1.434(5)
C(8)-H(8C)	0.9800	C(26)-C(27)	1.435(5)
C(8)-H(8B)	0.9800	C(26)-Fe	2.025(4)
C(8)-H(8A)	0.9800	C(27)-C(28)	1.408(6)
C(9)-P(2)	1.833(3)	C(27)-Fe	2.040(4)
C(9)-Si(4)	1.893(4)	C(27)-H(27A)	0.9500
C(9)-Si(3)	1.915(3)	C(28)-C(29)	1.412(6)
C(9)-H(9A)	1.0000	C(28)-Fe	2.054(4)
C(10)-Si(3)	1.875(4)	C(28)-H(28A)	0.9500
C(10)-H(10A)	0.9800	C(29)-C(30)	1.421(5)
C(10)-H(10B)	0.9800	C(29)-Fe	2.055(4)
C(10)-H(10C)	0.9800	C(29)-H(29A)	0.9500
C(11)-Si(3)	1.868(4)	C(30)-Fe	2.042(4)
C(11)-H(11A)	0.9800	C(30)-H(30A)	0.9500
C(11)-H(11B)	0.9800	C(31)-N(2)	1.153(5)
C(11)-H(11C)	0.9800	C(32)-O(6)	1.152(5)
C(12)-Si(3)	1.869(4)	C(32)-W(2)	1.970(4)
C(12)-H(12A)	0.9800	C(33)-O(7)	1.132(5)
C(12)-H(12B)	0.9800	C(33)-W(2)	2.042(4)
C(12)-H(12C)	0.9800	C(34)-O(8)	1.142(5)
C(13)-Si(4)	1.866(4)	C(34)-W(2)	2.045(3)
C(13)-H(13A)	0.9800	C(35)-O(9)	1.130(5)
C(13)-H(13B)	0.9800	C(35)-W(2)	2.038(4)
C(13)-H(13C)	0.9800	C(36)-O(10)	1.137(5)
C(14)-Si(4)	1.871(4)	C(36)-W(2)	2.050(4)
C(14)-H(14A)	0.9800	N(1)-P(2)	1.751(3)
C(14)-H(14B)	0.9800	N(2)-W(2)	2.177(3)

C(14)-H(14C)	0.9800	P(1)-P(2)	2.2543(11)
C(15)-Si(4)	1.875(4)	P(2)-W(1)	2.5188(8)
N(1)-C(1)-C(21)	122.8(3)	C(27)-C(28)-Fe	69.3(2)
N(1)-C(1)-P(1)	107.8(2)	C(29)-C(28)-Fe	69.9(2)
C(21)-C(1)-P(1)	128.9(2)	C(27)-C(28)-H(28A)	125.6
N(1)-C(1)-P(2)	46.71(16)	C(29)-C(28)-H(28A)	125.6
C(21)-C(1)-P(2)	166.3(2)	Fe-C(28)-H(28A)	126.7
P(1)-C(1)-P(2)	63.36(10)	C(28)-C(29)-C(30)	108.9(3)
P(1)-C(2)-Si(1)	123.30(18)	C(28)-C(29)-Fe	69.9(2)
P(1)-C(2)-Si(2)	105.50(16)	C(30)-C(29)-Fe	69.2(2)
Si(1)-C(2)-Si(2)	114.60(17)	C(28)-C(29)-H(29A)	125.6
P(1)-C(2)-H(2A)	103.7	C(30)-C(29)-H(29A)	125.6
Si(1)-C(2)-H(2A)	103.7	Fe-C(29)-H(29A)	126.9
Si(2)-C(2)-H(2A)	103.7	C(29)-C(30)-C(26)	106.7(3)
Si(1)-C(3)-H(3A)	109.5	C(29)-C(30)-Fe	70.2(2)
Si(1)-C(3)-H(3B)	109.5	C(26)-C(30)-Fe	68.7(2)
H(3A)-C(3)-H(3B)	109.5	C(29)-C(30)-H(30A)	126.6
Si(1)-C(3)-H(3C)	109.5	C(26)-C(30)-H(30A)	126.6
H(3A)-C(3)-H(3C)	109.5	Fe-C(30)-H(30A)	126.0
H(3B)-C(3)-H(3C)	109.5	N(2)-C(31)-C(26)	175.5(4)
Si(1)-C(4)-H(4A)	109.5	O(6)-C(32)-W(2)	175.7(4)
Si(1)-C(4)-H(4B)	109.5	O(7)-C(33)-W(2)	174.0(4)
H(4A)-C(4)-H(4B)	109.5	O(8)-C(34)-W(2)	175.7(3)
Si(1)-C(4)-H(4C)	109.5	O(9)-C(35)-W(2)	175.2(4)
H(4A)-C(4)-H(4C)	109.5	O(10)-C(36)-W(2)	176.2(4)
H(4B)-C(4)-H(4C)	109.5	C(26)-Fe-C(27)	41.34(14)
Si(1)-C(5)-H(5A)	109.5	C(26)-Fe-C(30)	41.31(14)
Si(1)-C(5)-H(5B)	109.5	C(27)-Fe-C(30)	69.43(16)
H(5A)-C(5)-H(5B)	109.5	C(26)-Fe-C(25)	156.57(14)
Si(1)-C(5)-H(5C)	109.5	C(27)-Fe-C(25)	160.06(14)
H(5A)-C(5)-H(5C)	109.5	C(30)-Fe-C(25)	119.98(15)
H(5B)-C(5)-H(5C)	109.5	C(26)-Fe-C(24)	162.43(15)
Si(2)-C(6)-H(6A)	109.5	C(27)-Fe-C(24)	123.05(15)
Si(2)-C(6)-H(6B)	109.5	C(30)-Fe-C(24)	152.82(15)
H(6A)-C(6)-H(6B)	109.5	C(25)-Fe-C(24)	40.68(14)
Si(2)-C(6)-H(6C)	109.5	C(26)-Fe-C(22)	110.38(15)
H(6A)-C(6)-H(6C)	109.5	C(27)-Fe-C(22)	120.65(15)
H(6B)-C(6)-H(6C)	109.5	C(30)-Fe-C(22)	129.44(15)
Si(2)-C(7)-H(7A)	109.5	C(25)-Fe-C(22)	68.75(15)

Si(2)-C(7)-H(7B)	109.5	C(24)-Fe-C(22)	68.31(15)
H(7A)-C(7)-H(7B)	109.5	C(26)-Fe-C(23)	127.17(16)
Si(2)-C(7)-H(7C)	109.5	C(27)-Fe-C(23)	106.34(16)
H(7A)-C(7)-H(7C)	109.5	C(30)-Fe-C(23)	166.33(15)
H(7B)-C(7)-H(7C)	109.5	C(25)-Fe-C(23)	68.44(15)
Si(2)-C(8)-H(8C)	109.5	C(24)-Fe-C(23)	40.43(16)
Si(2)-C(8)-H(8B)	109.5	C(22)-Fe-C(23)	40.63(14)
H(8C)-C(8)-H(8B)	109.5	C(26)-Fe-C(28)	68.34(15)
Si(2)-C(8)-H(8A)	109.5	C(27)-Fe-C(28)	40.23(16)
H(8C)-C(8)-H(8A)	109.5	C(30)-Fe-C(28)	68.47(17)
H(8B)-C(8)-H(8A)	109.5	C(25)-Fe-C(28)	123.54(15)
P(2)-C(9)-Si(4)	117.81(17)	C(24)-Fe-C(28)	104.52(16)
P(2)-C(9)-Si(3)	112.04(18)	C(22)-Fe-C(28)	153.17(16)
Si(4)-C(9)-Si(3)	115.67(17)	C(23)-Fe-C(28)	117.26(17)
P(2)-C(9)-H(9A)	102.9	C(26)-Fe-C(29)	68.34(15)
Si(4)-C(9)-H(9A)	102.9	C(27)-Fe-C(29)	68.09(17)
Si(3)-C(9)-H(9A)	102.9	C(30)-Fe-C(29)	40.60(15)
Si(3)-C(10)-H(10A)	109.5	C(25)-Fe-C(29)	106.68(16)
Si(3)-C(10)-H(10B)	109.5	C(24)-Fe-C(29)	117.27(16)
H(10A)-C(10)-H(10B)	109.5	C(22)-Fe-C(29)	166.28(16)
Si(3)-C(10)-H(10C)	109.5	C(23)-Fe-C(29)	151.19(16)
H(10A)-C(10)-H(10C)	109.5	C(28)-Fe-C(29)	40.19(18)
H(10B)-C(10)-H(10C)	109.5	C(26)-Fe-C(21)	122.83(14)
Si(3)-C(11)-H(11A)	109.5	C(27)-Fe-C(21)	156.83(14)
Si(3)-C(11)-H(11B)	109.5	C(30)-Fe-C(21)	110.11(14)
H(11A)-C(11)-H(11B)	109.5	C(25)-Fe-C(21)	41.00(13)
Si(3)-C(11)-H(11C)	109.5	C(24)-Fe-C(21)	68.45(14)
H(11A)-C(11)-H(11C)	109.5	C(22)-Fe-C(21)	40.71(13)
H(11B)-C(11)-H(11C)	109.5	C(23)-Fe-C(21)	68.36(14)
Si(3)-C(12)-H(12A)	109.5	C(28)-Fe-C(21)	162.65(16)
Si(3)-C(12)-H(12B)	109.5	C(29)-Fe-C(21)	127.56(16)
H(12A)-C(12)-H(12B)	109.5	C(1)-N(1)-P(2)	100.4(2)
Si(3)-C(12)-H(12C)	109.5	C(31)-N(2)-W(2)	170.6(3)
H(12A)-C(12)-H(12C)	109.5	C(1)-P(1)-C(2)	116.51(15)
H(12B)-C(12)-H(12C)	109.5	C(1)-P(1)-P(2)	69.74(10)
Si(4)-C(13)-H(13A)	109.5	C(2)-P(1)-P(2)	117.99(11)
Si(4)-C(13)-H(13B)	109.5	N(1)-P(2)-C(9)	109.07(15)
H(13A)-C(13)-H(13B)	109.5	N(1)-P(2)-P(1)	78.43(10)
Si(4)-C(13)-H(13C)	109.5	C(9)-P(2)-P(1)	108.39(11)
H(13A)-C(13)-H(13C)	109.5	N(1)-P(2)-C(1)	32.85(12)

H(13B)-C(13)-H(13C)	109.5	C(9)-P(2)-C(1)	122.09(13)
Si(4)-C(14)-H(14A)	109.5	P(1)-P(2)-C(1)	46.90(8)
Si(4)-C(14)-H(14B)	109.5	N(1)-P(2)-W(1)	110.65(10)
H(14A)-C(14)-H(14B)	109.5	C(9)-P(2)-W(1)	112.51(10)
Si(4)-C(14)-H(14C)	109.5	P(1)-P(2)-W(1)	131.35(4)
H(14A)-C(14)-H(14C)	109.5	C(1)-P(2)-W(1)	121.07(8)
H(14B)-C(14)-H(14C)	109.5	C(4)-Si(1)-C(3)	107.51(18)
Si(4)-C(15)-H(15A)	109.5	C(4)-Si(1)-C(5)	106.3(2)
Si(4)-C(15)-H(15B)	109.5	C(3)-Si(1)-C(5)	109.67(18)
H(15A)-C(15)-H(15B)	109.5	C(4)-Si(1)-C(2)	113.36(16)
Si(4)-C(15)-H(15C)	109.5	C(3)-Si(1)-C(2)	113.39(16)
H(15A)-C(15)-H(15C)	109.5	C(5)-Si(1)-C(2)	106.39(17)
H(15B)-C(15)-H(15C)	109.5	C(7)-Si(2)-C(8)	106.07(19)
O(1)-C(16)-W(1)	179.4(3)	C(7)-Si(2)-C(6)	108.47(19)
O(2)-C(17)-W(1)	175.4(3)	C(8)-Si(2)-C(6)	109.81(19)
O(3)-C(18)-W(1)	177.7(3)	C(7)-Si(2)-C(2)	113.13(18)
O(4)-C(19)-W(1)	172.6(3)	C(8)-Si(2)-C(2)	110.45(16)
O(5)-C(20)-W(1)	178.0(4)	C(6)-Si(2)-C(2)	108.84(16)
C(22)-C(21)-C(25)	107.6(3)	C(11)-Si(3)-C(12)	108.48(19)
C(22)-C(21)-C(1)	127.6(3)	C(11)-Si(3)-C(10)	109.83(18)
C(25)-C(21)-C(1)	124.8(3)	C(12)-Si(3)-C(10)	107.88(19)
C(22)-C(21)-Fe	69.44(19)	C(11)-Si(3)-C(9)	107.00(17)
C(25)-C(21)-Fe	68.95(19)	C(12)-Si(3)-C(9)	113.23(17)
C(1)-C(21)-Fe	129.2(2)	C(10)-Si(3)-C(9)	110.39(16)
C(23)-C(22)-C(21)	108.0(3)	C(13)-Si(4)-C(14)	111.11(19)
C(23)-C(22)-Fe	69.7(2)	C(13)-Si(4)-C(15)	105.4(2)
C(21)-C(22)-Fe	69.84(19)	C(14)-Si(4)-C(15)	109.6(2)
C(23)-C(22)-H(22A)	126.0	C(13)-Si(4)-C(9)	110.98(17)
C(21)-C(22)-H(22A)	126.0	C(14)-Si(4)-C(9)	111.51(17)
Fe-C(22)-H(22A)	126.0	C(15)-Si(4)-C(9)	108.01(18)
C(24)-C(23)-C(22)	108.2(3)	C(16)-W(1)-C(20)	91.41(18)
C(24)-C(23)-Fe	69.6(2)	C(16)-W(1)-C(17)	85.84(15)
C(22)-C(23)-Fe	69.7(2)	C(20)-W(1)-C(17)	90.03(17)
C(24)-C(23)-H(23A)	125.9	C(16)-W(1)-C(19)	87.78(15)
C(22)-C(23)-H(23A)	125.9	C(20)-W(1)-C(19)	83.91(17)
Fe-C(23)-H(23A)	126.4	C(17)-W(1)-C(19)	171.09(14)
C(23)-C(24)-C(25)	108.5(3)	C(16)-W(1)-C(18)	89.21(16)
C(23)-C(24)-Fe	70.0(2)	C(20)-W(1)-C(18)	179.00(16)
C(25)-C(24)-Fe	69.5(2)	C(17)-W(1)-C(18)	90.80(16)
C(23)-C(24)-H(24A)	125.8	C(19)-W(1)-C(18)	95.33(15)

C(25)-C(24)-H(24A)	125.8	C(16)-W(1)-P(2)	175.60(13)
Fe-C(24)-H(24A)	126.3	C(20)-W(1)-P(2)	84.39(13)
C(24)-C(25)-C(21)	107.8(3)	C(17)-W(1)-P(2)	92.85(10)
C(24)-C(25)-Fe	69.8(2)	C(19)-W(1)-P(2)	93.04(11)
C(21)-C(25)-Fe	70.05(19)	C(18)-W(1)-P(2)	95.01(10)
C(24)-C(25)-H(25A)	126.1	C(32)-W(2)-C(35)	89.32(17)
C(21)-C(25)-H(25A)	126.1	C(32)-W(2)-C(33)	83.76(16)
Fe-C(25)-H(25A)	125.6	C(35)-W(2)-C(33)	172.96(16)
C(31)-C(26)-C(30)	127.9(3)	C(32)-W(2)-C(34)	90.60(15)
C(31)-C(26)-C(27)	123.9(3)	C(35)-W(2)-C(34)	86.25(16)
C(30)-C(26)-C(27)	108.2(3)	C(33)-W(2)-C(34)	92.50(15)
C(31)-C(26)-Fe	124.9(3)	C(32)-W(2)-C(36)	88.84(15)
C(30)-C(26)-Fe	70.0(2)	C(35)-W(2)-C(36)	89.49(17)
C(27)-C(26)-Fe	69.9(2)	C(33)-W(2)-C(36)	91.67(17)
C(28)-C(27)-C(26)	107.4(3)	C(34)-W(2)-C(36)	175.71(16)
C(28)-C(27)-Fe	70.4(2)	C(32)-W(2)-N(2)	173.14(14)
C(26)-C(27)-Fe	68.8(2)	C(35)-W(2)-N(2)	97.13(14)
C(28)-C(27)-H(27A)	126.3	C(33)-W(2)-N(2)	89.84(14)
C(26)-C(27)-H(27A)	126.3	C(34)-W(2)-N(2)	92.16(13)
Fe-C(27)-H(27A)	126.0	C(36)-W(2)-N(2)	88.87(13)
C(27)-C(28)-C(29)	108.8(4)		

Table F.62: Anisotropic displacement parameters ($\text{Å}^2 \cdot 10^3$) for GSTR057. The anisotropic displacement factor exponent takes the form: $-2\pi^2[h^2a^{*2}U_{11} + ... + 2hka^*b^*U_{12}]$.

	U(11)	U(22)	U(33)	U(23)	U(13)	U(12)
C(1)	22(2)	20(1)	25(2)	-4(1)	-8(1)	1(1)
C(2)	23(2)	24(2)	22(1)	-3(1)	-7(1)	1(1)
C(3)	29(2)	33(2)	32(2)	-6(1)	-11(1)	2(1)
C(4)	34(2)	27(2)	42(2)	1(2)	-16(2)	-2(2)
C(5)	43(2)	34(2)	38(2)	-10(2)	-16(2)	11(2)
C(6)	35(2)	35(2)	35(2)	-4(2)	-11(2)	-8(2)
C(7)	28(2)	48(2)	43(2)	-1(2)	-5(2)	-3(2)
C(8)	35(2)	39(2)	31(2)	3(2)	-6(2)	-6(2)
C(9)	24(2)	22(2)	25(2)	-1(1)	-10(1)	-2(1)
C(10)	34(2)	36(2)	25(2)	-6(1)	-8(1)	0(2)
C(11)	40(2)	34(2)	34(2)	1(2)	-17(2)	1(2)
C(12)	41(2)	30(2)	38(2)	0(2)	-10(2)	-8(2)
C(13)	28(2)	44(2)	37(2)	-5(2)	-6(2)	4(2)

C(14)	40(2)	32(2)	35(2)	-8(2)	-12(2)	0(2)
C(15)	42(2)	37(2)	46(2)	-5(2)	-18(2)	11(2)
C(16)	45(2)	28(2)	42(2)	4(2)	-21(2)	-14(2)
C(17)	39(2)	27(2)	33(2)	3(1)	-18(2)	-6(2)
C(18)	34(2)	28(2)	31(2)	-3(1)	-10(2)	-3(2)
C(19)	31(2)	35(2)	31(2)	8(2)	-13(2)	-6(2)
C(20)	30(2)	42(2)	52(2)	6(2)	-15(2)	-6(2)
C(21)	23(2)	23(2)	22(1)	-4(1)	-3(1)	2(1)
C(22)	21(2)	33(2)	25(2)	-7(1)	-5(1)	3(1)
C(23)	29(2)	38(2)	29(2)	-9(2)	-10(1)	7(2)
C(24)	42(2)	28(2)	23(2)	-2(1)	-9(2)	5(2)
C(25)	32(2)	23(2)	26(2)	-2(1)	-6(1)	-2(1)
C(26)	32(2)	23(2)	26(2)	-5(1)	-5(1)	1(1)
C(27)	41(2)	29(2)	24(2)	-7(1)	-3(2)	1(2)
C(28)	43(2)	33(2)	28(2)	-6(2)	5(2)	5(2)
C(29)	25(2)	32(2)	44(2)	1(2)	6(2)	-1(2)
C(30)	24(2)	28(2)	34(2)	-1(1)	-5(1)	2(1)
C(31)	32(2)	26(2)	30(2)	-6(1)	-9(2)	0(1)
C(32)	37(2)	37(2)	24(2)	2(1)	-8(2)	-11(2)
C(33)	36(2)	33(2)	30(2)	-2(1)	-11(2)	1(2)
C(34)	40(2)	28(2)	29(2)	-6(1)	-14(2)	-2(2)
C(35)	35(2)	28(2)	42(2)	2(2)	-9(2)	5(2)
C(36)	41(2)	32(2)	26(2)	-8(1)	-1(2)	-13(2)
Fe	24(1)	23(1)	21(1)	-2(1)	-3(1)	-1(1)
N(1)	22(1)	25(1)	25(1)	-3(1)	-7(1)	0(1)
N(2)	33(2)	29(2)	29(1)	1(1)	-10(1)	-5(1)
O(1)	71(2)	35(2)	52(2)	3(1)	-30(2)	-25(2)
O(2)	55(2)	39(2)	43(2)	1(1)	-27(2)	-9(1)
O(3)	36(2)	47(2)	52(2)	-8(1)	-9(1)	1(1)
O(4)	41(2)	67(2)	42(2)	14(2)	-16(1)	-17(2)
O(5)	26(2)	74(3)	84(3)	13(2)	-8(2)	-3(2)
O(6)	48(2)	65(2)	29(1)	1(1)	-7(1)	-24(2)
O(7)	49(2)	54(2)	44(2)	-4(1)	-20(2)	6(2)
O(8)	64(2)	44(2)	42(2)	-8(1)	-21(2)	-3(2)
O(9)	54(2)	50(2)	68(2)	13(2)	-16(2)	8(2)
O(10)	65(2)	52(2)	42(2)	-14(2)	-1(2)	-23(2)
P(1)	20(1)	21(1)	23(1)	-2(1)	-6(1)	-2(1)
P(2)	21(1)	22(1)	23(1)	-2(1)	-7(1)	-2(1)
Si(1)	23(1)	25(1)	27(1)	-4(1)	-8(1)	1(1)
Si(2)	22(1)	31(1)	27(1)	-2(1)	-5(1)	-4(1)

Si(3)	30(1)	26(1)	25(1)	-1(1)	-10(1)	-2(1)
Si(4)	28(1)	26(1)	32(1)	-3(1)	-11(1)	4(1)
W(1)	26(1)	22(1)	31(1)	0(1)	-13(1)	-4(1)
W(2)	30(1)	24(1)	25(1)	-1(1)	-7(1)	-5(1)

Table F.63: Hydrogen coordinates (x 10^4) and isotropic displacement parameters ($\mathring{A}^2 \cdot 10^3$) for GSTR057.

	x	y	z	U(eq)
H(2A)	287	8828	3592	28
H(3A)	-1415	8740	1607	46
H(3B)	-172	8834	806	46
H(3C)	-1126	9710	995	46
H(4A)	1728	9840	1179	50
H(4B)	1365	10523	2041	50
H(4C)	831	10736	1158	50
H(5A)	-1041	10394	3605	57
H(5B)	-2049	10073	3219	57
H(5C)	-1330	10946	2695	57
H(6A)	-123	6538	2408	52
H(6B)	-1126	7186	2091	52
H(6C)	-1479	6372	2921	52
H(7A)	-2640	8632	3389	62
H(7B)	-2518	8702	4439	62
H(7C)	-3049	7811	4199	62
H(8C)	-1339	6567	4903	54
H(8B)	-800	7452	5146	54
H(8A)	44	6681	4490	54
H(9A)	4632	7703	3560	28
H(10A)	1439	8090	4578	47
H(10B)	2065	8428	5300	47
H(10C)	1183	7617	5646	47
H(11A)	4259	7498	5522	53
H(11B)	4670	6446	5241	53
H(11C)	3534	6660	6132	53
H(12A)	3060	5354	4592	55
H(12B)	2010	5869	4228	55
H(12C)	1867	5726	5353	55
H(13A)	6607	7180	1841	57
H(13B)	5698	7320	1222	57

H(13C)	6484	6356	1225	57
H(14A)	3395	6103	1983	53
H(14B)	3440	5329	2829	53
H(14C)	4399	5263	1798	53
H(15A)	5119	5325	3945	62
H(15B)	6142	6025	3663	62
H(15C)	6221	5175	3011	62
H(22A)	1062	7260	688	32
H(23A)	1260	7723	-1068	38
H(24A)	2939	8767	-1703	38
H(25A)	3804	8956	-354	33
H(27A)	2991	5826	-1577	39
H(28A)	4569	6911	-2414	46
H(29A)	5662	7207	-1257	45
H(30A)	4767	6315	335	36

Table F.64: Torsion angles [º] for GSTR057.

N(1)-C(1)-C(21)-C(22)	153.2(3)	C(27)-C(28)-Fe-C(29)	120.3(4)
P(1)-C(1)-C(21)-C(22)	−18.2(5)	C(27)-C(28)-Fe-C(21)	171.9(5)
P(2)-C(1)-C(21)-C(22)	−169.9(8)	C(29)-C(28)-Fe-C(21)	51.6(6)
N(1)-C(1)-C(21)-C(25)	−30.1(5)	C(28)-C(29)-Fe-C(26)	81.6(3)
P(1)-C(1)-C(21)-C(25)	158.4(3)	C(30)-C(29)-Fe-C(26)	-38.9(2)
P(2)-C(1)-C(21)-C(25)	6.7(13)	C(28)-C(29)-Fe-C(27)	37.0(2)
N(1)-C(1)-C(21)-Fe	60.0(4)	C(30)-C(29)-Fe-C(27)	-83.5(2)
P(1)-C(1)-C(21)-Fe	−111.4(3)	C(28)-C(29)-Fe-C(30)	120.5(3)
P(2)-C(1)-C(21)-Fe	96.9(10)	C(28)-C(29)-Fe-C(25)	-122.6(2)
C(25)-C(21)-C(22)-C(23)	−0.9(4)	C(30)-C(29)-Fe-C(25)	116.9(2)
C(1)-C(21)-C(22)-C(23)	176.2(3)	C(28)-C(29)-Fe-C(24)	-80.0(3)
Fe-C(21)-C(22)-C(23)	−59.5(2)	C(30)-C(29)-Fe-C(24)	159.5(2)
C(25)-C(21)-C(22)-Fe	58.6(2)	C(28)-C(29)-Fe-C(22)	169.0(6)
C(1)-C(21)-C(22)-Fe	−124.3(4)	C(30)-C(29)-Fe-C(22)	48.5(7)
C(21)-C(22)-C(23)-C(24)	0.5(4)	C(28)-C(29)-Fe-C(23)	-47.2(4)
Fe-C(22)-C(23)-C(24)	−59.1(3)	C(30)-C(29)-Fe-C(23)	-167.7(3)
C(21)-C(22)-C(23)-Fe	59.6(2)	C(30)-C(29)-Fe-C(28)	-120.5(3)
C(22)-C(23)-C(24)-C(25)	0.1(4)	C(28)-C(29)-Fe-C(21)	-162.9(2)
Fe-C(23)-C(24)-C(25)	−59.0(3)	C(30)-C(29)-Fe-C(21)	76.6(3)
C(22)-C(23)-C(24)-Fe	59.2(3)	C(22)-C(21)-Fe-C(26)	-83.4(2)
C(23)-C(24)-C(25)-C(21)	−0.7(4)	C(25)-C(21)-Fe-C(26)	157.2(2)
Fe-C(24)-C(25)-C(21)	−60.0(2)	C(1)-C(21)-Fe-C(26)	38.9(4)

C(23)-C(24)-C(25)-Fe	59.3(3)	C(22)-C(21)-Fe-C(27)	-43.2(5)
C(22)-C(21)-C(25)-C(24)	1.0(4)	C(25)-C(21)-Fe-C(27)	-162.5(4)
C(1)-C(21)-C(25)-C(24)	−176.2(3)	C(1)-C(21)-Fe-C(27)	79.1(5)
Fe-C(21)-C(25)-C(24)	59.9(3)	C(22)-C(21)-Fe-C(30)	-127.7(2)
C(22)-C(21)-C(25)-Fe	−58.9(2)	C(25)-C(21)-Fe-C(30)	113.0(2)
C(1)-C(21)-C(25)-Fe	123.9(3)	C(1)-C(21)-Fe-C(30)	-5.4(3)
C(31)-C(26)-C(27)-C(28)	179.4(4)	C(22)-C(21)-Fe-C(25)	119.3(3)
C(30)-C(26)-C(27)-C(28)	0.4(4)	C(1)-C(21)-Fe-C(25)	-118.4(4)
Fe-C(26)-C(27)-C(28)	60.1(3)	C(22)-C(21)-Fe-C(24)	81.4(2)
C(31)-C(26)-C(27)-Fe	119.3(4)	C(25)-C(21)-Fe-C(24)	-38.0(2)
C(30)-C(26)-C(27)-Fe	−59.7(3)	C(1)-C(21)-Fe-C(24)	-156.3(3)
C(26)-C(27)-C(28)-C(29)	−0.1(4)	C(25)-C(21)-Fe-C(22)	-119.3(3)
Fe-C(27)-C(28)-C(29)	59.0(3)	C(1)-C(21)-Fe-C(22)	122.3(4)
C(26)-C(27)-C(28)-Fe	−59.1(3)	C(22)-C(21)-Fe-C(23)	37.7(2)
C(27)-C(28)-C(29)-C(30)	−0.2(5)	C(25)-C(21)-Fe-C(23)	-81.6(2)
Fe-C(28)-C(29)-C(30)	58.4(3)	C(1)-C(21)-Fe-C(23)	160.0(3)
C(27)-C(28)-C(29)-Fe	−58.6(3)	C(22)-C(21)-Fe-C(28)	150.2(5)
C(28)-C(29)-C(30)-C(26)	0.5(4)	C(25)-C(21)-Fe-C(28)	30.9(6)
Fe-C(29)-C(30)-C(26)	59.3(2)	C(1)-C(21)-Fe-C(28)	-87.4(6)
C(28)-C(29)-C(30)-Fe	−58.8(3)	C(22)-C(21)-Fe-C(29)	-170.1(2)
C(31)-C(26)-C(30)-C(29)	−179.5(4)	C(25)-C(21)-Fe-C(29)	70.6(3)
C(27)-C(26)-C(30)-C(29)	−0.6(4)	C(1)-C(21)-Fe-C(29)	-47.8(4)
Fe-C(26)-C(30)-C(29)	−60.2(3)	C(21)-C(1)-N(1)-P(2)	168.7(3)
C(31)-C(26)-C(30)-Fe	−119.3(4)	P(1)-C(1)-N(1)-P(2)	-18.2(2)
C(27)-C(26)-C(30)-Fe	59.7(3)	C(26)-C(31)-N(2)-W(2)	-39(7)
C(30)-C(26)-C(31)-N(2)	−175(5)	N(1)-C(1)-P(1)-C(2)	126.8(2)
C(27)-C(26)-C(31)-N(2)	7(5)	C(21)-C(1)-P(1)-C(2)	-60.8(3)
Fe-C(26)-C(31)-N(2)	95(5)	P(2)-C(1)-P(1)-C(2)	112.02(13)
C(31)-C(26)-Fe-C(27)	−117.9(4)	N(1)-C(1)-P(1)-P(2)	14.8(2)
C(30)-C(26)-Fe-C(27)	119.2(3)	C(21)-C(1)-P(1)-P(2)	-172.8(3)
C(31)-C(26)-Fe-C(30)	122.9(4)	Si(1)-C(2)-P(1)-C(1)	1.3(3)
C(27)-C(26)-Fe-C(30)	−119.2(3)	Si(2)-C(2)-P(1)-C(1)	135.64(15)
C(31)-C(26)-Fe-C(25)	79.1(5)	Si(1)-C(2)-P(1)-P(2)	81.3(2)
C(30)-C(26)-Fe-C(25)	−43.8(4)	Si(2)-C(2)-P(1)-P(2)	-144.33(10)
C(27)-C(26)-Fe-C(25)	−163.0(3)	C(1)-N(1)-P(2)-C(9)	120.1(2)
C(31)-C(26)-Fe-C(24)	−86.7(6)	C(1)-N(1)-P(2)-P(1)	14.4(2)
C(30)-C(26)-Fe-C(24)	150.5(5)	C(1)-N(1)-P(2)-W(1)	-115.7(2)
C(27)-C(26)-Fe-C(24)	31.3(6)	Si(4)-C(9)-P(2)-N(1)	-7.1(2)
C(31)-C(26)-Fe-C(22)	−4.3(3)	Si(3)-C(9)-P(2)-N(1)	-144.95(15)
C(30)-C(26)-Fe-C(22)	−127.2(2)	Si(4)-C(9)-P(2)-P(1)	76.69(18)

C(27)-C(26)-Fe-C(22)	113.6(2)	Si(3)-C(9)-P(2)-P(1)	-61.20(17)
C(31)-C(26)-Fe-C(23)	−47.0(4)	Si(4)-C(9)-P(2)-C(1)	26.6(2)
C(30)-C(26)-Fe-C(23)	−169.9(2)	Si(3)-C(9)-P(2)-C(1)	-111.30(17)
C(27)-C(26)-Fe-C(23)	70.9(3)	Si(4)-C(9)-P(2)-W(1)	-130.24(14)
C(31)-C(26)-Fe-C(28)	−155.5(4)	Si(3)-C(9)-P(2)-W(1)	91.87(15)
C(30)-C(26)-Fe-C(28)	81.6(2)	C(1)-P(1)-P(2)-N(1)	-10.64(15)
C(27)-C(26)-Fe-C(28)	−37.6(2)	C(2)-P(1)-P(2)-N(1)	-120.68(16)
C(31)-C(26)-Fe-C(29)	161.1(4)	C(1)-P(1)-P(2)-C(9)	-117.10(16)
C(30)-C(26)-Fe-C(29)	38.2(2)	C(2)-P(1)-P(2)-C(9)	132.86(16)
C(27)-C(26)-Fe-C(29)	−81.0(3)	C(2)-P(1)-P(2)-C(1)	-110.04(16)
C(31)-C(26)-Fe-C(21)	39.4(4)	C(1)-P(1)-P(2)-W(1)	96.77(12)
C(30)-C(26)-Fe-C(21)	−83.4(2)	C(2)-P(1)-P(2)-W(1)	-13.26(14)
C(27)-C(26)-Fe-C(21)	157.4(2)	C(21)-C(1)-P(2)-N(1)	-43.8(10)
C(28)-C(27)-Fe-C(26)	−118.6(3)	P(1)-C(1)-P(2)-N(1)	160.5(3)
C(28)-C(27)-Fe-C(30)	−80.6(3)	N(1)-C(1)-P(2)-C(9)	-74.9(3)
C(26)-C(27)-Fe-C(30)	38.0(2)	C(21)-C(1)-P(2)-C(9)	-118.8(10)
C(28)-C(27)-Fe-C(25)	41.4(6)	P(1)-C(1)-P(2)-C(9)	85.60(16)
C(26)-C(27)-Fe-C(25)	160.0(4)	N(1)-C(1)-P(2)-P(1)	-160.5(3)
C(28)-C(27)-Fe-C(24)	72.2(3)	C(21)-C(1)-P(2)-P(1)	155.6(11)
C(26)-C(27)-Fe-C(24)	−169.2(2)	N(1)-C(1)-P(2)-W(1)	80.0(2)
C(28)-C(27)-Fe-C(22)	154.9(2)	C(21)-C(1)-P(2)-W(1)	36.1(11)
C(26)-C(27)-Fe-C(22)	−86.5(3)	P(1)-C(1)-P(2)-W(1)	-119.51(8)
C(28)-C(27)-Fe-C(23)	113.1(3)	P(1)-C(2)-Si(1)-C(4)	-41.1(3)
C(26)-C(27)-Fe-C(23)	−128.3(2)	Si(2)-C(2)-Si(1)-C(4)	-171.80(18)
C(26)-C(27)-Fe-C(28)	118.6(3)	P(1)-C(2)-Si(1)-C(3)	81.9(2)
C(28)-C(27)-Fe-C(29)	−36.9(3)	Si(2)-C(2)-Si(1)-C(3)	-48.9(2)
C(26)-C(27)-Fe-C(29)	81.7(2)	P(1)-C(2)-Si(1)-C(5)	-157.5(2)
C(28)-C(27)-Fe-C(21)	−173.8(3)	Si(2)-C(2)-Si(1)-C(5)	71.8(2)
C(26)-C(27)-Fe-C(21)	−55.2(5)	P(1)-C(2)-Si(2)-C(7)	-178.46(18)
C(29)-C(30)-Fe-C(26)	118.0(3)	Si(1)-C(2)-Si(2)-C(7)	-39.6(2)
C(29)-C(30)-Fe-C(27)	79.9(3)	P(1)-C(2)-Si(2)-C(8)	62.8(2)
C(26)-C(30)-Fe-C(27)	−38.0(2)	Si(1)-C(2)-Si(2)-C(8)	-158.29(19)
C(29)-C(30)-Fe-C(25)	−80.6(3)	P(1)-C(2)-Si(2)-C(6)	-57.8(2)
C(26)-C(30)-Fe-C(25)	161.5(2)	Si(1)-C(2)-Si(2)-C(6)	81.1(2)
C(29)-C(30)-Fe-C(24)	−43.0(4)	P(2)-C(9)-Si(3)-C(11)	-135.45(19)
C(26)-C(30)-Fe-C(24)	−161.0(3)	Si(4)-C(9)-Si(3)-C(11)	85.7(2)
C(29)-C(30)-Fe-C(22)	−166.7(2)	P(2)-C(9)-Si(3)-C(12)	105.1(2)
C(26)-C(30)-Fe-C(22)	75.3(3)	Si(4)-C(9)-Si(3)-C(12)	-33.8(2)
C(29)-C(30)-Fe-C(23)	154.2(6)	P(2)-C(9)-Si(3)-C(10)	-16.0(2)
C(26)-C(30)-Fe-C(23)	36.2(7)	Si(4)-C(9)-Si(3)-C(10)	-154.82(18)

C(29)-C(30)-Fe-C(28)	36.7(2)	P(2)-C(9)-Si(4)-C(13)	58.1(2)
C(26)-C(30)-Fe-C(28)	−81.3(2)	Si(3)-C(9)-Si(4)-C(13)	-165.53(19)
C(26)-C(30)-Fe-C(29)	−118.0(3)	P(2)-C(9)-Si(4)-C(14)	-66.4(2)
C(29)-C(30)-Fe-C(21)	−124.8(2)	Si(3)-C(9)-Si(4)-C(14)	70.0(2)
C(26)-C(30)-Fe-C(21)	117.3(2)	P(2)-C(9)-Si(4)-C(15)	173.2(2)
C(24)-C(25)-Fe-C(26)	−173.5(3)	Si(3)-C(9)-Si(4)-C(15)	-50.4(2)
C(21)-C(25)-Fe-C(26)	−54.8(4)	O(1)-C(16)-W(1)-C(20)	-109(37)
C(24)-C(25)-Fe-C(27)	41.1(6)	O(1)-C(16)-W(1)-C(17)	-19(37)
C(21)-C(25)-Fe-C(27)	159.7(4)	O(1)-C(16)-W(1)-C(19)	167(100)
C(24)-C(25)-Fe-C(30)	154.7(2)	O(1)-C(16)-W(1)-C(18)	72(37)
C(21)-C(25)-Fe-C(30)	−86.6(2)	O(1)-C(16)-W(1)-P(2)	-92(37)
C(21)-C(25)-Fe-C(24)	118.6(3)	O(5)-C(20)-W(1)-C(16)	-74(13)
C(24)-C(25)-Fe-C(22)	−81.0(2)	O(5)-C(20)-W(1)-C(17)	-159(13)
C(21)-C(25)-Fe-C(22)	37.6(2)	O(5)-C(20)-W(1)-C(19)	14(13)
C(24)-C(25)-Fe-C(23)	−37.3(2)	O(5)-C(20)-W(1)-C(18)	55(18)
C(21)-C(25)-Fe-C(23)	81.4(2)	O(5)-C(20)-W(1)-P(2)	108(13)
C(24)-C(25)-Fe-C(28)	72.0(3)	O(2)-C(17)-W(1)-C(16)	-16(5)
C(21)-C(25)-Fe-C(28)	−169.4(2)	O(2)-C(17)-W(1)-C(20)	75(5)
C(24)-C(25)-Fe-C(29)	112.7(2)	O(2)-C(17)-W(1)-C(19)	28(5)
C(21)-C(25)-Fe-C(29)	−128.7(2)	O(2)-C(17)-W(1)-C(18)	-105(5)
C(24)-C(25)-Fe-C(21)	−118.6(3)	O(2)-C(17)-W(1)-P(2)	160(5)
C(23)-C(24)-Fe-C(26)	51.6(6)	O(4)-C(19)-W(1)-C(16)	49(3)
C(25)-C(24)-Fe-C(26)	171.4(4)	O(4)-C(19)-W(1)-C(20)	-42(3)
C(23)-C(24)-Fe-C(27)	75.8(3)	O(4)-C(19)-W(1)-C(17)	5(4)
C(25)-C(24)-Fe-C(27)	−164.5(2)	O(4)-C(19)-W(1)-C(18)	138(3)
C(23)-C(24)-Fe-C(30)	−173.8(3)	O(4)-C(19)-W(1)-P(2)	-126(3)
C(25)-C(24)-Fe-C(30)	−54.0(4)	O(3)-C(18)-W(1)-C(16)	-32(9)
C(23)-C(24)-Fe-C(25)	−119.8(3)	O(3)-C(18)-W(1)-C(20)	-160(9)
C(23)-C(24)-Fe-C(22)	−37.6(2)	O(3)-C(18)-W(1)-C(17)	53(9)
C(25)-C(24)-Fe-C(22)	82.2(2)	O(3)-C(18)-W(1)-C(19)	-120(9)
C(25)-C(24)-Fe-C(23)	119.8(3)	O(3)-C(18)-W(1)-P(2)	146(9)
C(23)-C(24)-Fe-C(28)	115.2(2)	N(1)-P(2)-W(1)-C(16)	-78.3(15)
C(25)-C(24)-Fe-C(28)	−125.1(2)	C(9)-P(2)-W(1)-C(16)	44.0(15)
C(23)-C(24)-Fe-C(29)	156.2(2)	P(1)-P(2)-W(1)-C(16)	-170.9(15)
C(25)-C(24)-Fe-C(29)	−84.0(3)	C(1)-P(2)-W(1)-C(16)	-113.1(15)
C(23)-C(24)-Fe-C(21)	−81.5(2)	N(1)-P(2)-W(1)-C(20)	-61.17(17)
C(25)-C(24)-Fe-C(21)	38.2(2)	C(9)-P(2)-W(1)-C(20)	61.12(17)
C(23)-C(22)-Fe-C(26)	−123.8(2)	P(1)-P(2)-W(1)-C(20)	-153.81(14)
C(21)-C(22)-Fe-C(26)	117.1(2)	C(1)-P(2)-W(1)-C(20)	-95.98(16)
C(23)-C(22)-Fe-C(27)	−79.1(3)	N(1)-P(2)-W(1)-C(17)	-150.92(16)

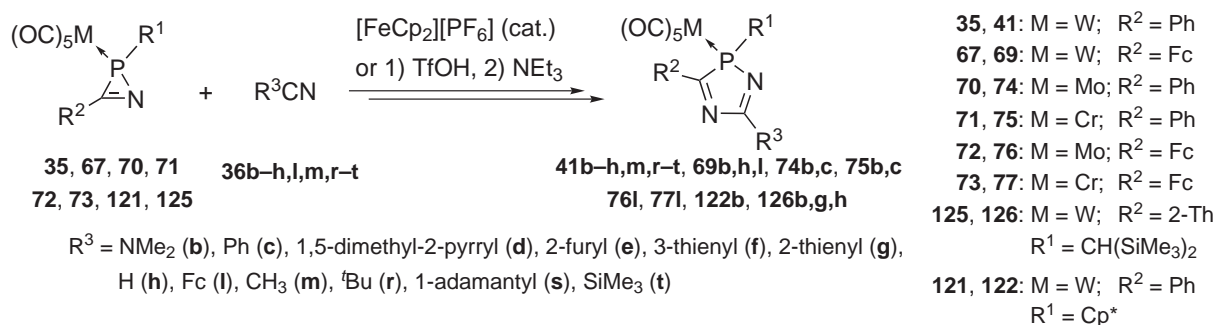|			
C(21)-C(22)-Fe-C(27)	161.8(2)	C(9)-P(2)-W(1)-C(17)	-28.63(17)
C(23)-C(22)-Fe-C(30)	−166.8(2)	P(1)-P(2)-W(1)-C(17)	116.44(13)
C(21)-C(22)-Fe-C(30)	74.1(3)	C(1)-P(2)-W(1)-C(17)	174.27(15)
C(23)-C(22)-Fe-C(25)	81.2(2)	N(1)-P(2)-W(1)-C(19)	22.40(16)
C(21)-C(22)-Fe-C(25)	−37.9(2)	C(9)-P(2)-W(1)-C(19)	144.69(16)
C(23)-C(22)-Fe-C(24)	37.4(2)	P(1)-P(2)-W(1)-C(19)	-70.24(12)
C(21)-C(22)-Fe-C(24)	−81.7(2)	C(1)-P(2)-W(1)-C(19)	-12.41(15)
C(21)-C(22)-Fe-C(23)	−119.1(3)	N(1)-P(2)-W(1)-C(18)	118.03(15)
C(23)-C(22)-Fe-C(28)	−41.8(4)	C(9)-P(2)-W(1)-C(18)	-119.69(16)
C(21)-C(22)-Fe-C(28)	−160.9(3)	P(1)-P(2)-W(1)-C(18)	25.38(12)
C(23)-C(22)-Fe-C(29)	154.1(6)	C(1)-P(2)-W(1)-C(18)	83.22(14)
C(21)-C(22)-Fe-C(29)	35.0(7)	O(6)-C(32)-W(2)-C(35)	-163(5)
C(23)-C(22)-Fe-C(21)	119.1(3)	O(6)-C(32)-W(2)-C(33)	18(5)
C(24)-C(23)-Fe-C(26)	−162.7(2)	O(6)-C(32)-W(2)-C(34)	110(5)
C(22)-C(23)-Fe-C(26)	77.7(3)	O(6)-C(32)-W(2)-C(36)	-74(5)
C(24)-C(23)-Fe-C(27)	−122.2(2)	O(6)-C(32)-W(2)-N(2)	-3(6)
C(22)-C(23)-Fe-C(27)	118.3(2)	O(9)-C(35)-W(2)-C(32)	-13(5)
C(24)-C(23)-Fe-C(30)	167.9(6)	O(9)-C(35)-W(2)-C(33)	-2(6)
C(22)-C(23)-Fe-C(30)	48.4(7)	O(9)-C(35)-W(2)-C(34)	78(5)
C(24)-C(23)-Fe-C(25)	37.5(2)	O(9)-C(35)-W(2)-C(36)	-102(5)
C(22)-C(23)-Fe-C(25)	−82.1(2)	O(9)-C(35)-W(2)-N(2)	170(5)
C(22)-C(23)-Fe-C(24)	−119.5(3)	O(7)-C(33)-W(2)-C(32)	-8(3)
C(24)-C(23)-Fe-C(22)	119.5(3)	O(7)-C(33)-W(2)-C(35)	-19(4)
C(24)-C(23)-Fe-C(28)	−80.2(2)	O(7)-C(33)-W(2)-C(34)	-99(3)
C(22)-C(23)-Fe-C(28)	160.2(2)	O(7)-C(33)-W(2)-C(36)	80(3)
C(24)-C(23)-Fe-C(29)	−48.0(4)	O(7)-C(33)-W(2)-N(2)	169(3)
C(22)-C(23)-Fe-C(29)	−167.6(3)	O(8)-C(34)-W(2)-C(32)	57(5)
C(24)-C(23)-Fe-C(21)	81.7(2)	O(8)-C(34)-W(2)-C(35)	-32(5)
C(22)-C(23)-Fe-C(21)	−37.8(2)	O(8)-C(34)-W(2)-C(33)	141(5)
C(27)-C(28)-Fe-C(26)	38.6(2)	O(8)-C(34)-W(2)-C(36)	-26(6)
C(29)-C(28)-Fe-C(26)	−81.6(3)	O(8)-C(34)-W(2)-N(2)	-130(5)
C(29)-C(28)-Fe-C(27)	−120.3(4)	O(10)-C(36)-W(2)-C(32)	-42(6)
C(27)-C(28)-Fe-C(30)	83.2(3)	O(10)-C(36)-W(2)-C(35)	47(6)
C(29)-C(28)-Fe-C(30)	−37.1(2)	O(10)-C(36)-W(2)-C(33)	-126(6)
C(27)-C(28)-Fe-C(25)	−164.3(2)	O(10)-C(36)-W(2)-C(34)	40(7)
C(29)-C(28)-Fe-C(25)	75.5(3)	O(10)-C(36)-W(2)-N(2)	144(6)
C(27)-C(28)-Fe-C(24)	−124.5(3)	C(31)-N(2)-W(2)-C(32)	3(3)
C(29)-C(28)-Fe-C(24)	115.3(2)	C(31)-N(2)-W(2)-C(35)	162.5(18)
C(27)-C(28)-Fe-C(22)	−54.0(5)	C(31)-N(2)-W(2)-C(33)	-18.5(18)
C(29)-C(28)-Fe-C(22)	−174.2(3)	C(31)-N(2)-W(2)-C(34)	-111.0(18)

C(27)-C(28)-Fe-C(23)	−83.2(3)	C(31)-N(2)-W(2)-C(36)	73.1(19)
C(29)-C(28)-Fe-C(23)	156.6(2)		

Summary – Electrophilic Ring Bond Activation of 2*H*-Azaphosphirene Complexes

In combined experimental and computational studies the scope of different strategies for P,N bond activation and ring expansion of 2*H*-azaphosphirene complexes was investigated.

First, a protocol using nitriles and catalytic amounts of SET oxidants such as [FeCp$_2$][PF$_6$] was explored, which leads to 2*H*-1,4,2-diazaphosphole complexes (**Scheme 1**); derivatives **41b,g** were isolated and structurally confirmed. Studies on the reaction course revealed evidence for a radical cation chain reaction mechanism. For reactions of **35** with **36d–g** it was demonstrated that the amount of [FeCp$_2$][PF$_6$] can be reduced to $0.05-0.025$ equivalents. In reactions of **35**, **67**, **70–73** with [FeCp$_2$][PF$_6$] in the *absence of nitriles* symmetrically 3,5-disubstituted 2*H*-1,4,2-diazaphosphole complexes **41c**, **69l**, **74c**, **75c**, **77l** were formed; complex **69l** was isolated and structurally confirmed. Here, the nitrile fragment that is required for their formation stems from the 2*H*-azaphosphirene complex. DFT calculations on the reaction mechanism revealed that the 2*H*-azaphosphirene complex is oxidized in the first step and the resulting cationic species is a metal-centered radical that shows *ligand-centered reactivity*, as nucleophilic attack of a nitrile causes ring opening followed by facile cyclization of the acyclic intermediate.

(OC)$_5$M⟍ R^1 [FeCp$_2$][PF$_6$] (cat.)   (OC)$_5$M⟍ R^1

P   or 1) TfOH, 2) NEt$_3$ R^2⟍P⟍N

R^2—N   +   R^{3}CN   ⟶   N⟍R^3

35, **67**, **70**, **71**   **36b–h,l,m,r–t**   **41b–h,m,r–t**, **69b,h,l**, **74b,c**, **75b,c**
72, **73**, **121**, **125**   **76l**, **77l**, **122b**, **126b,g,h**

R^3 = NMe$_2$ (**b**), Ph (**c**), 1,5-dimethyl-2-pyrryl (**d**), 2-furyl (**e**), 3-thienyl (**f**), 2-thienyl (**g**), H (**h**), Fc (**l**), CH$_3$ (**m**), ^{t}Bu (**r**), 1-adamantyl (**s**), SiMe$_3$ (**t**)

35, **41**: M = W; R^2 = Ph
67, **69**: M = W; R^2 = Fc
70, **74**: M = Mo; R^2 = Ph
71, **75**: M = Cr; R^2 = Ph
72, **76**: M = Mo; R^2 = Fc
73, **77**: M = Cr; R^2 = Fc
125, **126**: M = W; R^2 = 2-Th
      R^1 = CH(SiMe$_3$)$_2$
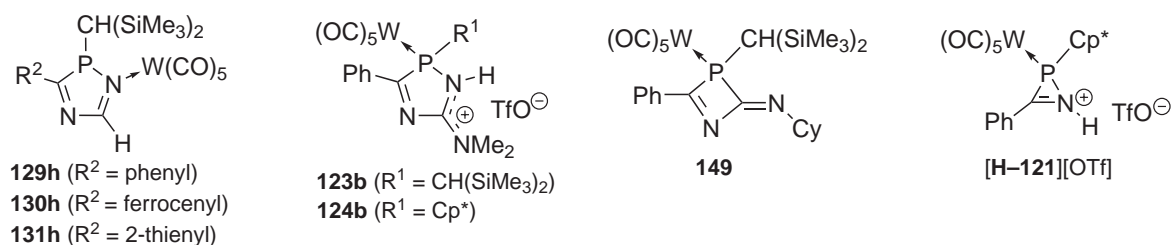**121**, **122**: M = W; R^2 = Ph
      R^1 = Cp*

Scheme 1.

The synthesis of complexes **41b,g,h,m,r–t**, **69b,l**, **74b**, **75b**, **122b**, **126b,g,h** from 2*H*-azaphosphirene complexes and nitriles was achieved by consecutive reaction with the strong acid TfOH and a base (**Scheme 1**); all products were isolated and unambiguously identified. This protocol offers new synthetic perspectives as even nitriles with high steric demand could successfully be employed, and it enabled access to the first *C*-SiMe$_3$ ring-functionalized 2*H*-1,4,2-diazaphosphole complex **41t**. By ^{31}P NMR spectroscopy evidence was obtained for the formation of 2*H*-1,4,2-diazaphospholium complexes. Derivatives **123b** and **124b** were isolated (**Figure 1**), and a single-crystal X-ray diffraction study was carried out on **123b**. Reactions with HCN afforded complexes **41h**, **69h**, **126h** each in the mixture with its κN-bonded coordination isomer **129h**, **130h**, or **131h**, respectively (**Figure 1**). A chemical equilibrium between the two haptomeric complexes was evidenced by ^{31}P{^{1}H} NMR spectroscopic measurements at varying temperatures. In ring expansion reactions of molybdenum and chromium complexes **70** and **71** with **36b** partial decomplexation was observed, but this could completely be prevented by adding the base at low temperature. On the other hand, after prolonged reaction times the N^1-protonated liberated 2*H*-1,4,2-diazaphosphole ligand was quantitatively formed and could be characterized by NMR spectroscopy. Subsequent deprotonation afforded the neutral heterocycle. Although it decomposed during column chromatography, all relevant NMR spectroscopic information was obtained from the raw product. Reaction of **35** with cyclohexyl isocyanide yielded the novel 2,3-dihydro-1,3-azaphosphete complex **149** (**Figure 1**); its molecular structure was confirmed by single-crystal X-ray diffractometry. Investigations on the applicability

of various Brønsted and Lewis acids to induce the reaction of **35** with **36b** showed that good results can be obtained also with CF_3CO_2H, $B(C_6F_5)_3$, and $Li[B(C_6F_5)_4]$.

Reaction of **35** with TfOH in the absence of trapping reagents resulted in partial desilylation of R^1 combined with ring opening, thus leading to coorination-isomeric N-protonated 1-aza-3-phosphabutadiene complexes. Their characterization was achieved by multinuclear NMR spectroscopy at low temperature. Subsequent reaction with nitrile **36b** and deprotonation yielded a $2H$-1,4,2-diazaphosphole complex with $R^1 = CH_2SiMe_3$, which was isolated and structurally confirmed. The first $2H$-azaphosphirenium complex [**H–121**][OTf] was observed in the reaction of **121** with TfOH (**Figure 1**). It was characterized by multinuclear one- and two-dimensional NMR experiments. Upon addition of nitrile **36b** ring expansion occurred with formation of **124b**. It was demonstrated that the protonation of **121** can be reversed through addition of NEt_3. On the basis of DFT calculations a mechanism for the acid-induced ring expansion of $2H$-azaphosphirene complexes with nitriles and isonitriles is proposed. Upon N-protonation the resulting $2H$-azaphosphirenium complex is prone to undergo spontaneous ring opening with formation of a phosphenium complex. Following nucleophilic attack of a nitrile or an isonitrile and subsequent cyclization and deprotonation yields the final products.

129h (R^2 = phenyl)
130h (R^2 = ferrocenyl)
131h (R^2 = 2-thienyl)

123b (R^1 = $CH(SiMe_3)_2$)
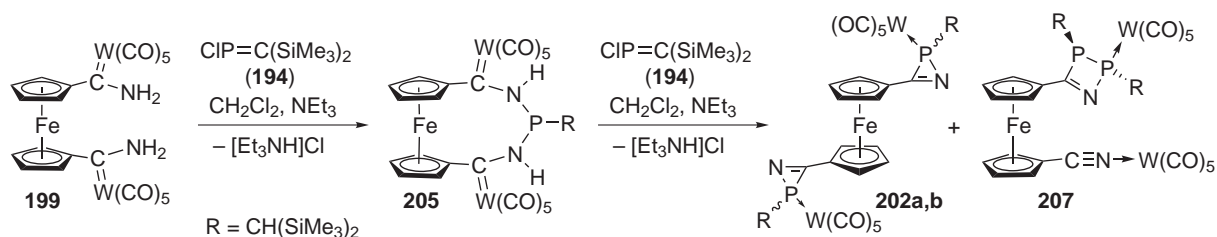**124b** (R^1 = Cp*)

149

[**H–121**][OTf]

Figure 1.

In their UV/Vis spectra $2H$-1,4,2-diazaphosphole complexes show absorption bands at very long wavelengths. This was interpreted on the basis of TD-DFT calclulations, which revealed that the lowest-lying transition is assigned to a metal−ligand charge transfer (MLCT) process.

In the reaction of **41h** and **129h** with MeOTf and TfOH methylation of the N^4-center occurred in combination with partial desilylation at the exocyclic P-substituent. Both $SiMe_3$ groups of **126h** and **131h** could be removed via reaction with [$^nBu_4N$]F in the presence of [Et_3NH][OTf], which afforded a P-methyl substituted $2H$-1,4,2-diazaphosphole complex.

Finally, the synthesis of bis-$2H$-azaphosphirene complexes **202a,b** is presented. Reaction of **199** with one equivalent of **194** and NEt_3 in a dilute CH_2Cl_2 solution yielded ferrocenophane complex **205**, which was isolated and structurally confirmed. Subsequent reaction with **194** and NEt_3 afforded a mixture of **202a,b** and 2,3-dihydro-1,2,3-azadiphosphete complex **207**. The structure of the latter was determined by a by single-crystal X-ray diffraction study. It could completely be separated, and a purified mixture of the complexes **202a,b** was obtained.

Scheme 2.